SPATIOTEMPORAL PARTICULATE MATTER CONCENTRATION PREDICTION USING MODIS AEROSOL OPTICAL DEPTH IN RURAL AND URBAN LANDSCAPES, THAILAND

PIRADA TONGPRASERT

A Thesis Submitted in Partial Fulfillment of the Requirements for the
Degree of Doctor of Philosophy in Geoinformatics
Suranaree University of Technology
Academic Year 2021

การประมาณค่าความเข้มข้นฝุ่นละอองขนาดเล็กเชิงพื้นที่และเชิงเวลา ด้วยข้อมูลความลึกเชิงแสงของละอองลอยในภูมิทัศน์ชนบทและภูมิทัศน์เมือง ประเทศไทย

นางสาวพิรฎา ทองประเสริฐ

วิทยานิพนธ์นี้เป็นส่วนหนึ่งของการศึกษาตามหลักสูตรปริญญาวิทยาศาสตรดุษฎีบัณฑิต
สาขาวิชาภูมิสารสนเทศ
มหาวิทยาลัยเทคโนโลยีสุรนารี
ปีการศึกษา 2564

SPATIOTEMPORAL PARTICULATE MATTER CONCENTRATION PREDICTION USING MODIS AEROSOL OPTICAL DEPTH IN RURAL AND URBAN LANDSCAPES, THAILAND

Suranaree University of Technology has approved this thesis submitted in partial fulfillment of the requirements for the Degree of Doctor of Philosophy.

Thesis Examining Committee

(Assoc. Prof. Dr. Sura Pattanakiat)
Chairperson

(Assoc. Prof. Dr. Suwit Ongsomwang)
Member (Thesis Advisor)

(Assoc. Prof. Dr. Songkot Dasananda)
Member

(Asst. Prof. Dr. Pantip Piyatadsananon)
Member

(Dr. Tanakorn Sritarapipat)
Member

(Dr. Siripon Kamontum)
Member

(Assoc. Prof. Dr. Chatchai Jothityangkoon)
Vice Rector for Academic Affairs
and Quality Assurance

(Prof. Dr. Santi Maensiri)
Dean of Institute of Science

พิรฎา ทองประเสริฐ : การประมาณค่าความเข้มข้นฝุ่นละอองขนาดเล็กเชิงพื้นที่และเชิงเวลาด้วยข้อมูลความลึกเชิงแสงของละอองลอยในภูมิทัศน์ชนบทและภูมิทัศน์เมือง ประเทศไทย (SPATIOTEMPORAL PARTICULATE MATTER CONCENTRATION PREDICTION USING MODIS AEROSOL OPTICAL DEPTH IN RURAL AND URBAN LANDSCAPES, THAILAND) อาจารย์ที่ปรึกษา : รองศาสตราจารย์ ดร.สุวิทย์ อ๋องสมหวัง, 395 หน้า.

คำสำคัญ: ความเข้มข้นฝุ่นละอองขนาดเล็ก/แบบจำลองการประมาณค่าความเข้มข้นฝุ่นละอองขนาดเล็ก/แบบจำลองที่เหมาะสม/ ภูมิทัศน์ชนบท/ ภูมิทัศน์เมือง

การประมาณค่าความเข้มข้นฝุ่นละอองขนาดเล็กเชิงพื้นที่และเชิงเวลาด้วยข้อมูลความลึกเชิงแสงของละอองลอยกับปัจจัยที่มีนัยสำคัญในภูมิทัศน์ชนบทและภูมิทัศน์เมืองในประเทศไทยนับว่าเป็นเรื่องสำคัญต่อสาธารณชน เนื่องจากจำนวนสถานีตรวจสอบติดตามทางภาคพื้นดินมีอย่างจำกัด การศึกษานี้จะให้รูปแบบเชิงพื้นที่ของความเข้มข้นฝุ่นละอองขนาดเล็กไม่เกิน 10 และ 2.5 ไมครอน และการจำแนกดัชนีคุณภาพอากาศระดับอำเภอในสองภูมิทัศน์ ทั้งในฤดูหนาวและฤดูร้อน ผลการศึกษาที่ได้รับสามารถนำมาใช้เป็นแนวทางสำหรับปรับปรุงคุณภาพอากาศและลดผลกระทบต่อสุขภาพของประชาชนได้ วัตถุประสงค์ของการวิจัย คือ (1) เพื่อระบุปัจจัยที่มีนัยสำคัญต่อความเข้มข้นของฝุ่นละอองขนาดเล็กไม่เกิน 10 ไมครอน ในภูมิทัศน์ชนบท และ 2.5 ไมครอน ในภูมิทัศน์เมือง ในฤดูหนาวและฤดูร้อน และความสัมพันธ์ระหว่างปัจจัยต่าง ๆ ด้วยการทดสอบภาวะร่วมเส้นตรงพหุและการวิเคราะห์เชิงเส้นกำลังสองน้อยที่สุด (2) เพื่อประมาณค่าความเข้มข้นฝุ่นละอองขนาดเล็กไม่เกิน 10 และ 2.5 ไมครอน ด้วยแบบจำลองถดถอยแบบถ่วงน้ำหนักและแบบจำลองอิทธิพลผสม และ (3) เพื่อประเมินหาแบบจำลองเชิงพื้นที่และเชิงเวลาที่เหมาะสมสำหรับการประมาณค่าความเข้มข้นฝุ่นละอองขนาดเล็กไม่เกิน 10 และ 2.5 ไมครอน และการตรวจสอบความถูกต้อง

การศึกษานี้เริ่มจากการเตรียมตัวแปรตามและตัวแปรอิสระ ซึ่งประกอบด้วย ความเข้มข้นของละอองขนาดเล็กทางภาคพื้นดิน ความชื้นสัมพัทธ์ อุณหภูมิ ความเร็วลม ความกดอากาศ ทัศนวิสัย อุณหภูมิความสว่างและพลังงานการแผ่รังสีของไฟ ด้วยวิธีการประมาณค่าในช่วงที่เหมาะสม ส่วนตัวแปรอิสระที่เหลือ ได้แก่ ข้อมูลความลึกเชิงแสงของละอองลอย ดัชนีความต่างพืชพรรณ ดัชนีสิ่งปลูกสร้าง ความหนาแน่นถนน ความหนาแน่นโรงงาน ระดับความสูง จุดความร้อน ความหนาแน่นประชากร ผลิตภัณฑ์มวลรวมระดับจังหวัด จัดเตรียมด้วยการวิเคราะห์เชิงพื้นที่ จากนั้น ทำการวิเคราะห์สถิติตามขอบเขตเพื่อคำนวณค่าเฉลี่ยและค่าเบี่ยงเบนมาตรฐานของตัวแปรทั้งหมดและปรับให้เป็นค่ามาตรฐานด้วยวิธีคะแนนมาตรฐาน จากนั้นนำตัวแปรตามและตัวแปรอิสระของความเข้มข้นฝุ่นละอองขนาดเล็กไม่เกิน 10 และ 2.5 ไมครอน ในภูมิทัศน์ชนบทและภูมิทัศน์เมือง ในฤดูหนาวและฤดูร้อน มาวิเคราะห์หาปัจจัยเชิงพื้นที่และเชิงเวลาพื้นที่ที่มีนัยสำคัญด้วยการทดสอบภาวะร่วม

เส้นตรงพหุและการวิเคราะห์เชิงเส้นกำลังสองน้อยที่สุด และนำปัจจัยที่มีนัยสำคัญที่ได้ไปใช้ประมาณค่าความเข้มข้นฝุ่นละอองขนาดเล็กไม่เกิน 10 และ 2.5 ไมครอนแบบรายเดือนและฤดูกาลด้วยแบบจำลองถดถอยแบบถ่วงน้ำหนักและแบบจำลองอิทธิพลผสม พร้อมกับเลือกแบบจำลองที่เหมาะสมสำหรับการประมาณค่าความเข้มข้นฝุ่นละอองขนาดเล็กด้วยเกณฑ์ข้อสนเทศของอาไคเคะและการตรวจสอบความถูกต้องด้วยการวิเคราะห์สหสัมพันธ์กับข้อมูลและปัจจัยที่มีนัยสำคัญชุดใหม่

ผลการศึกษา พบว่า การประมาณค่าความเข้มข้นฝุ่นละอองขนาดเล็กไม่เกิน 10 ไมครอน ในฤดูหนาว ด้วยแบบจำลองถดถอยแบบถ่วงน้ำหนักและแบบจำลองอิทธิพลผสม ให้ค่าระหว่าง 50.53 ถึง 85.79 ไมโครกรัมต่อลูกบาศก์เมตร และ 50.68 ถึง 84.59 ไมโครกรัมต่อลูกบาศก์เมตร ตามลำดับ และในฤดูร้อนให้ค่าระหว่าง 36.92 ถึง 51.32 ไมโครกรัมต่อลูกบาศก์เมตร และ 37.08 ถึง 50.81 ไมโครกรัมต่อลูกบาศก์เมตร ตามลำดับ ในขณะเดียวกัน การประมาณค่าความเข้มข้นฝุ่นละอองขนาดเล็กไม่เกิน 2.5 ไมครอน ในฤดูหนาว ด้วยแบบจำลองถดถอยแบบถ่วงน้ำหนักและแบบจำลองอิทธิพลผสม ให้ค่าระหว่าง 25.33 ถึง 44.37 ไมโครกรัมต่อลูกบาศก์เมตร และ 25.45 ถึง 44.36 ไมโครกรัมต่อลูกบาศก์เมตร ตามลำดับ และในฤดูร้อนให้ค่าระหว่าง 16.69 ถึง 24.04 ไมโครกรัมต่อลูกบาศก์เมตร และ 16.68 ถึง 23.75 ไมโครกรัมต่อลูกบาศก์เมตร ตามลำดับ นอกจากนี้ เกณฑ์ข้อสนเทศของอาไคเคะเฉลี่ยที่ได้จากแบบจำลองถดถอยแบบถ่วงน้ำหนักมีค่าน้อยกว่าแบบจำลองอิทธิพลผสม ดังนั้น แบบจำลองถดถอยแบบถ่วงน้ำหนักจึงเป็นแบบจำลองที่เหมาะสมสำหรับการประมาณค่าความเข้มข้นฝุ่นละอองขนาดเล็กไม่เกิน 10 และ 2.5 ไมครอน ในเชิงพื้นที่และเชิงเวลา การกระจายตัวเชิงพื้นที่ของความเข้มข้นฝุ่นละอองขนาดเล็กไม่เกิน 10 ไมครอน เกิดขึ้นบ่อยครั้งในพื้นที่ตอนกลางของภูมิทัศน์ชนบท โดยเฉพาะอย่างยิ่ง บริเวณตอนเหนือของจังหวัดสระบุรีและตอนใต้ของจังหวัดลพบุรี ในขณะที่ การกระจายเชิงพื้นที่ของความเข้มข้นฝุ่นละอองขนาดเล็กไม่เกิน 2.5 ไมครอนสูง เกิดขึ้นบ่อยครั้งทางตะวันตกของภูมิทัศน์เมือง โดยเฉพาะอย่างยิ่ง จังหวัดนครปฐม สมุทรสาคร นนทบุรี และทางตะวันตกของกรุงเทพ ฯ พร้อมกับการรายงานผลการจำแนกดัชนีคุณภาพอากาศตามมาตรฐานประเทศไทยและสำนักงานปกป้องสิ่งแวดล้อม สหรัฐอเมริกา รวมทั้ง ผลการวิเคราะห์สหสัมพันธ์เชิงพื้นที่ในการตรวจสอบความถูกต้องของแบบจำลองถดถอยแบบถ่วงน้ำหนักด้วยชุดข้อมูลใหม่ที่ให้ค่าสัมประสิทธิ์สหสัมพันธ์เฉลี่ยในการประมาณค่าความเข้มข้นฝุ่นละอองขนาดเล็กไม่เกิน 10 และ 2.5 ไมครอน มีค่าสูงกว่า 0.5 ตามที่คาดการณ์ไว้ ดังนั้น จึงสามารถนำแบบจำลองถดถอยแบบถ่วงน้ำหนักร่วมกับปัจจัยที่มีนัยสำคัญมาใช้ประมาณค่าความเข้มข้นฝุ่นละอองขนาดเล็กไม่เกิน 10 และ 2.5 ไมครอน ในภูมิทัศน์ชนบทและภูมิทัศน์เมืองในประเทศไทยได้

สาขาวิชาภูมิสารสนเทศ	ลายมือชื่อนักศึกษา__________
ปีการศึกษา 2564	ลายมือชื่ออาจารย์ที่ปรึกษา__________

PIRADA TONGPRASERT : SPATIOTEMPORAL PARTICULATE MATTER CONCENTRATION PREDICTION USING MODIS AEROSOL OPTICAL DEPTH IN RURAL AND URBAN LANDSCAPES, THAILAND. THESIS ADVISOR : ASSOC. PROF. SUWIT ONGSOMWANG, Ph.D. 395 PP.

Keyword: PARTICULATE MATTER CONCENTRATION/ PM CONCENTRATION PREDICTION MODEL/ OPTIMAL MODEL/ RURAL LANDSCAPE/ URBAN LANDSCAPE

Spatiotemporal PM concentration prediction using MODIS AOD with significant PM factors in rural and urban landscapes in Thailand is necessary to the public due to the limitation of the PM monitoring station. The study will provide the spatial pattern of PM10 and PM2.5 concentration and air quality index classification in both landscapes in the winter and summer seasons at the district level. The derived results can be used as a guideline for improving air quality and reducing impacts on human health. The research objectives were (1) to identify significant factors on PM10 concentration in the rural landscape and PM2.5 concentration in the urban landscape in the winter and summer seasons and their relationships using the multicollinearity test and the OLS regression analysis, (2) to predict spatiotemporal PM10 and PM2.5 concentration using GWR and MEM models, and (3) to evaluate a suitable spatiotemporal model for PM10 and PM2.5 concentration prediction and validation.

This study firstly prepared dependent and independent variables, including ground-level PM concentration, relative humidity, temperature, wind speed, pressure, visibility, brightness temperature and fire radiative power variables using the identified optimum interpolation method. The remaining independent variables, including MODIS AOD, NDVI, BUI, road density, factory density, elevation, fire hotspot, population density, and GPP, were prepared using spatial analysts. Then, the zonal statistics analysis extracted the mean and standard deviation values of all variables and then normalized them using the Z-score method. After that, the dependent and independent variables on PM10 concentration in the rural landscape and PM2.5 concentration in the urban landscape in the winter and summer seasons were applied to identify significant spatiotemporal factors based on a multicollinearity test and the OLS regression analysis. Then, the significant factors were separately applied to predict monthly and seasonally PM10 and PM2.5 concentration using GWR and MEM model. Finally, a suitable model for PM concentration prediction was identified based on the AICc values, and it was validated using correlation analysis with a new dataset and significant factors.

As a result, PM10 concentration predictions using the GWR and MEM models showed a value between 50.53 and 85.79 µg/m^3 and between 50.68 and 84.59 µg/m^3, respectively, in the winter and between 36.92 and 51.32 µg/m^3 and between 37.08 and 50.81 µg/m^3, respectively, in the summer. Meanwhile, PM2.5 concentration predictions using the GWR and MEM models showed a value between 25.33 and 44.37 µg/m^3 and between 25.45 and 44.36 µg/m^3, respectively, in the winter and between 16.69 and 24.04 µg/m^3 and between 16.68 and 23.75 µg/m^3, respectively, in the summer. Besides, the derived average AICc values of the GWR model for PM10 and PM2.5 prediction were lower than the MEM model. Thus, the GWR model was chosen as a suitable model for spatiotemporal PM10 and PM2.5 concentration prediction. The spatial distribution of PM10 concentration showed the high frequency of the high PM10 concentration that occurred in the central part of the rural landscape, particularly northern parts of Saraburi and the southern of Lop Buri province. In the meantime, the spatial distribution of PM2.5 concentration showed the high frequency of the high PM2.5 concentration that occurred in the western part of the urban landscape, particularly in Nakhon Pathom, Samut Sakhon, Nonthaburi, and the western side of Bangkok. Also, monthly AQI classifications were reported according to Thailand and US EPA standards. Furthermore, the result of spatial correlation analysis for GWR model validation based on the new dataset provided average correlation coefficient values for PM10 and PM2.5 concentration prediction higher than the expected value of 0.5. Subsequently, the GWR model with significant factors can predict spatiotemporal PM10 and PM2.5 concentration in rural and urban landscapes in Thailand.

School of Geoinformatics Student's Signature Pirada T.

Academic Year 2021 Advisor's Signature

ACKNOWLEDGEMENTS

First, I would like to express my deep gratitude to my advisor, Assoc. Prof. Dr. Suwit Ongsomwang, for the continuous support of my Ph.D. studies, offers patience, enthusiasm, advice, and knowledge during study and thesis writing. This thesis would not be successful without your guidance and supervision.

I also appreciate this thesis defense chairman and committee members: Assoc. Prof. Dr. Sura Pattanakiat, Assoc. Prof. Dr. Songkot Dasananda, Asst. Prof. Dr. Pantip Piyatadsananon, Dr. Tanakorn Sritarapipat, Dr. Siripon Kamontam and Dr. Nobphadon Suksangpanya for all suggestions and critical comments.

I would like to offer my special thanks to Kamphaeng Phet Rajabhat University for the opportunity to continue my education and provide a scholarship. And My gratitude is also extended to the Thai Pollution Control Department and Thai Meteorological department for PM concentration and meteorological data.

Besides, I wish to thank my friends in the School of Geoinformatics, especially Miss Wilawan Prasomsup and Mr. Athiwat Phinyoyang, for their help and kindness. You mean so much to me.

Finally, special thanks to my beloved family that always support me; Super-Dad, Mom, Somtum, Whan, Kao-tang, and Kao-chae; I love you all.

Pirada Tongprasert

CONTENTS

CONTENTS (Continued)

CONTENTS (Continued)

CONTENTS (Continued)

CONTENTS (Continued)

CONTENTS (Continued)

CONTENTS (Continued)

CONTENTS (Continued)

LIST OF TABLES

LIST OF TABLES (Continued)

LIST OF TABLES (Continued)

Table Page

LIST OF TABLES (Continued)

LIST OF TABLES (Continued)

LIST OF TABLES (Continued)

LIST OF TABLES (Continued)

LIST OF TABLES (Continued)

LIST OF TABLES (Continued)

Table Page

LIST OF TABLES (Continued)

Table Page

LIST OF TABLES (Continued)

LIST OF TABLES (Continued)

LIST OF TABLES (Continued)

LIST OF TABLES (Continued)

LIST OF FIGURES

LIST OF FIGURES (Continued)

LIST OF FIGURES (Continued)

LIST OF FIGURES (Continued)

LIST OF FIGURES (Continued)

LIST OF FIGURES (Continued)

LIST OF FIGURES (Continued)

LIST OF FIGURES (Continued)

LIST OF FIGURES (Continued)

LIST OF FIGURES (Continued)

LIST OF FIGURES (Continued)

LIST OF FIGURES (Continued)

LIST OF ABBREVIATIONS

AOD	Aerosol Optical Depth
BT	Brightness temperature
BUI	Built-up index
ELEV	Elevation
FD	Factory density
FH	Fire hotspot
FRP	Fire radiative power
GPP	Gross Provincial Product
GWR	Geographically Weighted Regression
LME	Linear mixed-effects
MEM	Mixed-Effect Model
NDBI	Normalized Difference Built-up Index
NDVI	Normalized difference vegetation index
NIR	Near-infrared
PM	Particulate Matter
Sig	Significance
SWIR	Short-wave infrared

CHAPTER I

INTRODUCTION

1.1 Background problems and significance of the study

Air pollution has been a significant problem in recent decades, which has a profound toxicological impact on human health and the environment (Ghorani, Riahi, and Balali, 2016). According to the World Health Organization (WHO) report, 3.7 million premature deaths related to ambient air pollution occurred worldwide in 2012. Premature deaths had increased to 4.2 million worldwide in 2016 (Chu et al., 2016; Zhang et al., 2019). Moreover, the Western Pacific and South-East Asia Region (SEAR) had 799,000 deaths in 2012 (Sonwani and Maurya, 2019).

Ambient air pollutants include particulate matter (PM), ozone, nitrogen dioxide, sulfur dioxide, and other contaminants. Typically, PM is a complex mixture of solid and liquid particles of primary and secondary origin, containing a wide range of inorganic and organic components. PM mass and composition are also highly variable in spatial-temporal terms and are strongly influenced by climatic and meteorological conditions (Wiseman and Zereini, 2010).

PM is measured as particles with an aerodynamic diameter of fewer than 10 micrometers (PM10) and less than 2.5 micrometers (PM2.5) (Kulshreshtha, 2019). Besides, they can be emitted from natural and human-made sources, including forest fires, dust storms, traffic, and industry. These are the most likely to impact human health as they are small enough to be inhaled and respired. Particles in PM10 are inhalable and may reach the upper part of the airways and lungs, while smaller PM2.5 particles are more able to penetrate the lungs and perhaps reach the alveoli deeply. Ultrafine, which has a cut-off of 0.1 micrometer, may make up a small proportion of the total mass but may have the most significant health impacts due to their ability to pass from the lung directly into the bloodstream and their larger reactive surface area, which may be capable of inducing more significant damage (Wiseman and Zereini, 2010).

Although PM exposure depends on physical characteristics, including breathing mode, rate, and volume of persons, the particles' size has been directly linked to the leading cause of health problems. Generally, the smaller a particle is, the more deeply it will penetrate to deposit on the respiratory tract at an increasing rate. In nasal breathing, the cilia and the mucus act as a very active filter for most particulates exceeding 10 micrometers, coarse PM. Because the coarse PM fraction settles quickly, it tends to lodge in the upper throat or the bronchi. If humans inhale this PM, it will be initially collected in the nose and throat. The body will then react to eliminate these intruding PMs through sneezing and coughing (Kim, Kabir, and Kabir, 2015).

While particles that have the most impact on human health have been acknowledged as those less than 10 micrometers in diameter, they can penetrate within the respiratory tract beginning with the nasal passages to the alveoli, deep within the lungs due to their excessive penetrability. Particles between approximately 5 and 10 micrometers are most likely deposited in the tracheobronchial tree. In comparison, those between 1 and 5 micrometers are deposited in the respiratory bronchioles and the alveoli, where gas exchange occurs. These particles can affect gas exchange within the lungs and even penetrate the lung. Eventually, these particles will escape into the bloodstream to cause significant health problems (Kim et al., 2015).

Besides, the Health Effects Institute (2020) presented the number of deaths attributable to PM2.5 in a given year reflects those deaths that likely occurred earlier than would be expected in the absence of PM2.5, computed based on nonlinear Integrated-Exposure-Response (IER) functions, all ages, for both sexes combined between 1990 and 2019 in Thailand are continually increasing shows in Table 1.1. However, Apte, Brauer, Cohen, Ezzati, and Pope (2018) presented that exposure to ambient fine particulate matter (PM2.5) air pollution is a significant risk for premature death. On the other hand, If PM2.5 in all countries met the World Health Organization Air Quality Guideline (10 μg/m3), the estimated life expectancy could increase by a population-weighted median of 0.6 years (interquartile range of 0.2–1.0 years).

Table 1.1 Number of deaths attributable to PM2.5 in Thailand between 1990 and 2019.

Year	Exposure lower	Exposure means	Exposure upper
1990	7,340	14,700	23,900
1995	10,600	19,300	29,200
2000	13,600	22,800	32,900
2005	16,900	24,600	32,700
2010	21,400	27,800	34,100
2011	21,400	27,800	33,600
2012	21,300	27,300	33,400
2013	21,000	26,800	32,400
2014	21,200	26,800	32,700
2015	21,600	27,200	33,100
2016	22,400	28,400	35,200
2017	21,700	29,200	37,800
2018	22,300	30,500	40,300
2019	23,200	32,200	43,400

Source: Health Effects Institute (2020).

PM has diverse effects on Thailand's economy, impacting tourism, property values, and medical treatment expense. According to the Kasikorn Research Center report in 2019, the smog could cost Thailand 6.6 billion baht in losses for the healthcare and tourism sectors due to the impact of air pollution (The Thaiger & The Nation, 2019). Thai Public Broadcasting Service reported the news about the effect of PM2.5 on medical expenses and the loss of tourism opportunities in and around Bangkok if PM2.5 does not ease within a month, medical expenses to be borne by each individual is an average of 1,000 baht for each medical visit and 22.50 baht per day for face masks. Total medical costs could range from 1,600 to 3,100 million baht, depending on the air pollution period (Thai PBS WORLD, 2019).

Therefore, the monitoring of PM10 and PM2.5 needs to be improved in many countries to assess population exposure and help local authorities improve air quality (World Health Organization, 2013). However, with many limitations, most pollutant concentration information is obtained from ground monitoring stations. For example, these stations are limited, unequally distributed, and have different measure frequency ranges. These limitations may affect the geographical and demographical range of studies, resulting in an information bias and reducing exposure-response studies (Chu et al., 2016).

Furthermore, the spatial-temporal variation of PM10 and PM2.5 is complex, and continuous monitoring is inattentive in many countries and regions. Thus, satellite-based remote sensing has become a widely used monitoring technique. Because it can provide extensive spatial coverage and a cost-effective way for studies, it acquires directly from the measured spectral Aerosol Optical Depth (AOD), which is the integral of the aerosol light extinction over the vertical path through the atmosphere (Levy, 2009). Consequently, spatiotemporal PM concentration prediction using MODIS AOD with significant PM factors in Thailand is necessary to the public due to PM monitoring station limitations.

In this study, spatiotemporal characteristics of PM concentration will be described according to two different landscape types: urban and rural and two different seasons: winter (October to February) and summer (March to May). Agricultural operations in a rural landscape, notably agricultural debris burning, generate massive sources of PM10 contribution. Arslan and Aybek (2012) stated that agricultural field operations cause dust production in conventional crop production, including soil tillage and seedbed preparation, planting, fertilizer, pesticide application, harvesting, and post-harvest processes (Arslan and Aybek, 2012). The high PM10 concentration distribution in the dust blown by the wind, especially on the surfaces without cement and asphalt (Li et al., 2017). On the contrary, the high PM2.5 concentration is mainly found with high population, rapid urban expansion and local economic growth (Lin et al., 2014). The PCD identified four critical air pollutant areas in Thailand, including (1) haze and smog in the Northern region, (2) PM10 concentration at Na Phra Lan district, Saraburi, (3) PM2.5 concentration in Bangkok Metropolitan and vicinity areas, and (4) volatile organic compounds (VOCs) at Map Ta Phut, Rayong. The PCD spent a budget of 95.04 million Baht to mitigate these pollutants in those areas (PCD, 2021). Thus, two study areas will be selected here according to the recent land use data of the Land Development Department (2019).

The expected results will provide significant spatiotemporal factors on PM10 and PM2.5 concentration in the rural and urban landscapes. The derived results will also provide the spatial pattern of PM10 and PM2.5 concentration in both landscapes at the district level in the winter and summer seasons. Additionally, the results can be used as a guideline for improving air quality and reducing impacts on human health in Thailand.

1.2 Research objectives

With a suitable prediction model, the research aims to predict spatiotemporal PM10 and PM2.5 concentration in the rural and urban landscape in the winter and summer seasons. The specific research objectives are as follows:

(1) To identify significant factors on PM10 concentration in the rural landscape and PM2.5 concentration in the urban landscape in the winter and summer seasons and their relationships using the multicollinearity test and the OLS regression analysis,

(2) To predict spatiotemporal PM10 and PM2.5 concentration using GWR and MEM models, and

(3) To evaluate a suitable spatiotemporal model for PM10 and PM2.5 concentration prediction and validation.

1.3 Scope of the study

The scope of the study can be summarized as follows:

(1) The multilinearity test and OLS regression analysis are applied to identify significant spatiotemporal factors and the relationship between PM10 concentration in the rural landscape and PM2.5 concentration in the urban landscape in winter (October 2019 to February 2020) and summer (March 2020 to May 2020) seasons.

(2) The GWR and MEM models are applied to predict monthly PM10 concentration in rural and PM2.5 concentration in urban landscapes.

(3) A suitable spatiotemporal PM10 and PM2.5 concentration prediction model is evaluated using AICc analysis.

(4) Suitable spatiotemporal model for PM10 and PM2.5 concentration prediction is validated based on the new dataset in winter (October 2020 to February 2021) and summer (March 2021 to May 2021) using Pearson correlation analysis.

1.4 Limitation of the study

The limitation of the study is summarized as follows:

(1) The interpolation result's accuracy depends on the number of meteorological and pollutant monitoring stations and their distributions.

(2) Due to cloud cover over remotely sensed imagers in the rainy season, spatiotemporal PM10 and PM2.5 concentration in rural and urban landscapes will focus on the winter and summer seasons.

(3) Due to the COVID-19 pandemic in Thailand, the new dataset (October 2020 to May 2021) is applied to validate the suitable spatiotemporal PM10 and PM2.5 models because of site visiting limitations by Government regulation.

1.5 Study area

Two study areas are chosen to serve two different studies on PM10 concentration in the rural landscape and PM2.5 concentration in the urban landscape, as shown in Figure 1.1. The supporting reason for choosing rural and urban landscapes is based on the recent land use data of the Land Development Department (2019).

According to the land use data of the Land Development Department (2019), the rural landscape covers approximately 15,827 sq. km with 60 districts from 6 provinces: Ang Thong, Lop Buri, Phra Nakhon Si Ayutthaya, Pathum Thani, Saraburi, and Sing Buri provinces. More than 65 percent of the rural landscape's total area in 2019 is agriculture, including paddy fields, field crops, orchards, and perennial trees. At the same time, urban, forest, waterbody and miscellaneous areas are about 13%, 12%, 4%, and 4%, respectively.

On the contrary, the urban landscape, including Bangkok and its vicinity, covers approximately 6,180 sq. km with 72 districts from 5 provinces, including Bangkok, Nakhon Pathom, Nonthaburi, Samut Prakan, and Samut Sakhon provinces. The urban areas cover about 39% of the total area, while agriculture, forest, waterbody and miscellaneous areas are about 49%, 1%, 4%, and 7%, respectively. This landscape, especially Bangkok, Thailand's capital city, has the highest population density of about 3,619 persons per sq. km (Bangkok GIS, 2018), heavy traffic congestion and rapid urban expansion.

1.6 Benefits of the study

The benefits of the study are summarized as follows:

(1) The optimum interpolated method for monthly mean PM concentration, meteorological (relative humidity, temperature, wind speed, pressure, visibility), and MODIS fire data (brightness temperature and fire radiative power).

(2) Identify significant monthly factors on PM concentration and characterize the spatiotemporal relationship between PM concentration and significant factors in the different landscapes in the winter and summer seasons.

(3) Predict PM concentration distribution and map monthly air quality index according to the Thai Air Quality and US EPA standards from the GWR and MEM models.

(4) Validate the suitable spatiotemporal model for the PM concentration prediction (GWR) based on the new dataset.

(5) Spatial relationship between PM10 and PM2.5 concentration and significant monthly factors in rural and urban landscapes during winter and summer.

(6) Spatial relationship between PM10 and PM2.5 concentration and land use type in winter and summer.

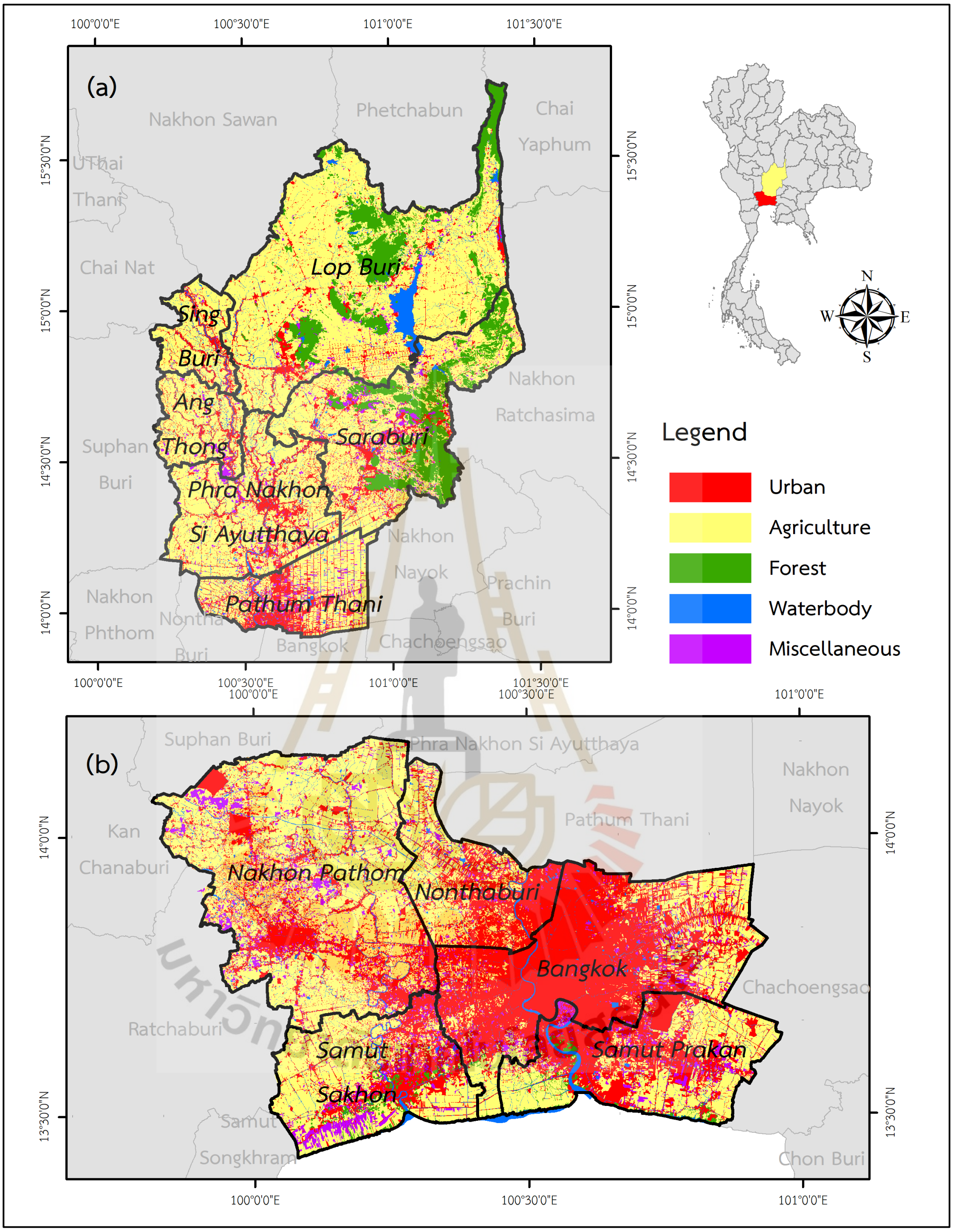

Figure 1.1 LULC classification and location map of the study area, (a) rural and (b) urban landscape.

CHAPTER II

BASIC CONCEPTS AND LITERATURE REVIEWS

Under this chapter, basic concepts and theories related to the research include (1) MODIS AOD, (2) significant spatiotemporal factor on PM concentration, (3) Geographically Weighted Regression (GWR), (4) Mixed-Effect Model (MEM), and (5) Spatial Interpolation Methods are here summarized.

2.1 MODIS AOD

The **MOD**erate resolution **I**maging **S**pectroradiometers (MODIS) was launched aboard NASA's Terra and Aqua satellites in December 1999 and May 2002. The MODIS mission is cross-disciplinary, addressing the Earth System from land, ocean, and atmosphere perspectives. The atmosphere focus encompasses aerosol, clouds, water vapor, atmospheric temperature sounding, the interaction between these parameters, and across disciplines, especially in understanding how these parameters affect the Earth as a system and its climate. MODIS AOD on Terra and Aqua is collocated with the **M**ultiangle **I**maging **S**pectro **R**adiometer (MISR). It flies information with a constellation of complementary sensors. Initially, MODIS aerosol algorithms are standalone procedures, but combining information from several sensors provides better retrievals and new products (Remer et al., 2013).

Terra crosses the equator in a descending orbit at the nominal local time of 10:30 am, while Aqua crosses in an ascending orbit three hours later. Each sensor is independent, but working with the twin sensors on two different platforms with equator crossing times 3 hours apart allows for some daily signal analysis and provides a cross-check on sensor calibration drift and artifacts. MODIS has 36 channels spanning the spectral range from 0.41 to 15 micrometers and representing three spatial resolutions: 250 meters (2 channels), 500 meters (5 channels), and 1 km (29 channels). The aerosol retrieval uses eight channels (0.41-2.13 micrometers) to retrieve aerosol characteristics and uses additional wavelengths in other parts of the spectrum to identify clouds and river sediments. MODIS scans cross-track, observing each target at only one angle per orbit. Swath width is 2,330 kilometers, which nearly covers the globe daily and provides multiple daily views of high latitude locations (Remer et al., 2013; Remer et al., 2005; Remer et al., 2012).

The primary MODIS aerosol data product is the aerosol optical depth (AOD, also known as aerosol optical thickness, AOT) at a wavelength of 550 nm. Besides, each algorithm provides additional information about the aerosol, such as single scattering albedo, spectral AOD, descriptions of relative aerosol size, and quality assurance information. Furthermore, the aerosol size distribution is derived over the oceans, and the aerosol type is derived over the continents. “Fine” aerosols (anthropogenic/pollution) and “course” aerosols (natural particles, e.g., dust) are also derived. Daily Level 2 (MOD_04) data are produced at a pixel array spatial resolution of 10 x 10 kilometers (at nadir). The aerosol product includes the “deep-blue” algorithm recently developed to get aerosol optical thickness over bright land areas (Levy and Hsu, 2019).

In general, the MODIS level-2 atmospheric aerosol product (MOD04_L2, MYD04_L2) provides full global coverage of aerosol properties from the Dark Target (DT) and Deep Blue (DB) algorithms. The DT algorithm is applied over the ocean and dark land (e.g., vegetation), while the DB algorithm in Collection 6 (C6) covers the entire land areas, including dark and bright surfaces. Both results are provided on a 10x10 pixel scale (10 km at nadir). Each MOD04_L2 product file covers a five-minute time interval. The output grid is 135 pixels in width by 203 pixels in length. Every tenth file is stored in Hierarchical Data Format (HDF-EOS). Based on C5 validation studies, many Science Data Sets (SDSs) have been deleted with C6 from the DT product (Angstrom_Exponent_Land, Optical_Depth_Small_Land, etc.), while many SDSs have been renamed or added. Several algorithm changes have led to significant changes in regional aerosol product statistics. For C6, the DT algorithm team now provides a new 3 km spatial resolution product intended for the air quality community; this is provided in a separate file (M*D04_3K) (Levy and Hsu, 2015). An example of an aerosol optical depth product at 3 km resolution is displayed in Figure 2.1.

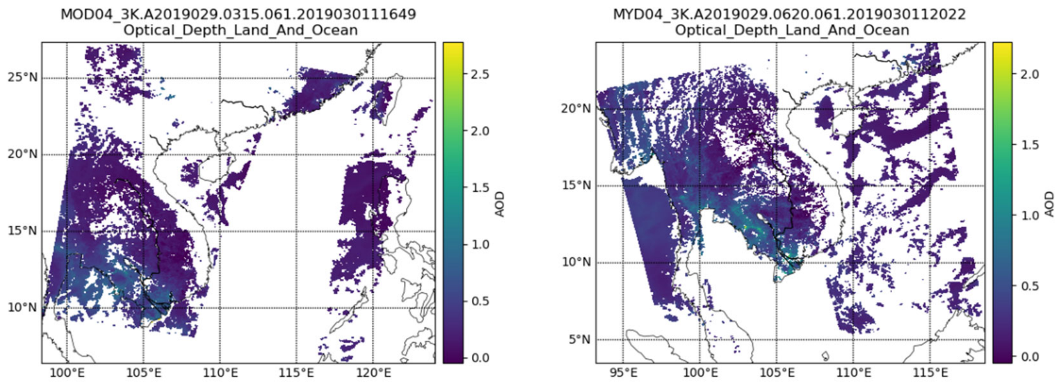

(a) (b)

Figure 2.1 The aerosol optical depth product retrieved from 29 January 2019 at 3 km spatial resolution (a) MOD04_3K and (b) MYD04_3K.

2.2 Significant spatiotemporal factor on PM concentration

PM concentration vary from place to place and depend on meteorological, biophysical, and socio-economic factors. The significant factors on PM concentration are reviewed from the previous studies with plus specif are summarized in Table 2.1.

Table 2.1 Significant factor in PM concentration.

Categories	Factors (Number of papers)	Reference	Data type
Meteorological data	Relative humidity (11)	Kloog, Koutrakis, Coull, Lee, and Schwartz (2011); Yuanai Guo and Zhang (2014); Meng et al. (2016); You, Zang, Pan, Zhang, and Chen (2015); Ma et al. (2016); You et al. (2016); Zheng, Zhang, Liu, Geng, and He (2016); Jiang, Sun, Yang, and Zhang (2017); Luo et al. (2017); Yuanxi Guo, Tang, Gong, and Zhang (2017); He and Huang (2018)	dynamic
	Temperature (10)	Kloog et al. (2011); Yuanai Guo and Zhang (2014); Meng et al. (2016); You et al. (2015); You et al. (2016); Zheng et al. (2016); Jiang et al. (2017); Luo et al. (2017); Yuanxi Guo et al. (2017); He and Huang (2018)	dynamic

Table 2.1 (Continued).

Categories	Factors (Number of papers)	Reference	Data type
Meteorological data	Wind direction* (2)	Meng et al. (2016); Yuanxi Guo et al. (2017)	dynamic
	Wind speed (11)	Kloog et al. (2011); Yuanai Guo and Zhang (2014); Meng et al. (2016); You et al. (2015); Ma et al. (2016); You et al. (2016); Zheng et al. (2016); Jiang et al. (2017); Luo et al. (2017); Yuanxi Guo et al. (2017); He and Huang (2018)	dynamic
	Precipitation* (1)	Luo et al. (2017)	dynamic
	Pressure (4)	Jiang et al. (2017); Luo et al. (2017); Yuanxi Guo et al. (2017); He and Huang (2018)	dynamic
	Visibility (5)	Kloog et al. (2011); Yuanai Guo and Zhang (2014); You et al. (2015); You et al. (2016); Jiang et al. (2017)	dynamic
	Planetary boundary layer height * (5)	Yuanxi Guo et al. (2017); Zheng et al. (2016); Kloog et al. (2011); He and Huang (2018); You et al. (2015)	dynamic
Biophysical data	MODIS AOD (14)	Kloog et al. (2011); You et al. (2015); Chu et al. (2016); Ma et al. (2016); Meng et al. (2016); You et al. (2016); Zheng et al. (2016); Yuanxi Guo et al. (2017); Jiang et al. (2017); Ni, Cao, Zhou, Cui, and Singh (2018); Xue et al. (2019); K. Zhang et al. (2019); Hamer, Franklin, Chau, Garay, and Kalashnikova (2020); He, Gu, and Zhang (2020)	dynamic
	Vegetation area/Green open space (7)	Meng et al. (2016); Ma et al. (2016); Jiang et al. (2017); Luo et al. (2017); Yuanxi Guo et al. (2017); He and Huang (2018); Kloog et al. (2011)	Static
	Urban area (3)	Kloog et al. (2011); Lin et al. (2014); Luo et al. (2017)	Static
	Pollutant point source/emission * (2)	Kloog et al. (2011); Meng et al. (2016)	Static
	Road density (by level)/ Traffic density (3)	Kloog et al. (2011); Meng et al. (2016); Luo et al. (2017)	Static
	Factory density (1)	Luo et al. (2017)	Static
	Brightness temperature (1)	Wiseman and Zereini (2010)	dynamic
	Fire radiative power (1)	Wiseman and Zereini (2010)	dynamic

Table 2.1 (Continued).

Categories	Factors (Number of papers)	Reference	Data type
Biophysical data	Fire hotspot (1)	Wiseman and Zereini (2010)	dynamic
	NO2 density * (1)	Zheng et al. (2016)	Static
	Elevation (5)	Kloog et al. (2011); Jiang et al. (2017); Luo et al. (2017); Yuanxi Guo et al. (2017); He and Huang (2018)	Static
	Aspect * (1)	Luo et al. (2017)	Static
	Slope * (1)	Luo et al. (2017)	Static
	Geomorphy feature (GEOM) * (1)	Jiang et al. (2017)	Static
Socio-economic data	Population data (6)	Kloog et al. (2011); Lin et al. (2014); Meng et al. (2016); Luo et al. (2017); Yuanxi Guo et al. (2017); He and Huang (2018)	dynamic
	GDP (GPP) (2)	Lin et al. (2014); Luo et al. (2017)	dynamic

Note: *These factors will not be applied in the tentative research framework.

2.2.1 Meteorological factor

Many researchers have reported that air pollution concentration vary depending on meteorological factors. They are vital factors guiding air movement. For example, significant factors on PM10 concentration are seasonal variation, daily time variation, wind speed, wind direction, rainfall, and relative humidity (Kliengchuay, Meeyai, Worakhunpiset, and Tantrakarnapa, 2018). Also, space-scale dependent relationships are found between PM pollution and meteorological elements. One example is when the temperature is about 15 °C, PM pollution is severe, and when the temperature is less or more than 15 °C, PM pollution is slight (Li et al., 2017). Moreover, the meteorological condition strongly affects the relationship between PM2.5 and AOD (He et al., 2020). The meteorological factor in the dispersion of air pollution include:

(1) Relative humidity (RH). The relative humidity quantifies humidity in terms of the mass of water vapor as a fraction of the maximum mass of water vapor that the air can hold, usually expressed as a percentage (Shonk, 2013).

(2) Temperature (TEMP). The temperature measures how hot or cold an object (or air mass) is. Initially, the Celsius scale runs from 0 °C to 100 °C between the freezing and boiling water points at standard atmospheric pressure (Shonk, 2013). Generally, the temperature is measured in Celsius.

(3) Wind speed (WS). The wind speed is the movement of the air from high to low pressure. An instrument for measuring wind speed is an anemometer (Giles, 2015). Generally, the wind speed is measured by knots.

(4) Air Pressure (P). The pressure is the force per unit area exerted by the atmosphere, and it also decreases with height through the atmosphere. Air pressure is measured using a barometer and reported in millibars (Shonk, 2013).

(5) Visibility (VIS). The visibility is the furthest distance at which objects can still clearly be seen. The visibility is stated in kilometers (Shonk, 2013).

2.2.2 Biophysical factor

The biophysical factors for studying PM concentration can be summarized as follows:

(1) MODIS AOD. The product names “MODIS/Terra and Aqua MAIAC Land Aerosol Optical Thickness Daily L2G Global 1km SIN Grid” or “MCD19A2” from MODIS Terra and Aqua combined Multi-Angle Implementation of Atmospheric Correction (MAIAC) at 1 km resolution will be downloaded and applied in this study. This new advanced algorithm uses time-series (TMS) analysis with a combination of pixel- and image-based processing to improve cloud detection accuracy, aerosol retrievals, and atmospheric correction (Lyapustin and Wang, 2018).

(2) Vegetation area. The normalized difference vegetation index (NDVI) describes agriculture and green open space. Generally, reflectance from a red channel centered around 660 nm and a near-infrared channel centered at 860 nm are used to calculate the NDVI. The near-infrared band empirically corresponds to the long-wavelength shoulder of the chlorophyll red edge, and the red band is associated with the maximum chlorophyll absorption. NDVI is derived using the following equation:

$$NDVI = \frac{NIR_{OLI5} - RED_{OLI4}}{NIR_{OLI5} + RED_{OLI4}} \tag{2.1}$$

The NDVI equation produces values in the range of –1.0 to 1.0. Increasing positive values indicate increasing green vegetation, and negative values indicate non-vegetated surfaces such as water, barren land, ice, snow, and clouds (Jensen, 2015).

(3) Urban area. The built-up index (BUI) was used to describe the urban area. The high positive value indicates built-up and barren land (Prasomsup, Piyatadsananon, Aunphoklang, and Boonrang, 2020). BUI is expressed as follows:

$$BUI=NDBI-NDVI \tag{2.2}$$

Where

$$NDBI = \frac{SWIR_{OLI6} - NIR_{OLI5}}{SWIR_{OLI6} + NIR_{OLI5}} \tag{2.3}$$

SWIR and NIR represent short-wavelength infrared radiometer and the near-infrared band of the spectrum bands of Landsat 8 OLI (Mehrotra, Bardhan, and Ramamritham, 2016).

(4) Road density (RD). The road density is a measurement of the road network per unit area and refers to the total road network's length in an area per sq. km.

(5) Factory density (FD). The factory density, which represents PM's non-point source, is measured by the number of factorial types (Type 1, 2, and 3) with the rank-sum weighting method to calculate factory density per sq. km in each district. In this study, each factorial type's weight is assigned a value of 1, 3, and 5 of Saaty's scale for Type 1, 2, and 3, respectively.

(6) Brightness temperature (BT). MODIS brightness temperature 31 or Bright_T31 is Channel 31 brightness temperature of the fire pixel measured in Kelvin. It is one product from MCD14DL MODIS/Aqua+Terra Thermal Anomalies/Fire locations 1 km at nadir by NASA's Land, Atmosphere Near real-time Capability for EOS Fire Information for Resource Management System (FIRMS) (Berrick, 2020).

(7) Fire radiative power (FRP). The FRP depicts the pixel-integrated fire radiative power from MCD14DL; MODIS/Aqua+Terra Thermal Anomalies/Fire; in megawatts (MW) (Berrick, 2020).

(8) Fire hotspot (FH). The accumulated fire hotspot in each month in each district is applied to calculate fire hotspot density (total point per sq. km) for representing fire activity in each district.

(9) Elevation (ELEV). The SRTM DEM data from the **S**huttle **R**ADAR **T**opography **M**ission describes digital elevation data. The Space Shuttle Endeavour acquired the SRTM data in 2000. SRTM acquired data for over 80 percent of the Earth's land surface between 60 degrees N and 56 degrees S latitude. The data have been released with one arc-second, or about 30 meters (98 feet) (Jensen, 2015).

2.2.3 Socio-economic factor

(1) Population data (POP). Population density is used to describe the population data. The population density is a measurement of populations per unit area and refers to the number of people living in an area per sq. km.

(2) Gross Provincial Product (GPP). At the national level, Gross Domestic Product (GDP) is the total output of goods and services for final use occurring within the domestic territory of a given country. It is frequently used as one of the socio-economic factors (World Health Organization, 2020). In this study, Gross Provincial Product from each province is chosen and applied as a significant factor on PM concentration.

2.3 Geographically Weighted Regression (GWR)

Fotheringham, Brunsdon, and Charlton (2002) defined the GWR model as a local statistic that produces a set of local parameter estimates and shows a relationship that varies over space. The GWR can be expressed as follows:

$$y_i=\beta_0+\sum_k \beta_k x_{ik}+\varepsilon_i \tag{2.4}$$

And GWR extends this traditional regression framework by allowing local rather than global parameters to be estimated so that the model is rewritten as:

$$y_i=\beta_0(u_i,v_i)+\sum_k \beta_k(u_i,v_i)x_{ik}+\varepsilon_i \tag{2.5}$$

Where (u_i,v_i) denotes the coordinates of the sample point in space and $\beta_k(u_i,v_i)$ is a realization of the continuous function $\beta_k(u,v)$ at point i. It allows for a continuous surface of parameter values, and measurements of this surface are taken at specific points to denote the surface's spatial variability. Equation (2.4) is a particular case of equation (2.5) in which the parameters are assumed to be spatially invariant. Thus, the GWR equation in (2.5) recognizes that spatial variations in relationships might exist and provide a way to be measured.

As it stands, though, there would appear to be problems in calibrating equation (2.5) because there are more unknowns than observed variables. However, models of this kind do occur in the statistical literature and discussions. Our approach borrows from the latter two, mainly because we do not assume the coefficients to be random. Instead, they are deterministic functions of some other variables – in our case, location in space. When handling such models, the general approach is to note that although an unbiased estimate of the local coefficients is not possible, estimates with only a slight bias can be provided.

Many researchers argue that GWR's calibration process can be a tradeoff between bias and standard error. Assuming the parameters exhibit some degree of spatial consistency, values near the one being estimated should have relatively similar magnitudes and signs. Thus, when estimating a parameter at a given location i, one can approximate (2.5) in the region of i by (2.4) and perform regression using a subset of the points in the data set close to i. Thus, the $\beta_k(u_i,v_i)$s are estimated for i in the usual way, and for the next i, a new subset of 'nearby' points is used, and so on. These estimates will have some degree of bias since the coefficients of (2.5) will exhibit some drift across the local calibration subset. However, if the local sample is large enough, this will allow calibration, albeit a biased one. The higher the size of the local calibration subset, the lower the standard errors of the coefficient estimates, but this must be offset against the fact that enlarging this subset increases the chance that the coefficient 'drift' introduces bias. One final adjustment to this approach may also be made to reduce this effect. Assuming that points in the calibration subset farther from i are more likely to have differing coefficients, a weighted calibration is used. More influence in the calibration is attributable to the points closer to i.

As noted above, the calibration of equation (2.4) assumes implicitly that observed data near location i have more of an influence in the estimation of the $\beta_k(u_i,v_i)$s than do data located farther from i. In essence, the equation measures the relationships inherent in the model *around each location* i. Hence weighted least squares provide a basis for understanding how GWR operates. In GWR, an observation is weighted by its proximity to location i so that the weighting of observation is no longer constant in the calibration but varies with i. Data from observations close to i are weighted more than from observations farther away. That is,

$$\hat{\boldsymbol{\beta}}_{(u_i,v_i)}=(X^TW_{(u_i,v_i)}X)^{-1}X^TW_{(u_i,v_i)}y \qquad (2.6)$$

where the bold type denotes a matrix, $\hat{\boldsymbol{\beta}}$ represents an estimate of $\boldsymbol{\beta}$, and $W_{(u_i,v_i)}$ is a n by n matrix whose off-diagonal elements are zero and whose diagonal elements denote the geographical weighting of each of the n observed data for regression point i.

This study applies the GWR model to predict spatiotemporal PM concentration in the rural and urban landscape in the winter and summer seasons.

2.4 Mixed-Effect Model (MEM)

Wu (2010) explained a mixed-effects model or random-effects model had been widely used in the regression model analysis of longitudinal data or clustered data that are often complex or incomplete, such as dropouts, missing data, measurement errors, censoring, and outliers. Furthermore, longitudinal studies are closely related to repeated measures studies, in which repeated or multiple measurements of one or more variables are made on each individual in the study. Still, these repeated measurements are not necessarily made over time. For example, air pollution may be measured at different city locations, so multiple measurements are made over space in different cities.

Moreover, there are many models considered as the MEM, including linear mixed-effects (LME) models, generalized linear mixed models (GLMMs), nonlinear mixed-effects (NLME) models, and frailty models. Still, in the LME model, the random effects are linear distribution. While the random effects are nonlinear in the other models, LME will be described below.

Let $y_{i=}\ \{y_1,y_{i2},\ldots,y_{in_i}\}^T$ be the n_i repeated measurements of the response variable y on individual i, i = 1; 2; · · ·; n: A general LME model can be written as:

$$y_i=X_i\boldsymbol{\beta}_i+Z_ib_i+e_i, \qquad i=1,2,\ldots,n \qquad (2.7)$$

$$b_i\sim N\big(0,D\big), \qquad e_i|\sim N\big(0,R_i\big) \qquad (2.8)$$

where $\boldsymbol{\beta}= (\boldsymbol{\beta}_1,\ldots,\boldsymbol{\beta}_p)^T$ is a p x 1 vector of fixed effects, $b_i=(b_{i1},\ldots,b_{iq})^T$ is a q x 1 vector of random effects, the n_i x p matrix X_i and the n_i x q matrix Z_i are known design matrices that may contain covariates, $e_i=(e_{i1},e_{i2}\ldots,e_{in_i})^T$represents random errors of the repeated measurements within individual i, D is a q x q covariance matrix of the random effects, and R_i is a n_i x n_i the covariance matrix of the within-individual errors.

In general, it is often assumed that $R_i = \sigma^2 I_{n_i}$ for simplicity, where I_{n_i} is the $n_i \times n_i$ identity matrix, i.e., the within-individual measurements, are assumed to be independent with constant variance. This assumption may be reasonable when the within-individual measurements are relatively far apart (so they are approximately independent). The repeated measurements within individuals roughly have a constant variance. The value of σ^2 represents the magnitude of the within-individual variation, and the values of the diagonal elements of D represent the magnitude of the between-individual variation. The simplified with-individual covariance structure R_i dramatically reduces the number of parameters and may avoid some identifiability problems.

The LME model, equations (2.7) and (2.8) is an extension of the corresponding linear regression model by adding the random effects b_i in the model. In other words, if the term with random effects b_i is omitted, LME model (2.7) and (2.8) reduces to a standard linear regression model. A vital characteristic of an LME model is that it is linear in both the mean parameters β and the random effects b_i. Therefore, many analytic or closed-form expressions of parameter estimates can be obtained for LME models, significantly reducing the computational burden. This critical advantage is unavailable for nonlinear models in the mean parameters, random effects, or both.

In the LME model, equations (2.7) and (2.8), the fixed effects β are population-level parameters and are the same for all individuals, as in a classical linear regression model for cross-sectional data, while the random effects b_i are individual-level "parameters" representing individual variations from population-level parameters. The random effects b_i measure between-individual variation, and the random errors e_i measure within-individual variation. Since each individual shares the same random effects, the multiple measurements within each individual or cluster are correlated.

In a mixed-effects model, the repeated measurements $\{y_{i1}, y_{i2}, \ldots, y_{in_i}\}$ of the response within each individual can be taken at different time points for different individuals, and the number of measurements n_i may also vary across individuals. In other words, an LME model allows unbalanced data in the response. This characteristic is an advantage of mixed-effects models.

In the LME model, equations (2.7) and (2.8), the design matrix Z_i is often a submatrix of the design matrix X_i. For example,

$$X_i=Z_i=\begin{bmatrix}1 & x_{i1}\\ 1 & x_{i2}\\ \vdots & \vdots\\ 1 & x_{in_i}\end{bmatrix}, \qquad b_i=\begin{bmatrix}b_{i0}\\ b_{i1}\end{bmatrix} \tag{2.9}$$

In the previous research, missing AOD data is essential in estimating PM2.5 from AOD. The method used to compensate for missing AOD data is essential in the derivation's precision and accuracy. Besides, several factors are also included in the model as covariates, including metrological variables and classic land-use variables. It also uses the inverse distance weight (IDW) and cluster analysis to deal with missing AOD values, so daily ground PM2.5 levels could be predicted in a wide range. If missing AOD presents a non-random distribution, AOD data needs to be corrected by meteorological factors using the inverse probability weight method (IPW) (Chu et al., 2016).

2.5 Spatial Interpolation Methods

Spatial interpolation is a crucial method to estimate unknown data by using known sample data. In this section, there are two main groupings of interpolation techniques. (1) Deterministic interpolation techniques create continuous surfaces from measured points, based on either the extent of similarity (inverse distance weighted) or the degree of smoothing (radial basis functions) and (2) Geostatistical interpolation techniques (kriging and Cokriging) utilize the statistical properties of the measured points. Geostatistical techniques quantify the spatial autocorrelation among measured points and account for the spatial configuration of the sample points around the prediction location (ESRI, 2015). These are summarized in the following section.

2.5.1 Inverse Distance Weighted (IDW) method

The IDW interpolation is used to determine pixel values by a linear combination of sampling points, which is assumed to be reduced by the distance between the mapped variables and the sampling locations (Zhang, Rui, and Fan, 2018; Zhang and Shen, 2015). The calculation formula is as follows:

$$Z_0 = \left[\sum_{i=1}^{n} \frac{Z_i}{d_i^k}\right] / \left[\sum_{i=1}^{n} \frac{1}{d_i^k}\right] \tag{2.10}$$

Where Z is the estimated value of 0, Z_i is the value of the control point i, d_i is the distance between 0 and i, n is used to estimate the number of control points, and k is the power, that is required to specify.

2.5.2 Global Polynomial Interpolation (GPI) method

The GPI interpolation fits a smooth surface defined by a mathematical function (a polynomial) to the input sample points. The GPI calculates predictions using the entire dataset instead of the measured points within neighborhoods. A first-order GPI fits a flat plane; a second-order GPI fits a surface, allowing for one bend; a third-order GPI allows for two bends; and so forth (ESRI, 2015; Wang et al., 2014).

2.5.3 Radial Basis Functions (RBF) method

RBF is a function that changes with distance from a location. RBFs are a series of exact interpolation techniques; the surface must pass through each measured sample value. RBF is conceptually fitting a rubber membrane through the measured sample values while minimizing the surface's total curvature (ESRI, 2015; Wang et al., 2014).

2.5.4 Ordinary Kriging (OK) method

The OK interpolation method assumes that sampling the point between the distance or direction can illustrate the spatial correlation of the surface changes, where the mathematical function with the specified number of points or designated radius in all points first principles to determine the location of each output value (Bardossy, 2002; G. Zhang, Rui, and Fan, 2018; P. Zhang and Shen, 2015). The calculation formula is as follows:

$$Z^*(x) = \sum_{i=1}^{n} \lambda_i Z(x_i) \tag{2.11}$$

Where Z(x) is the measurement of position i, λ_i is the unknown weight of the measurement value at position i, is the predicted position, and n is the number of measurements.

2.5.5 Simple Kriging (SK) method

The SK is an alternative to OK supposing the mean μ(x) is known (not necessarily constant) in the whole domain (Bardossy, 2002). In this case, the estimator formula is as follows:

$$Z^{*}(x)=\mu(x) + \sum_{i=1}^{n} \lambda_i \,(Z(x_i)-\mu(x_i)) \qquad (2.12)$$

2.5.6 Cokriging Kriging (CK) method

Cokriging uses information on several variable types. The primary variable of interest is Z_1, and both autocorrelation for Z_1 and cross-correlations between Z_1 and all other variable types are used to make better predictions (ESRI, 2015). Ordinary cokriging assumes the models:

$$Z_1(s)=\mu_1+\varepsilon_1(s) \qquad (2.13)$$

$$Z_2(s)= \mu_2+\varepsilon_2(s) \qquad (2.14)$$

Where μ_1 and μ_2 are unknown constants, $\varepsilon_1(s)$, $\varepsilon_2(s)$ are two types of random errors: autocorrelation for each of them and cross-correlation.

2.6 Literature review

2.6.1 Application of the GWR model

Lin et al. (2014) studied the spatiotemporal variation of PM2.5 concentration and their relationship with China's geographic and socio-economic factors. The GWR model was used to estimate PM2.5 concentration with MODIS AOD, population, GDP, and urban areas in 2001 and 2010. The results showed high concentration of PM2.5 were primarily found in high populations, the high value of GDP, and urban expansion, including the Beijing-Tianjin-Hebei region in North China, East China, and Henan province. The local R^2 values were 0.820 and 0.822 for 2001 and 2010, respectively. So, the three main driving forces that impact PM2.5 concentration are increasing populations, local economic growth, and urban expansion.

You et al. (2016) studied national-scale estimates of ground-level PM2.5 concentration in China using geographically weighted regression based on 3 km resolution MODIS AOD. This study used the GWR model to estimate ground-level PM2.5

concentration in China with MODIS AOD, wind speed, surface air temperature, horizontal visibility, and relative humidity. The result showed the annual mean PM2.5 concentration in industrial structures and densely populated areas such as the Beijing-Tianjin Metropolitan Region were higher than 85 μg/m^3, with the highest concentration greater than 135 μg/m^3. While in central China, PM concentration were greater than 75 μg/m^3. Intense human activity and rapid urbanization had led to the high production of PM2.5 concentration.

Jiang et al. (2017) studied seasonal GWR models of daily PM2.5 with proper auxiliary variables for the Yangtze River Delta. This study used the GWR model to estimate PM2.5 concentration for four-season and improve the retrieval model accuracy with MODIS AOD, temperature, wind speed, air pressure, vapor pressure, relative humidity, and horizontal surface visibility geomorphic feature, elevation, and MODIS NDVI. The results showed that meteorological or geographical factors significantly improved the GWR model accuracy for retrieving PM2.5 concentration from satellite AOD. Besides, the GWR models of “AOD+3” (WS, Vpre, VSB) performed better than the other GWR models. The seasonal models in summer and autumn performed better than in spring and winter.

Yuanxi Guo et al. (2017) studied ground-level PM2.5 concentration estimation in Beijing using satellite-based data and a geographically and temporally weighted regression model. The GWR model was used to estimate daily ground-level PM2.5 concentration and quantitatively evaluated the model’s performance with MODIS AOD, AERONET AOD, boundary layer height, relative humidity, surface pressure, temperature, wind direction, wind speed, NDVI, population data, elevation data. The results showed annual mean PM2.5 values ranged from 62 to 110 μg/m^3, with a mean of 79 μg/m^3, denoting very high pollution levels in Beijing. Highly polluted areas corresponded well with poorly vegetation-covered, heavily populated, and low-lying regions; The overall CV R^2 was valued at 0.58. The CV MPE and RMSE were valued at 21.01 and 30.81 μg/m^3, respectively.

Luo et al. (2017) studied the spatiotemporal pattern of PM2.5 concentration in Mainland China and analyzed its influencing factors. The GWR was used to analyze the spatiotemporal patterns of PM2.5 concentration in China at a high spatial resolution with (1) socio-economic factors including population density, GDP, road density, factory density, urban and agriculture area, and (2) natural geographic factors including altitude, slope, aspect, air temperature, air pressure, precipitation, relative humidity, wind speed. The result showed that the road, agriculture, population, industry, economy, and urban areas strongly correlated with PM2.5 concentration. In contrast, a significantly strong negative correlation was found in vegetation, topography, and climate on PM2.5.

The previous studies show the application of the GWR model with or without AOD. They use the model to estimate ground-level PM concentration (dependent variable) and improve the accuracy by finding the relationship between different meteorological, land use, and socio-economic factors (independent variables) in local scale areas. Finally, they found the GWR model can be applied to estimate the ground-level PM concentration in the areas with limited pollution data.

2.6.2 Application of the MEM model

Kloog et al. (2011) studied the assessing temporally and spatially resolved PM2.5 exposures for epidemiological studies using aerosol optical depth measurements in New England, USA. In this study, the LME model was used to estimate PM2.5 concentration with MODIS AOD data at 10 km resolution, a raster of open spaces at 30 m cell size, elevation, the sum of main road segment lengths in a 10 km grid, metrological data include; temperature, wind speed, visibility, PM2.5 point emission, area source PM2.5 emission, and daily PM2.5 concentration station. The results showed that on the days with available AOD data, they found high out-of-sample R^2 (mean out-of-sample R^2 = 0.830, year-to-year variation 0.725-0.904). Model performance was still excellent for days without AOD data (mean out-of-sample R^2 = 0.810, year-to-year variation 0.692-0.887). Significantly, these R^2 were for daily, rather than monthly or yearly, values. The model could investigate ambient particles' acute and chronic effects in short-term and long-term human exposures.

Next, Lee, Coull, Bell, and Koutrakis (2012) studied satellite-based aerosol optical depth and spatial clustering to predict ambient PM2.5 concentration in New England, USA. The MEM with random intercepts and slopes was used in the study to estimate daily PM2.5 concentration with only MODIS AOD data at 10 km resolution. The results showed that the daily intercepts and slopes varied by season: 8.43, 7.98, 11.02, and 8.99 for intercepts; and 8.18, 7.22, 9.25, 8.49 for slopes in winter, spring, summer, and fall, respectively. The model performances were high R^2 (0.83 and 0.73 for year and season, respectively). Finally, they suggested that AOD can be a robust predictor of PM2.5 in the mixed-effects model.

Yuanai Guo and Zhang (2014) studied the pollution characteristics and influence factors of PM2.5 in 24 capital cities on the Chinese mainland. This study used the LME with random intercept and LME with random intercept and a random slope to analyze PM2.5 concentration with the meteorological conditions data, including temperature, humidity, visibility, wind speed, rainfall, and weather conditions. The results showed that temperature, humidity, visibility, and wind speed were significant. PM2.5 had a position correlation with temperature and a negative correlation with humidity, visibility, and wind speed. Simultaneously, the most relevant factor was visibility, followed by wind speed, temperature, and humidity. Likewise, the PM2.5 level had a significant seasonal characteristic. The level in winter was higher than in spring. By the way, the weather conditions significantly affected the PM2.5 level. PM2.5 had a positive correlation with haze weather and a negative correlation with rainy and snowy conditions.

Meng et al. (2016) studied the estimated ground-level PM10 in a Chinese city by combining satellite data, meteorological information, and land-use regression models. In this study, the LME was used to estimate annual and seasonal mean PM10 concentration in 2008 with (1) MODIS AOD and (2) land use data, including green space, industrial land, commercial and residential land, water area, NDVI, road network, population data, and (3) meteorological data including temperature, relative humidity, wind speed, and wind direction. The results showed the annual mean predicted PM10 concentration was 90.70 $\mu g/m^3$. PM10 pollution was the most serious in winter, with a mean predicted concentration of 109.90 $\mu g/m^3$. While summer, spring, and autumn seasons were 59.40, 93.40, and 87.90 $\mu g/m^3$, respectively.

Ma et al. (2016) studied satellite-derived high-resolution PM2.5 concentration in China's Yangtze River Delta Region using an improved linear mixed-effects model with MODIS AOD, wind speed, relative humidity, and forest cover data. The result showed that the average PM2.5 concentration and AOD were 64.40 $\mu g/m^3$ and 0.71 for 10 km MODIS AOD data, respectively. For the 3 km MODIS AOD data, the mean PM2.5 and AOD were 57.62 $\mu g/m^3$ and 0.81, respectively. The MPE and RMSE values for the 3 km resolution model were smaller than the 10 km resolution model. Finally, the 3 km PM2.5 predictions could provide more spatial details than 10 km predictions for an urban scale.

In summary, the MEM model has been applied by many researchers to estimate PM concentration based on MODIS AOD, with different meteorological and land use data. Many studies attempt to improve the model prediction accuracy and study the relationship between PM concentration with MODIS AOD and other significant factors. Finally, the MEM model can assess human exposure for short-term and long-term epidemiological studies. Besides, it represents an attempt to adopt remote sensing technology to monitor on environmental field.

CHAPTER III
RESEARCH METHODOLOGY

The study on spatiotemporal PM concentration prediction using MODIS AOD with significant PM factors applied the GIS and remote sensing techniques to improve model prediction accuracy. In this study, the study area was separately identified into areas, including rural and urban landscapes, for studying the relationship between PM concentration and significant factors such as meteorological, biophysical, and socioeconomic data. However, PM concentration in this study is the atmospheric air quality measurement. Therefore, the sample is not collected directly influenced by the source of pollution. The height from the ground level to the end of the air sampling tube is more than 3 meters, and the distance of more than 1 meter from supporting structures is vertical and horizontal to avoid direct interference from the original, such as grilling and traffic.

The overview framework of the research methodology consisted of four components include (1) data collection and preparation, (2) identification of significant spatiotemporal factors on PM concentration and relationship, (3) prediction of spatiotemporal PM concentration, and (4) a suitable spatiotemporal model for PM concentration prediction and validation, as shown in Figure 3.1. Details of each component are separately described in the following sections.

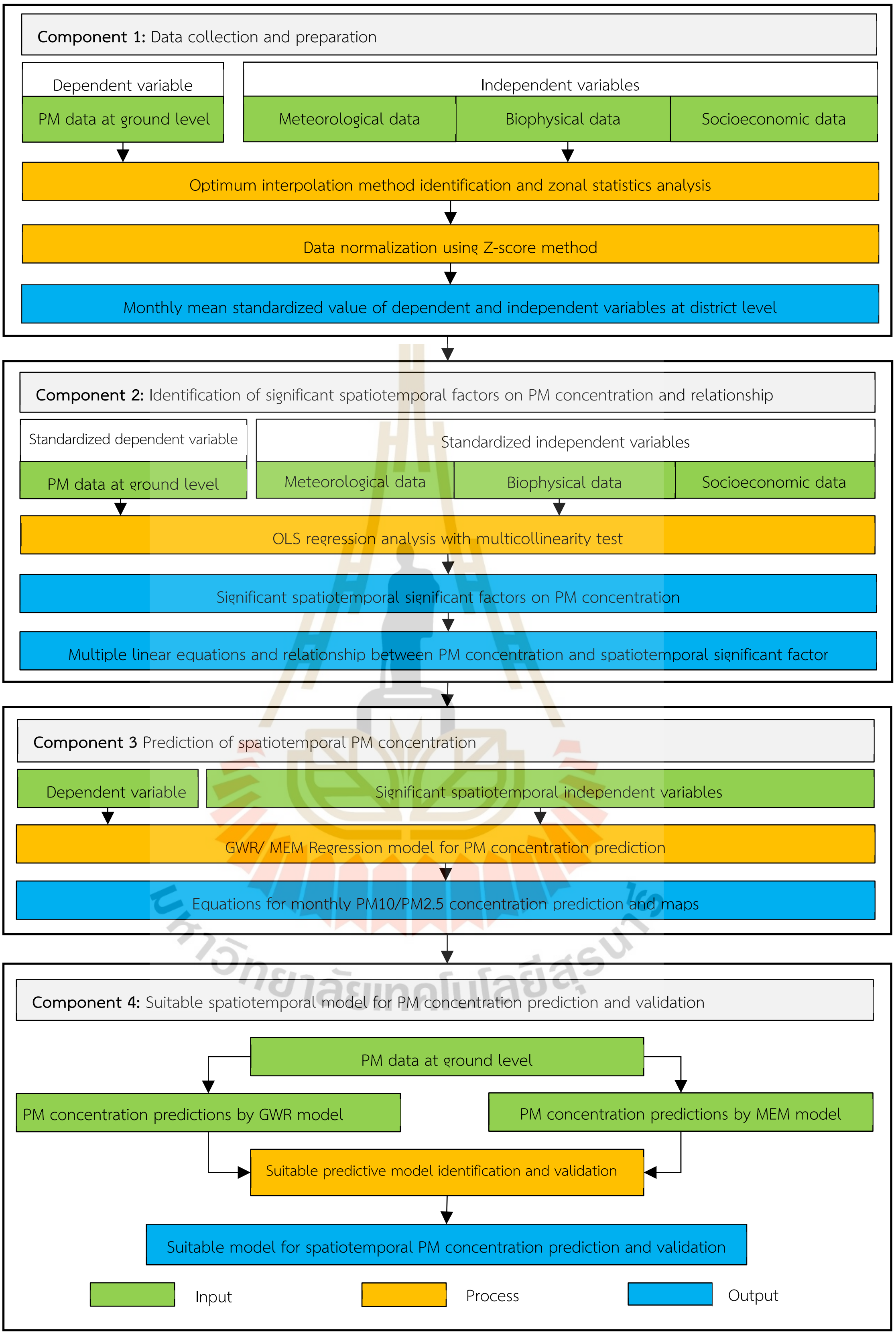

Figure 3.1 Overview of the research framework of the study.

3.1 Data collection and preparation

The required input data of the study, which are included ground-level PM data as dependent variables, and meteorological, biophysical, and socioeconomic data as independent variables from October 2019 to May 2020, were firstly collected from national and international organizations and prepared using standard tools under the ArcGIS software, as a summary in Table 3.1. This study transformed all dynamic daily input data into monthly mean data. On the contrary, road density in 2019, factory density in 2019, elevation in 2000, population density in 2019, and GPP in 2019 were applied as static input data. Likewise, selected Landsat data in December 2019 and March 2020 were represented as seasonal data for winter (October-February) and summer (March-May). The schematic workflow with input, process and output for data collection and preparation is exhibited in Figure 3.2.

In practice, available interpolation methods under the GIS environment, which many researchers subjectively choose, were examined to identify an optimum method for specific factors. In this study, seven interpolation methods, namely IDW, GPI, RBF, OK, OCK, SK, and SCK, were selected to examine an optimum interpolation method for appropriate dependent and independents variables, including average monthly PM data at ground level, meteorological data (relative humidity, temperature, wind speed, pressure, visibility) and MODIS fire data (brightness temperature and radiative firepower) based on the existing data between October 2019 to May 2020 using the Root Mean Squared Error (RMSE), which are reported by cross-validation under the ESRI ArcGIS environment.

The RMSE indicates how closely the model predicts the measured values. The RMSE value should be smaller and derived using Eq (3.1).

$$RMSE=\sqrt{\frac{\sum_{i=1}^{n}(\text{predicted-measured})^2}{n}} \tag{3.1}$$

Where, n is the number of measured data.

After that, all prepared variables were normalized using the Z-score method to identify significant spatiotemporal factors on PM concentration and relationships using the multicollinearity test and the OLS regression analysis.

Table 3.1 List of data collection and preparation for analysis and modeling in the study.

Categories	Variables	Source	Time-Frequency	Data preparation
PM data at ground level	PM10	PCD	Daily	Optimum interpolation method
		BMA	Daily	
	PM2.5	PCD	Daily	
		BMA	Daily	
Meteorological data	Relative humidity	TMD	Daily	Optimum interpolation method
	Temperatures	TMD	Daily	
	Wind speed	TMD	Daily	
	Pressure	TMD	Daily	
	Visibility	TMD	Monthly	
Biophysical data	MCD19A2	USGS	Daily	Raster Calculator
	NDVI	USGS	Seasonal (17/12/2019 and 26/03/2020)	Raster Calculator from Landsat 8 OLI data
	BUI	USGS	Seasonal (17/12/2019 and 26/03/2020)	
	Road density	MOT	-	Calculate geometry and field calculator
	Factory density	DIW	-	Spatial join and field calculator
	Elevation	USGS	-	Fill (Spatial analysis) from SRTM
	Brightness temperature	NASA	Daily	Optimum interpolation method
	Fire Radiative Power	NASA	Daily	
	Fire hotspot	NASA	Daily	Spatial join and field calculator
Socioeconomic data	Population density	NSO	Yearly (2019)	Field calculator (Extract from population data without non-registered people at district level)
	GPP	NESDC	Yearly (2019)	

Note: BMA: Bangkok Metropolitan Administration; DIW: Department of Industrial Works; MOT: Ministry of Transport; NASA: NASA's Earth Science Data Systems; NSO: National Statistical Office; NESDC: Office of the National Economic and Social Development Council; PCD: Pollution Control Department; TMD: Thai Meteorological Department; USGS: United States Geological Survey.

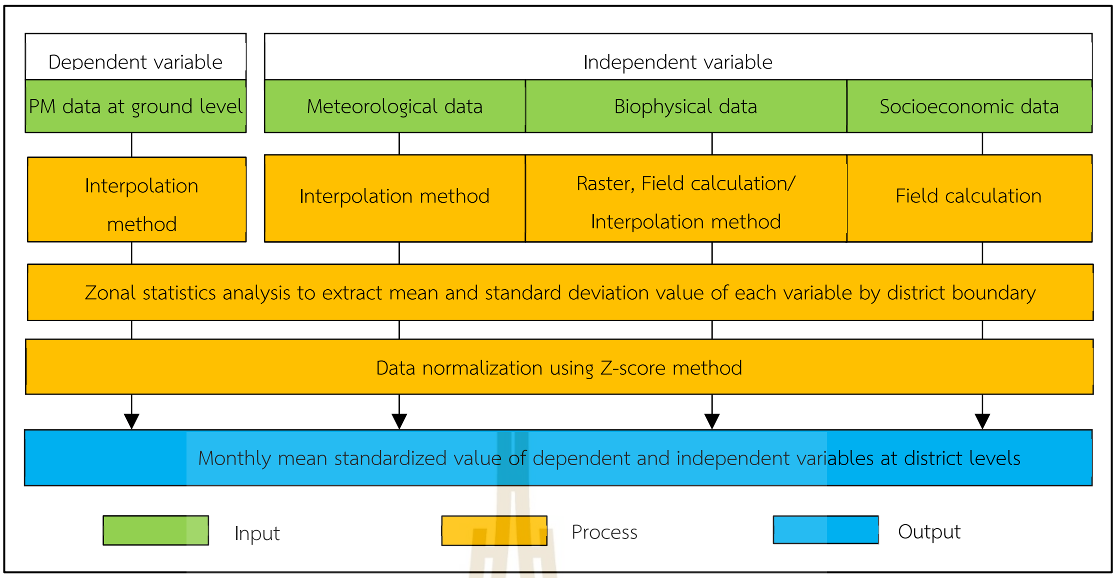

Figure 3.2 Workflow of data collection and preparation.

In practice, mean and standard deviation values at the district level of all dependent and independent variables were first extracted using the zonal statistics analysis. Then, they are further exported to the MS Excel spreadsheets and normalized using the Z-score method as:

$$Z = \frac{(X-\mu)}{\sigma} \tag{3.2}$$

Where Z is the standard score, X is the observed value, μ is the mean of the sample, and σ is the standard deviation of the sample. As a result, the mean values of all variables are zero, and their standard deviation values are one.

The schematic workflow of optimum interpolation method identification for PM, meteorological, and MODIS fire data preparation is displayed in Figure 3.3.

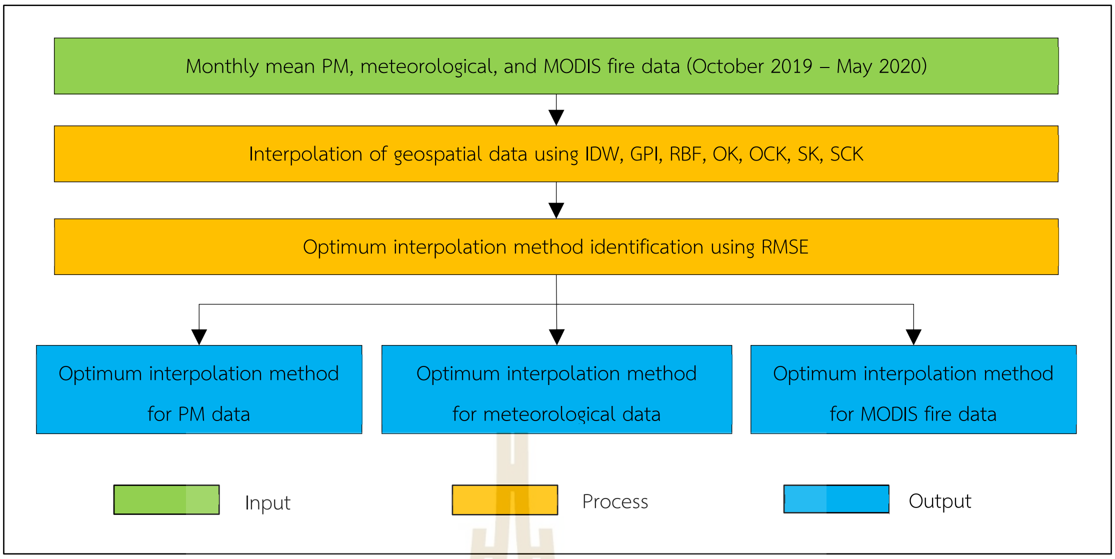

Figure 3.3 Workflow of optimum interpolation technique for PM, meteorological, and MODIS fire data preparation.

Besides, a specific week with the highest record of daily PM10 and PM2.5 concentration was prepared with the daily mean standardized value of dependent and independent variables at the district level to examine daily significant spatiotemporal factors.

3.2 Identification of significant spatiotemporal factor on PM concentration and relationship

Under this component, the dependent and independent variables on PM10 concentration in the rural landscape and PM2.5 concentration in the urban landscape in the winter season (October 2019 to February 2020) and summer season (March 2020 to May 2020) were applied to identify significant spatiotemporal factors using multicollinearity test with Variance Inflation Factor (VIF) value and ordinary least squares (OLS) regression analysis with a significance level of 0.01.

The VIF measures the amount of multicollinearity in a set of multiple regression variables. A high VIF value indicates that the associated independent variable is redundant with the other variables in the model. Therefore, the VIF value should be lower than 7.5 to avoid multicollinearity, as suggested in ArcGIS 10.3.1 Help (ESRI, 2015). The equation is shown as follows:

$$VIF_i = \frac{1}{1-R_i^2} \tag{3.3}$$

Where R_i^2 are the multiple coefficients of determination in a regression of the i^{th} predictor on the others.

The main output of this component is the significant spatiotemporal factors on PM10 concentration in the rural landscape and PM2.5 concentration in the urban landscape in the winter and summer seasons. Meanwhile, the regression coefficient values from multiple linear equations are applied to describe a positive or negative correlation of significant spatiotemporal factors on PM10 and PM2.5 concentration in different landscapes and seasons.

In this study, the relationship between the dependent variable (PM concentration) and independent variables (relative humidity, temperature, wind speed, pressure, visibility, MODIS AOD, brightness temperature, fire radiative power, fire hotspot, NDVI, BUI, road density, factory density, elevation, population density, and GPP) was assumed as linear form. The direction of the relationship between the dependent variable and sixteen candidate independent variables, which are categorized as a source of PM concentration, influencers on PM concentration and effect of PM concentration, are summarized in Table 3.2.

Table 3.2 Direction of the relationship between the dependent and independent variables based on the assumption of a linear relationship.

Categories	Independent variable	Relationship	Implication
Source of PM concentration	Brightness temperature	Positive	As these variables increase, PM concentration increase
	Fire radiative power	Positive	
	Fire hotspot	Positive	
	Road density	Positive	
	Factory density	Positive	
	Population density	Positive	
	GPP	Positive	
	BUI	Positive	

Table 3.2 (Continued).

Categories	Independent variable	Relationship	Implication
Influencers on PM concentration	Relative humidity	Positive	As these variables increase, PM concentration tends to increase
	Pressure	Positive	
	Wind speed	Negative	
	Temperature	Negative	
	NDVI	Negative	
	Elevation	Negative	
Effect of PM concentration	MODIS AOD	Negative	As PM concentration increases, these variables tend to decrease
	Visibility	Negative	

The schematic workflow of the significant spatiotemporal factors of PM (PM10 and PM2.5) concentration identification and relationship is displayed in Figure 3.4.

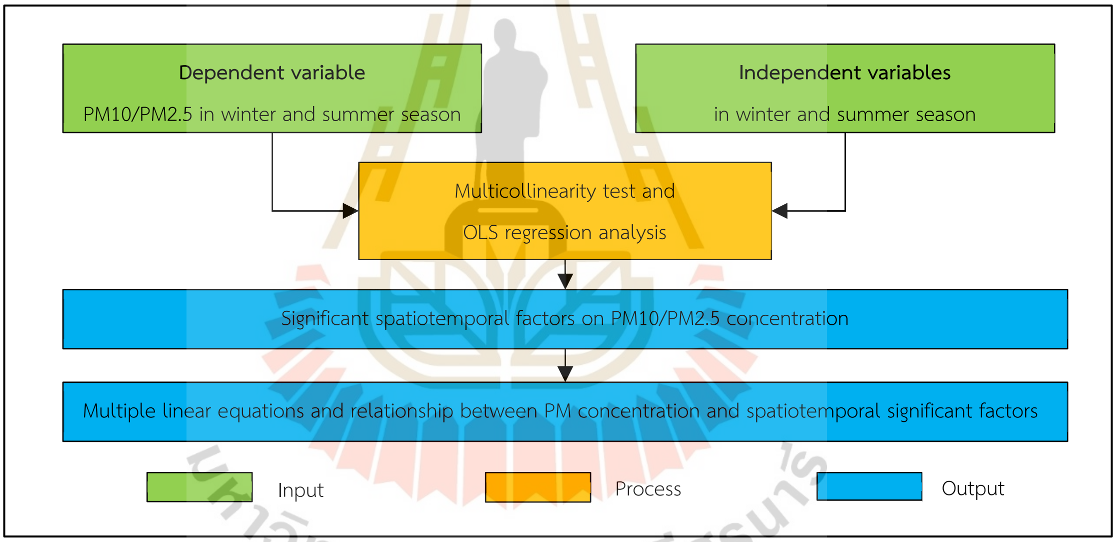

Figure 3.4 Workflow of identifying significant spatiotemporal factors on PM concentration and relationship.

The relation between a pair: PM concentration and Cokriging variable using Pearson's correlation. The range value of correlation coefficients varies between +1 to -1. The value -1 indicates a perfect negative linear relationship, while +1 indicates a perfect positive linear relationship. The value 0 shows no linear relationship. The interpretation of the correlation coefficient is described in Table 3.3.

Table 3.3 Interpretation of correlation coefficients.

Range of correlations coefficients	Interpretation
0.80 – 1.00	very strong positive
0.60 – 0.79	strong positive
0.40 – 0.59	moderate positive
0.20 – 0.39	weak positive
0.00 – 0.19	very weak positive
0.00 – (-0.19)	very weak negative
-0.20 – (-0.39)	weak negative
-0.40 – (-0.59)	moderate negative
-0.60 – (-0.79)	strong negative
-0.80 – (-1.00)	very strong negative

Source: Chowdhury, Debsarkar, and Chakrabarty (2015).

3.3 Prediction of spatiotemporal PM concentration

Under this component, primary input data (MODIS AOD) and significant spatiotemporal independent variables (the output from component 1) on PM10 and PM2.5 concentration in the rural and urban landscapes, respectively, are separately applied to predict monthly PM concentration in winter and summer seasons using the GWR and MEM models.

In practice, the GWR and MEM (fixed effect intercepts) models are first applied to predict monthly PM10 concentration in the rural landscape and PM2.5 concentration in the urban landscape in two seasons (winter and summer). Then, the efficiency of GWR models under the cross-validation process of ERSI ArcMap software is reported using the corrected Akaike Information Criterion (AICc), coefficient of determination (R^2), and Adjusted R-squared ($\bar{R}^2$) using the following equations.

$$\mathrm{AICc}=\left(-2\log(L)+2k\right)+\frac{2k(k+1)}{n-k-1} \tag{3.4}$$

$$R^2=1-\frac{SS_{res}}{SS_{tot}} \tag{3.5}$$

$$\bar{R}^2=1-\frac{SS_{res}/(n-k)}{SS_{tot}/(n-1)} \tag{3.6}$$

Where L is the maximum likelihood for the estimated model, k is the number of independent variables, n is the number of sample sizes, SS_{res} is the sum of squares of residual or calls the residual sum of squares, and SS_{tot} is the total sum of squares.

In the MEM model, the efficiency of models under the cross-validation process of SPSS statistical software is reported using the Akaike's Information Criterion (AIC), corrected Akaike information criterion (AICc) and Bayesian Information Criterion (BIC) as follows:

$$AIC=-2\log(L)+2k \tag{3.7}$$

$$BIC=-2\log(L)+k\log(N) \tag{3.8}$$

Where log(L) is the value of the log-likelihood function of the fitted model evaluated at the model estimate, k is the number of fitted model parameters, and N is the recorded measurements.

This component's significant output is the predictive equations for monthly PM10 concentration in the rural landscape and PM2.5 concentration in the urban landscape in winter and summer. Additionally, the distribution of monthly PM10 concentration in the rural landscape and PM2.5 concentration in the urban landscape over two seasons are presented according to the Thailand Air Quality Index (AQI) and US EPA standards, as described in Tables 3.4 to 3.5. In addition, The WHO has set guidelines on air pollution, especially PM10 and PM2.5 concentration levels, which are used as reference tools to set standards and goals to improve air quality for air quality management by policymakers worldwide, as described in Tables 3.6. For example, the WHO guidelines state that 24-hour average exposure for PM10 concentration should not exceed 45 μg/m^3, while PM2.5 concentration should not exceed 15 μg/m3. As a result, countries can reduce the disease burden from stroke, heart disease, lung cancer, and chronic and acute respiratory diseases, including asthma.

The schematic workflow of spatiotemporal PM concentration prediction is displayed in Figure 3.5.

Table 3.4 Thailand's Air Quality Index based on PM concentration.

Level of Thai AQI	Meaning	PM10 (μg/m^3)	PM2.5 (μg/m^3)
1	Excellent	0-50	0-25
2	Satisfactory	51-80	26-37
3	Moderate	81-120	38-50
4	Unhealthy	121-180	51-90
5	Very unhealthy	> 181	> 91

Source: Pollution Control Department (2018).

Table 3.5 The US EPA Air Quality Index based on PM concentration.

Level of AQI	Meaning	AQI	PM10 (μg/m^3)	PM2.5 (μg/m^3)
1	Good	0-50	0-54	0.0-12.0
2	Moderate	51-100	55-154	12.1-35.4
3	Unhealthy for Sensitive Groups	101-150	155-254	35.5-55.4
4	Unhealthy	151-200	255-354	55.5-150.4
5	Very Unhealthy	201–300	355–424	150.5–250.4
6	Hazardous	301-400	425-504	250.5-350.4
7		401-500	505-604	350.5-500.4

Source: (US Environmental Protection Agency, 2018)

Table 3.6 WHO air quality guidelines.

Pollutant	PM 10		PM2.5	
Averaging period	One day	One Year	One day	One Year
WHO guidelines (μg/m^3)	45 μg/m^3 Not to be exceeded on more than three days per year.	15 μg/m^3	15 μg/m^3 Not to be exceeded on more than three days per year.	5 μg/m^3
Air quality standards under the Air Quality Directive	Limit value, 50 μg/m^3 Not to be exceeded on more than 35 days per year.	Limit value, 40 μg/m^3		Limit value, 25 μg/m^3

Source: Antonis S. Manolis and Theodora A. Manolis (2013), European Environment Agency (2016); World Health Organization (2021)

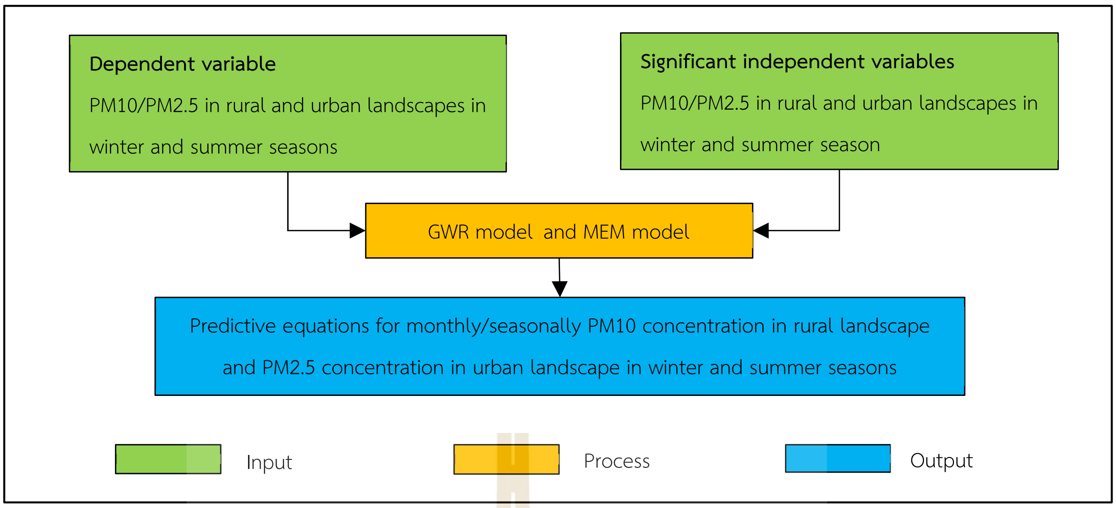

Figure 3.5 Workflow of spatiotemporal PM concentration prediction.

3.4 Suitable spatiotemporal model for PM concentration prediction and validation

Under this component, a suitable model for spatiotemporal PM10 and PM2.5 concentration prediction between GWR and MEM models was first identified based on their AICc values. (See also section 3.3). In general, the lower AICc value indicates a better fit model. In practice, average AICc values for PM10 concentration in the rural landscape and PM2.5 concentration in winter and summers from GWR and MEM models were calculated to identify the suitable model for spatiotemporal PM10 and PM2.5 concentration prediction in this study.

In addition, the suitable model for spatiotemporal PM10 and PM2.5 concentration prediction was validated with a new dataset (October 2020 to May 2021) using Pearson Correlation Analysis. The expected correlation coefficient value should be equal to or more than 0.5, which shows a strong linear relationship between the dependent and independent variables (Cohen, 1988).

Moreover, characteristics of predictive spatiotemporal PM concentration by the suitable model (GWR or MEM) were summarized in two aspects. Firstly, the relationship between PM10 and PM2.5 concentration and significant monthly factors was examined using spatial correlation analysis with the Spatial Modeler module under ERDAS Imagine software. Secondly, the relationship between PM10 and PM2.5 concentration classification in winter and summer with standard deviation method and land use data in 2019 by LDD were examined using overlay analysis under ESRI ArcMap.

The schematic workflow of a suitable spatiotemporal model for PM concentration prediction is displayed in Figure 3.6.

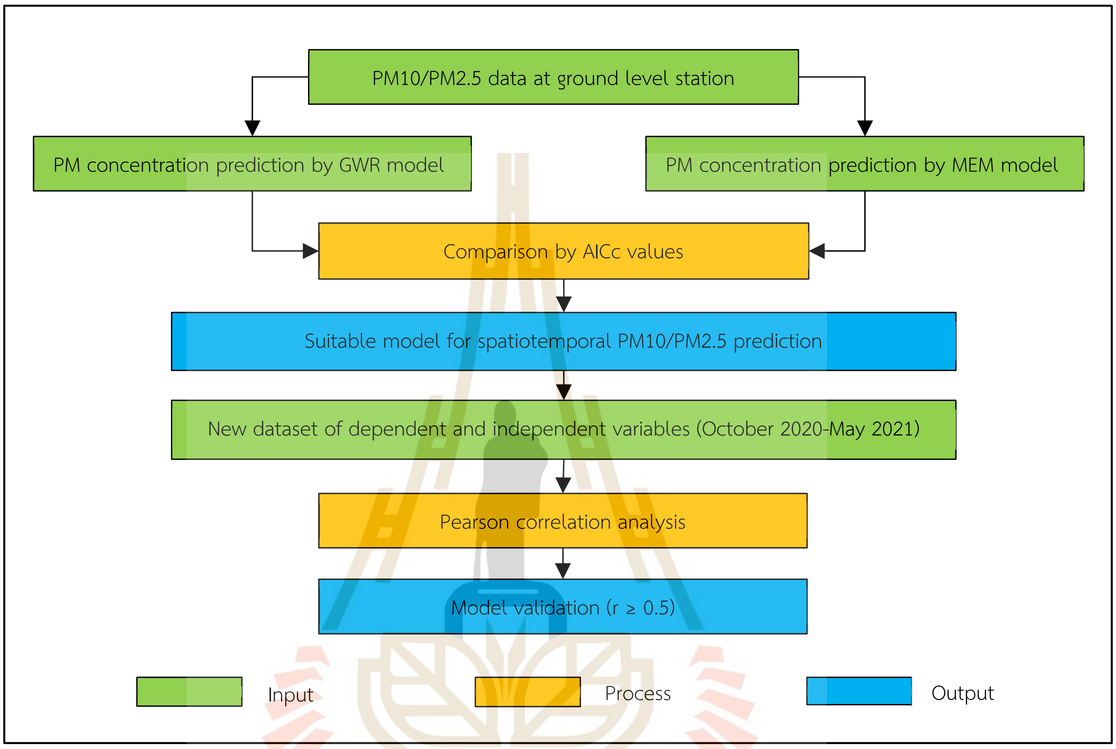

Figure 3.6 Workflow of a suitable spatiotemporal model for PM concentration prediction and validation.

The component's significant output is the suitable model for spatiotemporal PM10 and PM2.5 concentration prediction in the rural and urban landscapes in the winter and summer seasons and its spatiotemporal distribution characteristic. Additionally, the correlation coefficient value, which measures the strength and direction of a linear relationship of estimated and measured PM10 and PM2.5 in different landscapes and seasons, is validated to confirm the suitable model for PM10 and PM2.5 concentration prediction.

CHAPTER IV

DATA COLLECTION AND PREPARATION

This chapter presents the results of the first component of the research methodology focusing on data collection and preparation, particularly an optimum method for ground-level PM concentration, meteorological (relative humidity, temperature, wind speed, pressure, visibility), and MODIS fire data (brightness temperature and fire radiative power) interpolation. Details of each variable's result are explained and discussed in the following section.

4.1 Optimum method for monthly mean PM concentration interpolation

The statistical data of the ground-level monthly mean PM10 and PM2.5 concentration from the PCD and BMA between October 2019 to May 2020, which were applied to identify an optimum interpolation method, are summarized in Table 4.1, including minimum, maximum, mean, standard deviation (SD) values and the number of stations for interpolation. The spatial distribution of PM ground monitoring stations is displayed in Figure 4.1. Details of PM ground monitoring stations with geographic coordinates are reported in Table 1 in Appendix.

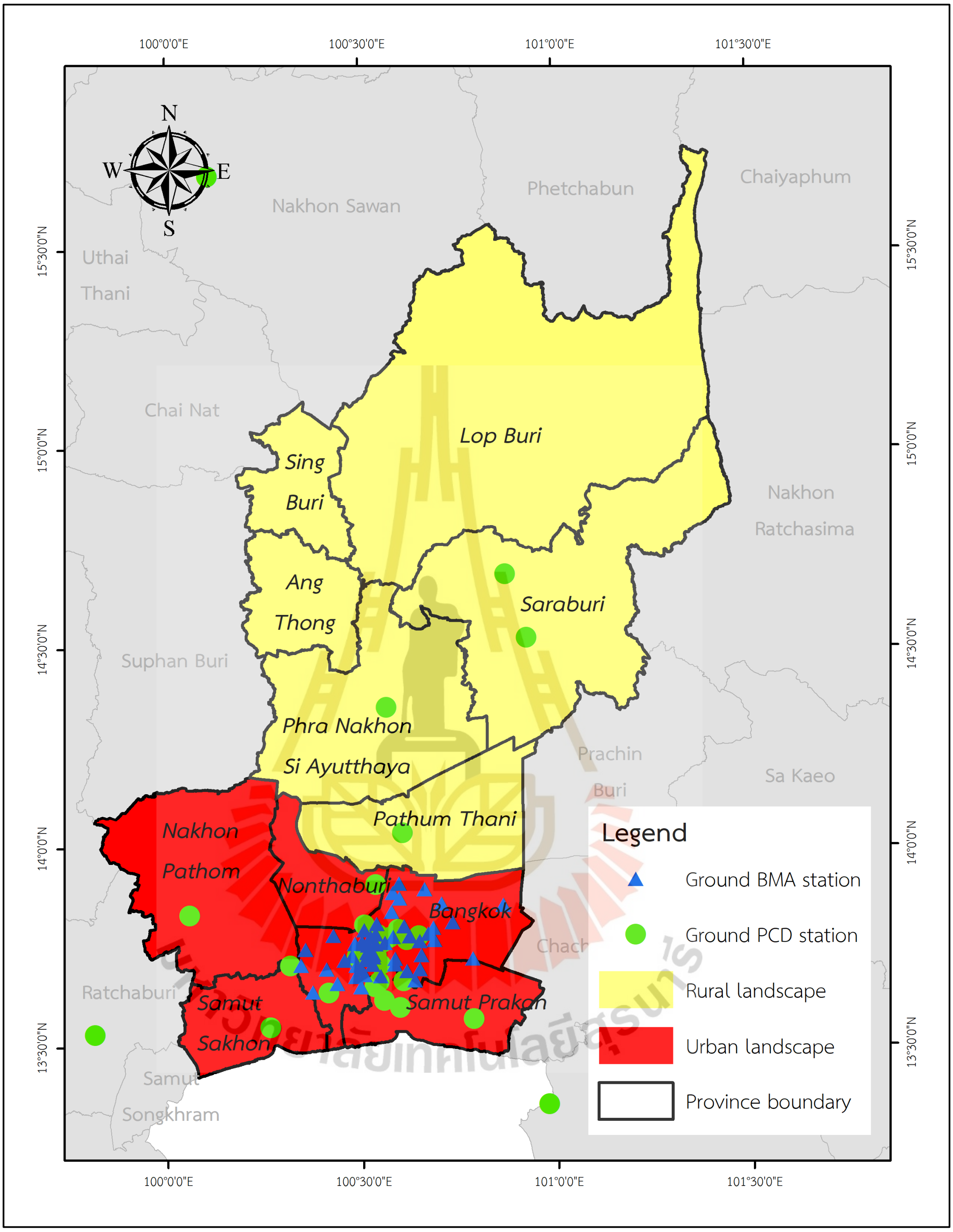

Figure 4.1 The spatial distribution of PM ground monitoring stations.

Table 4.1 Descriptive statistical data of the monthly mean PM10 and PM2.5 concentration.

Month	Season	PM10 concentration (µg/m^3)					PM2.5 concentration (µg/m^3)				
		Min.	Max.	Mean	SD.	Stations	Min.	Max.	Mean	SD.	Stations
Oct	Winter	29.84	151.43	51.53	17.17	64	13.66	41.52	25.82	6.59	64
Nov	Winter	41.80	176.23	64.08	18.23	64	20.53	46.33	32.97	6.39	64
Dec	Winter	45.89	179.49	74.07	18.62	64	27.27	54.10	39.29	6.67	64
Jan	Winter	48.23	202.36	78.46	20.81	68	29.77	67.23	43.61	8.07	77
Feb	Winter	50.42	213.11	79.51	20.79	68	19.72	63.23	44.11	7.51	85
Mar	Summer	24.55	121.55	48.49	15.86	68	14.17	50.46	23.54	6.15	91
Apr	Summer	22.64	104.07	43.00	13.02	68	13.65	37.41	21.98	4.90	91
May	Summer	17.74	84.34	37.14	11.25	68	9.15	28.32	16.75	4.17	91

According to the monthly mean basic statistical data, the monthly mean PM concentration is low in October. It gradually increases to the highest in February, then falls to the lowest in May. The maximum PM10 concentration is 213.11 µg/m^3 in February, while the maximum PM2.5 concentration is 67.23 µg/m^3 in January. In contrast, the minimum PM10 and PM2.5 concentrations were 17.74 µg/m^3 and 9.15 µg/m^3 in May, respectively. Additionally, the PM concentration is high in the winter season and low in the summer season. (See Table 4.1)

In the cokriging (OCK and SCK) method, the latitude and longitude variables were added to be the cokriging variable. The relationship between monthly mean PM10 and PM2.5 concentration and cokriging variables is summarized in Table 4.2.

Table 4.2 The Pearson's correlation coefficients between monthly mean PM10 and PM2.5 concentration with cokriging variables.

Variables		Oct	Nov	Dec	Jan	Feb	Mar	Apr	May
PM10	LAT	0.16	0.14	0.36**	0.36**	0.34**	0.50**	0.38**	0.32**
	LONG	-0.07	-0.11	-0.14	-0.07	0.07	0.17	0.17	0.15
PM2.5	LAT	0.13	0.06	0.38**	0.33**	0.27*	0.68**	0.54	0.34**
	LONG	-0.29*	-0.40**	-0.43**	-0.22	-0.10	0.10	0.02	0.04

Note: *correlation is significant at the 0.05 level (2-tailed), **correlation is significant at the 0.01 level (2-tailed).

As a result, the relationship between monthly mean PM10 concentration and latitude variable is a very weak positive linear relationship in October and November. Also, there is a statistically significant weak to moderate positive correlation ($p \leq 0.01$) from December to May. The relationship between monthly mean PM10 concentration and longitude variable indicates a weak negative linear relationship between October and January and a weak positive relationship between February and May.

Besides, the relationship between monthly mean PM2.5 concentration and latitude variable is a very weak positive linear relationship in October and November, same as the relationship between PM10 concentration. Additionally, a weak to moderate positive correlation is statistically significant ($p \leq 0.01$) from December to May. Except in February, there is statistically significant ($p \leq 0.05$). The relationship between monthly mean PM10 concentration and longitude variable indicates a negative linear relationship between October to February and a weak positive relationship between March and May.

The cross-validation RMSE for monthly mean PM10 and PM2.5 concentration interpolation with seven different methods (IDW, GPI, RBF, OK, OCK, SK, and SCK) is summarized in Tables 4.3 and 4.4, respectively.

Table 4.3 The cross-validation RMSE of the seven interpolation methods for mean PM10 concentration from October 2019 to May 2020.

Model	Function		RMSE (µg/m^3)								
			Oct	Nov	Dec	Jan	Feb	Mar	Apr	May	Avg.
IDW	Power 1	1 sector	17.55	18.88	17.32	19.97	20.04	14.90	12.39	11.00	16.51
		4 sectors	17.80	19.02	17.74	20.14	20.06	14.82	12.39	11.03	16.63
		4 sectors with 45-degree offset	17.55	18.78	17.26	19.77	19.83	14.74	12.32	10.90	16.39
		8 sectors	17.66	18.89	17.65	20.04	19.98	14.83	12.41	11.02	16.56

Table 4.3 (Continued).

Model	Function		RMSE (μg/m³)								
			Oct	Nov	Dec	Jan	Feb	Mar	Apr	May	Avg.
IDW	Power 2	1 sector	18.50	20.29	17.35	20.12	20.61	15.51	13.15	11.46	17.12
		4 sectors	18.38	20.07	17.38	20.00	20.35	15.37	13.03	11.40	17.00
		4 sectors with 45-degree offset	18.22	19.95	17.09	19.78	20.23	15.37	13.02	11.32	16.87
		8 sectors	18.2	19.89	17.23	19.85	20.19	15.35	12.98	11.34	16.88
GPI	Order 1		18.14	19.21	18.64	21.79	22.65	14.41	12.73	11.2	17.35
	Order 2		86.41	101.16	110.32	111.1	114.03	39.31	33.05	28.64	78.00
	Order 3		573.46	611.72	399.28	473.83	468.41	91.11	41.42	20.89	335.02
RBF	Completely Regularize spine	1 sector	17.73	19.34	17.15	20.03	20.15	14.82	12.52	11.04	16.60
		4 sectors	17.98	19.45	17.51	20.21	20.01	14.64	12.52	11.19	16.69
		4 sectors with 45-degree offset	17.68	19.16	17.08	19.92	19.82	14.51	12.43	11.05	16.46
		8 sectors	17.88	19.36	17.37	19.99	19.80	14.55	12.43	11.19	16.57
	Spline with tension	1 sector	17.84	19.55	17.19	20.12	20.03	14.6	12.48	11.11	16.62
		4 sectors	17.94	19.42	17.48	20.11	19.91	14.49	12.38	11.11	16.61
		4 sectors with 45-degree offset	17.73	19.21	17.09	19.85	19.69	14.43	12.35	11.05	16.43
		8 sectors	17.86	19.31	17.36	19.96	19.77	14.51	12.38	11.16	16.54
	multiquadric	1 sector	21.83	24.29	19.84	24.07	24.92	17.21	15.74	13.39	20.16
		4 sectors	20.59	22.67	18.67	22.51	23.33	16.75	15.23	12.91	19.08
		4 sectors with 45-degree offset	20.82	22.94	19.04	22.79	23.62	16.78	15.27	12.88	19.27
		8 sectors	20.75	22.84	18.97	22.66	23.46	16.77	15.21	12.92	19.20
	Inverse multiquadric	1 sector	17.65	18.97	17.41	20.27	19.92	14.38	11.95	10.77	16.42
		4 sectors	18.06	19.26	18.01	20.54	20.17	14.46	11.96	10.88	16.67
		4 sectors with 45-degree offset	17.80	19.04	17.36	20.22	19.85	14.35	11.96	10.78	16.42
		8 sectors	17.92	19.00	17.87	20.42	20.12	14.57	12.08	10.96	16.62

Table 4.3 (Continued).

Model	Function		RMSE (μg/m^3)								
			Oct	Nov	Dec	Jan	Feb	Mar	Apr	May	Avg.
RBF	Thin plate spine	1 sector	60.62	62.86	50.69	63.33	69.36	40.48	38.71	29.79	51.98
		4 sectors	41.23	46.38	36.9	44.84	51.11	31.82	29.52	22.36	38.02
		4 sectors with 45-degree offset	39.48	43.18	35.23	42.04	46.08	29.08	26.97	20.71	35.35
		8 sectors	37.02	41.38	33.31	40.08	44.21	27.81	25.54	19.92	33.66
OK*	Circular		86.46	101.34	109.86	114.5	117.96	38.39	32.20	28.62	78.67
	Spherical		86.46	101.25	109.81	110.62	117.94	38.5	32.27	28.62	78.18
	Tetraspherical		86.44	101.26	109.84	110.66	117.91	38.49	32.34	28.62	78.20
	Pentasherical		86.43	101.31	109.88	110.70	117.88	38.53	32.33	28.62	78.21
	Exponential		86.48	101.39	109.98	110.81	117.52	38.49	32.33	28.62	78.20
	Gaussian		86.41	101.10	109.62	114.68	118.31	38.60	32.17	28.62	78.69
	Rational Quadratic		86.57	101.53	110.11	110.97	117.66	39.34	32.99	28.62	78.47
	Hole Effect		86.13	100.56	109.69	115.01	118.57	39.58	33.71	28.62	78.98
	K-Bessel		86.50	101.45	109.98	110.81	118.24	38.51	32.32	28.62	78.30
	J-Bessel		85.95	100.25	109.81	115.25	118.89	38.69	33.65	27.90	78.80
	Stable		86.46	101.39	109.96	110.76	118.26	38.49	32.32	28.14	78.22
OCK*	Circular		77.31	94.14	102.32	114.46	113.76	33.9	33.92	27.56	74.67
	Spherical		82.51	97.77	102.37	111.32	115.19	33.91	34.05	28.62	75.72
	Tetraspherical		82.42	97.25	107.63	111.34	113.68	33.95	34.1	28.62	76.12
	Pentasherical		82.50	96.96	103.82	112.3	115.25	33.39	34.18	28.62	75.88
	Exponential		77.75	96.96	101.17	111.09	113.88	34.54	33.92	31.93	75.16
	Gaussian		77.51	91.67	101.1	114.65	113.91	34.11	33.97	27.38	74.29
	Rational Quadratic		77.55	91.75	100.78	91.58	114.83	33.77	34.04	28.56	71.61
	Hole Effect		83.49	94.28	106.49	92.53	114.46	33.89	32.30	27.85	73.16
	K-Bessel		77.22	92.83	101.16	110.8	113.06	34.12	30.73	29.15	73.63
	J-Bessel		82.71	96.77	106.68	103.6	118.88	37.75	30.86	27.61	75.61
	Stable		76.99	91.67	101.10	110.74	113.90	34.11	32.97	27.40	73.61
SK*	Circular		16.88	17.82	17.22	19.98	20.11	15.01	12.74	11.16	16.37
	Spherical		16.93	17.9	17.16	20.09	20.1	15.11	12.71	11.16	16.40
	Tetraspherical		16.92	17.88	17.19	20.17	20.09	15.37	12.73	11.17	16.44
	Pentaspherical		16.95	17.88	17.21	20.17	20.11	15.4	12.76	11.15	16.45
	Exponential		16.92	17.86	17.2	19.88	19.92	15.27	12.69	11.14	16.36
	Gaussian		16.88	17.83	17.75	20.16	20.25	14.79	12.76	11.17	16.45

Table 4.3 (Continued).

Model	Function	RMSE (μg/m³)								
		Oct	Nov	Dec	Jan	Feb	Mar	Apr	May	Avg.
SK*	Rational Quadratic	17.05	17.92	17.34	20.02	19.99	15.38	12.71	11.07	16.44
	Hole Effect	17.18	18.15	17.66	20.19	20.15	16.08	12.40	11.06	16.61
	K-Bessel	16.96	17.91	17.32	20.15	20.18	15.37	12.80	11.11	16.48
	J-Bessel	16.93	17.69	17.62	20.27	20.26	15.57	12.39	11.33	16.51
	Stable	17.00	17.92	17.40	20.16	20.25	15.26	12.74	11.10	16.48
SCK*	Circular	16.86	17.86	17.01	20.24	19.64	13.84	11.92	10.60	16.00
	Spherical	16.87	17.86	16.98	20.24	19.63	13.83	11.88	10.56	15.98
	Tetraspherical	16.87	17.86	16.96	20.24	19.63	13.82	11.84	10.55	15.97
	Pentaspherical	16.87	17.87	16.95	19.32	19.62	13.67	11.78	10.52	15.83
	Exponential	16.88	17.85	16.78	20.21	19.56	13.62	11.85	10.55	15.91
	Gaussian	16.87	17.89	17.06	20.24	19.69	13.96	11.93	11.25	16.11
	Rational Quadratic	16.87	17.85	16.77	20.26	19.55	13.54	11.7	10.48	15.88
	Hole Effect	16.84	17.79	17.08	19.22	19.54	13.46	11.29	10.62	15.73
	K-Bessel	16.84	17.87	16.57	19.34	19.41	13.41	11.85	10.55	15.73
	J-Bessel	16.80	17.87	17.02	19.24	19.75	13.47	11.55	10.41	15.76
	Stable	16.85	17.86	16.59	19.33	19.48	13.38	11.85	10.54	15.74

Note: * This model calculated new values for the parameters with optimized semivariogram

Table 4.4 The cross-validation RMSE of the seven different interpolation methods for mean PM2.5 concentration interpolation from October 2019 to May 2020.

Model	Function		RMSE (μg/m³)								
			Oct	Nov	Dec	Jan	Feb	Mar	Apr	May	Avg.
IDW	Power 1	1 sector	6.35	6.09	5.81	7.97	7.50	5.56	4.67	4.18	6.02
		4 sectors	6.19	6.00	5.81	7.77	7.42	5.43	4.56	4.16	5.92
		4 sectors with 45-degree offset	6.15	5.96	5.65	7.75	7.36	5.46	4.57	4.15	5.88
		8 sectors	6.20	6.03	5.85	7.73	7.39	5.46	4.56	4.14	5.92
	Power 2	1 sector	6.77	6.62	5.99	8.57	7.87	5.80	4.94	4.38	6.37
		4 sectors	6.63	6.50	5.92	8.34	7.74	5.67	4.83	4.32	6.24
		4 sectors with 45-degree offset	6.61	6.49	5.87	8.37	7.74	5.73	4.85	4.31	6.25
		8 sectors	6.62	6.50	5.94	8.31	7.71	5.70	4.82	4.29	6.24

Table 4.4 (Continued).

Model	Function		RMSE (µg/m³)								
			Oct	Nov	Dec	Jan	Feb	Mar	Apr	May	Avg.
GPI	Order 1		6.66	6.39	5.55	7.80	7.58	4.69	4.24	4.07	5.87
	Order 2		8.90	14.43	22.36	21.49	15.87	7.67	5.85	4.58	12.64
	Order 3		109.56	77.93	25.80	52.54	55.78	18.14	8.75	29.74	47.28
RBF	Completely Regularize spine	1 sector	6.63	6.39	5.94	8.37	7.83	5.68	4.88	4.34	6.26
		4 sectors	6.56	6.33	5.99	8.32	7.77	5.50	4.84	4.37	6.21
		4 sectors with 45-degree offset	6.48	6.26	5.82	8.31	7.79	5.56	4.87	4.36	6.18
		8 sectors	6.52	6.29	5.95	8.32	7.76	5.48	4.82	4.36	6.19
	Spline with tension	1 sector	6.69	6.41	5.97	8.35	7.73	5.63	4.88	4.41	6.26
		4 sectors	6.49	6.22	5.91	8.17	7.65	5.40	4.77	4.33	6.12
		4 sectors with 45-degree offset	6.43	6.18	5.74	8.17	7.66	5.49	4.81	4.33	6.10
		8 sectors	6.44	6.22	5.90	8.18	7.66	5.42	4.76	4.32	6.11
	multiquadric	1 sector	8.18	8.00	7.15	10.23	9.43	6.15	5.55	4.98	7.46
		4 sectors	7.67	7.57	6.76	9.96	9.04	6.09	5.46	4.91	7.18
		4 sectors with 45-degree offset	7.72	7.59	6.82	9.91	9.03	6.10	5.49	4.94	7.20
		8 sectors	7.69	7.59	6.79	9.86	8.96	6.11	5.49	4.93	7.18
	Inverse multiquadric	1 sector	6.37	6.05	5.80	7.91	7.43	5.54	4.63	4.34	6.01
		4 sectors	6.17	5.89	6.07	7.73	7.42	5.43	4.59	4.21	5.94
		4 sectors with 45-degree offset	6.24	5.97	5.81	7.66	7.35	5.46	4.58	4.19	5.91
		8 sectors	6.24	6.04	6.04	7.82	7.35	5.50	4.59	4.22	5.98
	Thin plate spine	1 sector	12.11	16.31	11.99	18.11	16.82	9.16	8.33	7.00	12.48
		4 sectors	11.11	11.60	9.90	15.70	13.51	7.59	6.81	6.28	10.31
		4 sectors with 45-degree offset	10.35	11.66	9.53	14.11	12.66	7.81	7.02	6.28	9.93
		8 sectors	10.40	10.93	9.22	14.24	12.50	7.88	7.12	6.49	9.85

Table 4.4 (Continued).

Model	Function	RMSE (μg/m³)								
		Oct	Nov	Dec	Jan	Feb	Mar	Apr	May	Avg.
OK*	Circular	8.98	14.40	22.36	21.60	15.95	7.65	5.77	4.74	12.68
	Spherical	8.98	14.40	22.36	21.60	15.95	7.65	5.77	4.75	12.68
	Tetraspherical	8.98	14.40	22.36	21.60	15.95	7.65	5.77	4.73	12.68
	Pentasherical	8.98	14.40	22.36	21.60	15.95	7.65	5.77	4.74	12.68
	Exponential	8.98	14.40	22.36	21.60	16.04	7.65	5.77	4.78	12.70
	Gaussian	8.98	14.40	22.36	21.60	15.95	7.76	5.77	4.75	12.70
	Rational Quadratic	8.98	14.40	22.36	21.60	15.95	7.65	5.77	4.77	12.69
	Hole Effect	8.98	14.40	22.36	21.60	15.95	7.65	5.77	4.79	12.69
	K-Bessel	8.98	14.40	22.36	21.60	16.12	7.75	5.77	4.75	12.72
	J-Bessel	8.98	14.40	22.36	21.60	16.02	7.65	5.77	4.72	12.69
	Stable	8.98	14.38	22.36	21.60	16.01	7.76	5.77	4.75	12.70
OCK*	Circular	8.98	14.40	21.25	21.60	14.11	7.65	5.05	4.50	12.19
	Spherical	8.98	14.40	21.26	21.60	15.61	7.46	5.05	4.50	12.36
	Tetraspherical	8.98	14.40	21.23	21.60	15.85	7.31	5.11	4.49	12.37
	Pentasherical	8.98	14.40	21.26	21.60	14.05	7.50	5.12	4.49	12.18
	Exponential	8.98	14.40	21.20	21.60	14.06	7.62	5.14	4.50	12.19
	Gaussian	8.98	14.25	21.20	19.30	14.14	7.73	4.90	4.45	11.87
	Rational Quadratic	8.98	14.40	21.16	21.60	13.95	7.56	5.31	4.49	12.18
	Hole Effect	8.98	14.40	20.00	21.60	14.52	7.65	5.05	4.45	12.08
	K-Bessel	8.64	14.40	22.11	19.32	14.11	7.64	4.94	4.48	11.96
	J-Bessel	8.81	13.84	22.09	19.12	14.38	7.22	5.09	4.51	11.88
	Stable	8.53	14.40	21.20	19.30	14.14	7.73	4.90	4.44	11.83
SK*	Circular	6.10	5.98	5.53	7.43	7.42	5.67	4.62	4.17	5.87
	Spherical	6.10	6.00	5.59	7.45	7.43	5.68	4.62	4.17	5.88
	Tetraspherical	6.16	6.02	5.60	7.50	7.39	5.70	4.68	4.17	5.90
	Pentaspherical	6.16	6.05	5.62	7.48	7.39	5.71	4.66	4.17	5.91
	Exponential	6.08	6.09	5.62	7.61	7.49	5.67	4.71	4.17	5.93
	Gaussian	6.10	6.01	5.54	7.24	7.36	5.44	4.62	4.17	5.81
	Rational Quadratic	6.10	5.95	5.60	7.42	7.45	5.56	4.72	4.17	5.87
	Hole Effect	6.15	6.15	5.70	7.36	7.61	5.56	4.70	4.16	5.92
	K-Bessel	6.07	6.08	5.53	7.34	7.71	5.45	4.60	4.17	5.87
	J-Bessel	6.24	6.05	5.78	7.48	7.60	5.52	4.68	4.17	5.94
	Stable	6.05	5.94	5.54	7.35	7.42	5.44	4.62	4.17	5.82

Table 4.4 (Continued).

Model	Function	RMSE (μg/m³)								
		Oct	Nov	Dec	Jan	Feb	Mar	Apr	May	Avg.
SCK*	Circular	6.09	5.83	5.74	8.07	7.51	5.81	4.73	4.17	5.99
	Spherical	6.08	5.84	5.75	8.07	7.51	5.80	4.73	4.17	5.99
	Tetraspherical	6.08	5.83	5.86	8.07	7.51	5.80	4.73	4.17	6.01
	Pentaspherical	6.09	5.83	5.76	8.07	7.51	5.80	4.73	4.17	6.00
	Exponential	6.09	5.88	5.93	8.07	7.51	5.76	4.90	4.17	6.04
	Gaussian	6.07	5.82	5.84	7.86	7.51	5.84	4.74	4.17	5.98
	Rational Quadratic	6.11	5.88	5.93	8.07	7.51	5.79	4.90	4.17	6.05
	Hole Effect	6.05	5.81	5.69	7.84	7.29	5.84	4.76	4.00	5.91
	K-Bessel	6.08	5.83	5.30	7.34	7.18	4.56	4.17	3.93	5.55
	J-Bessel	6.07	5.83	5.80	7.82	7.38	5.85	4.79	4.01	5.94
	Stable	6.08	5.82	5.36	7.86	7.18	4.57	4.18	3.93	5.62

Note: * This model calculated new values for the parameters with optimized semivariogram

As a result (Table 4.3), an average RMSE value of monthly mean PM10 concentration interpolation using seven different methods with various functions varies from 15.73 μg/m^3 using the SCK method with the Hole Effect or the K-Bessel function to 335.02 μg/m^3 using the GPI method with the Order 3 function. So, the SCK method with the Hole Effect or the K-Bessel function can be chosen as an optimum method for monthly mean PM10 concentration interpolation since both functions can provide the least RMSE value.

In the meantime, an average RMSE value of monthly mean PM2.5 concentration interpolation using the same methods with various functions varies from 15.73 μg/m^3 using the SCK method with the K-Bessel to 47.28 μg/m^3 using the GPI method with the Order 3 function. Therefore, the SCK method with the K-Bessel function is chosen as an optimum method for monthly mean PM2.5 concentration interpolation since it can provide the least RMSE value.

Nevertheless, previous research on an optimum interpolation method for predicting PM10 and PM2.5 concentration at international and national levels reported different methods. Sajjadi, Zolfaghari, Adab, Allahabadi, and Delsouz (2017) selected four interpolation methods (IDW, RBF, OK and UK) to identify an optimum method for predicting PM10 and PM2.5 in Sabzevar city of Razavi Khorasan province, Iran using RMSE, MAE, and MAPE. They found that IDW is the best interpolation method for PM10 and PM2.5 concentration prediction. Meanwhile, Vorapracha, Phonprasert, Khanaruksombat, and Pijarn (2015) selected three methods (IDW, OK and UK) to identify an optimum method for predicting PM10 in the Central Region of Thailand using RMSE. They also found that the most optimum method for PM10 prediction was IDW. Meanwhile. Wong, Yuan, and Perlin (2004) identified OK as the optimum method for PM10 prediction by comparing it with IDW. Likewise, Kumar et al. (2016) reported OK as the best interpolation method for PM10 concentration prediction among three selected methods (IDW, OK, spline).

According to the results mentioned above, it can be observed that the number of the selected interpolation methods to identify an optimum method for predicting PM10 and PM2.5 are less than in the current study. This study examines seven interpolation methods with various functions, namely IDW, GPI, RBF, OK, OCK, SK, and SCK, using RMSE. As a result, the SCK method, which applies the covariance between two or more realizations of cross-correlated random fields (Giraldo, Herrera, and Leiva, 2020), is the most optimum in this current.

4.2 Optimum method for monthly mean meteorological data interpolation

4.2.1 Relative humidity

The statistical data of relative humidity from 39 stations from TMD between October 2019 to May 2020 for identifying the optimum interpolation method are summarized in Table 4.5. Details of relative humidity measurement stations in geographic coordinates are reported in Table 2 in Appendix.

Table 4.5 Descriptive statistical data of the relative humidity.

Month	Season	Min. (%)	Max. (%)	Mean (%)	SD. (%)	Stations
Oct	Winter	69.39	83.58	77.14	3.67	39
Nov	Winter	57.15	77.03	69.51	4.58	39
Dec	Winter	54.35	76.13	65.76	5.06	39
Jan	Winter	58.61	77.87	69.32	5.57	39
Feb	Winter	51.62	75.41	64.89	6.29	39
Mar	Summer	55.94	81.35	70.15	6.21	39
Apr	Summer	56.90	82.93	70.70	6.84	39
May	Summer	65.32	85.03	73.82	4.69	39

According to the basic statistical data, the monthly mean relative humidity is the highest in October. After that, it gradually decreases to the lowest in February, then up to the high again in May. Thus, the maximum value of monthly relative humidity is 85.03% in May, while the minimum value of monthly relative humidity is 51.62% in February. Additionally, the mean relative humidity in the winter and summer seasons is insignificantly different.

In the cokriging (OCK and SCK) method, the latitude and longitude variables were added to be the cokriging variable. The relationship between monthly mean relative humidity and cokriging variables is summarized in Table 4.6.

Table 4.6 The Pearson's correlation coefficients between monthly mean relative humidity with cokriging variables.

Variables		Oct	Nov	Dec	Jan	Feb	Mar	Apr	May
RH	LAT	-0.46**	-0.34*	-0.44**	-0.73**	-0.83**	-0.86**	-0.91**	-0.71**
	LONG	0.28	-0.00	-0.06	0.01	0.05	0.38*	0.38*	0.53**

Note: *correlation is significant at the 0.05 level (2-tailed), **correlation is significant at the 0.01 level (2-tailed).

The relationship between monthly mean relative humidity and latitude variable has a moderate negative correlation from October to December. Additionally, January to May indicates strong negative linear relationships with statistically significant ($p \leq 0.01$). The correlation between relative humidity and longitude variable is relatively weak but noteworthy that there are moderate positive correlations with statistically significant ($p \leq 0.05$) in March and April ($p \leq 0.01$) in May.

The cross-validation RMSE for monthly mean relative humidity interpolation with seven different methods (IDW, GPI, RBF, OK, OCK, SK, and SCK) is summarized in Table 4.7.

Table 4.7 The cross-validation RMSE of the seven different interpolation methods for mean relative humidity interpolation from October 2019 to May 2020.

Model	Function		RMSE (%)								
			Oct	Nov	Dec	Jan	Feb	Mar	Apr	May	Avg.
IDW	Power 1	1 sector	3.32	4.56	4.97	4.43	4.04	3.76	3.72	3.24	4.01
		4 sectors	3.22	4.55	4.92	4.56	4.44	4.01	4.08	3.23	4.13
		4 sectors with 45-degree offset	3.25	4.54	4.84	4.52	4.43	4.15	4.18	3.40	4.16
		8 sectors	3.31	4.56	4.95	4.76	4.82	4.48	4.62	3.48	4.37
	Power 2	1 sector	3.54	4.87	5.33	4.84	4.23	3.76	3.74	3.27	4.20
		4 sectors	3.44	4.80	5.26	4.86	4.36	3.88	3.86	3.22	4.21
		4 sectors with 45-degree offset	3.46	4.79	5.24	4.85	4.37	3.91	3.90	3.29	4.23
		8 sectors	3.47	4.79	5.27	4.93	4.51	4.06	4.07	3.28	4.30
GPI	Order 1		3.49	3.49	4.63	4.75	3.78	3.32	3.52	3.13	3.76
	Order 2		3.80	3.80	4.54	4.93	3.93	3.42	3.02	2.99	3.80
	Order 3		4.01	4.01	6.77	5.55	4.32	3.98	3.94	3.54	4.52
RBF	Completely Regularize spine	1 sector	3.30	4.51	4.97	4.42	3.98	3.58	3.55	3.23	3.94
		4 sectors	3.19	4.43	4.91	4.47	4.11	3.65	3.62	3.19	3.95
		4 sectors with 45-degree offset	3.21	4.44	4.89	4.46	4.14	3.78	3.72	3.25	3.99
		8 sectors	3.20	4.44	4.91	4.49	4.18	3.78	3.73	3.24	4.00
	Spline with tension	1 sector	3.27	4.50	5.07	4.39	4.02	3.73	3.66	3.28	3.99
		4 sectors	3.16	4.41	4.90	4.43	4.11	3.63	3.61	3.18	3.93
		4 sectors with 45-degree offset	3.23	4.45	4.88	4.39	4.13	3.71	3.66	3.25	3.96
		8 sectors	3.18	4.43	4.88	4.46	4.18	3.76	3.71	3.24	3.98

Table 4.7 (Continued).

Model	Function		Oct	Nov	Dec	Jan	Feb	Mar	Apr	May	Avg.
			RMSE (%)								
RBF	multiquadric	1 sector	3.75	5.10	5.63	5.05	4.34	3.41	3.56	3.56	4.30
		4 sectors	3.76	5.07	5.53	4.93	4.22	3.20	3.39	3.56	4.21
		4 sectors with 45-degree offset	3.71	5.07	5.54	4.95	4.20	3.19	3.39	3.54	4.20
		8 sectors	3.75	5.07	5.53	4.92	4.20	3.18	3.37	3.54	4.20
	Inverse multiquadric	1 sector	3.25	4.51	4.97	4.29	3.92	4.09	4.04	3.36	4.05
		4 sectors	3.15	4.53	4.85	4.64	4.77	4.19	4.26	3.29	4.21
		4 sectors with 45-degree offset	3.25	4.56	4.74	4.42	4.50	4.25	4.30	3.46	4.19
		8 sectors	3.26	4.59	4.91	4.96	5.25	4.56	4.62	3.51	4.46
	Thin plate spine	1 sector	6.14	7.36	8.83	9.64	7.21	6.04	6.64	6.40	7.28
		4 sectors	5.23	7.05	7.97	7.59	6.41	4.80	5.36	5.25	6.21
		4 sectors with 45-degree offset	5.48	7.29	7.91	7.50	6.35	4.82	5.27	5.14	6.22
		8 sectors	5.50	7.35	8.04	7.48	6.40	4.66	5.21	5.15	6.22
OK*	Circular		3.84	4.56	5.00	3.96	3.46	2.90	3.02	3.90	3.83
	Spherical		3.77	4.56	5.00	3.96	3.46	2.90	3.02	3.89	3.82
	Tetraspherical		3.76	4.57	5.00	3.96	3.46	2.90	3.02	3.93	3.83
	Pentasherical		3.67	4.57	5.00	3.96	3.46	2.90	3.02	3.93	3.81
	Exponential		3.77	4.54	5.00	3.96	3.46	2.90	3.02	3.93	3.82
	Gaussian		3.72	4.56	5.00	3.96	3.46	2.90	3.02	3.90	3.82
	Rational Quadratic		3.70	4.61	5.00	3.96	3.46	2.90	3.02	3.93	3.82
	Hole Effect		3.42	4.48	5.00	3.96	3.46	2.90	3.02	3.93	3.77
	K-Bessel		3.78	4.45	5.00	3.96	3.46	2.90	3.02	3.74	3.79
	J-Bessel		3.36	4.71	5.00	3.96	3.46	2.90	3.02	3.93	3.79
	Stable		3.66	4.49	5.00	3.96	3.46	2.90	3.02	3.90	3.80

Table 4.7 (Continued).

Model	Function	RMSE (%)								
		Oct	Nov	Dec	Jan	Feb	Mar	Apr	May	Avg.
OCK*	Circular	3.61	4.56	5.00	3.96	3.46	2.90	3.02	3.78	3.79
	Spherical	3.53	4.56	5.00	3.96	3.46	2.90	3.02	3.83	3.78
	Tetraspherical	3.49	4.52	5.00	3.96	3.46	2.90	3.02	3.82	3.77
	Pentasherical	3.48	4.54	5.00	3.96	3.46	2.90	3.02	3.93	3.79
	Exponential	3.52	4.49	5.00	3.96	3.46	2.90	3.02	3.93	3.79
	Gaussian	3.67	4.56	5.00	3.96	3.46	2.90	3.02	3.82	3.80
	Rational Quadratic	3.53	4.56	5.00	3.96	3.46	2.90	3.02	3.94	3.80
	Hole Effect	3.34	4.47	5.00	3.96	3.46	2.90	3.02	3.10	3.66
	K-Bessel	3.53	4.41	5.00	3.96	3.46	2.90	3.02	3.68	3.75
	J-Bessel	3.26	4.49	5.00	3.96	3.46	2.90	3.02	3.47	3.70
	Stable	3.57	4.47	5.00	3.96	3.46	2.90	3.02	3.19	3.70
SK*	Circular	3.16	4.37	4.75	4.09	3.70	3.29	3.29	3.34	3.75
	Spherical	3.16	4.36	4.76	4.10	3.76	3.35	3.34	3.35	3.77
	Tetraspherical	3.16	4.33	4.77	4.12	3.71	3.40	3.39	3.36	3.78
	Pentaspherical	3.17	4.33	4.74	4.19	3.72	3.43	3.42	3.35	3.79
	Exponential	3.14	4.38	4.77	5.00	3.83	3.53	3.49	3.32	3.93
	Gaussian	3.03	4.27	4.74	3.96	3.51	3.15	3.15	3.46	3.66
	Rational Quadratic	3.16	4.35	4.77	4.22	3.78	3.55	3.53	3.44	3.85
	Hole Effect	3.14	4.38	4.72	4.05	3.54	3.41	3.27	3.43	3.74
	K-Bessel	3.05	4.29	4.73	3.97	3.55	3.15	3.16	3.47	3.67
	J-Bessel	2.97	4.36	4.72	4.03	3.53	3.30	3.33	3.45	3.71
	Stable	3.03	4.29	4.72	3.96	3.51	3.15	3.15	3.46	3.66
SCK*	Circular	3.06	4.28	4.44	3.66	3.20	3.15	2.88	2.94	3.45
	Spherical	3.07	4.29	4.45	3.68	3.18	3.15	2.87	2.93	3.45
	Tetraspherical	3.12	4.27	4.45	3.73	3.17	3.14	2.86	2.94	3.46
	Pentaspherical	3.09	4.27	4.45	3.74	3.16	3.14	2.87	2.95	3.46
	Exponential	3.18	4.36	4.47	5.57	3.14	3.15	2.88	2.97	3.72
	Gaussian	3.08	4.29	4.44	3.67	3.22	3.08	2.90	2.95	3.45
	Rational Quadratic	3.16	4.34	4.52	3.75	3.25	3.12	2.88	2.92	3.49
	Hole Effect	2.82	4.32	4.44	3.88	3.22	3.16	2.95	2.96	3.47
	K-Bessel	3.08	4.29	4.44	3.67	3.22	3.11	2.90	2.96	3.46
	J-Bessel	3.03	4.29	4.43	3.65	3.20	3.10	2.87	2.91	3.44
	Stable	3.06	4.28	4.44	3.67	3.22	3.08	2.90	2.96	3.45

Note: * This model calculated new values for the parameters with optimized semivariogram

As a result (Table 4.7), an average RMSE value of monthly mean relative humidity interpolation using seven different methods with various functions varies from 3.43 % using the SCK method with the J-Bessel function to 7.28% using the RBF method with the Thin Plate Spline and 1 Sector function. So, the SCK method with the J-Bessel function is selected as an optimum method for monthly mean relative humidity interpolation since it provides the least RMSE value.

4.2.2 Temperature

The statistical data of temperature from 37 stations between October 2019 to May 2020 for identifying the optimum interpolation method are summarized in Table 4.8. Details of temperature measurement stations in geographic coordinates are reported in Table 2 in Appendix.

Table 4.8 Descriptive statistical data of the temperature.

Month	Season	Min. (Celsius)	Max. (Celsius)	Mean (Celsius)	SD. (Celsius)	Stations
Oct	Winter	26.26	30.95	28.81	0.87	37
Nov	Winter	25.04	30.35	27.77	1.06	37
Dec	Winter	23.58	29.2	26.16	1.24	37
Jan	Winter	25.95	30.41	28.07	0.95	37
Feb	Winter	26.22	30.23	28.3	0.85	37
Mar	Summer	28.37	31.94	30.1	0.81	37
Apr	Summer	28.23	32.92	30.44	1.04	37
May	Summer	28.47	32.91	30.88	0.96	37

According to the basic statistical data, the monthly mean temperature is high in October and gradually decreases to the lowest in December, then to the highest in May. The maximum value of monthly temperature is 32.92 Celsius in April. In contrast, the minimum value of monthly temperature is 23.58 Celsius in December. In addition, the mean temperature in the summer season is obviously higher than in the winter.

In the cokriging (OCK and SCK) method, the latitude and longitude variables were added to be the cokriging variable. The relationship between monthly mean temperature and cokriging variables is summarized in Table 4.9.

Table 4.9 The Pearson's correlation coefficients between monthly mean temperature with cokriging variables.

Variables		Oct	Nov	Dec	Jan	Feb	Mar	Apr	May
TEMP	LAT	-0.01	-0.33*	-0.52**	-0.25	-0.03	0.64**	0.68**	0.42*
	LONG	-0.34*	-0.05	0.08	-0.04	-0.17	-0.31	-0.50**	-0.47**

Note: *correlation is significant at the 0.05 level (2-tailed), **correlation is significant at the 0.01 level (2-tailed).

The relationship between the monthly mean temperature and latitude variable is relatively weak from October to February but moderate to strong in March, April, and May. Also, the correlation between temperature and longitude variable is weak from November to February. There is a statistically significant between temperature and latitude variables in November, December, March, April, and May. At the same time, a statistically significant between temperature and longitude variable occurs in October, April, and May.

The cross-validation RMSE for monthly mean temperature interpolation with seven different methods (IDW, GPI, RBF, OK, OCK, SK, and SCK) is summarized in Table 4.10.

Table 4.10 The cross-validation RMSE of the seven interpolation methods for mean temperature from October 2019 to May 2020.

Model	Function		RMSE (Celsius)								
			Oct	Nov	Dec	Jan	Feb	Mar	Apr	May	Avg.
IDW	Power 1	1 sector	0.81	0.96	1.03	0.87	0.82	0.71	0.78	0.82	0.85
		4 sectors	0.80	0.97	1.06	0.87	0.80	0.70	0.79	0.79	0.85
		4 sectors with 45-degree offset	0.81	0.97	1.06	0.88	0.81	0.72	0.82	0.82	0.86
		8 sectors	0.81	0.98	1.07	0.88	0.81	0.72	0.84	0.82	0.87
	Power 2	1 sector	0.84	0.99	1.06	0.90	0.84	0.75	0.79	0.84	0.88
		4 sectors	0.83	0.99	1.06	0.89	0.82	0.74	0.79	0.82	0.87
		4 sectors with 45-degree offset	0.83	0.98	1.05	0.89	0.82	0.74	0.80	0.83	0.87
		8 sectors	0.84	0.99	1.06	0.89	0.82	0.74	0.80	0.83	0.87

Table 4.10 (Continued).

Model	Function		RMSE (Celsius)								
			Oct	Nov	Dec	Jan	Feb	Mar	Apr	May	Avg.
GPI	Order 1		0.88	1.07	1.13	0.99	0.91	0.67	0.78	0.89	0.92
	Order 2		0.91	1.03	1.07	0.93	0.86	0.74	0.83	1.00	0.92
	Order 3		1.12	1.85	1.95	1.65	1.56	0.78	0.88	1.03	1.35
RBF	Completely Regularize spine	1 sector	0.81	0.94	0.98	0.85	0.81	0.74	0.79	0.83	0.84
		4 sectors	0.79	0.93	0.98	0.83	0.79	0.72	0.78	0.80	0.83
		4 sectors with 45-degree offset	0.79	0.93	0.98	0.83	0.79	0.73	0.80	0.81	0.83
		8 sectors	0.79	0.93	0.97	0.83	0.79	0.73	0.80	0.81	0.83
	Spline with tension	1 sector	0.80	0.94	0.99	0.84	0.81	0.76	0.81	0.82	0.85
		4 sectors	0.78	0.92	0.98	0.83	0.78	0.72	0.79	0.80	0.83
		4 sectors with 45-degree offset	0.79	0.93	0.98	0.83	0.79	0.73	0.80	0.81	0.83
		8 sectors	0.79	0.92	0.97	0.83	0.78	0.73	0.80	0.81	0.83
	multiquadric	1 sector	0.96	1.08	1.12	1.00	0.94	0.88	0.88	0.97	0.98
		4 sectors	0.96	1.07	1.10	0.98	0.92	0.86	0.87	0.96	0.97
		4 sectors with 45-degree offset	0.95	1.08	1.11	0.98	0.92	0.86	0.87	0.96	0.97
		8 sectors	0.95	1.08	1.11	0.98	0.92	0.86	0.87	0.96	0.97
	Inverse multiquadric	1 sector	0.79	0.95	1.00	0.85	0.81	0.76	0.84	0.82	0.85
		4 sectors	0.78	0.95	1.02	0.84	0.79	0.71	0.82	0.80	0.84
		4 sectors with 45-degree offset	0.81	0.97	1.03	0.86	0.82	0.73	0.86	0.84	0.87
		8 sectors	0.81	0.96	1.04	0.85	0.79	0.74	0.86	0.83	0.86
	Thin plate spine	1 sector	1.53	1.77	1.87	1.70	1.51	1.48	1.36	1.56	1.60
		4 sectors	1.23	1.47	1.55	1.35	1.23	1.23	1.14	1.30	1.31
		4 sectors with 45-degree offset	1.28	1.51	1.59	1.39	1.25	1.27	1.17	1.36	1.35
		8 sectors	1.26	1.52	1.60	1.39	1.26	1.26	1.17	1.35	1.35

Table 4.10 (Continued).

Model	Function	RMSE (Celsius)								
		Oct	Nov	Dec	Jan	Feb	Mar	Apr	May	Avg.
OK*	Circular	0.86	0.95	1.02	0.87	0.84	0.73	0.81	0.94	0.88
	Spherical	0.91	0.97	1.03	0.88	0.84	0.75	0.83	0.93	0.89
	Tetraspherical	0.91	0.95	1.02	0.87	0.85	0.75	0.85	0.93	0.89
	Pentasherical	0.93	0.97	1.01	0.89	0.84	0.75	0.78	0.94	0.89
	Exponential	0.85	0.96	1.02	0.87	0.82	0.72	0.83	0.99	0.88
	Gaussian	0.92	0.94	1.02	0.86	0.82	0.73	0.78	0.92	0.87
	Rational Quadratic	0.87	0.95	1.00	0.88	0.86	0.77	0.83	0.97	0.89
	Hole Effect	0.93	0.99	1.03	0.89	0.82	0.82	0.82	0.98	0.91
	K-Bessel	0.91	0.95	1.01	0.86	0.81	0.75	0.82	0.94	0.88
	J-Bessel	0.88	0.99	1.04	0.89	0.86	0.75	0.82	0.97	0.90
	Stable	0.85	0.96	1.01	0.87	0.81	0.73	0.81	0.96	0.88
OCK*	Circular	0.83	0.94	1.00	0.87	0.82	0.71	0.75	0.87	0.85
	Spherical	0.80	0.93	1.01	0.87	0.82	0.71	0.71	0.83	0.84
	Tetraspherical	0.81	0.93	1.00	0.86	0.82	0.70	0.70	0.82	0.83
	Pentasherical	0.80	0.94	1.00	0.88	0.81	0.69	0.73	0.82	0.83
	Exponential	0.78	0.92	1.00	0.86	0.80	0.69	0.75	0.85	0.83
	Gaussian	0.89	0.94	1.01	0.86	0.83	0.72	0.77	0.86	0.86
	Rational Quadratic	0.81	0.93	1.00	0.85	0.82	0.70	0.73	0.84	0.84
	Hole Effect	0.82	0.99	1.02	0.88	0.80	0.74	0.74	0.82	0.85
	K-Bessel	0.83	0.93	1.00	0.85	0.81	0.72	0.75	0.86	0.84
	J-Bessel	0.83	0.96	1.07	0.91	0.81	0.69	0.72	0.81	0.85
	Stable	0.84	0.94	1.00	0.86	0.81	0.72	0.77	0.86	0.85
SK*	Circular	0.78	0.93	1.01	0.84	0.77	0.73	0.79	0.83	0.84
	Spherical	0.78	0.92	1.00	0.83	0.77	0.73	0.79	0.83	0.83
	Tetraspherical	0.78	0.92	1.00	0.83	0.77	0.73	0.79	0.83	0.83
	Pentaspherical	0.78	0.92	1.01	0.83	0.78	0.73	0.79	0.84	0.84
	Exponential	0.77	0.92	1.00	0.83	0.78	0.74	0.80	0.81	0.83
	Gaussian	0.78	0.93	1.02	0.83	0.77	0.71	0.80	0.81	0.83
	Rational Quadratic	0.77	0.93	1.01	0.82	0.77	0.75	0.82	0.82	0.84
	Hole Effect	0.76	0.94	1.02	0.82	0.73	0.71	0.80	0.79	0.82
	K-Bessel	0.77	0.92	1.00	0.83	0.77	0.71	0.80	0.83	0.83
	J-Bessel	0.74	0.93	1.02	0.83	0.76	0.72	0.81	0.81	0.83
	Stable	0.77	0.92	1.01	0.83	0.77	0.71	0.80	0.83	0.83

Table 4.10 (Continued).

Model	Function	RMSE (Celsius)								
		Oct	Nov	Dec	Jan	Feb	Mar	Apr	May	Avg.
SCK*	Circular	0.78	0.94	0.99	0.86	0.81	0.62	0.70	0.78	0.81
	Spherical	0.78	0.94	0.99	0.86	0.80	0.62	0.70	0.78	0.81
	Tetraspherical	0.78	0.95	1.00	0.87	0.81	0.62	0.70	0.78	0.81
	Pentaspherical	0.78	0.95	0.99	0.87	0.81	0.62	0.70	0.78	0.81
	Exponential	0.78	0.95	1.00	0.86	0.81	0.63	0.70	0.79	0.82
	Gaussian	0.78	0.94	1.00	0.86	0.80	0.62	0.71	0.77	0.81
	Rational Quadratic	0.78	0.94	1.01	0.87	0.81	0.62	0.70	0.78	0.81
	Hole Effect	0.74	0.90	0.92	0.82	0.74	0.64	0.76	0.76	0.79
	K-Bessel	0.77	0.92	0.96	0.84	0.78	0.63	0.70	0.77	0.80
	J-Bessel	0.78	0.94	0.99	0.85	0.79	0.63	0.71	0.77	0.81
	Stable	0.78	0.95	0.95	0.85	0.78	0.63	0.71	0.77	0.80

Note: * This model calculated new values for the parameters with optimized semivariogram

As a result (Table 4.10), an average RMSE value of monthly mean temperature interpolation using seven different methods with various functions varies from 0.79 Celsius using the SCK method with the Hole Effect function to 1.60 Celsius using the RBF method with the Thin Plate Spline and 1 Sector function. Consequently, the SCK method with the Hole Effect function is selected as an optimum method for monthly mean temperature interpolation since it provides the least RMSE value.

4.2.3 Wind speed

The statistical data of wind speed from 40 stations between October 2019 to May 2020 for identifying optimum interpolation methods are summarized in Table 4.11. Details of wind speed measurement stations in geographic coordinates are reported in Table 2 in Appendix.

Table 4.11 Descriptive statistical data of the wind speed.

Month	Season	Min. (knot)	Max. (knot)	Mean (knot)	SD. (knot)	Stations
Oct	Winter	0.17	6.71	2.13	1.40	40
Nov	Winter	0.50	7.47	2.60	1.52	40
Dec	Winter	0.88	8.23	2.80	1.58	40
Jan	Winter	0.57	6.74	2.27	1.44	40
Feb	Winter	0.77	9.72	2.95	1.76	40
Mar	Summer	0.70	11.39	3.46	2.41	40
Apr	Summer	0.61	9.07	3.13	1.94	40
May	Summer	0.46	9.71	2.88	1.96	40

Referring to the basic statistical data, the minimum value of the wind speed is 0.17 knot in October. In contrast, the maximum value of the wind speed is 11.39 knots in March. The monthly mean wind speed is the lowest in October, gradually increasing to the highest in March, then dropdown until May.

In the cokriging (OCK and SCK) method, the latitude and longitude variables were added to be the cokriging variable. The relationship between monthly mean wind speed and cokriging variables is summarized in Tables 4.12.

Table 4.12 The Pearson's correlation coefficients between monthly mean wind speed with cokriging variables.

Variables		Oct	Nov	Dec	Jan	Feb	Mar	Apr	May
WS	LAT	-0.25	-0.22	-0.29	-0.28	-0.16	-0.18	-0.09	-0.16
	LONG	0.02	0.06	0.07	0.00	-0.03	-0.16	-0.15	-0.12

Note: *correlation is significant at the 0.05 level (2-tailed), **correlation is significant at the 0.01 level (2-tailed).

The relationship between monthly mean wind speed and latitude variable is a relatively weak negative correlation. Likewise, the correlation between wind speed and longitude variables is very weak. The relationship between monthly mean wind speed and cokriging variables is also statistically insignificant.

The cross-validation RMSE for monthly mean wind speed interpolation with seven different methods (IDW, GPI, RBF, OK, OCK, SK, and SCK) is summarized in Table 4.13.

Table 4.13 The cross-validation RMSE of the seven interpolation methods for mean wind speed from October 2019 to May 2020.

Model	Function		RMSE (knot)								
			Oct	Nov	Dec	Jan	Feb	Mar	Apr	May	Avg.
IDW	Power 1	1 sector	1.31	1.45	1.48	1.32	1.66	2.23	1.81	1.80	1.63
		4 sectors	1.35	1.49	1.53	1.36	1.71	2.28	1.85	1.83	1.68
		4 sectors with 45-degree offset	1.35	1.48	1.53	1.36	1.71	2.29	1.87	1.84	1.68
		8 sectors	1.35	1.48	1.52	1.37	1.71	2.31	1.87	1.85	1.68
	Power 2	1 sector	1.29	1.44	1.48	1.29	1.59	2.22	1.79	1.72	1.60
		4 sectors	1.31	1.46	1.50	1.31	1.62	2.24	1.81	1.74	1.62
		4 sectors with 45-degree offset	1.30	1.46	1.50	1.30	1.62	2.24	1.80	1.74	1.62
		8 sectors	1.30	1.46	1.50	1.31	1.62	2.25	1.81	1.74	1.62
GPI	Order 1		1.44	1.44	1.58	1.61	1.46	1.84	2.47	2.03	1.73
	Order 2		1.48	1.48	1.57	1.59	1.47	1.82	2.40	2.04	1.73
	Order 3		2.36	2.36	2.65	2.71	2.75	3.31	4.33	3.81	3.04
RBF	Completely Regularize spine	1 sector	1.26	1.38	1.42	1.26	1.57	2.17	1.75	1.70	1.56
		4 sectors	1.27	1.40	1.44	1.27	1.58	2.18	1.76	1.69	1.57
		4 sectors with 45-degree offset	1.27	1.40	1.44	1.27	1.58	2.19	1.77	1.70	1.58
		8 sectors	1.27	1.40	1.44	1.27	1.58	2.20	1.77	1.71	1.58
	Spline with tension	1 sector	1.24	1.36	1.40	1.24	1.55	2.12	1.70	1.67	1.54
		4 sectors	1.27	1.40	1.44	1.28	1.58	2.18	1.77	1.71	1.58
		4 sectors with 45-degree offset	1.27	1.39	1.43	1.27	1.58	2.19	1.77	1.71	1.58
		8 sectors	1.27	1.40	1.44	1.27	1.58	2.20	1.77	1.72	1.58
	multiquadric	1 sector	1.40	1.51	1.56	1.39	1.69	2.45	1.96	1.88	1.73
		4 sectors	1.37	1.47	1.52	1.36	1.65	2.37	1.91	1.83	1.69
		4 sectors with 45-degree offset	1.37	1.48	1.52	1.36	1.65	2.37	1.91	1.82	1.69
		8 sectors	1.38	1.48	1.52	1.36	1.65	2.37	1.91	1.83	1.69

Table 4.13 (Continued).

Model	Function		RMSE (knot)								
			Oct	Nov	Dec	Jan	Feb	Mar	Apr	May	Avg.
RBF	Inverse multiquadric	1 sector	1.25	1.38	1.41	1.25	1.56	2.10	1.70	1.68	1.54
		4 sectors	1.35	1.50	1.52	1.35	1.68	2.28	1.87	1.78	1.67
		4 sectors with 45-degree offset	1.33	1.47	1.50	1.33	1.66	2.27	1.86	1.77	1.65
		8 sectors	1.34	1.48	1.52	1.35	1.67	2.30	1.88	1.78	1.67
	Thin plate spine	1 sector	1.89	2.11	2.12	1.82	2.09	3.16	2.64	2.36	2.27
		4 sectors	1.85	2.07	2.07	1.75	2.03	2.99	2.44	2.26	2.18
		4 sectors with 45-degree offset	1.87	2.12	2.09	1.78	2.05	2.96	2.44	2.25	2.20
		8 sectors	1.88	2.11	2.08	1.79	2.08	3.02	2.48	2.30	2.22
OK*	Circular		1.49	1.56	1.59	1.51	1.85	2.43	2.04	2.07	1.82
	Spherical		1.49	1.56	1.59	1.51	1.85	2.43	2.04	2.07	1.82
	Tetraspherical		1.49	1.56	1.59	1.51	1.85	2.43	2.04	1.90	1.80
	Pentasherical		1.49	1.56	1.59	1.51	1.85	2.43	2.04	1.89	1.80
	Exponential		1.45	1.56	1.50	1.51	1.68	2.43	1.84	1.81	1.72
	Gaussian		1.49	1.56	1.59	1.51	1.85	2.43	2.04	2.07	1.82
	Rational Quadratic		1.41	1.51	1.55	1.44	1.73	2.43	1.88	1.90	1.73
	Hole Effect		1.49	1.56	1.59	1.51	1.85	2.43	2.04	2.07	1.82
	K-Bessel		1.45	1.46	1.49	1.51	1.85	2.43	1.78	1.82	1.72
	J-Bessel		1.49	1.56	1.59	1.51	1.85	2.43	2.04	1.90	1.80
	Stable		1.43	1.42	1.47	1.32	1.67	2.43	1.82	1.84	1.68
OCK*	Circular		1.49	1.56	1.59	1.51	1.85	2.43	2.04	2.07	1.82
	Spherical		1.49	1.56	1.59	1.51	1.85	2.43	2.04	2.07	1.82
	Tetraspherical		1.49	1.56	1.59	1.51	1.85	2.43	2.04	2.07	1.82
	Pentasherical		1.49	1.56	1.59	1.51	1.85	2.43	2.04	2.07	1.82
	Exponential		1.49	1.44	1.59	1.51	1.85	2.43	2.04	2.07	1.80
	Gaussian		1.49	1.56	1.59	1.51	1.85	2.43	2.04	2.07	1.82
	Rational Quadratic		1.49	1.53	1.60	1.51	1.85	2.43	2.00	2.08	1.81
	Hole Effect		1.49	1.56	1.59	1.51	1.85	2.43	2.04	2.07	1.82
	K-Bessel		1.34	1.44	1.47	1.30	1.66	2.43	1.79	1.78	1.65
	J-Bessel		1.49	1.56	1.59	1.51	1.85	2.17	2.04	1.79	1.75
	Stable		1.39	1.40	1.56	1.30	1.64	2.21	1.77	1.79	1.63

Table 4.13 (Continued).

Model	Function	RMSE (knot)								
		Oct	Nov	Dec	Jan	Feb	Mar	Apr	May	Avg.
SK*	Circular	1.33	1.40	1.47	1.30	1.72	2.36	1.74	1.81	1.64
	Spherical	1.34	1.42	1.49	1.31	1.76	2.36	1.76	1.85	1.66
	Tetraspherical	1.35	1.42	1.56	1.33	1.73	2.36	1.77	1.86	1.67
	Pentaspherical	1.36	1.43	1.56	1.34	1.73	2.37	1.79	1.85	1.68
	Exponential	1.32	1.40	1.54	1.30	1.68	2.30	1.75	1.74	1.63
	Gaussian	1.34	1.41	1.48	1.31	1.72	2.31	1.76	1.77	1.64
	Rational Quadratic	1.36	1.44	1.55	1.34	1.69	2.31	1.78	1.78	1.66
	Hole Effect	1.39	1.49	1.55	1.40	1.76	2.39	1.89	1.91	1.72
	K-Bessel	1.28	1.38	1.47	1.27	1.63	2.23	1.74	1.70	1.59
	J-Bessel	1.36	1.46	1.55	1.42	1.74	2.38	1.91	1.95	1.72
	Stable	1.27	1.38	1.49	1.27	1.60	2.22	1.73	1.68	1.58
SCK*	Circular	1.34	1.43	1.49	1.37	1.73	2.28	1.81	1.75	1.65
	Spherical	1.35	1.44	1.49	1.35	1.75	2.27	1.81	1.80	1.66
	Tetraspherical	1.35	1.44	1.49	1.35	1.71	2.28	1.82	1.79	1.65
	Pentaspherical	1.35	1.45	1.49	1.37	1.71	2.29	1.83	1.83	1.67
	Exponential	1.34	1.44	1.47	1.35	1.64	2.22	1.79	1.70	1.62
	Gaussian	1.35	1.44	1.51	1.35	1.68	2.28	1.88	1.77	1.66
	Rational Quadratic	1.33	1.46	1.49	1.31	1.64	2.22	1.80	1.72	1.62
	Hole Effect	1.31	1.42	1.48	1.29	1.76	2.41	1.76	1.80	1.65
	K-Bessel	1.24	1.42	1.46	1.29	1.61	2.15	1.73	1.69	1.57
	J-Bessel	1.32	1.48	1.51	1.34	1.74	2.28	1.89	1.82	1.67
	Stable	1.24	1.43	1.46	1.24	1.59	2.12	1.73	1.66	1.56

Note: * This model calculated new values for the parameters with optimized semivariogram

As a result (Table 4.13), an average RMSE value of monthly mean wind speed interpolation using seven different methods with various functions varies from 1.54 knots using the RBF method with the Spline with Tension and 1 Sector to 3.30 knots using the GPI method with the Order 3 function. Therefore, the RBF method with the Spline with Tension and One Sector is chosen as an optimum method for monthly mean wind speed interpolation since it provides the least RMSE value.

4.2.4 Pressure

The statistical data of pressure from 40 stations from TMD between October 2019 to May 2020 for identifying the optimum interpolation method are summarized in Table 4.14. Details of pressure measurement stations in geographic coordinates are reported in Table 2 in Appendix.

Table 4.14 Descriptive statistical data of the pressure.

Month	Season	Min. (hPa)	Max. (hPa)	Mean (hPa)	SD. (hPa)	Stations
Oct	Winter	1009.81	1011.91	1010.39	0.47	40
Nov	Winter	1010.19	1012.80	1011.29	0.60	40
Dec	Winter	1012.01	1014.81	1013.29	0.67	40
Jan	Winter	1011.46	1013.48	1011.99	0.40	40
Feb	Winter	1012.40	1014.62	1012.91	0.38	40
Mar	Summer	1008.91	1011.81	1010.00	0.59	40
Apr	Summer	1009.34	1012.03	1010.21	0.44	40
May	Summer	1006.89	1009.62	1007.84	0.51	40

According to the basic statistical data, the minimum value of the pressure is 1,006.89 hectopascal in May. In contrast, the maximum value of the pressure is 1,014.81 hectopascal in December. Furthermore, mean pressure in winter and summer seasons is insignificantly different.

In the cokriging (OCK and SCK) method, the latitude and longitude variables were added to be the cokriging variable. The relationship between monthly mean pressure and cokriging variables is summarized in Table 4.15.

Table 4.15 The Pearson's correlation coefficients between monthly mean pressure with cokriging variables.

Variables		Oct	Nov	Dec	Jan	Feb	Mar	Apr	May
P	LAT	0.47**	0.71**	0.75**	0.19	0.14	-0.71**	-0.53**	-0.61**
	LONG	-0.02	-0.15	-0.11	-0.10	0.17	0.19	0.30	0.22

Note: *correlation is significant at the 0.05 level (2-tailed), **correlation is significant at the 0.01 level (2-tailed).

The relationship between monthly mean pressure and latitude variable is a moderate to strong correlation with a statistically significant ($p \leq 0.01$), except for the association in January and February, which is very weak. Besides, the relationship between pressure and longitude variable is a pretty weak correlation. Furthermore, the relationship between monthly mean pressure and cokriging variables (latitude and longitude) is statistically insignificant.

The cross-validation RMSE for monthly mean pressure interpolation with seven different methods (IDW, GPI, RBF, OK, OCK, SK, and SCK) is summarized in Table 4.16.

Table 4.16 The cross-validation RMSE of the seven interpolation methods for mean pressure from October 2019 to May 2020.

Model	Function		RMSE (hPa)								
			Oct	Nov	Dec	Jan	Feb	Mar	Apr	May	Avg.
IDW	Power 1	1 sector	0.45	0.48	0.50	0.42	0.42	0.47	0.42	0.45	0.45
		4 sectors	0.45	0.49	0.52	0.41	0.40	0.48	0.41	0.44	0.45
		4 sectors with 45-degree offset	0.44	0.48	0.51	0.41	0.40	0.49	0.41	0.45	0.45
		8 sectors	0.44	0.50	0.54	0.41	0.40	0.50	0.41	0.46	0.46
	Power 2	1 sector	0.46	0.48	0.49	0.44	0.43	0.49	0.43	0.47	0.46
		4 sectors	0.46	0.48	0.49	0.43	0.42	0.49	0.43	0.46	0.46
		4 sectors with 45-degree offset	0.45	0.47	0.49	0.43	0.41	0.50	0.43	0.47	0.46
		8 sectors	0.45	0.48	0.49	0.43	0.41	0.50	0.43	0.47	0.46
GPI	Order 1		0.43	0.43	0.44	0.46	0.41	0.39	0.45	0.39	0.43
	Order 2		0.45	0.45	0.45	0.45	0.44	0.41	0.52	0.44	0.45
	Order 3		0.52	0.52	0.52	0.52	0.47	0.46	0.59	0.48	0.51
RBF	Completely Regularize spine	1 sector	0.46	0.49	0.51	0.44	0.43	0.49	0.43	0.46	0.46
		4 sectors	0.46	0.49	0.51	0.43	0.42	0.48	0.42	0.46	0.46
		4 sectors with 45-degree offset	0.45	0.49	0.51	0.43	0.41	0.49	0.42	0.46	0.46
		8 sectors	0.45	0.49	0.51	0.43	0.41	0.49	0.42	0.46	0.46

Table 4.16 (Continued).

Model	Function		RMSE (hPa)								
			Oct	Nov	Dec	Jan	Feb	Mar	Apr	May	Avg.
RBF	Spline with tension	1 sector	0.48	0.51	0.53	0.46	0.44	0.50	0.43	0.47	0.48
		4 sectors	0.46	0.49	0.51	0.43	0.42	0.48	0.42	0.45	0.46
		4 sectors with 45-degree offset	0.45	0.48	0.50	0.42	0.41	0.49	0.42	0.46	0.45
		8 sectors	0.45	0.49	0.51	0.42	0.41	0.49	0.42	0.46	0.46
	multiquadric	1 sector	0.52	0.52	0.53	0.51	0.47	0.57	0.49	0.53	0.52
		4 sectors	0.53	0.54	0.55	0.52	0.48	0.57	0.49	0.53	0.53
		4 sectors with 45-degree offset	0.54	0.55	0.56	0.52	0.48	0.58	0.49	0.54	0.53
		8 sectors	0.53	0.54	0.56	0.52	0.48	0.57	0.49	0.54	0.53
	Inverse multiquadric	1 sector	0.48	0.52	0.54	0.45	0.44	0.50	0.44	0.47	0.48
		4 sectors	0.45	0.50	0.53	0.41	0.40	0.49	0.40	0.44	0.45
		4 sectors with 45-degree offset	0.44	0.49	0.51	0.40	0.39	0.50	0.41	0.46	0.45
		8 sectors	0.44	0.50	0.52	0.40	0.39	0.51	0.41	0.46	0.45
	Thin plate spine	1 sector	0.63	0.61	0.63	0.63	0.57	0.76	0.61	0.68	0.64
		4 sectors	0.63	0.63	0.64	0.64	0.57	0.73	0.61	0.66	0.64
		4 sectors with 45-degree offset	0.64	0.63	0.65	0.65	0.59	0.77	0.64	0.68	0.66
		8 sectors	0.64	0.63	0.65	0.65	0.58	0.75	0.63	0.66	0.65
OK*	Circular		0.45	0.45	0.46	0.44	0.42	0.53	0.45	0.49	0.46
	Spherical		0.45	0.45	0.46	0.44	0.42	0.53	0.45	0.49	0.46
	Tetraspherical		0.45	0.45	0.46	0.44	0.42	0.53	0.45	0.49	0.46
	Pentasherical		0.45	0.45	0.46	0.44	0.42	0.53	0.45	0.49	0.46
	Exponential		0.45	0.45	0.46	0.44	0.42	0.53	0.45	0.49	0.46
	Gaussian		0.45	0.45	0.46	0.44	0.42	0.53	0.45	0.49	0.46
	Rational Quadratic		0.46	0.45	0.46	0.44	0.42	0.53	0.45	0.49	0.46
	Hole Effect		0.46	0.45	0.46	0.44	0.42	0.53	0.45	0.49	0.46
	K-Bessel		0.45	0.45	0.46	0.44	0.42	0.53	0.45	0.49	0.46
	J-Bessel		0.46	0.45	0.46	0.44	0.42	0.53	0.46	0.49	0.46
	Stable		0.45	0.45	0.46	0.44	0.42	0.53	0.45	0.49	0.46

Table 4.16 (Continued).

Model	Function	RMSE (hPa)								
		Oct	Nov	Dec	Jan	Feb	Mar	Apr	May	Avg.
OCK*	Circular	0.45	0.45	0.46	0.44	0.42	0.49	0.43	0.49	0.45
	Spherical	0.45	0.45	0.46	0.44	0.42	0.49	0.45	0.45	0.45
	Tetraspherical	0.45	0.45	0.46	0.44	0.42	0.50	0.45	0.46	0.45
	Pentasherical	0.45	0.45	0.46	0.44	0.42	0.50	0.44	0.49	0.46
	Exponential	0.45	0.45	0.46	0.44	0.42	0.51	0.45	0.46	0.46
	Gaussian	0.45	0.45	0.46	0.44	0.42	0.50	0.43	0.45	0.45
	Rational Quadratic	0.46	0.45	0.46	0.44	0.42	0.50	0.45	0.46	0.46
	Hole Effect	0.46	0.45	0.46	0.44	0.42	0.50	0.45	0.49	0.46
	K-Bessel	0.45	0.45	0.46	0.44	0.42	0.49	0.44	0.47	0.45
	J-Bessel	0.46	0.45	0.46	0.44	0.42	0.51	0.44	0.46	0.46
	Stable	0.45	0.45	0.46	0.44	0.42	0.50	0.45	0.46	0.45
SK*	Circular	0.45	0.49	0.51	0.40	0.38	0.49	0.42	0.46	0.45
	Spherical	0.45	0.50	0.52	0.40	0.38	0.50	0.42	0.47	0.46
	Tetraspherical	0.45	0.50	0.60	0.40	0.38	0.50	0.42	0.47	0.47
	Pentaspherical	0.45	0.55	0.59	0.40	0.38	0.51	0.42	0.47	0.47
	Exponential	0.44	0.53	0.55	0.40	0.38	0.53	0.43	0.49	0.47
	Gaussian	0.45	0.46	0.48	0.40	0.38	0.47	0.41	0.45	0.44
	Rational Quadratic	0.45	0.55	0.57	0.40	0.38	0.52	0.44	0.49	0.48
	Hole Effect	0.45	0.48	0.49	0.40	0.38	0.48	0.44	0.46	0.45
	K-Bessel	0.44	0.52	0.55	0.40	0.38	0.47	0.44	0.48	0.46
	J-Bessel	0.45	0.49	0.51	0.40	0.38	0.48	0.44	0.46	0.45
	Stable	0.45	0.60	0.54	0.40	0.38	0.47	0.43	0.49	0.47
SCK*	Circular	0.41	0.42	0.44	0.38	0.37	0.42	0.37	0.40	0.40
	Spherical	0.41	0.43	0.44	0.38	0.37	0.42	0.37	0.40	0.40
	Tetraspherical	0.41	0.43	0.44	0.38	0.37	0.44	0.37	0.40	0.41
	Pentaspherical	0.41	0.44	0.45	0.38	0.37	0.45	0.37	0.40	0.41
	Exponential	0.42	0.46	0.50	0.38	0.37	0.46	0.39	0.43	0.43
	Gaussian	0.41	0.42	0.44	0.38	0.37	0.42	0.38	0.44	0.41
	Rational Quadratic	0.43	0.42	0.43	0.38	0.37	0.42	0.39	0.40	0.41
	Hole Effect	0.41	0.43	0.46	0.38	0.37	0.44	0.37	0.41	0.41
	K-Bessel	0.41	0.43	0.44	0.38	0.37	0.42	0.37	0.45	0.41
	J-Bessel	0.41	0.43	0.43	0.38	0.37	0.42	0.37	0.40	0.40
	Stable	0.41	0.42	0.44	0.38	0.37	0.42	0.37	0.40	0.40

Note: * This model calculated new values for the parameters with optimized semivariogram

As a result (Table 4.16), an average RMSE value of monthly mean pressure interpolation using seven different methods with various functions varies from 0.40 hPa using the SCK method with the Stable function to 0.66 hPa using the RBF method with the Thin Plate Spline and the Four Sectors with 45-degree offset function. Subsequently, the SCK method with the Stable function is selected as an optimum method for monthly mean pressure interpolation since it provides the least RMSE value.

4.2.5 Visibility

The statistical data of visibility from 41 stations from TMD between October 2019 to May 2020 for identifying the optimum interpolation method are summarized in Table 4.17. Details of visibility measurement stations in geographic coordinates are reported in Table 2 in Appendix.

Table 4.17 Descriptive statistical data of the visibility.

Month	Season	Min. (km)	Max. (km)	Mean (km)	SD. (km)	Stations
Oct	Winter	6.00	10.80	8.66	1.03	41
Nov	Winter	3.40	10.60	8.34	1.38	41
Dec	Winter	2.60	10.30	8.03	1.45	41
Jan	Winter	2.10	10.40	7.27	1.47	41
Feb	Winter	2.60	11.20	7.48	1.70	41
Mar	Summer	2.90	10.80	8.00	1.67	41
Apr	Summer	3.40	10.80	8.36	1.54	41
May	Summer	4.70	11.50	8.95	1.46	41

According to the basic statistical data, the minimum value is 2.10 km in January, and the maximum value is 11.5 km in May. Thus, the monthly mean visibility decreases from October until a minimum in January and gradually increases until a maximum in May.

In the cokriging (OCK and SCK) method, the latitude and longitude variables were added to be the cokriging variable. The relationship between monthly mean visibility and cokriging variables is summarized in Table 4.18.

Table 4.18 The Pearson's correlation coefficients between monthly mean pressure with cokriging variables.

Variables		Oct	Nov	Dec	Jan	Feb	Mar	Apr	May
VIS	LAT	-0.23	-0.06	-0.15	-0.26	-0.29	-0.40*	-0.34*	-0.17
	LONG	-0.15	0.03	0.08	0.15	-0.07	-0.01	-0.05	-0.35*

Note: *correlation is significant at the 0.05 level (2-tailed), **correlation is significant at the 0.01 level (2-tailed).

The relationship between monthly mean visibility and latitude variable is a relatively weak negative correlation. However, there is a negative correlation with statistically significant ($p \leq 0.05$) in March and April. The correlation between visibility and longitude variable is very weak, too. But there is a negative correlation with statistically significant ($p \leq 0.05$) only in May.

The cross-validation RMSE for monthly mean visibility interpolation with seven different methods (IDW, GPI, RBF, OK, OCK, SK, and SCK) is summarized in Table 4.19.

Table 4.19 The cross-validation RMSE of the seven interpolation methods for mean visibility interpolation from October 2019 to May 2020.

Model	Function		RMSE (km)								
			Oct	Nov	Dec	Jan	Feb	Mar	Apr	May	Avg.
IDW	Power 1	1 sector	1.02	1.46	1.49	1.48	1.63	1.55	1.41	1.34	1.42
		4 sectors	1.00	1.41	1.46	1.46	1.64	1.54	1.41	1.35	1.41
		4 sectors with 45-degree offset	0.99	1.41	1.43	1.45	1.64	1.54	1.40	1.34	1.40
		8 sectors	1.01	1.42	1.46	1.47	1.66	1.58	1.44	1.37	1.43
	Power 2	1 sector	1.08	1.53	1.51	1.51	1.65	1.56	1.40	1.38	1.45
		4 sectors	1.06	1.50	1.49	1.50	1.65	1.55	1.39	1.36	1.44
		4 sectors with 45-degree offset	1.06	1.49	1.47	1.49	1.65	1.55	1.39	1.36	1.43
		8 sectors	1.06	1.50	1.49	1.50	1.66	1.57	1.41	1.36	1.44
GPI	Order 1		1.05	1.47	1.54	1.52	1.76	1.68	1.61	1.42	1.51
	Order 2		1.01	1.49	1.50	1.48	1.84	1.54	1.35	1.28	1.44
	Order 3		1.00	1.57	1.72	1.65	1.61	1.43	1.24	1.43	1.46

Table 4.19 (Continued).

Model	Function		RMSE (km)								
			Oct	Nov	Dec	Jan	Feb	Mar	Apr	May	Avg.
RBF	Completely Regularize spine	1 sector	1.03	1.48	1.48	1.48	1.61	1.52	1.38	1.33	1.41
		4 sectors	1.03	1.47	1.47	1.48	1.62	1.52	1.39	1.34	1.42
		4 sectors with 45-degree offset	1.02	1.46	1.45	1.47	1.62	1.52	1.38	1.33	1.41
		8 sectors	1.03	1.47	1.47	1.49	1.63	1.54	1.39	1.33	1.42
RBF	Spline with tension	1 sector	1.05	1.50	1.52	1.52	1.65	1.57	1.38	1.36	1.44
		4 sectors	1.02	1.46	1.46	1.48	1.61	1.53	1.39	1.33	1.41
		4 sectors with 45-degree offset	1.01	1.45	1.45	1.46	1.61	1.51	1.39	1.31	1.40
		8 sectors	1.02	1.46	1.47	1.48	1.63	1.54	1.39	1.33	1.42
	multiquadric	1 sector	1.23	1.73	1.62	1.63	1.72	1.54	1.40	1.51	1.55
		4 sectors	1.21	1.71	1.58	1.60	1.69	1.53	1.41	1.52	1.53
		4 sectors with 45-degree offset	1.22	1.71	1.59	1.60	1.69	1.55	1.43	1.53	1.54
		8 sectors	1.22	1.70	1.58	1.60	1.69	1.53	1.41	1.52	1.53
	Inverse multiquadric	1 sector	1.03	1.48	1.52	1.52	1.67	1.60	1.41	1.36	1.45
		4 sectors	0.99	1.40	1.44	1.46	1.64	1.56	1.39	1.32	1.40
		4 sectors with 45-degree offset	0.98	1.39	1.42	1.44	1.64	1.53	1.36	1.30	1.38
		8 sectors	1.00	1.39	1.44	1.47	1.66	1.58	1.39	1.32	1.41
	Thin plate spine	1 sector	1.73	2.40	2.18	2.19	2.21	1.78	1.43	1.86	1.97
		4 sectors	1.60	2.19	1.98	1.94	1.97	1.66	1.49	1.82	1.83
		4 sectors with 45-degree offset	1.57	2.09	1.89	1.89	1.94	1.66	1.52	1.89	1.81
		8 sectors	1.56	2.08	1.88	1.86	1.89	1.62	1.47	1.83	1.77
OK*	Circular		1.03	1.51	1.49	1.54	1.67	1.50	1.37	1.30	1.43
	Spherical		1.03	1.51	1.55	1.54	1.66	1.52	1.33	1.30	1.43
	Tetraspherical		1.03	1.51	1.55	1.54	1.63	1.52	1.33	1.30	1.43
	Pentasherical		1.03	1.51	1.48	1.54	1.66	1.52	1.35	1.30	1.42
	Exponential		1.03	1.51	1.49	1.54	1.65	1.52	1.35	1.30	1.42
	Gaussian		1.03	1.51	1.55	1.54	1.67	1.50	1.35	1.30	1.43
	Rational Quadratic		1.03	1.51	1.48	1.54	1.72	1.52	1.34	1.30	1.43
	Hole Effect		1.03	1.73	1.47	1.62	1.70	1.42	1.35	1.32	1.46
	K-Bessel		1.03	1.51	1.55	1.54	1.65	1.52	1.35	1.30	1.43
	J-Bessel		1.03	1.51	1.45	1.54	1.69	1.43	1.35	1.33	1.42
	Stable		1.03	1.51	1.55	1.54	1.64	1.50	1.35	1.30	1.43

Table 4.19 (Continued).

Model	Function	RMSE (km)								
		Oct	Nov	Dec	Jan	Feb	Mar	Apr	May	Avg.
OCK*	Circular	1.03	1.51	1.55	1.54	1.74	1.52	1.35	1.30	1.44
	Spherical	1.03	1.51	1.55	1.54	1.57	1.52	1.35	1.30	1.42
	Tetraspherical	1.03	1.51	1.55	1.54	1.54	1.52	1.25	1.30	1.41
	Pentasherical	1.03	1.51	1.55	1.54	1.74	1.43	1.25	1.30	1.42
	Exponential	1.03	1.51	1.55	1.54	1.50	1.52	1.22	1.30	1.40
	Gaussian	1.03	1.51	1.55	1.54	1.49	1.52	1.35	1.30	1.41
	Rational Quadratic	1.03	1.51	1.55	1.54	1.50	1.52	1.35	1.27	1.41
	Hole Effect	0.98	1.51	1.45	1.48	1.45	1.27	1.11	1.30	1.32
	K-Bessel	1.03	1.51	1.55	1.54	1.48	1.52	1.20	1.30	1.39
	J-Bessel	1.03	1.51	1.45	1.54	1.48	1.28	1.31	1.30	1.36
	Stable	0.90	1.51	1.47	1.54	1.47	1.52	1.19	1.30	1.36
SK*	Circular	1.01	1.37	1.42	1.45	1.60	1.53	1.38	1.33	1.39
	Spherical	1.01	1.37	1.41	1.46	1.59	1.52	1.38	1.33	1.38
	Tetraspherical	1.01	1.37	1.40	1.46	1.60	1.53	1.38	1.33	1.39
	Pentaspherical	1.01	1.41	1.40	1.45	1.59	1.53	1.38	1.34	1.39
	Exponential	1.00	1.37	1.40	1.45	1.59	1.53	1.39	1.34	1.38
	Gaussian	1.01	1.37	1.40	1.47	1.61	1.51	1.38	1.33	1.39
	Rational Quadratic	1.01	1.40	1.40	1.45	1.59	1.59	1.37	1.34	1.39
	Hole Effect	1.05	1.46	1.43	1.46	1.59	1.50	1.38	1.33	1.40
	K-Bessel	0.98	1.37	1.45	1.45	1.61	1.53	1.38	1.34	1.39
	J-Bessel	1.03	1.45	1.42	1.45	1.60	1.52	1.38	1.35	1.40
	Stable	0.98	1.37	1.43	1.46	1.61	1.51	1.38	1.32	1.38
SCK*	Circular	0.96	1.37	1.44	1.42	1.57	1.49	1.40	1.27	1.37
	Spherical	0.96	1.37	1.40	1.42	1.57	1.49	1.40	1.27	1.36
	Tetraspherical	0.96	1.37	1.40	1.41	1.57	1.49	1.41	1.28	1.36
	Pentaspherical	0.96	1.42	1.39	1.41	1.58	1.49	1.41	1.28	1.37
	Exponential	0.96	1.37	1.39	1.41	1.57	1.50	1.40	1.29	1.36
	Gaussian	0.96	1.37	1.40	1.42	1.56	1.47	1.45	1.30	1.37
	Rational Quadratic	0.96	1.41	1.39	1.40	1.58	1.52	1.40	1.29	1.37
	Hole Effect	0.96	1.45	1.40	1.41	1.56	1.39	1.40	1.17	1.34
	K-Bessel	0.96	1.37	1.47	1.43	1.56	1.49	1.38	1.30	1.37
	J-Bessel	0.96	1.45	1.40	1.40	1.56	1.46	1.35	1.31	1.36
	Stable	0.96	1.37	1.43	1.42	1.56	1.47	1.45	1.30	1.37

Note: * This model calculated new values for the parameters with optimized semivariogram

As a result (Table 4.19), an average RMSE value of monthly mean visibility interpolation using seven different methods with various functions varies from 1.32 km using the OCK method with the Hole Effect function to 1.97 km using the RBF method with the Thin Plate Spline and the One Sector function. So, the OCK method with the Hole Effect function is selected as an optimum method for monthly mean visibility interpolation since it provides the least RMSE value. The average RMSE values from the seven interpolation methods of each monthly mean meteorological data are very similar.

In the meantime, the previous studies on an optimum interpolation method for predicting monthly mean meteorological data at international and national levels reported different methods. Prasomsup (2017) found that the SCK is the optimum method for monthly mean temperature in November, December, February, and March, while OCK is optimal in January and April. And Jantakat and Ongsomwang (2011) selected OCK for interpolated monthly mean temperature in January, November, and December, while they selected Distinctive cokriging (DCK) for February to October. At the same time, Ozturk and Kilic (2016) choose the OK for interpolated temperature and precipitation in 5-year periods. Like Cao, Hu, and Yu (2009) presented, the OK with exponential and spherical is the best interpolation precision.

Likewise, although Keskin and Özdoğu (2011) presented, OK performs better than the interpolation methods for wind speed data. In contrast, this study suggests RBF with Spline with Tension functions; the geometry of the search neighborhood is an ellipse. Follow the study of Gradka and Kwinta (2018). The RBF is conceptually like fitting a rubber membrane through the measured sample values while minimizing the surface's total curvature and selecting one function parameter to control the surface's smoothness using cross-validation. Also, the RBF represents an irregular surface using many linear functions that connect the node with the data point and can be alternative to kriging.

Equally, the other technique can be used to interpolate meteorological data. Still, the most commonly used technique is the kriging technique and additions of the cross-correlated variables to reduce the estimation error variance (Yalçin, 2005). However, Kuo, Huang, and Putra (2021) suggested kriging method was used to interpolate the temperature data but must focus on the optimal sample size of sensors. In addition, Deligiorgi and Philippopoulos (2011) reported that the most common kriging is simple kriging, which assumes a known constant mean, while ordinary kriging takes an unknown constant mean. As well, kriging is also known as the best linear unbiased estimator.

The reasonable supporting reasons for different suitable interpolation methods for predicting monthly mean meteorological data are the number of the selected interpolation methods and criteria in their studies for identifying an optimum method, as earlier mentioned in Section 4.1

4.3 Optimum method for monthly mean MODIS fire data interpolation

4.3.1 Brightness temperature

The statistical data of brightness temperature from USGS between October 2019 to May 2020 for identifying optimum interpolation methods are summarized in Table 4.20.

Table 4.20 Descriptive statistical data of the brightness temperature.

Month	Season	Min. (Kelvin)	Max. (Kelvin)	Mean (Kelvin)	SD. (Kelvin)	Count
Oct	Winter	284.50	305.30	298.29	3.26	209
Nov	Winter	285.60	309.90	300.41	3.89	331
Dec	Winter	283.40	312.00	300.93	4.19	1638
Jan	Winter	279.50	317.70	301.58	5.93	2381
Feb	Winter	269.40	321.30	301.15	7.06	2727
Mar	Summer	271.10	323.60	302.96	6.81	1791
Apr	Summer	275.90	317.00	301.83	6.31	501
May	Summer	278.40	304.70	295.49	6.31	112

According to the basic statistical data, brightness temperature decreases from October until a minimum in February and gradually increases until May.

In the cokriging (OCK and SCK) method, the latitude and longitude variables were added to be the cokriging variable. The relationship between monthly brightness temperature and cokriging variables is summarized in Table 4.21.

Table 4.21 The Pearson's correlation coefficients between monthly brightness temperature with cokriging variables.

Variables		Oct	Nov	Dec	Jan	Feb	Mar	Apr	May
BT	LAT	0.28**	0.27**	0.18**	0.14**	0.01	0.09**	0.14**	0.31**
	LONG	-0.06	-0.15**	-0.03	-0.01	0.14**	0.14**	0.02	-0.11

Note: *correlation is significant at the 0.05 level (2-tailed), **correlation is significant at the 0.01 level (2-tailed).

The relationship between monthly brightness temperature and latitude variable is relatively weak, positively correlated with statistical significance ($p \leq 0.01$), except in February. Also, the correlation between brightness temperature and longitude variable is a fragile relationship, but there are statistically significant ($p \leq 0.05$) in December, February, and March.

The cross-validation RMSE for monthly mean brightness temperature interpolation with seven different methods (IDW, GPI, RBF, OK, OCK, SK, and SCK) is summarized in Table 4.22.

Table 4.22 The cross-validation RMSE of the seven different interpolation methods of brightness temperature from October 2019 to May 2020.

Model	Function		RMSE (Kelvin)								
			Oct	Nov	Dec	Jan	Feb	Mar	Apr	May	Avg.
IDW	Power 1	1 sector	3.14	3.35	3.64	5.25	5.93	5.96	5.16	4.98	4.68
		4 sectors	3.09	3.31	3.65	5.27	6.00	5.94	5.15	4.98	4.67
		4 sectors with 45-degree offset	3.09	3.32	3.65	5.27	5.99	5.94	5.16	4.97	4.67
		8 sectors	3.09	3.33	3.67	5.32	6.08	5.98	5.24	4.95	4.71
	Power 2	1 sector	3.26	3.49	3.68	5.33	5.94	6.16	5.23	5.08	4.77
		4 sectors	3.20	3.41	3.63	5.24	5.86	6.01	5.12	4.98	4.68
		4 sectors with 45-degree offset	3.20	3.41	3.63	5.24	5.86	6.01	5.13	4.99	4.68
		8 sectors	3.19	3.39	3.62	5.22	5.85	5.98	5.10	4.92	4.66

Table 4.22 (Continued).

Model	Function		RMSE (Kelvin)								
			Oct	Nov	Dec	Jan	Feb	Mar	Apr	May	Avg.
GPI	Order 1		3.17	3.78	4.13	5.88	6.99	6.73	6.28	6.12	5.39
	Order 2		3.18	3.62	4.04	5.82	6.93	6.52	6.24	6.22	5.32
	Order 3		3.18	3.55	3.96	5.73	6.82	6.48	6.11	6.47	5.29
RBF	Complet	1 sector	3.15	3.37	3.63	5.26	5.94	6.04	5.21	4.85	4.68
	ely	4 sectors	3.12	3.32	3.60	5.22	5.87	5.96	5.13	4.79	4.63
	Regulariz	4 sectors with	3.12	3.32	3.60	5.22	5.87	5.95	5.14	4.77	4.62
	e spine	45-degree offset									
		8 sectors	3.12	3.32	3.60	5.22	5.87	5.96	5.14	4.77	4.63
	Spline	1 sector	3.18	3.46	3.67	5.39	6.02	6.13	5.35	4.93	4.77
	with	4 sectors	3.12	3.33	3.62	5.24	5.89	5.97	5.21	4.78	4.65
	tension	4 sectors with	3.11	3.31	3.61	5.24	5.90	5.97	5.20	4.75	4.64
		45-degree offset									
		8 sectors	3.11	3.32	3.61	5.23	5.88	5.96	5.18	4.75	4.63
	multiqua	1 sector	3.64	3.84	3.83	5.62	6.31	6.63	5.52	5.19	5.07
	dric	4 sectors	3.63	3.78	3.82	5.58	6.22	6.57	5.42	5.03	5.01
		4 sectors with	3.64	3.78	3.82	5.58	6.21	6.57	5.45	5.04	5.01
		45-degree offset									
		8 sectors	3.63	3.77	3.82	5.57	6.21	6.57	5.42	5.02	5.00
	Inverse	1 sector	3.26	3.52	4.79	5.72	7.71	6.42	5.61	4.92	5.24
	multiqua	4 sectors	3.14	3.38	4.89	5.57	7.70	6.28	5.45	4.75	5.15
	dric	4 sectors with	3.13	3.35	4.85	5.56	7.70	6.28	5.47	4.73	5.13
		45-degree offset									
		8 sectors	3.12	3.39	4.89	5.55	7.70	6.28	5.43	4.69	5.13
	Thin plate	1 sector	9.02	6.58	6.00	8.53	8.46	9.21	9.67	12.14	8.70
	spine	4 sectors	7.99	5.64	4.97	7.19	7.68	8.19	6.87	7.86	7.05
		4 sectors with	7.72	5.71	5.00	7.16	7.63	8.22	6.78	8.10	7.04
		45-degree offset									
		8 sectors	7.63	5.57	4.93	7.14	7.61	8.15	6.69	7.62	6.92
OK*	Circular		3.18	3.35	3.59	5.23	5.83	6.09	5.19	4.74	4.65
	Spherical		3.16	3.34	3.60	5.24	5.86	6.09	5.18	4.89	4.67
	Tetraspherical		3.15	3.35	3.59	5.22	5.87	6.00	5.17	4.88	4.65
	Pentasherical		3.15	3.35	3.59	5.23	5.85	6.00	5.18	4.84	4.65
	Exponential		3.15	3.37	3.60	5.22	5.84	6.08	5.21	4.83	4.66
	Gaussian		3.15	3.29	3.56	5.18	5.80	6.04	5.18	4.73	4.62
	Rational Quadratic		3.15	3.34	3.63	5.18	5.79	6.06	5.17	4.78	4.64
	Hole Effect		3.14	3.27	3.59	5.24	5.81	6.06	5.22	4.61	4.62

Table 4.22 (Continued).

Model	Function	RMSE (Kelvin)								
		Oct	Nov	Dec	Jan	Feb	Mar	Apr	May	Avg.
OK*	K-Bessel	3.16	3.33	3.56	5.19	5.87	6.05	5.19	4.78	4.64
	J-Bessel	3.15	3.34	3.62	5.20	5.80	5.98	5.22	4.83	4.64
	Stable	3.15	3.33	3.56	5.18	5.85	6.03	5.21	4.81	4.64
OCK*	Circular	3.21	3.47	3.78	5.51	6.21	6.20	5.54	5.64	4.95
	Spherical	3.20	3.46	3.77	5.51	6.19	6.18	5.63	5.64	4.95
	Tetraspherical	3.21	3.45	3.77	5.51	6.18	6.17	5.63	6.15	5.01
	Pentasherical	3.21	3.45	3.77	5.51	6.17	6.16	5.47	6.14	4.99
	Exponential	3.19	3.47	3.73	5.54	6.09	6.16	5.38	5.43	4.87
	Gaussian	3.22	3.52	3.83	5.51	6.30	6.25	5.70	5.64	5.00
	Rational Quadratic	3.19	3.49	3.78	5.51	6.18	6.17	5.38	5.47	4.90
	Hole Effect	3.20	3.54	3.83	5.51	6.31	6.26	5.74	5.50	4.99
	K-Bessel	3.17	3.42	3.68	5.42	5.87	6.04	5.23	4.95	4.72
	J-Bessel	3.33	3.54	3.83	5.51	6.31	6.26	5.65	5.37	4.98
	Stable	3.16	3.42	3.64	5.35	5.90	6.07	5.18	4.93	4.71
SK*	Circular	3.10	3.35	3.70	5.30	5.98	6.16	5.25	4.85	4.71
	Spherical	3.10	3.37	3.71	5.28	5.96	6.14	5.24	4.84	4.71
	Tetraspherical	3.10	3.37	3.71	5.26	5.93	6.13	5.24	4.83	4.70
	Pentaspherical	3.10	3.37	3.70	5.25	5.92	6.14	5.24	4.82	4.69
	Exponential	3.10	3.37	3.66	5.23	5.86	6.07	5.18	4.83	4.66
	Gaussian	3.09	3.28	3.66	5.26	5.94	6.14	5.23	4.76	4.67
	Rational Quadratic	3.09	3.29	3.69	5.18	5.82	6.05	5.16	4.77	4.63
	Hole Effect	3.13	3.34	3.75	5.33	6.09	6.26	5.32	4.82	4.76
	K-Bessel	3.09	3.29	3.65	5.24	5.86	5.96	5.15	4.77	4.63
	J-Bessel	3.09	3.32	3.67	5.23	5.89	6.15	5.24	4.73	4.67
	Stable	3.09	3.28	3.63	5.22	5.84	6.04	5.15	4.79	4.63
SCK*	Circular	3.01	3.28	3.62	5.28	5.99	6.20	5.23	4.63	4.66
	Spherical	3.01	3.29	3.67	5.28	5.97	6.20	5.22	4.62	4.66
	Tetraspherical	3.01	3.29	3.73	5.27	5.96	6.18	5.22	4.62	4.66
	Pentaspherical	3.02	3.30	3.73	5.26	5.94	6.17	5.22	4.61	4.66
	Exponential	3.04	3.29	3.69	5.22	5.89	6.11	5.17	4.59	4.63
	Gaussian	3.00	3.23	3.60	5.27	5.95	6.16	5.21	4.52	4.62
	Rational Quadratic	3.03	3.25	3.73	5.19	6.10	6.14	5.16	4.55	4.64
	Hole Effect	2.99	3.26	3.74	5.36	6.10	6.27	5.26	4.56	4.69
	K-Bessel	3.00	3.23	3.62	5.21	5.87	5.99	5.16	4.55	4.58
	J-Bessel	3.00	3.27	3.66	5.23	5.96	6.20	5.16	4.56	4.63
	Stable	3.00	3.23	3.61	5.19	5.85	5.95	5.15	4.52	4.56

Note: * This model calculated new values for the parameters with optimized semivariogram

As a result (Table 4.22), an average RMSE value of monthly mean brightness temperature interpolation using seven different methods with various functions varies from 4.56 Kelvin using the SCK method with the Stable function to 8.70 Kelvin using the RBF method with the Thin Plate Spline and the One Sector function. So, the SCK method with the Stable function is selected as an optimum method for monthly mean brightness temperature interpolation since it provides the least RMSE value.

4.3.2 Fire radiative power

The statistical data of fire radiative power from USGS between October 2019 to May 2020 for identifying optimum interpolation methods are summarized in Table 4.23.

Table 4.23 Descriptive statistical data of the monthly fire radiative power.

Month	Season	Min. (MW)	Max. (MW)	Mean (MW)	SD. (MW)	Count
Oct	Winter	3.90	44.20	9.59	4.70	209
Nov	Winter	4.20	151.00	14.91	14.35	331
Dec	Winter	3.10	465.40	18.73	22.41	1638
Jan	Winter	3.00	448.70	18.86	22.15	2381
Feb	Winter	2.40	1685.10	22.46	42.11	2727
Mar	Summer	3.60	371.50	23.96	30.02	1791
Apr	Summer	3.90	223.50	22.36	24.07	501
May	Summer	2.70	61.00	15.52	10.62	112

According to the basic statistical data, fire radiative power decreases from October until a minimum in February and gradually increases until May.

In the cokriging (OCK and SCK) method, the latitude and longitude variables were added to be the cokriging variable. The relationship between monthly fire radiative power and cokriging variables is summarized in Tables 4.24.

Table 4.24 The Pearson's correlation coefficients between monthly fire radiative power with cokriging variables.

Variables		Oct	Nov	Dec	Jan	Feb	Mar	Apr	May
FRP	LAT	-0.04	0.11	0.02	-0.02	-0.07**	-0.03	0.01	0.22*
	LONG	0.12	-0.10	-0.03	0.07**	0.02	-0.03	-0.05	-0.12

Note: *correlation is significant at the 0.05 level (2-tailed), **correlation is significant at the 0.01 level (2-tailed).

The relationship between monthly fire radiative power and latitude variable is a very weak correlation. Same with the correlation between fire radiative power and longitude variable. There is a very weak negative correlation, with a statistically significant ($p \leq 0.01$) in February and a statistically significant ($p \leq 0.05$) in May between fire radiative power and latitude. But between fire radiative power and longitude variable is a weak positive with statistically significant ($p \leq 0.01$) only in January.

The cross-validation RMSE for monthly mean fire radiative power interpolation with seven different methods (IDW, GPI, RBF, OK, OCK, SK, and SCK) is summarized in Table 4.25.

Table 4.25 The cross-validation RMSE of the seven interpolation methods for mean fire radiative power interpolation from October 2019 to May 2020.

Model	Function		RMSE (MW)								
			Oct	Nov	Dec	Jan	Feb	Mar	Apr	May	Avg.
IDW	Power 1	1 sector	4.94	12.15	20.61	21.73	39.86	28.47	22.57	8.72	19.88
		4 sectors	4.83	11.71	20.54	21.27	39.91	28.25	22.14	8.47	19.64
		4 sectors with 45-degree offset	4.83	11.74	20.58	21.29	39.94	28.23	22.14	8.48	19.65
		8 sectors	4.79	11.62	20.68	21.27	40.01	28.29	22.07	8.41	19.64
	Power 2	1 sector	5.18	12.47	20.80	22.94	42.30	29.79	23.94	9.19	20.83
		4 sectors	5.10	12.30	20.49	22.55	42.03	29.30	23.71	8.97	20.56
		4 sectors with 45-degree offset	5.10	12.30	20.49	22.56	42.02	29.29	23.70	8.96	20.55
		8 sectors	5.09	12.22	20.42	22.43	41.97	29.20	23.64	8.89	20.48

Table 4.25 (Continued).

Model	Function		RMSE (MW)								
			Oct	Nov	Dec	Jan	Feb	Mar	Apr	May	Avg.
GPI	Order 1		4.74	14.37	22.44	22.12	42.07	30.04	24.19	10.63	21.33
	Order 2		4.80	14.23	22.43	22.13	42.04	29.94	24.11	10.78	21.31
	Order 3		4.84	13.88	22.40	22.12	41.96	29.92	24.16	11.11	21.30
RBF	Completely Regularize spine	1 sector	4.88	11.54	20.32	21.74	39.70	29.18	22.06	8.65	19.76
		4 sectors	4.81	11.38	20.13	21.62	39.52	28.96	21.92	8.51	19.61
		4 sectors with 45-degree offset	4.81	11.40	20.14	21.63	39.55	28.97	21.92	8.53	19.62
		8 sectors	4.80	11.41	20.14	21.62	39.49	28.96	21.92	8.49	19.60
	Spline with tension	1 sector	4.97	11.80	20.32	21.79	39.63	28.98	22.69	8.84	19.88
		4 sectors	4.80	11.40	20.13	21.19	39.45	28.22	21.99	8.52	19.46
		4 sectors with 45-degree offset	4.82	11.41	20.14	21.21	39.48	28.22	21.98	8.51	19.47
		8 sectors	4.79	11.39	20.14	21.16	39.42	28.17	21.93	8.49	19.44
	multiquadric	1 sector	5.72	12.53	21.58	23.96	44.44	32.23	25.98	9.76	22.03
		4 sectors	5.52	12.13	21.53	23.69	44.27	31.81	25.28	9.93	21.77
		4 sectors with 45-degree offset	5.55	12.15	21.54	23.70	44.28	31.77	25.32	9.96	21.78
		8 sectors	5.52	12.12	21.54	23.69	44.24	31.79	25.28	9.89	21.76
	Inverse multiquadric	1 sector	4.92	11.67	21.95	22.35	42.25	29.37	22.36	8.64	20.44
		4 sectors	4.71	11.09	21.78	21.61	40.96	29.17	21.74	8.14	19.90
		4 sectors with 45-degree offset	4.72	11.13	21.78	21.62	40.95	29.20	21.75	8.15	19.91
		8 sectors	4.68	11.04	21.64	21.54	40.98	29.29	21.63	8.14	19.87
	Thin plate spine	1 sector	12.43	23.35	28.31	42.56	58.95	55.66	78.59	18.71	39.82
		4 sectors	10.05	16.82	26.51	32.14	56.88	41.06	43.43	15.53	30.30
		4 sectors with 45-degree offset	10.73	17.28	26.49	32.08	57.14	40.82	50.42	15.25	31.28
		8 sectors	10.34	16.40	26.43	31.92	57.17	40.45	42.05	15.27	30.00

Table 4.25 (Continued).

Model	Function	RMSE (MW)								
		Oct	Nov	Dec	Jan	Feb	Mar	Apr	May	Avg.
OK*	Circular	4.93	11.39	20.49	21.55	40.16	28.16	23.69	9.39	19.97
	Spherical	4.93	11.36	20.51	21.56	40.16	28.20	23.69	9.43	19.98
	Tetraspherical	4.91	11.38	20.49	21.58	40.16	28.25	23.69	9.37	19.98
	Pentasherical	4.90	11.61	20.49	21.59	40.16	28.27	23.69	9.20	19.99
	Exponential	4.89	11.35	20.34	21.53	40.16	28.45	23.69	9.23	19.96
	Gaussian	4.92	11.39	20.52	21.36	40.16	28.11	23.69	9.10	19.91
	Rational Quadratic	4.93	11.45	20.17	21.62	40.16	28.66	23.69	9.14	19.98
	Hole Effect	4.82	11.57	20.64	21.69	40.32	28.78	21.94	9.38	19.89
	K-Bessel	4.84	11.34	20.39	21.50	40.16	28.16	23.25	9.11	19.84
	J-Bessel	4.93	12.15	20.40	21.60	37.77	28.47	21.32	9.22	19.48
	Stable	4.82	11.30	20.46	21.36	40.16	28.13	23.46	9.13	19.85
OCK*	Circular	4.93	12.23	21.32	21.82	40.16	28.71	23.69	9.81	20.33
	Spherical	4.92	12.23	21.32	21.82	40.16	28.71	23.69	9.68	20.32
	Tetraspherical	4.90	12.23	21.32	21.82	40.16	28.71	23.69	9.64	20.31
	Pentasherical	4.89	12.23	21.32	21.82	40.16	28.71	23.69	9.59	20.30
	Exponential	4.89	12.12	21.32	21.82	40.16	28.71	23.69	9.34	20.26
	Gaussian	4.92	12.23	21.32	21.82	40.16	28.71	23.69	10.29	20.39
	Rational Quadratic	4.92	12.23	21.32	21.82	40.16	28.71	23.69	9.47	20.29
	Hole Effect	4.91	12.23	21.32	21.82	40.16	28.71	23.69	9.72	20.32
	K-Bessel	4.84	11.93	21.17	21.82	40.16	28.71	23.69	9.11	20.18
	J-Bessel	4.93	12.23	21.32	21.82	40.16	28.71	23.69	9.88	20.34
	Stable	4.88	11.90	21.32	21.82	40.16	28.71	23.69	9.13	20.20
SK*	Circular	4.66	11.07	20.36	21.60	39.71	28.40	23.61	8.70	19.76
	Spherical	4.66	11.30	20.36	21.61	39.76	28.46	23.69	8.75	19.82
	Tetraspherical	4.66	11.34	20.36	21.61	39.61	28.54	23.94	8.72	19.85
	Pentaspherical	4.66	11.32	20.35	21.62	40.02	28.69	24.07	8.69	19.93
	Exponential	4.67	11.52	20.19	21.64	39.92	28.53	24.07	8.70	19.91
	Gaussian	4.66	11.29	20.38	21.25	40.10	28.32	23.65	8.73	19.80
	Rational Quadratic	4.66	11.55	20.10	21.67	39.83	28.35	24.07	8.76	19.87
	Hole Effect	4.67	12.12	20.64	21.71	40.48	28.89	22.14	8.74	19.92
	K-Bessel	4.67	11.31	20.21	21.68	40.06	28.34	23.10	8.73	19.76
	J-Bessel	4.69	14.16	20.44	21.76	40.23	28.79	22.09	8.70	20.11
	Stable	4.66	11.26	20.29	21.25	40.10	28.33	23.47	8.73	19.76

Table 4.25 (Continued).

Model	Function	RMSE (MW)								
		Oct	Nov	Dec	Jan	Feb	Mar	Apr	May	Avg.
SCK*	Circular	4.63	11.13	20.36	21.62	39.71	28.55	23.61	8.65	19.78
	Spherical	4.63	11.22	20.36	21.61	39.76	28.59	23.69	8.62	19.81
	Tetraspherical	4.63	11.38	20.36	21.62	39.62	28.59	23.94	8.59	19.84
	Pentaspherical	4.63	11.35	20.35	21.64	40.02	28.71	24.04	8.59	19.92
	Exponential	4.63	11.55	20.19	21.52	39.96	28.21	24.07	8.55	19.84
	Gaussian	4.64	11.32	20.38	21.22	40.10	28.52	23.64	8.67	19.81
	Rational Quadratic	4.64	11.55	20.10	21.70	39.91	28.42	24.07	8.61	19.88
	Hole Effect	4.68	12.14	20.64	21.70	40.48	29.08	22.15	8.59	19.93
	K-Bessel	4.64	11.36	20.21	21.44	40.35	28.52	23.12	8.66	19.79
	J-Bessel	4.64	14.07	20.45	21.76	41.64	28.84	22.15	8.65	20.28
	Stable	4.64	11.33	20.32	21.22	40.10	28.52	23.64	8.67	19.81

Note: * This model calculated new values for the parameters with optimized semivariogram

As a result (Table 4.25), an average RMSE value of monthly mean fire radiative power interpolation using seven different methods with various functions varies from 19.44 MW using the RBF method with the Spline with Tension and Eight Sectors function to 39.82 MW using the RBF method with the Thin Plate Spline and One Sector function. Thus, the RBF method with the Spline with Tension and Eight Sector function is an optimum method for monthly mean fire radiative power interpolation since it provides the least RMSE value.

Several methods were used to interpolate MODIS fire data from the previous studies. For example, Veraverbeke et al. (2014) used kriging for interpolating the MODIS active fire because the kriging is based on local variogram analysis and allows an uncertainty analysis by spatially estimating the kriging standard error. Like Devkota (2021), Ponomarev, Shvetsov, and Usataya (2018) used kriging to interpolate the MODIS fire radiative power data. While, Loboda, Hall, and Baer (2017) used IDW to determine the fire spread from MODIS active fire points data.

Like Section 4.1 and 4.2, the rationale supporting reasons for different optimum interpolation methods for predicting monthly mean MODIS fire data are the number of the selected interpolation methods and criteria in their studies for identifying an optimum method.

Summary

An optimum interpolation method for the selected dependent and independent variables based on their corresponding data between October 2019 to May 2020 is summarized in Table 4.26 again. These methods will be applied to other datasets in this study. On the contrary, appropriate standard tools for Spatial Analyst under ArcMap software will be applied with other independent variables, as shown in Table 4.27.

Table 4.26 Summary of optimum interpolation method.

No.	Variable	Optimum interpolation method
1	PM10 concentration	SCK with K-Bessel function
2	PM2.5 concentration	SCK with K-Bessel function
3	Relative humidity	SCK with J-Bessel function
4	Temperature	SCK with Hole Effect function
5	Wind speed	RBF with Spline with Tension and One Sector
6	Pressure	SCK with Stable function
7	Visibility	OCK with Hole Effect function
8	Brightness temperature	SCK with Stable function
9	Fire radiative power	RBF with Spline with Tension and Eight Sector function

Table 4.27 Summary of the standard tools for other data preparation.

No.	Variable	Data preparation
1	MODIS AOD	Raster Calculator
2	NDVI	Raster Calculator from Landsat 8 OLI data
3	BUI	Raster Calculator from Landsat 8 OLI data
4	Road density	Calculate geometry and field calculator
5	Factory density	Spatial join and field calculator
6	Elevation	Fill (Spatial analysis) from SRTM
7	Fire hotspot	Spatial join and field calculator
8	Population density	Field calculator (Extract from population data at district level)
9	GPP	Field calculator (Extract from population data at district level)

After that, all prepared dependent and independent variables will be further applied to identify significant spatiotemporal factors on PM concentration using the multicollinearity test and OLS regression analysis.

CHAPTER V

SIGNIFICANT SPATIOTEMPORAL FACTORS ON PM CONCENTRATION

This chapter presents the study's first objective to identify significant factors on PM10 concentration in the rural landscape and PM2.5 concentration in the urban landscape during the winter and summer season and relationships using the multicollinearity test and the OLS regression analysis. The main results consist of (1) basic information on a dependent variable, (2) basic information on independent variables, (3) significant spatiotemporal factors on PM10 concentration in the rural landscape, (4) significant spatiotemporal factors on PM2.5 concentration in the urban landscape, (5) basic information of daily dependent and independent variables, (6) significant daily spatiotemporal factors on PM10 concentration in the rural landscape, and (7) significant daily spatiotemporal factors on PM25 concentration in the urban landscape, are here described and discussed in detail,

5.1 Basic information of dependent variable

The dependent variable, represented as dynamic data, includes (1) PM10 concentration in the rural landscape and (2) PM2.5 concentration in the urban landscape. The spatial distribution of monthly mean PM10 and PM2.5 in the rural and urban landscapes, which were interpolated using the SCK method with the K-Bessel function, is displayed in Figures 5.1 and 5.2.

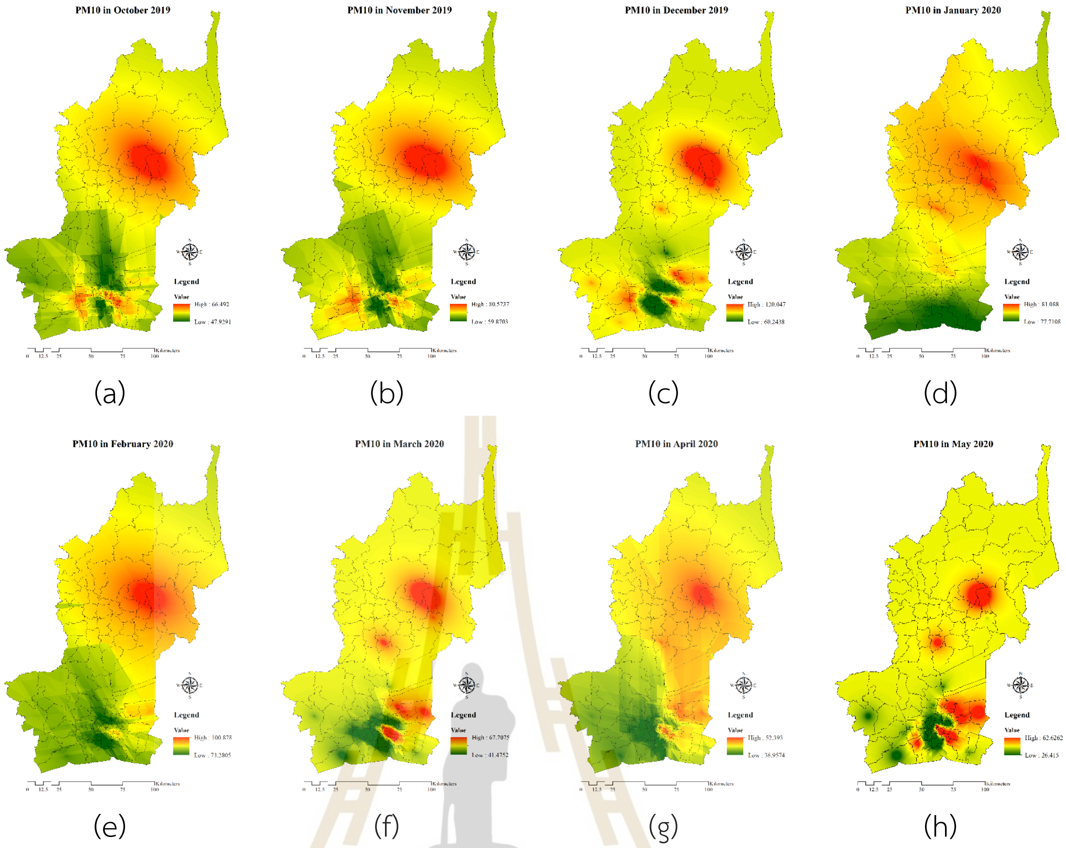

Figure 5.1 Spatial distribution of monthly mean PM10 concentration during October 2019 to May 2020: (a) October 2019, (b) November 2019, (c) December 2019, (d) January 2020, (e) February 2020, (f) March 2020, (g) April 2020, and (h) May 2020.

The output of PM10 concentration interpolation shows high value in the rural landscape, especially in Chaloem Phra Kiat and Phra Phuttabat – Saraburi province. Meanwhile, PM10 concentration in the urban landscape is lower than in rural landscapes, especially in Samut Sakhon and Nakhon Pathom province.

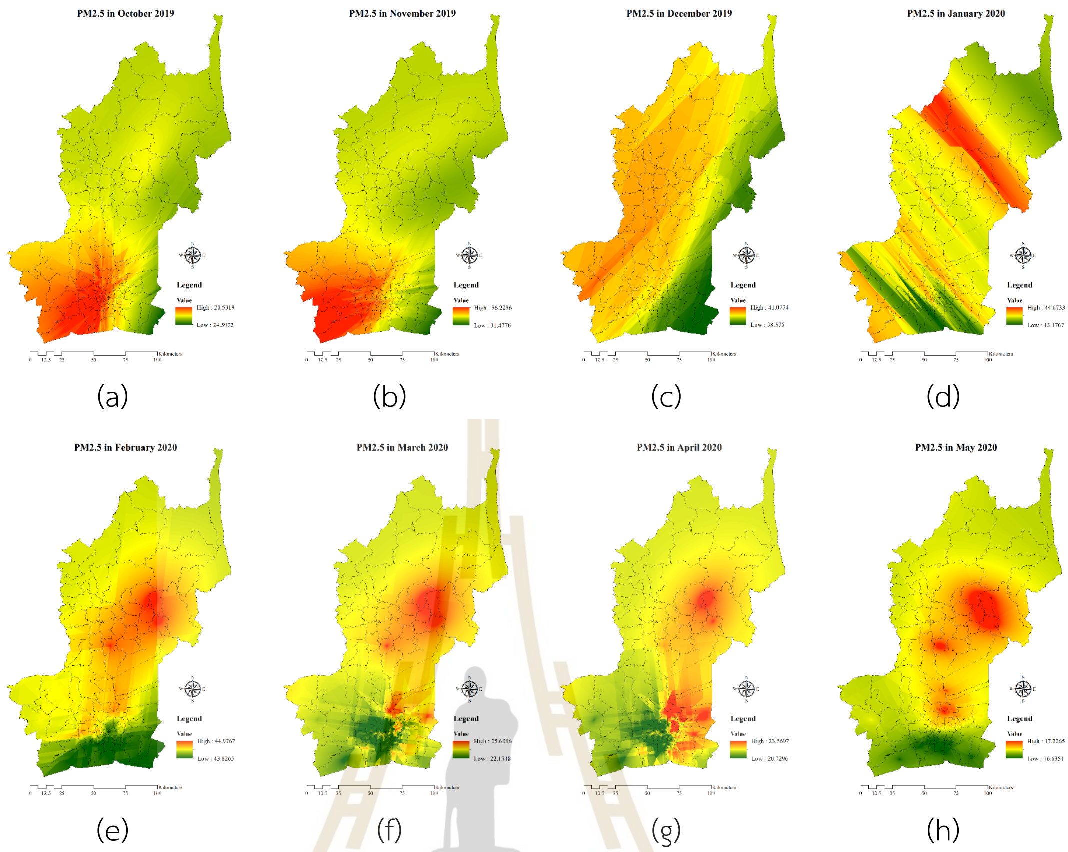

Figure 5.2 Spatial distribution of monthly mean PM2.5 concentration during October 2019 to May 2020: (a) October 2019, (b) November 2019, (c) December 2019, (d) January 2020, (e) February 2020, (f) March 2020, (g) April 2020, and (h) May 2020.

Primary statistics data of normalized PM concentration in rural and urban landscapes are summarized separately in Tables 5.1 and 5.2.

Table 5.1 Descriptive statistic data of PM10 concentration after normalization in rural landscape.

Statistics	Winter season					Summer season		
	Oct	Nov	Dec	Jan	Feb	Mar	Apr	May
Minimum	-2.30	-1.86	-0.99	-2.08	-1.98	-0.78	-1.97	-0.82
Maximum	3.72	3.84	5.39	2.87	3.36	5.55	3.28	5.83
Mean	0.00	0.00	0.00	0.00	0.00	0.00	0.00	0.00
SD.	1.00	1.00	1.00	1.00	1.00	1.00	1.00	1.00

Table 5.2 Descriptive statistic data of PM2.5 concentration after normalization in the urban landscape.

Statistics	Winter season					Summer season		
	Oct	Nov	Dec	Jan	Feb	Mar	Apr	May
Minimum	-2.93	-2.79	-2.40	-2.25	-1.75	-2.46	-2.20	-1.73
Maximum	1.33	2.00	1.63	1.51	1.82	2.22	2.29	2.31
Mean	0.00	0.00	0.00	0.00	0.00	0.00	0.00	0.00
SD.	1.00	1.00	1.00	1.00	1.00	1.00	1.00	1.00

5.2 Basic information of independent variable

The independent variables, which are represented as dynamic and static factors on PM concentration in rural and urban landscapes, includes (1) meteorological factor (relative humidity, temperature, wind speed, pressure, visibility), (2) biophysical factor (MODIS AOD, brightness temperature, fire radiative power, fire hotspot, NDVI, BUI, road density, factory density, elevation), and (3) socioeconomic factor (population density, GPP). Basic information on independent variables is separately described in the following sections.

5.2.1 Relative humidity

The spatial distribution of monthly mean relative humidity in the rural and urban landscapes, which were interpolated using the SCK method with the K-Bessel function, is displayed in Figure 5.3. Primary statistics data of normalized relative humidity in rural and urban landscapes are summarized separately in Tables 5.3 and 5.4.

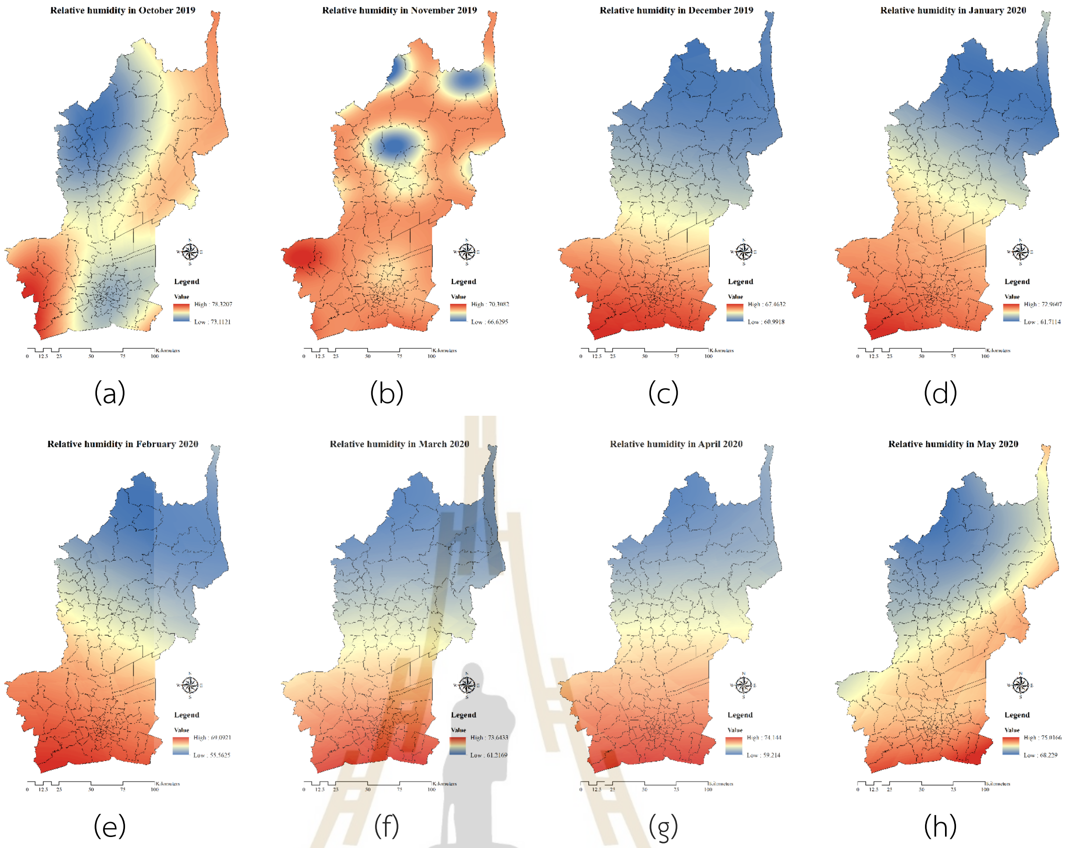

Figure 5.3 Spatial distribution of monthly mean relative humidity during October 2019 to May 2020: (a) October 2019, (b) November 2019, (c) December 2019, (d) January 2020, (e) February 2020, (f) March 2020, (g) April 2020, and (h) May 2020.

Table 5.3 Descriptive statistic data of relative humidity after normalization in rural landscape.

Statistics	Winter season					Summer season		
	Oct	Nov	Dec	Jan	Feb	Mar	Apr	May
Minimum	-1.82	-3.17	-1.62	-1.93	-1.81	-1.77	-2.01	-1.93
Maximum	1.87	1.02	1.99	1.49	1.70	1.89	1.72	1.46
Mean	0.00	0.00	0.00	0.00	0.00	0.00	0.00	0.00
SD.	1.00	1.00	1.00	1.00	1.00	1.00	1.00	1.00

Table 5.4 Descriptive statistic data of relative humidity after normalization in the urban landscape.

Statistics	Winter season					Summer season		
	Oct	Nov	Dec	Jan	Feb	Mar	Apr	May
Minimum	-0.86	-1.97	-1.91	-1.74	-2.04	-3.15	-2.68	-2.88
Maximum	3.26	3.49	2.21	3.22	2.65	1.79	1.88	3.36
Mean	0.00	0.00	0.00	0.00	0.00	0.00	0.00	0.00
SD.	1.00	1.00	1.00	1.00	1.00	1.00	1.00	1.00

5.2.2 Temperature

The spatial distribution of monthly mean temperature in the rural and urban landscapes, which were interpolated using the SCK method with the Hole Effect function, is displayed in Figure 5.4. Primary statistics data of normalized temperature in rural and urban landscapes are separately summarized in Tables 5.5 and 5.6, respectively.

Table 5.5 Descriptive statistic data of temperature after normalization in rural landscape.

Statistics	Winter season					Summer season		
	Oct	Nov	Dec	Jan	Feb	Mar	Apr	May
Minimum	-3.39	-3.68	-3.23	-3.46	-3.85	-2.23	-1.74	-2.70
Maximum	1.93	1.72	1.74	2.18	1.99	2.22	2.09	1.80
Mean	0.00	0.00	0.00	0.00	0.00	0.00	0.00	0.00
SD.	1.00	1.00	1.00	1.00	1.00	1.00	1.00	1.00

Table 5.6 Descriptive statistic data of temperature after normalization in the urban landscape.

Statistics	Winter season					Summer season		
	Oct	Nov	Dec	Jan	Feb	Mar	Apr	May
Minimum	-3.17	-2.95	-3.09	-2.97	-2.91	-3.31	-2.00	-3.18
Maximum	1.08	0.96	0.92	0.95	0.94	1.30	3.01	1.02
Mean	0.00	0.00	0.00	0.00	0.00	0.00	0.00	0.00
SD.	1.00	1.00	1.00	1.00	1.00	1.00	1.00	1.00

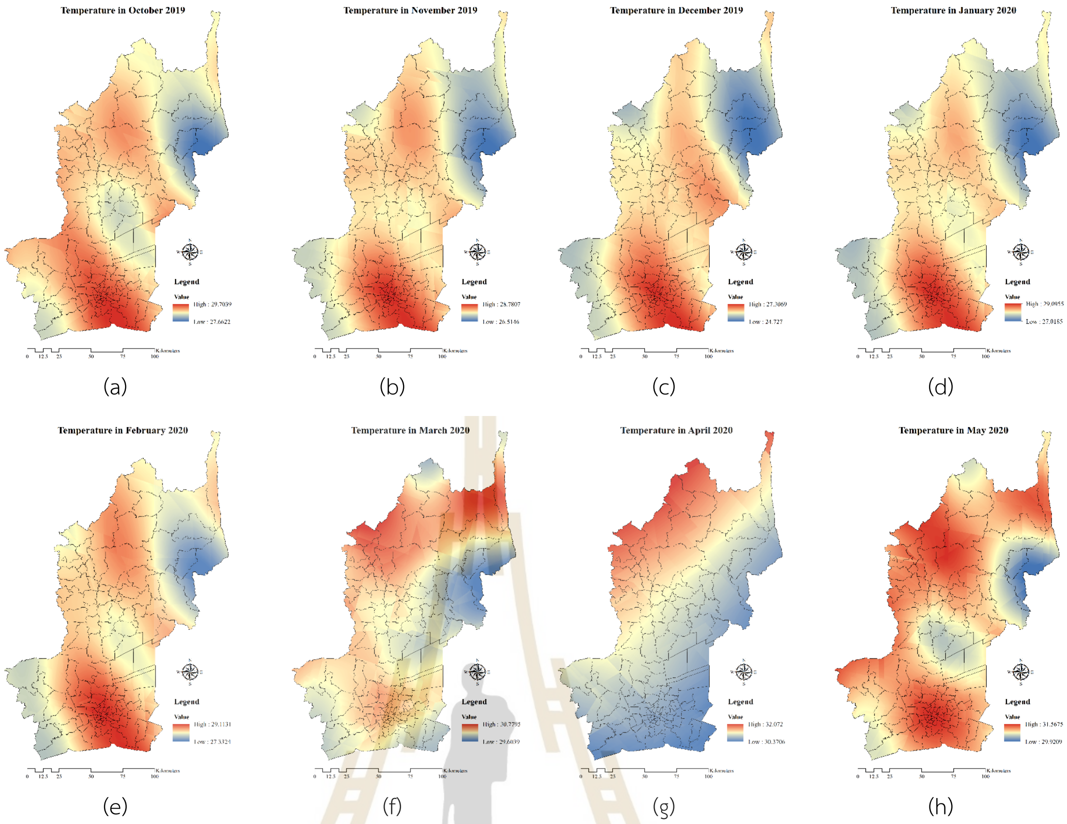

Figure 5.4 Spatial distribution of monthly mean temperature during October 2019 to May 2020: (a) October 2019, (b) November 2019, (c) December 2019, (d) January 2020, (e) February 2020, (f) March 2020, (g) April 2020, and (h) May 2020.

5.2.3 Wind speed

The spatial distribution of monthly mean wind speed in the rural and urban landscape, which were interpolated using the RBF method with Spline with Tension and One Sector function, is displayed in Figure 5.5. Primary statistics data of normalized wind speed in rural and urban landscapes are summarized separately in Tables 5.7 and 5.8.

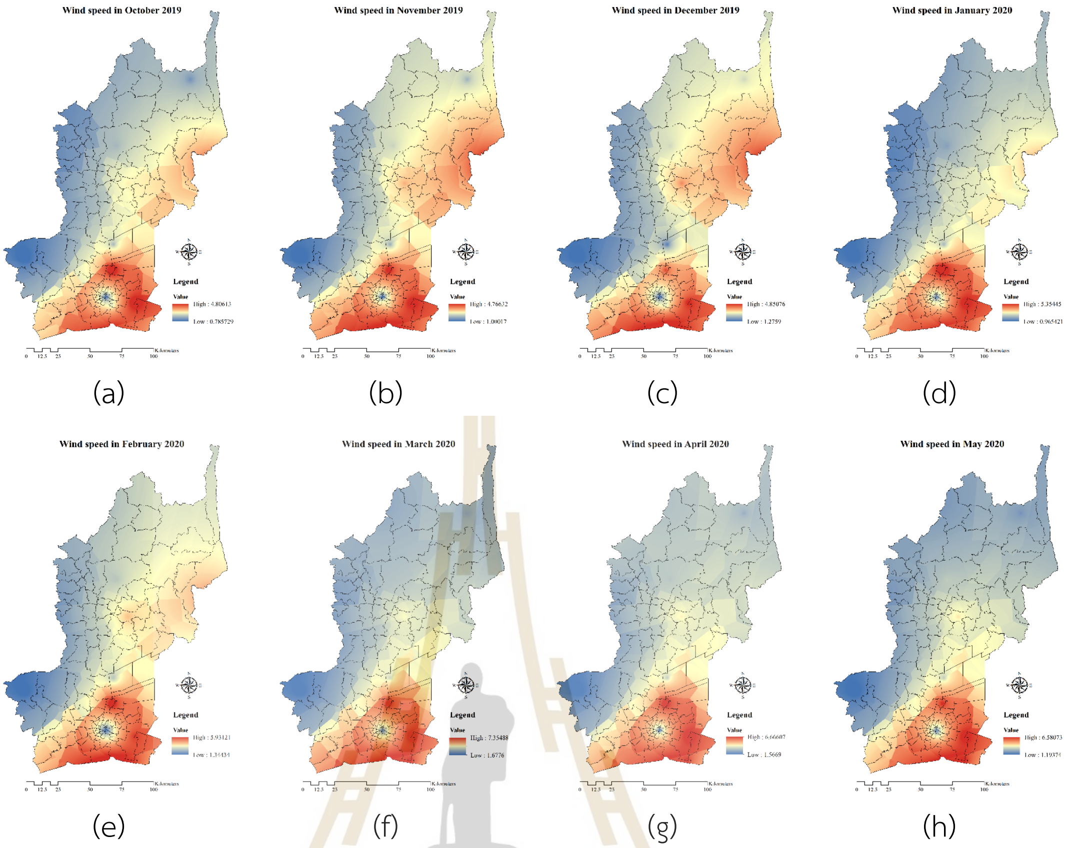

Figure 5.5 Spatial distribution of monthly mean wind speed during October 2019 to May 2020: (a) October 2019, (b) November 2019, (c) December 2019, (d) January 2020, (e) February 2020, (f) March 2020, (g) April 2020, and (h) May 2020.

Table 5.7 Descriptive statistic data of wind speed after normalization in rural landscape.

Statistics	Winter season					Summer season		
	Oct	Nov	Dec	Jan	Feb	Mar	Apr	May
Minimum	-1.55	-1.62	-1.56	-1.55	-1.73	-1.37	-1.44	-1.35
Maximum	2.15	1.91	1.99	2.53	2.01	2.81	2.96	2.67
Mean	0.00	0.00	0.00	0.00	0.00	0.00	0.00	0.00
SD.	1.00	1.00	1.00	1.00	1.00	1.00	1.00	1.00

Table 5.8 Descriptive statistic data of wind speed after normalization in the urban landscape.

Statistics	Winter season					Summer season		
	Oct	Nov	Dec	Jan	Feb	Mar	Apr	May
Minimum	-2.73	-2.90	-2.64	-2.93	-2.58	-2.99	-3.08	-3.03
Maximum	2.02	1.65	1.85	2.13	1.86	1.57	1.69	1.68
Mean	0.00	0.00	0.00	0.00	0.00	0.00	0.00	0.00
SD.	1.00	1.00	1.00	1.00	1.00	1.00	1.00	1.00

5.2.4 Pressure

The spatial distribution of monthly mean pressure in the rural and urban landscapes, which were interpolated using the SCK method with the Stable function, is displayed in Figure 5.6. Primary statistics data of normalized pressure in rural and urban landscapes are separately summarized in Tables 5.9 and 5.10, respectively.

Table 5.9 Descriptive statistic data of pressure after normalization in rural landscape.

Statistics	Winter season					Summer season		
	Oct	Nov	Dec	Jan	Feb	Mar	Apr	May
Minimum	-1.58	-1.34	-1.38	-1.71	-1.82	-2.29	-2.65	-2.55
Maximum	2.59	2.41	2.94	2.10	3.18	1.53	1.35	1.46
Mean	0.00	0.00	0.00	0.00	0.00	0.00	0.00	0.00
SD.	1.00	1.00	1.00	1.00	1.00	1.00	1.00	1.00

Table 5.10 Descriptive statistic data of pressure after normalization in the urban landscape.

Statistics	Winter season					Summer season		
	Oct	Nov	Dec	Jan	Feb	Mar	Apr	May
Minimum	-1.98	-2.21	-1.30	-2.37	-1.46	-2.54	-4.73	-3.65
Maximum	1.86	2.25	2.28	2.58	2.16	2.14	2.43	2.42
Mean	0.00	0.00	0.00	0.00	0.00	0.00	0.00	0.00
SD.	1.00	1.00	1.00	1.00	1.00	1.00	1.00	1.00

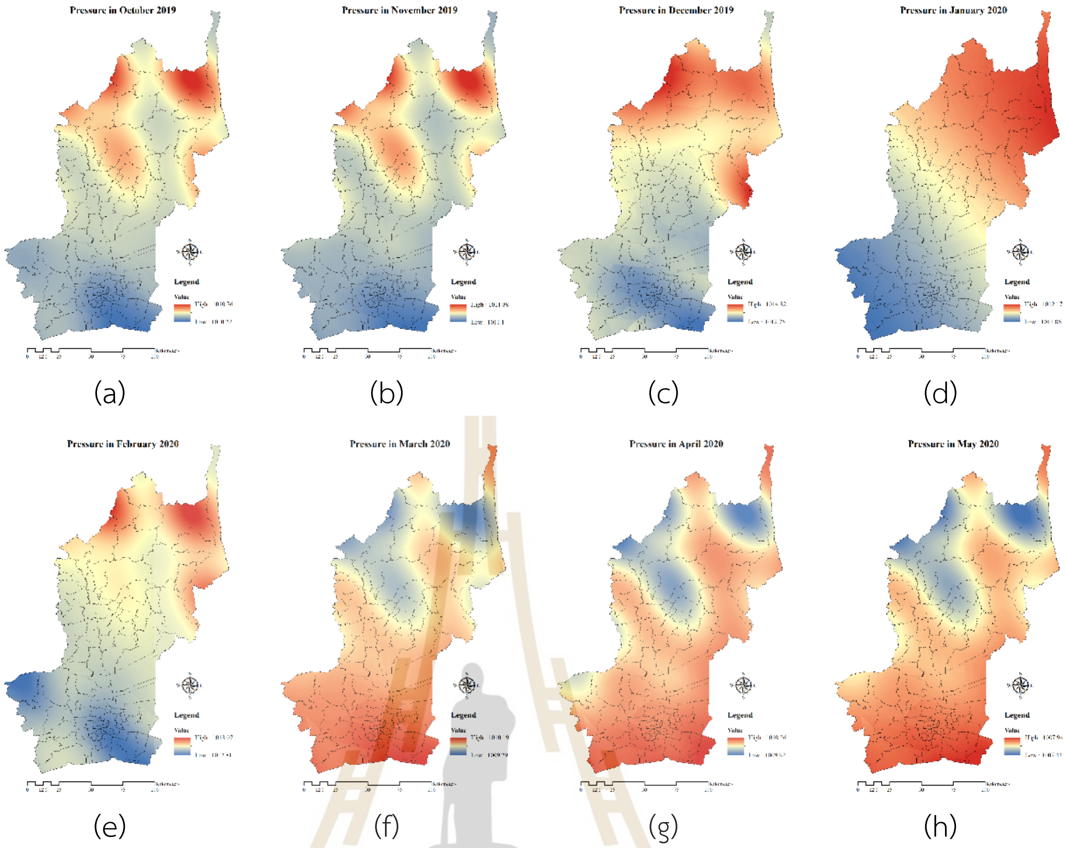

Figure 5.6 Spatial distribution of monthly mean pressure during October 2019 to May 2020: (a) October 2019, (b) November 2019, (c) December 2019, (d) January 2020, (e) February 2020, (f) March 2020, (g) April 2020, and (h) May 2020.

5.2.5 Visibility

The spatial distribution of monthly mean visibility in the rural and urban landscapes, which were interpolated using the OCK method with the Hole Effect function, is displayed in Figure 5.7. Primary statistics data of normalized visibility in rural and urban landscapes are separately summarized in Tables 5.11 and 5.12.

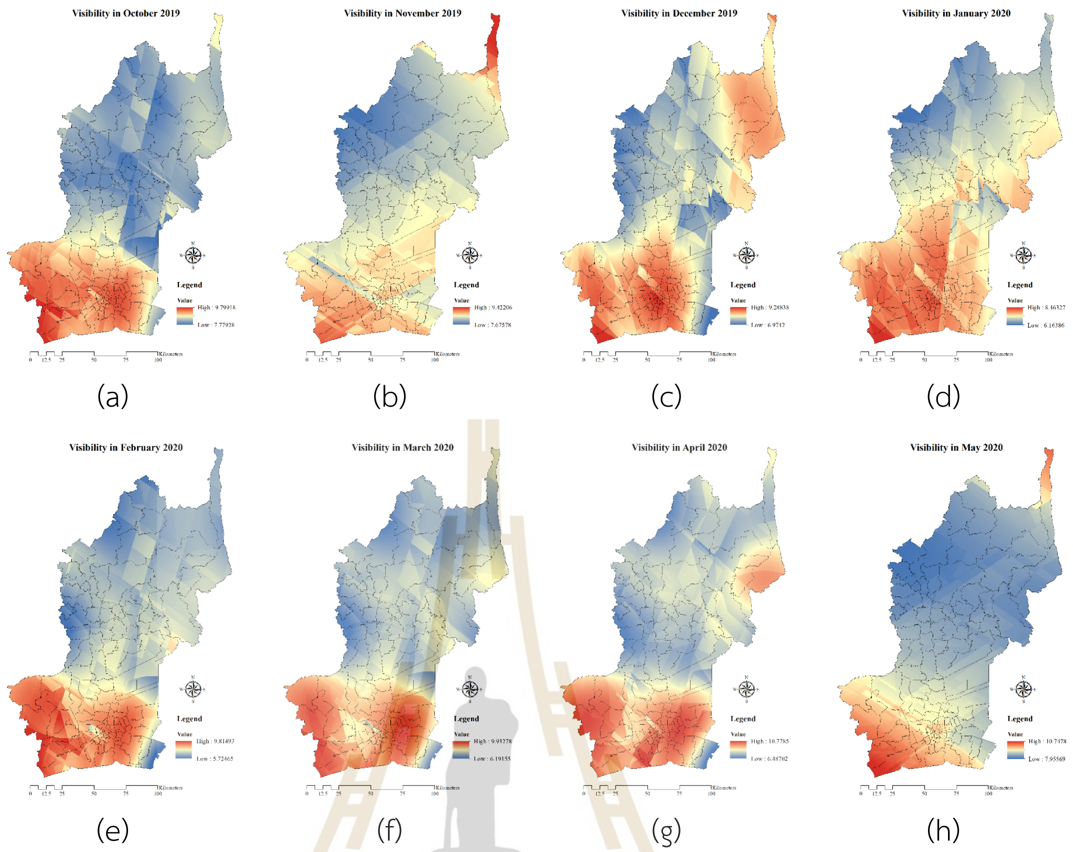

Figure 5.7 Spatial distribution of monthly mean visibility during October 2019 to May 2020: (a) October 2019, (b) November 2019, (c) December 2019, (d) January 2020, (e) February 2020, (f) March 2020, (g) April 2020, and (h) May 2020.

Table 5.11 Descriptive statistic data of visibility after normalization in rural landscape.

Statistics	Winter season				Summer season			
	Oct	Nov	Dec	Jan	Feb	Mar	Apr	May
Minimum	-1.58	-1.34	-1.38	-1.71	-1.82	-2.07	-1.93	-1.67
Maximum	2.59	2.41	2.94	2.10	3.18	3.03	2.68	2.99
Mean	0.00	0.00	0.00	0.00	0.00	0.00	0.00	0.00
SD.	1.00	1.00	1.00	1.00	1.00	1.00	1.00	1.00

Table 5.12 Descriptive statistic data of visibility after normalization in the urban landscape.

Statistics	Winter season					Summer season		
	Oct	Nov	Dec	Jan	Feb	Mar	Apr	May
Minimum	-4.31	-1.69	-4.31	-2.41	-4.77	-3.35	-4.70	-2.00
Maximum	1.45	2.39	1.16	1.54	1.20	1.75	1.32	3.29
Mean	0.00	0.00	0.00	0.00	0.00	0.00	0.00	0.00
SD.	1.00	1.00	1.00	1.00	1.00	1.00	1.00	1.00

5.2.6 MODIS AOD

The spatial distribution of monthly mean MODIS AOD in the rural and urban landscape, constructed using the Raster Calculator function of the ArcMap tool, is displayed in Figure 5.8. Primary statistics data of normalized MODIS AOD in rural and urban landscapes are separately summarized in Tables 5.13 and 5.14, respectively.

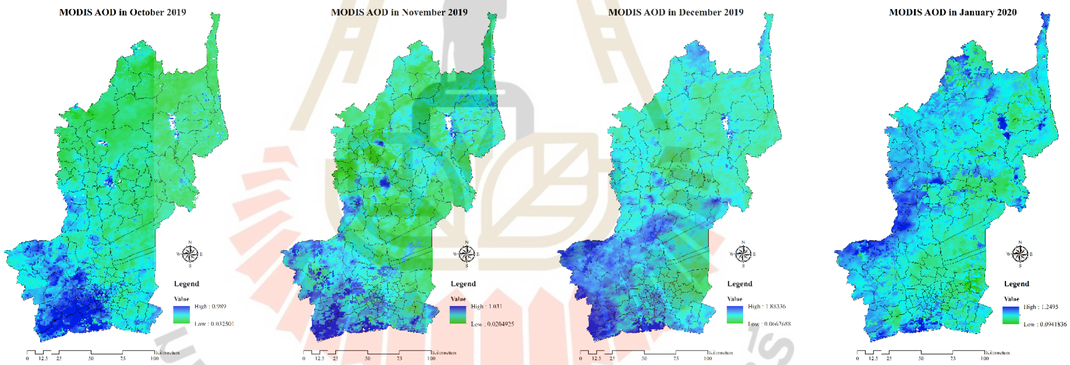

(a) (b) (c) (d)

Figure 5.8 Spatial distribution of monthly mean MODIS AOD during October 2019 to May 2020: (a) October 2019, (b) November 2019, (c) December 2019, (d) January 2020, (e) February 2020, (f) March 2020, (g) April 2020, and (h) May 2020.

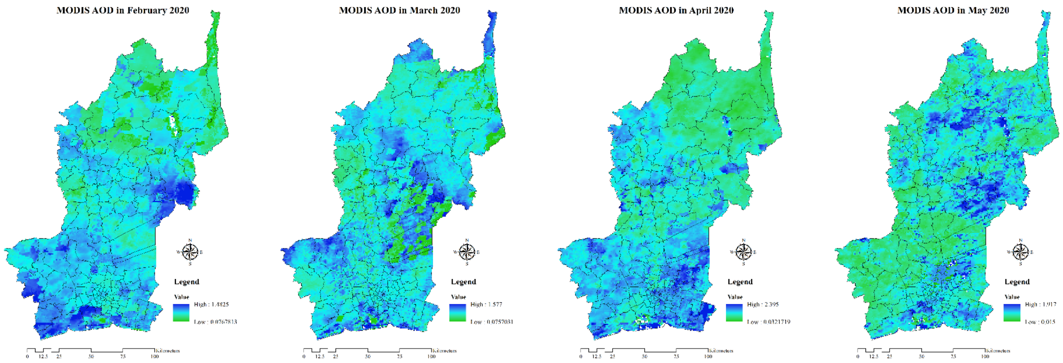

(e) (f) (g) (h)

Figure 5.8 (Continued).

Table 5.13 Descriptive statistic data of MODIS AOD after normalization in rural landscape.

Statistics	Winter season					Summer season		
	Oct	Nov	Dec	Jan	Feb	Mar	Apr	May
Minimum	-1.45	-2.28	-2.14	-1.77	-2.32	-0.96	-2.23	-1.74
Maximum	2.68	2.87	2.55	2.42	2.81	3.98	2.23	2.72
Mean	0.00	0.00	0.00	0.00	0.00	0.00	0.00	0.00
SD.	1.00	1.00	1.00	1.00	1.00	1.00	1.00	1.00

Table 5.14 Descriptive statistic data of MODIS AOD after normalization in the urban landscape.

Statistics	Winter season					Summer season		
	Oct	Nov	Dec	Jan	Feb	Mar	Apr	May
Minimum	-1.54	-2.27	2.36	-2.21	-1.65	-2.31	-2.00	-1.91
Maximum	2.21	2.51	2.36	2.52	3.29	3.10	3.29	2.31
Mean	0.00	0.00	0.00	0.00	0.00	0.00	0.00	0.00
SD.	1.00	1.00	1.00	1.00	1.00	1.00	1.00	1.00

5.2.7 Brightness temperature

The spatial distribution of monthly mean brightness temperature in the rural and urban landscape, which were interpolated using the SCK method with the Stable function, is displayed in Figure 5.9. Primary statistics data of normalized brightness temperature in rural and urban landscapes are separately summarized in Tables 5.15 and 5.16, respectively.

Table 5.15 Descriptive statistic data of brightness temperature after normalization in rural landscape.

Statistics	Winter season					Summer season		
	Oct	Nov	Dec	Jan	Feb	Mar	Apr	May
Minimum	-3.06	-2.50	-2.83	-2.23	-2.45	-2.79	-3.12	-3.24
Maximum	2.44	2.58	2.15	2.31	1.92	2.23	2.04	2.95
Mean	0.00	0.00	0.00	0.00	0.00	0.00	0.00	0.00
SD.	1.00	1.00	1.00	1.00	1.00	1.00	1.00	1.00

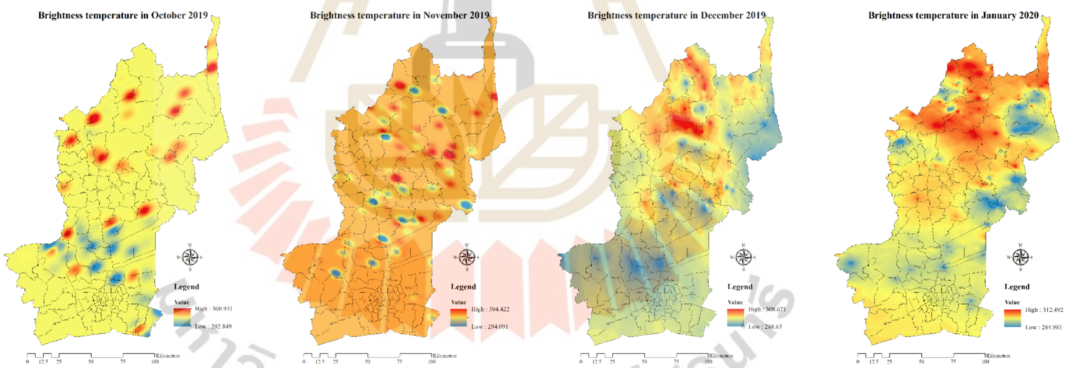

(a) (b) (c) (d)

Figure 5.9 Spatial distribution of monthly mean brightness temperature during October 2019 to May 2020: (a) October 2019, (b) November 2019, (c) December 2019, (d) January 2020, (e) February 2020, (f) March 2020, (g) April 2020, and (h) May 2020.

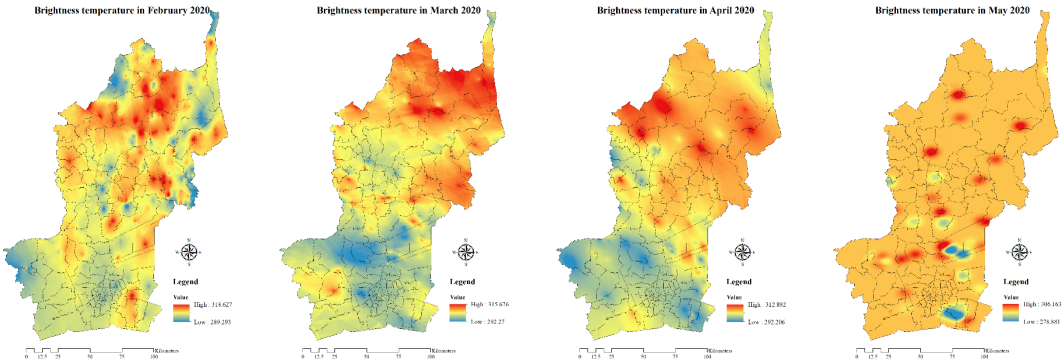

(e) (f) (g) (h)

Figure 5.9 (Continued).

Table 5.16 Descriptive statistic data of brightness temperature after normalization in the urban landscape.

Statistics	Winter season					Summer season		
	Oct	Nov	Dec	Jan	Feb	Mar	Apr	May
Minimum	-5.70	-6.37	-3.28	-2.42	-1.67	-1.91	-2.15	-6.05
Maximum	1.49	0.50	2.23	1.84	2.82	3.10	2.66	1.85
Mean	0.00	0.00	0.00	0.00	0.00	0.00	0.00	0.00
SD.	1.00	1.00	1.00	1.00	1.00	1.00	1.00	1.00

5.2.8 Fire radiative power

The spatial distribution of monthly mean fire radiative power in the rural and urban landscape, which were interpolated using the RBF method with the Spline with Tension and Eight Sector function, is displayed in Figure 5.10. Primary statistics data of normalized fire radiative power in rural and urban landscapes are summarized separately in Tables 5.17 and 5.18.

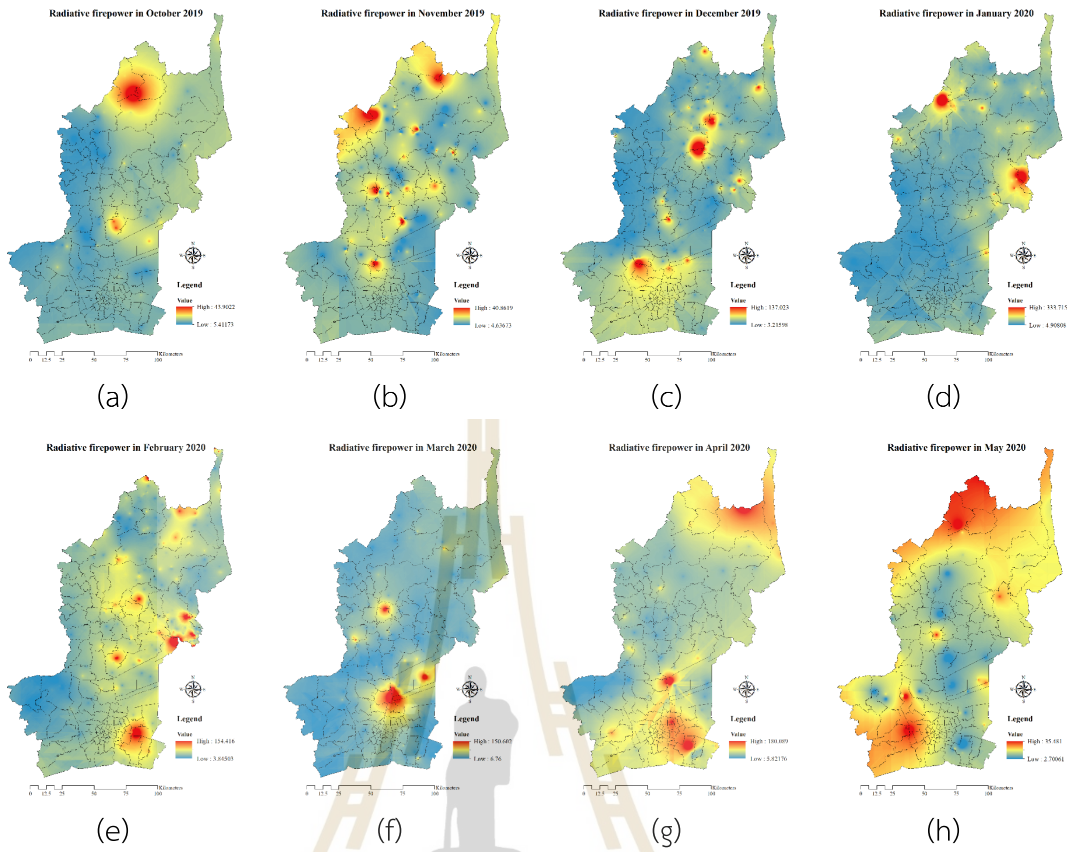

Figure 5.10 Spatial distribution of monthly mean fire radiative power during October 2019 to May 2020: (a) October 2019, (b) November 2019, (c) December 2019, (d) January 2020, (e) February 2020, (f) March 2020, (g) April 2020, and (h) May 2020.

Table 5.17 Descriptive statistic data of fire radiative power after normalization in rural landscape.

Statistics	Winter season					Summer season		
	Oct	Nov	Dec	Jan	Feb	Mar	Apr	May
Minimum	-1.26	-1.80	-2.83	-1.30	-1.50	-0.96	-1.20	-1.55
Maximum	3.50	3.15	2.15	3.51	3.86	3.98	3.07	3.22
Mean	0.00	0.00	0.00	0.00	0.00	0.00	0.00	0.00
SD.	1.00	1.00	1.00	1.00	1.00	1.00	1.00	1.00

Table 5.18 Descriptive statistic data of fire radiative power after normalization in the urban landscape.

Statistics	Winter season					Summer season		
	Oct	Nov	Dec	Jan	Feb	Mar	Apr	May
Minimum	-3.45	-2.13	-2.47	-2.42	-1.86	-1.34	-3.12	-1.78
Maximum	1.67	4.51	3.86	1.93	3.53	3.97	2.09	2.75
Mean	0.00	0.00	0.00	0.00	0.00	0.00	0.00	0.00
SD.	1.00	1.00	1.00	1.00	1.00	1.00	1.00	1.00

5.2.9 Fire hotspot

The spatial distribution of monthly fire hotspots in the rural and urban landscape, constructed using the Spatial join and field calculator function of the ArcMap software, is displayed in Figure 5.11. Primary statistics data of normalized fire hotspots in rural and urban landscapes are summarized separately in Tables 5.19 and 5.20.

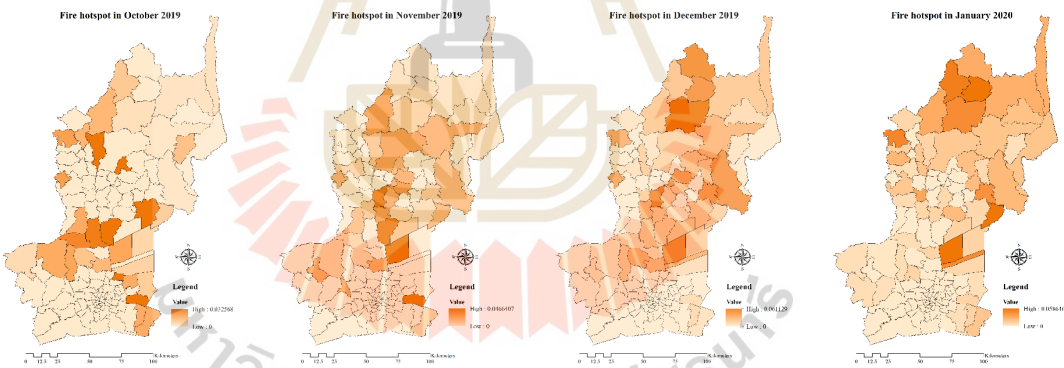

(a) (b) (c) (d)

Figure 5.11 Spatial distribution of monthly fire hotspot during October 2019 to May 2020: (a) October 2019, (b) November 2019, (c) December 2019, (d) January 2020, (e) February 2020, (f) March 2020, (g) April 2020, and (h) May 2020.

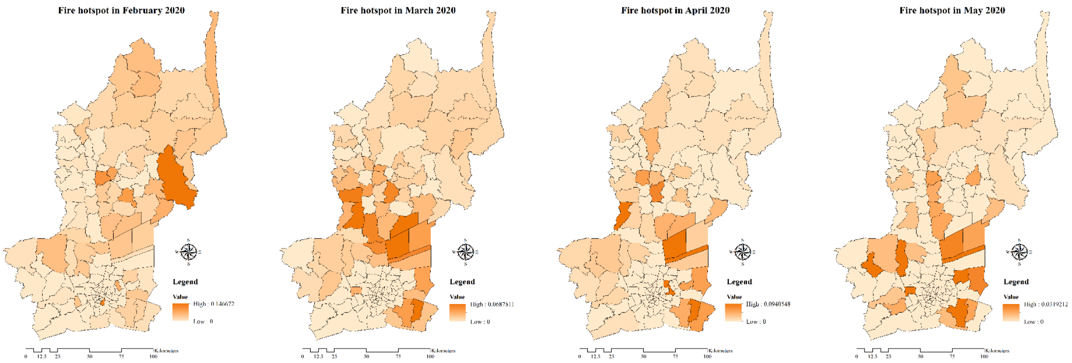

(e) (f) (g) (h)

Figure 5.11 (Continued).

Table 5.19 Descriptive statistic data of fire hotspots after normalization in rural landscape.

Statistics	Winter season					Summer season		
	Oct	Nov	Dec	Jan	Feb	Mar	Apr	May
Minimum	-0.55	-0.66	-1.00	-0.87	-0.72	-0.87	-0.50	-0.52
Maximum	4.20	4.14	3.22	3.25	5.62	3.93	4.29	4.15
Mean	0.00	0.00	0.00	0.00	0.00	0.00	0.00	0.00
SD.	1.00	1.00	1.00	1.00	1.00	1.00	1.00	1.00

Table 5.20 Descriptive statistic data of fire hotspots after normalization in the urban landscape.

Statistics	Winter season					Summer season		
	Oct	Nov	Dec	Jan	Feb	Mar	Apr	May
Minimum	-0.31	-0.20	-0.27	-0.37	-0.37	-0.33	-0.29	-0.36
Maximum	4.99	7.63	5.87	4.92	6.11	6.41	6.87	5.12
Mean	0.00	0.00	0.00	0.00	0.00	0.00	0.00	0.00
SD.	1.00	1.00	1.00	1.00	1.00	1.00	1.00	1.00

5.2.10 NDVI

The spatial distribution of monthly NDVI in the rural and urban landscape, constructed using the ArcMap tool's Raster Calculator function, is displayed in Figures 5.12(a) and 5.12(b). Primary statistics data of normalized NDVI in rural and urban landscapes are separately summarized in Tables 5.21 and 5.22, respectively.

5.2.11 BUI

The spatial distribution of monthly BUI in the rural and urban landscape, constructed using the ArcMap tool's Raster Calculator function, is displayed in Figures 5.12(c) and 5.12(d). Primary statistics data of normalized BUI in rural and urban landscapes are separately summarized in Tables 5.23 and 5.24.

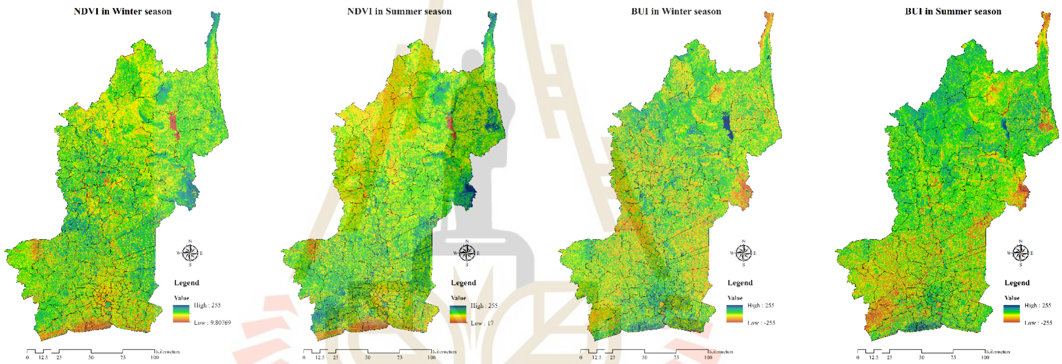

(a) (b) (c) (d)

Figure 5.12 Spatial distribution of mean NDVI and BUI during winter and summer season: (a) NDVI in the winter season, (b) NDVI in the summer season, (c) BUI in the winter season, (d) BUI in the summer season.

Table 5.21 Descriptive statistic data of NDVI after normalization in rural landscape.

Statistics	Winter season					Summer season		
	Oct	Nov	Dec	Jan	Feb	Mar	Apr	May
Minimum	-2.43	-2.43	-2.43	-2.43	-2.43	-2.27	-2.27	-2.27
Maximum	2.47	2.47	2.47	2.47	2.47	2.30	2.30	2.30
Mean	0.00	0.00	0.00	0.00	0.00	0.00	0.00	0.00
SD.	1.00	1.00	1.00	1.00	1.00	1.00	1.00	1.00

Table 5.22 Descriptive statistic data of NDVI after normalization in the urban landscape.

Statistics	Winter season					Summer season		
	Oct	Nov	Dec	Jan	Feb	Mar	Apr	May
Minimum	-2.45	-2.45	-2.45	-2.45	-2.45	-3.11	-3.11	-3.11
Maximum	2.40	2.40	2.40	2.40	2.40	2.11	2.11	2.11
Mean	0.00	0.00	0.00	0.00	0.00	0.00	0.00	0.00
SD.	1.00	1.00	1.00	1.00	1.00	1.00	1.00	1.00

Table 5.23 Descriptive statistic data of BUI after normalization in rural landscape.

Statistics	Winter season					Summer season		
	Oct	Nov	Dec	Jan	Feb	Mar	Apr	May
Minimum	-2.44	-2.44	-2.44	-2.44	-2.44	-2.45	-2.45	-2.45
Maximum	2.02	2.02	2.02	2.02	2.02	2.01	2.01	2.01
Mean	0.00	0.00	0.00	0.00	0.00	0.00	0.00	0.00
SD.	1.00	1.00	1.00	1.00	1.00	1.00	1.00	1.00

Table 5.24 Descriptive statistic data of BUI after normalization in the urban landscape.

Statistics	Winter season					Summer season		
	Oct	Nov	Dec	Jan	Feb	Mar	Apr	May
Minimum	-2.26	-2.26	-2.26	-2.26	-2.26	-2.77	-2.77	-2.77
Maximum	2.21	2.21	2.21	2.21	2.21	2.40	2.40	2.40
Mean	0.00	0.00	0.00	0.00	0.00	0.00	0.00	0.00
SD.	1.00	1.00	1.00	1.00	1.00	1.00	1.00	1.00

5.2.12 Road density

The spatial distribution of monthly road density in the rural and urban landscape, constructed using Calculate geometry and field calculator of ArcMap tool, is displayed in Figure 5.13(a). Primary statistics data of normalized road density in rural and urban landscapes are separately summarized in Tables 5.25 and 5.26, respectively.

5.2.13 Factory density

The spatial distribution of monthly factory density in the rural and urban landscape, constructed using Spatial join and field calculator of ArcMap tool, is displayed in Figure 5.13(b). Primary statistics data of normalized factory density in rural and urban landscapes are separately summarized in Tables 5.25 and 5.26, respectively.

5.2.14 Elevation

The spatial distribution of monthly elevation in the rural and urban landscape, constructed using Fill (Spatial analysis) from SRTM under ArcMap software, is displayed in Figure 5.13(c). Primary statistics data of normalized elevation in rural and urban landscapes are separately summarized in Tables 5.25 and 5.26, respectively.

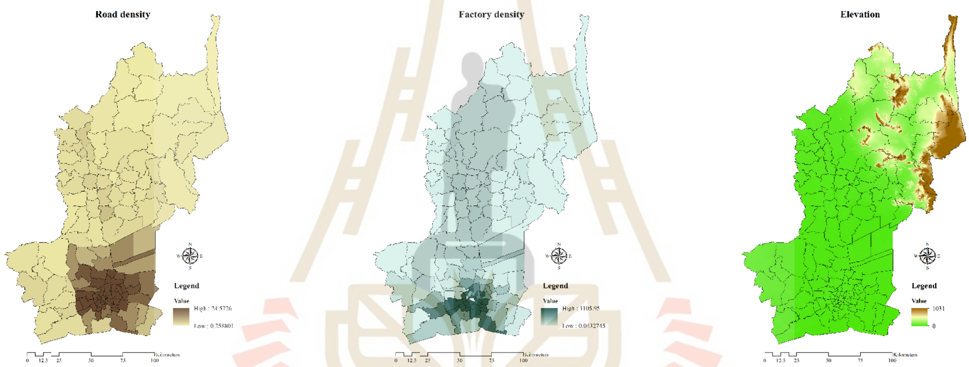

(a) (b) (c)

Figure 5.13 Spatial distribution of static data (a) road density, (b) factory density, and (c) elevation.

Table 5.25 Descriptive statistic data of road density, factory density, and elevation after normalization in rural landscape.

Statistics	Road density	Factory density	Elevation
Minimum	-0.82	-0.77	-0.54
Maximum	4.52	4.45	5.16
Mean	0.00	0.00	0.00
SD.	1.00	1.00	1.00

Table 5.26 Descriptive statistic data of road density, factory density, and elevation after normalization in the urban landscape.

Statistics	Road density	Factory density	Elevation
Minimum	-1.67	-0.79	-1.67
Maximum	2.21	3.21	3.29
Mean	0.00	0.00	0.00
SD.	1.00	1.00	1.00

5.2.15 Population density

The spatial distribution of monthly population density in the rural and urban landscape, extracted from population data at the district level and constructed using the field calculator function of the ArcMap tool, is displayed in Figure 5.14(a). Primary statistics data of normalized population density in rural and urban landscapes are separately summarized in Tables 5.27 and 5.28.

5.2.16 GPP

The spatial distribution of monthly GPP in the rural and urban landscape, extracted from district-level population data and constructed using the field calculator function of the ArcMap tool, is displayed in Figure 5.14(b). Primary statistics data of normalized GPP in rural and urban landscapes are separately summarized in Tables 5.27 and 5.28.

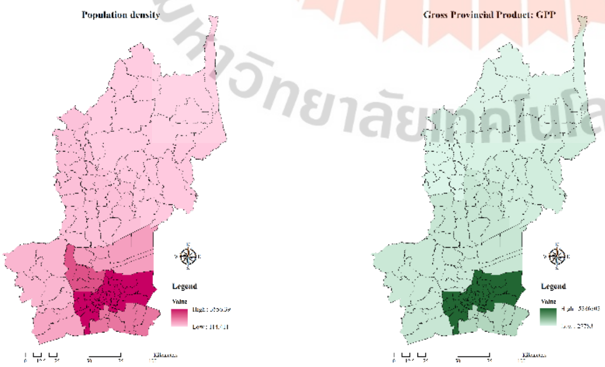

(a) (b)

Figure 5.14 Spatial distribution of static data (a) population density and (b) GPP.

Table 5.27 Descriptive statistic data of population density and GPP after normalization in rural landscape.

Statistics	Population density	GPP
Minimum	-0.95	-1.35
Maximum	2.51	1.13
Mean	0.00	0.00
SD.	1.00	1.00

Table 5.28 Descriptive statistic data of population density and GPP after normalization in urban landscape.

Statistics	Population density	GPP
Minimum	-2.06	-1.56
Maximum	0.63	0.66
Mean	0.00	0.00
SD.	1.00	1.00

5.3 Significant spatiotemporal factors on PM10 concentration in rural landscape

All normalized dependent and independent variables in rural landscape in the winter season (October 2019 to February 2020) and summer season (March 2020 to May 2020) were applied to identify significant spatiotemporal factors using multicollinearity test with the VIF values and the OLS regression analysis. The result of the multicollinearity test and the OLS regression analysis, including the derived equation, its coefficient, and its performance, is separately described and discussed by month and season.

If the VIF value of any factor is above 7.5, such a factor is removed from the model to avoid redundancy among explanatory variables (Section 3.2). The results of the multicollinearity test performed in the SPSS statistical software are reported in Tables 5.29.

Table 5.29 Results of multicollinearity test of explanatory variables on PM10 concentration.

No.	Variable	The VIF value							
		Winter season					Summer season		
		Oct 2019	Nov 2019	Dec 2019	Jan 2020	Feb 2020	Mar 2020	Apr 2020	May 2020
1	RH	5.50	4.84	22.76	44.83	22.93	22.23	38.47	15.69
2	TEMP	2.22	2.95	3.35	2.64	1.83	4.16	23.13	6.06
3	WS	4.54	3.81	4.01	16.13	5.85	8.43	9.10	8.12
4	P	2.65	6.46	7.24	63.79	8.65	5.42	2.42	4.96
5	VIS	3.05	3.90	3.66	9.76	5.03	6.62	3.93	4.51
6	AOD	4.61	2.49	3.48	6.35	2.63	2.15	3.99	2.47
7	NDVI	20.14	24.17	22.76	18.97	18.65	18.64	18.70	22.42
8	BUI	25.74	29.89	24.22	24.66	21.81	16.76	15.52	17.86
9	RD	12.18	13.25	12.05	11.97	10.92	11.41	15.53	15.58
10	FD	5.63	5.60	6.94	6.61	6.80	4.77	5.87	4.96
11	BT	3.47	3.00	3.07	2.87	1.63	7.33	4.32	1.30
12	FRP	1.92	2.76	2.94	3.34	3.22	2.70	3.62	4.04
13	FH	1.49	1.63	1.73	1.65	1.54	2.10	1.79	2.05
14	ELEV	3.50	3.54	4.74	5.58	4.22	4.14	5.73	3.98
15	POP	11.58	10.21	12.49	13.39	12.44	10.53	13.35	11.23
16	GPP	5.66	4.50	4.36	4.72	5.02	5.21	5.18	4.62
Total variables		12	12	11	8	10	10	9	10

As a result, the VIF values show that NDVI, BUI, road density, and population density are redundant with PM10 concentration. In addition, other redundant variables are cut each month differently. Hence, persistent independent variables with a VIF value less than 7.5 were applied for OLS regression analysis. The result of the OLS regression analysis in each month of each season are described separately and discussed below, particularly model performance and the relationship between PM10 concentration and their factors.

5.3.1 October 2019 in the winter season

The results of the OLS regression analysis are reported in Table 5.30. The model performance showed that AICc is 140.11. The multiple R-squared is 0.67, and the adjusted R-squared is 0.59.

Table 5.30 Summary of the OLS regression analysis between PM10 concentration and significant factors in October 2019.

No.	Factor	Coefficient	Std. Error	Probability	VIF
	Intercept	-0.00	0.08	1.00	--------
1	RH	0.17	0.16	0.31	3.82
2	TEMP	0.38	0.12	0.00*	1.96
3	WS	0.41	0.16	0.01*	3.67
4	P	0.19	0.13	0.15	2.35
5	VIS	-0.66	0.14	0.00*	2.61
6	AOD	-0.04	0.15	0.81	3.13
7	FD	0.05	0.13	0.72	2.47
8	BT	0.20	0.14	0.18	2.91
9	FRP	-0.20	0.11	0.08	1.73
10	FH	-0.11	0.10	0.29	1.39
11	ELEV	0.22	0.15	0.15	3.23
12	GPP	0.06	0.19	0.76	5.03

Note: an asterisk (*) at the significance level of 0.01.

As a result of OLS regression analysis in Table 5.30, if the probability at the confident level of 99% is not considered (ignored), the relationship between PM10 concentration and selected factors by VIF value can be explained into two types: positive and negative. The positive relationship between PM10 concentration and their factors occurred with relative humidity, temperature, wind speed, pressure, factory density, brightness temperature, elevation, and GPP. This finding indicates that if these variables increase, the PM10 concentration increase. In contrast, the negative relationship between PM10 concentration and their factors is found with visibility, MODIS AOD, fire radiative power, and fire hotspot. So, with the increase of these factors, the PM10 concentration decrease.

When the probability at the confident level of 99% is considered, the significant factors on PM10 concentration in October 2019 are temperature, wind speed, and visibility.

5.3.2 November 2019 in the winter season

The results of the OLS regression analysis are reported in Table 5.31. The model performance showed that AICc is 150.90. The multiple R-squared is 0.60, while the adjusted R-squared is 0.50.

Table 5.31 Summary of the OLS regression analysis between PM10 concentration and significant factors in November 2019.

No.	Factor	Coefficient	Std. Error	Probability	VIF
	Intercept	0.00	0.09	1.00	--------
1	RH	-0.21	0.19	0.29	4.52
2	TEMP	0.13	0.15	0.39	2.77
3	WS	0.88	0.15	0.00*	2.71
4	P	-0.13	0.22	0.56	5.87
5	VIS	-0.63	0.17	0.00*	3.39
6	AOD	0.24	0.12	0.05*	1.69
7	FD	-0.20	0.12	0.10	1.72
8	BT	-0.02	0.14	0.90	2.42
9	FRP	0.07	0.14	0.61	2.44
10	FH	-0.03	0.11	0.76	1.41
11	ELEV	-0.10	0.16	0.54	3.02
12	GPP	-0.24	0.18	0.20	3.99

Note: an asterisk (*) at the significance level of 0.01.

As a result of OLS regression analysis in Table 5.31, if the probability at the confident level of 99% is not considered (ignored), the relationship between PM10 concentration and selected factors by VIF value can be explained into two types: positive and negative. The positive relationship between PM10 concentration and their factors occurred with temperature, wind speed, MODIS AOD, and fire radiative power. This finding indicates that if these variables increase, the PM10 concentration increase. In contrast, the negative relationship between PM10 concentration and their factors is found with relative humidity, pressure, visibility, factory density, brightness temperature, fire hotspot, elevation, and GPP. So, with the increase of these factors, the PM10 concentration decrease.

When the probability at the confident level of 99% is considered, the significant factors on PM10 concentration in November 2019 are wind speed, visibility, and MODIS AOD.

5.3.3 December 2019 in the winter season

The results of the OLS regression analysis are reported in Table 5.32. The model performance showed that AICc is 166.42. The multiple R-squared is 0.46, while the adjusted R-squared is 0.33.

Table 5.32 Summary of the OLS regression analysis between PM10 concentration and significant factors in December 2019.

No.	Variable	Coefficient	Std. Error	Probability	VIF
	Intercept	0.00	0.11	1.00	--------
1	TEMP	0.34	0.16	0.04*	2.37
2	WS	0.37	0.18	0.05*	2.84
3	P	-0.03	0.21	0.88	3.99
4	VIS	-0.41	0.19	0.03*	3.13
5	AOD	-0.09	0.16	0.57	2.33
6	FD	0.07	0.14	0.62	1.80
7	BT	0.22	0.16	0.17	2.26
8	FRP	0.29	0.16	0.07	2.18
9	FH	-0.19	0.13	0.16	1.51
10	ELEV	0.28	0.21	0.19	3.87
11	GPP	0.04	0.18	0.84	2.86

Note: an asterisk (*) at the significance level of 0.01.

As a result of OLS regression analysis in Table 5.32, if the probability at the confident level of 99% is not considered (ignored), the relationship between PM10 concentration and selected factors by VIF value can be explained into two types: positive and negative. The positive relationship between PM10 concentration and their factors occurred with temperature, wind speed, factory density, brightness temperature, fire radiative power, elevation, and GPP. This finding indicates that if these variables increase, the PM10 concentration increase. In contrast, the negative relationship between PM10 concentration and their factors are found with pressure, visibility, MODIS AOD, and fire hotspot. So, with the increase of these factors, the PM10 concentration decrease.

When the probability at the confident level of 99% is considered, the significant factors on PM10 concentration in December 2019 are temperature, wind speed, and visibility.

5.3.4 January 2020 in the winter season

The results of the OLS regression analysis are reported in Table 5.33. The model performance showed that AICc is 178.47. The multiple R-squared is 0.26, while the adjusted R-squared is 0.13.

Table 5.33 Summary of the OLS regression analysis between PM10 concentration and significant factors in January 2020.

No.	Factor	Coefficient	Std. Error	Probability	VIF
	Intercept	0.00	0.12	1.00	--------
1	TEMP	0.36	0.17	0.04*	2.04
2	AOD	-0.36	0.16	0.02*	1.82
3	FD	-0.13	0.23	0.48	1.87
4	BT	0.24	0.15	0.08	1.52
5	FRP	0.26	0.20	0.22	2.81
6	FH	-0.23	0.15	0.06	1.56
7	ELEV	-0.20	0.20	0.41	2.75
8	GPP	-0.16	0.23	0.32	3.53

Note: an asterisk (*) at the significance level of 0.01.

As a result of OLS regression analysis in Table 5.33, if the probability at the confident level of 99% is not considered (ignored), the relationship between PM10 concentration and selected factors by VIF value can be explained into two types: positive and negative. The positive relationship between PM10 concentration and their factors occurred with temperature, brightness temperature, and fire radiative power. This finding indicates that if these variables increase, the PM10 concentration increase. In contrast, the negative relationship between PM10 concentration and their factors is found with MODIS AOD, factory density, fire hotspot, elevation, and GPP. So, with the increase of these factors, the PM10 concentration decrease.

When the probability at the confident level of 99% is considered, the significant factors on PM10 concentration in January 2020 are temperature and MODIS AOD.

5.3.5 February 2020 in the winter season

The results of the OLS regression analysis are reported in Table 5.34. The model performance showed that AICc is 159.75. The multiple R-squared is 0.49, while the adjusted R-squared is 0.38.

Table 5.34 Summary of the OLS regression analysis between PM10 concentration and significant factors in February 2020.

No.	Factor	Coefficient	Std. Error	Probability	VIF
	Intercept	0.00	0.10	1.00	--------
1	TEMP	-0.04	0.13	0.75	1.66
2	WS	0.43	0.21	0.04*	4.15
3	VIS	-0.37	0.21	0.08	4.07
4	AOD	0.08	0.15	0.57	2.05
5	FD	-0.09	0.16	0.60	2.51
6	BT	0.19	0.11	0.10	1.24
7	FRP	0.47	0.16	0.00*	2.34
8	FH	-0.07	0.12	0.57	1.42
9	ELEV	-0.05	0.17	0.79	2.77
10	GPP	-0.19	0.16	0.25	2.57

Note: an asterisk (*) at the significance level of 0.01.

As a result of OLS regression analysis in Table 5.34, if the probability at the confident level of 99% is not considered (ignored), the relationship between PM10 concentration and selected factors by VIF value can be explained into two types: positive and negative. The positive relationship between PM10 concentration and their factors occurred with wind speed, MODIS AOD, brightness temperature, and fire radiative power. This finding indicates that if these variables increase, the PM10 concentration increase. In contrast, the negative relationship between PM10 concentration and their factors is found with temperature, visibility, factory density, fire hotspot, elevation, and GPP. So, with the increase of these factors, the PM10 concentration decrease.

When the probability at the confident level of 99% is considered, the significant factors on PM10 concentration in February 2020 are wind speed and fire radiative power.

5.3.6 March 2020 in the summer season

The results of the OLS regression analysis are reported in Table 5.35. The model performance showed that AICc is 157.49. The multiple R-squared is 0.53, while the adjusted R-squared is 0.43.

Table 5.35 Summary of the OLS regression analysis between PM10 concentration and significant factors in March 2020.

No.	Factor	Coefficient	Std. Error	Probability	VIF
	Intercept	-0.00	0.10	1.00	--------
1	TEMP	-0.58	0.18	0.00*	3.19
2	P	-0.26	0.17	0.13	2.88
3	VIS	-0.05	0.24	0.82	5.87
4	AOD	0.34	0.14	0.02*	1.92
5	FD	0.50	0.16	0.00*	2.57
6	BT	0.14	0.20	0.48	3.92
7	FRP	-0.17	0.14	0.25	2.06
8	FH	-0.16	0.14	0.25	1.92
9	ELEV	-0.18	0.17	0.28	2.80
10	GPP	0.14	0.17	0.40	2.93

Note: an asterisk (*) at the significance level of 0.01.

As a result of OLS regression analysis in Table 5.35, if the probability at the confident level of 99% is not considered (ignored), the relationship between PM10 concentration and selected factors by VIF value can be explained into two types: positive and negative. The positive relationship between PM10 concentration and their factors occurred with MODIS AOD, NDVI, BUI, factory density, brightness temperature and GPP. This finding indicates that if these variables increase, the PM10 concentration increase. In contrast, the negative relationship between PM10 concentration and their factors is found with temperature, wind speed, pressure, visibility, fire radiative power, fire hotspot, and elevation. So, with the increase of these factors, the PM10 concentration decrease.

When the probability at the confident level of 99% is considered, the significant factors on PM10 concentration in March 2020 are temperature, MODIS AOD, and factory density.

5.3.7 April 2020 in the summer season

The results of the OLS regression analysis are reported in Table 5.36. The model performance showed that AICc is 160.62. The multiple R-squared is 0.45, while the adjusted R-squared is 0.35.

Table 5.36 Summary of the OLS regression analysis between PM10 concentration and significant factors in April 2020.

No.	Factor	Coefficient	Std. Error	Probability	VIF
	Intercept	-0.00	0.10	1.00	--------
1	P	0.07	0.13	0.58	1.60
2	VIS	0.02	0.15	0.91	2.10
3	AOD	0.14	0.15	0.35	2.14
4	FD	0.15	0.14	0.23	1.85
5	BT	0.65	0.14	0.00*	1.75
6	FRP	-0.22	0.14	0.13	1.78
7	FH	-0.12	0.12	0.34	1.32
8	ELEV	-0.05	0.18	0.79	3.07
9	GPP	0.15	0.12	0.24	1.37

Note: an asterisk (*) at the significance level of 0.01.

As a result of OLS regression analysis in Table 5.36, if the probability at the confident level of 99% is not considered (ignored), the relationship between PM10 concentration and selected factors by VIF value can be explained into two types: positive and negative. The positive relationship between PM10 concentration and their factors occurred with pressure, visibility MODIS AOD, factory density, brightness temperature, and GPP. This finding indicates that if these variables increase, the PM10 concentration increase. In contrast, the negative relationship between PM10 concentration and their factors is found with fire radiative power, fire hotspot, and elevation. So, with the increase of these factors, the PM10 concentration decrease.

When the probability at the confident level of 99% is considered, the significant factor on PM10 concentration in April 2020 is brightness temperature.

5.3.8 May 2020 in the summer season

The results of the OLS regression analysis are reported in Table 5.37. The model performance showed AICc is 187.73. The multiple R-squared is 0.18, while the adjusted R-squared is 0.02.

Table 5.37 Summary of the OLS regression analysis between PM10 concentration and significant factors in May 2020.

No.	Factor	Coefficient	Std. Error	Probability	VIF
	Intercept	-0.00	0.13	1.00	--------
1	TEMP	0.05	0.25	0.85	3.82
2	P	-0.05	0.22	0.82	2.91
3	VIS	-0.39	0.22	0.04*	3.02
4	AOD	0.09	0.14	0.53	1.18
5	FD	0.30	0.16	0.06	1.50
6	BT	0.19	0.14	0.18	1.10
7	FRP	0.01	0.18	0.94	1.99
8	FH	0.01	0.15	0.97	1.34
9	ELEV	0.21	0.21	0.32	2.57
10	GPP	0.42	0.26	0.11	3.94

Note: an asterisk (*) at the significance level of 0.01.

As a result of OLS regression analysis in Table 5.37, if the probability at the confident level of 99% is not considered (ignored), the relationship between PM10 concentration and selected factors by VIF value can be explained into two types: positive and negative. The positive relationship between PM10 concentration and their factors occurred with temperature, MODIS AOD, factory density, brightness temperature, fire radiative power, fire hotspot, elevation, and GPP. This finding indicates that if these variables increase, the PM10 concentration increase. In contrast, the negative relationship between PM10 concentration and their factors is found with pressure and visibility. So, with the increase of these factors, the PM10 concentration decrease.

When the probability at the confident level of 99% is considered, the significant factor on PM10 concentration in May 2020 is visibility.

Referring to significant spatiotemporal factors on PM10 concentration reported in Tables 5.30 to 5.37, the significant factors on PM10 concentration in rural and urban landscapes in winter and summer seasons can be summarized with frequency in Tables 5.38 and 5.39.

Table 5.38 Frequency of significant factors on PM10 concentration in the winter season.

No.	Significant factor	October 2019	November 2019	December 2019	January 2020	February 2020	Frequency
1	WS	Yes	Yes	Yes		Yes	4 of 5
2	TEMP	Yes		Yes	Yes		3 of 5
3	VIS	Yes	Yes	Yes			3 of 5
4	AOD		Yes		Yes		2 of 5
5	FRP					Yes	1 of 5

Table 5.39 Frequency of significant factors on PM10 concentration in the summer season.

No.	Significant factor	March 2020	April 2020	May 2020	Frequency
1	FD	Yes			2 of 3
2	TEMP	Yes			1 of 3
3	AOD	Yes			1 of 3
4	BT		Yes		1 of 3
5	VIS			Yes	1 of 3

As reported in Tables 5.38 and 5.39, the number of the significant factors on PM10 concentration in winter and summer are five and five factors with their varieties. Three common factors on PM10 concentration, namely temperature, visibility, and MODIS AOD, are identified in both seasons. Two significant factors on PM10 concentration are only found in the winter season, including wind speed and fire radiative power. On the contrary, two significant factors on PM10 concentration, factory density and brightness temperature, are only found in the summer season.

The significant factors on PM10 concentration in this study are similar to the previous study by Harnkijroong and Panich (2013). They reported that PM10 concentration at the roadside of Bangkok is most relevant to temperature, followed by wind speed. And they also found that rainfall did not influence PM10 concentration.

Furthermore, Unal, Toros, Deniz, and Incecik (2011) suggested that PM10 concentration were associated with wind speed, and high PM10 concentration were found in high pressure and low wind speed. Likewise, the most significant meteorological factors, including planetary boundary layer height, temperature, wind speed, and precipitation influenced by the seasonal dynamics of PM10 concentration, were reported by Czernecki et al. (2017).

In addition, many studies reported the relationship between MODIS AOD and PM10 concentration (Ferrero et al., 2019; Grgurić et al., 2014; Kanabkaew, 2013; Syafrijon, Marzuki, Emriadi, and Pratama, 2018). Especially, Ferrero et al. (2019) found a high relationship and developed high accuracy algorithm to predict ground PM concentration based on AOD mixing height and wind speed. At the same time, Kanabkaew (2013) reported that the relationship between AOD and hourly PM improved accuracy when corrected with meteorological factors, including relative humidity and temperature data.

5.4 Significant spatiotemporal factors on PM2.5 concentration in the urban landscape

Like PM10 concentration in the rural landscape, all normalized dependent and independent variables in the urban landscape in the winter and summer season (October 2019 to May 2020) were applied to identify significant spatiotemporal factors using the multicollinearity test and the OLS regression analysis. The multicollinearity test and the OLS regression analysis, including the derived equation and its coefficient and performance, are separately described and discussed by month and season.

If the VIF value of any factor is above 7.5, such a factor is removed from the model to avoid redundancy among explanatory variables (Section 3.2). The results of the multicollinearity test performed in the SPSS statistical software are reported in Table 5.40.

Table 5.40 Results of multicollinearity test of explanatory variables on PM2.5 concentration.

No.	Variable	The VIF value							
		Winter season					Summer season		
		Oct 2019	Nov 2019	Dec 2019	Jan 2020	Feb 2020	Mar 2020	Apr 2020	May 2020
1	RH	11.88	6.51	15.56	25.58	2.50	20.80	16.97	41.35
2	TEMP	11.69	9.87	28.18	7.19	9.30	5.47	13.14	9.45
3	WS	4.03	4.81	4.83	4.94	3.38	6.10	4.46	4.24
4	P	7.11	8.70	16.09	26.68	6.10	17.24	16.03	38.35
5	VIS	2.11	1.86	6.65	4.26	1.46	2.19	3.62	6.06
6	AOD	2.41	2.43	8.33	5.60	2.07	1.50	2.82	2.47
7	NDVI	42.06	48.43	75.04	73.29	48.76	24.12	32.56	27.57
8	BUI	76.13	79.61	105.99	110.25	88.86	38.65	49.40	42.13
9	RD	20.30	15.60	16.47	16.43	17.19	14.29	16.94	13.31
10	FD	2.88	2.59	2.63	4.12	2.88	2.51	3.55	2.62
11	BT	2.39	1.56	13.88	8.11	3.55	3.48	2.68	2.96
12	FRP	4.13	4.28	7.87	5.12	3.55	4.50	6.25	5.90
13	FH	2.07	1.25	2.42	2.20	1.18	2.10	1.45	1.91
14	ELEV	5.89	5.29	5.73	5.49	5.83	5.46	6.19	5.11
15	POP	44.96	38.81	46.98	36.86	37.13	28.17	25.59	30.01
16	GPP	28.92	30.98	36.30	27.77	25.59	19.19	20.42	18.67
Total variables		9	9	5	8	10	9	8	8

As a result, the VIF value shows that NDVI, BUI, road density, population density, and GPP are redundant for PM2.5 concentration models. In addition, other redundant variables are cut each month differently. Hence, persist independent variables with a VIF value less than 7.5 are applied for OLS regression analysis. The result of the OLS regression analysis in each month of each season are described separately and discussed below, particularly model performance and the relationship between PM2.5 concentration and their factors.

5.4.1 October 2019 in the winter season

The results of the OLS regression analysis are reported in Table 5.41. The model performance showed that AICc is 114.36. The multiple R-squared is 0.80, and the adjusted R-squared is 0.77.

Table 5.41 Summary of the OLS regression analysis between PM2.5 concentration and significant factors in October 2019.

No.	Factor	Coefficient	Std Error	Probability	VIF
	Intercept	0.00	0.06	1.00	--------
1	WS	0.27	0.09	0.00*	2.33
2	P	0.20	0.08	0.00*	1.81
3	VIS	0.23	0.08	0.04*	1.95
4	AOD	0.67	0.07	0.00*	1.60
5	FD	0.13	0.08	0.06	1.96
6	BT	-0.17	0.08	0.01*	1.98
7	FRP	-0.20	0.09	0.02*	2.30
8	FH	-0.18	0.08	0.00*	1.92
9	ELEV	0.42	0.08	0.00*	2.03

Note: an asterisk (*) at the significance level of 0.01.

As a result of OLS regression analysis in Table 5.41, if the probability at the confident level of 99% is not considered (ignored), the relationship between PM2.5 concentration and selected factors by VIF value can be explained into two types: positive and negative. The positive relationship between PM2.5 concentration and their factors occurred with wind speed, pressure, visibility, MODIS AOD, factory density, and elevation. This finding indicates that if these variables increase, the PM2.5 concentration increase. In contrast, the negative relationship between PM2.5

concentration and their factors is found with brightness temperature, fire radiative power, and fire hotspot. So, with the increase of these factors, the PM2.5 concentration decrease.

When the probability at the confident level of 99% is considered, the significant factors on PM2.5 concentration in October 2019 are wind speed, pressure, visibility, MODIS AOD, brightness temperature, fire radiative power, fire hotspot, and elevation.

5.4.2 November 2019 in the winter season

The results of the OLS regression analysis are reported in Table 5.42. The model performance showed that AICc is 133.92. The multiple R-squared is 0.80, while the adjusted R-squared is 0.75.

Table 5.42 Summary of the OLS regression analysis between PM2.5 concentration and significant factors in November 2019.

No.	Factor	Coefficient	Std. Error	Probability	VIF
	Intercept	0.00	0.08	1.00	--------
1	RH	0.21	0.16	0.19	3.45
2	WS	-0.23	0.16	0.16	3.77
3	VIS	0.31	0.10	0.00*	1.52
4	AOD	0.21	0.11	0.07	1.76
5	FD	0.18	0.10	0.08	1.36
6	BT	0.09	0.10	0.39	1.49
7	FRP	0.44	0.12	0.00*	1.89
8	FH	0.08	0.09	0.38	1.20
9	ELEV	-0.08	0.16	0.61	3.46

Note: an asterisk (*) at the significance level of 0.01.

As a result of OLS regression analysis in Table 5.42, if the probability at the confident level of 99% is not considered (ignored), the relationship between PM2.5 concentration and selected factors by VIF value can be explained into two types: positive and negative. The positive relationship between PM2.5 concentration and their factors occurred with relative humidity, visibility, MODIS AOD, factory density, brightness temperature, fire radiative power, and fire hotspot. This finding indicates that if these variables increase, the PM2.5 concentration increase. In contrast, the negative relationship between PM2.5 concentration and their factors is found with wind speed and elevation. So, with the increase of these factors, the PM2.5 concentration decrease.

When the probability at the confident level of 99% is considered, the significant factors on PM2.5 concentration in November 2019 are visibility and fire radiative power.

5.4.3 December 2019 in the winter season

The results of the OLS regression analysis are reported in Table 5.43. The model performance showed that AICc is 190.87. The multiple R-squared is 0.32, while the adjusted R-squared is 0.27.

Table 5.43 Summary of the OLS regression analysis between PM2.5 concentration and significant factors in December 2019.

No.	Factor	Coefficient	Std. Error	Probability	VIF
	Intercept	-0.00	0.10	1.00	--------
1	WS	-0.43	0.14	0.00*	1.86
2	VIS	0.40	0.16	0.01*	2.41
3	FD	-0.21	0.12	0.09	1.45
4	FH	0.08	0.13	0.53	1.53
5	ELEV	-0.05	0.17	0.78	2.67

Note: an asterisk (*) at the significance level of 0.01.

As a result of OLS regression analysis in Table 5.43, if the probability at the confident level of 99% is not considered (ignored), the relationship between PM2.5 concentration and selected factors by VIF value can be explained into two types: positive and negative. The positive relationship between PM2.5 concentration and their factors occurred with visibility and fire hotspots. This finding indicates that if these variables increase, the PM2.5 concentration increase. In contrast, the negative relationship between PM2.5 concentration and their factors is found with wind speed, factory density, and elevation. So, with the increase of these factors, the PM2.5 concentration decrease.

When the probability at the confident level of 99% is considered, the significant factors on PM2.5 concentration in December 2019 are wind speed and visibility.

5.4.4 January 2020 in the winter season

The results of the OLS regression analysis are reported in Table 5.44. The model performance showed that AICc is 194.85. The multiple R-squared is 0.36, while the adjusted R-squared is 0.28.

Table 5.44 Summary of the OLS regression analysis between PM2.5 concentration and significant factors in January 2020.

No.	Factor	Coefficient	Std. Error	Probability	VIF
	Intercept	-0.00	0.10	1.00	--------
1	TEMP	-0.39	0.15	0.01*	2.20
2	WS	0.17	0.15	0.25	2.23
3	VIS	0.30	0.15	0.05*	2.16
4	AOD	-0.46	0.14	0.00*	1.99
5	FD	-0.12	0.14	0.39	1.91
6	FRP	-0.08	0.13	0.53	1.63
7	FH	0.30	0.12	0.02*	1.50
8	ELEV	0.48	0.15	0.00*	2.21

Note: an asterisk (*) at the significance level of 0.01.

As a result of OLS regression analysis in Table 5.44, if the probability at the confident level of 99% is not considered (ignored), the relationship between PM2.5 concentration and selected factors by VIF value can be explained into two types: positive and negative. The positive relationship between PM2.5 concentration and their factors occurred with wind speed, visibility, fire hotspot, and elevation. This finding indicates that if these variables increase, the PM2.5 concentration increase. In contrast, the negative relationship between PM2.5 concentration and their factors is found with temperature, MODIS AOD, factory density, and fire radiative power. So, with the increase of these factors, the PM2.5 concentration decrease.

When the probability at the confident level of 99% is considered, the significant factors for PM2.5 concentration in January 2020 are temperature, visibility, MODIS AOD, fire hotspot, and elevation.

5.4.5 February 2020 in the winter season

The results of the OLS regression analysis are reported in Table 5.45. The model performance showed that AICc is 137.64. The multiple R-squared is 0.73, while the adjusted R-squared is 0.69.

Table 5.45 Summary of the OLS regression analysis between PM2.5 concentration and significant factors in February 2020.

No.	Factor	Coefficient	Std. Error	Probability	VIF
	Intercept	-0.00	0.07	1.00	--------
1	RH	-0.52	0.09	0.00*	1.65
2	WS	0.37	0.10	0.00*	2.41
3	P	0.30	0.11	0.01*	2.86
4	VIS	0.05	0.07	0.51	1.27
5	AOD	-0.16	0.09	0.08	1.84
6	FD	-0.07	0.09	0.45	1.69
7	BT	0.22	0.12	0.06	3.05
8	FRP	-0.64	0.11	0.00*	2.77
9	FH	-0.06	0.07	0.39	1.13
10	ELEV	0.44	0.12	0.00*	3.40

Note: an asterisk (*) at the significance level of 0.01.

As a result of OLS regression analysis in Table 5.45, if the probability at the confident level of 99% is not considered (ignored), the relationship between PM2.5 concentration and selected factors by VIF value can be explained into two types: positive and negative. The positive relationship between PM2.5 concentration and their factors occurred with wind speed, pressure, visibility, brightness temperature, and elevation. This finding indicates that if these variables increase, the PM2.5 concentration increase. In contrast, the negative relationship between PM2.5 concentration and their factors is found with relative humidity, MODIS AOD, factory density, fire radiative power, and fire hotspot. So, with the increase of these factors, the PM2.5 concentration decrease.

When the probability at the confident level of 99% is considered, the significant factors on PM2.5 concentration in February 2020 are relative humidity, wind speed, pressure, fire radiative power, and elevation.

5.4.6 March 2020 in the summer season

The results of the OLS regression analysis are reported in Table 5.46. The model performance showed that AICc is 192.42. The multiple R-squared is 0.40, while the adjusted R-squared is 0.32.

Table 5.46 Summary of the OLS regression analysis between PM2.5 concentration and significant factors in March 2020.

No.	Factor	Coefficient	Std. Error	Probability	VIF
	Intercept	-0.00	0.10	1.00	--------
1	TEMP	-0.36	0.18	0.05	3.53
2	WS	-0.20	0.15	0.17	2.24
3	VIS	-0.12	0.12	0.34	1.54
4	AOD	-0.07	0.11	0.53	1.15
5	FD	-0.05	0.12	0.71	1.53
6	BT	0.28	0.15	0.07	2.45
7	FRP	0.63	0.16	0.00*	2.59
8	FH	0.12	0.13	0.35	1.70
9	ELEV	-0.23	0.16	0.16	2.75

Note: an asterisk (*) at the significance level of 0.01.

As a result of OLS regression analysis in Table 5.46, if the probability at the confident level of 99% is not considered (ignored), the relationship between PM2.5 concentration and selected factors by VIF value can be explained into two types: positive and negative. The positive relationship between PM2.5 concentration and their factors occurred with brightness temperature, fire radiative power, and fire hotspot. This finding indicates that if these variables increase, the PM2.5 concentration increase. In contrast, the negative relationship between PM2.5 concentration and their factors is found with temperature, wind speed, visibility, MODIS AOD, factory density, and elevation. So, with the increase of these factors, the PM2.5 concentration decrease.

When the probability at the confident level of 99% is considered, the significant factor on PM2.5 concentration in March 2020 is only fire radiative power.

5.4.7 April 2020 in the summer season

The multiple R-squared is 0.56, while the adjusted R-squared is 0.50. The results of the OLS regression analysis are reported in Table 5.47. The model performance showed that AICc is 168.59.

Table 5.47 Summary of the OLS regression analysis between PM2.5 concentration and significant factors in April 2020.

No.	Factor	Coefficient	Std. Error	Probability	VIF
	Intercept	0.00	0.08	1.00	--------
1	WS	0.60	0.13	0.00*	2.54
2	VIS	0.45	0.11	0.00*	1.59
3	AOD	0.25	0.10	0.01*	1.30
4	FD	-0.27	0.11	0.01*	1.56
5	BT	-0.29	0.10	0.00*	1.49
6	FRP	-0.44	0.13	0.00*	2.49
7	FH	0.26	0.09	0.01*	1.15
8	ELEV	0.10	0.12	0.42	1.95

Note: an asterisk (*) at the significance level of 0.01.

As a result of OLS regression analysis in Table 5.47, if the probability at the confident level of 99% is not considered (ignored), the relationship between PM2.5 concentration and selected factors by VIF value can be explained into two types: positive and negative. The positive relationship between PM2.5 concentration and their factors occurred with wind speed, visibility, MODIS AOD, fire hotspot, and elevation. This finding indicates that if these variables increase, the PM2.5 concentration increase. In contrast, the negative relationship between PM2.5 concentration and their factors is found with factory density, brightness temperature, and fire radiative power. So, with the increase of these factors, the PM2.5 concentration decrease.

When the probability at the confident level of 99% is considered, the significant factors on PM2.5 concentration in April 2020 are wind speed, visibility, MODIS AOD, factory density, brightness temperature, fire radiative power, and fire hotspot.

5.4.8 May 2020 in the summer season

The model performance showed that AICc is 174.99. The multiple R-squared is 0.51, while the adjusted R-squared is 0.45. The results of the OLS regression analysis are reported in Table 5.48.

Table 5.48 Summary of the OLS regression analysis between PM2.5 concentration and significant factors in May 2020.

No.	Factor	Coefficient	Std. Error	Probability	VIF
	Intercept	-0.00	0.09	1.00	--------
1	WS	0.34	0.14	0.00*	2.37
2	VIS	-0.20	0.14	0.01*	2.48
3	AOD	-0.14	0.12	0.19	1.77
4	FD	-0.57	0.11	0.00*	1.54
5	BT	0.28	0.13	0.02*	2.12
6	FRP	-0.11	0.15	0.35	2.99
7	FH	0.06	0.11	0.50	1.67
8	ELEV	0.51	0.12	0.00*	1.92

Note: an asterisk (*) at the significance level of 0.01.

As a result of OLS regression analysis in Table 5.48, if the probability at the confident level of 99% is not considered (ignored), the relationship between PM2.5 concentration and selected factors by VIF value can be explained into two types: positive and negative. The positive relationship between PM2.5 concentration and their factors occurred with wind speed, brightness temperature, fire hotspot and elevation. This finding indicates that if these variables increase, the PM2.5 concentration increase. In contrast, the negative relationship between PM2.5 concentration and their factors is found with visibility, MODIS AOD, factory density and fire radiative power. So, with the increase of these factors, the PM2.5 concentration decrease.

When the probability at the confident level of 99% is considered, the significant factors on PM2.5 concentration in May 2020 are wind speed, visibility, factory density and brightness temperature, and elevation.

In the case of PM2.5 concentration in the urban landscape (Tables 5.49 and 5.50), the significant factors on PM2.5 in winter and summer are ten and eight factors. Furthermore, many meteorological factors significantly influenced PM2.5 than PM10 concentration (Chen et al., 2017). As a result, there are seven common factors on PM2.5 concentration in both seasons: wind speed, visibility, brightness temperature, fire radiative power, MODIS AOD, fire hotspot, and elevation. Furthermore, it was found that three significant factors on PM2.5 concentration are only found in the winter season, including relative humidity, temperature, and pressure. In contrast, one significant factor in PM2.5 concentration, factory density, is only found in the summer season.

Table 5.49 Frequency of significant factors on PM2.5 concentration in the winter season.

No.	Significant factor	October 2019	November 2019	December 2019	January 2020	February 2020	Frequency
1	VIS	Yes	Yes	Yes	Yes		4 of 5
2	WS	Yes		Yes		Yes	3 of 5
3	FRP	Yes	Yes			Yes	3 of 5
4	ELEV	Yes			Yes	Yes	3 of 5
5	P	Yes				Yes	2 of 5
6	AOD	Yes			Yes		2 of 5
7	FH	Yes			Yes		2 of 5
8	RH					Yes	1 of 5
9	TEMP				Yes		1 of 5
10	BT	Yes					1 of 5

Table 5.50 Frequency of significant factors on PM2.5 concentration in the summer season.

No.	Significant factor	March 2020	April 2020	May 2020	Frequency
1	WS		Yes	Yes	2 of 3
2	VIS		Yes	Yes	2 of 3
3	FD		Yes	Yes	2 of 3
4	BT		Yes	Yes	2 of 3
5	FRP	Yes	Yes		2 of 3
6	AOD		Yes		1 of 3
7	FH		Yes		1 of 3
8	ELEV			Yes	1 of 3

The findings show similar results to the previous study of Guo and Zhang (2014), who reported that PM2.5 concentration is most relevant to visibility, followed by the wind speed. The least pertinent factors are temperature and relative humidity. Likewise, these findings are consistent with the previous work of Chen et al. (2017), who showed the strong influence of wind speed on local PM2.5 concentration. They also observed strong interactions between wind speed and other meteorological factors influencing PM2.5 concentration. While Galindo, Varea, Gil-Moltó, Yubero, and Nicolás (2011) found that the winter wind speed is the main effect of the dilution of atmospheric aerosols. At the same time, temperature and solar radiation strongly influenced coarse particles. That means the meteorological data, solar heating at the earth's surface, or active fire data significantly affect PM2.5 concentration. In addition, MODIS AOD had a strong correlation with PM2.5 concentration (Gu, 2019; Kong, Xin, Zhang, and Wang, 2016). Like Lee, Liu, Coull, Schwartz, and Koutrakis (2011) reported and potentially helpful in predicting PM2.5 concentration. And Chudnovsky et al. (2014) predicted PM2.5 concentration with MODIS AOD and improved the accuracy with land use and meteorological data. However, Chu et al. (2016) suggested using higher-resolution AOD data to estimate PM2.5 in a relatively small area more accurately.

5.5 Basic information of daily dependent and independent variables

For daily significant spatiotemporal factors identification, PM10 and PM2.5 concentration' highest records of specific days were selected to display on the chart comparatively. Figure 5.15 shows the maximum record values of PM10 and PM2.5 concentration from October 2019 to May 2020.

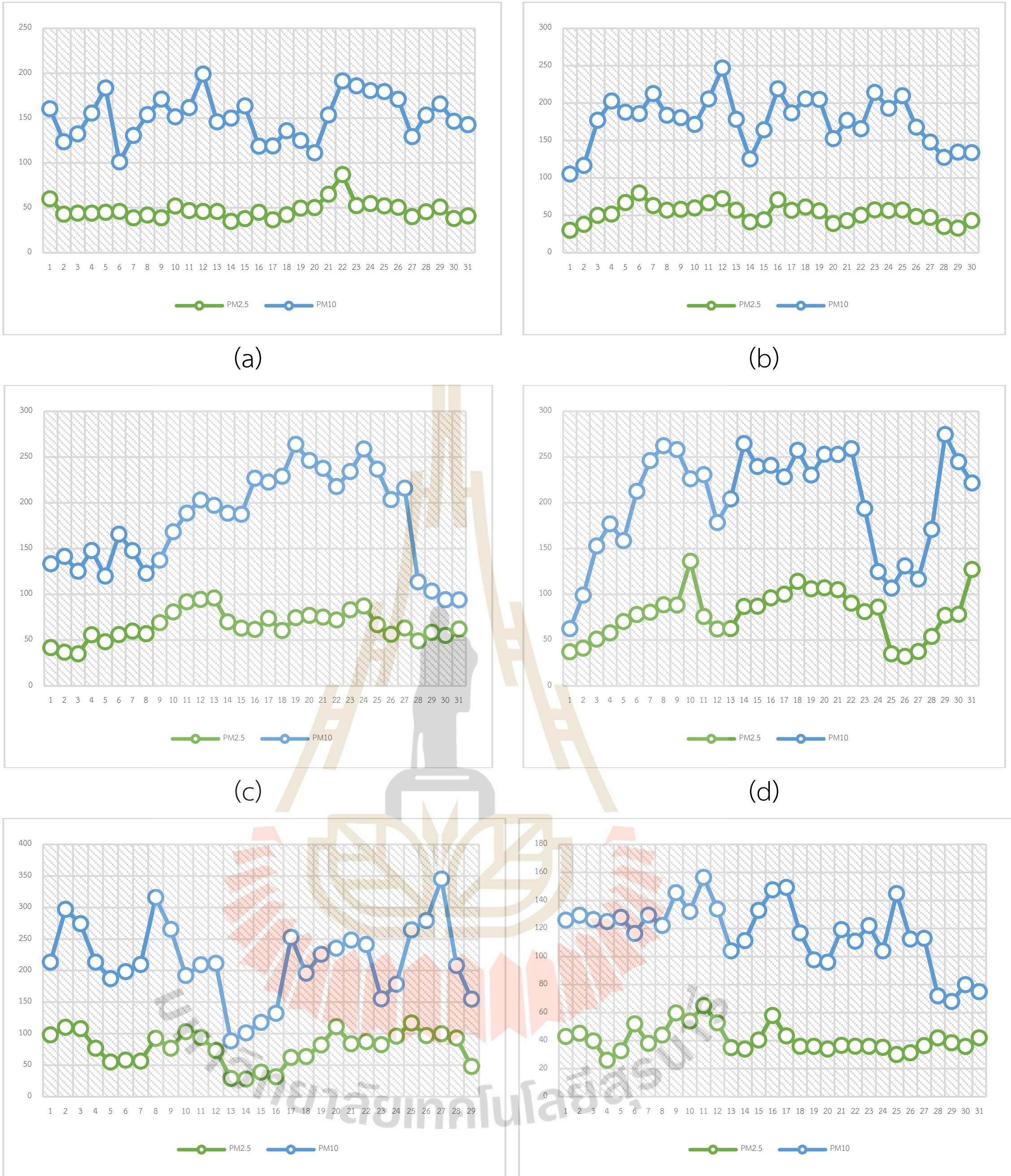

(a) (b) (c) (d) (e) (f)

Figure 5.15 The maximum recorded value of daily PM10 and PM2.5 concentration during October 2019 to May 2020: (a) October 2019 (b) November 2019 (c) December 2019 (d) January 2020 (e) February 2020 (f) March 2020 (g) April 2020 (h) May 2020.

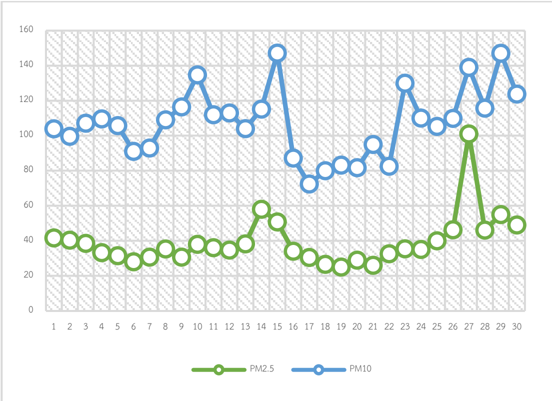

(g)

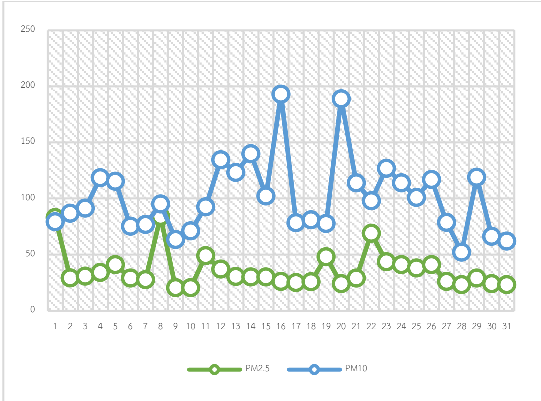

(h)

Figure 5.15 (Continued).

As a result, it can be observed that the maximum record value of PM10 concentration is 345.17 μg/m^3 on 27 February 2020 at Na Phra Lan Police Station, Station ID: 24t, in Na Phra Lan, Chaloem Phra Kiat, Saraburi (Figure 15(e)). At the same time, the maximum record value of PM2.5 concentration is 136.00 μg/m^3 on 10 January 2020 at Phra Nakhon District Office, Station ID: b92, in Samsen Roadside, Phra Nakhon, Bangkok (Figure 15(d)).

Hence, a specific week for examining daily significant spatiotemporal factors was prepared between 24 February and 1 March 2020 for PM10 concentration and between 7 and 13 January 2020 for PM2.5 concentration, as shown in Figures 5.16 and 5.17 and Tables 5.51 and 5.52, respectively. At the same time, significant daily factors on PM10 in the rural landscape and PM2.5 in the urban landscape, including relative humidity, temperature, wind speed, pressure, brightness temperature, fire radiative power, and fire hotspot, were prepared as shown in Figures 5.18 to 5.24 and summarized in Tables 5.53 to 5.66, respectively.

5.5.1 PM10 concentration

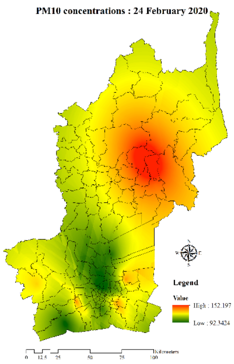

(a)

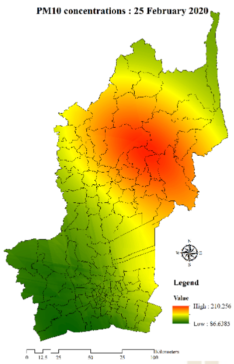

(b)

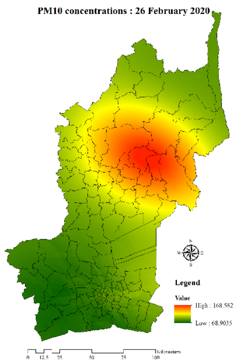

(c)

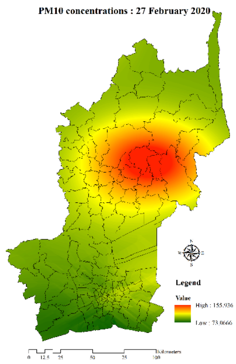

(d)

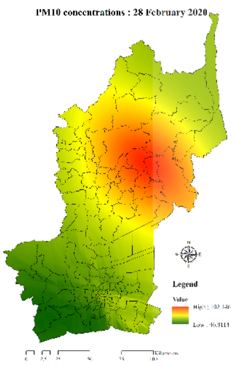

(e)

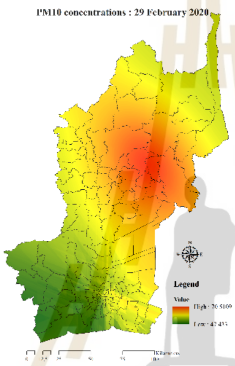

(f)

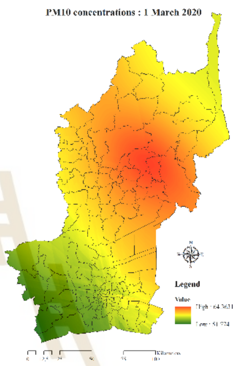

(g)

Figure 5.16 Spatial distribution of daily mean PM10 concentration during 24 February to 1 March 2020: (a) 24 February, (b) 25 February, (c) 26 February, (d) 27 February, (e) 28 February, (f) 29 February, (g) 1 March.

Table 5.51 Descriptive statistic data of daily mean PM10 concentration after normalization in the rural landscape.

	24 Feb	25 Feb	26 Feb	27 Feb	28 Feb	29 Feb	1 Mar
Minimum	-2.19	-1.85	-1.47	-1.23	-1.48	-1.83	-2.01
Maximum	2.96	2.01	2.45	2.53	2.34	2.21	1.98
Mean	0.00	0.00	0.00	0.00	0.00	0.00	0.00
SD.	1.00	1.00	1.00	1.00	1.00	1.00	1.00

5.5.2 PM2.5 concentration

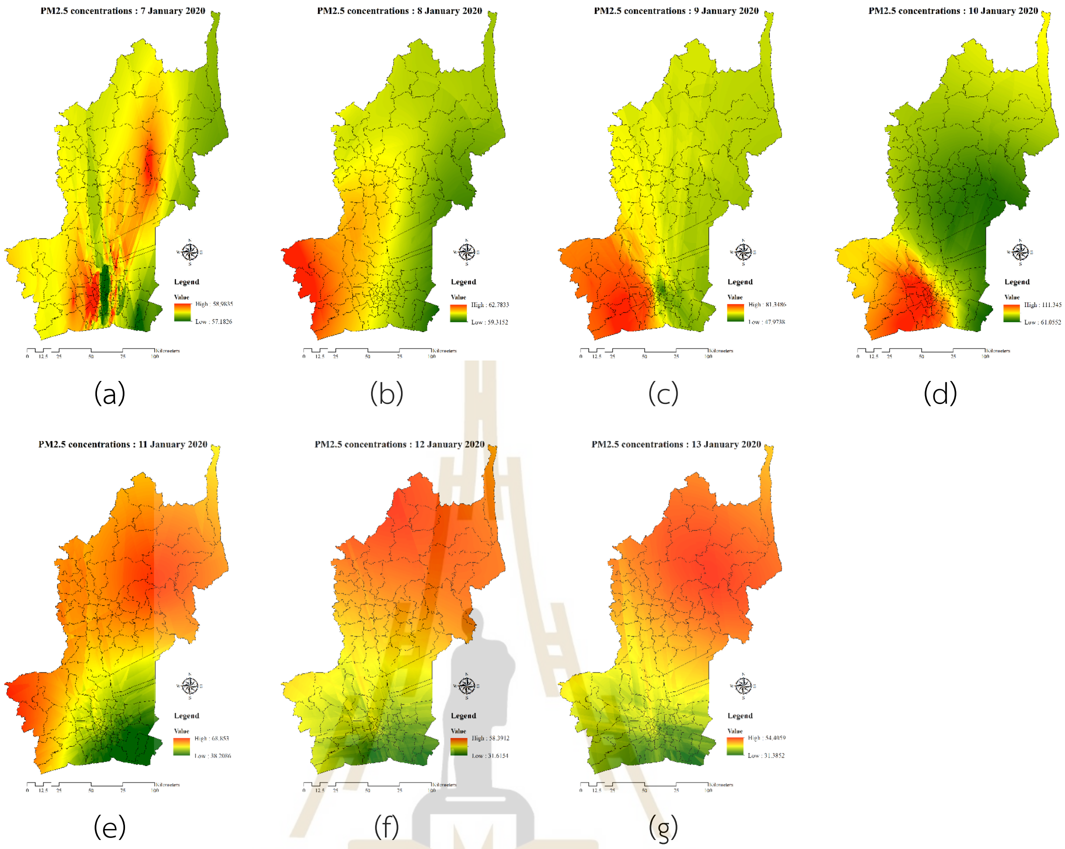

Figure 5.17 Spatial distribution of daily mean PM2.5 concentration during 7 to 13 January 2020: (a) 7 January, (b) 8 January, (c) 9 January, (d) 10 January, (e) 11 January, (f) 12 January, (g) 13 January.

Table 5.52 Descriptive statistic data of daily mean PM2.5 concentration after normalization in the urban landscape.

	7 Jan	8 Jan	9 Jan	10 Jan	11 Jan	12 Jan	13 Jan
Minimum	-2.48	-2.24	-1.57	-2.25	-2.19	-2.36	-2.16
Maximum	2.02	2.85	1.59	1.61	2.83	2.18	1.65
Mean	0.00	0.00	0.00	0.00	0.00	0.00	0.00
SD.	1.00	1.00	1.00	1.00	1.00	1.00	1.00

5.5.3 Relative humidity

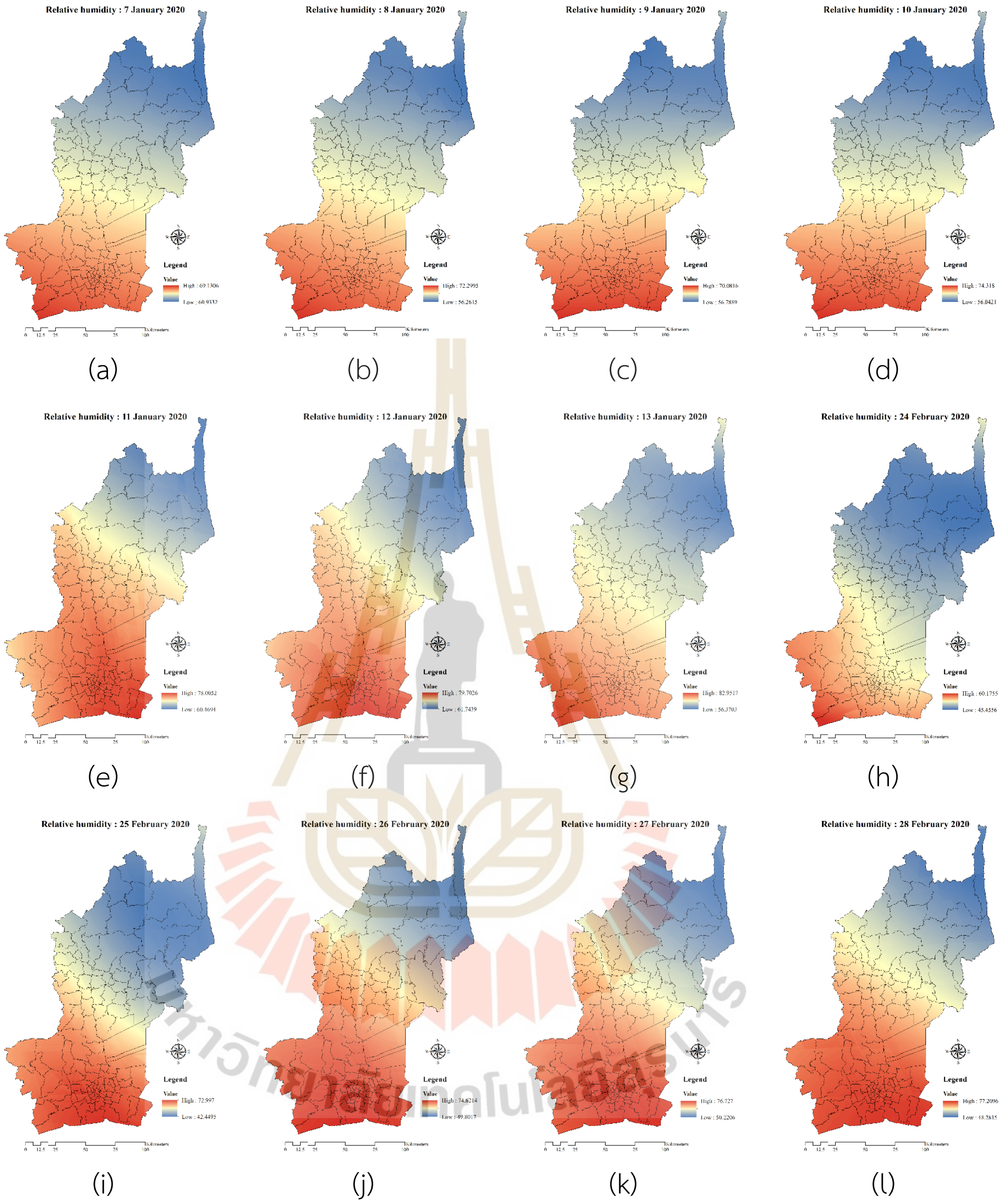

Figure 5.18 Spatial distribution of daily mean relative humidity during 7 to 13 January and 24 February to 1 March 2020: (a) 7 January, (b) 8 January, (c) 9 January, (d) 10 January, (e) 11 January, (f) 12 January, (g) 13 January, (h) 24 February, (i) 25 February, (j) 26 February, (k) 27 February, (l) 28 February, (m) 29 February, (n) 1 March.

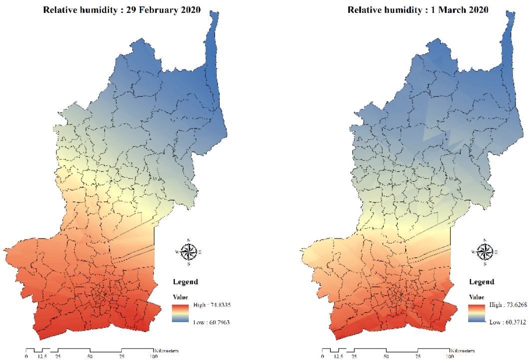

(m) (n)

Figure 5.18 (Continued).

Table 5.53 Descriptive statistic data of daily mean relative humidity after normalization in the rural landscape.

	24 Feb	25 Feb	26 Feb	27 Feb	28 Feb	29 Feb	1 Mar
Minimum	-1.84	-1.71	-2.31	-2.14	-2.40	-2.23	-1.93
Maximum	1.86	1.91	1.59	1.69	1.54	1.79	2.18
Mean	0.00	0.00	0.00	0.00	0.00	0.00	0.00
SD.	1.00	1.00	1.00	1.00	1.00	1.00	1.00

Table 5.54 Descriptive statistic data of daily mean relative humidity after normalization in the urban landscape.

	7 Jan	8 Jan	9 Jan	10 Jan	11 Jan	12 Jan	13 Jan
Minimum	-1.78	-1.82	-2.66	-2.43	-3.75	-3.78	-2.04
Maximum	2.80	2.88	2.13	2.44	1.26	1.43	3.30
Mean	0.00	0.00	0.00	0.00	0.00	0.00	0.00
SD.	1.00	1.00	1.00	1.00	1.00	1.00	1.00

5.5.4 Temperature

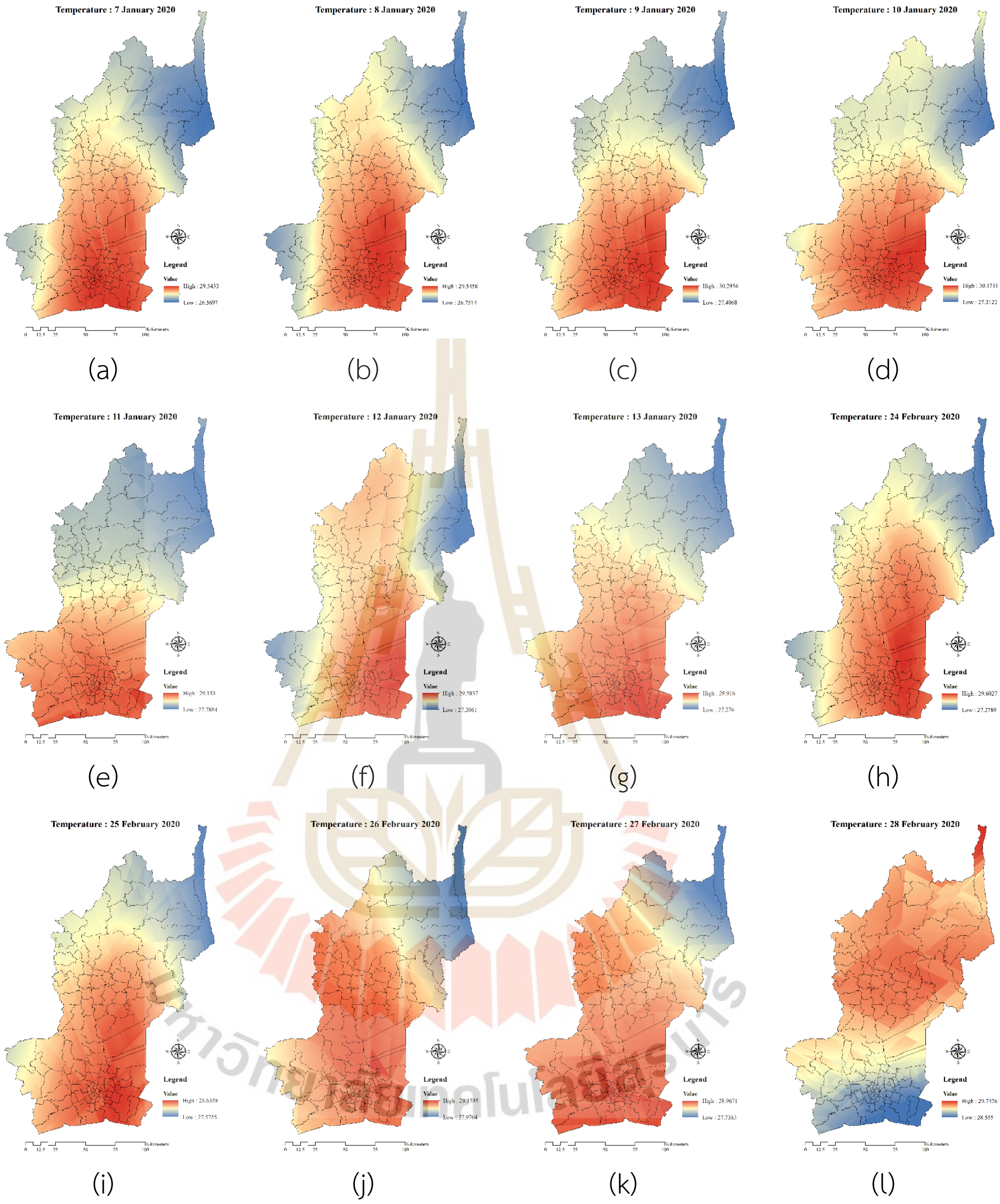

Figure 5.19 Spatial distribution of daily mean relative humidity during 7 to 13 January and 24 February to 1 March 2020: (a) 7 January, (b) 8 January, (c) 9 January, (d) 10 January, (e) 11 January, (f) 12 January, (g) 13 January, (h) 24 February, (i) 25 February, (j) 26 February, (k) 27 February, (l) 28 February, (m) 29 February, (n) 1 March.

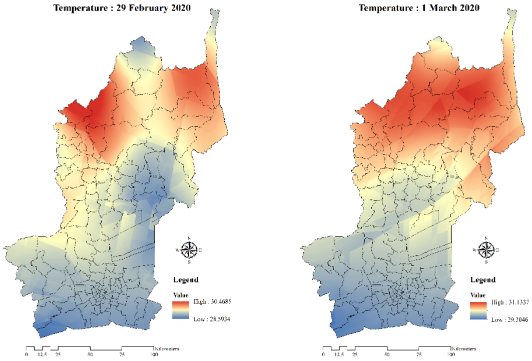

(m) (n)

Figure 5.19 (Continued).

Table 5.55 Descriptive statistic data of daily mean temperature after normalization in the rural landscape.

	24 Feb	25 Feb	26 Feb	27 Feb	28 Feb	29 Feb	1 Mar
Minimum	-3.08	-3.10	-3.51	-3.96	-2.82	-1.71	-1.30
Maximum	1.56	1.41	0.90	1.02	1.23	2.71	2.06
Mean	0.00	0.00	0.00	0.00	0.00	0.00	0.00
SD.	1.00	1.00	1.00	1.00	1.00	1.00	1.00

Table 5.56 Descriptive statistic data of daily mean temperature after normalization in the urban landscape.

	7 Jan	8 Jan	9 Jan	10 Jan	11 Jan	12 Jan	13 Jan
Minimum	-4.00	-3.66	-4.30	-3.92	-3.94	-3.54	-3.97
Maximum	0.68	0.86	0.82	1.03	1.38	1.19	1.49
Mean	0.00	0.00	0.00	0.00	0.00	0.00	0.00
SD.	1.00	1.00	1.00	1.00	1.00	1.00	1.00

5.5.5 Wind speed

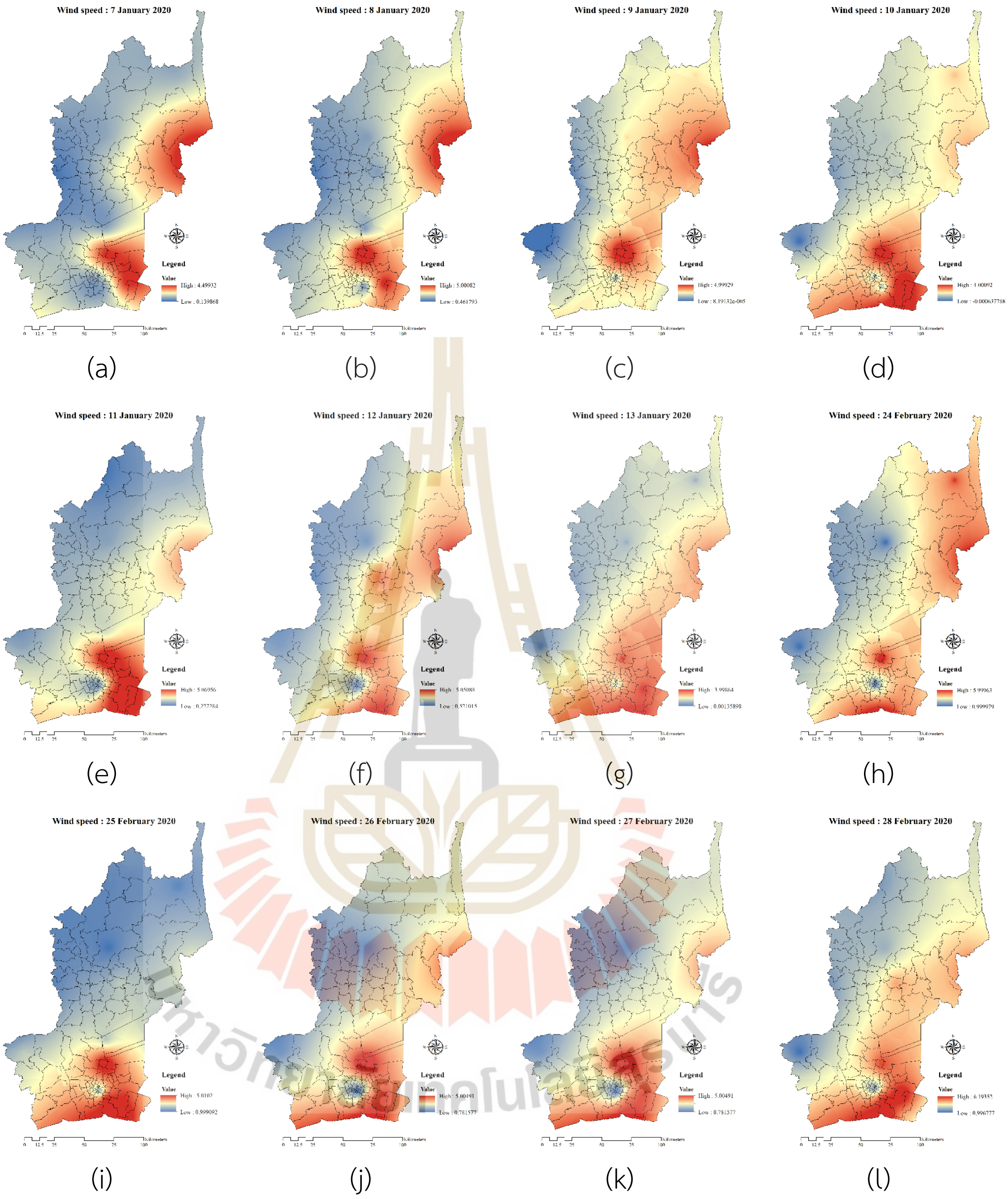

Figure 5.20 Spatial distribution of daily mean wind speed during 7 to 13 January and 24 February to 1 March 2020: (a) 7 January, (b) 8 January, (c) 9 January, (d) 10 January, (e) 11 January, (f) 12 January, (g) 13 January, (h) 24 February, (i) 25 February, (j) 26 February, (k) 27 February, (l) 28 February, (m) 29 February, (n) 1 March.

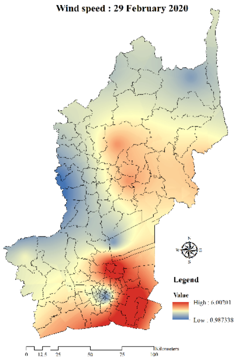

(m)

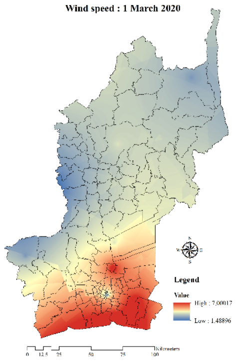

(n)

Figure 5.20 (Continued).

Table 5.57 Descriptive statistic data of daily mean wind speed after normalization in rural landscape.

	24 Feb	25 Feb	26 Feb	27 Feb	28 Feb	29 Feb	1 Mar
Minimum	-1.49	-1.14	-1.30	-1.30	-1.58	-2.37	-2.03
Maximum	2.27	3.28	2.81	2.81	1.75	1.89	3.02
Mean	0.00	0.00	0.00	0.00	0.00	0.00	0.00
SD.	1.00	1.00	1.00	1.00	1.00	1.00	1.00

Table 5.58 Descriptive statistic data of daily mean wind speed after normalization in the urban landscape.

	7 Jan	8 Jan	9 Jan	10 Jan	11 Jan	12 Jan	13 Jan
Minimum	-1.07	-1.98	-2.81	-2.65	-1.28	-1.53	-3.37
Maximum	2.18	3.08	4.08	2.47	2.05	2.40	1.87
Mean	0.00	0.00	0.00	0.00	0.00	0.00	0.00
SD.	1.00	1.00	1.00	1.00	1.00	1.00	1.00

5.5.6 Pressure

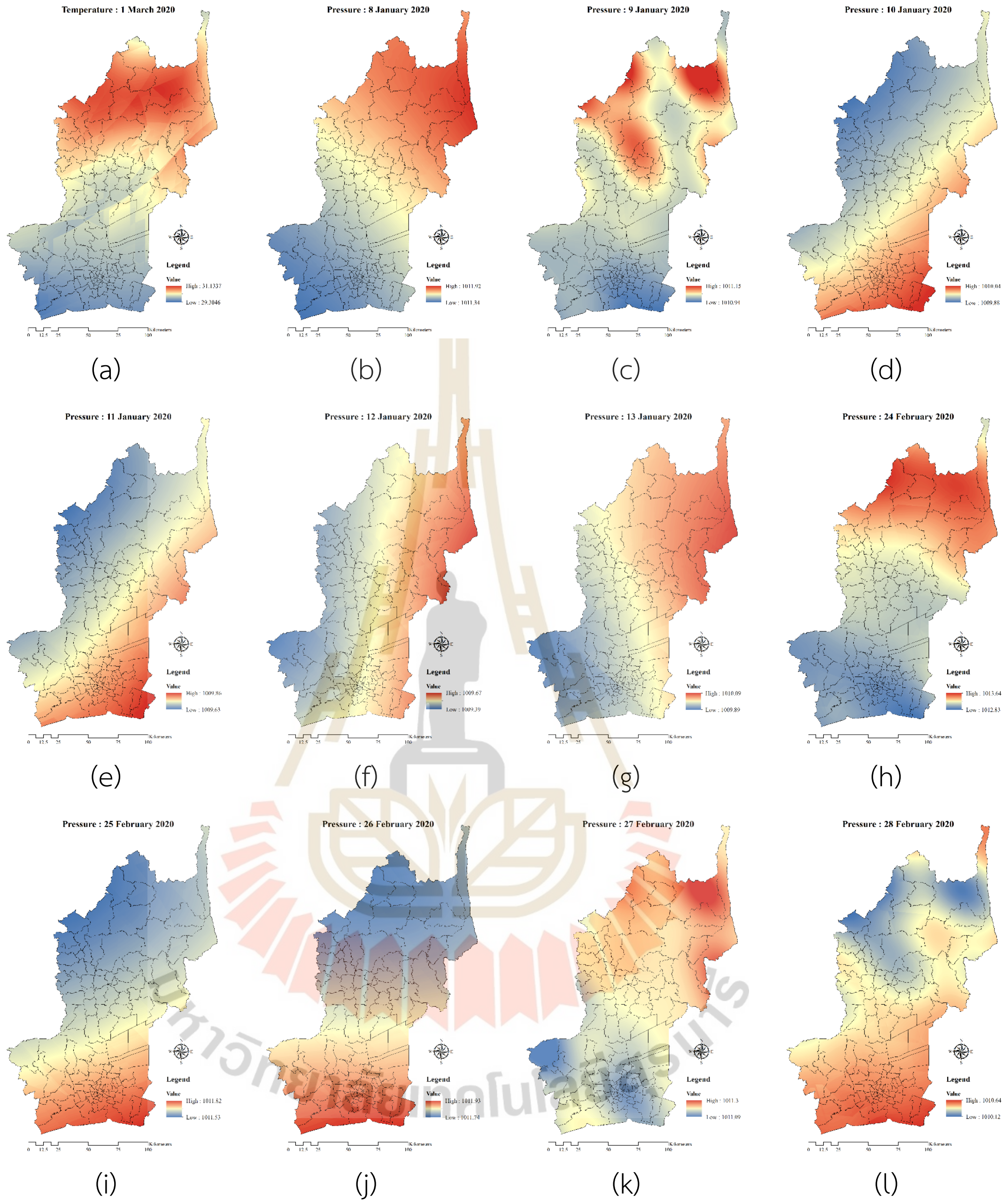

Figure 5.21 Spatial distribution of daily mean pressure during 7 to 13 January and 24 February to 1 March 2020: (a) 7 January, (b) 8 January, (c) 9 January, (d) 10 January, (e) 11 January, (f) 12 January, (g) 13 January, (h) 24 February, (i) 25 February, (j) 26 February, (k) 27 February, (l) 28 February, (m) 29 February, (n) 1 March.

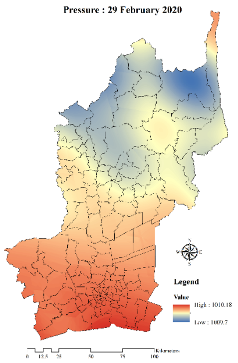

(m)

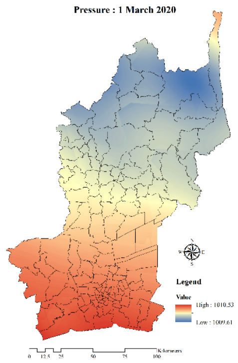

(n)

Figure 5.21 (Continued).

Table 5.59 Descriptive statistic data of daily mean pressure after normalization in the rural landscape.

	24 Feb	25 Feb	26 Feb	27 Feb	28 Feb	29 Feb	1 Mar
Minimum	-1.28	-1.73	-1.73	-2.10	-2.67	-2.31	-2.19
Maximum	2.49	2.29	2.06	3.27	1.79	1.80	1.91
Mean	0.00	0.00	0.00	0.00	0.00	0.00	0.00
SD.	1.00	1.00	1.00	1.00	1.00	1.00	1.00

Table 5.60 Descriptive statistic data of daily mean pressure after normalization in the urban landscape.

	7 Jan	8 Jan	9 Jan	10 Jan	11 Jan	12 Jan	13 Jan
Minimum	-2.31	-2.43	-2.25	-3.39	-3.29	-2.94	-2.38
Maximum	2.62	2.62	1.91	2.42	2.46	2.39	2.34
Mean	0.00	0.00	0.00	0.00	0.00	0.00	0.00
SD.	1.00	1.00	1.00	1.00	1.00	1.00	1.00

5.5.7 Brightness temperature

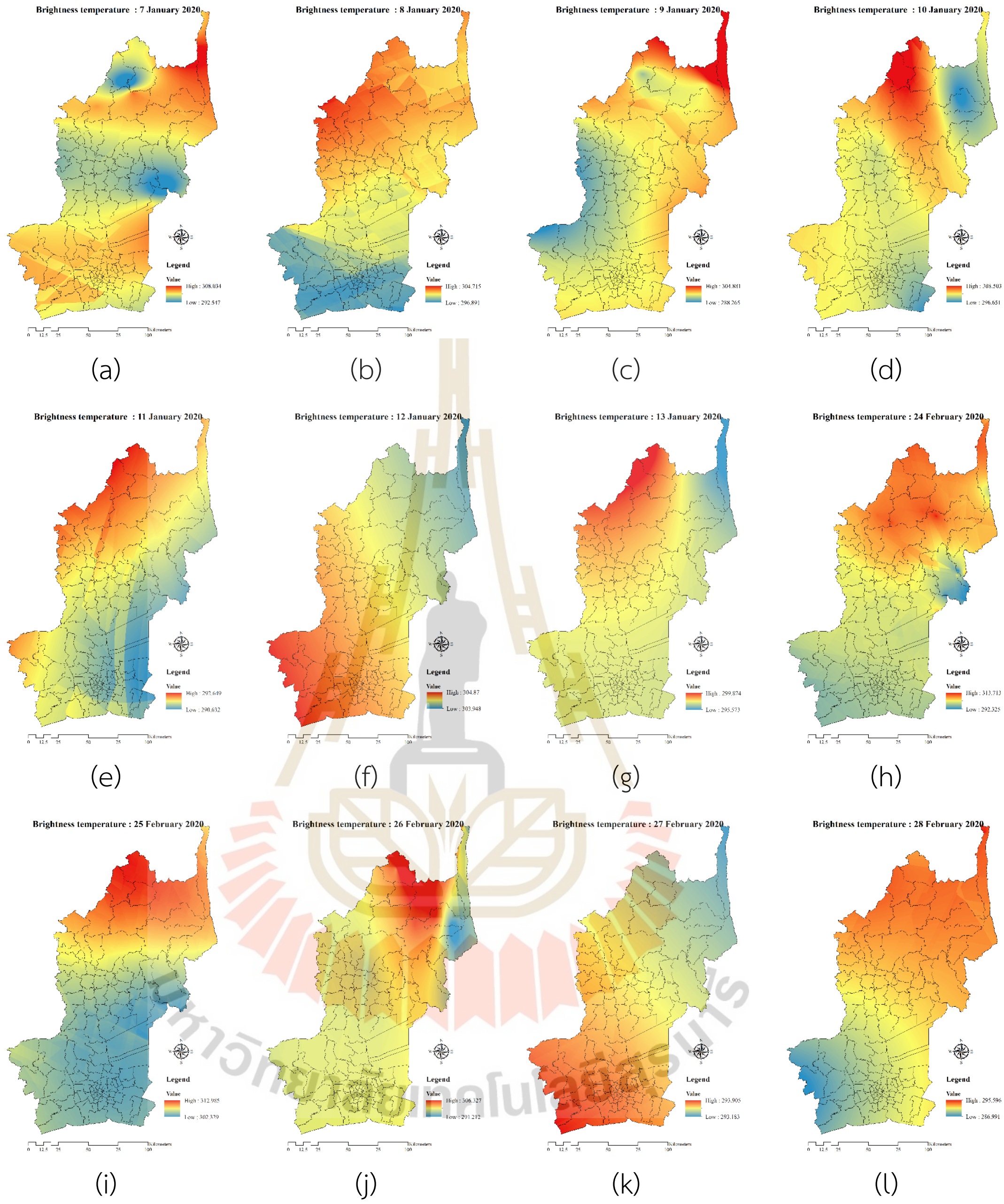

Figure 5.22 Spatial distribution of daily mean brightness temperature during 7 to 13 January and 24 February to 1 March 2020: (a) 7 January, (b) 8 January, (c) 9 January, (d) 10 January, (e) 11 January, (f) 12 January, (g) 13 January, (h) 24 February, (i) 25 February, (j) 26 February, (k) 27 February, (l) 28 February, (m) 29 February, (n) 1 March.

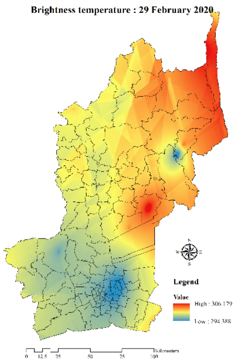

(m)

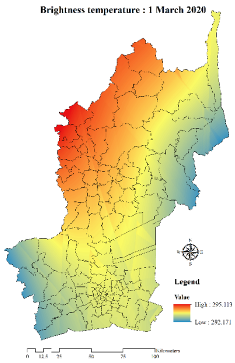

(n)

Figure 5.22 (Continued).

Table 5.61 Descriptive statistic data of daily mean brightness temperature after normalization in the rural landscape.

	24 Feb	25 Feb	26 Feb	27 Feb	28 Feb	29 Feb	1 Mar
Minimum	-1.88	-1.17	-1.87	-3.03	-2.14	-1.85	-2.47
Maximum	2.07	2.43	4.78	1.69	1.80	2.86	2.01
Mean	0.00	0.00	0.00	0.00	0.00	0.00	0.00
SD.	1.00	1.00	1.00	1.00	1.00	1.00	1.00

Table 5.62 Descriptive statistic data of daily mean brightness temperature after normalization in the urban landscape.

	7 Jan	8 Jan	9 Jan	10 Jan	11 Jan	12 Jan	13 Jan
Minimum	-3.40	-1.17	-4.66	-3.48	-1.87	-2.22	-2.19
Maximum	1.81	2.47	1.59	1.92	3.42	2.59	3.23
Mean	0.00	0.00	0.00	0.00	0.00	0.00	0.00
SD.	1.00	1.00	1.00	1.00	1.00	1.00	1.00

5.5.8 Fire radiative power

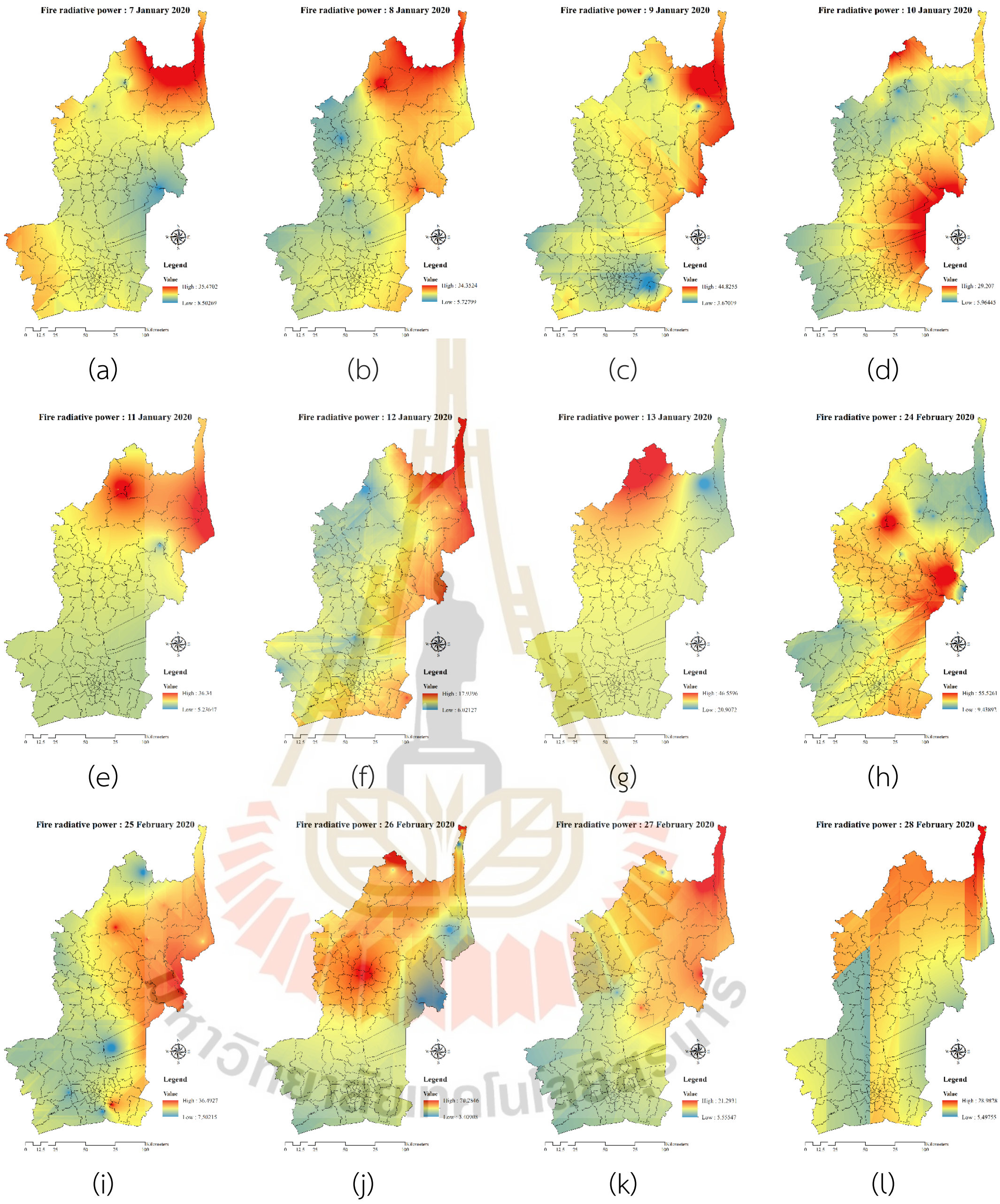

Figure 5.23 Spatial distribution of daily mean fire radiative power during 7 to 13 January and 24 February to 1 March 2020: (a) 7 January, (b) 8 January, (c) 9 January, (d) 10 January, (e) 11 January, (f) 12 January, (g) 13 January, (h) 24 February, (i) 25 February, (j) 26 February, (k) 27 February, (l) 28 February, (m) 29 February, (n) 1 March.

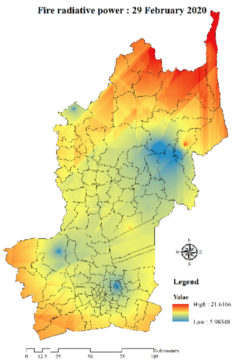

(m)

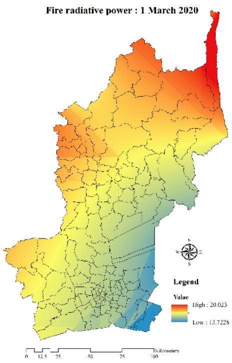

(n)

Figure 5.23 (Continued).

Table 5.63 Descriptive statistic data of daily mean fire radiative power after normalization in rural landscape.

	24 Feb	25 Feb	26 Feb	27 Feb	28 Feb	29 Feb	1 Mar
Minimum	-2.45	-1.70	-2.16	-1.23	-1.71	-1.98	-2.05
Maximum	2.43	2.03	2.72	3.15	2.58	3.77	3.10
Mean	0.00	0.00	0.00	0.00	0.00	0.00	0.00
SD.	1.00	1.00	1.00	1.00	1.00	1.00	1.00

Table 5.64 Descriptive statistic data of daily mean fire radiative power after normalization in the urban landscape.

	7 Jan	8 Jan	9 Jan	10 Jan	11 Jan	12 Jan	13 Jan
Minimum	-2.02	-3.39	-2.13	-2.21	-2.49	-2.22	-2.50
Maximum	3.65	2.86	2.81	3.00	3.01	2.99	3.04
Mean	0.00	0.00	0.00	0.00	0.00	0.00	0.00
SD.	1.00	1.00	1.00	1.00	1.00	1.00	1.00

5.5.9 Fire hotspot

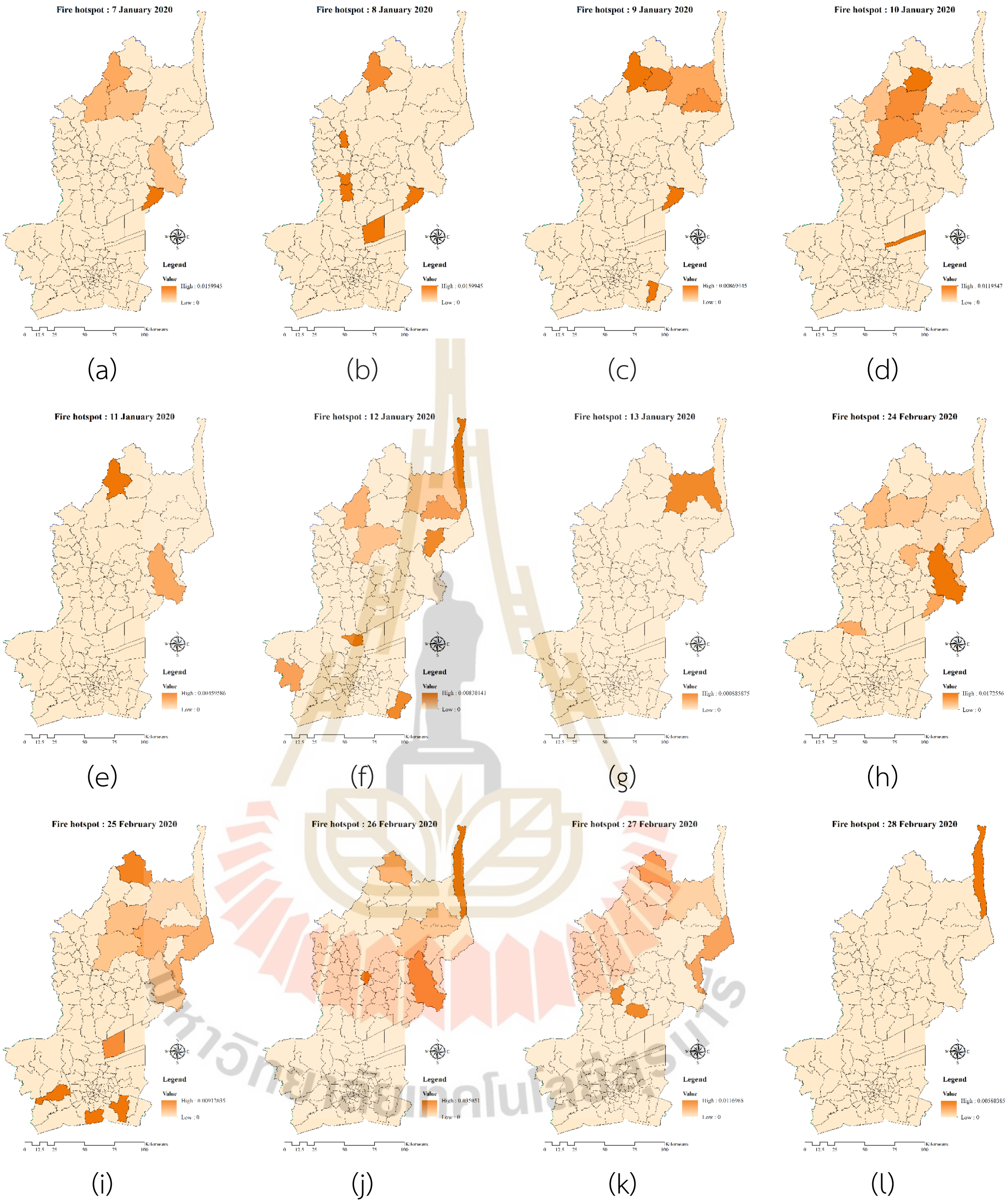

Figure 5.24 Spatial distribution of daily mean fire hotspot during 7 to 13 January and 24 February to 1 March 2020: (a) 7 January, (b) 8 January, (c) 9 January, (d) 10 January, (e) 11 January, (f) 12 January, (g) 13 January, (h) 24 February, (i) 25 February, (j) 26 February, (k) 27 February, (l) 28 February, (m) 29 February, (n) 1 March.

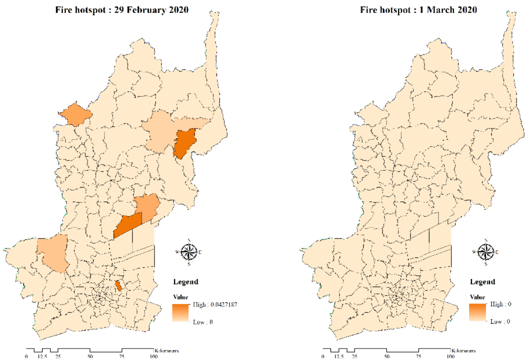

(m) (n)

Figure 5.24 (Continued).

Table 5.65 Descriptive statistic data of daily mean fire hotspot after normalization in the rural landscape.

	24 Feb	25 Feb	26 Feb	27 Feb	28 Feb	29 Feb	1 Mar
Minimum	-0.29	-0.35	-0.20	-0.23	-0.13	-0.23	-
Maximum	6.64	4.35	7.31	6.21	7.62	6.33	-
Mean	0.00	0.00	0.00	0.00	0.00	0.00	-
SD.	1.00	1.00	1.00	1.00	1.00	1.00	-

Table 5.66 Descriptive statistic data of daily mean fire hotspot after normalization in the urban landscape.

	7 Jan	8 Jan	9 Jan	10 Jan	11 Jan	12 Jan	13 Jan
Minimum	-	-	-0.12	-	-	-0.16	-
Maximum	-	-	8.37	-	-	7.30	-
Mean	-	-	0.00	-	-	0.00	-
SD.	-	-	1.00	-	-	1.00	-

There is no data on fire hotspots in the rural landscape on 1 March 2020. In addition, in the urban landscape, there is no data on 7, 8, 10, 11, and 13 January 2020. So that the calculation of the fire hotspot data is in the same standard, therefore, use the monthly mean variables replacement.

In addition, the daily MODIS AOD on the selected day lacks coverage in orbit-scanning gaps and cloud obscuration (Zhang et al., 2017). Therefore, the variables: Visibility, MODIS AOD, Fire hotspot, NDVI, BUI, Road density, Factory density, Elevation, Population density, and GPP use the monthly mean variables.

5.6 Significant daily spatiotemporal factors on PM10 concentration in the rural landscape

The multicollinearity test of daily explanatory variables performed in the SPSS statistical software is reported in Table 5.67. In this study, any variable with a VIF value above 7.5 is removed from the model to avoid redundancy among explanatory variables (Section 3.2).

Table 5.67 Results of multicollinearity test of explanatory variables on daily PM10 concentration.

No.	Variable	The VIF value						
		24 Feb	25 Feb	26 Feb	27 Feb	28 Feb	29 Feb	1 Mar
1	RH	25.51	33.25	72.42	76.94	32.38	30.32	48.61
2	TEMP	14.12	19.04	31.69	14.48	2.93	6.07	10.25
3	WS	9.12	34.12	23.05	11.28	8.76	5.59	8.18
4	P	16.68	33.76	39.32	10.28	4.85	12.66	28.71
5	VIS	5.76	4.81	4.76	4.42	5.88	6.67	5.74
6	AOD	3.98	3.98	3.00	2.92	2.81	3.32	2.17
7	NDVI	18.67	16.59	23.43	23.00	20.14	18.52	15.94
8	BUI	23.03	20.29	30.73	26.94	23.60	21.04	13.17
9	RD	11.05	11.17	10.68	12.34	11.80	11.18	11.73
10	FD	6.22	6.90	5.98	6.32	6.33	5.52	4.74
11	BT	18.24	38.63	2.18	116.60	33.44	3.71	7.94
12	FRP	6.20	10.93	4.19	15.88	3.61	4.27	8.45
13	FH	1.82	1.53	1.48	1.52	1.46	1.47	2.18
14	ELEV	7.83	8.55	8.15	5.31	5.04	5.48	5.41
15	POP	10.58	12.92	12.48	12.36	12.11	10.52	13.67
16	GPP	5.43	5.10	4.94	4.03	6.99	4.10	5.39
Total variables		6	5	7	6	9	10	5

As a result, the VIF values show that relative humidity, NDVI, BUI, road density, and population density are redundant for PM10 concentration models. In addition, other redundant variables are cut each day differently. Hence, persist independent variables with a VIF value less than 7.5 are applied for OLS regression analysis. The result of the OLS regression analysis of PM10 concentration in the rural landscape daily is separately described and discussed below

5.6.1 On 24 February 2020

The model performance showed that AICc is 154.16. The multiple R-squared is 0.43, while the adjusted R-squared is 0.37. The results of the OLS regression analysis are reported in Table 5.68.

Table 5.68 Summary of the OLS regression analysis between PM10 concentration and significant factors on 24 February 2020.

No.	Factor	Coefficient	Std. Error	Probability	VIF
	Intercept	0.00	0.10	1.00	--------
1	VIS	0.30	0.19	0.12	3.44
2	AOD	-0.39	0.15	0.01*	2.14
3	FD	0.71	0.13	0.00*	1.47
4	FRP	-0.35	0.14	0.01*	1.73
5	FH	-0.14	0.14	0.32	1.75
6	GPP	0.02	0.11	0.87	1.17

Note: an asterisk (*) at the significance level of 0.01.

As a result of OLS regression analysis in Table 5.68, if the probability at the confident level of 99% is not considered (ignored), the relationship between PM10 concentration and selected factors by VIF value can be explained into two types: positive and negative. The positive relationship between PM10 concentration and their factors occurred with visibility, factory density, and GPP. This finding indicates that if these variables increase, the PM10 concentration increase. In contrast, the negative relationship between PM10 concentration and their factors is found with MODIS AOD, fire radiative, and fire hotspot. So, with the increase of these factors, the PM10 concentration decrease.

When the probability at the confident level of 99% is considered, the significant factors on PM10 concentration on 24 February 2020 are MODIS AOD, factory density, and fire radiative power.

5.6.2 On 25 February 2020

The model performance showed that AICc is 174.05. The multiple R-squared is 0.17, while the adjusted R-squared is 0.10. The results of the OLS regression analysis are reported in Table 5.69.

Table 5.69 Summary of the OLS regression analysis between PM10 concentration and significant factors on 25 February 2020.

No.	Factor	Coefficient	Std. Error	Probability	VIF
	Intercept	0.00	0.12	1.00	--------
1	VIS	0.32	0.23	0.17	3.34
2	AOD	0.03	0.16	0.83	1.58
3	FD	-0.28	0.16	0.09	1.69
4	FH	0.14	0.13	0.29	1.14
5	GPP	-0.41	0.16	0.01*	1.75

Note: an asterisk (*) at the significance level of 0.01.

As a result of OLS regression analysis in Table 5.69, if the probability at the confident level of 99% is not considered (ignored), the relationship between PM10 concentration and selected factors by VIF value can be explained into two types: positive and negative. The positive relationship between PM10 concentration and their factors occurred with visibility, MODIS AOD, and fire hotspots. This finding indicates that if these variables increase, the PM10 concentration increase. In contrast, the negative relationship between PM10 concentration and their factors is found with factory density and GPP. So, with the increase of these factors, the PM10 concentration decrease.

When the probability at the confident level of 99% is considered, the significant factor on PM10 concentration on 25 February 2020 is only GPP.

5.6.3 On 26 February 2020

The model performance showed that AICc is 182.05. The multiple R-squared is 0.14, while the adjusted R-squared is 0.02. The results of the OLS regression analysis are reported in Table 5.70.

Table 5.70 Summary of the OLS regression analysis between PM10 concentration and significant factors on 26 February 2020.

No.	Factor	Coefficient	Std. Error	Probability	VIF
	Intercept	-0.00	0.13	1.00	--------
1	VIS	0.28	0.24	0.25	3.47
2	AOD	0.13	0.17	0.43	1.67
3	FD	-0.22	0.17	0.94	1.17
4	BT	-0.01	0.14	0.13	1.38
5	FRP	0.23	0.15	0.19	1.71
6	FH	0.11	0.14	0.11	1.78
7	GPP	-0.28	0.17	0.44	1.24

Note: an asterisk (*) at the significance level of 0.01.

As a result of OLS regression analysis in Table 5.70, if the probability at the confident level of 99% is not considered (ignored), the relationship between PM10 concentration and selected factors by VIF value can be explained into two types: positive and negative. The positive relationship between PM10 concentration and their factors occurred with visibility, MODIS AOD, fire radiative power, and fire hotspot. This finding indicates that if these variables increase, the PM10 concentration increase. In contrast, the negative relationship between PM10 concentration and their factors is found with factory density, brightness temperature and GPP. So, with the increase of these factors, the PM10 concentration decrease.

When the probability at the confident level of 99% is considered, no significant factors on PM10 concentration on PM10 concentration were found on 26 February 2020.

5.6.4 On 27 February 2020

The model performance showed that AICc is 184.84. The multiple R-squared is 0.05, while the adjusted R-squared is -0.05. The results of the OLS regression analysis are reported in Table 5.71.

Table 5.71 Summary of the OLS regression analysis between PM10 concentration and significant factors on 27 February 2020.

No.	Factor	Coefficient	Std. Error	Probability	VIF
	Intercept	-0.00	0.13	1.00	--------
1	VIS	0.06	0.25	0.81	3.59
2	AOD	0.17	0.19	0.37	2.03
3	FD	-0.19	0.18	0.29	1.77
4	FH	0.00	0.16	0.99	1.37
5	ELEV	0.02	0.17	0.93	1.62
6	GPP	0.00	0.19	0.99	1.94

Note: an asterisk (*) at the significance level of 0.01.

As a result of OLS regression analysis in Table 5.71, if the probability at the confident level of 99% is not considered (ignored), the relationship between PM10 concentration and selected factors by VIF value can be explained into two types: positive and negative. The positive relationship between PM10 concentration and their factors occurred with visibility, MODIS AOD, fire hotspot, elevation, and GPP. This finding indicates that if these variables increase, the PM10 concentration increase. In contrast, the negative relationship between PM10 concentration and their factors is found with factory density. So, with the increase of these factors, the PM10 concentration decrease.

When the probability at the confident level of 99% is considered, no significant factors on PM10 concentration were found on 26 February 2020.

5.6.5 On 28 February 2020

The model performance showed that AICc is 124.98. The multiple R-squared is 0.70, while the adjusted R-squared is 0.64. The results of the OLS regression analysis are reported in Table 5.72.

Table 5.72 Summary of the OLS regression analysis between PM10 concentration and significant factors on 28 February 2020.

No.	Factor	Coefficient	Std. Error	Probability	VIF
	Intercept	0.00	0.08	1.00	--------
1	TEMP	0.82	0.10	0.00*	1.50
2	P	-0.25	0.13	0.07	2.87
3	VIS	0.46	0.16	0.00*	3.98
4	AOD	0.15	0.12	0.22	2.33
5	FD	0.03	0.11	0.78	2.02
6	FRP	-0.02	0.10	0.83	1.82
7	FH	0.10	0.09	0.28	1.43
8	ELEV	0.03	0.10	0.77	1.72
9	GPP	-0.05	0.12	0.69	2.45

Note: an asterisk (*) at the significance level of 0.01.

As a result of OLS regression analysis in Table 5.72, if the probability at the confident level of 99% is not considered (ignored), the relationship between PM10 concentration and selected factors by VIF value can be explained into two types: positive and negative. The positive relationship between PM10 concentration and their factors occurred with temperature, visibility, MODIS AOD, factory density, fire hotspot, and elevation. This finding indicates that if these variables increase, the PM10 concentration increase. In contrast, the negative relationship between PM10 concentration and their factors is found with pressure, fire radiative power, and GPP. So, with the increase of these factors, the PM10 concentration decrease.

When the probability at the confident level of 99% is considered, the significant factors on PM10 concentration on 28 February 2020 are temperature and visibility.

5.6.6 On 29 February 2020

The model performance showed that AICc is 56.64. The multiple R-squared is 0.91, while the adjusted R-squared is 0.89. The results of the OLS regression analysis are reported in Table 5.73.

Table 5.73 Summary of the OLS regression analysis between PM10 concentration and significant factors on 29 February 2020.

No.	Factor	Coefficient	Std. Error	Probability	VIF
	Intercept	0.00	0.04	1.00	--------
1	TEMP	0.01	0.08	0.94	3.06
2	WS	0.69	0.07	0.00*	2.36
3	VIS	-0.39	0.10	0.00*	4.91
4	AOD	-0.10	0.07	0.18	2.80
5	FD	-0.13	0.06	0.04*	2.17
6	BT	0.30	0.07	0.00*	2.72
7	FRP	-0.61	0.07	0.00*	2.48
8	FH	0.09	0.05	0.09	1.38
9	ELEV	-0.16	0.06	0.01*	2.13
10	GPP	-0.12	0.08	0.14	3.12

Note: an asterisk (*) at the significance level of 0.01.

As a result of OLS regression analysis in Table 5.73, if the probability at the confident level of 99% is not considered (ignored), the relationship between PM10 concentration and selected factors by VIF value can be explained into two types: positive and negative. The positive relationship between PM10 concentration and their factors occurred with temperature, wind speed, brightness temperature, and fire hotspot. This finding indicates that if these variables increase, the PM10 concentration increase. In contrast, the negative relationship between PM10 concentration and their factors is found with visibility, MODIS AOD, factory density, fire radiative power, elevation, and GPP. So, with the increase of these factors, the PM10 concentration decrease.

When the probability at the confident level of 99% is considered, the significant factors on PM10 concentration on 28 February 2020 are wind speed, visibility, factory density, brightness temperature, fire radiative power and elevation.

5.6.7 On 1 March 2020

The model performance showed that AICc is 170.08. The multiple R-squared is 0.26, while the adjusted R-squared is 0.18. The results of the OLS regression analysis are reported in Table 5.74.

Table 5.74 Summary of the OLS regression analysis between PM10 concentration and significant factors on 1 March 2020.

No.	Factor	Coefficient	Std. Error	Probability	VIF
	Intercept	-0.00	0.12	1.00	--------
1	VIS	-0.09	0.19	0.65	2.58
2	AOD	0.43	0.14	0.00*	1.33
3	FD	-0.07	0.17	0.68	2.06
4	FH	-0.22	0.15	0.16	1.70
5	ELEV	-0.12	0.13	0.34	1.18
6	GPP	0.02	0.17	0.92	2.05

Note: an asterisk (*) at the significance level of 0.01.

As a result of OLS regression analysis in Table 5.74, if the probability at the confident level of 99% is not considered (ignored), the relationship between PM10 concentration and selected factors by VIF value can be explained into two types: positive and negative. The positive relationship between PM10 concentration and their factors occurred with MODIS AOD and GPP. This finding indicates that if these variables increase, the PM10 concentration increase. In contrast, the negative relationship between PM10 concentration and their factors is found with visibility, factory density, fire hotspot, and elevation. So, with the increase of these factors, the PM10 concentration decrease.

When the probability at the confident level of 99% is considered, the significant factors on PM10 concentration on 1 March 2020 is only MODIS AOD.

5.7 Significant daily spatiotemporal factors on PM2.5 concentration in the urban landscape

The multicollinearity test of daily explanatory variables performed in the SPSS statistical software is reported in Tables 5.75.

Table 5.75 Results of multicollinearity test of explanatory variables on PM2.5 concentration.

No.	Variable	The VIF value						
		7 Jan	8 Jan	9 Jan	10 Jan	11 Jan	12 Jan	13 Jan
1	RH	7.90	27.51	17.34	123.57	19.49	15.99	17.51
2	TEMP	21.06	37.12	12.66	23.35	9.03	94.88	18.51
3	WS	8.06	5.87	4.75	4.18	4.84	4.42	9.14
4	P	33.42	50.41	10.96	277.71	33.31	31.28	37.11
5	VIS	5.00	4.25	2.79	4.32	3.37	5.22	5.34
6	AOD	5.42	4.77	6.02	4.99	5.20	5.23	5.22
7	NDVI	65.68	68.78	68.81	77.46	71.44	63.88	66.28
8	BUI	100.42	103.48	110.88	111.13	108.61	93.81	96.91
9	RD	16.48	16.53	16.18	16.58	16.59	16.31	17.34
10	FD	3.84	4.01	3.71	4.05	4.03	3.98	3.62
11	BT	4.32	7.94	16.15	37.65	15.19	40.33	82.71
12	FRP	15.67	25.76	2.62	69.82	28.87	5.84	134.32
13	FH	2.64	3.32	1.86	3.08	2.00	3.39	2.51
14	ELEV	5.17	4.76	5.86	5.52	5.96	6.05	7.47
15	POP	44.72	53.92	31.73	34.20	31.06	30.98	26.57
16	GPP	31.18	32.59	23.32	27.69	23.45	22.30	20.22
Total variables		6	6	6	6	6	6	5

As a result, the VIF analysis shows that relative humidity, temperature, pressure, NDVI, BUI, road density, population density, and GPP are redundant for PM2.5 concentration models. Additionally, other redundant variables are cut each month differently. Hence, persist independent variables with a VIF value less than 7.5 are applied for OLS regression analysis. The result of the OLS regression analysis of PM2.5 concentration in the urban landscape daily is separately described and discussed below.

5.7.1 On 7 January 2020

The model performance showed that AICc is 201.22. The multiple R-squared is 0.25, while the adjusted R-squared is 0.18. The results of the OLS regression analysis are reported in Table 5.76.

Table 5.76 Summary of the OLS regression analysis between PM2.5 concentration and significant factors on 7 January 2020.

No.	Variable	Coefficient	Std. Error	Probability	VIF
	Intercept	-0.00	0.11	1.00	--------
1	VIS	0.38	0.16	0.04*	2.08
2	AOD	-0.03	0.13	0.83	1.45
3	FD	0.15	0.14	0.35	1.78
4	BT	0.20	0.13	0.01*	1.36
5	FH	0.04	0.13	0.60	1.53
6	ELEV	-0.45	0.13	0.00*	1.36

Note: an asterisk (*) at the significance level of 0.01.

As a result of OLS regression analysis in Table 5.76, if the probability at the confident level of 99% is not considered (ignored), the relationship between PM2.5 concentration and selected factors by VIF value can be explained into two types: positive and negative. The positive relationship between PM2.5 concentration and their factors occurred with visibility, factory density, brightness temperature, and fire hotspot. This finding indicates that if these variables increase, the PM2.5 concentration increase. In contrast, the negative relationship between PM2.5 concentration and their factors is found with MODIS AOD and elevation. So, with the increase of these factors, the PM2.5 concentration decrease.

When the probability at the confident level of 99% is considered, the significant factors on PM2.5 concentration on 7 January 2020 are visibility, brightness temperature, and elevation.

5.7.2 On 8 January 2020

The model performance showed that AICc is 154.40. The multiple R-squared is 0.61, while the adjusted R-squared is 0.57. The results of the OLS regression analysis are reported in Table 5.77.

Table 5.77 Summary of the OLS regression analysis between PM2.5 concentration and significant factors on 8 January 2020.

No.	Variable	Coefficient	Std. Error	Probability	VIF
	Intercept	0.00	0.08	1.00	--------
1	WS	-0.49	0.10	0.00*	1.69
2	VIS	0.33	0.11	0.01*	2.07
3	AOD	0.16	0.11	0.23	1.93
4	FD	-0.46	0.10	0.00*	1.52
5	FH	-0.03	0.09	0.79	1.46
6	ELEV	0.18	0.09	0.17	1.30

Note: an asterisk (*) at the significance level of 0.01.

As a result of OLS regression analysis in Table 5.77, if the probability at the confident level of 99% is not considered (ignored), the relationship between PM2.5 concentration and selected factors by VIF value can be explained into two types: positive and negative. The positive relationship between PM2.5 concentration and their factors occurred with visibility, MODIS AOD, and elevation. This finding indicates that if these variables increase, the PM2.5 concentration increase. In contrast, the negative relationship between PM2.5 concentration and their factors is found with wind speed, factory density, and fire hotspots. So, with the increase of these factors, the PM2.5 concentration decrease.

When the probability at the confident level of 99% is considered, the significant factors on PM2.5 concentration on 8 January 2020 are wind speed, visibility, and factory density.

5.7.3 On 9 January 2020

The model performance showed that AICc is 132.47. The multiple R-squared is 0.72, while the adjusted R-squared is 0.69. The results of the OLS regression analysis are reported in Table 5.78.

Table 5.78 Summary of the OLS regression analysis between PM2.5 concentration and significant factors on 9 January 2020.

No.	Variable	Coefficient	Std. Error	Probability	VIF
	Intercept	-0.00	0.07	1.00	--------
1	WS	-0.34	0.09	0.00*	1.85
2	VIS	0.66	0.10	0.00*	2.31
3	AOD	-0.02	0.10	0.81	2.19
4	FD	-0.14	0.09	0.12	1.69
5	FRP	0.34	0.08	0.00*	1.57
6	FH	0.01	0.08	0.94	1.65
7	ELEV	-0.11	0.08	0.25	1.47

Note: an asterisk (*) at the significance level of 0.01.

As a result of OLS regression analysis in Table 5.78, if the probability at the confident level of 99% is not considered (ignored), the relationship between PM2.5 concentration and selected factors by VIF value can be explained into two types: positive and negative. The positive relationship between PM2.5 concentration and their factors occurred with visibility, fire radiative power, and fire hotspot. This finding indicates that if these variables increase, the PM2.5 concentration increase. In contrast, the negative relationship between PM2.5 concentration and their factors is found with wind speed, MODIS AOD, factory density, and elevation. So, with the increase of these factors, the PM2.5 concentration decrease.

When the probability at the confident level of 99% is considered, the significant factors on PM2.5 concentration on 9 January 2020 are wind speed, visibility, and fire radiative power.

5.7.4 On 10 January 2020

The model performance showed that AICc is 87.61. The multiple R-squared is 0.84, while the adjusted R-squared is 0.83. The results of the OLS regression analysis are reported in Table 5.79.

Table 5.79 Summary of the OLS regression analysis between PM2.5 concentration and significant factors on 10 January 2020.

No.	Factor	Coefficient	Std. Error	Probability	VIF
	Intercept	0.00	0.05	1.00	--------
1	WS	-0.43	0.07	0.00*	1.93
2	VIS	0.70	0.07	0.00*	2.06
3	AOD	0.01	0.06	0.89	1.68
4	FD	0.10	0.06	0.09	1.53
5	FH	-0.05	0.06	0.45	1.47
6	ELEV	-0.20	0.07	0.00*	1.85

Note: an asterisk (*) at the significance level of 0.01.

As a result of OLS regression analysis in Table 5.79, if the probability at the confident level of 99% is not considered (ignored), the relationship between PM2.5 concentration and selected factors by VIF value can be explained into two types: positive and negative. The positive relationship between PM2.5 concentration and their factors occurred with visibility, MODIS AOD, and factory density. This finding indicates that if these variables increase, the PM2.5 concentration increase. In contrast, the negative relationship between PM2.5 concentration and their factors is found with wind speed, fire hotspots, and elevation. So, with the increase of these factors, the PM2.5 concentration decrease.

When the probability at the confident level of 99% is considered, the significant factors on PM2.5 concentration on 10 January 2020 are wind speed, visibility, and elevation.

5.7.5 On 11 January 2020

The model performance showed that AICc is 175.58. The multiple R-squared is 0.47, while the adjusted R-squared is 0.42. The results of the OLS regression analysis are reported in Table 5.80.

Table 5.80 Summary of the OLS regression analysis between PM2.5 concentration and significant factors on 11 January 2020.

No.	Factor	Coefficient	Std. Error	Probability	VIF
	Intercept	-0.00	0.09	1.00	--------
1	WS	-0.59	0.16	0.00*	3.26
2	VIS	0.15	0.14	0.36	2.32
3	AOD	0.07	0.12	0.64	1.83
4	FD	-0.57	0.11	0.00*	1.55
5	FH	0.02	0.11	0.85	1.46
6	ELEV	0.12	0.12	0.46	1.81

Note: an asterisk (*) at the significance level of 0.01.

As a result of OLS regression analysis in Table 5.80, if the probability at the confident level of 99% is not considered (ignored), the relationship between PM2.5 concentration and selected factors by VIF value can be explained into two types: positive and negative. The positive relationship between PM2.5 concentration and their factors occurred with visibility, MODIS AOD, fire hotspot, and elevation. This finding indicates that if these variables increase, the PM2.5 concentration increase. In contrast, the negative relationship between PM2.5 concentration and their factors is found with wind speed and factory density. So, with the increase of these factors, the PM2.5 concentration decrease.

When the probability at the confident level of 99% is considered, the significant factors on PM2.5 concentration on 11 January 2020 are wind speed and factory density

5.7.6 On 12 January 2020

The model performance showed that AICc is 103.86. The multiple R-squared is 0.81, while the adjusted R-squared is 0.79. The results of the OLS regression analysis are reported in Table 5.81.

Table 5.81 Summary of the OLS regression analysis between PM2.5 concentration and significant factors on 12 January 2020.

No.	Factor	Coefficient	Std. Error	Probability	VIF
	Intercept	-0.00	0.05	1.00	--------
1	WS	-0.23	0.09	0.00*	2.64
2	VIS	0.02	0.08	0.82	2.25
3	AOD	-0.05	0.07	0.63	1.73
4	FD	-0.11	0.08	0.08	1.92
5	FRP	-0.76	0.07	0.00*	1.69
6	FH	0.13	0.07	0.05*	1.47
7	ELEV	0.12	0.08	0.16	2.40

Note: an asterisk (*) at the significance level of 0.01.

As a result of OLS regression analysis in Table 5.81, if the probability at the confident level of 99% is not considered (ignored), the relationship between PM2.5 concentration and selected factors by VIF value can be explained into two types: positive and negative. The positive relationship between PM2.5 concentration and their factors occurred with visibility, fire hotspot, and elevation. This finding indicates that if these variables increase, the PM2.5 concentration increase. In contrast, the negative relationship between PM2.5 concentration and their factors is found with wind speed, MODIS AOD, factory density, and fire radiative power. So, with the increase of these factors, the PM2.5 concentration decrease.

When the probability at the confident level of 99% is considered, the significant factors on PM2.5 concentration on 12 January 2020 are wind speed, fire radiative power, and fire hotspot.

5.7.7 On 13 January 2020

The model performance showed that AICc is 192.53. The multiple R-squared is 0.31, while the adjusted R-squared is 0.26. The results of the OLS regression analysis are reported in Table 5.82.

Table 5.82 Summary of the OLS regression analysis between PM2.5 concentration and significant factors on 13 January 2020.

No.	Variable	Coefficient	Std. Error	Probability	VIF
	Intercept	-0.00	0.10	1.00	--------
1	VIS	0.32	0.15	0.05	2.06
2	AOD	-0.23	0.12	0.14	1.35
3	FD	-0.27	0.13	0.01*	1.52
4	FH	0.09	0.12	0.44	1.46
5	ELEV	0.54	0.12	0.00*	1.30

Note: an asterisk (*) at the significance level of 0.01.

As a result of OLS regression analysis in Table 5.82, if the probability at the confident level of 99% is not considered (ignored), the relationship between PM2.5 concentration and selected factors by VIF value can be explained into two types: positive and negative. The positive relationship between PM2.5 concentration and their factors occurred with visibility, fire hotspot, and elevation. This finding indicates that if these variables increase, the PM2.5 concentration increase. In contrast, the negative relationship between PM2.5 concentration and their factors is found with MODIS AOD and factory density. So, with the increase of these factors, the PM2.5 concentration decrease.

When the probability at the confident level of 99% is considered, the significant factors on PM2.5 concentration on 13 January 2020 are factory density and elevation.

Summary

According to significant spatiotemporal factors reports on PM10 and PM2.5 concentration in Sections 5.3 and 5.4, the significant factors on PM10 and PM2.5 concentration in rural and urban landscapes in the winter and summer seasons can be summarized with frequency in Tables 5.83 to 5.86.

Table 5.83 Frequency of significant factors on PM10 concentration in the winter season.

No.	Significant factor	Oct-19	Nov-19	Dec-19	Jan-20	Feb-20	Frequency
1	WS	Yes	Yes	Yes		Yes	4 of 5
2	TEMP	Yes		Yes	Yes		3 of 5
3	VIS	Yes	Yes	Yes			3 of 5
4	AOD		Yes		Yes		2 of 5
5	FRP					Yes	1 of 5

Table 5.84 Frequency of significant factors on PM10 concentration in the summer season.

No.	Significant factor	Mar-20	Apr-20	May-20	Frequency
1	FD	Yes			2 of 3
2	TEMP	Yes			1 of 3
3	AOD	Yes			1 of 3
4	BT		Yes		1 of 3
5	VIS			Yes	1 of 3

Table 5.85 Frequency of significant factors on PM2.5 concentration in the winter season.

No.	Significant factor	Oct-19	Nov-19	Dec-19	Jan-20	Feb-20	Frequency
1	VIS	Yes	Yes	Yes	Yes		4 of 5
2	WS	Yes		Yes		Yes	3 of 5
3	FRP	Yes	Yes			Yes	3 of 5
4	ELEV	Yes			Yes	Yes	3 of 5
5	P	Yes				Yes	2 of 5
6	AOD	Yes			Yes		2 of 5
7	FH	Yes			Yes		2 of 5
8	RH					Yes	1 of 5
9	TEMP				Yes		1 of 5
10	BT	Yes					1 of 5

Table 5.86 Frequency of significant factors on PM2.5 concentration in the summer season.

No.	Significant factor	Mar-20	Apr-20	May-20	Frequency
1	WS		Yes	Yes	2 of 3
2	VIS		Yes	Yes	2 of 3
3	FD		Yes	Yes	2 of 3
4	BT		Yes	Yes	2 of 3
5	FRP	Yes	Yes		2 of 3
6	AOD		Yes		1 of 3
7	FH		Yes		1 of 3
8	ELEV			Yes	1 of 3

In the case of PM10 concentration in the rural landscape (Tables 5.83 and 5.84), the number of significant factors on PM10 concentration in winter and summer are five and five factors. As a result, three common factors on PM10 concentration, namely temperature, visibility, and MODIS AOD, are identified in both seasons. Two significant factors on PM10 concentration are only found in the winter season, including wind speed and fire radiative power. On the contrary, two significant factors on PM10 concentration, factory density and brightness temperature, are only found in the summer season.

The significant factors on PM10 concentration in this study are similar to the previous study by Harnkijroong and Panich (2013). They reported that PM10 concentration at the roadside of Bangkok is most relevant to temperature, followed by wind speed. And also found that rainfall did not influence PM10 concentration. Furthermore, Unal, Toros, Deniz, and Incecik (2011) suggested that PM10 concentration are associated with wind speed. Moreover, Czernecki et al. (2017) also suggested that the most significant meteorological factors include planetary boundary layer height, temperature, wind speed, and precipitation influenced by the seasonal dynamics of PM10 concentration. In addition, many studies show the relationship between MODIS AOD and PM10 concentration (Ferrero et al., 2019; Grgurić et al., 2014; Kanabkaew, 2013; Syafrijon, Marzuki, Emriadi, and Pratama, 2018). Ferrero et al. (2019) especially report the high relationship and developed a high accuracy algorithm to predict ground PM concentration based on AOD mixing height and wind speed. At the same time, Kanabkaew (2013) reported that the relationship between AOD and hourly PM improved accuracy when corrected with meteorological factors, including relative humidity and temperature data. In contrast, the study of the relationship between PM10 concentration and MODIS fire data was incomprehensive.

In the case of PM2.5 concentration in the urban landscape (Tables 5.85 and 5.86), the significant factors on PM2.5 in winter and summer are ten and eight factors. Furthermore, many meteorological factors significantly influenced PM2.5 than PM10 concentration (Chen et al., 2017). As a result, there are seven common factors on PM2.5 concentration in both seasons: wind speed, visibility, brightness temperature, fire radiative power, MODIS AOD, fire hotspot, and elevation. Furthermore, it was found that three significant factors on PM2.5 concentration are only found in the winter season, including relative humidity, temperature, and pressure. In contrast, one significant factor in PM2.5 concentration, factory density, is only found in the summer season.

The findings show similar results to the previous study of Guo and Zhang (2014), who reported that PM2.5 concentration is most relevant to visibility, followed by the wind speed. The least pertinent factors are temperature and relative humidity. Additionally, these findings are consistent with the previous work of Chen et al. (2017), who showed the strong influence of wind speed on local PM2.5 concentration. The wind speed also strongly interacts with other meteorological factors, influencing PM2.5 concentration. While Galindo, Varea, Gil-Moltó, Yubero, and Nicolás (2011) found that the winter wind speed is the main effect of the dilution of atmospheric aerosols. At the same time, temperature and solar radiation strongly influenced coarse particles. That means the meteorological data, solar heating at the earth's surface, or active fire data significantly affect PM2.5 concentration. In addition, MODIS AOD had a strong correlation with PM2.5 concentration (Gu, 2019; Kong, Xin, Zhang, and Wang, 2016). Like Lee, Liu, Coull, Schwartz, and Koutrakis (2011) reported and potentially helpful in predicting PM2.5 concentration. And Chudnovsky et al. (2014) predicted PM2.5 concentration with MODIS AOD and improved the accuracy with land use and meteorological data. However, Chu et al. (2016) suggested using higher-resolution AOD data to estimate PM2.5 in a relatively small area more accurately.

Furthermore, the significant factors on daily PM10 and PM2.5 concentration in rural and urban landscapes can be summarized with their frequency in Tables 5.87 to 5.88.

Table 5.87 Frequency of significant daily factors on PM10 concentration.

No.	Significant factor	Winter season						Summer season	Frequency
		24 Feb	25 Feb	26 Feb	27 Feb	28 Feb	29 Feb	1 Mar	
1	VIS					Yes	Yes		2 of 7
2	AOD	Yes						Yes	2 of 7
3	FD	Yes					Yes		2 of 7
4	FRP	Yes					Yes		2 of 7
5	GPP		Yes						1 of 7
6	TEMP					Yes			1 of 7
7	WS						Yes		1 of 7
8	BT						Yes		1 of 7
9	ELEV						Yes		1 of 7

Table 5.88 Frequency of significant daily factors on PM2.5 concentration.

No.	Significant factor	Winter season							Frequency
		7 Jan	8 Jan	9 Jan	10 Jan	11 Jan	12 Jan	13 Jan	
1	WS		Yes	Yes	Yes	Yes	Yes		5 of 7
2	VIS	Yes	Yes	Yes	Yes				4 of 7
3	ELEV	Yes			Yes			Yes	3 of 7
4	FD		Yes			Yes		Yes	3 of 7
5	FRP			Yes			Yes		2 of 7

As a result, there are nine daily factors on PM10 concentration in the rural landscape in the winter and summer seasons (Table 5.87). Besides, only one common daily factor, MODIS AOD, is found in both seasons. The frequency of daily factors from both seasons is relatively low, varying from 1 of 7 to 2 of 7.

Besides, by comparing the significant daily factors and significant monthly factors on PM10 concentration in the winter season, all five monthly significant factors on PM10 concentration in the winter season (Table 5.83) are identified as daily significant on PM10 concentration, including wind speed, temperature, visibility, MODIS AOD, and fire radiative. Likewise, all five monthly significant factors on PM10 concentration in the summer season (Table 5.84) are daily significant on PM10 concentration, including factory density, temperature, MODIS AOD, brightness temperature, and visibility. Additionally, only two daily significant factors on PM10 concentration: GPP and elevation, are not identified in both seasons.

Besides, by comparing the significant daily factors and significant monthly factors on PM2.5 concentration in the winter season, only four monthly significant factors on PM2.5 concentration in the winter season (Table 5.85) are identified as daily significant on PM2.5 concentration, including visibility, wind speed, fire radiative and elevation. Additionally, only one daily significant on PM10 concentration, factory density is not identified as a significant monthly factor under this season. Interestingly, six-monthly significant factors on PM2.5 concentration, including pressure, MODIS AOD, fire hotspot, relative humidity, temperature, and brightness temperature, are not significant daily factors on PM2.5 concentration.

Consequently, the derivation of significant monthly factors on PM10 and PM2.5 concentration in winter and summer seasons, which cover almost daily significant factors, are further applied to predict monthly and seasonally PM10 and PM2.5 concentration using GWR and MEM models in the next component. This study will apply significant monthly factors to predict PM concentration in the corresponding month. Meanwhile, all significant monthly factors in each season will be combined and applied to predict PM concentration in the corresponding season. The next chapter will report the monthly and seasonally PM concentration prediction using GWR and MEM.

CHAPTER VI
PREDICTION OF SPATIOTEMPORAL PM CONCENTRATION

This chapter presents the study's second objective to predict spatiotemporal PM10 and PM2.5 concentration using GWR and MEM models. The significant monthly and seasonal factors on PM10 and PM2.5 concentration from Chapter 5 were separately applied to predict PM concentration. The standard function of the GWR model with the adaptive kernel type and AICc bandwidth was applied to predict PM concentration under the ArcMap software environment. At the same time, the MEM model with fixed effects intercepts and scaled identity covariance type was applied to predict PM concentration under the IBM SPSS Statistics Version 25 (Bruin, 2006; SPSS Inc., 2005). Herein, the estimation of the linear mixed model was using the restricted maximum likelihood (REML) method. The main results consist of (1) the predictive equations and their distribution map for spatiotemporal PM10 concentration in the rural landscape using the GWR model, (2) the predictive equations and their distribution map for spatiotemporal PM2.5 concentration in the urban landscape using the GWR model, (3) the predictive equations and their distribution for spatiotemporal PM10 concentration in the rural landscape using the MEM model, and (4) the predictive equations and their distribution map for spatiotemporal PM2.5 concentration in the urban landscape using the MEM model and (5) comparison of spatiotemporal patterns of particulate matter concentration using GWR and MEM models, are here described and discussed in detail.

6.1 The predictive equations and their distribution map for spatiotemporal PM10 concentration in the rural landscape using the GWR model

Under this section, the GWR model with the significant derived factors was applied to predict monthly PM10 concentration in winter and summer in the rural landscape. The generic equations for PM10 concentration in winter and summer in the rural landscape are shown in Equations 6.1 and 6.2.

$$y_{(i,j)}=\beta o_{i,j}+\beta k_{1(i,j)}TEMP+\beta k_{2(i,j)}WS+\beta k_{3(i,j)}VIS+\beta k_{4(i,j)}FRP+\beta k_{5(i,j)}AOD+\varepsilon_{(i,j)} \quad (6.1)$$

$$y_{(i,j)}=\beta o_{i,j}+\beta k_{1(i,j)}TEMP+\beta k_{3(i,j)}VIS+\beta k_{5(i,j)}AOD+\beta k_{6(i,j)}BT+\beta k_{7(i,j)}FD+\varepsilon_{(i,j)} \quad (6.2)$$

Where $\beta o_{i,j}$ denotes intercept value at district i, month j; $\beta k_{1(i,j)}$ denotes the coefficients of temperature; $\beta k_{2(i,j)}$ denotes the coefficients of wind speed; $\beta k_{3(i,j)}$ denotes the coefficients of visibility; $\beta k_{4(i,j)}$ denotes the coefficients of fire radiative power; $\beta k_{5(i,j)}$ denotes the coefficients of MODIS AOD; $\beta k_{6(i,j)}$ denotes the coefficients of brightness temperature; $\beta k_{7(i,j)}$ denotes the coefficients of factory density; $\varepsilon_{(i,j)}$ is residual values. TEMP, WS, VIS, FRP, AOD, BT, and FD are significant normalization variables.

The monthly predictive equation of PM10 concentration in winter and summer in rural landscapes is systematically reported in a table in the following sections. As a result, columns, namely Intercept, Regression coefficient, and Residual, summarize a fitting regression equation for every district of sixty districts—columns LocalR^2 and Predicted (μg/m^3) display local R squares and predicted value in microgram per cubic meter. Meanwhile, the performance of the GWR model for spatiotemporal PM10 concentration prediction is reported, including AICc, R-square, and adjusted R-square.

6.1.1 October 2019 in the winter season

The result of the GWR model for PM10 concentration prediction in October 2019 in the winter season is summarized in Table 6.1. The model performance shows that AICc, R-square, and adjusted R-square values are 89.88, 0.93, and 0.88, respectively.

Table 6.1 The predictive equations of PM10 concentration in October 2019.

No.	District	Intercept	Regression coefficient			Residual	LocalR2	Predicted
			WS	TEMP	VIS			(µg/m³)
1	Chaiyo	0.64	0.82	0.75	0.23	0.00	0.85	52.56
2	Mueang Ang Thong	0.16	0.65	0.35	-0.27	-0.01	0.82	52.40
3	Pa Mok	-0.10	0.45	0.09	-0.47	0.10	0.93	52.10
4	Pho Thong	1.02	1.05	0.80	0.53	0.09	0.73	52.20
5	Samko	-0.16	0.00	-0.37	-0.21	-0.16	0.21	52.13
6	Sawaeng Ha	1.20	1.07	0.62	0.58	0.06	0.77	52.15
7	Wiset Chai Chan	-0.20	0.20	-0.26	-0.42	-0.12	0.62	52.14
8	Ban Mi	0.06	0.34	0.67	0.04	-0.26	0.67	52.77
9	Chai Badan	0.60	1.51	0.56	-0.46	0.20	0.82	51.79
10	Khok Charoen	0.41	1.09	0.44	-0.22	-0.06	0.71	51.93
11	Khok Samrong	0.51	1.56	0.63	-0.56	-0.21	0.85	52.88
12	Lam Sonthi	0.50	1.37	0.48	-0.49	-0.09	0.80	51.80
13	Mueang Lop Buri	0.81	1.67	0.90	0.13	-0.28	0.71	53.74
14	Nong Muang	0.46	0.70	0.52	0.42	-0.04	0.77	52.13
15	Phatthana Nikhom	0.87	1.51	0.73	-0.13	0.01	0.73	52.94
16	Sa Bot	0.58	1.40	0.51	-0.22	-0.12	0.89	52.24
17	Tha Luang	0.69	1.45	0.59	-0.46	0.25	0.77	51.86
18	Tha Wung	0.61	0.73	0.69	0.15	0.00	0.91	52.79
19	Khlong Luang	-0.86	0.06	-0.28	-0.28	-0.21	0.78	51.66
20	Lam Luk Ka	-0.80	0.17	-0.14	-0.36	0.37	0.67	51.47
21	Lat Lum Kaeo	-0.86	-0.26	-0.12	-0.18	0.47	0.59	50.77
22	Mueang Pathum Thani	-0.64	-0.09	-0.13	-0.30	-0.37	0.62	50.53
23	Nong Suea	-0.38	0.13	0.32	-0.37	-0.31	0.52	52.35
24	Sam Khok	-0.63	-0.13	-0.10	-0.33	-0.45	0.65	50.94
25	Thanyaburi	-0.80	0.15	-0.17	-0.35	-0.09	0.70	51.69
26	Ban Phraek	0.37	0.75	0.78	-0.08	0.01	0.93	52.75
27	Bang Ban	-0.36	0.09	-0.13	-0.55	-0.03	0.96	51.87
28	Bang Pa-In	-0.67	-0.21	-0.31	-0.42	0.01	0.96	51.40
29	Bang Pahan	0.05	0.49	0.36	-0.34	0.08	0.96	52.20
30	Bang Sai	-0.82	-0.24	-0.17	-0.22	-0.22	0.68	51.40
31	Bang Sai	-0.39	0.20	0.03	-0.45	-0.23	0.79	51.41
32	Lat Bua Luang	-1.18	-0.44	-0.20	0.01	-0.04	0.68	51.28
33	Maha Rat	0.25	0.64	0.53	-0.18	-0.02	0.93	52.58

Table 6.1 (Continued).

No.	District	Intercept	Regression coefficient			Residual	LocalR2	Predicted
			WS	TEMP	VIS			($\mu g/m^3$)
34	Nakhon Luang	0.20	0.50	0.54	-0.25	0.09	0.95	52.48
35	Phachi	0.47	0.06	0.75	-0.42	-0.06	0.78	52.76
36	Phak Hai	-0.38	0.10	-0.26	-0.48	0.10	0.92	51.81
37	Phra Nakhon Si Ayutthaya	-0.42	-0.02	-0.15	-0.54	0.03	0.92	51.71
38	Sena	-0.46	0.06	-0.02	-0.44	-0.03	0.75	51.48
39	Tha Ruea	0.78	0.53	1.02	0.20	-0.08	0.83	53.22
40	Uthai	0.20	-0.01	0.48	-0.50	0.13	0.85	52.20
41	Wang Noi	-0.31	-0.06	0.11	-0.46	-0.18	0.65	52.24
42	Ban Mo	1.70	0.52	1.63	1.14	0.09	0.79	53.61
43	Chaloem Phra Kiat	3.87	-1.30	0.91	1.90	1.02	0.53	55.03
44	Don Phut	0.65	0.76	1.02	0.20	-0.22	0.89	53.19
45	Kaeng Khoi	4.20	-2.39	0.36	0.53	0.59	0.47	52.99
46	Muak Lek	0.97	0.71	0.40	-0.85	-0.07	0.67	52.48
47	Mueang Saraburi	3.45	-1.95	0.63	0.58	0.15	0.33	53.46
48	Nong Don	0.79	1.23	1.55	0.54	0.05	0.73	53.76
49	Nong Khae	1.80	-1.32	1.20	-0.59	-0.12	0.58	52.77
50	Nong Saeng	2.01	-1.09	1.20	0.01	-0.11	0.55	53.27
51	Phra Phutthabat	1.30	1.16	1.47	0.95	0.58	0.44	54.64
52	Sao Hai	4.07	-1.78	1.04	1.80	0.48	0.59	53.86
53	Wang Muang	1.14	0.81	0.57	-0.39	0.41	0.67	52.38
54	Wihan Daeng	1.99	-1.24	0.76	-0.21	-0.42	0.21	53.01
55	Bang Rachan	1.01	0.80	0.18	0.30	-0.10	0.72	52.31
56	In Buri	0.91	0.65	-0.08	0.04	0.00	0.74	52.29
57	Khai Bang Rachan	1.15	1.03	0.60	0.54	-0.04	0.79	52.32
58	Mueang Sing Buri	0.86	0.70	0.17	0.17	0.13	0.78	52.37
59	Phrom Buri	0.84	0.88	0.74	0.39	0.00	0.91	52.62
60	Tha Chang	1.02	0.98	0.69	0.50	0.07	0.85	52.42

From Table 6.1, the maximum value is 55.03 $\mu g/m^3$ in Chaloem Phra Kiat District, Saraburi province. In contrast, the minimum value is 50.53 $\mu g/m^3$ in Mueang Pathum Thani District, Pathum Thani province. The classification maps of prediction values for PM10 concentration using the GWR model according to the Thailand Air Quality Index and the U.S. EPA Air Quality Index are displayed in Figure 6.1.

As a result, the predicted values of PM10 concentration in October 2019 are satisfactory at level 2, according to Thailand AQI. Still, according to the EPA AQI, they are good at level 1. However, the predicted value in the rural landscape in October 2019 from the GWR model is more than the one-day mean of WHO guidelines (Table 3.5).

In addition, a spatial distribution map of PM10 concentration in October 2019 using the SCK interpolation technique is displayed in Figure 6.2. As a result, the high PM10 concentration occur on agricultural land in the central part of the study area, particularly in Lob Buri and Saraburi province.

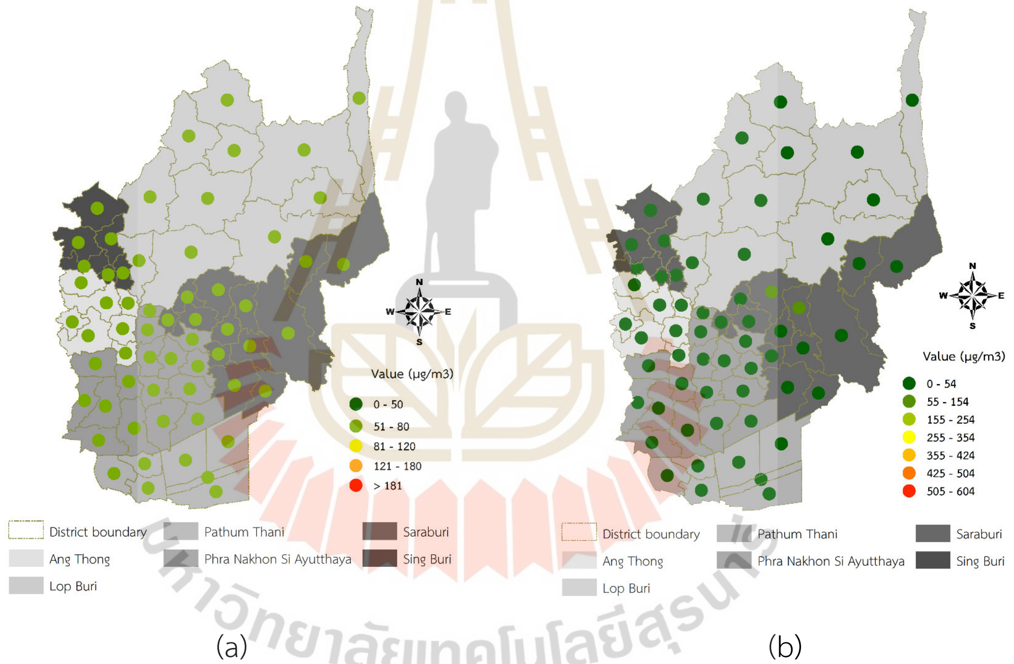

Figure 6.1 The classification map of PM10 concentration prediction using the GWR model in October 2019 according to the (a) Thailand AQI and (b) EPA AQI.

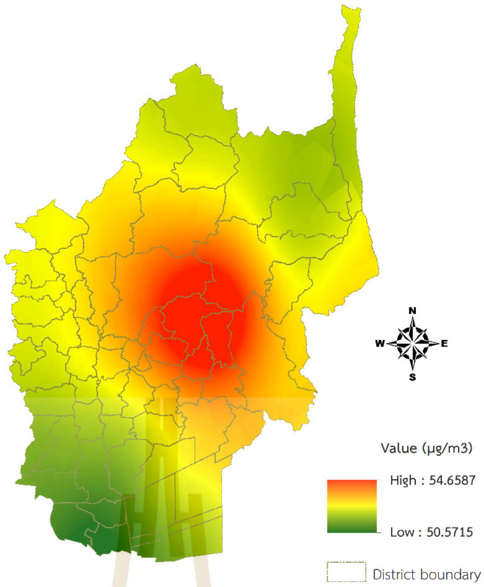

Figure 6.2 Spatial distribution of PM10 concentration in October 2019.

6.1.2 November 2019 in the winter season

The result of the GWR model for PM10 concentration prediction in November 2019 in the winter season is summarized in Table 6.2. The model performance shows that AICc, R-square, and adjusted R-square values are 91.16, 0.96, and 0.91, respectively.

Table 6.2 The predictive equations of PM10 concentration in November 2019.

No.	District	Intercept	Regression coefficient			Residual	LocalR2	Predicted ($\mu g/m^3$)
			WS	VIS	AOD			
1	Chaiyo	0.35	0.57	-0.35	0.01	0.00	0.95	65.22
2	Mueang Ang Thong	0.31	0.65	-0.47	0.03	0.11	0.91	64.86
3	Pa Mok	0.24	0.68	-0.75	0.04	0.09	0.80	64.64
4	Pho Thong	0.43	0.73	-0.42	0.01	0.05	0.93	64.91
5	Samko	0.53	0.89	-0.52	0.02	0.00	0.93	64.70
6	Sawaeng Ha	0.52	0.78	-0.37	-0.02	0.06	0.91	64.83
7	Wiset Chai Chan	0.55	0.95	-0.60	0.03	-0.06	0.91	64.60
8	Ban Mi	0.53	0.20	0.18	-0.05	-0.11	0.19	65.12
9	Chai Badan	-0.32	0.47	-0.20	-0.04	-0.05	0.69	64.58
10	Khok Charoen	-0.30	0.66	-0.28	-0.04	-0.08	0.58	64.44
11	Khok Samrong	0.08	0.72	-0.40	0.55	-0.27	0.47	65.41
12	Lam Sonthi	-0.34	0.44	-0.16	-0.04	0.05	0.75	64.22

Table 6.2 (Continued).

No.	District	Intercept	Regression coefficient			Residual	LocalR2	Predicted
			WS	VIS	AOD			(μg/m³)
13	Mueang Lop Buri	2.41	-0.41	1.61	0.55	-0.03	0.78	66.12
14	Nong Muang	-0.39	0.71	-0.55	-0.01	-0.26	0.55	64.82
15	Phatthana Nikhom	-0.81	0.29	-1.58	1.94	-0.25	0.43	65.82
16	Sa Bot	-0.34	0.77	-0.47	0.02	-0.07	0.58	64.68
17	Tha Luang	-0.23	0.35	-0.31	0.10	-0.33	0.40	65.04
18	Tha Wung	0.49	0.85	-0.48	0.05	-0.03	0.90	65.48
19	Khlong Luang	-0.31	0.22	-0.86	-0.27	-0.09	0.63	63.86
20	Lam Luk Ka	-0.45	0.15	-0.72	-0.39	-0.02	0.63	64.15
21	Lat Lum Kaeo	-0.82	-0.07	-0.55	-0.01	0.20	0.74	63.48
22	Mueang Pathum Thani	-0.27	0.14	-0.90	-0.12	-0.28	0.54	63.37
23	Nong Suea	-0.25	0.40	-0.85	-0.28	0.35	0.49	63.96
24	Sam Khok	-0.49	0.06	-0.77	-0.09	-0.18	0.63	63.34
25	Thanyaburi	-0.55	0.16	-0.66	-0.41	0.04	0.64	63.94
26	Ban Phraek	0.53	0.64	-0.21	-0.07	0.00	0.70	65.47
27	Bang Ban	0.32	0.76	-1.70	-0.01	0.02	0.96	64.42
28	Bang Pa-In	0.07	0.72	-1.31	-0.03	-0.29	0.77	64.20
29	Bang Pahan	0.14	0.52	-0.90	0.07	0.05	0.94	64.84
30	Bang Sai	-0.50	0.07	-0.79	-0.10	-0.05	0.83	63.85
31	Bang Sai	-0.12	0.46	-0.99	-0.03	-0.10	0.85	63.91
32	Lat Bua Luang	-0.66	0.00	-0.67	-0.04	-0.06	0.80	63.78
33	Maha Rat	0.19	0.53	-0.68	0.06	-0.01	0.84	65.22
34	Nakhon Luang	0.11	0.62	-0.72	0.11	-0.03	0.92	65.09
35	Phachi	0.14	0.74	-0.74	0.25	0.04	0.84	65.07
36	Phak Hai	0.49	1.11	-1.02	0.07	0.11	0.79	64.39
37	Phra Nakhon Si Ayutthaya	0.37	0.85	-1.72	0.02	-0.02	0.85	64.35
38	Sena	-0.18	0.30	-1.07	-0.07	-0.08	0.88	64.08
39	Tha Ruea	0.07	0.93	-0.87	0.21	-0.38	0.60	66.05
40	Uthai	0.03	0.81	-0.82	0.16	0.06	0.88	64.62
41	Wang Noi	-0.19	0.86	-1.02	-0.12	0.01	0.68	64.36
42	Ban Mo	-0.09	1.29	-1.25	0.58	-0.01	0.33	66.38
43	Chaloem Phra Kiat	-0.22	1.79	-2.13	1.26	0.62	0.72	68.23
44	Don Phut	0.20	0.68	-1.07	0.03	-0.31	0.65	65.97
45	Kaeng Khoi	5.13	-2.01	-2.28	0.18	0.16	0.78	66.00
46	Muak Lek	0.48	0.10	-1.10	0.44	-0.38	0.11	65.49
47	Mueang Saraburi	1.11	0.80	-1.89	0.58	0.26	0.71	65.64
48	Nong Don	-0.38	1.70	-1.62	0.71	0.50	0.27	66.13

Table 6.2 (Continued).

No.	District	Intercept	Regression coefficient			Residual	LocalR2	Predicted
			WS	VIS	AOD			($\mu g/m^3$)
49	Nong Khae	0.58	0.71	-1.24	0.26	0.00	0.85	65.01
50	Nong Saeng	0.05	1.15	-1.07	0.34	-0.33	0.66	65.91
51	Phra Phutthabat	-1.08	2.31	-2.15	1.58	0.18	0.71	67.85
52	Sao Hai	-0.02	1.54	-1.66	0.90	-0.15	0.62	66.99
53	Wang Muang	0.28	-0.01	-0.52	1.07	-0.38	0.18	65.88
54	Wihan Daeng	1.34	0.46	-1.72	0.30	-0.03	0.86	65.02
55	Bang Rachan	0.84	0.56	0.03	0.02	-0.01	0.85	64.88
56	In Buri	0.91	0.23	0.35	-0.01	0.02	0.72	64.82
57	Khai Bang Rachan	0.64	0.69	-0.21	-0.01	0.02	0.90	64.93
58	Mueang Sing Buri	0.81	0.37	0.18	-0.02	0.05	0.75	65.02
59	Phrom Buri	0.48	0.66	-0.28	-0.05	-0.01	0.98	65.28
60	Tha Chang	0.49	0.67	-0.28	-0.04	0.04	0.97	65.08

From Table 6.2, the maximum value is 68.23 $\mu g/m^3$ in Chaloem Phra Kiat District, Saraburi province. In contrast, the minimum value is 63.34 $\mu g/m^3$ in Sam Khok District, Pathum Thani province. The classification maps of prediction values for PM10 concentration using the GWR according to the Thailand Air Quality Index and the U.S. EPA Air Quality Index are displayed in Figure 6.3.

As a result, the predicted values of PM10 concentration are satisfactory at level 2 according to Thailand AQI and moderate at level 2 according to EPA AQI. However, the predicted values in rural landscape in November 2019 obtained from the GWR model are more than the WHO guideline.

In addition, a spatial distribution map of PM10 concentration in November 2019 using the SCK interpolation technique is displayed in Figure 6.4. As a result, the high PM10 concentration occur on agricultural land in the central part of the study area, particularly Lob Buri and Saraburi province.

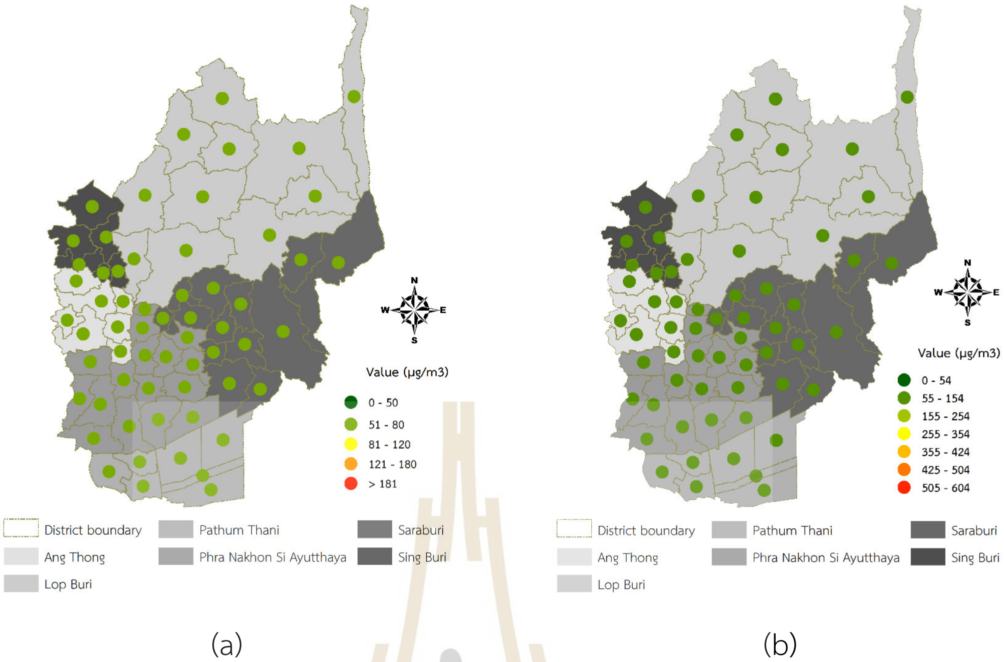

Figure 6.3 The classification map of PM10 concentration prediction using the GWR model in November 2019 according to the (a) Thailand AQI and (b) EPA AQI.

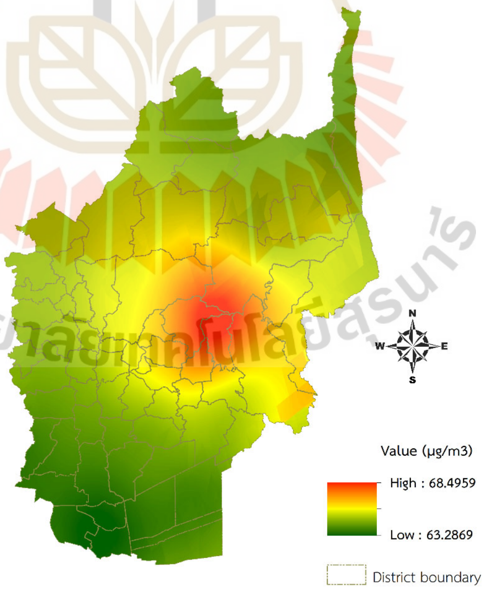

Figure 6.4 Spatial distribution of PM10 concentration in November 2019.

6.1.3 December 2019 in the winter season

The result of the GWR model for PM10 concentration prediction in December 2019 in the winter season is summarized in Table 6.3. The model performance shows that AICc, R-square, and adjusted R-square values are 123.24, 0.90, and 0.80, respectively.

Table 6.3 The predictive equations of PM10 concentration in December 2019.

No.	District	Intercept	Regression coefficient			Residual	LocalR2	Predicted
			TEMP	WS	VIS			(µg/m^3)
1	Chaiyo	-0.10	0.15	0.30	-0.11	0.00	0.75	74.42
2	Mueang Ang Thong	-0.13	0.25	0.13	0.05	-0.04	0.91	74.41
3	Pa Mok	-0.08	-0.03	0.03	0.26	-0.01	0.68	74.46
4	Pho Thong	-0.12	-0.01	0.25	-0.04	0.00	0.96	74.23
5	Samko	-0.13	0.03	0.20	-0.02	0.00	0.90	74.15
6	Sawaeng Ha	-0.11	0.00	0.22	-0.02	-0.01	0.96	74.18
7	Wiset Chai Chan	-0.14	0.08	0.14	0.04	0.00	0.81	74.21
8	Ban Mi	-0.14	0.10	0.01	0.13	-0.11	0.29	74.42
9	Chai Badan	-0.13	0.63	1.02	0.16	0.36	0.42	73.53
10	Khok Charoen	-0.37	0.03	0.41	-0.16	0.00	0.26	74.08
11	Khok Samrong	-0.24	0.46	1.21	-0.32	-0.53	0.46	75.17
12	Lam Sonthi	-0.21	0.39	0.81	-0.02	-0.25	0.34	74.47
13	Mueang Lop Buri	-0.88	0.65	2.50	-3.27	-0.34	0.70	75.96
14	Nong Muang	-0.38	-0.01	0.30	-0.16	-0.12	0.16	74.29
15	Phatthana Nikhom	0.29	1.09	1.44	0.22	-0.18	0.62	75.13
16	Sa Bot	-0.26	0.31	0.66	0.07	-0.11	0.38	74.27
17	Tha Luang	0.19	0.91	1.05	0.36	0.46	0.49	73.38
18	Tha Wung	0.06	0.09	0.77	-0.44	0.03	0.84	74.52
19	Khlong Luang	-0.34	-0.06	0.06	-0.20	-0.25	0.52	73.95
20	Lam Luk Ka	-0.37	-0.02	0.13	-0.20	0.19	0.61	74.24
21	Lat Lum Kaeo	-0.27	-0.12	0.05	-0.17	0.10	0.55	73.54
22	Mueang Pathum Thani	-0.30	-0.07	0.06	-0.20	0.06	0.54	73.39
23	Nong Suea	-0.41	-0.03	0.17	-0.18	-0.08	0.53	74.27
24	Sam Khok	-0.28	-0.15	0.03	-0.16	-0.17	0.52	73.52
25	Thanyaburi	-0.36	-0.03	0.11	-0.20	-0.10	0.58	74.14
26	Ban Phraek	-0.24	1.40	0.12	-0.37	-0.02	0.82	74.72

Table 6.3 (Continued).

No.	District	Intercept	Regression coefficient			Residual	LocalR2	Predicted
			TEMP	WS	VIS			($\mu g/m^3$)
27	Bang Ban	0.11	-1.03	0.08	0.40	-0.02	0.59	74.71
28	Bang Pa-In	0.01	-0.86	-0.06	0.01	-0.06	0.43	74.46
29	Bang Pahan	-0.19	0.83	-0.04	0.25	-0.10	0.70	74.83
30	Bang Sai	-0.01	-0.62	0.07	0.02	-0.09	0.57	74.22
31	Bang Sai	0.09	-0.87	0.12	0.29	-0.08	0.72	74.21
32	Lat Bua Luang	-0.09	-0.48	0.09	0.01	0.00	0.61	73.92
33	Maha Rat	-0.31	1.53	0.04	-0.26	-0.06	0.85	74.64
34	Nakhon Luang	-0.22	0.99	-0.07	0.31	-0.08	0.69	74.84
35	Phachi	-0.30	1.43	-0.21	0.43	-0.06	0.59	74.86
36	Phak Hai	-0.02	-0.85	0.02	0.32	0.02	0.68	74.24
37	Phra Nakhon Si Ayutthaya	0.13	-0.86	0.14	0.23	0.37	0.29	74.84
38	Sena	0.08	-0.91	0.10	0.27	0.04	0.66	74.12
39	Tha Ruea	-0.35	2.18	-0.39	0.11	0.04	0.63	75.22
40	Uthai	-0.16	0.35	0.06	0.17	0.09	0.32	74.56
41	Wang Noi	-0.31	0.17	-0.06	-0.20	-0.14	0.19	74.55
42	Ban Mo	-0.56	1.97	0.58	-2.62	0.45	0.54	75.67
43	Chaloem Phra Kiat	1.10	-1.20	1.65	-4.39	1.79	0.43	80.60
44	Don Phut	-0.46	2.46	-0.14	-0.59	0.01	0.86	74.97
45	Kaeng Khoi	3.78	0.53	-1.94	0.66	-0.36	0.15	76.81
46	Muak Lek	2.10	0.34	0.12	-0.94	0.08	0.65	74.30
47	Mueang Saraburi	0.61	0.89	0.03	0.60	-0.24	0.04	77.48
48	Nong Don	-1.04	2.05	1.40	-3.91	-0.14	0.77	76.78
49	Nong Khae	-0.25	1.19	-0.02	0.83	-0.18	0.45	75.02
50	Nong Saeng	-0.29	1.68	-0.17	0.51	-0.76	0.23	76.70
51	Phra Phutthabat	-0.36	-1.28	3.15	-6.15	0.70	0.69	79.22
52	Sao Hai	0.28	-0.06	1.11	-1.79	0.35	0.13	77.74
53	Wang Muang	1.61	0.36	0.58	-1.07	-0.02	0.64	74.65
54	Wihan Daeng	-0.26	1.11	0.22	1.08	-0.29	0.34	75.14
55	Bang Rachan	-0.14	0.00	0.10	0.09	0.00	0.86	74.17
56	In Buri	-0.13	0.02	0.11	0.08	0.02	0.55	74.13
57	Khai Bang Rachan	-0.10	0.01	0.22	0.00	0.00	0.96	74.19
58	Mueang Sing Buri	-0.08	0.04	0.24	-0.02	0.02	0.69	74.23
59	Phrom Buri	-0.07	-0.01	0.31	-0.06	-0.01	0.90	74.41
60	Tha Chang	-0.09	0.00	0.25	-0.02	0.00	0.96	74.29

From Table 6.3, the maximum value is 80.60 μg/m^3 in Chaloem Phra Kiat District, Saraburi province. In contrast, the minimum value is 73.38 μg/m^3 in Tha Luang District, Lop Buri province. The classification maps of prediction values for PM10 concentration using the GWR model according to the Thailand Air Quality Index and the U.S. EPA Air Quality Index are displayed in Figure 6.5.

As a result, the predicted values of PM10 concentration are satisfactory at level 2 based on Thailand AQI and moderate at level 2 according to EPA AQI. However, the predicted value in the rural landscape in December 2019 obtained from the GWR model is more than the one-day mean of WHO guidelines (Table 5.3).

In addition, a spatial distribution map of PM10 concentration in December 2019 using the SCK interpolation technique is displayed in Figure 6.6. As a result, the high PM10 concentration occur on agricultural land in the central part of the study area, particularly in Saraburi province.

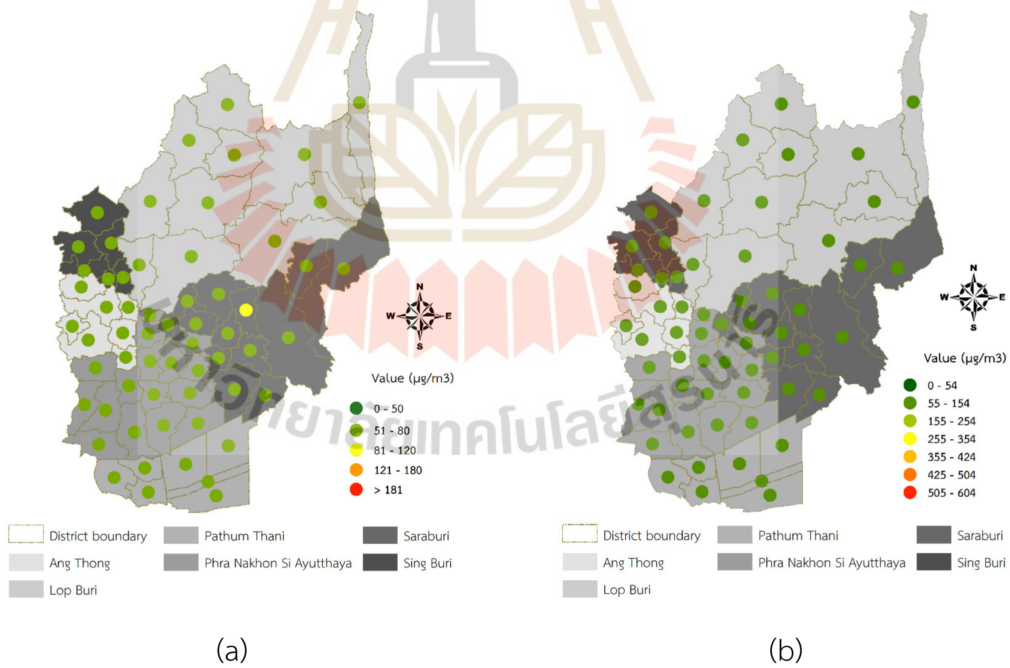

Figure 6.5 The classification map of PM10 concentration prediction using the GWR model in December 2019 according to the (a) Thailand AQI and (b) EPA AQI.

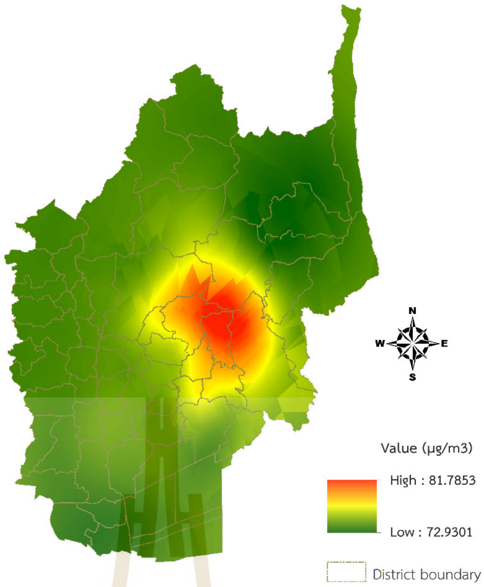

Figure 6.6 Spatial distribution of PM10 concentration in December 2019.

6.1.4 January 2020 in the winter season

The result of the GWR model for PM10 concentration prediction in January 2020 in the winter season is summarized in Table 6.4. The model performance shows that AICc, R-square, and adjusted R-square values are 106.85, 0.91, and 0.83, respectively.

Table 6.4 The predictive equations of PM10 concentration in January 2020.

No.	District	Intercept	Regression coefficient		Residual	LocalR2	Predicted
			TEMP	AOD			(µg/m³)
1	Chaiyo	0.18	1.07	-0.27	0.01	0.25	79.16
2	Mueang Ang Thong	-0.02	1.33	-0.17	0.03	0.34	79.12
3	Pa Mok	0.15	0.79	-0.17	-0.04	0.28	79.11
4	Pho Thong	0.27	0.57	-0.46	-0.12	0.20	79.09
5	Samko	0.08	-0.59	-0.16	-0.08	0.12	79.02
6	Sawaeng Ha	0.10	0.00	-0.32	-0.52	0.13	79.07
7	Wiset Chai Chan	0.63	-1.42	-0.33	-0.16	0.40	79.06
8	Ban Mi	0.07	0.23	-0.12	-0.07	0.14	79.11
9	Chai Badan	-0.96	0.12	-0.18	-0.29	0.03	78.88
10	Khok Charoen	-0.55	0.46	-0.22	-0.19	0.47	78.95
11	Khok Samrong	-0.04	0.68	-1.22	-0.27	0.64	79.07

Table 6.4 (Continued).

No.	District	Intercept	Regression coefficient		Residual	LocalR2	Predicted
			TEMP	AOD			(μg/m³)
12	Lam Sonthi	-1.22	0.08	-0.45	-0.74	0.04	78.84
13	Mueang Lop Buri	1.09	-0.12	-1.87	-0.54	0.48	79.36
14	Nong Muang	-0.41	0.45	0.26	-0.06	0.53	79.03
15	Phatthana Nikhom	0.71	0.68	-0.79	-0.32	0.59	79.06
16	Sa Bot	-0.42	0.45	-0.31	-0.05	0.56	78.94
17	Tha Luang	-0.84	0.05	0.16	-0.27	0.03	78.88
18	Tha Wung	0.62	0.20	-0.63	0.01	0.65	79.20
19	Khlong Luang	-0.57	-0.05	0.09	-0.19	0.05	78.96
20	Lam Luk Ka	-0.51	0.05	0.22	-0.25	0.08	78.94
21	Lat Lum Kaeo	-0.66	-0.23	-0.17	-0.31	0.25	78.91
22	Mueang Pathum Thani	-0.88	-0.04	-0.12	0.20	0.12	78.95
23	Nong Suea	0.88	0.49	1.22	-0.28	0.28	79.03
24	Sam Khok	-0.75	-0.13	-0.13	0.18	0.18	78.94
25	Thanyaburi	-0.48	0.04	0.24	-0.14	0.10	78.94
26	Ban Phraek	-0.23	1.93	0.00	-0.09	0.85	79.24
27	Bang Ban	0.32	-2.56	-0.01	0.06	0.84	79.12
28	Bang Pa-In	-0.22	-0.62	0.09	-0.22	0.27	79.05
29	Bang Pahan	0.27	0.61	-0.08	-0.20	0.14	79.17
30	Bang Sai	-0.24	-0.59	-0.17	-0.22	0.41	78.96
31	Bang Sai	0.32	-1.90	-0.16	-0.19	0.89	78.96
32	Lat Bua Luang	-0.17	-0.64	-0.25	-0.30	0.44	78.91
33	Maha Rat	0.05	1.69	-0.18	0.19	0.80	79.15
34	Nakhon Luang	0.39	0.86	-0.09	-0.17	0.44	79.18
35	Phachi	0.59	1.17	0.01	-0.03	0.59	79.16
36	Phak Hai	0.52	-2.22	-0.18	-0.09	0.73	79.05
37	Phra Nakhon Si Ayutthaya	0.04	-1.53	0.19	0.45	0.36	79.15
38	Sena	0.17	-1.39	-0.18	-0.01	0.71	78.94
39	Tha Ruea	0.27	1.71	-0.30	-0.16	0.79	79.32
40	Uthai	0.51	0.60	0.22	0.26	0.21	79.10
41	Wang Noi	0.05	-0.52	0.43	-0.10	0.25	79.07
42	Ban Mo	0.25	1.79	-0.39	0.08	0.66	79.40
43	Chaloem Phra Kiat	2.00	0.56	0.14	0.74	0.20	79.52
44	Don Phut	0.15	1.67	-0.22	0.01	0.90	79.27

Table 6.4 (Continued).

No.	District	Intercept	Regression coefficient		Residual	LocalR2	Predicted
			TEMP	AOD			($\mu g/m^3$)
45	Kaeng Khoi	2.00	0.69	0.39	0.05	0.41	79.30
46	Muak Lek	2.03	0.90	0.45	0.04	0.81	78.90
47	Mueang Saraburi	1.44	0.70	0.11	0.70	0.11	79.41
48	Nong Don	0.55	1.20	-0.43	-0.12	0.54	79.44
49	Nong Khae	-0.77	0.53	-1.21	-0.70	0.44	79.29
50	Nong Saeng	0.42	1.83	-0.24	-0.43	0.59	79.35
51	Phra Phutthabat	1.91	-0.23	-0.29	0.49	0.07	79.45
52	Sao Hai	1.10	1.30	-0.09	0.42	0.23	79.50
53	Wang Muang	1.98	0.87	0.39	0.54	0.83	78.86
54	Wihan Daeng	-0.89	0.13	-1.43	-0.26	0.28	79.22
55	Bang Rachan	0.16	0.14	-0.40	-0.14	0.10	79.08
56	In Buri	0.23	0.23	-0.40	-0.05	0.16	79.09
57	Khai Bang Rachan	0.17	0.08	-0.41	-0.21	0.12	79.08
58	Mueang Sing Buri	0.33	0.28	-0.51	0.32	0.22	79.06
59	Phrom Buri	0.53	0.28	-0.65	0.06	0.28	79.15
60	Tha Chang	0.49	0.18	-0.70	0.12	0.24	79.10

From Table 6.4, the maximum value is 79.52 $\mu g/m^3$ in Chaloem Phra Kiat District, Saraburi province. In contrast, the minimum value is 78.84 $\mu g/m^3$ in Lam Sonthi District, Lop Buri province. The classification maps of prediction values for PM10 concentration using the GWR model according to the Thailand Air Quality Index and the U.S. EPA Air Quality Index are displayed in Figure 6.7.

As a result, the predicted values of PM10 concentration are satisfactory at level 2 based on Thailand AQI and moderate at level 2 according to EPA AQI. However, the predicted value in the rural landscape in January 2020 taken from the GWR model is more than the one-day mean of WHO guidelines. See Table 5.3.

In addition, a spatial distribution map of PM10 concentration in January 2020 using the SCK interpolation technique is displayed in Figure 6.8. As a result, the high PM10 concentration occur on agricultural land in the central part of the study area, particularly in Saraburi province.

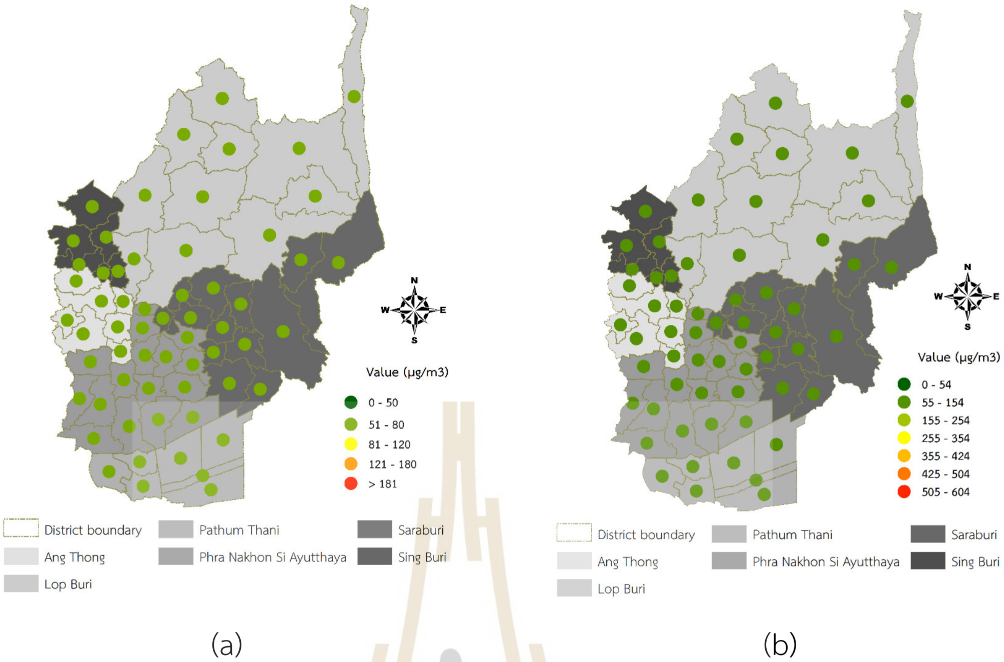

Figure 6.7 The classification map of PM10 concentration prediction using the GWR model in January 2020 according to the (a) Thailand AQI and (b) EPA AQI.

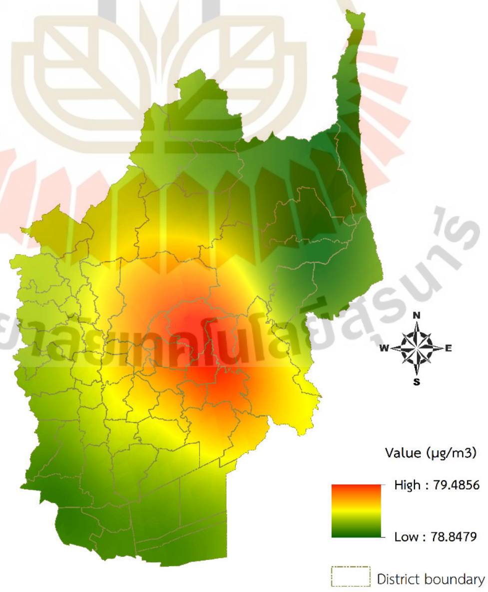

Figure 6.8 Spatial distribution of PM10 concentration in January 2020.

6.1.5 February 2020 in the winter season

The result of the GWR model for PM10 concentration prediction in February 2020 in the winter season is summarized in Table 6.5. The model performance shows that AICc, R-square, and adjusted R-square values are 78.45, 0.92, and 0.87, respectively.

Table 6.5 The predictive equations of PM10 concentration in February 2020.

No.	District	Intercept	Regression coefficient		Residual	LocalR2	Predicted
			WS	FRP			($\mu g/m^3$)
1	Chaiyo	0.25	0.11	0.29	0.01	0.93	82.18
2	Mueang Ang Thong	0.31	0.28	0.26	0.04	0.93	81.81
3	Pa Mok	0.25	0.43	0.11	-0.01	0.65	81.62
4	Pho Thong	0.20	0.05	0.44	0.04	0.86	81.44
5	Samko	0.33	0.08	0.60	-0.19	0.84	80.85
6	Sawaeng Ha	0.16	-0.10	0.65	0.07	0.87	81.27
7	Wiset Chai Chan	0.30	0.21	0.42	0.07	0.77	80.99
8	Ban Mi	0.49	0.18	0.58	-0.13	0.91	81.96
9	Chai Badan	-0.44	0.56	-0.05	-0.28	0.21	81.27
10	Khok Charoen	-0.34	0.04	0.08	-0.38	0.02	81.19
11	Khok Samrong	0.65	0.40	0.75	0.13	0.85	81.73
12	Lam Sonthi	-0.55	0.60	-0.07	-0.48	0.27	81.01
13	Mueang Lop Buri	0.98	1.10	0.27	0.03	0.68	83.30
14	Nong Muang	-0.07	-0.14	0.35	0.00	0.22	81.01
15	Phatthana Nikhom	0.39	0.72	0.72	-0.11	0.32	82.70
16	Sa Bot	-0.20	0.21	0.11	-0.14	0.08	81.26
17	Tha Luang	-0.36	0.73	0.14	-0.50	0.20	81.93
18	Tha Wung	1.00	0.81	-0.05	0.04	0.86	82.39
19	Khlong Luang	-1.08	0.17	0.34	-0.07	0.16	80.32
20	Lam Luk Ka	-1.02	0.18	0.35	0.08	0.17	80.94
21	Lat Lum Kaeo	-1.31	-0.16	0.46	-0.26	0.39	79.07
22	Mueang Pathum Thani	-1.35	0.10	0.37	-0.51	0.30	79.88
23	Nong Suea	-0.44	0.01	0.24	0.27	0.24	81.08
24	Sam Khok	-1.34	-0.04	0.38	-0.34	0.33	79.79
25	Thanyaburi	-1.01	0.17	0.34	0.15	0.15	80.54
26	Ban Phraek	0.35	0.26	0.33	-0.21	0.82	83.00
27	Bang Ban	-0.05	0.77	-0.27	0.28	0.34	80.83

Table 6.5 (Continued).

No.	District	Intercept	Regression coefficient		Residual	LocalR2	Predicted
			WS	FRP			($\mu g/m^3$)
28	Bang Pa-In	-0.78	0.23	0.11	-0.34	0.12	80.90
29	Bang Pahan	0.19	0.40	0.12	0.11	0.59	81.87
30	Bang Sai	-1.24	-0.36	0.52	-0.02	0.44	79.81
31	Bang Sai	-1.21	-0.81	0.69	-0.31	0.13	80.28
32	Lat Bua Luang	-1.27	-0.42	0.55	-0.37	0.43	79.62
33	Maha Rat	0.32	0.29	0.28	-0.01	0.88	82.41
34	Nakhon Luang	0.16	0.39	0.20	0.01	0.61	82.32
35	Phachi	-0.07	0.58	0.30	-0.21	0.45	82.89
36	Phak Hai	-0.09	0.36	0.04	0.11	0.14	80.83
37	Phra Nakhon Si Ayutthaya	-0.13	0.76	-0.41	0.20	0.57	80.97
38	Sena	-1.07	-0.47	0.49	-0.21	0.12	80.25
39	Tha Ruea	0.26	0.24	0.53	-0.15	0.52	83.51
40	Uthai	-0.13	0.89	-0.48	-0.04	0.74	82.13
41	Wang Noi	-0.68	0.47	0.15	0.00	0.15	81.48
42	Ban Mo	0.70	0.35	0.30	-0.07	0.09	84.24
43	Chaloem Phra Kiat	3.38	-0.94	-0.65	0.87	0.26	85.79
44	Don Phut	0.30	0.28	0.41	-0.21	0.74	83.40
45	Kaeng Khoi	4.94	-3.17	-0.05	0.22	0.37	83.53
46	Muak Lek	-0.19	0.96	0.57	-0.45	0.24	82.60
47	Mueang Saraburi	3.10	-1.29	-0.29	0.24	0.22	83.71
48	Nong Don	1.00	0.59	0.06	0.25	0.18	83.79
49	Nong Khae	-1.32	2.04	-0.14	-0.38	0.40	83.17
50	Nong Saeng	0.18	0.59	0.26	-0.15	0.11	83.53
51	Phra Phutthabat	2.43	0.39	-0.78	0.86	0.29	84.60
52	Sao Hai	2.78	-0.77	-0.49	0.54	0.13	84.13
53	Wang Muang	0.40	0.61	0.69	0.21	0.28	82.12
54	Wihan Daeng	-1.66	2.53	-0.22	-0.11	0.27	82.77
55	Bang Rachan	0.23	-0.01	0.54	-0.01	0.88	81.44
56	In Buri	0.25	-0.02	0.57	-0.02	0.93	81.49
57	Khai Bang Rachan	0.22	0.00	0.53	-0.01	0.87	81.55
58	Mueang Sing Buri	0.28	0.04	0.48	0.09	0.90	81.71
59	Phrom Buri	0.26	0.07	0.35	0.05	0.90	82.11
60	Tha Chang	0.22	0.03	0.44	0.07	0.88	81.81

From Table 6.5, the maximum value is 85.79 μg/m^3 in Chaloem Phra Kiat District, Saraburi province. In contrast, the minimum value is 79.07 μg/m^3 in Lat Lum Kaeo District, Pathum Thani province. The classification maps of prediction values for PM10 concentration using the GWR model according to the Thailand Air Quality Index and the U.S. EPA Air Quality Index are displayed in Figure 6.9.

Most predicted PM10 concentration are moderate at levels 3 of Thailand AQI and 2 of EPA AQI. However, the predicted value in rural landscape in February 2020 from the GWR model is more than the one-day mean of WHO guidelines. See Table 5.3.

In addition, a spatial distribution map of PM10 concentration in February 2020 using the SCK interpolation technique is displayed in Figure 6.10. As a result, the high PM10 concentration occur on agricultural land in the central part of the study area, particularly in Saraburi province.

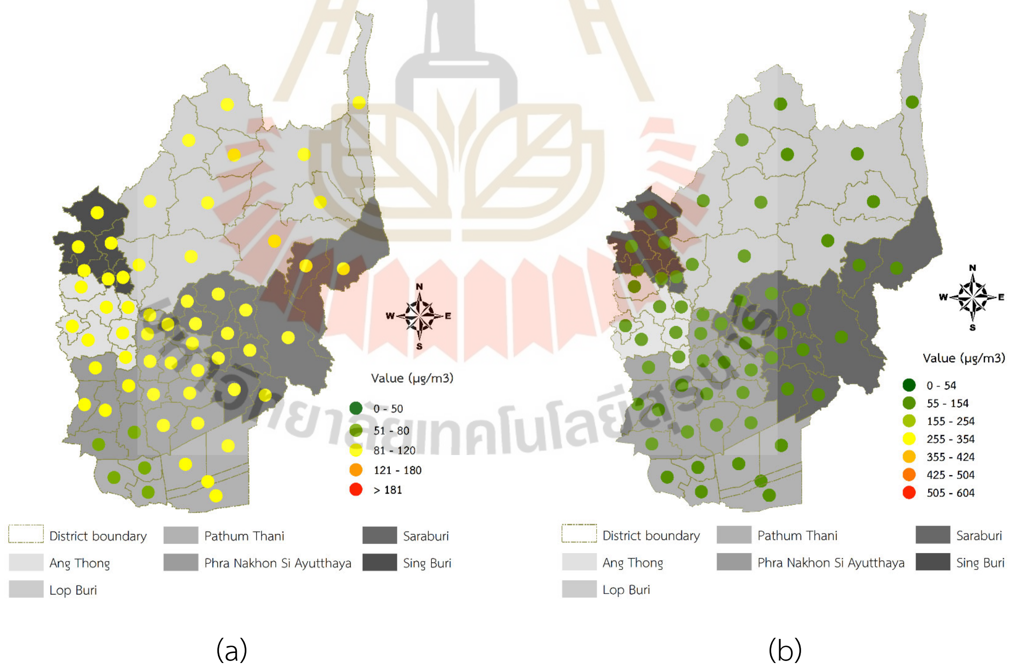

Figure 6.9 The classification map of PM10 concentration prediction using the GWR model in February 2020 according to the (a) Thailand AQI and (b) EPA AQI.

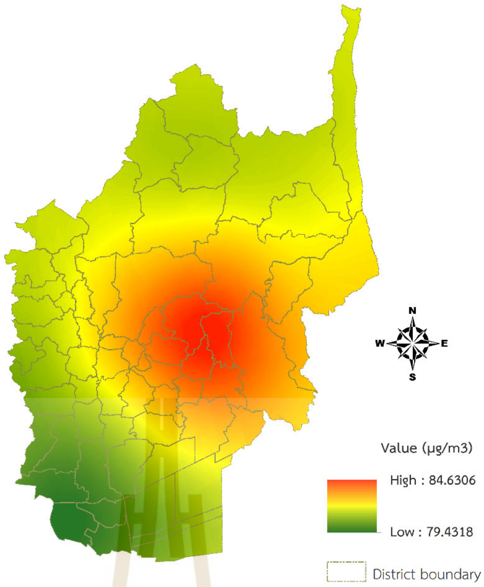

Figure 6.10 Spatial distribution of PM10 concentration in February 2020.

6.1.6 March 2020 in the summer season

The result of the GWR model for PM10 concentration prediction in March 2020 in the summer season is summarized in Table 6.6. The model performance shows that AICc, R-square, and adjusted R-square values are 119.61, 0.81, and 0.72, respectively.

Table 6.6 The predictive equations of PM10 concentration in March 2020.

No.	District	Intercept	Regression coefficient			Residual	LocalR2	Predicted ($\mu g/m^3$)
			TEMP	AOD	FD			
1	Chaiyo	-0.01	-0.30	0.18	0.07	-0.17	0.48	48.69
2	Mueang Ang Thong	0.00	-0.33	0.18	0.11	-0.19	0.54	48.73
3	Pa Mok	0.03	-0.55	0.23	0.12	-0.21	0.58	48.88
4	Pho Thong	-0.09	-0.26	0.13	0.05	-0.01	0.53	48.55
5	Samko	-0.12	-0.27	0.10	0.07	0.06	0.50	48.49
6	Sawaeng Ha	-0.18	-0.20	0.09	0.04	-0.05	0.46	48.54
7	Wiset Chai Chan	-0.04	-0.33	0.14	0.09	-0.07	0.52	48.61
8	Ban Mi	0.46	-0.55	0.31	0.40	0.37	0.52	48.33
9	Chai Badan	1.43	-0.14	0.15	2.53	0.06	0.87	48.46
10	Khok Charoen	0.84	-0.28	0.07	1.61	-0.35	0.55	48.70
11	Khok Samrong	1.11	-0.54	0.28	1.61	0.24	0.74	48.43
12	Lam Sonthi	1.42	-0.13	0.13	2.54	-0.02	0.87	48.50

Table 6.6 (Continued).

No.	District	Intercept	Regression coefficient			Residual	LocalR2	Predicted
			TEMP	AOD	FD			(μg/m³)
13	Mueang Lop Buri	1.06	-0.77	0.38	1.43	-0.25	0.78	49.09
14	Nong Muang	0.51	-0.34	0.15	1.00	0.01	0.42	48.49
15	Phatthana Nikhom	1.35	-0.10	0.29	2.35	-0.01	0.85	48.74
16	Sa Bot	1.17	-0.30	0.11	2.05	0.11	0.70	48.43
17	Tha Luang	1.40	-0.09	0.21	2.47	0.06	0.88	48.47
18	Tha Wung	0.21	-0.44	0.27	0.17	0.10	0.47	48.57
19	Khlong Luang	-0.26	-0.31	0.20	-0.02	-0.15	0.15	48.64
20	Lam Luk Ka	-0.25	-0.27	0.19	-0.02	0.51	0.15	48.68
21	Lat Lum Kaeo	-0.32	-0.61	0.13	-0.05	-0.29	0.25	48.56
22	Mueang Pathum Thani	-0.32	-0.46	0.14	-0.03	-0.11	0.18	48.55
23	Nong Suea	-0.03	-0.06	0.32	-0.03	-0.22	0.33	48.73
24	Sam Khok	-0.31	-0.51	0.17	-0.04	-0.68	0.21	48.76
25	Thanyaburi	-0.24	-0.26	0.19	-0.02	0.21	0.15	48.59
26	Ban Phraek	0.04	-0.32	0.28	0.19	-0.27	0.44	48.82
27	Bang Ban	-0.02	-0.55	0.28	0.16	0.43	0.52	48.76
28	Bang Pa-In	-0.18	-0.38	0.30	-0.03	0.25	0.24	48.75
29	Bang Pahan	0.01	-0.50	0.34	0.22	0.10	0.61	48.85
30	Bang Sai	-0.26	-0.66	0.22	-0.06	-0.02	0.30	48.61
31	Bang Sai	-0.15	-0.95	0.11	-0.06	-0.23	0.44	48.73
32	Lat Bua Luang	-0.28	-0.81	0.14	-0.08	-0.13	0.34	48.55
33	Maha Rat	0.03	-0.39	0.27	0.17	-0.49	0.53	48.95
34	Nakhon Luang	0.00	-0.37	0.42	0.27	-0.03	0.55	48.85
35	Phachi	0.00	-0.34	0.51	0.45	0.28	0.47	48.59
36	Phak Hai	0.00	-0.54	0.18	0.11	0.04	0.55	48.61
37	Phra Nakhon Si Ayutthaya	0.01	-0.26	0.37	0.20	0.72	0.44	49.35
38	Sena	-0.18	-0.81	0.16	-0.06	-0.04	0.38	48.63
39	Tha Ruea	0.00	-0.64	0.60	0.64	-0.40	0.55	49.08
40	Uthai	0.11	0.01	0.43	0.13	-0.13	0.50	48.99
41	Wang Noi	0.00	-0.05	0.36	-0.03	-0.46	0.33	49.00
42	Ban Mo	0.19	-0.57	0.68	1.04	-0.40	0.62	49.43
43	Chaloem Phra Kiat	0.74	-0.14	0.52	1.85	1.24	0.66	51.32
44	Don Phut	0.13	-0.56	0.52	0.48	-0.04	0.56	48.77
45	Kaeng Khoi	0.58	-0.16	0.49	1.61	0.08	0.63	49.12
46	Muak Lek	1.13	-0.05	0.36	2.04	0.05	0.79	48.55
47	Mueang Saraburi	0.43	-0.18	0.51	1.48	-1.33	0.56	50.17

Table 6.6 (Continued).

No.	District	Intercept	Regression coefficient			Residual	LocalR2	Predicted
			TEMP	AOD	FD			($\mu g/m^3$)
48	Nong Don	0.40	-0.54	0.68	1.23	0.29	0.68	49.07
49	Nong Khae	-0.08	-0.35	0.56	0.33	-0.94	0.43	49.25
50	Nong Saeng	0.16	-0.32	0.57	0.99	0.54	0.51	48.59
51	Phra Phutthabat	0.78	-0.24	0.56	1.96	1.73	0.72	49.77
52	Sao Hai	0.49	-0.18	0.57	1.57	-0.10	0.59	49.98
53	Wang Muang	1.21	-0.05	0.35	2.13	0.06	0.81	48.60
54	Wihan Daeng	-0.12	-0.39	0.59	0.36	0.32	0.42	48.48
55	Bang Rachan	-0.16	-0.20	0.11	0.02	-0.22	0.39	48.63
56	In Buri	0.03	-0.32	0.19	0.06	0.02	0.39	48.50
57	Khai Bang Rachan	-0.14	-0.22	0.11	0.03	-0.13	0.45	48.59
58	Mueang Sing Buri	0.07	-0.35	0.20	0.07	-0.03	0.42	48.56
59	Phrom Buri	0.04	-0.34	0.20	0.07	0.09	0.44	48.52
60	Tha Chang	-0.04	-0.28	0.16	0.04	0.15	0.44	48.45

From Table 6.6, the maximum value is 51.32 $\mu g/m^3$ in Chaloem Phra Kiat District, Saraburi province. In contrast, the minimum value is 48.33 $\mu g/m^3$ in Ban Mi District, Lop Buri province. The classification maps of prediction values for PM10 concentration using the GWR model according to the Thailand Air Quality Index and the U.S. EPA Air Quality Index are displayed in Figure 6.11.

As a result, most predicted PM10 concentration are excellent at level 1 of Thailand AQI and good at level 1 of the EPA AQI. However, the predicted value in the rural landscape in March 2020 from the GWR model is higher than the one-day mean of WHO guidelines. See Table 5.3.

In addition, a spatial distribution map of PM10 concentration in March 2020 using the SCK interpolation technique is displayed in Figure 6.12. As a result, the high PM10 concentration occur on agricultural land in the central part of the study area, particularly in Saraburi province.

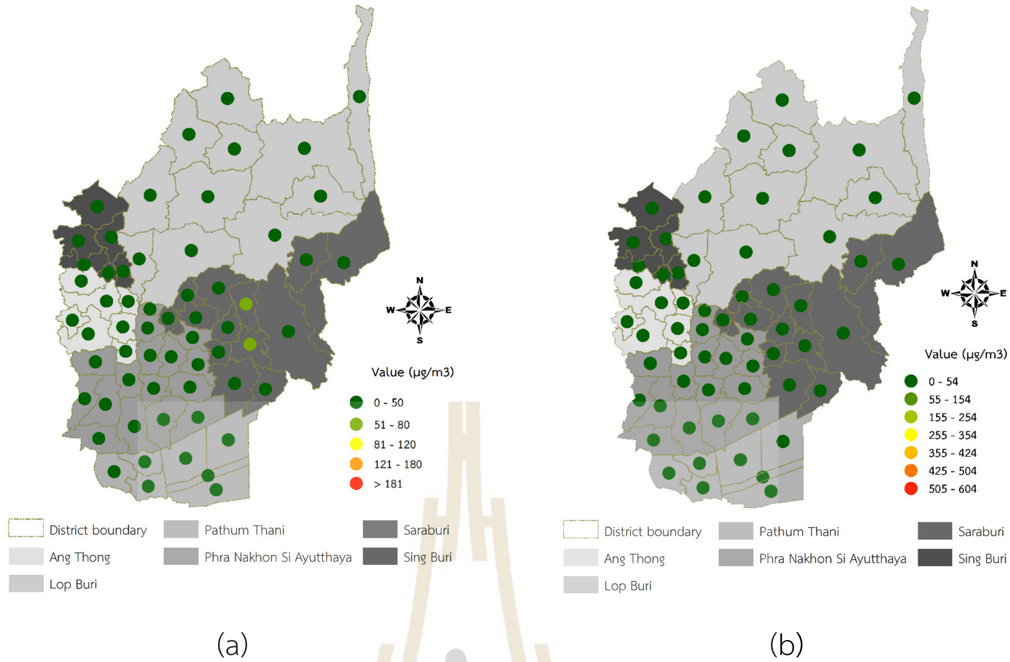

Figure 6.11 The classification map of PM10 concentration prediction using the GWR model in March 2020 according to the (a) Thailand AQI and (b) EPA AQI.

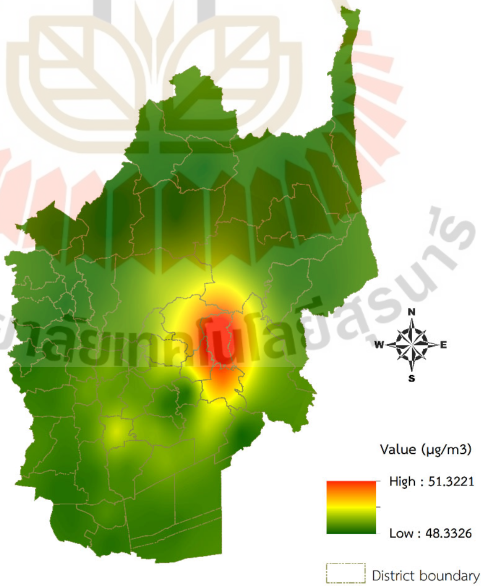

Figure 6.12 Spatial distribution of PM10 concentration in March 2020.

6.1.7 April 2020 in the summer season

The result of the GWR model for PM10 concentration prediction in April 2020 in the summer season is summarized in Table 6.7. The model performance shows that AICc, R-square, and adjusted R-square values are 64.75, 0.93, and 0.89, respectively.

Table 6.7 The predictive equations of PM10 concentration in April 2020.

No.	District	Intercept	Regression coefficient	Residual	LocalR2	Predicted
			BT			($\mu g/m^3$)
1	Chaiyo	0.12	0.24	0.03	0.45	44.01
2	Mueang Ang Thong	0.09	0.20	0.10	0.21	43.89
3	Pa Mok	0.03	0.19	0.07	0.11	43.96
4	Pho Thong	-0.13	0.12	-0.02	0.11	43.84
5	Samko	-0.51	-0.12	-0.19	0.12	43.74
6	Sawaeng Ha	-0.29	0.06	-0.05	0.08	43.78
7	Wiset Chai Chan	-0.56	-0.23	-0.01	0.28	43.70
8	Ban Mi	-0.02	-0.14	-0.01	0.09	43.84
9	Chai Badan	-0.91	0.43	-0.11	0.43	43.52
10	Khok Charoen	-0.88	0.39	-0.31	0.32	43.62
11	Khok Samrong	-0.05	0.04	0.00	0.00	44.01
12	Lam Sonthi	-0.94	0.40	0.00	0.55	43.21
13	Mueang Lop Buri	0.66	0.37	-0.04	0.03	44.55
14	Nong Muang	-0.69	0.25	-0.03	0.14	43.64
15	Phatthana Nikhom	-0.24	0.54	-0.16	0.01	44.21
16	Sa Bot	-0.78	0.40	-0.06	0.17	43.65
17	Tha Luang	-0.87	0.46	-0.53	0.19	43.85
18	Tha Wung	-0.04	-0.01	0.01	0.00	43.99
19	Khlong Luang	0.57	1.02	0.54	0.72	43.85
20	Lam Luk Ka	0.71	1.02	0.54	0.73	44.09
21	Lat Lum Kaeo	-0.54	0.54	0.26	0.57	42.65
22	Mueang Pathum Thani	0.27	0.86	0.01	0.71	42.99
23	Nong Suea	0.52	0.26	-0.02	0.12	44.29
24	Sam Khok	-0.02	0.77	-0.55	0.66	43.20
25	Thanyaburi	0.70	1.03	-0.37	0.71	44.43
26	Ban Phraek	0.38	0.48	-0.05	0.63	44.22
27	Bang Ban	0.01	1.01	-0.31	0.59	44.03

Table 6.7 (Continued).

No.	District	Intercept	Regression coefficient	Residual	LocalR2	Predicted
			BT			(μg/m³)
28	Bang Pa-In	0.26	1.25	-0.25	0.73	44.16
29	Bang Pahan	0.30	0.49	-0.04	0.58	44.25
30	Bang Sai	-0.22	0.83	-0.42	0.75	43.39
31	Bang Sai	-0.38	0.88	-0.22	0.73	43.27
32	Lat Bua Luang	-0.60	0.56	-0.08	0.68	43.00
33	Maha Rat	0.37	0.46	-0.17	0.73	44.23
34	Nakhon Luang	0.33	0.83	-0.13	0.65	44.56
35	Phachi	0.62	0.58	-0.10	0.21	44.54
36	Phak Hai	-0.34	0.32	-0.10	0.09	43.75
37	Phra Nakhon Si Ayutthaya	0.09	1.30	0.06	0.78	44.37
38	Sena	-0.26	0.93	-0.30	0.75	43.39
39	Tha Ruea	0.44	1.11	-0.14	0.27	44.68
40	Uthai	0.52	0.52	0.11	0.24	44.43
41	Wang Noi	0.52	0.56	0.26	0.30	44.30
42	Ban Mo	0.28	1.80	0.00	0.67	44.79
43	Chaloem Phra Kiat	0.14	2.28	0.50	0.68	45.73
44	Don Phut	0.49	0.75	-0.16	0.60	44.51
45	Kaeng Khoi	0.39	1.32	-0.67	0.25	44.97
46	Muak Lek	0.53	-0.39	-0.64	0.01	44.09
47	Mueang Saraburi	0.35	1.84	-0.10	0.63	44.68
48	Nong Don	0.37	1.69	0.32	0.78	44.58
49	Nong Khae	0.60	0.84	0.01	0.49	44.32
50	Nong Saeng	0.46	1.44	0.08	0.50	44.57
51	Phra Phutthabat	0.15	2.25	-0.27	0.81	45.74
52	Sao Hai	0.15	2.32	0.29	0.80	44.97
53	Wang Muang	1.09	-0.69	-0.46	0.01	44.22
54	Wihan Daeng	0.58	0.86	-0.25	0.44	44.48
55	Bang Rachan	-0.32	0.01	-0.13	0.01	43.83
56	In Buri	-0.29	-0.01	-0.17	0.00	43.83
57	Khai Bang Rachan	-0.30	0.04	-0.06	0.07	43.83
58	Mueang Sing Buri	-0.25	-0.01	0.03	0.00	43.86
59	Phrom Buri	-0.13	0.06	0.12	0.09	43.94
60	Tha Chang	-0.19	0.07	0.02	0.14	43.89

From Table 6.7, the maximum value is 45.74 μg/m^3 in Phra Phutthabat District, Saraburi province. In contrast, the minimum value is 42.65 μg/m^3 in Lat Lum Kaeo District, Pathum Thani province. The classification maps of prediction values for PM10 concentration using the GWR model according to the Thailand Air Quality Index and the U.S. EPA Air Quality Index are displayed in Figure 6.13.

As a result, the predicted values of PM10 concentration are excellent at level 1 of Thailand AQI and good at level 1 of the EPA AQI. In addition, the predicted value in rural landscape in April 2020 from the GWR model is less than the one-day mean of WHO guidelines. See Table 5.3.

In addition, a spatial distribution map of PM10 concentration in April 2020 using the SCK interpolation technique is displayed in Figure 6.14. As a result, the high PM10 concentration occur on agricultural land in the central part of the study area, particularly in Saraburi province.

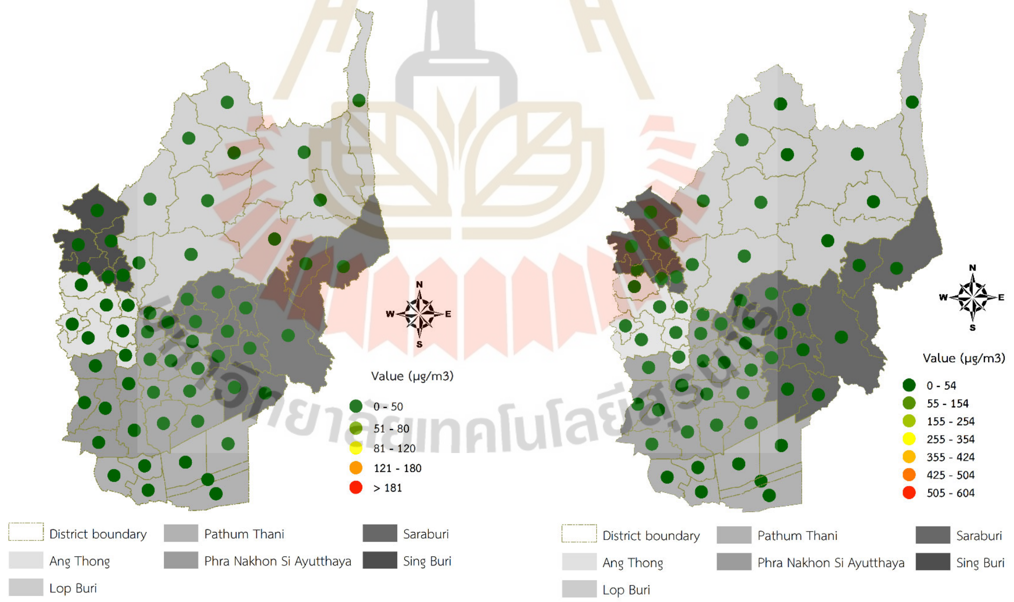

(a) (b)

Figure 6.13 The classification map of PM10 concentration prediction using the GWR model in April 2020 according to the (a) Thailand AQI and (b) EPA AQI.

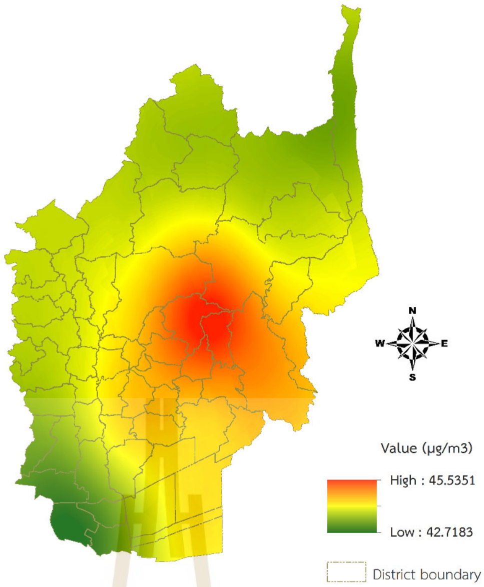

Figure 6.14 Spatial distribution of PM10 concentration in April 2020.

6.1.8 May 2020 in the summer season

The result of the GWR model for PM10 concentration prediction in May 2020 in the summer season is summarized in Table 6.8. The model performance shows that AICc, R-square, and adjusted R-square values are 154.74, 0.62, and 0.45, respectively.

Table 6.8 The predictive equations of PM10 concentration in May 2020.

No.	District	Intercept	Regression coefficient	Residual	LocalR2	Predicted
			VIS			(μg/m³)
1	Chaiyo	-0.28	0.09	-0.02	0.53	37.17
2	Mueang Ang Thong	-0.24	0.20	-0.09	0.27	37.23
3	Pa Mok	-0.12	0.71	-0.20	0.14	37.39
4	Pho Thong	-0.32	0.06	-0.01	0.50	37.15
5	Samko	-0.34	0.06	-0.01	0.48	37.15
6	Sawaeng Ha	-0.36	0.02	-0.01	0.42	37.14
7	Wiset Chai Chan	-0.31	0.11	-0.05	0.29	37.18
8	Ban Mi	-0.26	0.08	-0.02	0.10	37.15
9	Chai Badan	-0.28	-0.07	-0.10	0.02	37.20
10	Khok Charoen	-0.38	-0.02	-0.02	0.04	37.14
11	Khok Samrong	-0.06	0.18	-0.14	0.01	37.24
12	Lam Sonthi	-0.34	-0.03	0.02	0.03	37.12

Table 6.8 (Continued).

No.	District	Intercept	Regression coefficient VIS	Residual	LocalR2	Predicted ($\mu g/m^3$)
13	Mueang Lop Buri	2.31	2.27	-0.24	0.30	37.47
14	Nong Muang	-0.38	-0.02	-0.03	0.03	37.15
15	Phatthana Nikhom	0.35	-0.37	-0.56	0.00	37.70
16	Sa Bot	-0.36	-0.05	-0.06	0.02	37.17
17	Tha Luang	-0.14	-0.16	-0.24	0.02	37.29
18	Tha Wung	-0.20	0.13	0.00	0.21	37.15
19	Khlong Luang	0.38	-0.46	-0.33	0.22	37.20
20	Lam Luk Ka	0.11	-0.21	0.91	0.05	37.25
21	Lat Lum Kaeo	0.43	-0.56	0.20	0.52	36.95
22	Mueang Pathum Thani	0.43	-0.52	-0.07	0.35	36.92
23	Nong Suea	-0.26	0.11	-0.18	0.03	37.29
24	Sam Khok	0.45	-0.57	-0.15	0.52	37.01
25	Thanyaburi	0.14	-0.24	0.13	0.06	37.25
26	Ban Phraek	-0.19	0.09	-0.07	0.02	37.24
27	Bang Ban	0.43	-0.37	0.00	0.01	37.55
28	Bang Pa-In	1.07	-1.18	-0.16	0.35	37.56
29	Bang Pahan	0.02	1.92	-0.07	0.33	37.54
30	Bang Sai	0.94	-0.94	-0.34	0.45	37.45
31	Bang Sai	0.06	-0.28	-0.03	0.07	37.26
32	Lat Bua Luang	0.47	-0.59	0.00	0.41	37.15
33	Maha Rat	-0.10	0.30	-0.14	0.13	37.31
34	Nakhon Luang	0.19	1.44	-0.10	0.25	37.55
35	Phachi	0.17	-0.10	-0.26	0.00	37.48
36	Phak Hai	-0.21	0.17	-0.17	0.04	37.29
37	Phra Nakhon Si Ayutthaya	0.56	-0.23	1.73	0.00	37.67
38	Sena	0.51	-0.70	-0.20	0.20	37.35
39	Tha Ruea	0.08	-0.93	-0.28	0.11	37.57
40	Uthai	0.13	0.46	-0.04	0.03	37.52
41	Wang Noi	0.30	-0.52	-0.26	0.14	37.38
42	Ban Mo	-0.11	-2.61	-0.44	0.14	38.00
43	Chaloem Phra Kiat	0.17	-5.64	3.19	0.19	39.00
44	Don Phut	-0.07	-0.23	-0.16	0.03	37.38
45	Kaeng Khoi	0.18	-2.85	-1.69	0.11	38.48
46	Muak Lek	-0.01	-0.84	-0.77	0.02	37.63
47	Mueang Saraburi	0.01	-4.64	-0.44	0.31	37.54

Table 6.8 (Continued).

No.	District	Intercept	Regression coefficient	Residual	LocalR2	Predicted
			VIS			($\mu g/m^3$)
48	Nong Don	0.44	-0.42	-0.38	0.01	37.79
49	Nong Khae	-0.01	-0.65	-0.26	0.15	37.34
50	Nong Saeng	0.03	-3.34	-0.26	0.32	37.51
51	Phra Phutthabat	1.80	0.13	1.36	0.00	38.44
52	Sao Hai	-0.24	-6.02	0.46	0.35	38.18
53	Wang Muang	0.23	-0.80	-0.91	0.01	37.78
54	Wihan Daeng	0.07	-0.90	-0.39	0.13	37.39
55	Bang Rachan	-0.37	0.02	0.00	0.25	37.14
56	In Buri	-0.33	0.05	0.00	0.14	37.13
57	Khai Bang Rachan	-0.36	0.03	-0.01	0.39	37.14
58	Mueang Sing Buri	-0.33	0.05	0.00	0.17	37.14
59	Phrom Buri	-0.31	0.06	0.00	0.52	37.14
60	Tha Chang	-0.34	0.04	0.00	0.45	37.14

From Table 6.8, the maximum value is 39.00 $\mu g/m^3$ in Chaloem Phra Kiat District, Saraburi province. In contrast, the minimum value is 36.92 $\mu g/m^3$ in Mueang Pathum Thani District, Pathum Thani province. The classification maps of prediction values for PM10 concentration using the GWR model according to the Thailand Air Quality Index and the U.S. EPA Air Quality Index are displayed in Figure 6.15.

As a result, the predicted values of PM10 concentration are excellent at level 1 of Thailand AQI and good at level 1 of the EPA AQI. In addition, the predicted value in rural landscape in May 2020 from the GWR model is less than the one-day mean of WHO guidelines. See Table 5.3.

In addition, a spatial distribution map of PM10 concentration in May 2020 using the SCK interpolation technique is displayed in Figure 6.16. As a result, the high PM10 concentration occur on agricultural land in the central part of the study area, particularly in Saraburi province.

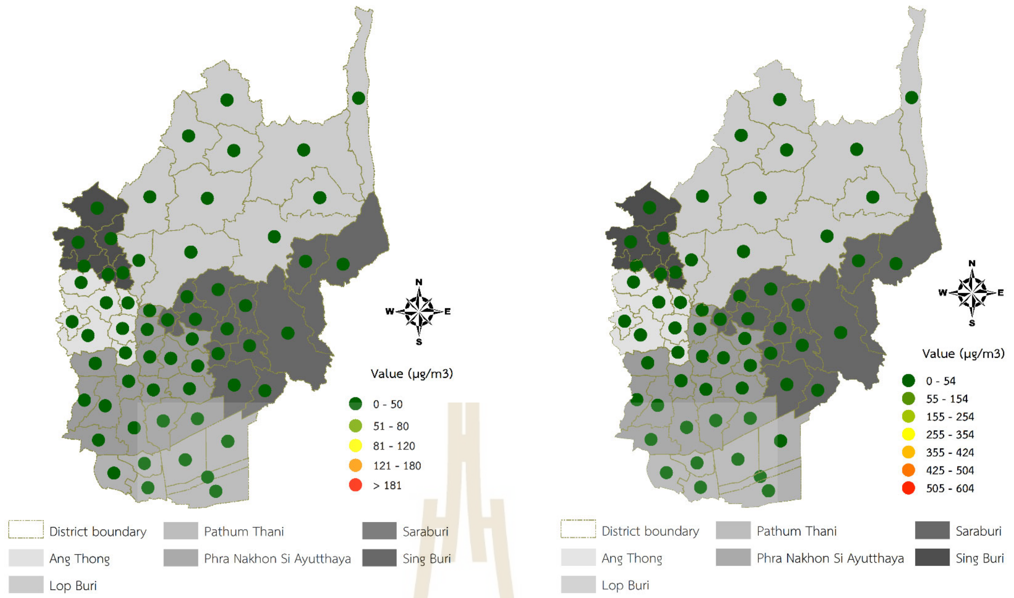

(a) (b)

Figure 6.15 The classification map of PM10 concentration prediction using the GWR model in May 2020 according to the (a) Thailand AQI and (b) EPA AQI.

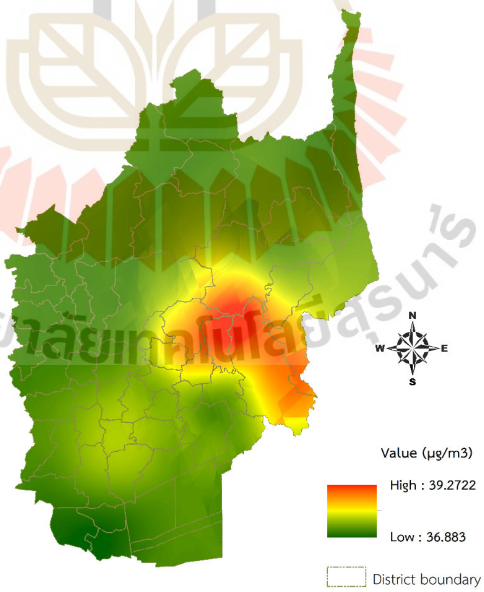

Figure 6.16 Spatial distribution of PM10 concentration in May 2020.

6.1.9 Winter season

The result of the GWR model for PM10 concentration prediction in the winter season (October to February) is summarized in Table 6.9. The model performance shows that AICc, R-square, and adjusted R-square values are 132.89, 0.70, and 0.61, respectively.

Table 6.9 The predictive equations of PM10 concentration in the winter season.

No.	District	Intercept	Regression coefficient					Residual	Local R2	Predicted (μg/m^3)
			TEMP	WS	VIS	FRP	AOD			
1	Chaiyo	0.23	0.68	0.62	-0.46	0.25	-0.04	0.20	0.66	70.51
2	Mueang Ang Thong	0.16	0.68	0.58	-0.60	0.32	-0.02	0.05	0.71	70.49
3	Pa Mok	0.12	0.54	0.53	-0.74	0.38	0.02	-0.04	0.70	70.45
4	Pho Thong	0.22	0.57	0.66	-0.52	0.23	-0.03	0.09	0.68	70.32
5	Samko	0.17	0.39	0.70	-0.66	0.23	0.01	-0.21	0.70	70.30
6	Sawaeng Ha	0.25	0.42	0.71	-0.50	0.17	-0.03	0.02	0.65	70.30
7	Wiset Chai Chan	0.15	0.43	0.64	-0.67	0.27	0.01	-0.17	0.73	70.36
8	Ban Mi	0.62	0.46	0.49	0.23	0.10	0.03	-0.35	0.51	70.89
9	Chai Badan	0.46	0.48	1.07	-0.27	-0.14	0.15	0.10	0.53	69.95
10	Khok Charoen	0.51	0.44	0.89	-0.17	-0.05	0.21	-0.45	0.51	70.43
11	Khok Samrong	0.61	0.49	0.69	0.10	0.04	0.08	-0.68	0.51	71.32
12	Lam Sonthi	0.44	0.46	1.12	-0.33	-0.17	0.17	-0.39	0.54	70.21
13	Mueang Lop Buri	0.58	0.48	0.62	0.05	0.15	-0.03	-0.24	0.50	71.77
14	Nong Muang	0.56	0.45	0.75	-0.03	0.00	0.17	-0.68	0.50	70.86
15	Phatthana Nikhom	0.45	0.52	0.94	-0.09	-0.06	-0.04	0.14	0.46	70.83
16	Sa Bot	0.52	0.46	0.88	-0.14	-0.05	0.16	-0.35	0.51	70.53
17	Tha Luang	0.37	0.49	1.11	-0.31	-0.15	0.05	0.13	0.49	70.04
18	Tha Wung	0.41	0.48	0.66	-0.24	0.16	-0.03	0.08	0.57	70.81
19	Khlong Luang	0.14	0.40	0.23	-0.89	0.40	-0.06	0.00	0.65	69.58
20	Lam Luk Ka	0.19	0.42	0.17	-0.91	0.38	-0.11	0.15	0.66	69.94
21	Lat Lum Kaeo	0.03	0.27	0.31	-0.82	0.37	0.04	-0.05	0.69	69.28
22	Mueang Pathum Thani	0.07	0.33	0.27	-0.85	0.39	0.00	-0.46	0.67	69.44

Table 6.9 (Continued).

No.	District	Intercept	Regression coefficient					Residual	Local R2	Predicted (μg/m³)
			TEMP	WS	VIS	FRP	AOD			
23	Nong Suea	0.24	0.40	0.20	-0.93	0.40	-0.12	-0.51	0.61	70.72
24	Sam Khok	0.07	0.34	0.30	-0.86	0.39	0.01	0.02	0.66	69.01
25	Thanyaburi	0.17	0.41	0.19	-0.91	0.39	-0.10	-0.31	0.65	70.18
26	Ban Phraek	0.22	0.75	0.59	-0.47	0.27	-0.05	-0.03	0.63	70.99
27	Bang Ban	0.08	0.39	0.42	-0.82	0.40	0.04	0.54	0.68	69.72
28	Bang Pa-In	0.10	0.41	0.31	-0.88	0.41	-0.02	-0.28	0.64	70.10
29	Bang Pahan	0.13	0.61	0.46	-0.77	0.41	-0.02	0.27	0.65	70.32
30	Bang Sai	0.06	0.34	0.33	-0.85	0.39	0.02	0.11	0.67	69.44
31	Bang Sai	0.02	0.24	0.44	-0.79	0.35	0.09	0.03	0.71	69.52
32	Lat Bua Luang	0.00	0.23	0.34	-0.79	0.36	0.07	0.24	0.71	69.10
33	Maha Rat	0.16	0.80	0.54	-0.57	0.34	-0.04	0.09	0.66	70.69
34	Nakhon Luang	0.15	0.63	0.41	-0.80	0.42	-0.07	0.33	0.60	70.42
35	Phachi	0.21	0.66	0.30	-0.85	0.42	-0.16	-0.36	0.54	71.23
36	Phak Hai	0.09	0.31	0.55	-0.73	0.32	0.05	0.04	0.74	70.10
37	Phra Nakhon Si Ayutthaya	0.10	0.44	0.37	-0.87	0.41	-0.01	0.36	0.64	70.04
38	Sena	0.02	0.25	0.38	-0.79	0.37	0.08	0.18	0.71	69.51
39	Tha Ruea	0.22	0.71	0.46	-0.64	0.36	-0.13	-0.30	0.52	71.64
40	Uthai	0.18	0.54	0.27	-0.91	0.43	-0.11	-0.34	0.60	70.94
41	Wang Noi	0.19	0.48	0.22	-0.92	0.41	-0.11	-0.64	0.62	70.92
42	Ban Mo	0.29	0.54	0.61	-0.55	0.28	-0.12	-0.03	0.48	72.03
43	Chaloem Phra Kiat	0.35	0.38	0.72	-0.51	0.19	-0.21	2.99	0.34	71.94
44	Don Phut	0.21	0.87	0.53	-0.45	0.31	-0.07	-0.17	0.61	71.37
45	Kaeng Khoi	0.30	0.24	0.64	-0.98	0.30	-0.20	0.38	0.33	71.44
46	Muak Lek	0.22	0.45	1.07	-0.42	-0.06	-0.10	-0.24	0.40	70.80
47	Mueang Saraburi	0.34	0.25	0.50	-0.99	0.37	-0.22	-0.15	0.37	72.21
48	Nong Don	0.35	0.51	0.70	-0.41	0.21	-0.08	0.08	0.50	72.04
49	Nong Khae	0.31	0.34	0.30	-0.96	0.40	-0.16	-0.70	0.51	71.54
50	Nong Saeng	0.30	0.46	0.40	-0.88	0.39	-0.19	-0.09	0.44	71.45
51	Phra Phutthabat	0.42	0.44	0.73	-0.31	0.18	-0.14	1.34	0.40	72.43
52	Sao Hai	0.33	0.34	0.59	-0.78	0.33	-0.20	0.71	0.37	72.07

Table 6.9 (Continued).

No.	District	Intercept	Regression coefficient					Residual	Local R2	Predicted (μg/m^3)
			TEMP	WS	VIS	FRP	AOD			
53	Wang Muang	0.31	0.48	0.98	-0.25	-0.05	-0.12	0.39	0.40	70.46
54	Wihan Daeng	0.38	0.24	0.29	-1.01	0.39	-0.19	-1.04	0.47	71.88
55	Bang Rachan	0.33	0.37	0.67	-0.32	0.12	-0.04	0.13	0.57	70.21
56	In Buri	0.46	0.39	0.51	0.01	0.10	-0.03	0.42	0.52	69.94
57	Khai Bang Rachan	0.29	0.41	0.70	-0.42	0.15	-0.04	0.00	0.61	70.40
58	Mueang Sing Buri	0.40	0.42	0.64	-0.20	0.12	-0.03	0.27	0.55	70.28
59	Phrom Buri	0.32	0.51	0.68	-0.37	0.17	-0.04	0.18	0.60	70.54
60	Tha Chang	0.30	0.49	0.68	-0.40	0.17	-0.04	0.17	0.62	70.41

From Table 6.9, the maximum value is 72.43 μg/m^3 in Phra Phutthabat District, Saraburi province. In contrast, the minimum value is 69.01 μg/m^3 in Sam Khok District, Pathum Thani province. The classification maps of prediction values for PM10 concentration using the GWR model according to the Thailand Air Quality Index and the U.S. EPA Air Quality Index are displayed in Figure 6.17.

As a result, the predicted values of PM10 concentration are satisfactory at level 2 of Thailand AQI and moderate at level 2 of the EPA AQI. However, the predicted value in rural landscape in the winter season from the GWR model is more than the one-day mean of WHO guidelines. See Table 5.3.

In addition, a spatial distribution map of PM10 concentration in the winter season using the SCK interpolation technique is displayed in Figure 6.18. As a result, the high PM10 concentration occur on agricultural land in the central part of the study area, particularly Lob Buri and Saraburi province.

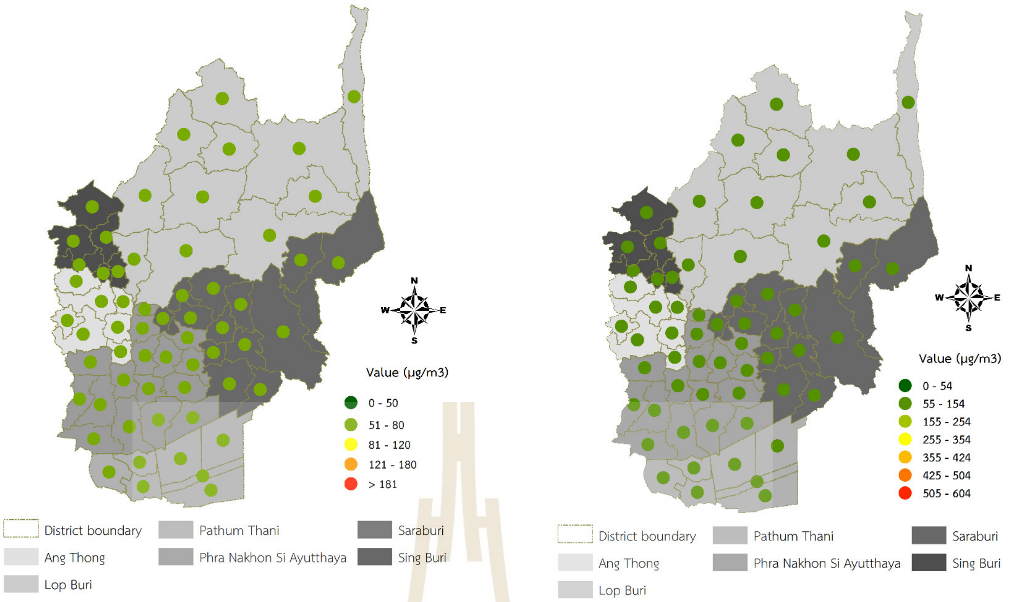

(a) (b)

Figure 6.17 The classification map of PM10 concentration prediction using the GWR model in the winter season according to the (a) Thailand AQI and (b) EPA AQI.

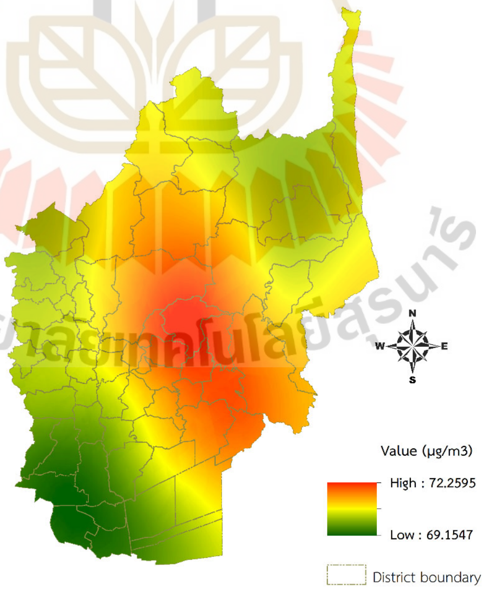

Figure 6.18 Spatial distribution of PM10 concentration in the winter season.

6.1.10 Summer season

The result of the GWR model for PM10 concentration prediction in the summer season (March to May) is summarized in Table 6.10. The model performance shows that AICc, R-square, and adjusted R-square values are 120.34, 0.79, and 0.70, respectively.

Table 6.10 The predictive equations of PM10 concentration in the summer season.

No.	District	Intercept	Regression coefficient					Residual	Local	Predicted
			TEMP	VIS	AOD	BT	FD		R2	(μg/m^3)
1	Chaiyo	0.48	-0.34	0.40	0.14	0.45	0.35	0.03	0.54	43.24
2	Mueang Ang Thong	0.35	-0.25	0.26	0.17	0.55	0.29	0.10	0.57	43.19
3	Pa Mok	0.29	-0.13	0.17	0.17	0.66	0.25	-0.03	0.66	43.36
4	Pho Thong	0.39	-0.37	0.29	0.16	0.42	0.29	0.31	0.54	42.99
5	Samko	0.19	-0.34	0.10	0.16	0.41	0.18	0.05	0.58	43.07
6	Sawaeng Ha	0.38	-0.41	0.28	0.13	0.35	0.22	0.32	0.53	42.95
7	Wiset Chai Chan	0.19	-0.29	0.10	0.17	0.46	0.19	-0.22	0.63	43.26
8	Ban Mi	0.70	-0.50	0.31	0.22	0.26	0.79	0.43	0.53	42.93
9	Chai Badan	0.88	-0.19	-0.02	0.23	0.16	1.82	-0.04	0.67	43.05
10	Khok Charoen	0.76	-0.40	-0.13	0.27	0.16	1.46	-0.14	0.60	43.10
11	Khok Samrong	0.77	-0.35	0.10	0.30	0.24	1.46	0.14	0.60	43.17
12	Lam Sonthi	0.94	-0.20	-0.07	0.20	0.11	1.89	0.04	0.69	42.93
13	Mueang Lop Buri	0.80	-0.21	0.78	0.22	0.34	1.21	-0.14	0.59	43.68
14	Nong Muang	0.69	-0.47	-0.08	0.30	0.20	1.24	0.55	0.55	42.78
15	Phatthana Nikhom	0.87	0.02	0.26	0.24	0.26	1.90	0.23	0.66	43.28
16	Sa Bot	0.78	-0.34	-0.06	0.28	0.19	1.55	-0.02	0.62	43.10
17	Tha Luang	0.96	-0.09	0.04	0.20	0.16	1.99	-0.14	0.70	43.13
18	Tha Wung	0.73	-0.51	0.56	0.07	0.38	0.41	-0.17	0.57	43.36
19	Khlong Luang	0.21	-0.13	0.07	0.13	0.69	0.08	0.41	0.62	43.01
20	Lam Luk Ka	0.26	-0.07	0.09	0.12	0.73	0.09	0.46	0.57	43.47

Table 6.10 (Continued).

No.	District	Intercept	Regression coefficient					Residual	Local	Predicted
			TEMP	VIS	AOD	BT	FD		R2	(μg/m^3)
21	Lat Lum Kaeo	0.08	-0.29	-0.01	0.17	0.57	0.05	0.20	0.76	42.64
22	Mueang Pathum Thani	0.10	-0.25	0.02	0.16	0.60	0.05	-0.36	0.71	42.99
23	Nong Suea	0.40	0.08	0.13	0.07	0.84	0.15	0.08	0.52	43.31
24	Sam Khok	0.10	-0.26	0.01	0.16	0.60	0.06	-0.47	0.72	42.98
25	Thanyaburi	0.26	-0.07	0.09	0.12	0.73	0.09	-0.07	0.58	43.45
26	Ban Phraek	0.55	-0.25	0.53	0.12	0.53	0.44	-0.09	0.55	43.40
27	Bang Ban	0.20	-0.16	0.06	0.15	0.67	0.14	-0.15	0.76	43.55
28	Bang Pa-In	0.21	-0.14	0.06	0.12	0.70	0.09	0.43	0.65	43.21
29	Bang Pahan	0.39	0.04	0.29	0.16	0.77	0.35	-0.22	0.63	43.67
30	Bang Sai	0.14	-0.23	0.02	0.15	0.63	0.07	-0.25	0.73	43.13
31	Bang Sai	0.11	-0.27	-0.01	0.16	0.59	0.08	-0.21	0.78	43.11
32	Lat Bua Luang	0.09	-0.29	-0.02	0.17	0.57	0.06	0.16	0.79	42.76
33	Maha Rat	0.47	-0.11	0.43	0.15	0.64	0.41	-0.06	0.57	43.37
34	Nakhon Luang	0.49	0.19	0.38	0.12	0.88	0.44	-0.44	0.57	43.85
35	Phachi	0.57	0.32	0.29	0.04	1.03	0.43	-0.34	0.50	43.71
36	Phak Hai	0.17	-0.23	0.05	0.17	0.59	0.15	-0.06	0.73	43.21
37	Phra Nakhon Si Ayutthaya	0.23	-0.11	0.07	0.13	0.72	0.14	0.48	0.67	44.03
38	Sena	0.12	-0.26	-0.01	0.16	0.60	0.09	-0.08	0.79	43.05
39	Tha Ruea	0.63	0.33	0.62	0.10	0.91	0.74	-0.33	0.54	43.80
40	Uthai	0.43	0.12	0.17	0.06	0.90	0.22	-0.08	0.53	43.68
41	Wang Noi	0.36	0.03	0.13	0.08	0.83	0.15	0.42	0.55	43.23
42	Ban Mo	0.65	0.22	0.80	0.13	0.74	0.93	0.23	0.53	43.78
43	Chaloem Phra Kiat	0.68	0.36	0.54	0.23	0.64	1.49	1.71	0.55	45.38
44	Don Phut	0.60	-0.03	0.64	0.12	0.68	0.59	0.03	0.55	43.46
45	Kaeng Khoi	0.62	0.39	-0.09	0.18	0.92	1.17	0.00	0.49	43.73
46	Muak Lek	0.80	0.10	0.22	0.22	0.33	1.88	-0.14	0.66	43.22
47	Mueang Saraburi	0.63	0.49	0.05	0.11	1.08	0.90	-1.26	0.48	44.48

Table 6.10 (Continued).

No.	District	Intercept	Regression coefficient					Residual	Local	Predicted
			TEMP	VIS	AOD	BT	FD		R2	(μg/m^3)
48	Nong Don	0.69	-0.04	0.88	0.15	0.48	0.94	0.44	0.54	43.61
49	Nong Khae	0.69	0.44	0.18	-0.04	1.07	0.42	-0.54	0.46	43.71
50	Nong Saeng	0.66	0.47	0.31	0.03	1.10	0.68	-0.37	0.49	43.84
51	Phra Phutthabat	0.70	0.24	0.91	0.24	0.52	1.46	1.94	0.56	44.11
52	Sao Hai	0.65	0.45	0.46	0.16	0.91	1.11	0.14	0.52	44.43
53	Wang Muang	0.80	0.12	0.30	0.23	0.34	1.86	0.17	0.65	43.17
54	Wihan Daeng	0.75	0.53	0.05	0.00	1.05	0.51	-0.37	0.45	43.59
55	Bang Rachan	0.52	-0.49	0.35	0.10	0.32	0.21	-0.14	0.53	43.21
56	In Buri	0.63	-0.53	0.38	0.13	0.28	0.38	-0.17	0.53	43.22
57	Khai Bang Rachan	0.46	-0.45	0.33	0.10	0.33	0.19	0.00	0.53	43.15
58	Mueang Sing Buri	0.66	-0.53	0.44	0.09	0.34	0.33	-0.44	0.55	43.43
59	Phrom Buri	0.61	-0.47	0.47	0.08	0.38	0.30	0.03	0.55	43.23
60	Tha Chang	0.53	-0.45	0.40	0.10	0.36	0.25	0.15	0.54	43.11

From Table 6.10, the maximum value is 45.38 μg/m^3 in Chaloem Phra Kiat District, Saraburi province. In contrast, the minimum value is 42.64 μg/m^3 in Lat Lum Kaeo District, Pathum Thani province. The classification maps of prediction values for PM10 concentration using the GWR model according to the Thailand Air Quality Index and the U.S. EPA Air Quality Index are displayed in Figure 6.19.

As a result, the predicted values of PM10 concentration are excellent at level 1 of Thailand AQI and good at level 1 of the EPA AQI. In addition, the predicted value in rural landscape in the summer season from the GWR model is less than the one-day mean of WHO guidelines. See Table 5.3.

In addition, a spatial distribution map of PM10 concentration in the summer season using the SCK interpolation technique is displayed in Figure 6.20. As a result, the high PM10 concentration occur on agricultural land in the central part of the study area, particularly in Saraburi province.

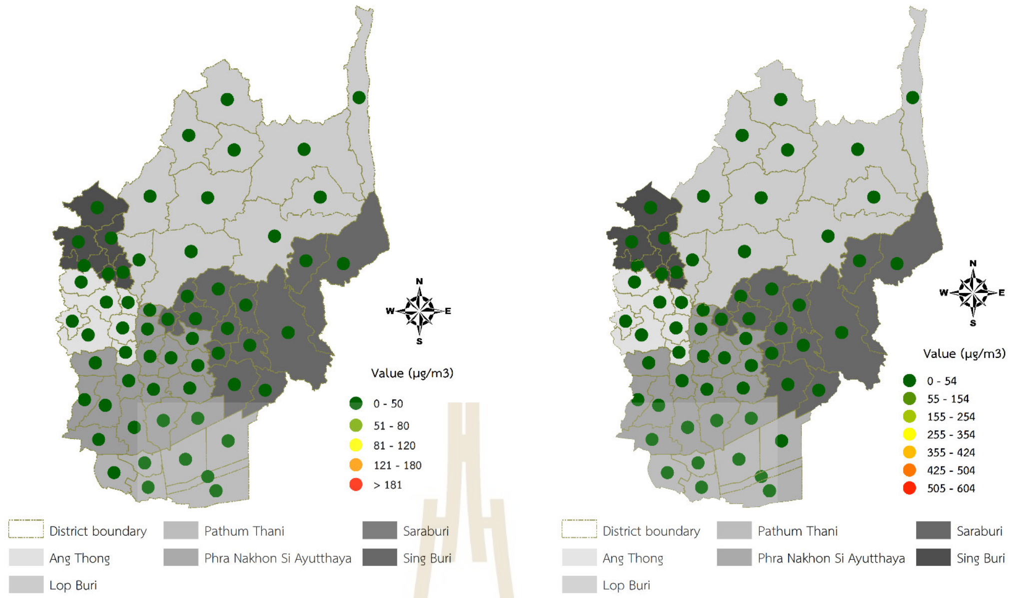

(a) (b)

Figure 6.19 The classification map of PM10 concentration prediction using the GWR model in the summer season according to the (a) Thailand AQI and (b) EPA AQI.

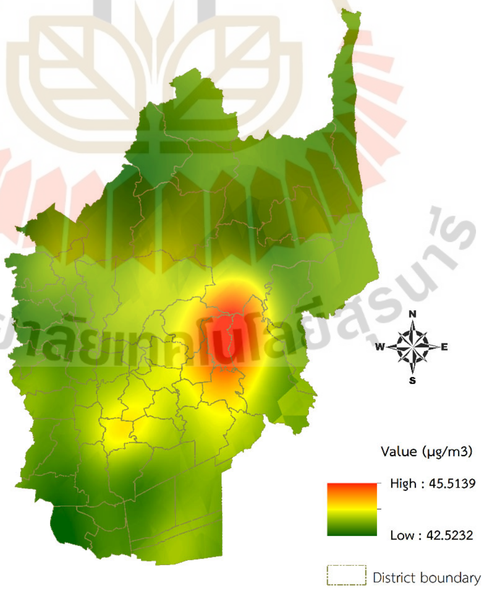

Figure 6.20 Spatial distribution of PM10 concentration in the summer season.

6.2 The predictive equations and their distribution map for spatiotemporal PM2.5 concentration in the urban landscape using the GWR model

Under this section, the GWR model with the significant derived factors was applied to predict the urban landscape's monthly PM2.5 concentration in winter and summer. The generic equations for PM2.5 concentration in winter and summer in urban landscapes are shown in Equations 6.3 and 6.4.

$$y_{(i,j)} = \beta o_{i,j} + \beta k_{1(i,j)}RH + \beta k_{2(i,j)}TEMP + \beta k_{3(i,j)}WS + \beta k_{4(i,j)}P + \beta k_{5(i,j)}VIS + \beta k_{6(i,j)}BT + \beta k_{7(i,j)}FRP + \beta k_{8(i,j)}FH + \beta k_{9(i,j)}AOD + \beta k_{10(i,j)}ELEV + \varepsilon_{(i.j)} \quad (6.3)$$

$$y_{(i,j)} = \beta o_{i,j} + \beta k_{3(i,j)}WS + \beta k_{5(i,j)}VIS + \beta k_{6(i,j)}BT + \beta k_{7(i,j)}FRP + \beta k_{8(i,j)}FH + \beta k_{9(i,j)}AOD + \beta k_{11(i,j)}FD + \beta k_{10(i,j)}ELEV + \varepsilon_{(i.j)} \quad (6.4)$$

Where $\beta o_{i,j}$ denotes intercept value at district i, month j; $\beta k_{1(i,j)}$ denotes the coefficients of relative humidity; $\beta k_{2(i,j)}$ denotes the coefficients of temperature; $\beta k_{3(i,j)}$ denotes the coefficients of wind speed; $\beta k_{4(i,j)}$ denotes the coefficients of pressure; $\beta k_{5(i,j)}$ denotes the coefficients of visibility; $\beta k_{6(i,j)}$ denotes the coefficients of brightness temperature; $\beta k_{7(i,j)}$ denotes the coefficients of fire radiative power; $\beta k_{8(i,j)}$ denotes the coefficients of fire hotspot; $\beta k_{9(i,j)}$ denotes the coefficients of MODIS AOD; $\beta k_{10(i,j)}$ denotes the coefficients of elevation; $\beta k_{11(i,j)}$ denotes the coefficients of factory density; and $\varepsilon_{(i.j)}$ is residual values. RH, TEMP, WS, P, VIS, BT, FRP, FH, AOD, ELEV, and FD are significant normalized variables.

The monthly predictive equation of PM2.5 concentration in winter and summer in urban landscapes is systematically reported in a tabular form in the following sections. As a result, columns, namely Intercept, Regression coefficient, and Residual, summarize a fitting regression equation for every district of seventy-two districts—columns LocalR2 and Predicted (μg/m^3) display local R squares and predicted value in microgram per cubic meter. Meanwhile, the performance of the GWR model for spatiotemporal PM10 concentration prediction is reported, including AICc, R-square, and adjusted R-square.

6.2.1 October 2019 in the winter season

The result of the GWR model for PM2.5 concentration prediction in October 2019 in the winter season is summarized in Table 6.11. The model performance shows that AICc, R-square, and adjusted R-square values are 73.70, 0.91, and 0.88, respectively.

Table 6.11 The predictive equations of PM2.5 concentration in October 2019.

No.	District	Intercept	Regression coefficient								Resi-	Local	Predicted
			WS	P	VIS	BT	FRP	AOD	FH	ELEV	dual	R2	(μg/m^3)
1	Bang Bon	0.28	0.27	0.19	-0.29	0.06	-0.12	0.42	-0.11	0.41	-0.39	0.86	28.38
2	Bang Kapi	-0.03	0.36	0.04	0.17	-0.22	-0.29	0.66	-0.21	0.52	-0.15	0.80	26.40
3	Bang Khae	0.28	0.32	0.17	-0.27	0.08	-0.13	0.41	-0.11	0.41	0.00	0.85	28.04
4	Bang Khen	0.00	0.35	-0.03	0.11	-0.23	-0.33	0.61	-0.22	0.51	-0.43	0.78	27.30
5	Bang Kho Laem	0.19	0.17	0.17	-0.22	-0.11	-0.19	0.50	-0.27	0.40	-0.03	0.84	27.63
6	Bang Khun Thian	0.14	0.18	0.23	-0.32	0.02	-0.13	0.42	-0.64	0.38	0.16	0.88	27.81
7	Bang Na	0.02	0.30	0.14	0.15	-0.19	-0.25	0.68	-0.24	0.47	0.16	0.83	26.41
8	Bang Phlat	0.22	0.30	0.06	-0.25	-0.03	-0.21	0.44	-0.15	0.41	0.45	0.83	27.49
9	Bang Rak	0.16	0.18	0.14	-0.18	-0.14	-0.20	0.52	-0.27	0.41	-0.29	0.83	27.77
10	Bang Sue	0.16	0.26	0.01	-0.21	-0.13	-0.24	0.48	-0.22	0.41	0.69	0.81	27.06
11	Bangkok Noi	0.26	0.30	0.11	-0.27	0.03	-0.18	0.42	-0.10	0.41	0.01	0.84	27.92
12	Bangkok Yai	0.27	0.26	0.15	-0.29	0.03	-0.17	0.42	-0.10	0.40	0.18	0.85	27.74
13	Bueng Kum	-0.04	0.39	0.01	0.19	-0.22	-0.31	0.66	-0.20	0.53	-0.32	0.80	26.55
14	Chatuchak	0.09	0.27	0.00	-0.09	-0.19	-0.27	0.54	-0.24	0.45	0.81	0.80	26.81
15	Chom Thong	0.27	0.22	0.19	-0.30	0.03	-0.15	0.43	-0.12	0.39	0.24	0.86	27.94
16	Din Daeng	0.11	0.22	0.07	-0.12	-0.18	-0.24	0.55	-0.26	0.43	-0.11	0.81	27.36
17	Don Mueang	0.06	0.30	-0.08	0.01	-0.22	-0.34	0.55	-0.22	0.47	-0.12	0.77	27.19
18	Dusit	0.18	0.25	0.07	-0.22	-0.10	-0.22	0.48	-0.21	0.41	-0.01	0.82	27.75
19	Huai Khwang	0.09	0.22	0.07	-0.09	-0.20	-0.24	0.56	-0.26	0.43	0.17	0.81	26.82
20	Khan Na Yao	-0.06	0.42	0.01	0.24	-0.22	-0.32	0.67	-0.19	0.55	-0.82	0.80	26.85
21	Khlong Sam Wa	-0.07	0.43	0.02	0.30	-0.22	-0.34	0.68	-0.17	0.56	-0.30	0.80	26.43

Table 6.11 (Continued).

No.	District	Intercept	Regression coefficient								Resi-dual	Local R2	Predicted (µg/m³)
			WS	P	VIS	BT	FRP	AOD	FH	ELEV			
22	Khlong San	0.21	0.20	0.15	-0.24	-0.07	-0.18	0.48	-0.22	0.40	0.31	0.84	27.68
23	Khlong Toei	0.15	0.13	0.16	-0.16	-0.17	-0.22	0.54	-0.29	0.39	-0.30	0.83	26.97
24	Lak Si	0.09	0.29	-0.06	-0.07	-0.20	-0.31	0.53	-0.23	0.45	0.18	0.78	27.09
25	Lat Krabang	-0.12	0.47	0.04	0.36	-0.20	-0.30	0.73	-0.14	0.57	0.31	0.83	25.60
26	Lat Phrao	0.02	0.32	-0.02	0.04	-0.22	-0.30	0.60	-0.23	0.49	0.00	0.79	26.88
27	Min Buri	-0.10	0.46	0.02	0.33	-0.21	-0.32	0.71	-0.16	0.57	-0.29	0.82	26.22
28	Nong Chok	-0.12	0.47	0.02	0.37	-0.21	-0.33	0.71	-0.14	0.58	-0.45	0.82	25.97
29	Nong Khaem	0.27	0.36	0.18	-0.28	0.16	-0.10	0.37	-0.26	0.40	-0.03	0.86	28.09
30	Pathum Wan	0.16	0.18	0.13	-0.19	-0.14	-0.21	0.52	-0.26	0.40	-0.24	0.83	27.72
31	Phasi Charoen	0.28	0.29	0.16	-0.28	0.06	-0.15	0.42	-0.08	0.41	-0.14	0.85	28.17
32	Phaya Thai	0.15	0.22	0.06	-0.19	-0.15	-0.23	0.51	-0.24	0.41	0.27	0.82	27.27
33	Phra Khanong	0.04	0.26	0.13	0.09	-0.20	-0.25	0.65	-0.25	0.46	0.28	0.82	26.36
34	Phra Nakhon	0.22	0.25	0.11	-0.25	-0.05	-0.19	0.46	-0.18	0.41	0.10	0.84	27.84
35	Pom Prap Sattru Phai	0.20	0.22	0.11	-0.24	-0.08	-0.20	0.48	-0.21	0.40	0.14	0.83	27.78
36	Prawet	-0.07	0.41	0.07	0.28	-0.20	-0.28	0.72	-0.18	0.54	0.34	0.83	26.04
37	Rat Burana	0.21	0.16	0.20	-0.24	-0.08	-0.18	0.48	-0.27	0.39	-0.37	0.85	27.84
38	Ratchathewi	0.16	0.20	0.10	-0.19	-0.14	-0.21	0.51	-0.25	0.41	-0.50	0.83	27.76
39	Sai Mai	-0.01	0.36	-0.03	0.16	-0.23	-0.35	0.62	-0.20	0.52	0.11	0.78	26.69
40	Samphanthawong	0.20	0.21	0.13	-0.23	-0.08	-0.19	0.48	-0.22	0.40	-0.02	0.84	27.87
41	Saphan Sung	-0.07	0.43	0.04	0.28	-0.21	-0.30	0.70	-0.18	0.55	0.29	0.81	26.01
42	Sathon	0.16	0.17	0.15	-0.18	-0.15	-0.20	0.53	-0.28	0.40	-0.16	0.84	27.49
43	Suan Luang	0.00	0.31	0.08	0.13	-0.21	-0.27	0.66	-0.23	0.49	0.44	0.81	26.11
44	Taling Chan	0.25	0.32	0.12	-0.25	0.02	-0.17	0.44	-0.12	0.41	0.18	0.84	27.88
45	Thawi Watthana	0.30	0.41	0.15	-0.24	0.16	-0.11	0.38	-0.13	0.40	0.18	0.84	27.66
46	Thon Buri	0.25	0.22	0.17	-0.28	-0.01	-0.17	0.45	-0.16	0.40	0.20	0.85	27.91
47	Thung Khru	0.20	0.14	0.23	-0.24	-0.08	-0.17	0.48	-0.34	0.38	0.19	0.86	27.42
48	Vadhana	0.13	0.15	0.13	-0.13	-0.19	-0.22	0.55	-0.28	0.40	-0.47	0.83	27.09

Table 6.11 (Continued).

No.	District	Intercept	Regression coefficient								Resi-dual	Local R2	Predicted (μg/m³)
			WS	P	VIS	BT	FRP	AOD	FH	ELEV			
49	Wang Thonglang	0.03	0.29	0.04	0.04	-0.22	-0.27	0.61	-0.24	0.48	-0.34	0.80	26.73
50	Yan Nawa	0.17	0.14	0.18	-0.19	-0.14	-0.20	0.52	-0.30	0.39	0.10	0.84	27.10
51	Bang Len	0.37	0.37	0.11	-0.15	0.16	0.03	0.42	-0.11	0.26	-0.06	0.83	26.73
52	Don Tum	0.38	0.37	0.13	-0.18	0.21	0.06	0.37	-0.15	0.26	0.08	0.85	26.86
53	Kamphaeng Saen	0.40	0.37	0.12	-0.16	0.21	0.08	0.36	-0.14	0.23	-0.30	0.86	26.87
54	Mueang Nakhon Pathom	0.38	0.37	0.16	-0.22	0.25	0.08	0.32	-0.21	0.28	0.32	0.87	26.91
55	Nakhon Chai Si	0.35	0.38	0.16	-0.22	0.23	0.03	0.34	-0.20	0.32	0.13	0.86	27.19
56	Phutthamonthon	0.33	0.39	0.14	-0.21	0.17	-0.07	0.37	-0.17	0.37	-0.16	0.85	27.51
57	Sam Phran	0.31	0.37	0.17	-0.26	0.22	-0.04	0.33	-0.27	0.37	0.07	0.87	27.55
58	Bang Bua Thong	0.26	0.34	0.04	-0.19	0.00	-0.19	0.45	-0.13	0.39	-0.30	0.80	27.48
59	Bang Kruai	0.26	0.36	0.09	-0.23	0.04	-0.18	0.43	-0.11	0.42	0.37	0.83	27.51
60	Bang Yai	0.30	0.41	0.10	-0.20	0.11	-0.14	0.41	-0.09	0.40	-0.03	0.82	27.62
61	Mueang Nonthaburi	0.20	0.30	-0.02	-0.22	-0.09	-0.25	0.46	-0.17	0.41	0.45	0.80	27.22
62	Pak Kret	0.18	0.27	-0.10	-0.20	-0.15	-0.29	0.47	-0.20	0.40	0.18	0.78	27.28
63	Sai Noi	0.32	0.37	0.08	-0.17	0.09	-0.07	0.45	-0.10	0.33	-0.01	0.81	26.87
64	Bang Bo	-0.12	0.47	0.07	0.40	-0.18	-0.26	0.78	-0.12	0.56	-0.37	0.86	25.33
65	Bang Phli	-0.09	0.44	0.08	0.35	-0.18	-0.26	0.77	-0.15	0.54	-0.45	0.85	26.25
66	Bang Sao Thong	-0.12	0.46	0.06	0.38	-0.19	-0.27	0.77	-0.13	0.56	-0.03	0.85	25.59
67	Mueang Samut Prakan	-0.04	0.39	0.14	0.29	-0.16	-0.24	0.75	-0.19	0.51	-0.20	0.85	26.42
68	Phra Pradaeng	0.17	0.12	0.22	-0.15	-0.15	-0.20	0.54	-0.33	0.38	-0.09	0.85	27.05
69	Phra Samut Chedi	0.10	0.16	0.24	-0.13	-0.05	-0.17	0.55	-0.46	0.39	0.13	0.86	27.09
70	Ban Phaeo	0.29	0.36	0.20	-0.27	0.16	-0.03	0.34	-0.32	0.38	-0.09	0.86	27.53

Table 6.11 (Continued).

No.	District	Intercept	Regression coefficient								Resi-dual	Local R2	Predicted (μg/m³)
			WS	P	VIS	BT	FRP	AOD	FH	ELEV			
71	Krathum Baen	0.26	0.35	0.19	-0.28	0.17	-0.09	0.35	-0.32	0.40	0.00	0.87	27.89
72	Mueang Samut Sakhon	0.21	0.25	0.21	-0.31	0.06	-0.11	0.41	-0.38	0.40	-0.08	0.87	27.83

From Table 6.11, the maximum value is 28.38 μg/m^3 in Bang Bon District, Bangkok. In contrast, the minimum value is 25.33 μg/m^3 in Bang Bo District, Samut Prakan province. The classification maps of predicted values for PM2.5 concentration using the GWR model according to the Thailand Air Quality Index and the U.S. EPA Air Quality Index are displayed in Figure 6.21.

As a result, the predicted n values of PM2.5 concentration are satisfactory at level 2 of Thailand AQI and moderate at level 2 of the EPA AQI. However, the predicted value in an urban landscape in October 2019 from the GWR model is more than the one-day mean of WHO guidelines. See Table 5.3.

In addition, a spatial distribution map of PM2.5 concentration in October 2019 using the SCK interpolation technique is displayed in Figure 6.22. As a result, the high PM2.5 concentration occur in urban areas in the central part of the study area, particularly Bangkok Metropolitan.

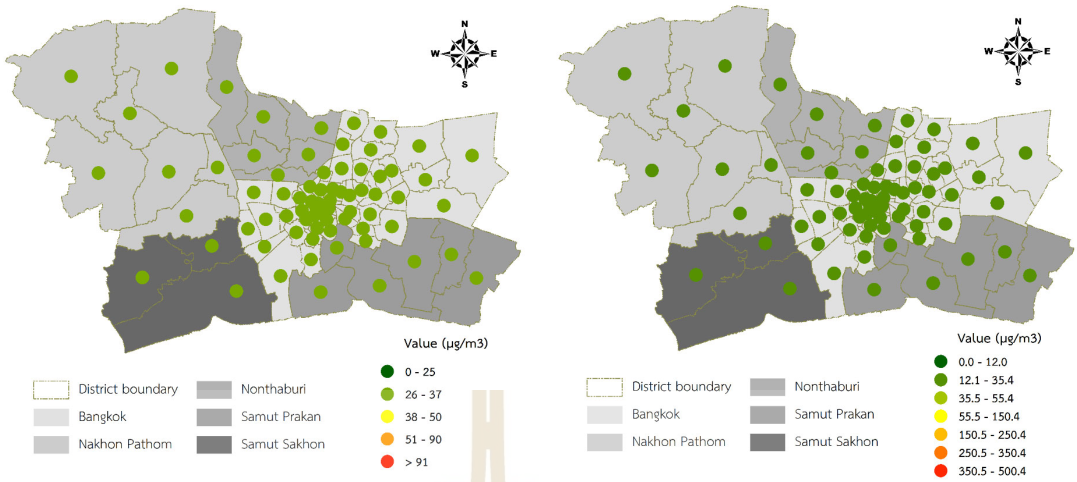

(a) (b)

Figure 6.21 The classification map of PM2.5 concentration prediction using the GWR model in October 2019 according to the (a) Thailand AQI and (b) EPA AQI.

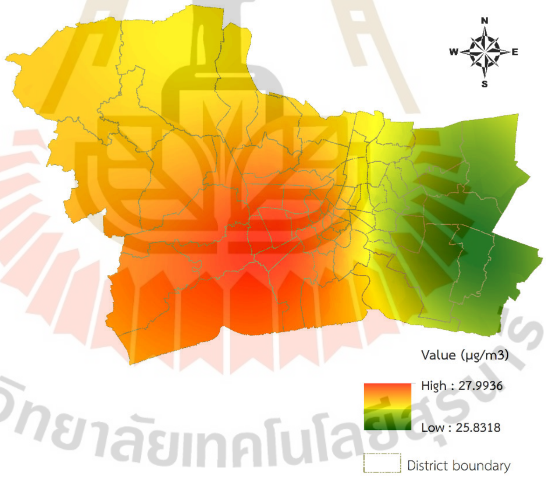

Figure 6.22 Spatial distribution of PM2.5 concentration in October 2019.

6.2.2 November 2019 in the winter season

The result of the GWR model for PM2.5 concentration prediction in November 2019 in the winter season is summarized in Table 6.12. The model performance shows that AICc, R-square, and adjusted R-square values are 10.54, 0.97, and 0.95, respectively.

Table 6.12 The predictive equations of PM2.5 concentration in November 2019.

No.	District	Intercept	Regression coefficient		Residual	Local	Predicted
			VIS	FRP		R2	(μg/m^3)
1	Bang Bon	0.76	0.32	0.56	0.15	0.61	35.24
2	Bang Kapi	-0.79	-0.16	0.75	-0.17	0.61	33.54
3	Bang Khae	0.82	0.22	0.13	0.00	0.50	35.22
4	Bang Khen	-0.70	0.01	0.40	-0.03	0.69	33.77
5	Bang Kho Laem	0.28	-0.09	-0.15	0.09	0.03	34.56
6	Bang Khun Thian	0.68	0.42	1.51	0.25	0.47	34.72
7	Bang Na	-0.30	-0.04	1.02	0.00	0.35	33.58
8	Bang Phlat	0.09	-0.41	0.22	0.14	0.47	34.47
9	Bang Rak	0.13	-0.25	-0.07	-0.09	0.21	34.52
10	Bang Sue	-0.09	-0.50	0.27	-0.13	0.57	34.55
11	Bangkok Noi	0.38	-0.18	-0.01	0.01	0.13	34.65
12	Bangkok Yai	0.45	-0.07	-0.15	0.08	0.04	34.66
13	Bueng Kum	-0.79	-0.06	0.59	-0.13	0.78	33.54
14	Chatuchak	-0.48	-0.34	0.45	-0.03	0.58	34.10
15	Chom Thong	0.56	0.14	0.06	0.15	0.13	34.85
16	Din Daeng	-0.37	-0.40	0.51	-0.21	0.35	33.96
17	Don Mueang	-0.49	-0.52	0.28	0.09	0.63	34.12
18	Dusit	-0.01	-0.40	0.23	0.18	0.44	34.21
19	Huai Khwang	-0.55	-0.36	0.72	-0.14	0.31	33.74
20	Khan Na Yao	-0.76	0.02	0.50	-0.01	0.81	33.45
21	Khlong Sam Wa	-0.73	0.12	0.42	0.16	0.88	33.27
22	Khlong San	0.29	-0.14	-0.16	0.23	0.10	34.57
23	Khlong Toei	-0.28	-0.33	0.55	-0.06	0.16	34.08
24	Lak Si	-0.37	-0.55	0.26	0.19	0.57	34.21
25	Lat Krabang	-0.77	-0.11	0.71	-0.02	0.79	32.83
26	Lat Phrao	-0.80	-0.13	0.70	-0.08	0.81	33.76
27	Min Buri	-0.78	0.09	0.44	0.13	0.83	32.90
28	Nong Chok	-0.74	0.05	0.53	0.07	0.83	32.74
29	Nong Khaem	0.89	0.23	0.09	0.04	0.56	35.32

Table 6.12 (Continued).

No.	District	Intercept	Regression coefficient		Residual	Local R2	Predicted (μg/m³)
			VIS	FRP			
30	Pathum Wan	-0.02	-0.38	0.17	-0.06	0.35	34.07
31	Phasi Charoen	0.66	0.13	-0.08	0.22	0.15	34.79
32	Phaya Thai	-0.19	-0.44	0.35	-0.12	0.41	34.11
33	Phra Khanong	-0.44	-0.11	0.79	-0.29	0.23	33.71
34	Phra Nakhon	0.22	-0.27	0.00	0.25	0.25	34.41
35	Pom Prap Sattru Phai	0.14	-0.29	0.03	0.20	0.25	34.17
36	Prawet	-0.67	-0.12	0.82	0.00	0.63	33.15
37	Rat Burana	0.39	0.01	0.11	0.10	0.00	34.53
38	Ratchathewi	-0.09	-0.43	0.28	-0.06	0.39	33.98
39	Sai Mai	-0.68	0.06	0.36	0.18	0.72	33.66
40	Samphanthawong	0.21	-0.23	-0.06	-0.34	0.18	34.62
41	Saphan Sung	-0.80	0.01	0.49	-0.11	0.75	33.19
42	Sathon	0.10	-0.24	-0.10	0.02	0.18	34.49
43	Suan Luang	-0.64	-0.18	0.81	-0.19	0.34	33.60
44	Taling Chan	0.66	0.00	-0.02	0.26	0.00	34.77
45	Thawi Watthana	0.96	0.12	-0.07	0.08	0.30	34.99
46	Thon Buri	0.42	-0.04	-0.16	0.34	0.03	34.61
47	Thung Khru	0.52	0.24	1.10	0.16	0.15	34.47
48	Vadhana	-0.46	-0.38	0.81	-0.15	0.20	33.95
49	Wang Thonglang	-0.77	-0.23	0.82	-0.18	0.54	33.63
50	Yan Nawa	0.08	-0.14	0.06	-0.01	0.05	34.32
51	Bang Len	0.84	0.49	-0.06	-0.13	0.64	34.34
52	Don Tum	0.82	0.44	-0.02	0.00	0.74	34.59
53	Kamphaeng Saen	0.79	0.46	-0.02	-0.23	0.78	34.48
54	Mueang Nakhon Pathom	0.85	0.41	0.03	-0.25	0.79	35.31
55	Nakhon Chai Si	0.95	0.33	-0.02	0.11	0.67	35.16
56	Phutthamonthon	1.07	0.17	-0.15	-0.04	0.59	35.17
57	Sam Phran	1.10	0.23	0.05	0.21	0.61	35.41
58	Bang Bua Thong	0.59	-0.27	-0.06	-0.01	0.18	34.65
59	Bang Kruai	0.67	-0.10	0.03	0.24	0.05	34.88
60	Bang Yai	0.95	0.00	-0.13	0.20	0.23	34.93
61	Mueang Nonthaburi	0.14	-0.67	0.09	0.29	0.63	34.78
62	Pak Kret	-0.11	-0.92	0.15	-0.14	0.64	34.61
63	Sai Noi	0.94	0.49	-0.11	-0.32	0.35	34.61
64	Bang Bo	-0.61	-0.24	1.01	-0.18	0.89	32.05

Table 6.12 (Continued).

No.	District	Intercept	Regression coefficient		Residual	Local	Predicted
			VIS	FRP		R2	(µg/m^3)
65	Bang Phli	-0.55	-0.17	1.03	-0.09	0.87	32.84
66	Bang Sao Thong	-0.65	-0.24	0.98	-0.01	0.88	32.43
67	Mueang Samut Prakan	-0.02	0.02	1.52	-0.42	0.64	33.25
68	Phra Pradaeng	0.19	0.10	0.86	-0.26	0.10	34.14
69	Phra Samut Chedi	1.01	0.62	3.57	-0.60	0.53	34.07
70	Ban Phaeo	1.08	0.26	0.27	0.16	0.59	35.77
71	Krathum Baen	1.01	0.24	0.12	0.21	0.51	35.45
72	Mueang Samut Sakhon	0.65	0.43	0.84	-0.13	0.50	35.63

From Table 6.12, the maximum value is 35.77 µg/m^3 in Ban Phaeo District, Samut Sakhon province. In contrast, the minimum value is 32.05 µg/m^3 in Bang Bo District, Samut Prakan province. The classification maps of predicted values for PM2.5 concentration using the GWR model according to the Thailand Air Quality Index and the U.S. EPA Air Quality Index are displayed in Figure 6.23.

As a result, the predicted values of PM2.5 concentration are satisfactory at level 2 of Thailand AQI, but they are moderate and unhealthy for sensitive groups at levels 2 and 3 of EPA AQI. However, the predicted value in an urban landscape in November 2019 from the GWR model is more than the one-day mean of WHO guidelines. See Table 5.3.

In addition, a spatial distribution map of PM2.5 concentration in November 2019 using the SCK interpolation technique is displayed in Figure 6.24. As a result, the high PM2.5 concentration occur in urban areas in the western part of the study area, particularly in Nakhon Pathom and Samut Sakhon province.

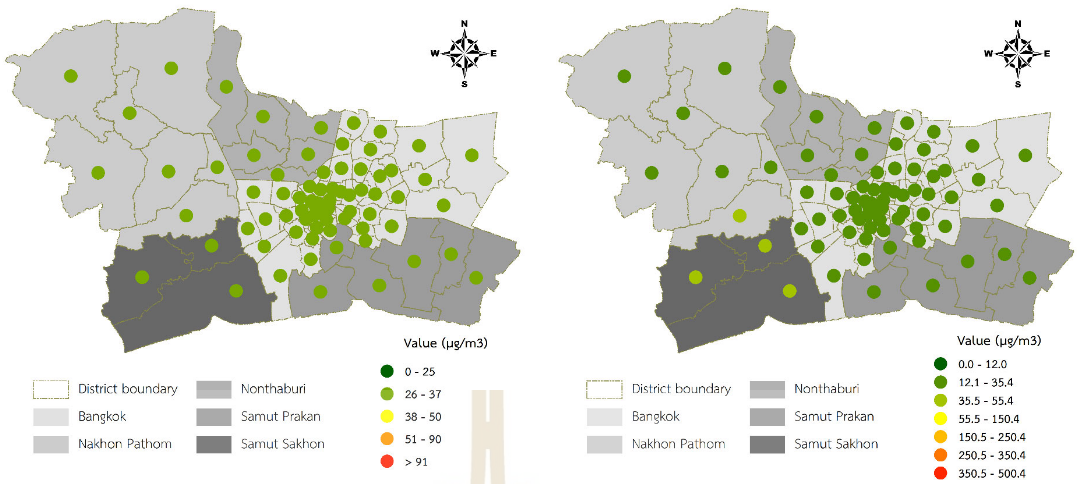

(a) (b)

Figure 6.23 The classification map of PM2.5 concentration prediction using the GWR model in November 2019 according to the (a) Thailand AQI and (b) EPA AQI.

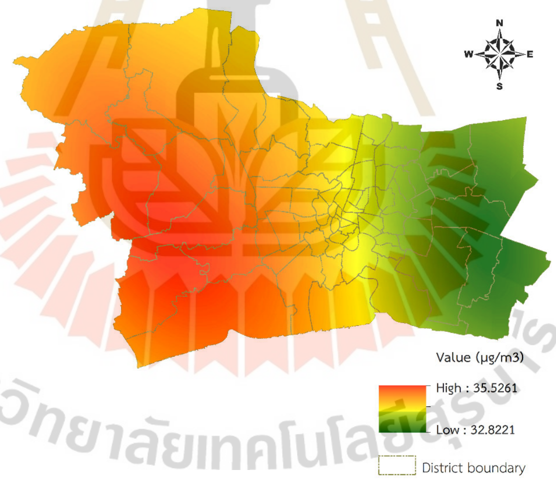

Figure 6.24 Spatial distribution of PM2.5 concentration in November 2019.

6.2.3 December 2019 in the winter season

The result of the GWR model for PM2.5 concentration prediction in December 2019 in the winter season is summarized in Table 6.13. The model performance shows that AICc, R-square, and adjusted R-square values are 24.44, 0.97, and 0.95, respectively.

Table 6.13 The predictive equations of PM2.5 concentration in December 2019.

No.	District	Intercept	Regression coefficient		Residual	Local	Predicted
			WS	VIS		R2	(μg/m^3)
1	Bang Bon	1.20	-0.85	-0.93	0.10	0.50	40.00
2	Bang Kapi	-1.13	0.25	1.34	-0.25	0.57	39.53
3	Bang Khae	0.93	-0.38	-0.44	0.05	0.31	40.11
4	Bang Khen	-0.87	1.01	1.41	-0.13	0.50	39.90
5	Bang Kho Laem	-1.09	0.49	1.34	-0.23	0.20	39.87
6	Bang Khun Thian	1.54	-1.31	-1.77	0.08	0.62	39.76
7	Bang Na	-1.32	-0.12	0.53	-0.11	0.77	39.31
8	Bang Phlat	0.73	0.59	0.07	0.13	0.67	40.17
9	Bang Rak	0.21	0.53	0.30	0.00	0.34	39.85
10	Bang Sue	0.58	0.60	0.13	0.10	0.44	40.13
11	Bangkok Noi	0.81	0.28	-0.17	0.18	0.35	40.14
12	Bangkok Yai	0.31	0.48	0.29	0.01	0.33	40.09
13	Bueng Kum	-1.00	0.51	1.26	-0.20	0.48	39.59
14	Chatuchak	0.17	0.41	0.21	0.09	0.15	40.01
15	Chom Thong	0.69	-0.10	-0.57	0.02	0.05	39.98
16	Din Daeng	-0.22	0.64	1.03	-0.08	0.40	39.81
17	Don Mueang	0.22	0.11	0.67	0.39	0.12	40.04
18	Dusit	0.61	0.74	0.24	0.20	0.68	40.06
19	Huai Khwang	-1.15	0.32	1.91	0.04	0.45	39.61
20	Khan Na Yao	-0.99	0.64	0.91	-0.21	0.49	39.51
21	Khlong Sam Wa	-0.83	0.52	0.63	0.00	0.61	39.32
22	Khlong San	-0.04	0.49	0.52	0.02	0.27	39.97
23	Khlong Toei	-1.26	0.01	0.97	-0.16	0.52	39.51
24	Lak Si	0.42	0.12	0.06	0.35	0.01	40.08
25	Lat Krabang	-0.98	-0.21	0.26	0.02	0.86	39.03
26	Lat Phrao	-1.10	0.67	2.09	-0.14	0.48	39.82
27	Min Buri	-0.88	0.01	0.40	-0.09	0.62	39.21
28	Nong Chok	-0.68	-0.11	0.42	0.07	0.70	38.98

Table 6.13 (Continued).

No.	District	Intercept	Regression coefficient		Residual	Local	Predicted
			WS	VIS		R2	(μg/m³)
29	Nong Khaem	0.99	-0.53	-0.38	0.04	0.68	40.13
30	Pathum Wan	0.40	0.71	0.34	0.24	0.54	39.74
31	Phasi Charoen	0.29	0.37	0.27	0.10	0.11	40.11
32	Phaya Thai	0.30	0.80	0.61	0.03	0.50	39.94
33	Phra Khanong	-1.32	-0.08	0.77	-0.07	0.64	39.34
34	Phra Nakhon	0.84	0.58	-0.11	0.13	0.68	40.09
35	Pom Prap Sattru Phai	0.78	0.61	-0.06	0.15	0.64	40.01
36	Prawet	-1.19	-0.05	0.41	-0.09	0.69	39.24
37	Rat Burana	-1.61	0.53	1.81	-0.24	0.15	39.83
38	Ratchathewi	0.41	0.81	0.49	0.27	0.65	39.81
39	Sai Mai	-0.79	1.03	1.19	0.17	0.59	39.77
40	Samphanthawong	0.77	0.56	-0.12	0.12	0.53	39.98
41	Saphan Sung	-1.01	0.06	0.48	-0.17	0.56	39.33
42	Sathon	-0.62	0.37	0.86	-0.22	0.33	39.80
43	Suan Luang	-1.27	0.11	1.19	-0.10	0.62	39.38
44	Taling Chan	0.90	-0.10	-0.31	-0.05	0.30	40.13
45	Thawi Watthana	0.90	-0.30	-0.25	0.08	0.81	40.23
46	Thon Buri	-0.49	0.64	1.01	0.02	0.26	40.01
47	Thung Khru	-0.51	-0.02	0.26	-0.19	0.05	39.66
48	Vadhana	-1.14	0.15	1.21	0.00	0.49	39.46
49	Wang Thonglang	-1.38	0.30	2.22	-0.36	0.57	39.71
50	Yan Nawa	-1.58	0.08	1.37	-0.50	0.38	39.73
51	Bang Len	0.94	-0.24	0.02	0.07	0.65	40.49
52	Don Tum	1.00	-0.23	0.07	0.16	0.61	40.51
53	Kamphaeng Saen	1.03	-0.21	0.09	-0.25	0.51	40.52
54	Mueang Nakhon Pathom	1.03	-0.24	0.14	0.08	0.71	40.52
55	Nakhon Chai Si	0.94	-0.25	-0.01	-0.21	0.78	40.42
56	Phutthamonthon	0.89	-0.14	-0.20	0.06	0.76	40.31
57	Sam Phran	0.88	-0.22	-0.16	0.10	0.70	40.28
58	Bang Bua Thong	0.90	-0.16	-0.10	-0.07	0.81	40.37
59	Bang Kruai	0.91	-0.19	-0.28	-0.01	0.64	40.22
60	Bang Yai	0.89	-0.17	-0.16	0.06	0.77	40.30
61	Mueang Nonthaburi	0.81	0.23	-0.18	-0.04	0.29	40.24
62	Pak Kret	0.79	-0.07	-0.19	0.18	0.06	40.19
63	Sai Noi	0.89	-0.26	-0.01	-0.02	0.89	40.45
64	Bang Bo	-1.18	-0.20	0.20	-0.02	0.97	38.76

Table 6.13 (Continued).

No.	District	Intercept	Regression coefficient		Residual	Local	Predicted
			WS	VIS		R2	(μg/m^3)
65	Bang Phli	-1.24	-0.18	0.19	0.01	0.96	39.03
66	Bang Sao Thong	-1.17	-0.20	0.21	-0.03	0.95	38.88
67	Mueang Samut Prakan	-1.25	-0.08	0.36	-0.19	0.71	39.19
68	Phra Pradaeng	-1.50	0.10	1.17	-0.36	0.51	39.52
69	Phra Samut Chedi	-0.88	0.04	0.51	-0.25	0.12	39.46
70	Ban Phaeo	0.95	-0.31	-0.02	0.11	0.74	40.20
71	Krathum Baen	0.92	-0.43	-0.25	0.03	0.78	40.23
72	Mueang Samut Sakhon	1.04	-0.81	-0.77	0.12	0.71	40.02

From Table 6.13, the maximum value is 40.52 μg/m^3 in Kamphaeng Saen District, Nakhon Pathom province. In contrast, the minimum value is 38.76 μg/m^3 in Bang Bo District, Samut Prakan province. The classification maps of predicted values for PM2.5 concentration using the GWR model according to the Thailand Air Quality Index and the U.S. EPA Air Quality Index are displayed in Figure 6.25.

As a result, the predicted values of PM2.5 concentration are moderate at level 3 of Thailand AQI and unhealthy for sensitive groups at level 3 of EPA AQI. On the contrary, the predicted value in an urban landscape in December 2019 from the GWR model is more than the one-day mean of WHO guidelines. See Table 5.3.

In addition, a spatial distribution map of PM2.5 concentration in December 2019 using the SCK interpolation technique is displayed in Figure 6.26. As a result, the high PM2.5 concentration occur in urban areas in the northwestern part of the study area, particularly in Nakhon Pathom and Nonthaburi province.

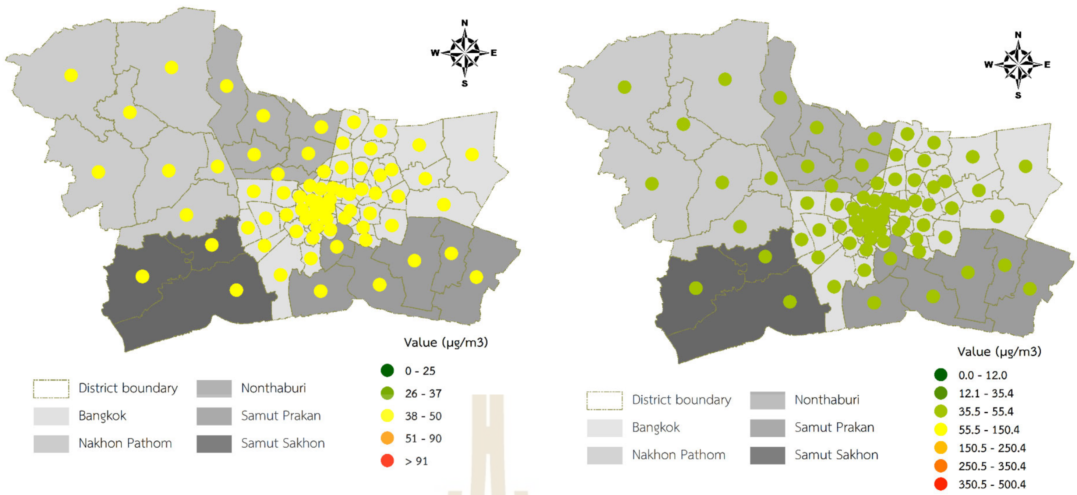

(a) (b)

Figure 6.25 The classification map of PM2.5 concentration prediction using the GWR model in December 2019 according to the (a) Thailand AQI and (b) EPA AQI.

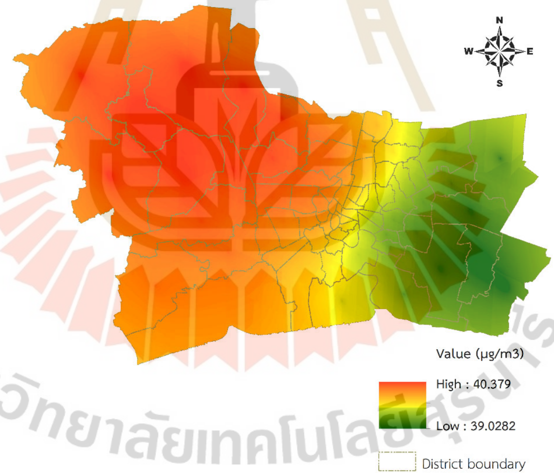

Figure 6.26 Spatial distribution of PM2.5 concentration in December 2019.

6.2.4 January 2020 in the winter season

The result of the GWR model for PM2.5 concentration prediction in January 2020 in the winter season is summarized in Table 6.14. The model performance shows that AICc, R-square, and adjusted R-square values are 177.81, 0.58, and 0.46, respectively.

Table 6.14 The predictive equations of PM2.5 concentration in January 2020.

No.	District	Intercept	Regression coefficient					Residual	Local	Predicted
			TEMP	VIS	AOD	FH	ELEV		R2	(μg/m^3)
1	Bang Bon	-0.44	-0.12	0.54	-0.52	0.44	0.43	-0.99	0.38	43.53
2	Bang Kapi	0.38	-1.04	0.55	-0.56	0.13	0.31	-0.05	0.42	43.67
3	Bang Khae	-0.43	0.08	0.60	-0.69	0.51	0.36	-1.05	0.40	43.57
4	Bang Khen	0.35	-0.84	0.55	-0.59	0.09	0.25	0.92	0.41	43.69
5	Bang Kho Laem	-0.52	0.29	0.59	-0.73	0.44	0.28	0.63	0.41	43.59
6	Bang Khun Thian	-0.40	-0.17	0.50	-0.44	0.56	0.44	-0.10	0.40	43.36
7	Bang Na	0.12	-0.75	0.51	-0.64	0.34	0.38	-1.17	0.40	43.62
8	Bang Phlat	-0.27	0.01	0.60	-0.95	0.39	0.31	0.35	0.37	43.72
9	Bang Rak	-0.42	0.18	0.61	-0.82	0.42	0.29	-0.49	0.38	43.71
10	Bang Sue	0.04	-0.49	0.57	-0.89	0.30	0.36	-0.01	0.36	43.57
11	Bangkok Noi	-0.43	0.29	0.62	-0.91	0.45	0.27	0.80	0.41	43.74
12	Bangkok Yai	-0.50	0.37	0.62	-0.83	0.50	0.27	0.87	0.42	43.63
13	Bueng Kum	0.38	-0.95	0.56	-0.54	0.08	0.26	1.04	0.42	43.70
14	Chatuchak	0.32	-0.88	0.55	-0.72	0.23	0.34	-0.77	0.38	43.69
15	Chom Thong	-0.46	0.16	0.58	-0.66	0.53	0.33	-1.40	0.41	43.53
16	Din Daeng	0.14	-0.70	0.56	-0.78	0.28	0.38	-0.27	0.36	43.50
17	Don Mueang	0.33	-0.74	0.53	-0.66	0.18	0.26	0.11	0.39	43.81
18	Dusit	-0.14	-0.22	0.59	-0.91	0.36	0.34	0.71	0.36	43.58
19	Huai Khwang	0.29	-0.96	0.56	-0.69	0.19	0.37	-0.64	0.38	43.52
20	Khan Na Yao	0.39	-0.89	0.57	-0.51	0.07	0.21	0.35	0.43	43.76
21	Khlong Sam Wa	0.37	-0.74	0.57	-0.51	0.10	0.16	-0.22	0.41	43.76
22	Khlong San	-0.57	0.46	0.62	-0.81	0.50	0.25	0.99	0.41	43.67
23	Khlong Toei	0.01	-0.51	0.54	-0.74	0.38	0.37	0.58	0.37	43.44
24	Lak Si	0.30	-0.79	0.53	-0.72	0.22	0.31	0.13	0.39	43.82
25	Lat Krabang	0.25	-0.73	0.55	-0.57	0.21	0.25	-0.04	0.43	43.77
26	Lat Phrao	0.41	-1.01	0.56	-0.58	0.09	0.29	1.53	0.42	43.53
27	Min Buri	0.35	-0.79	0.57	-0.51	0.15	0.20	-0.42	0.42	43.81
28	Nong Chok	0.34	-0.68	0.58	-0.51	0.16	0.16	-0.87	0.41	43.82
29	Nong Khaem	-0.40	-0.14	0.54	-0.57	0.44	0.44	-0.43	0.36	43.53

Table 6.14 (Continued).

No.	District	Intercept	Regression coefficient					Residual	Local	Predicted
			TEMP	VIS	AOD	FH	ELEV		R2	(μg/m^3)
30	Pathum Wan	-0.20	-0.15	0.59	-0.83	0.40	0.33	-0.02	0.36	43.62
31	Phasi Charoen	-0.49	0.27	0.62	-0.76	0.53	0.30	-1.20	0.43	43.61
32	Phaya Thai	0.09	-0.60	0.58	-0.83	0.31	0.37	-0.32	0.35	43.60
33	Phra Khanong	0.18	-0.83	0.53	-0.65	0.31	0.38	-0.73	0.39	43.55
34	Phra Nakhon	-0.43	0.27	0.63	-0.90	0.46	0.28	0.19	0.39	43.77
35	Pom Prap Sattru Phai	-0.37	0.16	0.62	-0.88	0.44	0.29	0.02	0.38	43.73
36	Prawet	0.29	-0.96	0.53	-0.56	0.22	0.34	-0.10	0.44	43.53
37	Rat Burana	-0.51	0.21	0.57	-0.65	0.47	0.31	-0.77	0.41	43.53
38	Ratchathewi	-0.08	-0.34	0.59	-0.84	0.37	0.35	0.20	0.35	43.60
39	Sai Mai	0.39	-0.78	0.56	-0.55	0.07	0.18	0.22	0.41	43.73
40	Samphanthawong	-0.48	0.35	0.63	-0.86	0.48	0.27	-0.08	0.39	43.67
41	Saphan Sung	0.33	-0.90	0.55	-0.54	0.16	0.27	1.15	0.43	43.66
42	Sathon	-0.41	0.15	0.59	-0.78	0.41	0.29	-0.09	0.38	43.66
43	Suan Luang	0.38	-1.12	0.54	-0.58	0.20	0.37	-0.75	0.42	43.53
44	Taling Chan	-0.55	0.48	0.68	-0.97	0.49	0.25	0.17	0.46	43.69
45	Thawi Watthana	-0.34	0.11	0.59	-0.82	0.52	0.33	-0.78	0.40	43.58
46	Thon Buri	-0.58	0.45	0.62	-0.77	0.54	0.26	0.10	0.43	43.67
47	Thung Khru	-0.42	0.00	0.52	-0.56	0.49	0.36	-1.50	0.40	43.51
48	Vadhana	0.12	-0.71	0.54	-0.72	0.32	0.38	-0.95	0.37	43.63
49	Wang Thonglang	0.43	-1.13	0.56	-0.58	0.11	0.33	-0.20	0.42	43.58
50	Yan Nawa	-0.40	0.11	0.57	-0.72	0.45	0.30	0.17	0.38	43.63
51	Bang Len	0.28	0.09	-0.09	-0.06	0.30	0.07	0.65	0.18	43.65
52	Don Tum	0.11	-0.02	0.02	-0.08	0.35	0.16	-0.21	0.17	43.62
53	Kamphaeng Saen	0.12	0.00	0.04	-0.03	0.35	0.09	-0.29	0.16	43.72
54	Mueang Nakhon Pathom	-0.09	-0.18	0.17	-0.16	0.36	0.29	0.08	0.20	43.78
55	Nakhon Chai Si	-0.03	-0.18	0.10	-0.24	0.37	0.37	-0.77	0.20	43.71
56	Phutthamonthon	-0.03	-0.11	0.17	-0.43	0.42	0.39	0.18	0.23	43.58
57	Sam Phran	-0.24	-0.33	0.30	-0.35	0.37	0.53	-0.16	0.27	43.60
58	Bang Bua Thong	0.18	-0.25	0.26	-0.60	0.32	0.24	-0.30	0.22	43.83
59	Bang Kruai	-0.42	0.36	0.66	-1.06	0.48	0.26	0.23	0.45	43.68
60	Bang Yai	-0.12	0.01	0.42	-0.79	0.46	0.31	0.78	0.33	43.63
61	Mueang Nonthaburi	0.00	-0.36	0.56	-0.95	0.34	0.35	-0.04	0.36	43.69
62	Pak Kret	0.20	-0.63	0.51	-0.83	0.30	0.34	0.04	0.37	43.76

Table 6.14 (Continued).

No.	District	Intercept	Regression coefficient					Residual	Local R2	Predicted (μg/m³)
			TEMP	VIS	AOD	FH	ELEV			
63	Sai Noi	0.28	-0.02	-0.02	-0.23	0.28	0.12	0.44	0.15	43.72
64	Bang Bo	0.14	-0.69	0.52	-0.58	0.27	0.30	-0.04	0.47	43.63
65	Bang Phli	0.17	-0.82	0.51	-0.57	0.27	0.34	0.01	0.45	43.51
66	Bang Sao Thong	0.18	-0.73	0.53	-0.58	0.26	0.30	0.38	0.46	43.65
67	Mueang Samut Prakan	-0.03	-0.58	0.47	-0.58	0.37	0.37	0.36	0.42	43.40
68	Phra Pradaeng	-0.42	0.11	0.55	-0.64	0.51	0.31	0.43	0.40	43.44
69	Phra Samut Chedi	-0.36	-0.14	0.48	-0.48	0.55	0.39	0.27	0.41	43.27
70	Ban Phaeo	-0.46	-0.45	0.42	-0.26	0.25	0.59	1.01	0.36	43.70
71	Krathum Baen	-0.43	-0.37	0.48	-0.40	0.33	0.56	-0.89	0.33	43.66
72	Mueang Samut Sakhon	-0.52	-0.40	0.46	-0.33	0.16	0.55	0.93	0.38	43.57

From Table 6.14, the maximum value is 43.83 μg/m^3 in Bang Bua Thong District, Nonthaburi province. In contrast, the minimum value is 43.27 μg/m^3 in Phra Samut Chedi District, Samut Prakan province. The classification maps of predicted values for PM2.5 concentration using the GWR model according to the Thailand Air Quality Index and the U.S. EPA Air Quality Index are displayed in Figure 6.27.

Thus, the predicted values of PM2.5 concentration are moderate at level 3 of Thailand AQI and unhealthy for sensitive groups at level 3 of EPA AQI. Meanwhile, the predicted value in an urban landscape in January 2020 from the GWR model is more than the one-day mean of WHO guidelines. See Table 5.3.

In addition, a spatial distribution map of PM2.5 concentration in January 2020 using the SCK interpolation technique is displayed in Figure 6.28. As a result, the high PM2.5 concentration occur in urban areas in the northern part of the study area, particularly Bangkok Metropolitan and Nonthaburi province.

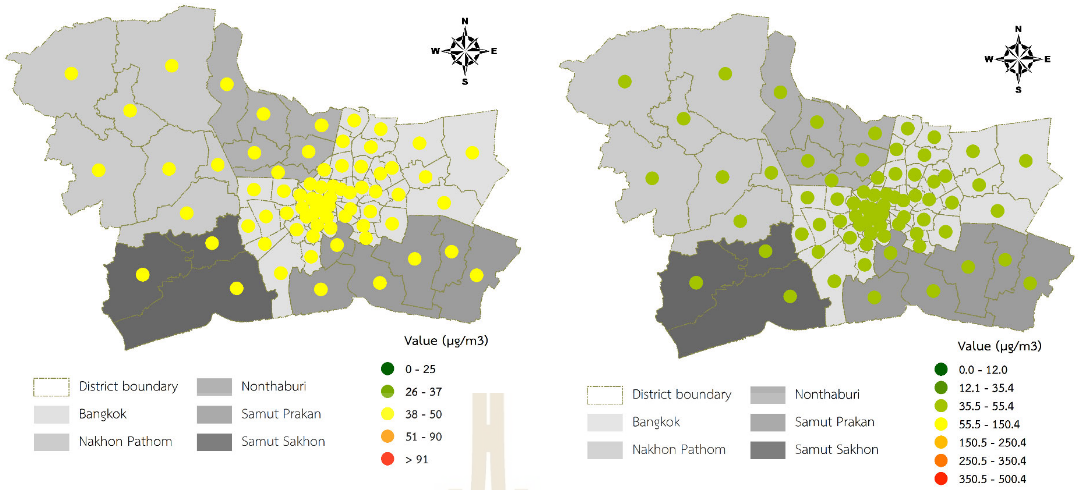

(a) (b)

Figure 6.27 The classification map of PM2.5 concentration prediction using the GWR model in January 2020 according to the (a) Thailand AQI and (b) EPA AQI.

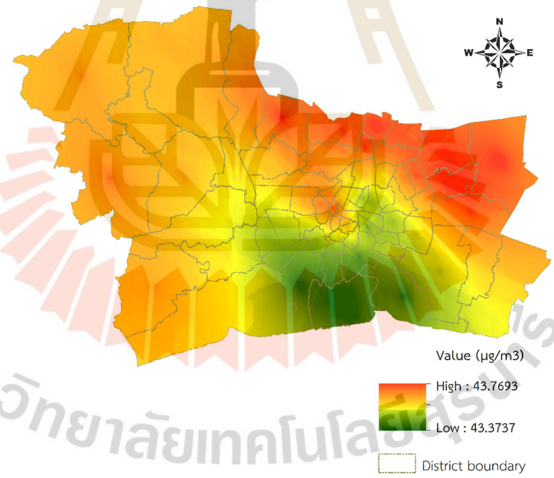

Figure 6.28 Spatial distribution of PM2.5 concentration in January 2020.

6.2.5 February 2020 in the winter season

The result of the GWR model for PM2.5 concentration prediction in February 2020 in the winter season is summarized in Table 6.15. The model performance shows that AICc, R-square, and adjusted R-square values are 82.82, 0.92, and 0.88, respectively.

Table 6.15 The predictive equations of PM2.5 concentration in February 2020.

No.	District	Intercept	Regression coefficient					Residual	Local	Predicted
			RH	WS	P	FRP	ELEV		R2	(μg/m^3)
1	Bang Bon	-0.24	-1.08	0.22	0.09	-2.25	0.25	-0.78	0.81	44.09
2	Bang Kapi	0.12	-0.35	0.43	0.40	-0.35	0.14	0.44	0.81	44.13
3	Bang Khae	-0.72	-0.93	0.48	-0.41	-2.99	0.31	-0.11	0.81	44.22
4	Bang Khen	0.96	0.65	0.88	0.51	-0.59	0.01	0.05	0.90	44.29
5	Bang Kho Laem	0.20	-1.28	0.64	0.12	-1.16	0.26	-0.14	0.68	44.06
6	Bang Khun Thian	0.52	-1.49	0.31	0.51	-1.10	0.21	-0.16	0.77	44.01
7	Bang Na	-0.03	-0.84	0.31	0.44	-0.29	0.26	-0.10	0.71	43.98
8	Bang Phlat	-0.30	-0.55	0.65	-0.31	-2.11	0.19	0.08	0.74	44.23
9	Bang Rak	0.33	-0.78	0.50	0.54	-0.83	0.28	-0.52	0.63	44.14
10	Bang Sue	0.65	0.36	0.85	0.53	-0.64	0.21	0.03	0.82	44.22
11	Bangkok Noi	-0.78	-0.88	0.56	-0.70	-3.14	0.19	0.29	0.77	44.26
12	Bangkok Yai	-0.52	-1.05	0.53	-0.45	-2.72	0.19	0.69	0.75	44.20
13	Bueng Kum	0.35	0.00	0.70	0.27	-0.47	0.11	0.33	0.86	44.21
14	Chatuchak	1.02	0.68	0.77	0.91	-0.31	0.15	-0.12	0.87	44.21
15	Chom Thong	-0.04	-1.46	0.65	-0.20	-2.11	0.22	0.04	0.79	44.08
16	Din Daeng	1.09	0.48	0.54	1.39	-0.10	0.24	-0.43	0.71	44.09
17	Don Mueang	1.03	0.69	0.82	0.63	-0.59	-0.01	-0.16	0.91	44.37
18	Dusit	0.20	-0.27	0.69	0.24	-1.10	0.24	0.13	0.69	44.17
19	Huai Khwang	0.74	0.15	0.45	1.08	-0.26	0.21	-0.12	0.71	44.08
20	Khan Na Yao	0.11	-0.20	0.75	0.06	-0.45	0.14	0.16	0.87	44.22
21	Khlong Sam Wa	-0.51	-0.69	0.88	-0.38	-0.26	0.34	0.02	0.86	44.24
22	Khlong San	0.09	-1.06	0.54	0.14	-1.54	0.23	0.38	0.68	44.12
23	Khlong Toei	0.35	-0.57	0.38	0.79	-0.33	0.30	0.38	0.62	44.00
24	Lak Si	1.20	0.87	0.77	0.94	-0.40	0.06	0.22	0.92	44.30
25	Lat Krabang	-1.23	-1.41	0.59	-0.59	-0.05	0.47	0.05	0.85	44.05
26	Lat Phrao	1.09	0.78	0.82	0.77	-0.46	0.05	-0.23	0.89	44.21
27	Min Buri	-1.69	-1.80	0.64	-0.85	0.12	0.57	0.20	0.87	44.15
28	Nong Chok	-1.46	-1.54	0.75	-0.77	0.05	0.60	-0.31	0.88	44.15

Table 6.15 (Continued).

No.	District	Intercept	Regression coefficient					Residual	Local	Predicted
			RH	WS	P	FRP	ELEV		R2	(μg/m³)
29	Nong Khaem	-0.56	-0.81	0.28	-0.11	-2.52	0.35	-0.43	0.79	44.22
30	Pathum Wan	0.44	-0.53	0.48	0.74	-0.63	0.28	-0.19	0.62	44.11
31	Phasi Charoen	-0.76	-1.07	0.61	-0.68	-3.16	0.23	0.55	0.81	44.18
32	Phaya Thai	0.77	0.30	0.73	0.87	-0.34	0.25	-0.53	0.71	44.13
33	Phra Khanong	0.10	-0.66	0.26	0.65	-0.24	0.25	0.15	0.69	44.00
34	Phra Nakhon	-0.16	-0.75	0.51	-0.03	-1.97	0.21	0.38	0.70	44.20
35	Pom Prap Sattru Phai	0.15	-0.64	0.55	0.31	-1.24	0.25	0.23	0.65	44.19
36	Prawet	-0.43	-1.03	0.26	0.04	-0.33	0.14	-0.11	0.83	44.03
37	Rat Burana	0.35	-1.58	0.67	0.11	-1.22	0.24	-0.61	0.72	44.05
38	Ratchathewi	0.51	-0.28	0.52	0.80	-0.54	0.28	-0.24	0.63	44.11
39	Sai Mai	0.87	0.57	0.94	0.34	-0.63	-0.03	0.15	0.90	44.32
40	Samphanthawong	0.12	-0.79	0.54	0.26	-1.28	0.25	0.56	0.66	44.15
41	Saphan Sung	-0.76	-1.20	0.30	-0.20	-0.22	0.15	0.30	0.86	44.10
42	Sathon	0.39	-0.87	0.48	0.62	-0.71	0.28	0.03	0.63	44.05
43	Suan Luang	0.11	-0.51	0.23	0.66	-0.23	0.19	0.39	0.75	44.05
44	Taling Chan	-1.22	-0.89	0.68	-1.13	-3.93	0.22	-0.09	0.83	44.30
45	Thawi Watthana	-0.99	-0.69	0.50	-0.70	-3.34	0.30	-0.02	0.77	44.31
46	Thon Buri	-0.11	-1.20	0.60	-0.16	-1.88	0.22	0.34	0.71	44.13
47	Thung Khru	0.66	-1.84	0.69	0.27	-1.03	0.22	-0.33	0.77	44.00
48	Vadhana	0.45	-0.33	0.34	0.94	-0.24	0.27	-0.01	0.64	44.05
49	Wang Thonglang	0.72	0.20	0.46	0.92	-0.33	0.13	0.11	0.79	44.12
50	Yan Nawa	0.32	-1.08	0.51	0.46	-0.67	0.29	-0.15	0.64	44.01
51	Bang Len	0.73	-0.21	0.34	-0.08	-0.35	-0.04	-0.10	0.47	44.25
52	Don Tum	0.60	-0.28	0.28	-0.02	-0.34	0.03	0.03	0.35	44.23
53	Kamphaeng Saen	0.57	-0.27	0.28	-0.02	-0.36	0.01	-0.15	0.38	44.24
54	Mueang Nakhon Pathom	0.22	-0.44	0.34	0.22	-0.56	0.32	0.07	0.46	44.21
55	Nakhon Chai Si	0.25	-0.50	0.46	0.21	-0.76	0.55	0.23	0.47	44.20
56	Phutthamonthon	-0.11	-0.51	0.56	-0.12	-1.55	0.43	-0.01	0.49	44.23
57	Sam Phran	0.05	-0.83	0.47	0.53	-1.01	0.88	0.26	0.69	44.21
58	Bang Bua Thong	-0.11	-0.34	0.79	-0.24	-1.77	0.22	0.01	0.76	44.28
59	Bang Kruai	-1.04	-0.78	0.72	-1.03	-3.53	0.20	-0.09	0.82	44.29
60	Bang Yai	-0.76	-0.59	0.71	-0.84	-3.01	0.19	0.31	0.74	44.24
61	Mueang Nonthaburi	0.12	-0.04	0.84	0.04	-1.55	0.22	-0.17	0.88	44.29

Table 6.15 (Continued).

No.	District	Intercept	Regression coefficient					Residual	Local	Predicted
			RH	WS	P	FRP	ELEV		R2	(μg/m^3)
62	Pak Kret	0.75	0.40	0.72	0.66	-0.60	0.15	0.18	0.90	44.28
63	Sai Noi	0.56	-0.22	0.51	-0.10	-0.64	-0.08	0.01	0.60	44.25
64	Bang Bo	-0.82	-1.00	0.43	-0.25	-0.16	0.41	0.00	0.78	43.98
65	Bang Phli	-0.52	-1.11	0.30	-0.07	-0.35	0.18	0.06	0.81	43.99
66	Bang Sao Thong	-0.92	-1.17	0.42	-0.34	-0.17	0.34	-0.29	0.81	44.03
67	Mueang Samut Prakan	-0.21	-0.97	0.37	0.16	-0.41	0.25	0.08	0.68	43.97
68	Phra Pradaeng	0.30	-1.32	0.54	0.34	-0.65	0.28	-0.31	0.68	43.99
69	Phra Samut Chedi	0.60	-1.60	0.59	0.45	-0.67	0.28	0.16	0.72	43.97
70	Ban Phaeo	0.32	-1.00	0.33	0.77	-0.54	0.80	0.34	0.75	44.10
71	Krathum Baen	-0.22	-0.78	0.27	0.32	-1.56	0.61	0.13	0.76	44.12
72	Mueang Samut Sakhon	-0.29	-0.82	0.00	0.23	-1.89	0.29	0.09	0.79	44.01

From Table 6.15, the maximum value is 44.37 μg/m^3 in Don Mueang District, Bangkok. In contrast, the minimum value is 43.97 μg/m^3 in Phra Samut Chedi District, Samut Prakan province. The classification maps of predicted values for PM2.5 concentration using the GWR model according to the Thailand Air Quality Index and the U.S. EPA Air Quality Index are displayed in Figure 6.29.

Thus, the predicted values of PM2.5 concentration are moderate at level 3 of Thailand AQI and unhealthy for sensitive groups at level 3 of EPA AQI. In contrast, the predicted value in an urban landscape in February 2020 from the GWR model is more than the one-day mean of WHO guidelines. See Table 5.3.

In addition, a spatial distribution map of PM2.5 concentration in February 2020 using the SCK interpolation technique is displayed in Figure 6.30. As a result, the high PM2.5 concentration occur in urban areas in the northern part of the study area, mainly in Bangkok Metropolitan and Nonthaburi province.

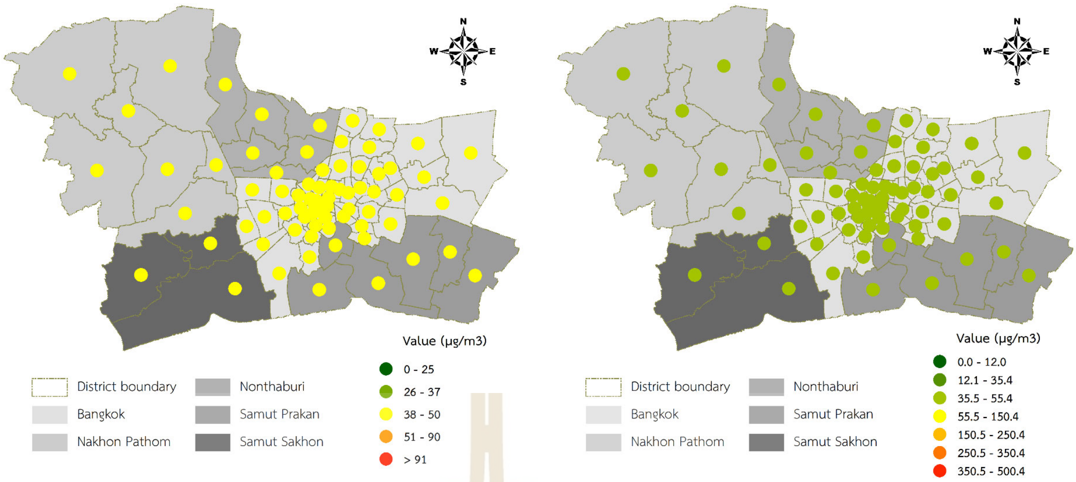

(a) (b)

Figure 6.29 The classification map of PM2.5 concentration prediction using the GWR model in February 2020 according to the (a) Thailand AQI and (b) EPA AQI.

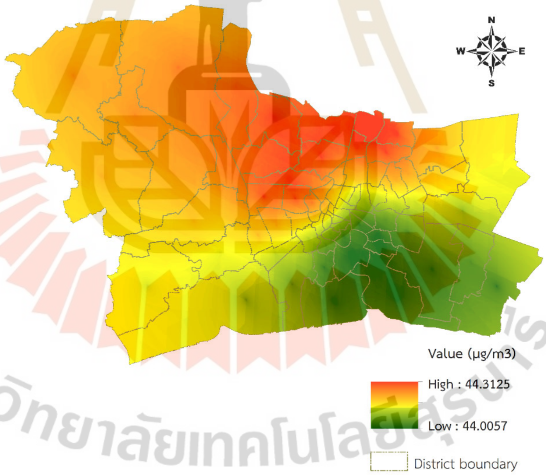

Figure 6.30 Spatial distribution of PM2.5 concentration in February 2020.

6.2.6 March 2020 in the summer season

The result of the GWR model for PM2.5 concentration prediction in March 2020 in the summer season is summarized in Table 6.16. The model performance shows that AICc, R-square, and adjusted R-square values are 114.63, 0.92, and 0.85, respectively.

Table 6.16 The predictive equations of PM2.5 concentration in March 2020.

No.	District	Intercept	Regression coefficient FRP	Residual	LocalR2	Predicted ($\mu g/m^3$)
1	Bang Bon	-0.45	-0.43	0.40	0.03	23.31
2	Bang Kapi	0.42	0.30	0.71	0.02	23.51
3	Bang Khae	-0.96	-0.77	-0.20	0.21	23.25
4	Bang Khen	-0.02	0.68	0.41	0.58	23.73
5	Bang Kho Laem	0.46	6.26	0.11	0.92	23.13
6	Bang Khun Thian	-0.62	-1.18	0.72	0.11	23.29
7	Bang Na	-0.28	0.89	0.21	0.12	23.20
8	Bang Phlat	-1.18	-1.12	-0.55	0.18	22.90
9	Bang Rak	0.18	-2.34	0.51	0.24	23.38
10	Bang Sue	-3.04	1.85	-0.09	0.68	23.09
11	Bangkok Noi	-0.91	-2.08	-0.23	0.38	23.09
12	Bangkok Yai	-0.43	-0.68	0.30	0.04	23.26
13	Bueng Kum	0.50	0.32	0.47	0.07	23.57
14	Chatuchak	-2.93	1.91	-0.17	0.72	23.26
15	Chom Thong	0.13	3.81	-0.12	0.40	23.08
16	Din Daeng	-0.49	-2.02	-0.16	0.20	22.86
17	Don Mueang	-0.13	0.66	-0.25	0.62	24.04
18	Dusit	-0.92	-1.90	-0.34	0.34	22.83
19	Huai Khwang	-0.14	-1.83	0.33	0.17	23.05
20	Khan Na Yao	0.57	0.39	-0.38	0.24	23.62
21	Khlong Sam Wa	0.90	0.34	0.13	0.49	23.67
22	Khlong San	-0.07	0.79	0.16	0.04	23.32
23	Khlong Toei	-0.45	-0.28	-0.04	0.01	23.23
24	Lak Si	-1.21	1.02	0.49	0.71	23.72
25	Lat Krabang	0.54	-0.29	-0.03	0.37	23.60
26	Lat Phrao	-0.36	0.67	-0.21	0.14	23.48
27	Min Buri	0.82	0.05	-0.09	0.01	23.58
28	Nong Chok	1.10	-0.04	0.37	0.01	23.67
29	Nong Khaem	-1.07	-1.10	-0.06	0.19	23.33

Table 6.16 (Continued).

No.	District	Intercept	Regression coefficient FRP	Residual	LocalR2	Predicted ($\mu g/m^3$)
30	Pathum Wan	0.41	-5.28	0.05	0.84	23.22
31	Phasi Charoen	-0.58	0.20	0.00	0.01	23.17
32	Phaya Thai	-1.48	-0.69	-0.53	0.05	22.82
33	Phra Khanong	-0.32	0.89	-0.38	0.13	23.22
34	Phra Nakhon	-0.19	-3.98	-0.35	0.49	23.16
35	Pom Prap Sattru Phai	0.25	-5.08	0.09	0.72	23.21
36	Prawet	0.20	0.85	0.22	0.14	23.35
37	Rat Burana	0.50	6.42	-0.32	0.79	22.95
38	Ratchathewi	0.23	-4.24	-0.30	0.90	23.01
39	Sai Mai	0.49	0.50	0.17	0.63	23.88
40	Samphanthawong	0.02	-2.81	0.52	0.27	23.33
41	Saphan Sung	0.55	0.40	-0.15	0.19	23.51
42	Sathon	0.03	1.78	0.13	0.18	23.35
43	Suan Luang	-0.15	1.13	0.34	0.20	23.34
44	Taling Chan	-1.05	-0.81	-0.22	0.23	23.15
45	Thawi Watthana	-0.73	-0.35	-0.16	0.08	23.22
46	Thon Buri	0.32	4.12	0.00	0.78	23.22
47	Thung Khru	-1.36	-1.07	-0.02	0.02	23.05
48	Vadhana	-0.46	-0.86	-0.02	0.21	23.20
49	Wang Thonglang	-0.01	-0.08	0.11	0.00	23.34
50	Yan Nawa	0.02	3.40	0.01	0.63	23.20
51	Bang Len	0.44	-0.25	0.05	0.29	23.55
52	Don Tum	0.41	-0.25	0.01	0.09	23.56
53	Kamphaeng Saen	0.64	-0.10	0.25	0.01	23.57
54	Mueang Nakhon Pathom	-0.09	-0.60	-0.03	0.25	23.56
55	Nakhon Chai Si	-0.42	-0.80	-0.04	0.59	23.52
56	Phutthamonthon	-0.30	-0.52	0.12	0.19	23.40
57	Sam Phran	-0.95	-1.27	0.10	0.47	23.44
58	Bang Bua Thong	0.31	0.07	0.17	0.02	23.45
59	Bang Kruai	-0.80	-0.22	0.11	0.03	23.14
60	Bang Yai	-0.15	0.03	0.35	0.00	23.31
61	Mueang Nonthaburi	-2.10	1.45	0.45	0.68	23.21
62	Pak Kret	-1.18	0.96	0.04	0.80	23.57
63	Sai Noi	0.45	-0.18	0.05	0.21	23.52
64	Bang Bo	0.49	-0.21	-0.23	0.06	23.56
65	Bang Phli	-0.06	-0.93	0.31	0.46	23.54

Table 6.16 (Continued).

No.	District	Intercept	Regression coefficient FRP	Residual	LocalR2	Predicted (µg/m³)
66	Bang Sao Thong	0.42	-0.32	0.03	0.18	23.57
67	Mueang Samut Prakan	-1.27	-3.09	0.24	0.67	23.47
68	Phra Pradaeng	-0.25	2.30	0.14	0.40	23.03
69	Phra Samut Chedi	-1.63	-3.06	-0.03	0.27	23.33
70	Ban Phaeo	-0.44	-0.80	0.02	0.44	23.47
71	Krathum Baen	-0.66	-0.93	0.20	0.12	23.39
72	Mueang Samut Sakhon	0.34	0.23	0.02	0.04	23.39

From Table 6.16, the maximum value is 24.04 µg/m^3 in Don Mueang District, Bangkok. In contrast, the minimum value is 22.82 µg/m^3 in Phaya Thai District, Bangkok. The classification maps of predicted values for PM2.5 concentration using the GWR model according to the Thailand Air Quality Index and the U.S. EPA Air Quality Index are displayed in Figure 6.31.

Thus, the predicted values of PM2.5 concentration are excellent at level 1 of Thailand AQI and moderate at level 2 of EPA AQI. However, the predicted value in an urban landscape in March 2020 from the GWR model is more than the one-day mean of WHO guidelines. See Table 5.3.

In addition, a spatial distribution map of PM2.5 concentration in March 2020 using the SCK interpolation technique is displayed in Figure 6.32. As a result, the high PM2.5 concentration occur in urban areas in the northern part of the study area, mainly in Bangkok Metropolitan.

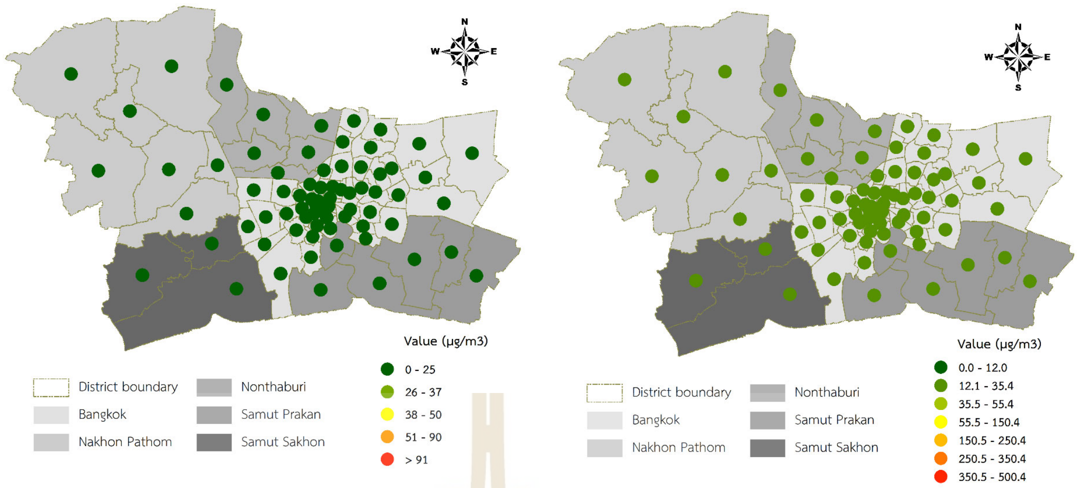

(a) (b)

Figure 6.31 The classification map of PM2.5 concentration prediction using the GWR model in March 2020 according to the (a) Thailand AQI and (b) EPA AQI.

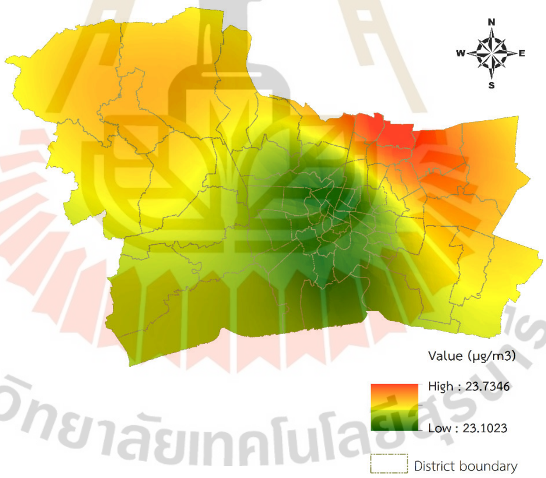

Figure 6.32 Spatial distribution of PM2.5 concentration in March 2020.

6.2.7 April 2020 in the summer season

The result of the GWR model for PM2.5 concentration prediction in April 2020 in the summer season is summarized in Table 6.17. The model performance shows that AICc, R-square, and adjusted R-square values are 162.63, 0.70, and 0.60, respectively.

Table 6.17 The predictive equations of PM2.5 concentration in April 2020.

No.	District	Intercept	Regression coefficient							Residual	Local	Predicted
			WS	VS	BT	FRP	AOD	FH	FD		R2	(μg/m^3)
1	Bang Bon	-0.41	0.08	0.11	0.01	-0.08	0.07	0.34	-0.12	0.60	0.13	21.71
2	Bang Kapi	-0.23	0.73	0.49	-0.23	-0.12	0.33	0.21	-0.09	0.62	0.64	22.31
3	Bang Khae	-0.39	0.08	0.15	-0.06	-0.20	0.05	0.34	-0.11	0.03	0.11	21.72
4	Bang Khen	-0.09	0.86	0.46	-0.19	-0.20	0.34	0.21	-0.10	1.05	0.67	22.25
5	Bang Kho Laem	-0.38	0.49	0.19	-0.20	0.15	0.15	0.21	-0.05	-0.68	0.37	21.71
6	Bang Khun Thian	-0.38	0.27	0.06	-0.02	0.14	0.10	0.28	-0.11	0.52	0.23	21.83
7	Bang Na	-0.39	0.55	0.35	-0.29	0.07	0.26	0.21	-0.05	-0.20	0.58	21.94
8	Bang Phlat	-0.19	0.75	0.31	-0.37	-0.13	0.29	0.23	-0.03	-0.84	0.47	21.69
9	Bang Rak	-0.35	0.57	0.26	-0.31	0.07	0.19	0.21	-0.03	0.96	0.42	21.64
10	Bang Sue	-0.15	0.84	0.39	-0.40	-0.19	0.35	0.23	-0.03	-0.04	0.58	21.75
11	Bangkok Noi	-0.23	0.63	0.24	-0.30	-0.07	0.23	0.23	-0.05	-0.37	0.37	21.80
12	Bangkok Yai	-0.31	0.53	0.20	-0.24	0.02	0.17	0.22	-0.05	0.63	0.32	21.73
13	Bueng Kum	-0.15	0.81	0.47	-0.13	-0.14	0.32	0.20	-0.11	0.65	0.66	22.21
14	Chatuchak	-0.16	0.86	0.42	-0.37	-0.18	0.36	0.22	-0.03	0.08	0.63	21.84
15	Chom Thong	-0.36	0.40	0.13	-0.12	0.12	0.13	0.23	-0.08	-0.59	0.27	21.69
16	Din Daeng	-0.22	0.76	0.39	-0.38	-0.13	0.32	0.23	-0.03	-0.90	0.58	21.83
17	Don Mueang	-0.03	0.88	0.45	-0.32	-0.32	0.37	0.24	-0.08	0.22	0.68	22.43
18	Dusit	-0.21	0.76	0.34	-0.39	-0.11	0.29	0.23	-0.03	-1.32	0.50	21.90
19	Huai Khwang	-0.24	0.74	0.42	-0.36	-0.12	0.32	0.22	-0.04	0.18	0.59	21.82
20	Khan Na Yao	-0.11	0.81	0.45	-0.06	-0.13	0.31	0.19	-0.15	-0.62	0.66	22.42
21	Khlong Sam Wa	-0.04	0.82	0.40	0.03	-0.13	0.28	0.18	-0.19	-0.32	0.67	22.46
22	Khlong San	-0.33	0.56	0.22	-0.26	0.07	0.18	0.21	-0.05	0.34	0.38	21.70

Table 6.17 (Continued).

No.	District	Intercept	Regression coefficient							Residual	Local	Predicted
			WS	VS	BT	FRP	AOD	FH	FD		R2	(µg/m³)
23	Khlong Toei	-0.31	0.63	0.35	-0.33	-0.01	0.25	0.21	-0.05	0.33	0.54	21.62
24	Lak Si	-0.09	0.90	0.43	-0.36	-0.25	0.38	0.23	-0.04	0.58	0.66	22.23
25	Lat Krabang	-0.12	0.69	0.38	-0.02	-0.09	0.30	0.19	-0.21	0.27	0.64	22.17
26	Lat Phrao	-0.16	0.85	0.45	-0.27	-0.17	0.35	0.21	-0.06	-0.14	0.66	22.26
27	Min Buri	-0.07	0.79	0.35	0.08	-0.05	0.28	0.17	-0.21	-0.40	0.66	22.37
28	Nong Chok	-0.01	0.81	0.31	0.15	-0.04	0.24	0.15	-0.25	0.59	0.67	22.17
29	Nong Khaem	-0.40	0.00	0.14	-0.02	-0.27	0.04	0.37	-0.12	0.26	0.13	21.73
30	Pathum Wan	-0.29	0.65	0.31	-0.35	-0.01	0.24	0.22	-0.03	0.73	0.48	21.61
31	Phasi Charoen	-0.31	0.41	0.17	-0.17	-0.02	0.13	0.25	-0.08	-0.02	0.24	21.74
32	Phaya Thai	-0.20	0.77	0.36	-0.37	-0.13	0.32	0.23	-0.04	-1.27	0.56	21.82
33	Phra Khanong	-0.37	0.58	0.41	-0.33	0.00	0.27	0.22	-0.05	-0.61	0.58	21.96
34	Phra Nakhon	-0.28	0.64	0.27	-0.33	-0.02	0.22	0.22	-0.03	-0.29	0.40	21.79
35	Pom Prap Sattru Phai	-0.29	0.64	0.28	-0.34	-0.01	0.22	0.22	-0.03	0.61	0.43	21.72
36	Prawet	-0.28	0.62	0.42	-0.24	-0.06	0.33	0.22	-0.11	-0.24	0.62	22.20
37	Rat Burana	-0.42	0.41	0.13	-0.12	0.22	0.12	0.21	-0.06	-1.53	0.33	21.72
38	Ratchathewi	-0.25	0.71	0.34	-0.37	-0.07	0.28	0.22	-0.03	-0.38	0.52	21.74
39	Sai Mai	-0.04	0.88	0.44	-0.12	-0.21	0.32	0.20	-0.12	0.67	0.69	22.36
40	Samphanthawong	-0.31	0.60	0.26	-0.31	0.03	0.20	0.21	-0.03	0.89	0.40	21.71
41	Saphan Sung	-0.18	0.72	0.44	-0.12	-0.11	0.33	0.20	-0.15	-0.58	0.64	22.28
42	Sathon	-0.36	0.55	0.25	-0.29	0.09	0.18	0.21	-0.03	0.49	0.43	21.63
43	Suan Luang	-0.33	0.64	0.48	-0.33	-0.07	0.31	0.22	-0.06	0.23	0.61	22.03
44	Taling Chan	-0.22	0.53	0.24	-0.27	-0.18	0.20	0.26	-0.07	-0.42	0.28	21.77
45	Thawi Watthana	-0.28	0.24	0.23	-0.19	-0.39	0.10	0.35	-0.10	-0.06	0.16	21.72
46	Thon Buri	-0.36	0.47	0.18	-0.20	0.10	0.14	0.21	-0.05	0.14	0.31	21.70
47	Thung Khru	-0.44	0.36	0.07	-0.05	0.27	0.12	0.22	-0.07	-0.89	0.31	21.80
48	Vadhana	-0.29	0.67	0.39	-0.33	-0.05	0.28	0.21	-0.05	0.05	0.57	21.74
49	Wang Thonglang	-0.24	0.77	0.48	-0.33	-0.13	0.34	0.22	-0.04	0.60	0.63	22.02
50	Yan Nawa	-0.40	0.50	0.22	-0.24	0.15	0.17	0.21	-0.04	-0.59	0.43	21.68

Table 6.17 (Continued).

No.	District	Intercept	Regression coefficient							Residual	Local R2	Predicted (μg/m³)
			WS	VS	BT	FRP	AOD	FH	FD			
51	Bang Len	0.00	0.71	0.33	-0.30	-0.71	0.34	0.40	-0.06	0.00	0.52	21.96
52	Don Tum	-0.19	0.42	0.19	-0.19	-0.51	0.18	0.36	-0.07	-0.06	0.43	21.96
53	Kamphaeng Saen	-0.14	0.47	0.21	-0.21	-0.53	0.20	0.37	-0.08	-0.07	0.47	22.04
54	Mueang Nakhon Pathom	-0.35	0.16	0.09	-0.07	-0.34	0.07	0.32	-0.09	-0.02	0.40	21.93
55	Nakhon Chai Si	-0.35	0.18	0.10	-0.09	-0.37	0.08	0.33	-0.08	0.21	0.33	21.86
56	Phutthamonthon	-0.31	0.27	0.16	-0.17	-0.47	0.11	0.35	-0.06	0.17	0.25	21.80
57	Sam Phran	-0.47	-0.01	0.04	0.03	-0.29	0.04	0.34	-0.09	0.20	0.26	21.81
58	Bang Bua Thong	0.09	0.76	0.54	-0.39	-0.75	0.39	0.37	-0.12	0.01	0.54	21.88
59	Bang Kruai	-0.09	0.64	0.34	-0.34	-0.38	0.28	0.30	-0.09	-0.37	0.37	21.76
60	Bang Yai	-0.06	0.58	0.39	-0.32	-0.61	0.28	0.36	-0.10	0.29	0.35	21.77
61	Mueang Nonthaburi	-0.05	0.84	0.42	-0.42	-0.36	0.37	0.27	-0.05	-0.31	0.57	21.87
62	Pak Kret	0.00	0.85	0.46	-0.43	-0.42	0.39	0.27	-0.07	-0.20	0.64	22.01
63	Sai Noi	0.07	0.77	0.43	-0.35	-0.76	0.39	0.39	-0.08	0.34	0.55	21.85
64	Bang Bo	-0.19	0.55	0.37	-0.13	-0.07	0.32	0.21	-0.22	0.14	0.62	21.98
65	Bang Phli	-0.30	0.55	0.37	-0.21	-0.01	0.33	0.22	-0.13	-0.07	0.62	22.25
66	Bang Sao Thong	-0.20	0.59	0.39	-0.14	-0.08	0.32	0.21	-0.19	-0.48	0.62	22.30
67	Mueang Samut Prakan	-0.42	0.48	0.21	-0.20	0.20	0.23	0.20	-0.07	0.31	0.59	22.03
68	Phra Pradaeng	-0.42	0.46	0.18	-0.19	0.21	0.16	0.21	-0.05	-0.96	0.45	21.82
69	Phra Samut Chedi	-0.42	0.38	0.04	-0.04	0.30	0.12	0.24	-0.09	-0.25	0.37	21.94
70	Ban Phaeo	-0.48	-0.07	0.03	0.10	-0.24	0.06	0.37	-0.11	0.14	0.30	21.86
71	Krathum Baen	-0.48	-0.10	0.06	0.09	-0.28	0.05	0.40	-0.11	0.33	0.20	21.78
72	Mueang Samut Sakhon	-0.37	0.05	0.10	0.03	-0.15	0.08	0.41	-0.14	0.00	0.16	21.86

From Table 6.17, the maximum value is 22.46 µg/m^3 in Khlong Sam Wa District, Bangkok. In contrast, the minimum value is 21.61 µg/m^3 in Pathum Wan District, Bangkok. The classification maps of predicted values for PM2.5 concentration using the GWR model according to the Thailand Air Quality Index and the U.S. EPA Air Quality Index are displayed in Figure 6.33.

As a result, the predicted values of PM2.5 concentration are excellent at level 1 of Thailand AQI and moderate at level 2 of EPA AQI. On the contrary, the predicted value in an urban landscape in April 2020 from the GWR model is more than the one-day mean of WHO guidelines. See Table 5.3.

In addition, a spatial distribution map of PM2.5 concentration in April 2020 using the SCK interpolation technique is displayed in Figure 6.34. As a result, the high PM2.5 concentration occur in urban areas in the northern part of the study area, mainly in Bangkok Metropolitan.

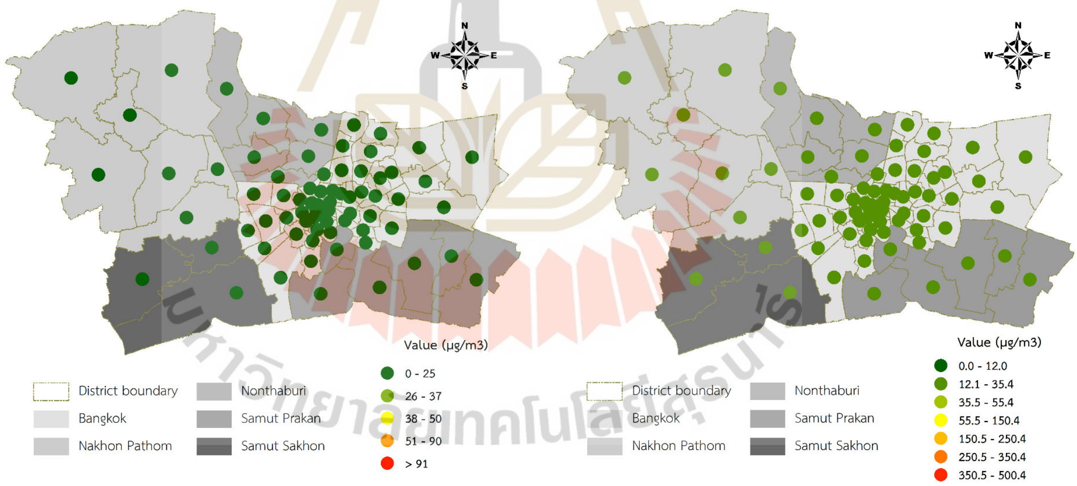

(a) (b)

Figure 6.33 The classification map of PM2.5 concentration prediction using the GWR model in April 2020 according to the (a) Thailand AQI and (b) EPA AQI.

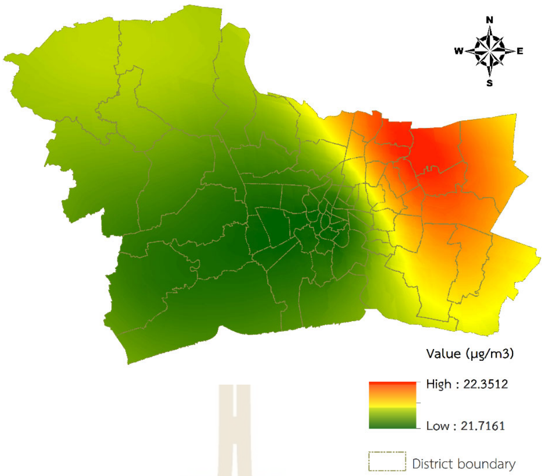

Figure 6.34 Spatial distribution of PM2.5 concentration in April 2020.

6.2.8 May 2020 in the summer season

The result of the GWR model for PM2.5 concentration prediction in May 2020 in the summer season is summarized in Table 6.18. The model performance shows that AICc, R-square, and adjusted R-square values are 90.38, 0.93, and 0.88, respectively.

Table 6.18 The predictive equations of PM2.5 concentration in May 2020.

No.	District	Intercept	Regression coefficient					Residual	Local	Predicted
			WS	VIS	BT	FD	ELEV		R2	(µg/m^3)
1	Bang Bon	-0.63	0.19	-0.05	0.32	-0.33	0.42	0.17	0.61	16.69
2	Bang Kapi	0.68	1.29	1.04	1.23	-0.35	0.15	0.06	0.86	16.77
3	Bang Khae	-0.19	0.14	-0.42	0.08	-0.40	0.25	-0.09	0.67	16.73
4	Bang Khen	0.96	1.52	0.98	0.21	-0.21	0.18	0.29	0.82	16.83
5	Bang Kho Laem	-0.56	0.36	-0.16	0.66	-0.35	0.40	-0.04	0.49	16.69
6	Bang Khun Thian	-1.00	0.28	0.13	0.38	-0.23	0.50	-0.06	0.59	16.71
7	Bang Na	-0.48	0.37	-0.11	0.25	-0.45	0.40	-0.49	0.46	16.71
8	Bang Phlat	0.52	0.77	0.05	-0.93	-0.39	0.15	0.38	0.47	16.77
9	Bang Rak	-0.24	0.55	0.15	1.08	-0.42	0.30	-0.61	0.49	16.75
10	Bang Sue	1.04	1.09	0.30	-1.22	-0.25	-0.04	0.52	0.65	16.78
11	Bangkok Noi	0.12	0.53	-0.18	-0.28	-0.41	0.24	-0.16	0.45	16.77
12	Bangkok Yai	-0.15	0.49	-0.29	0.01	-0.41	0.34	0.19	0.48	16.73
13	Bueng Kum	0.84	1.61	1.07	0.37	-0.28	0.36	0.10	0.81	16.80

Table 6.18 (Continued).

No.	District	Intercept	Regression coefficient					Residual	Local	Predicted
			WS	VIS	BT	FD	ELEV		R2	(μg/m^3)
14	Chatuchak	0.91	1.22	0.61	0.71	-0.16	-0.08	0.08	0.82	16.81
15	Chom Thong	-0.62	0.50	-0.35	0.33	-0.30	0.47	-0.14	0.58	16.70
16	Din Daeng	0.15	1.05	0.72	4.32	-0.32	-0.01	0.44	0.73	16.77
17	Don Mueang	1.01	1.18	0.55	0.27	-0.18	0.03	-0.05	0.77	16.85
18	Dusit	1.69	0.94	0.24	-7.74	-0.41	0.10	0.04	0.56	16.78
19	Huai Khwang	0.59	1.10	0.88	1.58	-0.30	-0.01	0.08	0.76	16.77
20	Khan Na Yao	0.84	1.69	1.09	0.22	-0.34	0.52	-0.03	0.82	16.80
21	Khlong Sam Wa	0.53	1.14	0.46	0.08	-0.93	0.92	0.09	0.77	16.80
22	Khlong San	-0.51	0.44	-0.02	1.79	-0.38	0.33	0.06	0.48	16.71
23	Khlong Toei	-0.07	0.63	0.37	0.84	-0.47	0.26	0.27	0.56	16.71
24	Lak Si	1.02	1.12	0.37	0.19	-0.12	-0.04	0.42	0.80	16.83
25	Lat Krabang	-0.19	0.46	-0.24	0.07	-1.71	1.44	-0.05	0.59	16.76
26	Lat Phrao	0.88	1.46	0.94	0.66	-0.15	0.11	0.22	0.84	16.80
27	Min Buri	0.18	0.80	0.30	0.20	-1.60	1.05	0.16	0.64	16.77
28	Nong Chok	-0.08	0.60	-0.28	0.04	-1.86	1.73	0.11	0.71	16.77
29	Nong Khaem	-0.19	-0.21	-0.23	0.07	-0.42	0.18	-0.16	0.70	16.73
30	Pathum Wan	0.00	0.71	0.32	1.22	-0.44	0.23	-0.69	0.53	16.77
31	Phasi Charoen	-0.29	0.49	-0.48	0.17	-0.38	0.39	-0.20	0.57	16.74
32	Phaya Thai	0.25	1.05	0.59	3.42	-0.32	0.00	0.24	0.67	16.78
33	Phra Khanong	-0.12	0.61	0.23	0.66	-0.53	0.33	-0.53	0.57	16.73
34	Phra Nakhon	0.58	0.69	0.09	-2.80	-0.43	0.23	-0.51	0.49	16.78
35	Pom Prap Sattru Phai	-0.02	0.67	0.27	1.09	-0.42	0.22	0.87	0.49	16.72
36	Prawet	0.02	0.75	0.34	0.37	-0.76	0.50	-0.44	0.57	16.74
37	Rat Burana	-0.75	0.32	-0.21	0.48	-0.28	0.44	-0.31	0.54	16.69
38	Ratchathewi	-0.07	0.86	0.47	3.55	-0.41	0.12	0.09	0.58	16.76
39	Sai Mai	0.96	1.47	0.93	0.17	-0.27	0.28	-0.02	0.81	16.84
40	Samphanthawong	-0.24	0.57	0.09	1.57	-0.42	0.27	-0.14	0.48	16.74
41	Saphan Sung	0.62	1.37	1.03	0.53	-0.78	0.47	-0.09	0.74	16.77
42	Sathon	-0.33	0.47	0.03	0.79	-0.41	0.34	-0.02	0.48	16.71
43	Suan Luang	0.32	0.97	0.66	1.02	-0.55	0.25	-0.10	0.72	16.74
44	Taling Chan	0.08	0.28	-0.54	-0.06	-0.41	0.21	-0.35	0.49	16.78
45	Thawi Watthana	0.09	-0.11	-0.48	-0.05	-0.41	0.12	0.03	0.68	16.76
46	Thon Buri	-0.41	0.44	-0.25	0.53	-0.37	0.38	-0.27	0.50	16.72
47	Thung Khru	-1.00	0.29	-0.05	0.24	-0.19	0.44	-0.34	0.60	16.70
48	Vadhana	0.22	0.86	0.56	1.02	-0.48	0.20	0.07	0.63	16.74

Table 6.18 (Continued).

No.	District	Intercept	Regression coefficient					Residual	Local	Predicted
			WS	VIS	BT	FD	ELEV		R2	(μg/m³)
49	Wang Thonglang	0.68	1.25	0.99	1.37	-0.29	0.05	-0.12	0.82	16.79
50	Yan Nawa	-0.58	0.30	-0.08	0.56	-0.35	0.38	-0.23	0.49	16.70
51	Bang Len	0.40	0.14	-0.31	-0.12	-0.31	0.15	-0.10	0.46	16.77
52	Don Tum	0.03	0.04	-0.22	-0.04	-0.50	0.10	-0.04	0.61	16.76
53	Kamphaeng Saen	0.01	0.04	-0.20	-0.03	-0.50	0.07	-0.14	0.58	16.77
54	Mueang Nakhon Pathom	-0.19	-0.05	-0.17	0.05	-0.50	0.07	0.19	0.79	16.75
55	Nakhon Chai Si	-0.04	-0.03	-0.23	-0.01	-0.53	0.24	0.06	0.82	16.75
56	Phutthamonthon	0.10	-0.11	-0.35	-0.07	-0.46	0.28	-0.04	0.75	16.76
57	Sam Phran	-0.12	-0.16	-0.20	0.06	-0.45	0.25	0.09	0.87	16.74
58	Bang Bua Thong	0.51	0.45	-0.92	-0.10	-0.20	0.22	-0.09	0.63	16.78
59	Bang Kruai	0.26	0.16	-0.63	-0.13	-0.35	0.12	0.00	0.42	16.78
60	Bang Yai	0.28	0.12	-0.70	-0.10	-0.33	0.18	-0.05	0.52	16.77
61	Mueang Nonthaburi	0.89	0.87	-0.15	-0.71	-0.21	-0.03	-0.23	0.58	16.81
62	Pak Kret	0.94	0.85	-0.21	-0.18	-0.12	-0.02	0.20	0.76	16.80
63	Sai Noi	0.56	0.20	-0.53	-0.16	-0.31	0.35	0.06	0.58	16.77
64	Bang Bo	-0.46	0.16	-0.39	0.01	-0.99	0.93	-0.13	0.54	16.73
65	Bang Phli	-0.56	0.20	-0.26	0.08	-0.63	0.57	0.09	0.48	16.71
66	Bang Sao Thong	-0.42	0.22	-0.35	0.03	-1.10	1.01	-0.60	0.53	16.75
67	Mueang Samut Prakan	-0.85	0.14	-0.25	0.04	-0.35	0.34	0.07	0.49	16.70
68	Phra Pradaeng	-0.78	0.19	-0.18	0.24	-0.29	0.40	-0.43	0.51	16.70
69	Phra Samut Chedi	-1.05	0.20	0.10	0.03	-0.20	0.41	0.16	0.52	16.70
70	Ban Phaeo	-0.29	-0.17	-0.11	0.17	-0.41	0.29	0.04	0.86	16.74
71	Krathum Baen	-0.22	-0.27	-0.14	0.10	-0.42	0.27	0.01	0.82	16.73
72	Mueang Samut Sakhon	-0.75	-0.01	0.10	0.38	-0.31	0.41	-0.07	0.65	16.73

From Table 6.18, the maximum value is 16.85 μg/m^3 in Don Mueang District, Bangkok. In contrast, the minimum value is 16.69 μg/m^3 in Bang Bon District, Bangkok. The classification maps of predicted values for PM2.5 concentration using the GWR model according to the Thailand Air Quality Index and the U.S. EPA Air Quality Index are displayed in Figure 6.35.

Thus, the predicted values of PM2.5 concentration are excellent at level 1 of Thailand AQI and moderate at level 2 of EPA AQI. In contrast, the predicted value in an urban landscape in May 2020 from the GWR model is more than the one-day mean of WHO guidelines. See Table 5.3.

In addition, a spatial distribution map of PM2.5 concentration in May 2020 using the SCK interpolation technique is displayed in Figure 6.36. As a result, the high PM2.5 concentration occur in urban areas in the northern part of the study area, mainly in Bangkok Metropolitan.

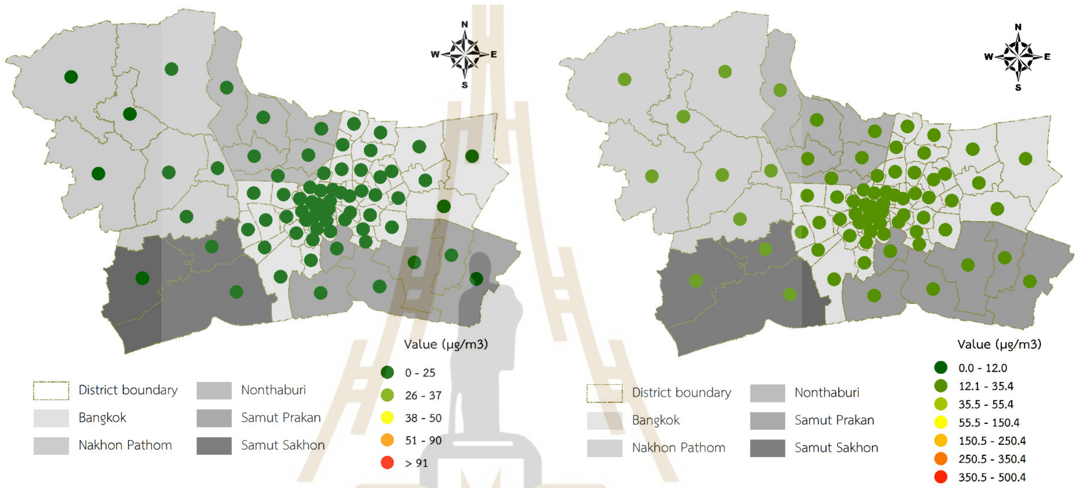

(a) (b)

Figure 6.35 The classification map of PM2.5 concentration prediction using the GWR model in May 2020 according to the (a) Thailand AQI and (b) EPA AQI.

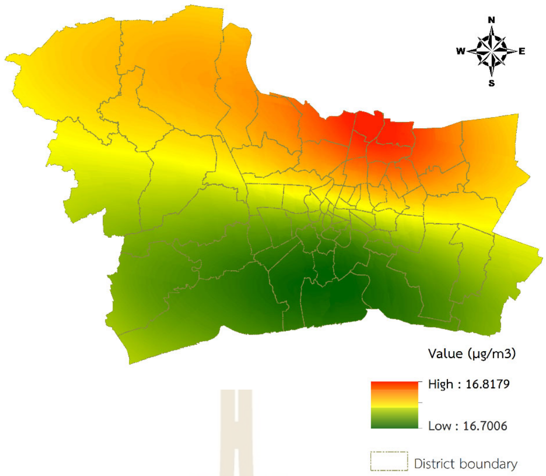

Figure 6.36 Spatial distribution of PM10 concentration in May 2020.

6.2.9 Winter season

The result of the GWR model for PM2.5 concentration prediction in the winter season (October to February) is summarized in Table 6.19. The model performance shows that AICc, R-square, and adjusted R-square values are 79.58, 0.91, and 0.88, respectively.

Table 6.19 The predictive equations of PM2.5 concentration in the winter season.

No.	District	Intercept	Regression coefficient										Residual	Local R2	Predicted ($\mu g/m^3$)
			RH	TEMP	WS	P	VIS	BT	FRP	FH	AOD	ELEV			
1	Bang Bon	0.49	0.28	-0.47	0.33	-0.31	-0.71	-0.63	-0.74	-0.11	0.00	0.22	-0.14	0.77	38.23
2	Bang Kapi	-0.09	1.20	2.42	0.08	1.94	-0.16	-0.05	-0.58	-0.03	-0.07	0.29	-0.19	0.74	37.46
3	Bang Khae	0.45	0.48	-0.21	0.34	-0.18	-0.74	-0.63	-0.71	-0.12	-0.06	0.21	0.26	0.76	38.10
4	Bang Khen	-0.08	1.48	2.82	0.18	2.18	-0.28	-0.08	-0.51	-0.04	-0.08	0.26	-0.07	0.79	37.77
5	Bang Kho Laem	0.32	0.56	0.66	0.04	0.57	-0.54	-0.34	-0.93	-0.15	-0.07	0.17	0.06	0.75	37.93
6	Bang Khun Thian	0.43	0.25	-0.21	0.18	-0.04	-0.54	-0.52	-0.86	-0.15	0.01	0.21	-0.08	0.76	38.03
7	Bang Na	-0.02	0.88	1.78	0.04	1.52	-0.06	-0.04	-0.68	-0.04	-0.04	0.31	0.09	0.71	37.32
8	Bang Phlat	0.27	0.91	0.82	0.20	0.59	-0.60	-0.50	-0.71	-0.16	-0.12	0.18	0.58	0.76	37.90
9	Bang Rak	0.29	0.66	0.86	0.05	0.69	-0.57	-0.34	-0.89	-0.15	-0.09	0.17	-0.46	0.75	38.09
10	Bang Sue	0.18	1.13	1.33	0.20	1.00	-0.52	-0.42	-0.64	-0.14	-0.14	0.20	0.03	0.76	37.98

Table 6.19 (Continued).

No.	District	Intercept	Regression coefficient										Residual	Local R2	Predicted (µg/m^3)
			RH	TEMP	WS	P	VIS	BT	FRP	FH	AOD	ELEV			
11	Bangkok Noi	0.33	0.74	0.45	0.22	0.30	-0.67	-0.54	-0.75	-0.16	-0.10	0.18	0.12	0.77	38.15
12	Bangkok Yai	0.33	0.67	0.47	0.17	0.35	-0.63	-0.50	-0.80	-0.16	-0.09	0.18	-0.06	0.76	38.17
13	Bueng Kum	-0.11	1.30	2.63	0.10	2.08	-0.19	-0.05	-0.54	-0.03	-0.07	0.29	-0.30	0.76	37.59
14	Chatuchak	0.07	1.24	2.03	0.20	1.47	-0.49	-0.27	-0.63	-0.10	-0.11	0.20	0.05	0.79	37.84
15	Chom Thong	0.35	0.56	0.32	0.14	0.29	-0.58	-0.48	-0.84	-0.16	-0.07	0.18	0.46	0.75	37.91
16	Din Daeng	0.10	1.06	1.79	0.10	1.36	-0.43	-0.24	-0.72	-0.10	-0.10	0.21	-0.19	0.75	37.74
17	Don Mueang	0.03	1.66	2.73	0.32	2.03	-0.41	-0.19	-0.47	-0.07	-0.10	0.22	-0.10	0.85	37.98
18	Dusit	0.22	0.95	1.07	0.16	0.81	-0.54	-0.43	-0.72	-0.15	-0.12	0.19	0.34	0.75	37.90
19	Huai Khwang	0.02	1.12	2.10	0.08	1.65	-0.30	-0.14	-0.69	-0.07	-0.10	0.24	-0.27	0.73	37.64
20	Khan Na Yao	-0.13	1.32	2.70	0.11	2.14	-0.17	-0.03	-0.51	-0.02	-0.06	0.30	-0.25	0.77	37.53
21	Khlong Sam Wa	-0.17	1.39	2.88	0.13	2.28	-0.17	-0.01	-0.45	-0.01	-0.05	0.31	0.01	0.80	37.38
22	Khlong San	0.31	0.66	0.68	0.09	0.55	-0.58	-0.40	-0.86	-0.16	-0.09	0.17	0.30	0.75	38.01
23	Khlong Toei	0.07	0.91	1.77	0.02	1.45	-0.24	-0.11	-0.78	-0.08	-0.08	0.24	-0.42	0.71	37.72
24	Lak Si	0.07	1.48	2.26	0.27	1.67	-0.45	-0.28	-0.52	-0.09	-0.12	0.22	0.10	0.81	37.96
25	Lat Krabang	-0.16	1.15	2.34	0.09	1.93	-0.07	-0.03	-0.45	0.00	-0.03	0.34	0.35	0.78	36.96
26	Lat Phrao	-0.05	1.35	2.56	0.14	1.97	-0.29	-0.11	-0.57	-0.05	-0.09	0.25	-0.23	0.76	37.75
27	Min Buri	-0.16	1.25	2.59	0.09	2.09	-0.12	-0.02	-0.46	0.00	-0.04	0.32	-0.10	0.78	37.26
28	Nong Chok	-0.20	1.28	2.71	0.10	2.17	-0.12	-0.01	-0.41	0.00	-0.03	0.33	-0.18	0.80	37.12
29	Nong Khaem	0.45	0.51	-0.19	0.41	-0.14	-0.72	-0.60	-0.61	-0.10	-0.06	0.26	0.38	0.72	38.09
30	Pathum Wan	0.25	0.74	1.06	0.06	0.82	-0.56	-0.32	-0.87	-0.14	-0.09	0.17	-0.26	0.75	37.93
31	Phasi Charoen	0.36	0.63	0.19	0.23	0.14	-0.65	-0.58	-0.76	-0.16	-0.09	0.19	0.26	0.76	38.07
32	Phaya Thai	0.17	0.99	1.45	0.14	1.07	-0.53	-0.33	-0.74	-0.12	-0.11	0.19	-0.16	0.76	37.88
33	Phra Khanong	-0.02	0.95	1.93	0.04	1.61	-0.10	-0.05	-0.68	-0.04	-0.06	0.30	0.03	0.71	37.34
34	Phra Nakhon	0.27	0.81	0.78	0.15	0.59	-0.57	-0.46	-0.77	-0.16	-0.11	0.18	0.46	0.75	37.96
35	Pom Prap Sattru Phai	0.27	0.80	0.87	0.12	0.67	-0.56	-0.42	-0.80	-0.15	-0.11	0.18	0.21	0.75	37.97

Table 6.19 (Continued).

No.	District	Intercept	Regression coefficient										Residual	Local R2	Predicted (μg/m^3)
			RH	TEMP	WS	P	VIS	BT	FRP	FH	AOD	ELEV			
36	Prawet	-0.10	1.04	2.09	0.07	1.74	-0.06	-0.04	-0.56	-0.02	-0.04	0.33	0.34	0.74	37.10
37	Rat Burana	0.34	0.48	0.53	0.03	0.49	-0.51	-0.34	-0.95	-0.16	-0.06	0.17	0.12	0.74	37.81
38	Ratchathewi	0.22	0.84	1.21	0.09	0.92	-0.55	-0.32	-0.82	-0.13	-0.10	0.18	-0.30	0.76	37.91
39	Sai Mai	-0.09	1.58	3.00	0.20	2.33	-0.26	-0.06	-0.46	-0.03	-0.08	0.27	0.07	0.81	37.68
40	Samphanthawong	0.28	0.74	0.79	0.11	0.62	-0.57	-0.41	-0.82	-0.15	-0.10	0.17	0.01	0.75	38.02
41	Saphan Sung	-0.13	1.19	2.43	0.08	1.97	-0.11	-0.03	-0.52	-0.01	-0.05	0.32	0.40	0.76	37.15
42	Sathon	0.28	0.64	0.92	0.03	0.75	-0.52	-0.30	-0.91	-0.14	-0.08	0.17	-0.38	0.74	38.01
43	Suan Luang	-0.06	1.07	2.16	0.05	1.77	-0.12	-0.05	-0.63	-0.03	-0.06	0.30	0.05	0.73	37.33
44	Taling Chan	0.38	0.72	0.24	0.30	0.10	-0.74	-0.60	-0.71	-0.14	-0.11	0.18	-0.18	0.77	38.29
45	Thawi Watthana	0.39	0.89	0.34	0.40	0.16	-0.72	-0.59	-0.59	-0.12	-0.18	0.22	0.12	0.72	38.13
46	Thon Buri	0.33	0.62	0.52	0.12	0.42	-0.59	-0.45	-0.85	-0.16	-0.08	0.17	0.33	0.75	38.03
47	Thung Khru	0.27	0.47	0.77	-0.02	0.76	-0.30	-0.20	-0.96	-0.14	-0.05	0.21	0.09	0.71	37.76
48	Vadhana	0.03	1.01	1.97	0.04	1.59	-0.22	-0.10	-0.73	-0.07	-0.08	0.25	-0.51	0.71	37.71
49	Wang Thonglang	-0.05	1.21	2.37	0.09	1.87	-0.23	-0.08	-0.62	-0.05	-0.09	0.27	-0.48	0.74	37.63
50	Yan Nawa	0.20	0.69	1.23	-0.01	1.05	-0.33	-0.18	-0.91	-0.12	-0.08	0.21	0.28	0.71	37.62
51	Bang Len	0.28	1.70	1.62	0.30	1.14	-0.54	-0.47	-0.47	-0.15	-0.39	0.15	-0.03	0.74	37.90
52	Don Tum	0.32	1.61	1.48	0.26	1.05	-0.51	-0.39	-0.44	-0.16	-0.45	0.16	-0.08	0.65	38.01
53	Kamphaeng Saen	0.32	1.62	1.50	0.25	1.06	-0.50	-0.39	-0.43	-0.16	-0.46	0.15	-0.14	0.67	37.90
54	Mueang Nakhon Pathom	0.32	1.46	1.33	0.26	1.00	-0.48	-0.31	-0.42	-0.15	-0.46	0.24	0.07	0.57	38.13
55	Nakhon Chai Si	0.32	1.45	1.27	0.30	0.93	-0.54	-0.36	-0.43	-0.15	-0.42	0.23	0.27	0.60	38.03
56	Phutthamonthon	0.33	1.36	1.07	0.35	0.74	-0.63	-0.46	-0.45	-0.15	-0.34	0.22	-0.03	0.66	38.15
57	Sam Phran	0.34	1.15	0.84	0.36	0.66	-0.57	-0.36	-0.42	-0.13	-0.32	0.31	0.21	0.58	38.18
58	Bang Bua Thong	0.30	1.59	1.44	0.36	1.02	-0.62	-0.52	-0.45	-0.15	-0.25	0.17	0.15	0.82	38.00
59	Bang Kruai	0.35	0.98	0.58	0.35	0.32	-0.73	-0.58	-0.63	-0.13	-0.17	0.18	0.41	0.77	38.06
60	Bang Yai	0.31	1.32	1.00	0.37	0.65	-0.68	-0.54	-0.50	-0.14	-0.26	0.21	0.46	0.75	38.03
61	Mueang Nonthaburi	0.26	1.19	1.15	0.32	0.76	-0.68	-0.49	-0.58	-0.13	-0.15	0.18	0.20	0.81	38.07

Table 6.19 (Continued).

No.	District	Inter cept	RH	TEMP	WS	P	VIS	BT	FRP	FH	AOD	ELEV	Resi-dual	Local R2	Predicted (µg/m^3)
			Regression coefficient												
62	Pak Kret	0.18	1.58	1.99	0.37	1.42	-0.56	-0.36	-0.48	-0.10	-0.14	0.19	-0.02	0.86	38.06
63	Sai Noi	0.29	1.68	1.59	0.33	1.13	-0.57	-0.49	-0.46	-0.15	-0.32	0.16	-0.14	0.79	37.99
64	Bang Bo	-0.15	0.93	1.78	0.10	1.55	0.04	-0.06	-0.44	0.00	0.02	0.38	-0.44	0.77	36.84
65	Bang Phli	-0.11	0.90	1.77	0.08	1.53	0.03	-0.05	-0.53	-0.01	0.00	0.36	-0.01	0.75	37.05
66	Bang Sao Thong	-0.15	0.98	1.92	0.09	1.65	0.01	-0.05	-0.46	0.00	0.00	0.36	0.01	0.77	36.91
67	Mueang Samut Prakan	-0.03	0.67	1.34	0.06	1.23	0.07	-0.04	-0.66	-0.03	0.02	0.35	-0.72	0.73	37.43
68	Phra Pradaeng	0.12	0.69	1.40	-0.03	1.25	-0.15	-0.07	-0.87	-0.09	-0.06	0.26	-0.19	0.70	37.62
69	Phra Samut Chedi	0.22	0.27	0.70	-0.04	0.79	-0.05	-0.04	-1.00	-0.12	0.02	0.27	-1.06	0.71	37.89
70	Ban Phaeo	0.32	1.05	0.86	0.36	0.76	-0.47	-0.29	-0.43	-0.12	-0.30	0.37	0.26	0.55	38.22
71	Krathum Baen	0.43	0.62	-0.01	0.47	0.05	-0.67	-0.49	-0.44	-0.10	-0.10	0.34	0.32	0.65	38.16
72	Mueang Samut Sakhon	0.50	0.18	-0.54	0.43	-0.28	-0.64	-0.60	-0.63	-0.08	0.05	0.30	-0.05	0.74	38.24

From Table 6.19, the maximum value is 38.29 µg/m^3 in Taling Chan District, Bangkok. In contrast, the minimum value is 36.84 µg/m^3 in Bang Bo District, Samut Prakan province. The classification maps of predicted values for PM2.5 concentration using the GWR model according to the Thailand Air Quality Index and the U.S. EPA Air Quality Index are displayed in Figure 6.37.

Thus, the predicted values of PM2.5 concentration are moderate at level 3 of Thailand AQI and unhealthy for sensitive groups at level 3 of EPA AQI. However, the predicted value in an urban landscape in the winter season from the GWR model is more than the one-day mean of WHO guidelines. See Table 5.3.

In addition, a spatial distribution map of PM2.5 concentration in the winter season using the SCK interpolation technique is displayed in Figure 6.38. As a result, the high PM2.5 concentration occur in urban areas in the western part of the study area, particularly in Nakhon Pathom and Samut Sakhon province.

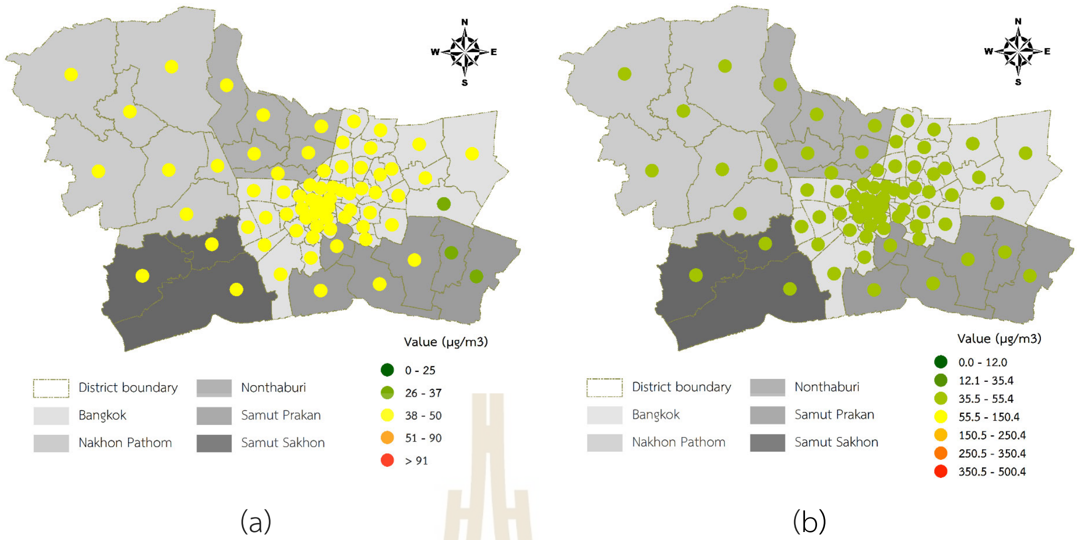

Figure 6.37 The classification map of PM2.5 concentration prediction using the GWR model winter season according to the (a) Thailand AQI and (b) EPA AQI.

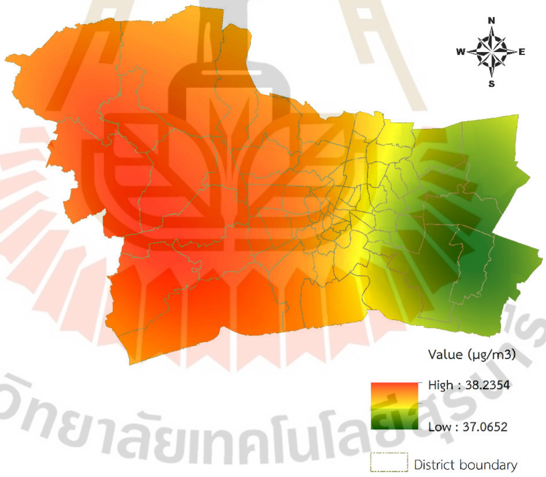

Figure 6.38 Spatial distribution of PM2.5 concentration in the winter season.

6.2.10 Summer season

The result of the GWR model for PM2.5 concentration prediction in the summer season (March to May) is summarized in Table 6.20. The model performance shows that AICc, R-square, and adjusted R-square values are 181.86, 0.65, and 0.51, respectively.

Table 6.20 The predictive equations of PM2.5 concentration in the summer season.

No.	District	Intercept	Regression coefficient								Residual	Local R2	Predicted (μg/m³)
			VIS	WS	BT	FRP	FH	AOD	FD	ELEV			
1	Bang Bon	-0.48	0.28	0.23	0.21	0.03	0.27	-0.22	-0.12	0.16	0.43	0.18	20.58
2	Bang Kapi	-0.40	0.29	1.05	0.13	0.29	0.19	0.15	-0.06	0.32	0.87	0.55	20.82
3	Bang Khae	-0.62	0.13	0.07	0.36	0.32	0.10	-0.23	-0.07	0.10	-0.16	0.17	20.58
4	Bang Khen	-0.19	0.00	0.91	0.21	0.33	0.15	0.23	-0.06	0.09	0.77	0.59	20.93
5	Bang Kho Laem	-0.57	0.36	0.63	0.08	0.29	0.26	-0.09	-0.06	0.29	-0.18	0.29	20.49
6	Bang Khun Thian	-0.41	0.43	0.39	0.10	-0.19	0.45	-0.23	-0.14	0.26	0.46	0.23	20.64
7	Bang Na	-0.49	0.36	0.86	0.01	0.25	0.27	0.03	-0.09	0.35	-0.13	0.44	20.64
8	Bang Phlat	-0.69	-0.07	0.37	0.29	0.88	0.01	0.02	0.02	0.07	-1.35	0.38	20.58
9	Bang Rak	-0.66	0.29	0.66	0.10	0.47	0.18	-0.03	-0.02	0.28	0.69	0.33	20.59
10	Bang Sue	-0.57	-0.02	0.56	0.17	0.73	0.05	0.13	0.00	0.07	-0.67	0.46	20.66
11	Bangkok Noi	-0.69	-0.03	0.30	0.34	0.82	0.02	-0.05	0.00	0.09	-0.26	0.30	20.54
12	Bangkok Yai	-0.62	0.11	0.41	0.25	0.60	0.11	-0.07	-0.03	0.15	0.76	0.27	20.52
13	Bueng Kum	-0.27	0.16	1.03	0.21	0.28	0.17	0.19	-0.06	0.23	0.47	0.59	20.87
14	Chatuchak	-0.46	0.07	0.78	0.08	0.53	0.10	0.18	-0.03	0.13	-0.59	0.52	20.74
15	Chom Thong	-0.51	0.30	0.44	0.17	0.23	0.26	-0.16	-0.09	0.21	-0.59	0.21	20.53
16	Din Daeng	-0.55	0.18	0.82	0.03	0.51	0.14	0.13	-0.03	0.23	-1.26	0.47	20.63
17	Don Mueang	-0.12	-0.15	0.69	0.13	0.37	0.15	0.29	-0.06	-0.08	0.01	0.55	21.10
18	Dusit	-0.62	0.04	0.57	0.15	0.70	0.08	0.07	0.00	0.13	-1.41	0.41	20.61
19	Huai Khwang	-0.55	0.25	0.91	0.03	0.45	0.16	0.13	-0.03	0.28	0.03	0.50	20.59
20	Khan Na Yao	-0.20	0.12	1.00	0.24	0.26	0.16	0.19	-0.09	0.19	-0.48	0.59	20.94
21	Khlong Sam Wa	-0.09	0.07	0.94	0.26	0.24	0.14	0.16	-0.14	0.12	0.29	0.60	20.90
22	Khlong San	-0.62	0.23	0.56	0.15	0.47	0.18	-0.06	-0.04	0.23	0.56	0.29	20.52
23	Khlong Toei	-0.59	0.36	0.88	0.00	0.38	0.21	0.05	-0.05	0.34	0.97	0.44	20.37
24	Lak Si	-0.29	-0.06	0.70	0.10	0.48	0.11	0.25	-0.03	-0.01	0.74	0.54	20.89
25	Lat Krabang	-0.14	0.12	0.91	0.18	0.22	0.15	0.09	-0.20	0.20	0.29	0.55	20.81
26	Lat Phrao	-0.35	0.11	0.93	0.13	0.38	0.15	0.20	-0.05	0.18	-0.64	0.55	20.94
27	Min Buri	-0.15	0.13	0.97	0.22	0.22	0.15	0.13	-0.16	0.19	0.02	0.58	20.86
28	Nong Chok	-0.07	0.11	0.93	0.24	0.20	0.13	0.11	-0.20	0.15	1.23	0.58	20.73
29	Nong Khaem	-0.59	0.14	0.03	0.32	0.14	0.12	-0.23	-0.08	0.10	-0.30	0.20	20.67

Table 6.20 (Continued).

No.	District	Intercept	Regression coefficient								Residual	Local R2	Predicted (μg/m^3)
			VIS	WS	BT	FRP	FH	AOD	FD	ELEV			
30	Pathum Wan	-0.65	0.25	0.72	0.06	0.53	0.16	0.03	-0.01	0.27	0.29	0.38	20.54
31	Phasi Charoen	-0.59	0.12	0.28	0.31	0.52	0.11	-0.14	-0.06	0.12	0.07	0.21	20.53
32	Phaya Thai	-0.56	0.12	0.73	0.06	0.58	0.12	0.12	-0.02	0.18	-1.74	0.45	20.64
33	Phra Khanong	-0.52	0.36	0.93	0.02	0.30	0.25	0.06	-0.07	0.36	-0.23	0.47	20.58
34	Phra Nakhon	-0.67	0.06	0.46	0.25	0.72	0.07	-0.02	0.00	0.15	-0.24	0.33	20.55
35	Pom Prap Sattru Phai	-0.65	0.12	0.56	0.17	0.65	0.11	0.01	-0.01	0.19	0.20	0.35	20.59
36	Prawet	-0.33	0.15	0.90	0.09	0.29	0.21	0.11	-0.13	0.26	0.15	0.50	20.73
37	Rat Burana	-0.52	0.45	0.59	0.08	0.10	0.33	-0.16	-0.10	0.30	-1.44	0.26	20.55
38	Ratchathewi	-0.61	0.18	0.72	0.06	0.57	0.14	0.08	-0.02	0.22	-0.73	0.42	20.58
39	Sai Mai	-0.08	-0.08	0.85	0.25	0.31	0.14	0.25	-0.08	0.01	0.26	0.60	21.06
40	Samphanthawong	-0.64	0.15	0.56	0.16	0.59	0.13	-0.01	-0.02	0.20	0.93	0.33	20.55
41	Saphan Sung	-0.25	0.17	0.99	0.18	0.25	0.18	0.14	-0.12	0.25	-0.03	0.55	20.79
42	Sathon	-0.64	0.37	0.69	0.05	0.37	0.22	-0.05	-0.03	0.31	0.76	0.33	20.48
43	Suan Luang	-0.46	0.29	0.97	0.06	0.31	0.22	0.11	-0.08	0.33	0.71	0.50	20.62
44	Taling Chan	-0.64	-0.07	0.11	0.37	0.80	0.01	-0.09	-0.02	0.00	-0.03	0.25	20.50
45	Thawi Watthana	-0.63	-0.05	-0.16	0.34	0.50	0.04	-0.19	-0.03	-0.05	-0.60	0.16	20.66
46	Thon Buri	-0.57	0.21	0.50	0.17	0.44	0.18	-0.08	-0.06	0.20	0.10	0.26	20.54
47	Thung Khru	-0.46	0.57	0.56	0.06	-0.15	0.44	-0.24	-0.13	0.34	-0.84	0.28	20.59
48	Vadhana	-0.57	0.32	0.92	0.01	0.40	0.20	0.08	-0.05	0.33	0.22	0.47	20.52
49	Wang Thonglang	-0.44	0.23	0.96	0.07	0.37	0.18	0.14	-0.06	0.27	0.32	0.52	20.72
50	Yan Nawa	-0.60	0.44	0.74	0.02	0.26	0.27	-0.07	-0.06	0.34	0.04	0.34	20.46
51	Bang Len	-0.01	0.17	-0.29	-0.06	0.16	0.06	0.16	-0.22	-0.26	0.00	0.24	20.76
52	Don Tum	-0.27	0.06	-0.32	0.02	0.08	-0.02	0.01	-0.15	-0.17	-0.06	0.31	20.77
53	Kamphaeng Saen	-0.22	0.07	-0.33	0.00	0.08	-0.04	0.05	-0.17	-0.17	0.28	0.34	20.75
54	Mueang Nakhon Pathom	-0.47	-0.02	-0.24	0.10	-0.08	-0.08	-0.08	-0.11	-0.09	-0.13	0.42	20.77
55	Nakhon Chai Si	-0.48	-0.01	-0.28	0.12	0.00	-0.03	-0.11	-0.08	-0.13	-0.13	0.34	20.75
56	Phutthamonthon	-0.48	0.00	-0.33	0.15	0.22	0.06	-0.14	-0.05	-0.18	0.07	0.20	20.67
57	Sam Phran	-0.56	0.01	-0.17	0.21	-0.04	0.03	-0.16	-0.08	-0.02	0.01	0.32	20.69
58	Bang Bua Thong	-0.16	-0.12	-0.22	0.09	0.53	0.14	0.21	-0.06	-0.38	0.47	0.27	20.63
59	Bang Kruai	-0.61	-0.19	-0.05	0.34	0.88	0.02	-0.04	0.00	-0.12	-0.57	0.26	20.64
60	Bang Yai	-0.48	-0.17	-0.32	0.22	0.65	0.09	-0.02	-0.01	-0.25	0.07	0.17	20.67

Table 6.20 (Continued).

No.	District	Intercept	Regression coefficient								Residual	Local R2	Predicted (μg/m³)
			VIS	WS	BT	FRP	FH	AOD	FD	ELEV			
61	Mueang Nonthaburi	-0.50	-0.22	0.29	0.14	0.79	0.06	0.18	0.01	-0.10	-0.28	0.42	20.69
62	Pak Kret	-0.28	-0.21	0.41	0.02	0.58	0.12	0.29	-0.02	-0.17	0.21	0.48	20.75
63	Sai Noi	0.07	0.17	-0.26	-0.04	0.25	0.11	0.23	-0.15	-0.42	0.30	0.24	20.69
64	Bang Bo	-0.15	0.06	0.78	0.09	0.24	0.16	0.01	-0.25	0.18	0.25	0.50	20.70
65	Bang Phli	-0.25	0.08	0.79	0.06	0.28	0.19	0.05	-0.19	0.21	-0.09	0.48	20.87
66	Bang Sao Thong	-0.16	0.07	0.82	0.10	0.25	0.16	0.04	-0.23	0.19	-0.58	0.51	20.93
67	Mueang Samut Prakan	-0.35	0.10	0.66	-0.01	0.26	0.24	0.01	-0.16	0.21	0.29	0.42	20.73
68	Phra Pradaeng	-0.54	0.52	0.78	0.01	0.14	0.32	-0.10	-0.09	0.37	-0.46	0.37	20.52
69	Phra Samut Chedi	-0.44	0.56	0.60	0.03	-0.16	0.43	-0.21	-0.14	0.35	0.15	0.34	20.60
70	Ban Phaeo	-0.60	0.00	-0.05	0.23	-0.22	0.01	-0.13	-0.10	0.08	0.11	0.42	20.68
71	Krathum Baen	-0.62	0.06	-0.03	0.29	-0.09	0.06	-0.19	-0.08	0.11	0.00	0.32	20.68
72	Mueang Samut Sakhon	-0.43	0.27	0.22	0.14	-0.23	0.38	-0.20	-0.13	0.19	-0.20	0.24	20.70

From Table 6.20, the maximum value is 21.10 μg/m^3 in Don Mueang District, Bangkok. In contrast, the minimum value is 20.37 μg/m^3 in Khlong Toei District, Bangkok. The classification maps of predicted values for PM2.5 concentration using the GWR model according to the Thailand Air Quality Index and the U.S. EPA Air Quality Index are displayed in Figure 6.39.

Thus, the predicted values of PM2.5 concentration are excellent at level 1 of Thailand AQI and moderate at level 2 of EPA AQI. In contrast, the predicted value in an urban landscape in the summer season from the GWR model is more than the one-day mean of WHO guidelines. See Table 5.3.

In addition, a spatial distribution map of PM2.5 concentration in the summer season using the SCK interpolation technique is displayed in Figure 6.40. As a result, the high PM2.5 concentration occur in urban areas in the northern part of the study area, mainly in Bangkok Metropolitan.

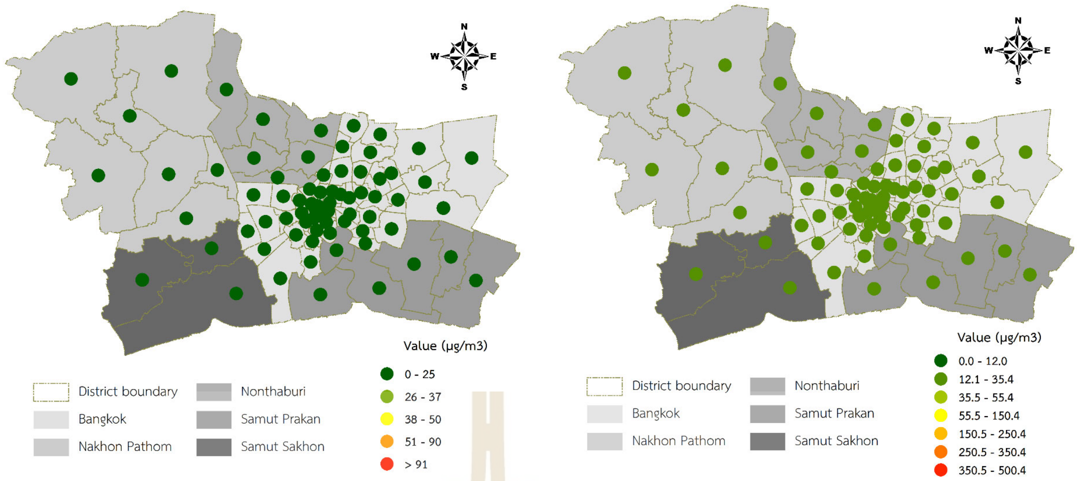

(a) (b)

Figure 6.39 The classification map of PM2.5 concentration prediction using the GWR model summer season according to the (a) Thailand AQI and (b) EPA AQI.

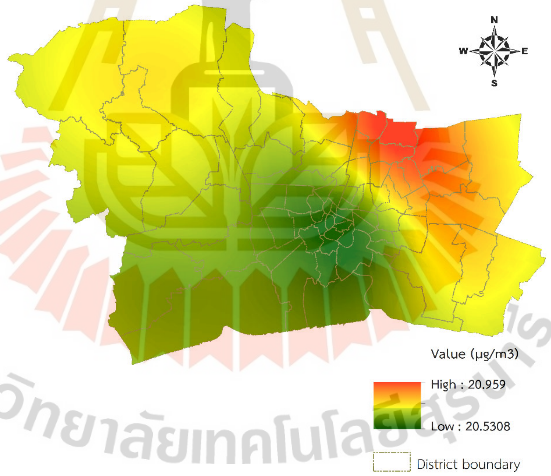

Figure 6.40 Spatial distribution of PM10 concentration in the summer season.

6.3 The predictive equations and their distribution map for spatiotemporal PM10 concentration in the rural landscape using the MEM model

Under this section, the MEM model with the significant derived factors was applied to predict the rural landscape's PM10 concentration in winter and summer. The model structure for PM10 concentration in the winter and summer is shown in Equations 6.5 and 6.6.

$$PM10_{i,j}=\mu+\beta_1 TEMP_{i,j}+\beta_2 WS_{i,j}+\beta_3 VIS_{i,j}+\beta_4 FRP_{i,j}+\beta_5 AOD_{i,j}+\varepsilon \tag{6.5}$$

Where $PM10_{i,j}$ is the averaged PM10 concentration at district i on month j in the winter season; μ is the fixed intercept; β_1 - β_5 are coefficients of fixed effect for independent variables; $TEMP_{i,j}$, $WS_{i,j}$, $VIS_{i,j}$, $FRP_{i,j}$, $AOD_{i,j}$ are temperature, wind speed, visibility, fire radiative power, MODIS AOD at district i on month j, respectively and ε is the residual error.

$$PM10_{i,j}=\mu+\beta_1 TEMP_{i,j}+\beta_2 VIS_{i,j}+\beta_3 AOD_{i,j}+\beta_4 BT_{i,j}+\beta_5 FD_{i,j}+\varepsilon \tag{6.6}$$

Where $PM10_{i,j}$ is the averaged PM10 concentration at district i on month j in the summer season; μ is the fixed intercept; β_1-β_5 are coefficients of fixed effect for independent variables; $TEMP_{i,j}$, $VIS_{i,j}$, $AOD_{i,j}$, $BT_{i,j}$, $FD_{i,j}$ are temperature, visibility, MODIS AOD, brightness temperature, factory density at district i on month j, respectively and ε is the residual error.

The summary of the predicted PM10 concentration (in microgram per cubic meter) in each month and season by the district in a rural landscape using the MEM model is reported in Table 6.21.

Table 6.21 The predictive value of PM10 concentration in each month and season using the MEM model.

No.	DISTRICT	PROVINCE	OCT	NOV	DEC	JAN	FEB	MAR	APR	MAY	WINTER	SUMMER
1	Chaiyo	Ang Thong	52.68	65.12	74.42	79.12	82.03	48.62	43.94	37.29	70.61	43.21
2	Mueang Ang Thong	Ang Thong	52.60	64.80	74.37	79.10	81.68	48.60	43.74	37.28	70.53	43.25
3	Pa Mok	Ang Thong	52.22	64.43	74.42	79.08	81.47	48.71	43.89	37.32	70.33	43.36
4	Pho Thong	Ang Thong	52.45	64.78	74.19	79.07	81.28	48.41	43.69	37.28	70.39	43.12
5	Samko	Ang Thong	52.33	64.49	74.11	79.03	80.61	48.32	43.74	37.28	70.24	43.19
6	Sawaeng Ha	Ang Thong	52.25	64.81	74.19	79.03	81.14	48.40	43.62	37.28	70.40	43.09
7	Wiset Chai Chan	Ang Thong	52.33	64.45	74.23	79.05	80.94	48.49	43.83	37.27	70.31	43.30
8	Ban Mi	Lop Buri	52.52	65.36	74.46	79.10	81.58	48.48	44.26	37.29	70.98	43.30
9	Chai Badan	Lop Buri	51.98	64.61	73.82	78.91	81.55	48.35	43.77	37.25	70.08	43.10
10	Khok Charoen	Lop Buri	52.09	64.48	74.29	78.99	80.97	48.77	43.81	37.25	70.46	43.18
11	Khok Samrong	Lop Buri	52.61	65.47	74.81	79.07	81.56	48.51	44.18	37.29	70.95	43.33
12	Lam Sonthi	Lop Buri	51.64	63.50	74.14	78.88	80.84	48.62	43.47	37.19	69.86	42.90
13	Mueang Lop Buri	Lop Buri	53.17	65.94	75.39	79.21	82.79	48.96	44.36	37.37	71.28	43.47
14	Nong Muang	Lop Buri	52.33	65.02	74.59	79.06	80.84	48.50	43.87	37.27	70.77	43.04
15	Phatthana Nikhom	Lop Buri	52.72	65.75	74.87	79.00	82.06	48.79	44.23	37.38	70.94	43.45
16	Sa Bot	Lop Buri	52.35	64.77	74.41	78.99	80.99	48.47	43.90	37.26	70.50	43.22
17	Tha Luang	Lop Buri	51.86	65.14	73.81	78.89	81.55	48.48	43.98	37.26	70.08	43.19
18	Tha Wung	Lop Buri	52.73	65.38	74.51	79.15	82.20	48.62	44.09	37.30	70.72	43.33
19	Khlong Luang	Pathum Thani	51.87	64.01	73.95	79.04	81.05	48.69	43.97	37.15	69.83	43.26
20	Lam Luk Ka	Pathum Thani	51.90	64.46	75.05	79.02	81.67	48.94	44.13	37.55	70.45	43.61
21	Lat Lum Kaeo	Pathum Thani	50.94	63.84	73.61	79.04	79.88	48.64	42.91	37.18	69.18	42.69

Table 6.21 (Continued).

No.	DISTRICT	PROVINCE	OCT	NOV	DEC	JAN	FEB	MAR	APR	MAY	WINTER	SUMMER
22	Mueang Pathum Thani	Pathum Thani	50.68	63.90	73.98	79.14	80.50	48.78	43.14	37.08	69.40	43.06
23	Nong Suea	Pathum Thani	52.73	64.26	74.68	79.04	81.66	48.69	44.10	37.25	70.56	43.41
24	Sam Khok	Pathum Thani	50.87	63.48	73.47	79.10	80.65	48.75	43.17	37.11	69.11	42.83
25	Thanyaburi	Pathum Thani	52.01	64.36	74.63	79.04	81.30	48.79	44.10	37.32	70.38	43.68
26	Ban Phraek	Phra Nakhon Si Ayutthaya	52.87	65.43	74.79	79.16	82.71	48.78	44.08	37.30	70.91	43.31
27	Bang Ban	Phra Nakhon Si Ayutthaya	51.85	64.32	74.31	79.10	81.47	48.85	43.93	37.46	69.94	43.47
28	Bang Pa-In	Phra Nakhon Si Ayutthaya	51.36	64.11	74.20	79.06	81.65	48.86	44.01	37.41	69.80	43.30
29	Bang Pahan	Phra Nakhon Si Ayutthaya	52.34	64.80	74.64	79.12	81.67	48.89	44.15	37.44	70.42	43.55
30	Bang Sai	Phra Nakhon Si Ayutthaya	51.30	64.04	73.95	79.00	80.55	48.64	43.42	37.29	69.57	42.99
31	Bang Sai	Phra Nakhon Si Ayutthaya	51.30	64.04	73.95	79.00	80.55	48.62	43.42	37.29	69.57	42.95
32	Lat Bua Luang	Phra Nakhon Si Ayutthaya	51.13	63.74	73.78	78.98	80.02	48.71	43.18	37.23	69.25	42.76
33	Maha Rat	Phra Nakhon Si Ayutthaya	52.75	65.34	74.73	79.12	82.22	48.87	44.06	37.30	70.89	43.47
34	Nakhon Luang	Phra Nakhon Si Ayutthaya	52.67	65.01	75.05	79.13	82.00	48.83	44.36	37.43	70.66	43.60

Table 6.21 (Continued).

No.	DISTRICT	PROVINCE	OCT	NOV	DEC	JAN	FEB	MAR	APR	MAY	WIN TER	SUM MER
35	Phachi	Phra Nakhon Si Ayutthaya	53.01	65.02	75.40	79.13	82.46	48.74	44.31	37.35	71.06	43.60
36	Phak Hai	Phra Nakhon Si Ayutthaya	51.98	64.59	74.23	79.03	80.86	48.53	43.81	37.27	70.21	43.16
37	Phra Nakhon Si Ayutthaya	Phra Nakhon Si Ayutthaya	51.65	64.23	74.80	79.16	81.79	49.56	44.27	38.05	70.07	44.11
38	Sena	Phra Nakhon Si Ayutthaya	51.48	64.05	74.03	78.99	80.48	48.65	43.48	37.28	69.63	43.03
39	Tha Ruea	Phra Nakhon Si Ayutthaya	53.28	65.73	75.73	79.22	82.96	48.91	44.40	37.40	71.36	43.64
40	Uthai	Phra Nakhon Si Ayutthaya	52.54	64.59	75.19	79.12	82.16	48.99	44.31	37.43	70.81	43.76
41	Wang Noi	Phra Nakhon Si Ayutthaya	52.53	64.30	74.85	79.08	81.99	48.96	44.22	37.28	70.62	43.50
42	Ban Mo	Saraburi	53.62	66.13	76.18	79.28	83.64	49.17	44.49	37.57	71.67	43.67
43	Chaloem Phra Kiat	Saraburi	54.50	67.46	79.97	79.39	84.59	50.81	45.22	39.18	73.26	45.22
44	Don Phut	Saraburi	53.11	65.78	75.31	79.19	82.97	48.80	44.29	37.33	71.22	43.44
45	Kaeng Khoi	Saraburi	53.22	66.01	76.06	79.19	83.28	49.31	44.43	37.43	71.63	43.91
46	Muak Lek	Saraburi	52.13	65.70	74.60	78.91	81.56	48.81	44.03	37.28	70.47	43.35
47	Mueang Saraburi	Saraburi	53.39	65.64	76.94	79.36	83.54	49.48	44.39	37.33	71.97	44.00
48	Nong Don	Saraburi	53.74	66.16	76.10	79.29	83.61	49.17	44.45	37.48	71.74	43.68
49	Nong Khae	Saraburi	52.91	64.97	75.73	79.15	82.54	48.94	44.15	37.28	71.23	43.64
50	Nong Saeng	Saraburi	53.22	65.53	75.91	79.21	82.94	48.84	44.37	37.37	71.41	43.64
51	Phra Phutthabat	Saraburi	54.23	66.98	78.22	79.36	84.34	50.02	44.98	38.34	72.68	44.39
52	Sao Hai	Saraburi	53.85	66.33	77.44	79.38	83.83	49.80	44.69	37.93	72.19	44.38
53	Wang Muang	Saraburi	52.33	65.93	74.65	78.94	81.72	48.88	44.16	37.31	70.72	43.37

Table 6.21 (Continued).

No.	DISTRICT	PROVINCE	OCT	NOV	DEC	JAN	FEB	MAR	APR	MAY	WIN TER	SUM MER
54	Wihan Daeng	Saraburi	52.63	65.05	75.91	79.17	83.68	48.68	44.21	37.26	71.49	43.52
55	Bang Rachan	Sing Buri	52.05	65.07	74.04	79.05	81.22	48.65	43.91	37.30	70.38	43.29
56	In Buri	Sing Buri	51.99	65.07	74.05	79.05	81.26	48.56	44.17	37.30	70.40	43.32
57	Khai Bang Rachan	Sing Buri	52.20	65.06	74.22	79.06	81.32	48.53	43.83	37.29	70.52	43.19
58	Mueang Sing Buri	Sing Buri	52.34	65.06	74.15	79.08	81.54	48.58	44.26	37.30	70.45	43.36
59	Phrom Buri	Sing Buri	52.58	65.20	74.40	79.13	81.94	48.51	44.04	37.29	70.56	43.14
60	Tha Chang	Sing Buri	52.41	65.08	74.29	79.10	81.64	48.37	43.91	37.29	70.51	42.98

The monthly predictive equation for PM10 concentration in the rural landscape using the MEM model with the significant derived factors in winter and summer is systematically reported in two table forms in the following sections. The first table shows the intercept's value of the parameter associated with the rural area in each month (columns 1 and 2) and the standard error of the sample mean, degree of freedom to determine the observed significance level (columns 3 to 5) and the smallest and largest value that exceeds the lower and upper bound fall outside the confidence interval range (columns 6 and 7). Meanwhile, the second table shows parameter estimates associated with a covariance matrix in column 2 and the standard error of a parameter estimate associated with a covariance matrix in column 3. Besides, the performance of the MEM model for PM10 concentration is reported, including AIC, AICc, and BIC.

6.3.1 October 2019 in the winter season

The MEM model results are shown in Tables 6.22 and Table 6.23. The model performance shows that AIC, AICc, and BIC values are 140.62, 140.84, and 144.67, respectively.

Table 6.22 Estimates of Fixed Effects in October 2019.

Parameter	Estimate	St. Error	df	Sig.	95% Confidence Interval	
					Lower Bound	Upper Bound
Intercept	0.00	0.09	56.00	1.00	-0.18	0.18
Wind speed	0.40	0.10	56.00	0.00	0.20	0.61
Temperature	0.19	0.10	56.00	0.06	-0.01	0.40
Visibility	-0.74	0.10	56.00	0.00	-0.93	-0.54

Table 6.23 Estimates of covariance parameters in October 2019.

Parameter		Estimate	Std. Error
Residual		0.25	0.10
Intercept [subject = ID_district]	Variance	0.25	0.00

From Table 6.21, the maximum value is 54.50 μg/m^3 in Chaloem Phra Kiat District, Pathum Thani province. In contrast, the minimum value is 50.68 μg/m^3 in Mueang Pathum Thani District, Pathum Thani province. The classification maps of predicted values for PM10 concentration using the MEM model according to the Thailand Air Quality Index and the U.S. EPA Air Quality Index are displayed in Figure 6.41.

Thus, the predicted values of PM10 concentration are satisfactory at level 2 of Thailand AQI and good at level 1 of EPA AQI. Additionally, the predicted value in the rural landscape in October 2019 from the MEM model is more than the one-day mean of WHO guidelines. See Table 5.3.

In addition, a spatial distribution map of PM10 concentration in October 2019 using the SCK interpolation technique is displayed in Figure 6.42. As a result, the high PM10 concentration occur on agricultural land in the central part of the study area, particularly in Saraburi province.

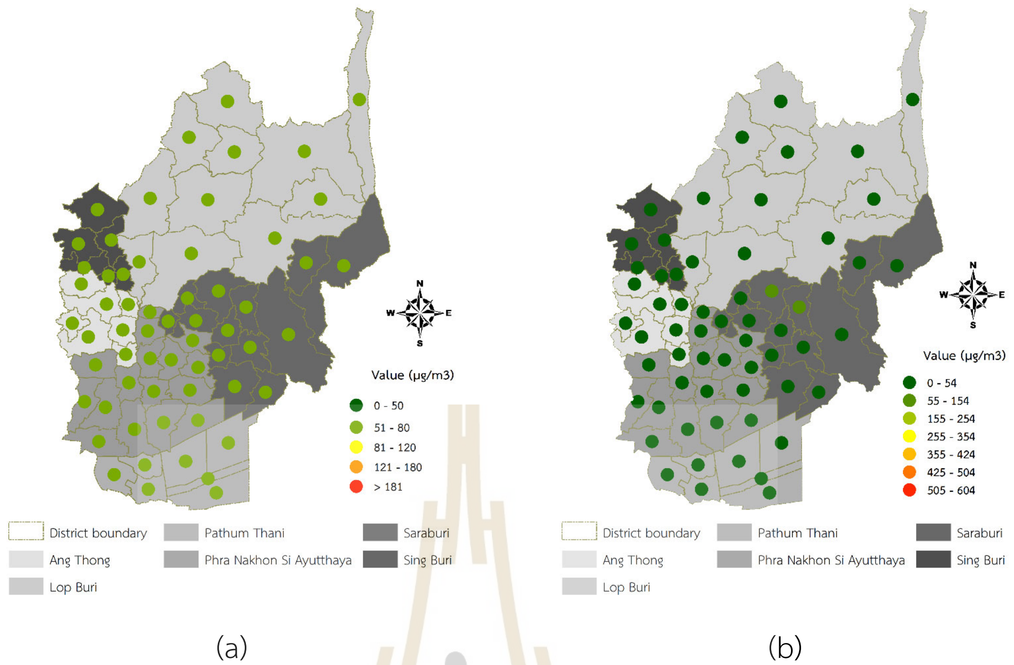

Figure 6.41 The classification map of PM10 concentration prediction using the MEM model in October 2019 according to the (a) Thailand AQI and (b) EPA AQI.

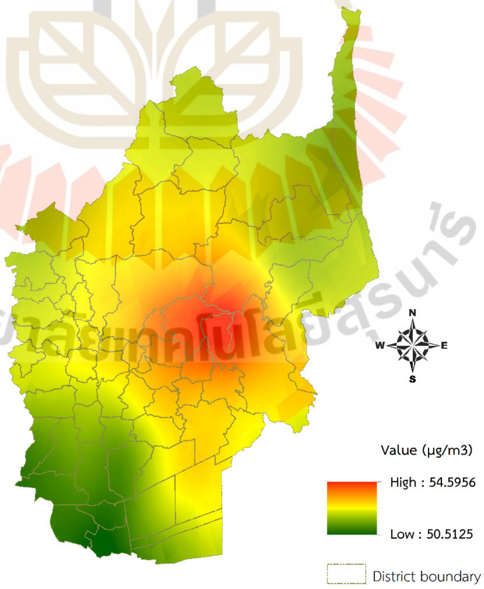

Figure 6.42 Spatial distribution of PM10 concentration in October 2019.

6.3.2 November 2019 in the winter season

The MEM model results are shown in Table 6.24 and Table 6.25. The model performance shows that AIC, AICc, and BIC values are 140.77, 140.99, and 144.82, respectively.

Table 6.24 Estimates of Fixed Effects in November 2019.

Parameter	Estimate	St. Error	df	Sig.	95% Confidence Interval	
					Lower Bound	Upper Bound
Intercept	0.00	0.09	56.00	1.00	-0.18	0.18
Wind speed	0.77	0.12	56.00	.00	0.54	1.00
Visibility	-0.82	0.12	56.00	.00	-1.06	-0.59
MODIS AOD	0.22	0.09	56.00	.02	0.03	0.41

Table 6.25 Estimates of covariance parameters in November 2019.

Parameter		Estimate	Std. Error
Residual		0.25	0.10
Intercept [subject = ID_district]	Variance	0.25	0.00

From Table 6.21, the maximum value is 67.46 μg/m^3 in Chaloem Phra Kiat District, Saraburi province. At the same time, the minimum value is 63.48 μg/m^3 in Sam Khok District, Pathum Thani province. The classification maps of prediction values for PM10 concentration using the MEM model according to the Thailand Air Quality Index and the U.S. EPA Air Quality Index are displayed in Figure 6.43.

Thus, the predicted values of PM10 concentration are satisfactory at level 2 of Thailand AQI and moderate at level 2 of EPA AQI. The predicted value in the MEM model's rural landscape in November 2019 is more than the one-day mean of WHO guidelines. See Table 5.3.

In addition, a spatial distribution map of PM10 concentration in November 2019 using the SCK interpolation technique is displayed in Figure 6.44. As a result, the high PM10 concentration occur on agricultural land in the central part of the study area, particularly in Saraburi province.

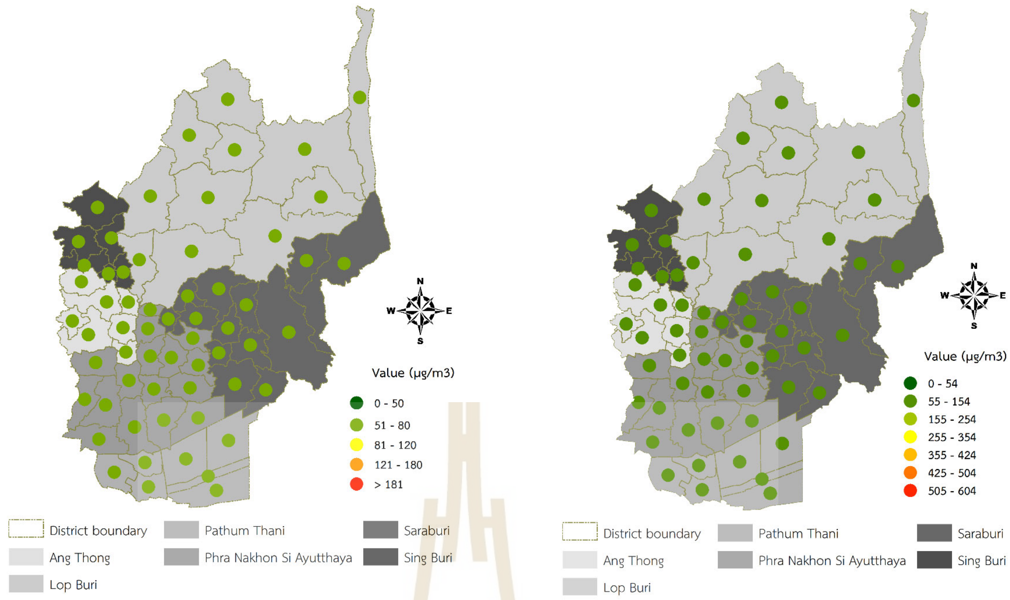

(a) (b)

Figure 6.43 The classification map of PM10 concentration prediction using the MEM model in November 2019 according to the (a) Thailand AQI and (b) EPA AQI.

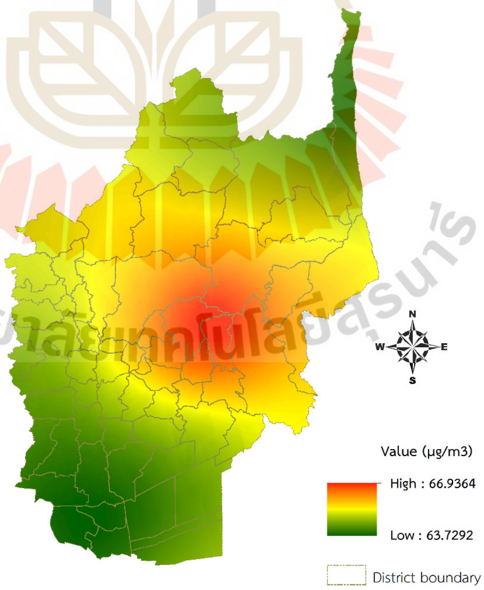

Figure 6.44 Spatial distribution of PM10 concentration in November 2019.

6.3.3 December 2019 in the winter season

The MEM model results are shown in Table 6.26 and Table 6.27. The model performance shows that AIC, AICc, and BIC values are 158.40, 158.62, and 162.45, respectively.

Table 6.26 Estimates of Fixed Effects in December 2019.

Parameter	Estimate	St. Error	df	Sig.	95% Confidence Interval	
					Lower Bound	Upper Bound
Intercept	0.00	0.11	56.00	1.00	-0.22	0.22
Wind speed	0.60	0.12	56.00	0.00	0.36	0.85
Temperature	0.22	0.11	56.00	0.05	0.00	0.44
Visibility	-0.34	0.12	56.00	0.01	-0.59	-0.10

Table 6.27 Estimates of covariance parameters in December 2019.

Parameter		Estimate	Std. Error
Residual		0.35	0.13
Intercept [subject = ID_district]	Variance	0.35	0.00

From Table 6.21, the maximum value is 79.97 µg/m^3 in Chaloem Phra Kiat District, Pathum Thani province. In contrast, the minimum value is 73.47 µg/m^3 in Sam Khok District, Pathum Thani province. The classification maps of prediction values for PM10 concentration using the MEM model according to the Thailand Air Quality Index and the U.S. EPA Air Quality Index are displayed in Figure 6.45.

Thus, most predicted PM10 concentration are satisfactory at level 2 of Thailand AQI and moderate at level 2 of EPA AQI. However, the predicted value in the rural landscape in December 2019 from the MEM model is more than the one-day mean of WHO guidelines. See Table 5.3.

In addition, a spatial distribution map of PM10 concentration in December 2019 using the SCK interpolation technique is displayed in Figure 6.46. As a result, the high PM10 concentration occur on agricultural land in the central part of the study area, particularly in Saraburi province.

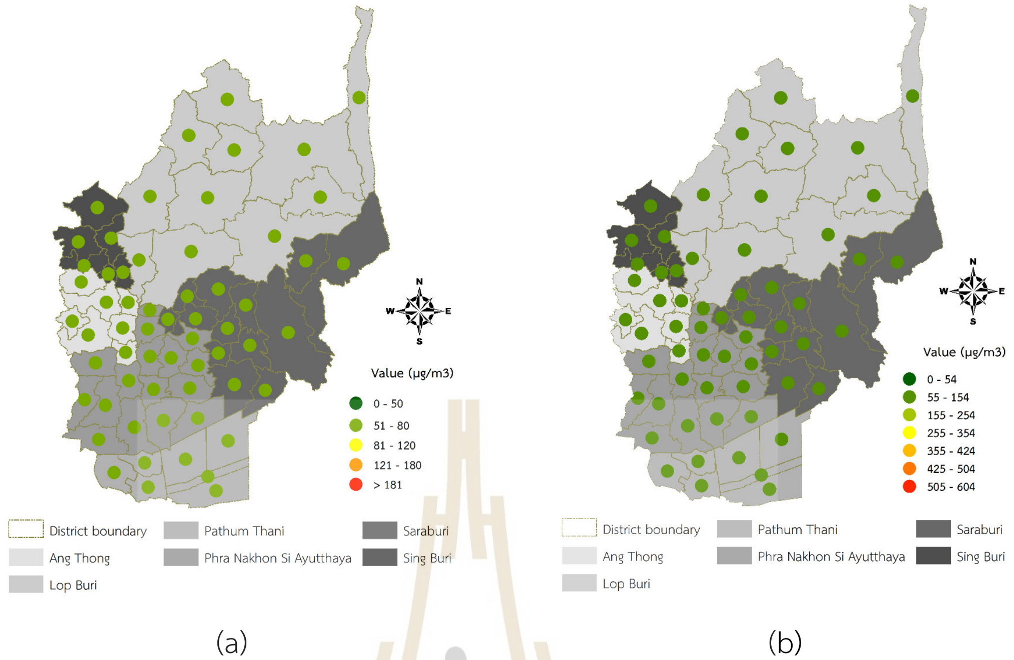

Figure 6.45 The classification map of PM10 concentration prediction using the MEM model in December 2019 according to the (a) Thailand AQI and (b) EPA AQI.

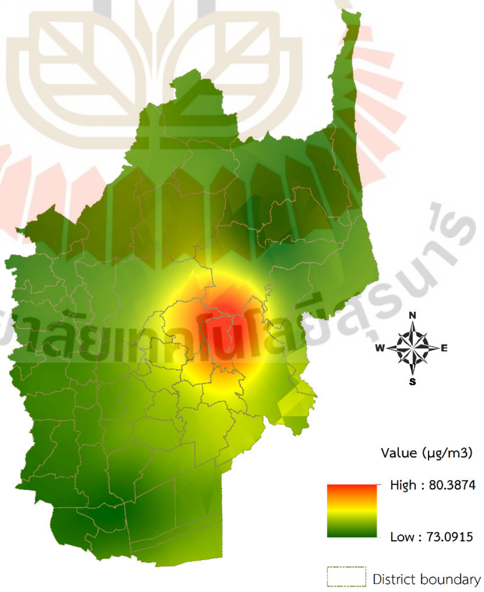

Figure 6.46 Spatial distribution of PM10 concentration in December 2019.

6.3.4 January 2020 in the winter season

The MEM model results are shown in Table 6.28 and Table 6.29. The model performance shows AIC, AICc, and BIC values are 172.84, 173.06 and 176.92, respectively.

Table 6.28 Estimates of Fixed Effects in January 2020.

Parameter	Estimate	St. Error	df	Sig.	95% Confidence Interval	
					Lower Bound	Upper Bound
Intercept	0.00	0.12	57.00	1.00	-0.25	0.25
Temperature	0.31	0.12	57.00	0.02	0.06	0.56
MODIS AOD	-0.17	0.12	57.00	0.17	-0.42	0.08

Table 6.29 Estimates of covariance parameters in January 2020.

Parameter		Estimate	Std. Error
Residual		0.46	0.17
Intercept [subject = ID_district]	Variance	0.46	0.00

From Table 6.21, the maximum value is 79.39 µg/m^3 in Chaloem Phra Kiat District, Saraburi province. In contrast, the minimum value is 78.88 µg/m^3 in Lam Sonthi District, Lop Buri province. The classification maps of prediction values for PM10 concentration using the MEM model according to the Thailand Air Quality Index and the U.S. EPA Air Quality Index are displayed in Figure 6.47.

Thus, the predicted values of PM10 concentration are satisfactory at level 2 of Thailand AQI and moderate at level 2 of EPA AQI. The predicted value in the rural landscape in January 2020 from the MEM model is more than the one-day mean of WHO guidelines. See Table 5.3.

In addition, a spatial distribution map of PM10 concentration in January 2020 using the SCK interpolation technique is displayed in Figure 6.48. As a result, the high PM10 concentration occur on agricultural land in the central part of the study area, particularly in Saraburi province.

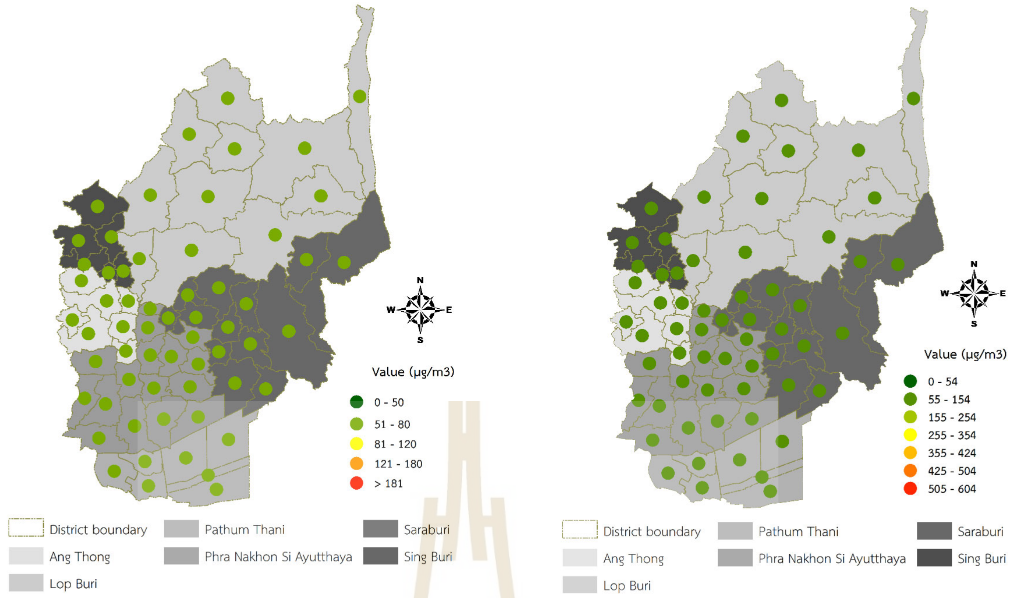

(a) (b)

Figure 6.47 The classification map of PM10 concentration prediction using the MEM model in January 2020 according to the (a) Thailand AQI and (b) EPA AQI.

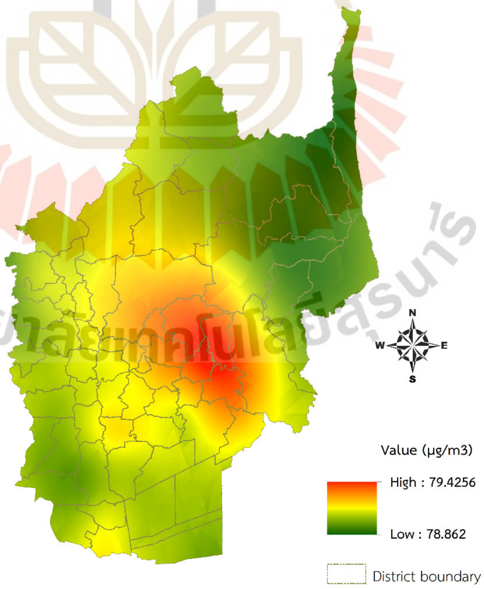

Figure 6.48 Spatial distribution of PM10 concentration in January 2020.

6.3.5 February 2020 in the winter season

The MEM model results are shown in Table 6.30 and Table 6.31. The model performance shows that AIC, AICc, and BIC values are 163.70, 163.92, and 167.78, respectively.

Table 6.30 Estimates of Fixed Effects in February 2020.

Parameter	Estimate	St. Error	df	Sig.	95% Confidence Interval	
					Lower Bound	Upper Bound
Intercept	0.00	0.11	57.00	1.00	-0.23	0.23
Wind speed	0.07	0.14	57.00	0.60	-0.20	0.34
Fire radiative power	0.45	0.14	57.00	0.00	0.18	0.72

Table 6.31 Estimates of covariance parameters in February 2020.

Parameter		Estimate	Std. Error
Residual		0.39	0.15
Intercept [subject = ID_district]	Variance	0.39	0.00

From Table 6.21, the maximum value is 84.59 μg/m^3 in Chaloem Phra Kiat District, Saraburi province. In contrast, the minimum value is 79.88 μg/m^3 in Lat Lum Kaeo District, Pathum Thani province. The classification maps of prediction values for PM10 concentration using the MEM model according to the Thailand Air Quality Index and the U.S. EPA Air Quality Index are displayed in Figure 6.49.

Thus, the predicted values of PM10 concentration are satisfactory and moderate at levels 2 and 3 of Thailand AQI standard and moderate at level 2 of EPA AQI standard. The predicted value in the rural landscape in February 2020 from the MEM model is more than the one-day mean of WHO guidelines. See Table 5.3.

In addition, a spatial distribution map of PM10 concentration in February 2020 using the SCK interpolation technique is displayed in Figure 6.50. As a result, the high PM10 concentration occur on agricultural land in the central part of the study area, particularly in Saraburi province.

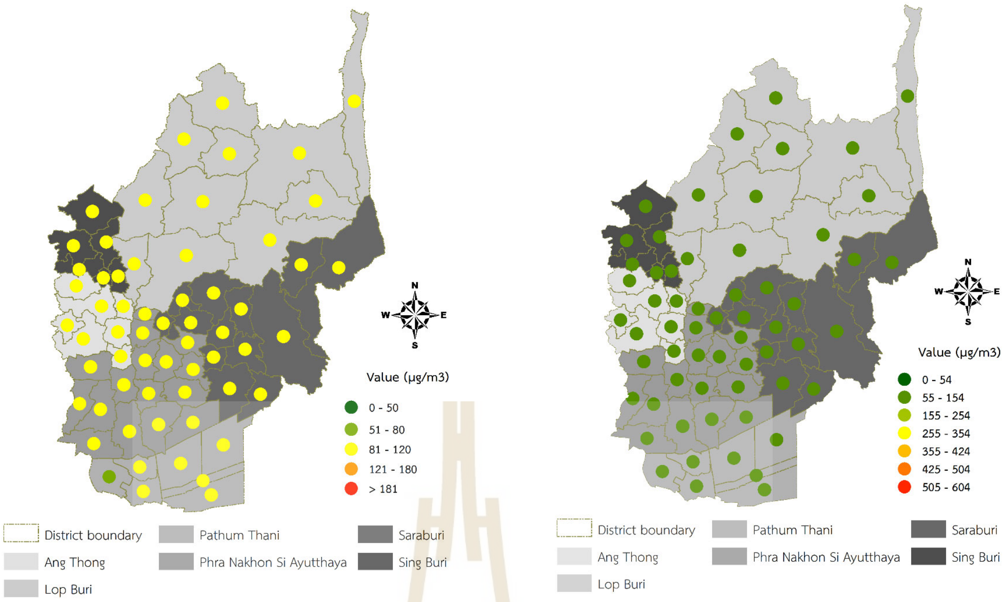

(a) (b)

Figure 6.49 The classification map of PM10 concentration prediction using the MEM model in February 2019 according to the (a) Thailand AQI and (b) EPA AQI.

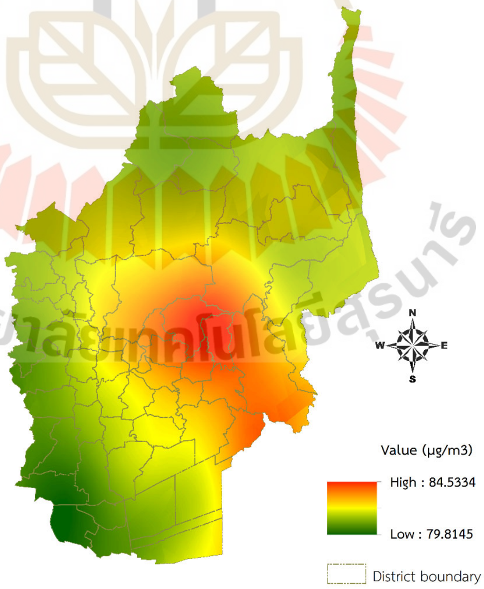

Figure 6.50 Spatial distribution of PM10 concentration in February 2020.

6.3.6 March 2020 in the summer season

The MEM model results are shown in Table 6.32 and Table 6.33. The model performance shows that AIC, AICc, and BIC values are 157.09, 157.31, and 161.14, respectively.

Table 6.32 Estimates of Fixed Effects in March 2020.

Parameter	Estimate	St. Error	df	Sig.	95% Confidence Interval	
					Lower Bound	Upper Bound
Intercept	0.00	0.11	56.00	1.00	-0.21	0.21
Temperature	-0.33	0.11	56.00	0.00	-0.55	-0.11
MODIS AOD	0.43	0.11	56.00	0.00	0.21	0.65
Factory density	0.09	0.11	56.00	0.41	-0.13	0.31

Table 6.33 Estimates of covariance parameters in March 2020.

Parameter		Estimate	Std. Error
Residual		0.34	0.13
Intercept [subject = ID_district]	Variance	0.34	0.00

From Table 6.21, the maximum value is 50.81 μg/m^3 in Chaloem Phra Kiat District, Saraburi province. In contrast, the minimum value is 48.32 μg/m^3 in Samko District, Ang Thong province. The classification maps of prediction values for PM10 concentration using the MEM model according to the Thailand Air Quality Index and the U.S. EPA Air Quality Index are displayed in Figure 6.51.

Thus, the predicted values of PM10 concentration are excellent at level 1, satisfactory at level 2 of Thailand AQI, and good at level 1of EPA AQI. In addition, the predicted value in rural landscape in March 2020 from the MEM model is more than the one-day mean of WHO guidelines. See Table 5.3.

In addition, a spatial distribution map of PM10 concentration in March 2020 using the SCK interpolation technique is displayed in Figure 6.52. As a result, the high PM10 concentration occur on agricultural land in the central part of the study area, particularly in Saraburi province.

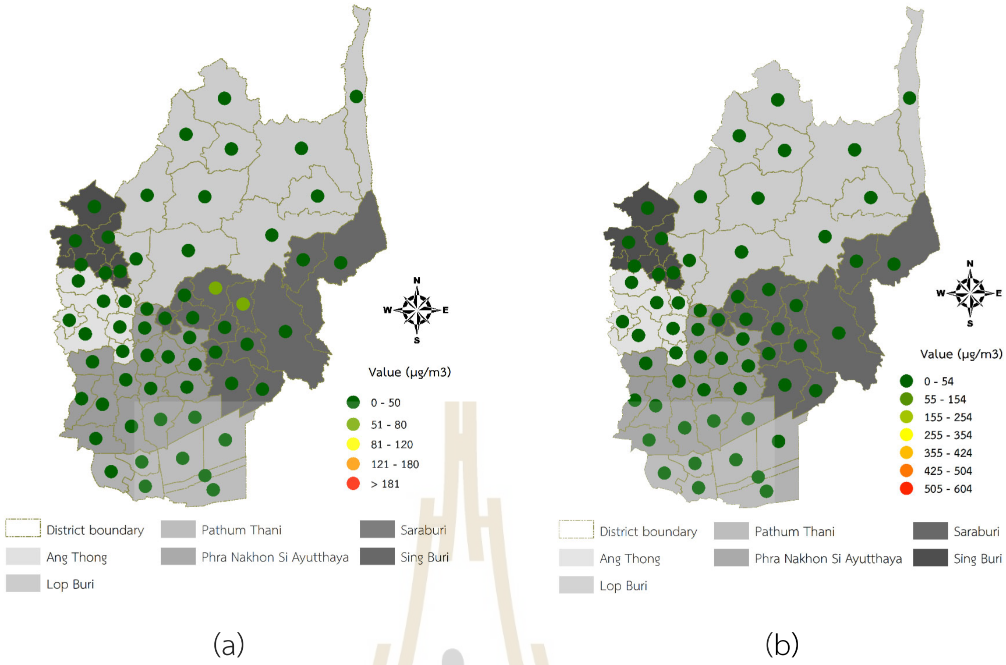

Figure 6.51 The classification map of PM10 concentration prediction using the MEM model in March 2020 according to the (a) Thailand AQI and (b) EPA AQI.

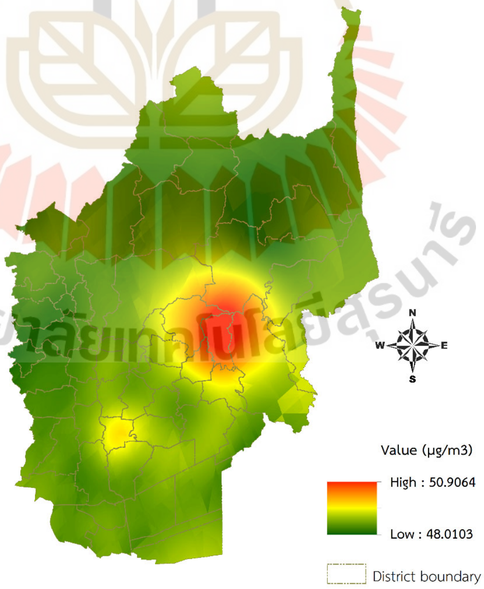

Figure 6.52 Spatial distribution of PM10 concentration in March 2020.

6.3.7 April 2020 in the summer season

The MEM model results are shown in Table 6.34 and Table 6.35. The model performance shows that AIC, AICc, and BIC values are 159.16, 159.37, and 163.28, respectively.

Table 6.34 Estimates of Fixed Effects in April 2020.

Parameter	Estimate	St. Error	df	Sig.	95% Confidence Interval	
					Lower Bound	Upper Bound
Intercept	0.00	0.11	58.00	1.00	-0.22	0.22
Brightness temperature	0.52	0.11	58.00	0.00	0.30	0.75

Table 6.35 Estimates of covariance parameters in April 2020.

Parameter		Estimate	Std. Error
Residual		0.37	0.14
Intercept [subject = ID_district]	Variance	0.37	0.00

From Table 6.21, the maximum value is 45.22 μg/m^3 in Chaloem Phra Kiat District, Pathum Thani province. In contrast, the minimum value is 42.91 μg/m^3 in Lat Lum Kaeo District, Pathum Thani province. The classification maps of prediction values for PM10 concentration using the MEM model according to the Thailand Air Quality Index and the U.S. EPA Air Quality Index are displayed in Figure 6.53.

Thus, the predicted values of PM10 concentration are excellent at level 1 of Thailand AQI and good at level 1 of EPA AQI. On the other hand, the predicted value in rural landscape in April 2020 from the MEM model is less than the one-day mean of WHO guidelines. See Table 5.3.

In addition, a spatial distribution map of PM10 concentration in April 2020 using the SCK interpolation technique is displayed in Figure 6.54. As a result, the high PM10 concentration occur on agricultural land in the central part of the study area, particularly in Saraburi province.

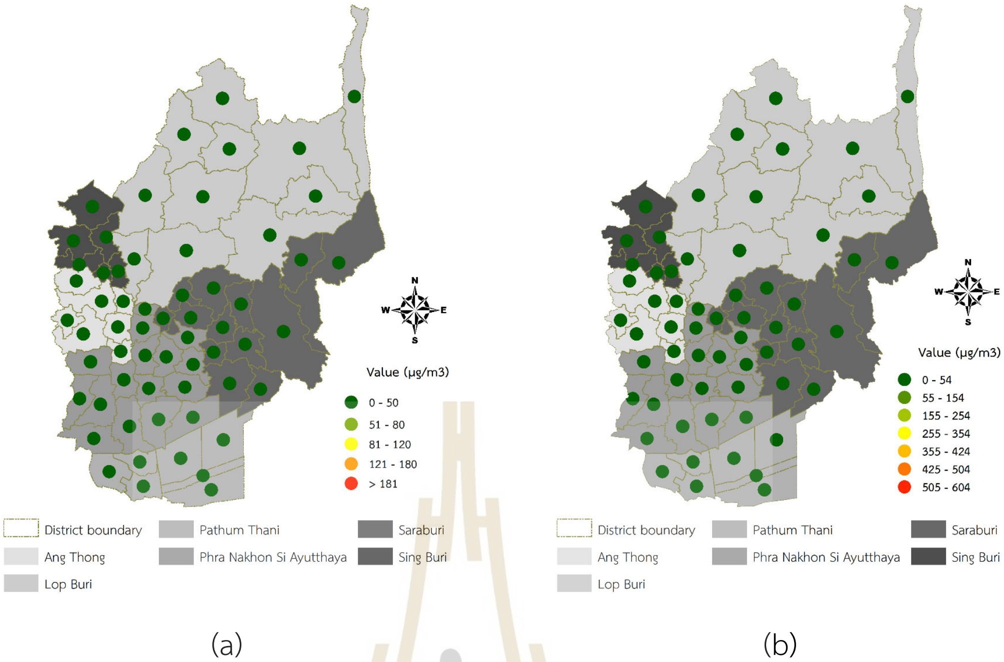

Figure 6.53 The classification map of PM10 concentration prediction using the MEM model in April 2020 according to the (a) Thailand AQI and (b) EPA AQI.

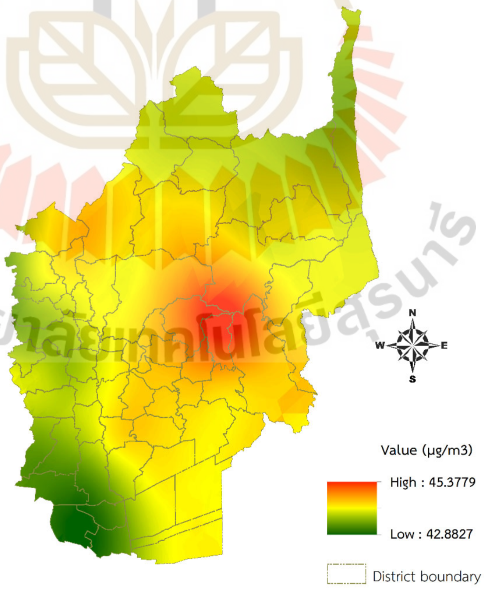

Figure 6.54 Spatial distribution of PM10 concentration in April 2020.

6.3.8 May 2020 in the summer season

The MEM model results are shown in Table 6.36 and Table 6.37. The model performance shows that AIC, AICc, and BIC values are 177.40, 177.62, and 181.52, respectively.

Table 6.36 Estimates of Fixed Effects in May 2020.

Parameter	Estimate	St. Error	df	Sig.	95% Confidence Interval	
					Lower Bound	Upper Bound
Intercept	0.00	0.13	58.00	1.00	-0.26	0.26
Visibility	-0.08	0.13	58.00	0.55	-0.34	0.18

Table 6.37 Estimates of covariance parameters in May 2020.

Parameter		Estimate	Std. Error
Residual		0.51	0.19
Intercept [subject = ID_district]	Variance	0.51	0.00

From Table 6.21, the maximum value is 39.18 μg/m^3 in Chaloem Phra Kiat District, Saraburi province. In contrast, the minimum value is 37.08 μg/m^3 in Mueang Pathum Thani District, Pathum Thani province. The classification maps of prediction values for PM10 concentration using the MEM model according to the Thailand Air Quality Index and the U.S. EPA Air Quality Index are displayed in Figure 6.55.

Thus, the predicted values of PM10 concentration are excellent at level 1 of Thailand AQI and good at level 1 of EPA AQI. On the other hand, the predicted value in rural landscape in May 2020 from the MEM model is less than the one-day mean of WHO guidelines. See Table 5.3.

In addition, a spatial distribution map of PM10 concentration in May 2020 using the SCK interpolation technique is displayed in Figure 6.56. As a result, the high PM10 concentration occur on agricultural land in the central part of the study area, particularly in Saraburi province.

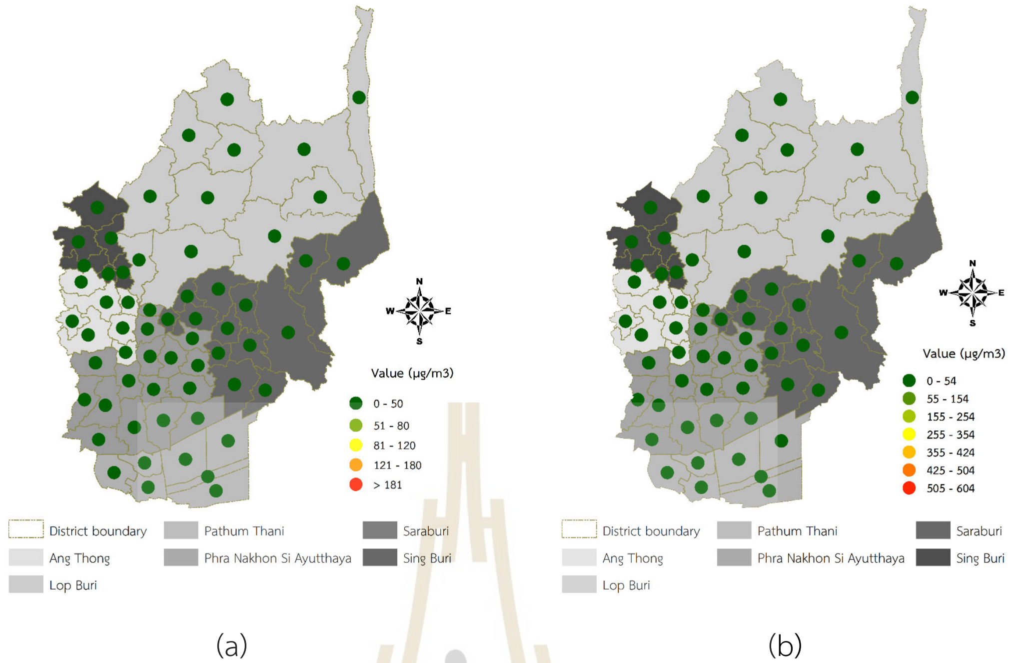

Figure 6.55 The classification map of PM10 concentration prediction using the MEM model in May 2020 according to the (a) Thailand AQI and (b) EPA AQI.

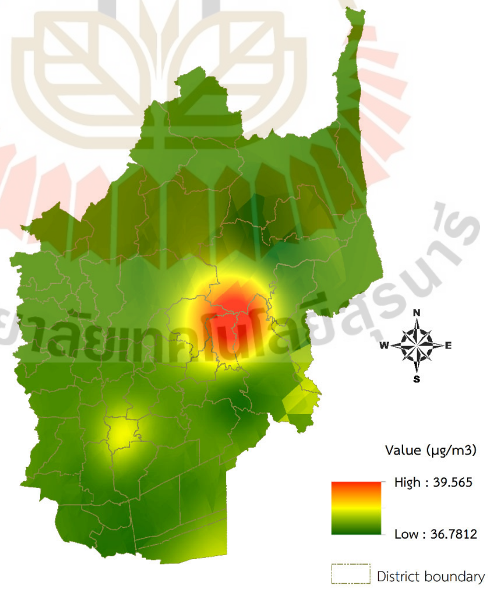

Figure 6.56 Spatial distribution of PM10 concentration in May 2020.

6.3.9 Winter season

The result of the MEM model for PM10 concentration prediction in the winter season (October to February) is summarized in Table 6.38 and Table 6.39. The model performance shows that AIC, AICc, and BIC values are 151.00, 151.24, and 154.98, respectively.

Table 6.38 Estimates of Fixed Effects in the winter season.

Parameter	Estimate	St. Error	df	Sig.	95% Confidence Interval	
					Lower Bound	Upper Bound
Intercept	0.00	0.10	54.00	1.00	-.20	0.20
Temperature	0.17	0.11	54.00	.14	-0.05	0.39
Wind speed	0.79	0.17	54.00	.00	0.45	1.13
Visibility	-0.83	0.15	54.00	.00	-1.13	-0.53
Fire radiative power	0.14	0.14	54.00	.32	-0.14	0.41
MODIS AOD	0.16	0.13	54.00	.24	-0.11	0.42

Table 6.39 Estimates of covariance parameters in the winter season.

Parameter		Estimate	Std. Error
Residual		0.29	0.11
Intercept [subject = ID_district]	Variance	0.29	0.00

From Table 6.21, the maximum value is 73.26 μg/m^3 in Chaloem Phra Kiat District, Saraburi province. In contrast, the minimum value is 69.11 μg/m^3 in Sam Khok District, Pathum Thani province. The classification maps of prediction values for PM10 concentration using the MEM model according to the Thailand Air Quality Index and the U.S. EPA Air Quality Index are displayed in Figure 6.57.

Thus, the predicted values of PM10 concentration are satisfactory at level 2 of Thailand AQI and moderate at level 2 of EPA AQI. Meanwhile, the predicted value in rural landscape in the winter season from the MEM model is more than the one-day mean of WHO guidelines. See Table 5.3.

In addition, a spatial distribution map of PM10 concentration in the winter season using the SCK interpolation technique is displayed in Figure 6.58. As a result, the high PM10 concentration occur on agricultural land in the central part of the study area, particularly in Saraburi province.

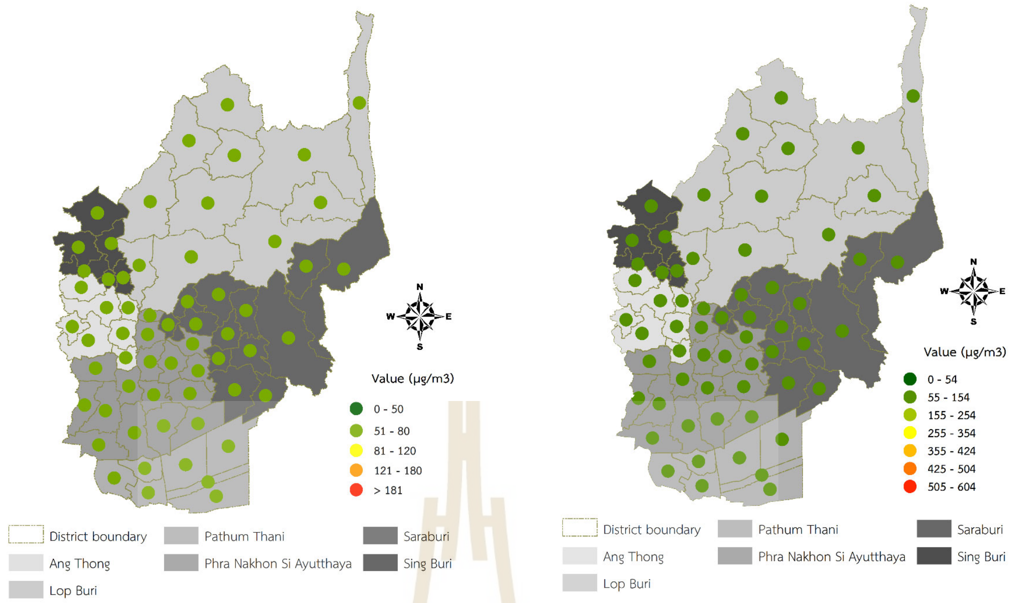

(a) (b)

Figure 6.57 The classification map of PM10 concentration prediction using the MEM model in the winter season according to the (a) Thailand AQI and (b) EPA AQI.

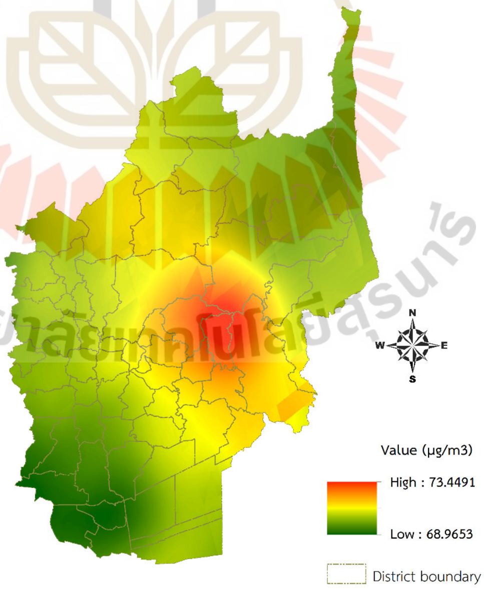

Figure 6.58 Spatial distribution of PM10 concentration in the winter season.

6.3.10 Summer season

The result of the MEM model for PM10 concentration prediction in the summer season (March to May) is summarized in Table 6.40 and Table 6.41. The model performance shows that AIC, AICc, and BIC values are 158.46, 158.70, and 162.44, respectively.

Table 6.40 Estimates of Fixed Effects in the summer season.

Parameter	Estimate	St. Error	df	Sig.	95% Confidence Interval	
					Lower Bound	Upper Bound
Intercept	0.00	0.11	54.00	1.00	-0.21	0.21
Temperature	-0.32	0.13	54.00	0.01	-0.58	-0.07
Visibility	-0.26	0.15	54.00	0.09	-0.57	0.05
MODIS AOD	0.39	0.11	54.00	0.00	0.16	0.61
Brightness temperature	0.42	0.12	54.00	0.00	0.18	0.67
Factory density	0.31	0.13	54.00	0.03	0.04	0.58

Table 6.41 Estimates of covariance parameters in the summer season.

Parameter		Estimate	Std. Error
Residual		0.33	0.13
Intercept [subject = ID_district]	Variance	0.33	0.00

From Table 6.21, the maximum value is 45.22 μg/m^3 in Chaloem Phra Kiat District, Saraburi province. In contrast, the minimum value is 42.69 μg/m^3 in Lat Lum Kaeo District, Pathum Thani province.

The classification maps of prediction values for PM10 concentration using the MEM model according to the Thailand Air Quality Index and the U.S. EPA Air Quality Index are displayed in Figure 6.59.

Thus, the predicted values of PM10 concentration are excellent at level 1 of Thailand AQI and good at level 1 of EPA AQI. Additionally, the predicted value in rural landscape in the summer season from the MEM model is less than the one-day mean of WHO guidelines. See Table 5.3.

In addition, a spatial distribution map of PM10 concentration in the summer season using the SCK interpolation technique is displayed in Figure 6.60. As a result, the high PM10 concentration occur on agricultural land in the central part of the study area, particularly in Saraburi province.

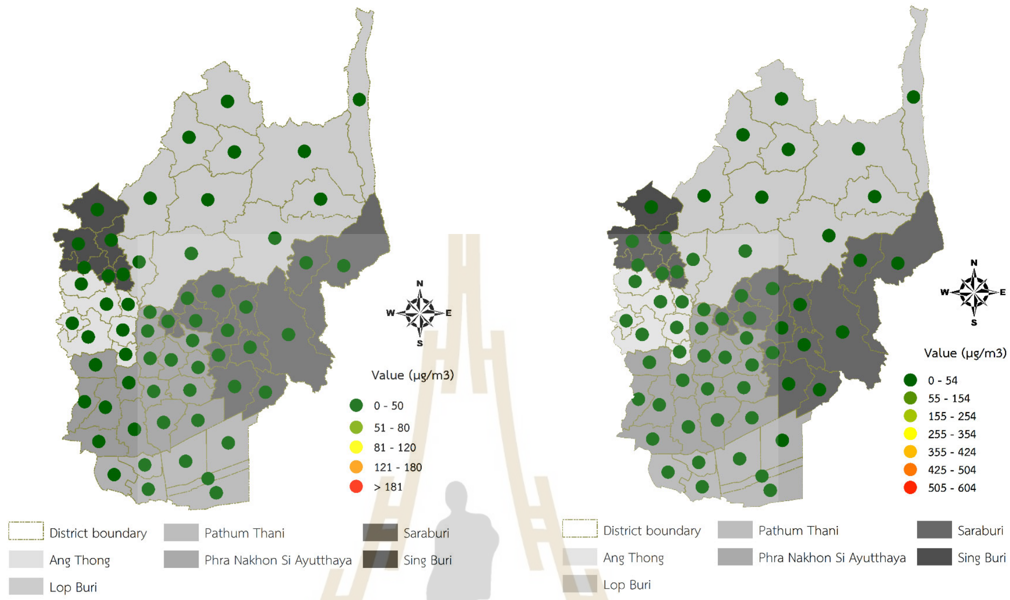

(a) (b)

Figure 6.59 The classification map of PM10 concentration prediction using the MEM model in the summer season according to the (a) Thailand AQI and (b) EPA AQI.

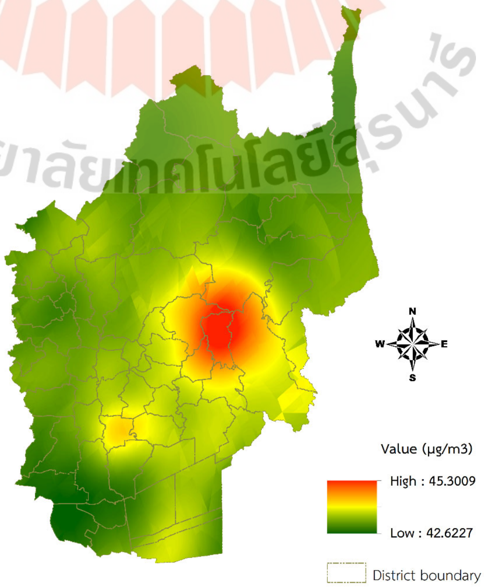

Figure 6.60 Spatial distribution of PM10 concentration in the summer season.

6.4 The predictive equations and their distribution map for spatiotemporal PM2.5 concentration in the urban landscape using the MEM model

Under this section, the MEM model with the significant derived factors was applied to predict the urban landscape's monthly PM2.5 concentration in winter and summer. The model structure for PM2.5 concentration in the winter and summer is shown in Equations 6.7 and 6.8.

$$PM2.5_{i,j}=\mu+\beta_1 RH_{i,j}+\beta_2 TEMP_{i,j}+\beta_3 WS_{i,j}+\beta_4 P_{i.j}+\beta_5 VIS_{i,j}+\beta_6 BT_{i,j} + \beta_7 FRP_{i,j}+\beta_8 FH_{i,j}+\beta_9 AOD_{i,j}+\beta_{10} ELEV_{i,j}+\varepsilon \quad (6.7)$$

Where $PM2.5_{i,j}$ is the averaged PM2.5 concentration at district i on month j in the winter season; μ is the fixed intercept; β_1 - β_{10} are coefficients of fixed effect for independent variables; $RH_{i,j}$, $TEMP_{i,j}$, $WS_{i,j}$, $P_{i.j}$, $VIS_{i,j}$, $BT_{i,j}$, $FRP_{i,j}$, $FH_{i,j}$, $AOD_{i,j}$, $ELEV_{i,j}$ are relative humidity, temperature, wind speed, pressure, visibility, brightness temperature, fire radiative power, fire hotspot, MODIS AOD, elevation at district i on month j, respectively and **ε** is the residual error.

$$PM2.5_{i,j}=\mu+\beta_1 VIS_{i,j}+\beta_2 WS_{i,j}+\beta_3 BT_{i,j}+\beta_4 FRP_{i.j}+\beta_5 FH_{i,j}+\beta_6 AOD_{i,j} + \beta_7 FD_{i,j}+\beta_8 ELEV_{i,j}+\varepsilon \quad (6.8)$$

Where $PM2.5_{i,j}$ is the averaged PM2.5 concentration at district i on month j in the summer season; μ is the fixed intercept; β_1 - β_8 are coefficients of fixed effect for independent variables; $VIS_{i,j}$, $WS_{i,j}$, $BT_{i,j}$, $FRP_{i,j}$, $FH_{i,j}$, $AOD_{i,j}$, $FD_{i,j}$, $ELEV_{i,j}$ are visibility, wind speed, brightness temperature, fire radiative power, fire hotspot, MODIS AOD, factory density, and elevation at district i on month j, respectively and **ε** is the residual error.

The monthly predictive equation for PM2.5 concentration in the urban landscape using the MEM model with the significant derived factors in winter and summer is systematically reported in two tabular forms in the following sections. The first table shows the intercept's value of the parameter associated with the rural area in each month (columns 1 and 2) and the standard error of the sample mean, degree of freedom to determine the observed significance level (columns 3 to 5) and the smallest and largest value that exceeds the lower and upper bound fall outside the confidence interval range (columns 6 and 7). Meanwhile, the second table shows parameter estimates associated with a covariance matrix in column 2 and the standard error of a parameter estimate associated with a covariance matrix in column 3. Besides, the performance of the MEM model for PM2.5 concentration in the urban landscape is reported, including AIC, AICc, and BIC.

The summary of PM2.5 concentration in micrograms per cubic meter using the MEM model in an urban landscape is shown in Table 6.42.

Table 6.42 The prediction value of PM2.5 concentration in each month and season using the MEM model.

No.	DISTRICT	PROVINCE	OCT	NOV	DEC	JAN	FEB	MAR	APR	MAY	WINTER	SUMMER
1	Bang Bon	Bangkok	28.16	35.09	39.84	43.49	44.07	23.37	21.76	16.69	38.14	20.61
2	Bang Kapi	Bangkok	26.40	33.73	39.63	43.67	44.15	23.54	22.35	16.77	37.47	20.90
3	Bang Khae	Bangkok	27.99	34.99	39.93	43.51	44.19	23.26	21.71	16.74	38.06	20.59
4	Bang Khen	Bangkok	27.09	34.03	39.77	43.74	44.30	23.64	22.34	16.82	37.79	20.92
5	Bang Kho Laem	Bangkok	27.64	34.26	39.88	43.63	44.06	23.26	21.60	16.69	37.87	20.47
6	Bang Khun Thian	Bangkok	27.76	34.76	39.68	43.37	44.04	23.41	22.00	16.72	38.14	20.73
7	Bang Na	Bangkok	26.47	33.82	39.58	43.55	43.98	23.30	21.90	16.71	37.38	20.64
8	Bang Phlat	Bangkok	27.73	34.57	40.08	43.71	44.21	23.06	21.58	16.77	38.04	20.47
9	Bang Rak	Bangkok	27.58	34.20	40.00	43.68	44.13	23.44	21.79	16.75	38.06	20.63
10	Bang Sue	Bangkok	27.29	34.46	40.02	43.58	44.21	23.24	21.74	16.77	37.97	20.57
11	Bangkok Noi	Bangkok	27.71	34.41	40.08	43.77	44.24	23.19	21.79	16.77	38.09	20.56
12	Bangkok Yai	Bangkok	27.66	34.28	40.02	43.69	44.21	23.35	21.83	16.73	38.02	20.58
13	Bueng Kum	Bangkok	26.49	33.84	39.63	43.77	44.23	23.55	22.23	16.79	37.56	20.86
14	Chatuchak	Bangkok	27.10	34.34	39.97	43.62	44.21	23.31	21.87	16.79	37.88	20.67
15	Chom Thong	Bangkok	27.95	34.80	39.91	43.43	44.10	23.19	21.59	16.70	37.98	20.48
16	Din Daeng	Bangkok	27.41	34.17	39.91	43.51	44.10	23.10	21.70	16.77	37.73	20.52
17	Don Mueang	Bangkok	27.06	34.41	39.92	43.78	44.36	23.75	22.39	16.82	37.93	20.95
18	Dusit	Bangkok	27.88	34.50	40.06	43.64	44.18	23.06	21.73	16.78	37.97	20.52
19	Huai Khwang	Bangkok	26.95	34.06	39.82	43.49	44.08	23.26	21.86	16.77	37.60	20.64
20	Khan Na Yao	Bangkok	26.58	33.78	39.55	43.77	44.22	23.45	22.26	16.79	37.51	20.81

Table 6.42 (Continued).

No.	DISTRICT	PROVINCE	OCT	NOV	DEC	JAN	FEB	MAR	APR	MAY	WIN TER	SUM MER
21	Khlong Sam Wa	Bangkok	26.31	33.68	39.44	43.71	44.27	23.55	22.34	16.78	37.40	20.88
22	Khlong San	Bangkok	27.69	34.37	40.00	43.72	44.14	23.36	21.75	16.72	38.00	20.56
23	Khlong Toei	Bangkok	26.89	34.04	39.84	43.51	44.04	23.29	21.69	16.73	37.64	20.58
24	Lak Si	Bangkok	27.06	34.54	40.00	43.78	44.31	23.66	22.28	16.82	37.98	20.89
25	Lat Krabang	Bangkok	25.79	33.02	39.21	43.75	44.03	23.45	22.23	16.77	36.97	20.81
26	Lat Phrao	Bangkok	26.95	34.06	39.79	43.65	44.20	23.42	22.23	16.79	37.72	20.88
27	Min Buri	Bangkok	26.22	33.11	39.34	43.75	44.16	23.44	22.32	16.78	37.24	20.82
28	Nong Chok	Bangkok	26.01	33.05	39.25	43.74	44.20	23.54	22.22	16.78	37.14	20.88
29	Nong Khaem	Bangkok	28.08	35.07	39.90	43.54	44.18	23.31	21.71	16.73	38.14	20.63
30	Pathum Wan	Bangkok	27.69	34.23	40.03	43.63	44.12	23.30	21.77	16.78	37.97	20.64
31	Phasi Charoen	Bangkok	28.08	34.62	39.99	43.52	44.20	23.26	21.76	16.74	38.00	20.57
32	Phaya Thai	Bangkok	27.43	34.32	39.98	43.59	44.12	23.03	21.67	16.79	37.87	20.50
33	Phra Khanong	Bangkok	26.48	33.69	39.63	43.52	44.00	23.23	21.85	16.73	37.38	20.60
34	Phra Nakhon	Bangkok	27.86	34.47	40.08	43.75	44.21	23.21	21.81	16.77	38.08	20.59
35	Pom Prap Sattru Phai	Bangkok	27.85	34.44	40.07	43.72	44.20	23.30	21.75	16.73	38.10	20.52
36	Prawet	Bangkok	26.18	33.39	39.44	43.54	43.99	23.38	22.13	16.74	37.18	20.75
37	Rat Burana	Bangkok	27.73	34.40	39.81	43.47	44.03	23.10	21.50	16.68	37.82	20.39
38	Ratchathe wi	Bangkok	27.69	34.21	40.02	43.63	44.12	23.15	21.71	16.77	37.91	20.54
39	Sai Mai	Bangkok	26.69	34.02	39.74	43.71	44.34	23.71	22.38	16.82	37.71	20.95
40	Samphant hawong	Bangkok	27.78	34.12	40.05	43.66	44.19	23.42	21.85	16.74	38.00	20.63
41	Saphan Sung	Bangkok	26.18	33.26	39.46	43.74	44.09	23.42	22.17	16.77	37.22	20.78
42	Sathon	Bangkok	27.38	34.22	39.94	43.64	44.08	23.37	21.69	16.72	37.92	20.56
43	Suan Luang	Bangkok	26.28	33.63	39.62	43.49	44.06	23.40	22.03	16.75	37.36	20.72
44	Taling Chan	Bangkok	27.78	34.51	39.98	43.68	44.24	23.21	21.73	16.77	38.07	20.58
45	Thawi Watthana	Bangkok	27.75	34.61	40.03	43.54	44.25	23.25	21.71	16.77	38.05	20.65

Table 6.42 (Continued).

No.	DISTRICT	PROVINCE	OCT	NOV	DEC	JAN	FEB	MAR	APR	MAY	WIN TER	SUM MER
46	Thon Buri	Bangkok	27.96	34.45	39.99	43.66	44.15	23.28	21.73	16.72	38.02	20.54
47	Thung Khru	Bangkok	27.49	34.55	39.65	43.40	44.01	23.19	21.75	16.72	37.84	20.58
48	Vadhana	Bangkok	26.98	33.94	39.80	43.58	44.07	23.28	21.77	16.76	37.64	20.61
49	Wang Thonglang	Bangkok	26.70	34.01	39.74	43.58	44.14	23.38	22.05	16.77	37.56	20.74
50	Yan Nawa	Bangkok	27.10	34.20	39.79	43.63	44.02	23.27	21.59	16.70	37.72	20.50
51	Bang Len	Nakhon Pathom	26.53	33.82	40.31	43.63	44.26	23.44	21.90	16.76	37.94	20.69
52	Don Tum	Nakhon Pathom	26.85	34.11	40.40	43.62	44.22	23.43	21.94	16.75	37.99	20.72
53	Kamphaeng Saen	Nakhon Pathom	27.03	33.98	40.33	43.68	44.24	23.47	22.00	16.77	37.85	20.69
54	Mueang Nakhon Pathom	Nakhon Pathom	27.15	34.82	40.38	43.80	44.20	23.42	21.95	16.75	38.18	20.70
55	Nakhon Chai Si	Nakhon Pathom	27.24	34.76	40.19	43.67	44.20	23.41	21.90	16.75	38.08	20.71
56	Phuttham onthon	Nakhon Pathom	27.41	34.46	40.10	43.62	44.22	23.38	21.82	16.76	38.07	20.67
57	Sam Phran	Nakhon Pathom	27.60	35.10	40.07	43.61	44.20	23.39	21.84	16.74	38.20	20.69
58	Bang Bua Thong	Nonthab uri	27.25	34.80	40.14	43.77	44.28	23.43	21.87	16.77	37.93	20.67
59	Bang Kruai	Nonthab uri	27.60	34.67	40.03	43.68	44.25	23.26	21.72	16.77	38.08	20.60
60	Bang Yai	Nonthab uri	27.62	34.69	40.14	43.69	44.25	23.38	21.82	16.76	38.06	20.66
61	Mueang Nonthaburi	Nonthab uri	27.24	34.89	40.00	43.66	44.26	23.37	21.84	16.79	38.05	20.66
62	Pak Kret	Nonthab uri	27.14	35.07	40.08	43.72	44.30	23.52	21.97	16.79	38.00	20.74
63	Sai Noi	Nonthab uri	26.52	34.27	40.25	43.72	44.27	23.43	21.86	16.77	38.01	20.69
64	Bang Bo	Samut Prakan	25.45	32.64	38.93	43.64	44.02	23.40	22.01	16.75	36.84	20.71
65	Bang Phli	Samut Prakan	26.09	33.31	39.21	43.53	43.98	23.47	22.22	16.71	37.05	20.87

Table 6.42 (Continued).

No.	DISTRICT	PROVINCE	OCT	NOV	DEC	JAN	FEB	MAR	APR	MAY	WINTER	SUMMER
66	Bang Sao Thong	Samut Prakan	25.69	32.87	39.04	43.68	44.02	23.44	22.30	16.75	36.94	20.88
67	Mueang Samut Prakan	Samut Prakan	26.33	33.60	39.30	43.45	43.99	23.44	22.12	16.70	37.32	20.77
68	Phra Pradaeng	Samut Prakan	27.03	34.13	39.63	43.48	43.99	23.20	21.71	16.70	37.60	20.54
69	Phra Samut Chedi	Samut Prakan	27.12	34.00	39.41	43.30	44.02	23.33	22.01	16.72	37.85	20.70
70	Ban Phaeo	Samut Sakhon	27.70	35.54	40.00	43.78	44.11	23.39	21.93	16.73	38.31	20.72
71	Krathum Baen	Samut Sakhon	28.05	35.19	39.96	43.64	44.13	23.38	21.76	16.72	38.23	20.68
72	Mueang Samut Sakhon	Samut Sakhon	27.73	35.27	39.81	43.66	44.05	23.35	21.87	16.72	38.32	20.70

6.4.1 October 2019 in the winter season

The MEM model results are shown in Table 6.43 and Table 6.44. The model performance shows that AIC, AICc, and BIC values are 127.83, 128.03, and 132.11, respectively.

Table 6.43 Estimates of Fixed Effects in October 2019.

Parameter	Estimate	St. Error	df	Sig.	95% Confidence Interval	
					Lower Bound	Upper Bound
Intercept	0.00	0.06	63.00	1.00	-0.11	0.11
Wind speed	0.27	0.09	63.00	0.00	0.09	0.44
Pressure	0.15	0.07	63.00	0.04	0.01	0.29
Visibility	0.21	0.08	63.00	0.01	0.05	0.37
Brightness temperature	-0.17	0.08	63.00	0.04	-0.33	-0.01
Fire radiative power	-0.18	0.09	63.00	0.04	-0.36	-0.01
MODIS AOD	0.71	0.07	63.00	0.00	0.58	0.85
Fire hotspot	-0.18	0.08	63.00	0.03	-0.34	-0.02
Elevation	0.46	0.08	63.00	0.00	0.31	0.62

Table 6.44 Estimates of covariance parameters in October 2019.

Parameter		Estimate	Std. Error
Residual		0.12	0.04
Intercept [subject = ID_district]	Variance	0.12	0.00

From Table 6.42, the maximum value is 28.16 μg/m^3 in Bang Bon, Bangkok. In contrast, the minimum value is 25.45 μg/m^3 in Bang Bo District, Samut Prakan province. The classification maps of prediction values for PM2.5 concentration using the MEM model according to the Thailand Air Quality Index and the U.S. EPA Air Quality Index are displayed in Figure 6.61.

Thus, predicted values of PM2.5 concentration are satisfactory at level 2 of Thailand AQI and moderate at level 2 of EPA AQI. On the other hand, the predicted value in an urban landscape in October 2019 from the MEM model is more than the one-day mean of WHO guidelines. See Table 5.3.

In addition, a spatial distribution map of PM2.5 concentration in October 2019 using the SCK interpolation technique is displayed in Figure 6.62. As a result, the high PM2.5 concentration occur in urban areas in the central part of the study area, particularly in Bangkok Metropolitan and Samut Sakhon province.

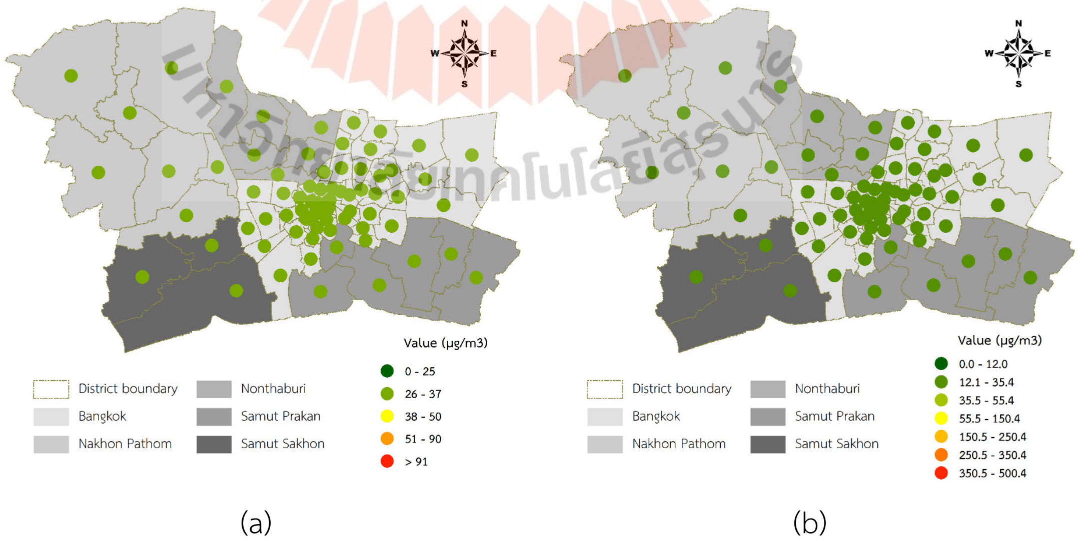

Figure 6.61 The classification map of PM2.5 concentration prediction using the MEM model in October 2019 according to the (a) Thailand AQI and (b) EPA AQI.

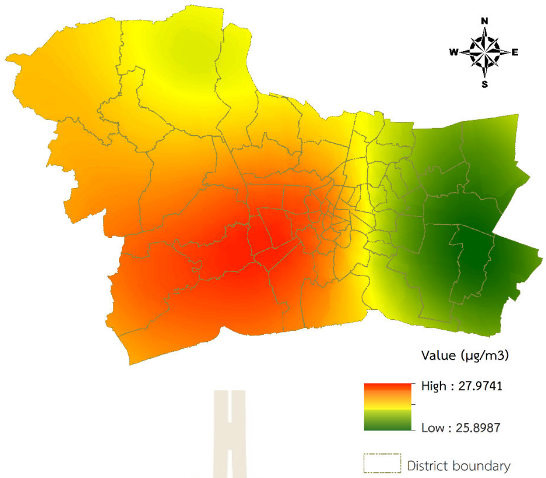

Figure 6.62 Spatial distribution of PM2.5 concentration in October 2019.

6.4.2 November 2019 in the winter season

The MEM model results are shown in Table 6.45 and Table 6.46. The model performance shows that AIC, AICc, and BIC values are 187.15, 187.33, and 191.62, respectively.

Table 6.45 Estimates of Fixed Effects in November 2019.

Parameter	Estimate	St. Error	df	Sig.	95% Confidence Interval	
					Lower Bound	Upper Bound
Intercept	0.00	0.10	69.00	1.00	-0.20	0.20
Visibility	0.40	0.10	69.00	0.00	0.20	0.60
Fire radiative power	0.37	0.10	69.00	0.00	0.17	0.57

Table 6.46 Estimates of covariance parameters in November 2019.

Parameter		Estimate	Std. Error
Residual		0.35	0.12
Intercept [subject = ID_district]	Variance	0.35	0.00

From Table 6.42, the maximum value is 35.54 µg/m^3 in Ban Phaeo District, Samut Sakhon province. In contrast, the minimum value is 32.64 µg/m^3 in Bang Bo District, Samut Sakhon province. The classification maps of prediction values for PM2.5 concentration using the MEM model according to the Thailand Air Quality Index and the U.S. EPA Air Quality Index are displayed in Figure 6.63.

Thus, the predicted values of PM2.5 concentration are satisfactory at level 2 of Thailand AQI and moderate at level 2 and unhealthy for sensitive groups at level 3 of EPA AQI. On the other hand, the predicted value in an urban landscape in November 2019 from the MEM model is more than the one-day mean of WHO guidelines. See Table 5.3.

In addition, a spatial distribution map of PM2.5 concentration in November 2019 using the SCK interpolation technique is displayed in Figure 6.64. As a result, the high PM2.5 concentration occur in urban areas in the western part of the study area, mainly in Samut Sakhon province and Bangkok Metropolitan.

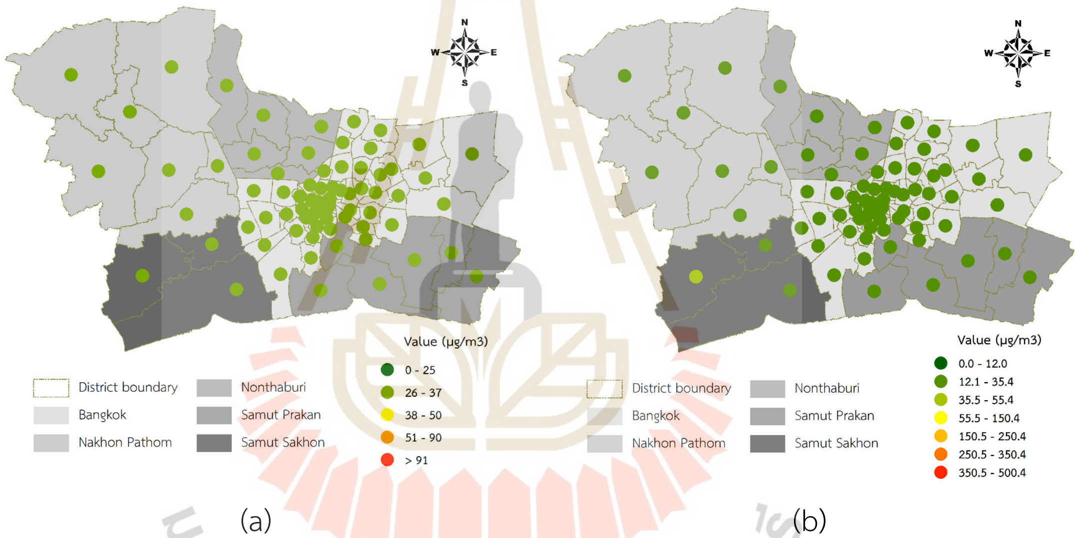

Figure 6.63 The classification map of PM2.5 concentration prediction using the MEM model in November 2019 according to the (a) Thailand AQI and (b) EPA AQI.

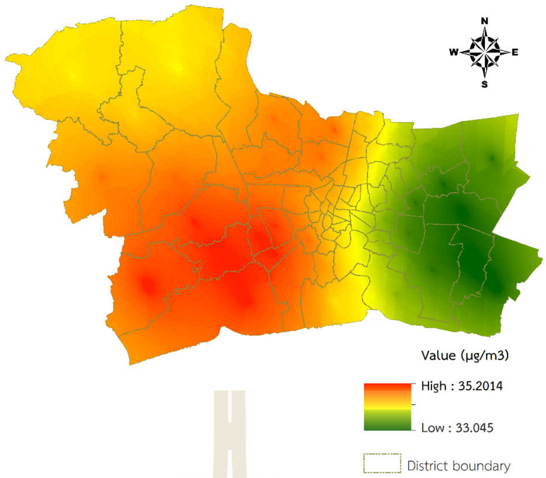

Figure 6.64 Spatial distribution of PM2.5 concentration in November 2019.

6.4.3 December 2019 in the winter season

The MEM model results are shown in Table 6.47 and Table 6.48. The model performance shows that AIC, AICc, and BIC values are 191.28, 191.46, and 195.75, respectively.

Table 6.47 Estimates of Fixed Effects in December 2019.

Parameter	Estimate	St. Error	df	Sig.	95% Confidence Interval	
					Lower Bound	Upper Bound
Intercept	0.00	0.10	69.00	1.00	-0.20	0.20
Wind speed	-0.43	0.11	69.00	0.00	-0.64	-0.22
Visibility	0.22	0.11	69.00	0.04	0.01	0.43

Table 6.48 Estimates of covariance parameters in December 2019.

Parameter		Estimate	Std. Error
Residual		0.37	0.13
Intercept [subject = ID_district]	Variance	0.37	0.00

From Table 6.42, the maximum value is 40.40 µg/m^3 in Don Tum District, Nakhon Pathom province. In contrast, the minimum value is 38.93 µg/m^3 in Bang Bo District, Samut Prakan province. The classification maps of prediction values for PM2.5 concentration using the MEM model according to the Thailand Air Quality Index and the U.S. EPA Air Quality Index are displayed in Figure 6.65.

Thus, the predicted values of PM2.5 concentration are moderate at level 3 of Thailand AQI and unhealthy for sensitive groups at level 3 of EPA AQI. On the other hand, the predicted value in an urban landscape in December 2019 from the MEM model is more than the one-day mean of WHO guidelines. See Table 5.3.

In addition, a spatial distribution map of PM2.5 concentration in December 2019 using the SCK interpolation technique is displayed in Figure 6.66. As a result, the high PM2.5 concentration occur in urban areas in the central and western parts of the study area, mainly in Bangkok Metropolitan and Samut Sakhon province.

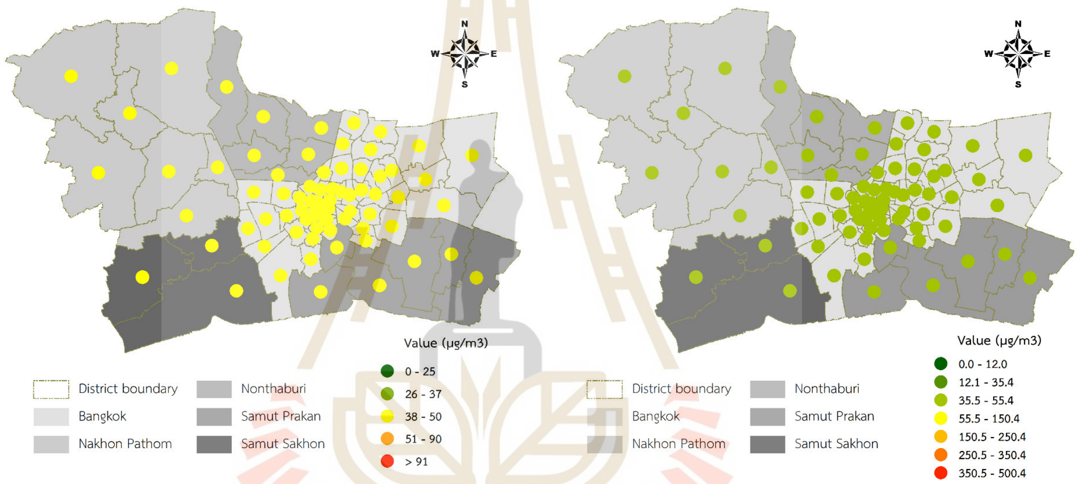

(a) (b)

Figure 6.65 The classification map of PM2.5 concentration prediction using the MEM model in December 2019 according to the (a) Thailand AQI and (b) EPA AQI.

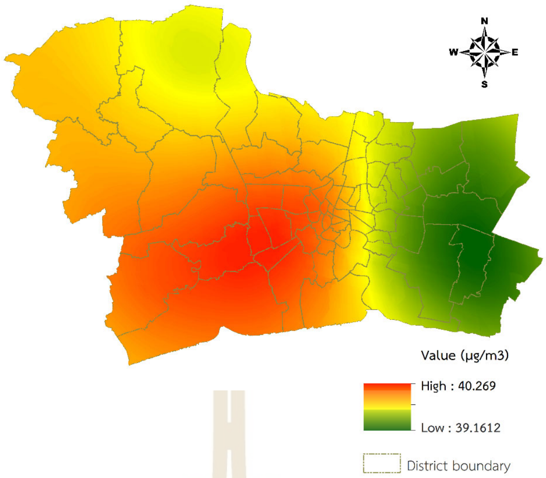

Figure 6.66 Spatial distribution of PM2.5 concentration in December 2019.

6.4.4 January 2020 in the winter season

The MEM model results are shown in Table 6.49 and Table 6.50. The model performance shows that AIC, AICc, and BIC values are 194.09, 194.28, and 198.47, respectively.

Table 6.49 Estimates of Fixed Effects in January 2020.

Parameter	Estimate	St. Error	df	Sig.	95% Confidence Interval	
					Lower Bound	Upper Bound
Intercept	0.00	0.10	66.00	1.00	-0.20	0.20
Temperature	-0.43	0.12	66.00	0.00	-0.66	-0.19
Visibility	0.29	0.14	66.00	0.04	0.02	0.56
MODIS AOD	-0.57	0.12	66.00	0.00	-0.81	-0.32
Fire hotspot	0.28	0.12	66.00	0.03	0.03	0.52
Elevation	0.38	0.11	66.00	0.00	0.15	0.61

Table 6.50 Estimates of covariance parameters in January 2020.

Parameter		Estimate	Std. Error
Residual		0.36	0.13
Intercept [subject = ID_district]	Variance	0.36	0.00

From Table 6.42, the maximum value is 43.80 μg/m^3 in Mueang Nakhon Pathom District, Samut Prakan province. In contrast, the minimum value is 43.30 μg/m^3 in Phra Samut Chedi District, Samut Prakan province. The classification maps of prediction values for PM2.5 concentration using the MEM model according to the Thailand Air Quality Index and the U.S. EPA Air Quality Index are displayed in Figure 6.67.

Thus, the predicted values of PM2.5 concentration are moderate at level 3 of Thailand AQI and unhealthy for sensitive groups at level 3 of EPA AQI. On the other hand, the predicted value in an urban landscape in January 2020 from the MEM model is more than the one-day mean of WHO guidelines. See Table 5.3.

In addition, a spatial distribution map of PM2.5 concentration in January 2020 using the SCK interpolation technique is displayed in Figure 6.68. As a result, the high PM2.5 concentration occur in urban areas in the central and western parts of the study area, mainly in Bangkok Metropolitan and Samut Sakhon province.

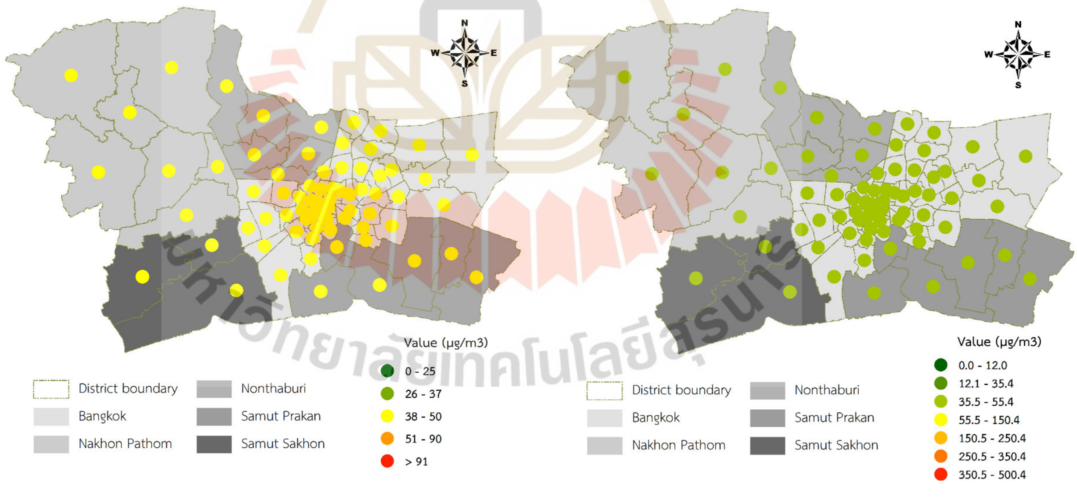

(a) (b)

Figure 6.67 The classification map of PM2.5 concentration prediction using the MEM model in January 2020 according to the (a) Thailand AQI and (b) EPA AQI.

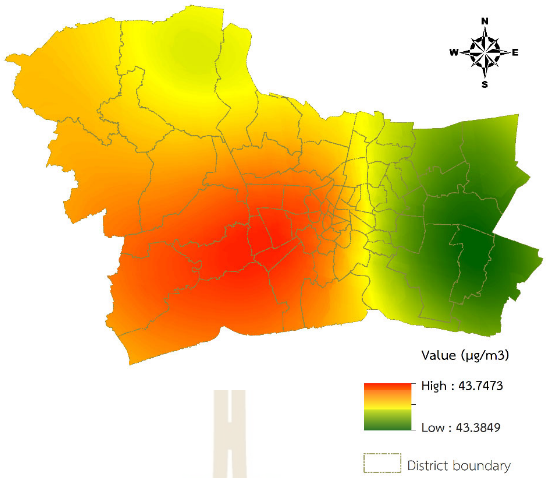

Figure 6.68 Spatial distribution of PM2.5 concentration in January 2020.

6.4.5 February 2020 in the winter season

The result of the MEM model is shown in Tables 6.51 and 6.52. The model performance shows that AIC, AICc, and BIC values are 141.76, 141.95, and 146.14, respectively.

Table 6.51 Estimates of Fixed Effects in February 2020.

Parameter	Estimate	St. Error	df	Sig.	95% Confidence Interval	
					Lower Bound	Upper Bound
Intercept	0.00	0.07	66.00	1.00	-0.13	0.13
Relative humidity	-0.59	0.07	66.00	0.00	-0.73	-0.44
Wind speed	0.32	0.10	66.00	0.00	0.13	0.52
Pressure	0.29	0.09	66.00	0.00	0.11	0.48
Fire radiative power	-0.54	0.09	66.00	0.00	-0.73	-0.36
Elevation	0.33	0.10	66.00	0.00	0.13	0.53

Table 6.52 Estimates of covariance parameters in February 2020.

Parameter		Estimate	Std. Error
Residual		0.16	0.06
Intercept [subject = ID_district]	Variance	0.16	0.00

From Table 6.42, the maximum value is 44.36 μg/m^3 in Don Mueang District, Bangkok. In contrast, the minimum value is 43.98 μg/m^3 in Bang Na District, Bangkok. The classification maps of prediction values for PM2.5 concentration using the MEM model according to the Thailand Air Quality Index and the U.S. EPA Air Quality Index are displayed in Figure 6.69.

Thus, the predicted values of PM2.5 concentration are moderate at level 3 of Thailand AQI and unhealthy for sensitive groups at level 3 of EPA AQI. On the other hand, the predicted value in an urban landscape in February 2020 from the MEM model is still more than the one-day mean of WHO guidelines. See Table 5.3.

In addition, a spatial distribution map of PM2.5 concentration in February 2020 using the SCK interpolation technique is displayed in Figure 6.70. As a result, the high PM2.5 concentration occur in urban areas in the central and western parts of the study area, mainly in Bangkok Metropolitan and Samut Sakhon province.

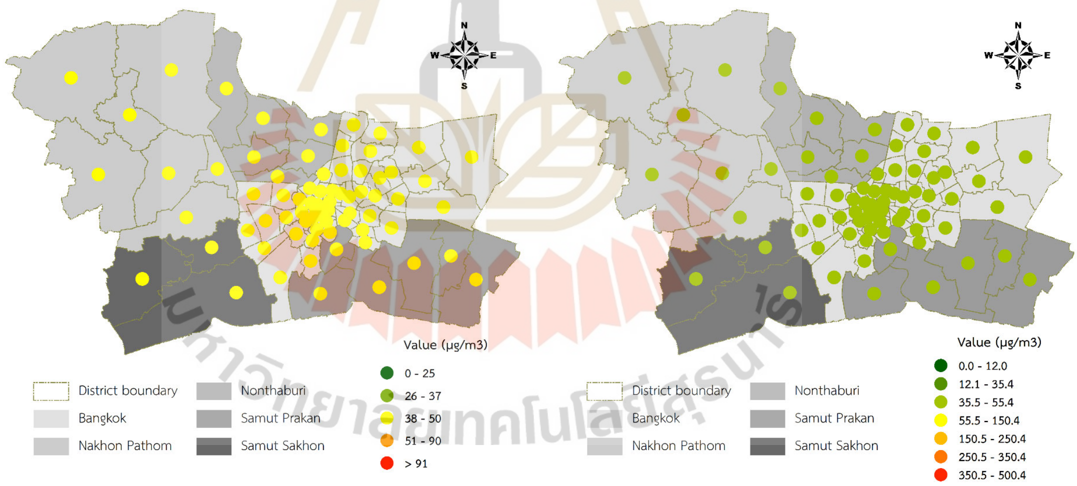

(a) (b)

Figure 6.69 The classification map of PM2.5 concentration prediction using the MEM model in February 2020 according to the (a) Thailand AQI and (b) EPA AQI.

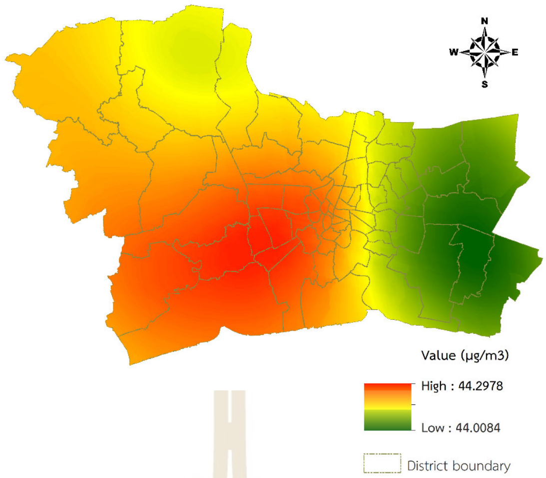

Figure 6.70 Spatial distribution of PM2.5 concentration in February 2020.

6.4.6 March 2020 in the summer season

The MEM model results are shown in Table 6.53 and Table 6.54. The model performance shows that AIC, AICc, and BIC values are 210.44, 210.62, and 214.94, respectively.

Table 6.53 Estimates of Fixed Effects in March 2020.

Parameter	Estimate	St. Error	df	Sig.	95% Confidence Interval	
					Lower Bound	Upper Bound
Intercept	0.00	0.12	70.00	1.00	-0.23	0.23
Fire radiative power	0.16	0.12	70.00	0.19	-0.08	0.39

Table 6.54 Estimates of covariance parameters in March 2020.

Parameter		Estimate	Std. Error
Residual		0.49	0.17
Intercept [subject = ID_district]	UN (1,1)	0.49	0.00

From Table 6.42, the maximum value is 23.75 µg/m^3 in Don Mueang District, Bangkok. In contrast, the minimum value is 23.03 µg/m^3 in Phaya Thai District, Bangkok. The classification maps of prediction values for PM2.5 concentration using the MEM model according to the Thailand Air Quality Index and the U.S. EPA Air Quality Index are displayed in Figure 6.71.

Thus, the predicted values of PM2.5 concentration are excellent at level 1 of Thailand AQI but moderate at level 2 of EPA AQI. Additionally, the predicted value in an urban landscape in March 2020 from the MEM model is more than the one-day mean of WHO guidelines. See Table 5.3.

In addition, a spatial distribution map of PM2.5 concentration in March 2020 using the SCK interpolation technique is displayed in Figure 6.72. As a result, the high PM2.5 concentration occur in urban areas in the northern part of the study area, mainly in Bangkok Metropolitan.

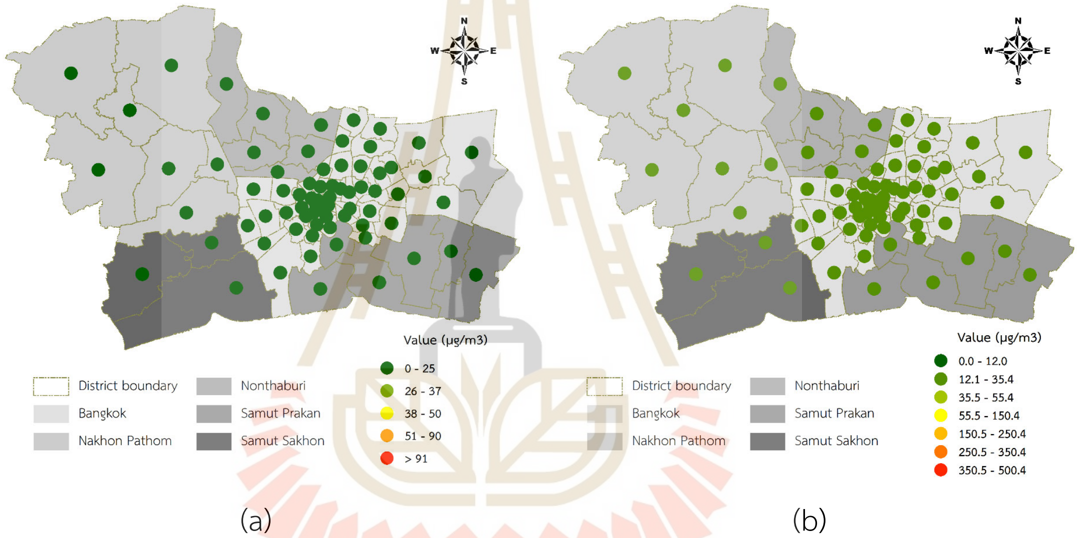

Figure 6.71 The classification map of PM2.5 concentration prediction using the MEM model in March 2020 according to the (a) Thailand AQI and (b) EPA AQI.

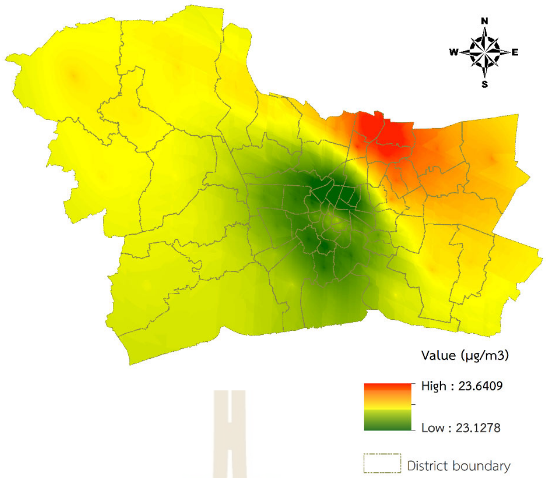

Figure 6.72 Spatial distribution of PM2.5 concentration in March 2020.

6.4.7 April 2020 in the summer season

The MEM model results are shown in Table 6.55 and Table 6.56. The model performance shows that AIC, AICc, and BIC values are 175.16, 175.35, and 179.54, respectively.

Table 6.55 Estimates of Fixed Effects in April 2020.

Parameter	Estimate	St. Error	df	Sig.	95% Confidence Interval	
					Lower Bound	Upper Bound
Intercept	0.00	0.08	64.00	1.00	-0.17	0.17
Wind speed	0.54	0.11	64.00	0.00	0.31	0.76
Visibility	0.45	0.11	64.00	0.00	0.24	0.66
Brightness temperature	-0.29	0.10	64.00	0.01	-0.50	-0.09
Fire radiative power	-0.41	0.13	64.00	0.00	-0.66	-0.15
MODIS AOD	0.24	0.10	64.00	0.01	0.05	0.43
Fire hotspot	0.25	0.09	64.00	0.01	0.07	0.42
Factory density	-0.24	0.10	64.00	0.02	-0.43	-0.04

Table 6.56 Estimates of covariance parameters in April 2020.

Parameter		Estimate	Std. Error
Residual		0.25	0.09
Intercept [subject = ID_district]	Variance	0.25	0.00

From Table 6.42, the maximum value is 22.39 µg/m^3 in Don Mueang District, Bangkok. In contrast, the minimum value is 21.50 µg/m^3 in Rat Burana District, Bangkok. The classification maps of prediction values for PM2.5 concentration using the MEM model presented according to the Thailand Air Quality Index and the U.S. EPA Air Quality Index are displayed in Figure 6.73.

Thus, the predicted values of PM2.5 concentration are excellent at level 1 of Thailand AQI but moderate at level 2 of EPA AQI. However, the predicted value in an urban landscape in April 2020 from the MEM model is more than the one-day mean of WHO guidelines. See Table 5.3.

In addition, a spatial distribution map of PM2.5 concentration in April 2020 using the SCK interpolation technique is displayed in Figure 6.74. As a result, the high PM2.5 concentration occur in urban areas in the northern part of the study area, mainly in Bangkok Metropolitan.

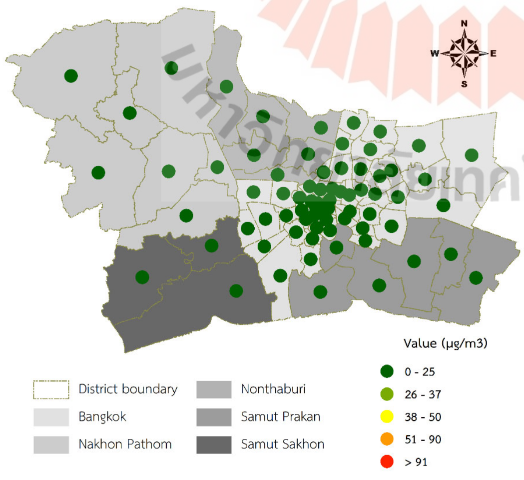

(a)

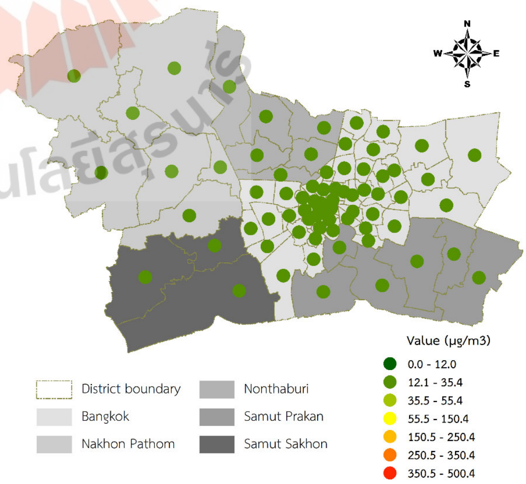

(b)

Figure 6.73 The classification map of PM2.5 concentration prediction using the MEM model in April 2020 according to the (a) Thailand AQI and (b) EPA AQI.

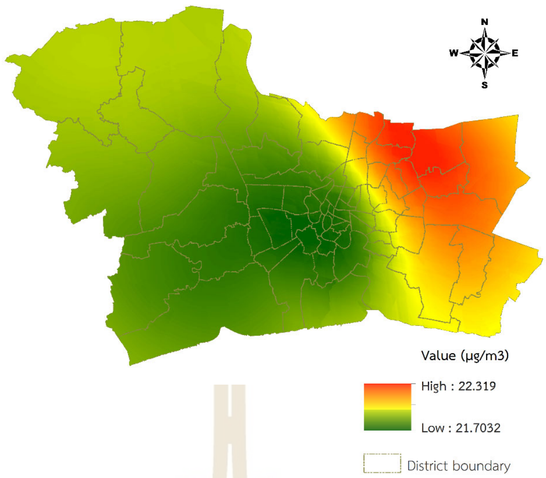

Figure 6.74 Spatial distribution of PM2.5 concentration in April 2020.

6.4.8 May 2020 in the summer season

The MEM model results are shown in Table 6.57 and Table 6.58. The model performance shows that AIC, AICc, and BIC values are 175.16, 175.35, and 179.54, respectively.

Table 6.57 Estimates of Fixed Effects in May 2020.

Parameter	Estimate	St. Error	df	Sig.	95% Confidence Interval	
					Lower Bound	Upper Bound
Intercept	0.00	0.09	66.00	1.00	-0.17	0.17
Wind speed	0.24	0.11	66.00	0.03	0.02	0.46
Visibility	-0.29	0.09	66.00	0.00	-0.47	-0.11
Brightness temperature	0.21	0.09	66.00	0.02	0.03	0.40
Factory density	-0.62	0.10	66.00	0.00	-0.82	-0.43
Elevation	0.48	0.11	66.00	0.00	0.25	0.70

Table 6.58 Estimates of covariance parameters in May 2020.

Parameter			Estimate	Std. Error
Residual			0.27	0.09
Intercept	[subject = ID_district]	Variance	0.27	0.00

From Table 6.42, the maximum value is 16.82 μg/m^3 in Don Mueang District, Bangkok. In contrast, the minimum value is 16.68 μg/m^3 in Rat Burana District, Bangkok. The classification maps of prediction values for PM2.5 concentration using the MEM model according to the Thailand Air Quality Index and the U.S. EPA Air Quality Index are displayed in Figure 6.75.

Thus, the predicted values of PM2.5 concentration are excellent at level 1 of Thailand AQI and moderate at level 2 of EPA AQI. However, the predicted value in an urban landscape in May 2020 from the MEM model is more than the one-day mean of WHO guidelines. See Table 5.3.

In addition, a spatial distribution map of PM2.5 concentration in May 2020 using the SCK interpolation technique is displayed in Figure 6.76. As a result, the high PM2.5 concentration occur in urban areas in the northern part of the study area, mainly in Bangkok Metropolitan.

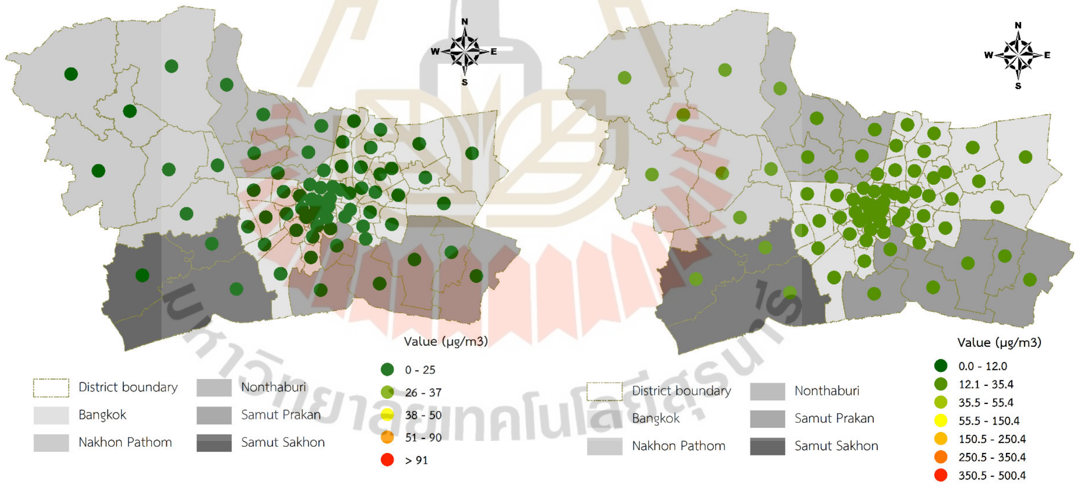

(a) (b)

Figure 6.75 The classification map of PM2.5 concentration prediction using the MEM model in May 2020 according to the (a) Thailand AQI and (b) EPA AQI.

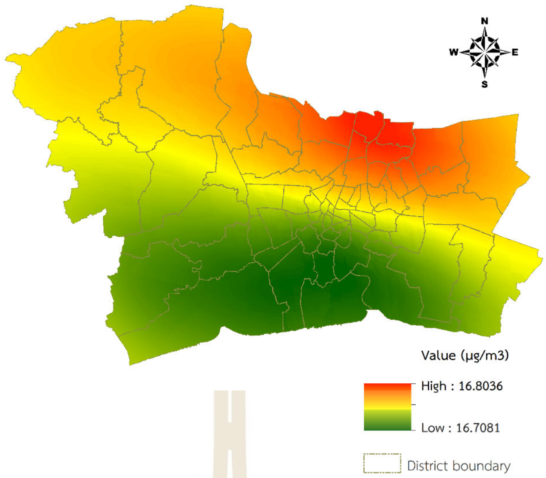

Figure 6.76 Spatial distribution of PM2.5 concentration in May 2020.

6.4.9 Winter season

The result of the MEM model for PM2.5 concentration prediction in the winter season (October to February) is summarized in Table 6.59 and Table 6.60. The model performance shows that AIC, AICc, and BIC values are 143.14, 143.34, and 147.36, respectively.

Table 6.59 Estimates of Fixed Effects in the winter season.

Parameter	Estimate	St. Error	df	Sig.	95% Confidence Interval	
					Lower Bound	Upper Bound
Intercept	0.00	0.06	61.00	1.00	-0.13	0.13
Relative humidity	1.25	0.28	61.00	0.00	0.70	1.81
Temperature	1.81	0.33	61.00	0.00	1.16	2.46
Wind speed	0.10	0.11	61.00	0.34	-0.11	0.32
Pressure	1.62	0.28	61.00	0.00	1.06	2.18
Visibility	0.00	0.10	61.00	0.96	-0.19	0.20
Brightness temperature	-0.19	0.11	61.00	0.11	-0.42	0.04
Fire radiative power	-0.47	0.13	61.00	0.00	-0.73	-0.22
Fire hotspot	-0.06	0.08	61.00	0.45	-0.22	0.10
MODIS AOD	-0.15	0.17	61.00	0.40	-0.49	0.20
Elevation	0.35	0.12	61.00	0.01	0.11	0.59

Table 6.60 Estimates of covariance parameters in the winter season.

Parameter		Estimate	Std. Error
Residual		0.15	0.05
Intercept [subject = ID_district]	Variance	0.15	0.00

From Table 6.42, the maximum value is 38.32 μg/m^3 in Mueang Samut Sakhon District, Samut Sakhon province. In contrast, the minimum value is 36.84 μg/m^3 in Bang Bo District, Samut Prakan province. The classification maps of prediction values for PM2.5 concentration using the MEM model according to the Thailand Air Quality Index and the U.S. EPA Air Quality Index are displayed in Figure 6.77.

Thus, the predicted values of PM2.5 concentration are moderate at level 3 of Thailand AQI and unhealthy for sensitive groups at level 3 of EPA AQI. The predicted value in an urban landscape using the MEM model in the winter is more than the one-day mean of WHO guidelines. See Table 5.3.

In addition, a spatial distribution map of PM2.5 concentration in the winter season using the SCK interpolation technique is displayed in Figure 6.78. As a result, the high PM2.5 concentration occur in urban areas in the western part of the study area, mainly in Nakhon Pathom and Samut Sakhon province.

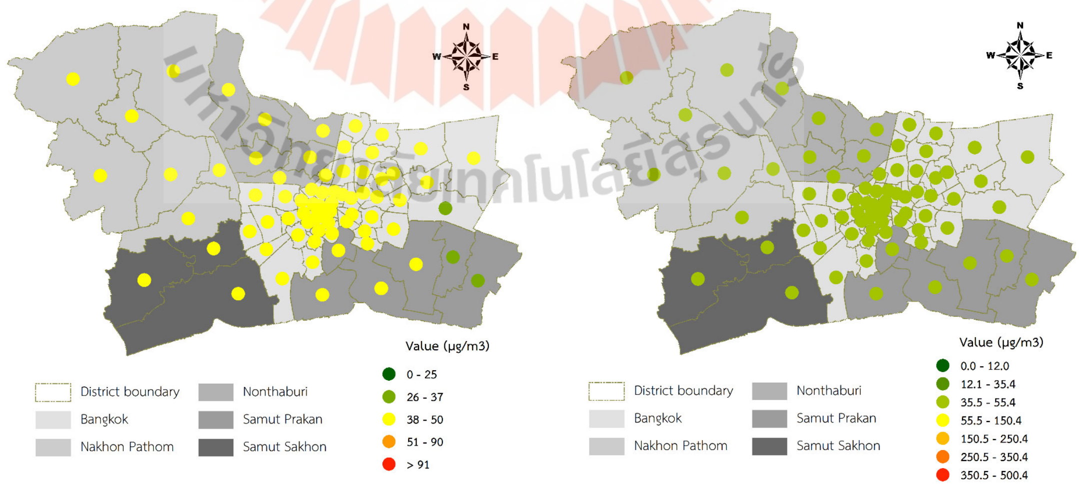

(a) (b)

Figure 6.77 The classification map of PM2.5 concentration prediction using the MEM model in the winter season according to the (a) Thailand AQI and (b) EPA AQI.

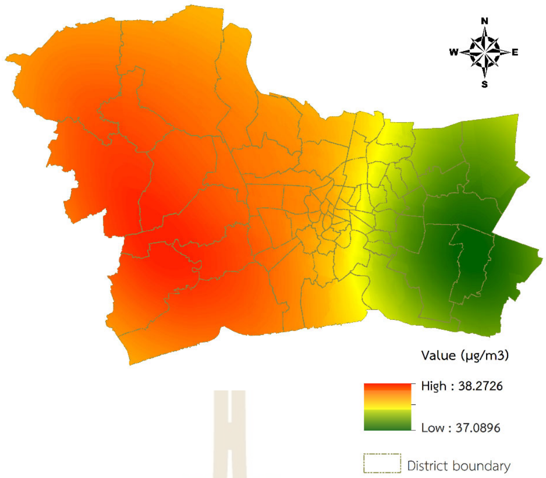

Figure 6.78 Spatial distribution of PM2.5 concentration in the winter season.

6.4.10 Summer season

The result of the MEM model for PM2.5 concentration prediction in the summer season (March to May) is summarized in Tables 6.61 and 6.62. The model performance shows that AIC, AICc, and BIC values are 204.10, 204.30 and 208.38, respectively.

Table 6.61 Estimates of Fixed Effects in the summer season.

Parameter	Estimate	St. Error	df	Sig.	95% Confidence Interval	
					Lower Bound	Upper Bound
Intercept	.00	.10	63.00	1.00	-.21	.21
Visibility	.14	.12	63.00	.24	-.10	.38
Wind speed	.16	.18	63.00	.38	-.21	.53
Brightness temperature	.01	.12	63.00	.91	-.22	.24
Fire radiative power	.07	.16	63.00	.65	-.25	.40
Fire hotspot	.25	.12	63.00	.05	.00	.49
MODIS AOD	.04	.12	63.00	.72	-.19	.28
Factory density	-.35	.12	63.00	.01	-.59	-.11
Elevation	-.01	.17	63.00	.94	-.36	.33

Table 6.62 Estimates of covariance parameters in the summer season.

Parameter		Estimate	Std. Error
Residual		0.39	0.14
Intercept [subject = ID_district]	Variance	0.39	0.00

From Table 6.42, the maximum value is 20.95 µg/m^3 in Sai Mai District, Bangkok. In contrast, the minimum value is 20.39 µg/m^3 in Rat Burana District, Bangkok. The classification maps of prediction values for PM2.5 concentration using the MEM model according to the Thailand Air Quality Index and the U.S. EPA Air Quality Index are displayed in Figure 6.79.

Thus, the predicted values of PM2.5 concentration are excellent at level 1 of Thailand AQI and moderate at level 2 of EPA AQI. Additionally, the predicted value in an urban landscape in the summer season from the MEM model is more than the one-day mean of WHO guidelines. See Table 5.3.

In addition, a spatial distribution map of PM2.5 concentration in the summer season using the SCK interpolation technique is displayed in Figure 6.80. As a result, the high PM2.5 concentration occur in urban areas in the northern part of the study area, mainly in Bangkok Metropolitan.

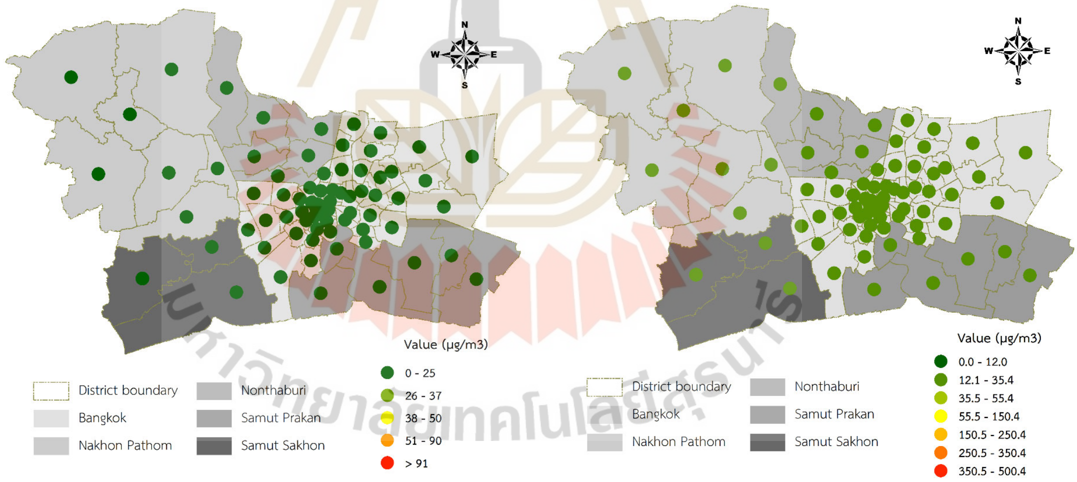

(a) (b)

Figure 6.79 The classification map of PM2.5 concentration prediction using the MEM model in the summer season according to the (a) Thailand AQI and (b) EPA AQI.

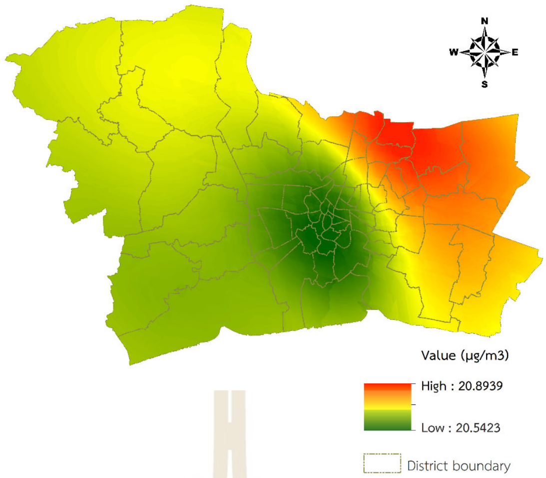

Figure 6.80 Spatial distribution of PM2.5 concentration in the summer season.

6.5 Comparison of spatiotemporal patterns of PM concentration using GWR and MEM models

The spatiotemporal patterns of PM10 and PM2.5 concentration using the GWR model as a local model and MEM model as a global model are summarized in terms of similarity/dissimilarity based on the derived results in Sections 6.1 to 6.4.

6.5.1 Monthly air quality index classification

Overall monthly AQI classification according to Thailand and US EPA standards of PM10 and PM2.5 concentration using the GWR and MEM models is summarized in Table 6.63 and Table 6.64, respectively.

As a result, in Tables 6.63 to 6.64, it can be observed that monthly AQI classifications according to Thailand and US EPA standards are similar. The interpretation of each AQI class from two standards should see the quantitative information in corresponding tables because the number of AQI classes and the quantity of PM10 and PM2.5 concentration are slightly different. Nevertheless, as a local model, the GWR model can provide the predictive equation for each district.

Table 6.63 Comparison of monthly AQI classification according to Thailand and US EPA standards of PM10 concentration using GWR and MEM model.

Month	AQI Classification by GWR model		AQI Classification by MEM model		Compare
	Thailand	US EPA	Thailand	US EPA	
October	Satisfactory	Good	Satisfactory	Good	Similarity
November	Satisfactory	Moderate	Satisfactory	Moderate	Similarity
December	Satisfactory	Moderate	Satisfactory	Moderate	Similarity
January	Satisfactory	Moderate	Satisfactory	Moderate	Similarity
February	Moderate	Moderate	Moderate	Moderate	Similarity
March	Excellent	Good	Excellent	Good	Similarity
April	Excellent	Good	Excellent	Good	Similarity
May	Excellent	Good	Excellent	Good	Similarity

Table 6.64 Comparison of monthly AQI classification according to Thailand and US EPA standards of PM2.5 concentration using GWR and MEM model.

Month	GWR model		MEM model		Compare
	Thailand	US EPA	Thailand	US EPA	
October	Satisfactory	Moderate	Satisfactory	Moderate	Similarity
November	Satisfactory	Moderate	Satisfactory	Moderate	Similarity
December	Moderate	Unhealthy for sensitive group	Moderate	Unhealthy for sensitive group	Similarity
January	Moderate	Unhealthy for sensitive group	Moderate	Unhealthy for sensitive group	Similarity
February	Moderate	Unhealthy for sensitive group	Moderate	Unhealthy for sensitive group	Similarity
March	Excellent	Moderate	Excellent	Moderate	Similarity
April	Excellent	Moderate	Excellent	Moderate	Similarity
May	Excellent	Moderate	Excellent	Moderate	Similarity

6.5.2 Seasonally air quality index classification

According to Thailand and US EPA standards of PM10 and PM2.5 concentration using the GWR and MEM models, seasonally, AQI classification is summarized in Table 6.65.

Table 6.65 Comparison of seasonally AQI classification according to Thailand and US EPA standards of PM10 and PM2.5 concentration using GWR and MEM model.

Season	GWR model		MEM model		Comparison
	Thailand	US EPA	Thailand	US EPA	
			PM10 concentration		
Winter	Satisfactory	Moderate	Satisfactory	Moderate	Similarity
Summer	Excellent	Good	Excellent	Good	Similarity
			PM2.5 concentration		
Winter	Moderate	Unhealthy for sensitive group	Moderate	Unhealthy for sensitive group	Similarity
Summer	Excellent	Moderate	Excellent	Moderate	Similarity

As a result, in Table 6.65, it can be observed that seasonally AQI classifications according to Thailand and US EPA standards are similar. As mentioned in Section 6.5.1, the interpretation of each AQI class from two standards should see the quantitative information in corresponding tables because the number of AQI classes and the quantity of PM10 and PM2.5 concentration are slightly different. Nevertheless, the GWR model, as a local model, can provide the predictive equation for each district.

CHAPTER VII
SUITABLE SPATIOTEMPORAL MODEL FOR PM CONCENTRATION PREDICTION AND VALIDATION

This chapter presents the study's third objective to evaluate a suitable model for predicting spatiotemporal PM10 and PM2.5 concentration between GWR and MEM models and validation. The reported AICc values from Chapter 6 were used to determine how well a model fits the data generated, compare different possible models, and decide which model best works for the data (Bevans, 2021). The lower AICc values indicate a better fit model. At the same time, the Pearson correlation analysis was used to measure how strong a relationship is between the derived patterns of PM concentration based on the existing dataset (October 2019 to May 2020) and the new dataset (October 2020 to May 2021) for suitable model validation. The value -1 and 1 of the Pearson correlation indicates a strong relationship. Additionally, spatial correlation analysis was applied to characterize the relationship between predictive PM concentration and their significant factors. The main results of this chapter consist of (1) a suitable model for spatiotemporal PM concentration prediction, (2) validation of a suitable model for spatiotemporal PM concentration prediction and (3) specific characteristics of predictive spatiotemporal PM concentration.

7.1 Suitable model for spatiotemporal PM concentration prediction

Suitable models for predicting spatiotemporal PM10 and PM2.5 concentration are summarized separately and discussed in the following section.

7.1.1 Suitable models for spatiotemporal PM10 concentration prediction

The AICc values of PM10 concentration prediction on sixty districts in rural landscapes in the winter and summer compared between the GWR and MEM model are summarized in Table 7.1 and Table 7.2, respectively. As shown in a table, column one displays the month in each season; column two indicates the sum of the districts in each landscape for the model calculation; and columns three and four display the AICc value of the GWR and MEM model, respectively.

Table 7.1 Monthly and seasonally AICc value and the average for two competing models for PM10 concentration prediction in the winter season.

Month	N	GWR model	MEM model
October	60	89.88	140.84
November	60	91.16	140.99
December	60	123.24	158.62
January	60	106.85	173.06
February	60	78.45	163.92
Average	60	97.92	155.49
Winter season	60	132.89	151.24

Table 7.2 Monthly and seasonally AICc value and the average for two competing models for PM10 concentration prediction in the summer season.

Month	N	GWR model	MEM model
March	60	119.61	157.31
April	60	64.75	159.37
May	60	154.74	177.62
Average	60	113.03	164.77
Summer season	60	120.34	158.70

As a result, Table 7.1 and Table 7.2 show that the average AICc value of PM10 concentration in winter and summer using the GWR model is lower than the MEM model. So, the GWR model is suitable for spatiotemporal PM10 concentration prediction in both seasons.

7.1.2 Suitable models for spatiotemporal PM2.5 concentration prediction

The AICc values of PM2.5 concentration prediction on seventy-two districts in urban landscapes in the winter and summer compared to GWR and MEM models are reported in Table 7.3 and Table 7.4, respectively.

Table 7.3 Monthly and seasonally AICc value and the average for two competing models for PM2.5 concentration prediction in the winter season.

Month	N	GWR model	MEM model
October	72	73.70	128.03
November	72	10.54	187.33
December	72	24.44	191.46
January	72	177.81	194.28
February	72	82.82	141.95
Average	72	73.86	168.61
Winter season	72	79.58	143.34

Table 7.4 Monthly and seasonally AICc value and the average for two competing models for PM2.5 concentration prediction in the summer season.

Month	N	GWR model	MEM model
March	72	114.63	210.62
April	72	162.63	174.03
May	72	90.38	175.35
Average	72	122.55	186.67
Summer season	72	181.86	204.30

As a result, in Table 7.3 and Table 7.4, the average AICc value of PM2.5 concentration in winter and summer using the GWR model is lower than in the MEM model. So, the GWR model is suitable for spatiotemporal PM2.5 concentration prediction in both seasons.

In summary, it can be concluded that the GWR model is suitable for monthly PM10 and PM2.5 concentration in the rural and urban landscape in the winter and summer seasons. This finding is consistent with many previous studies. Chu et al. (2016) concluded that GWR was suitable for PM2.5 concentration prediction at a regional scale. Like, Wei et al. (2019) suggested that the GWR model could provide a better spatiotemporal PM2.5 concentration prediction than the MEM model. Also, Gu (2019) stated that the GWR generated the best performance compared with the MEM (Mixed linear regression) model.

7.2 Validation of a suitable model for spatiotemporal PM concentration prediction

Under this section, a newly collected and prepared dataset in the winter and summer seasons (between October 2020 and May 2021) was reapplied to validate the spatiotemporal PM10 and PM2.5 concentration prediction using the GWR a suitable model.

7.2.1 Validation of PM10 concentration prediction

Using the GWR as a suitable model, the predictive value of monthly PM10 concentration in the winter season at the centroid of each district from the existing dataset (October 2019 to February 2020) and the new dataset (October 2020 to February 2021) was extracted as a summary in Table 7.5 and Table 7.6. The result of spatial correlation analysis between the predictive value of monthly PM10 concentration in the winter season from the existing dataset and the new dataset is summarized in Table 7.7.

Table 7.5 The predictive value of monthly PM10 concentration in the winter season at the centroid of each district from the existing dataset (October 2019 to February 2020).

No.	District	October	November	December	January	February
1	Chaiyo	52.56	65.22	74.42	79.16	82.18
2	Mueang Ang Thong	52.40	64.86	74.41	79.12	81.81
3	Pa Mok	52.10	64.64	74.46	79.11	81.62
4	Pho Thong	52.20	64.91	74.23	79.09	81.44
5	Samko	52.13	64.70	74.15	79.02	80.85
6	Sawaeng Ha	52.15	64.83	74.18	79.07	81.27
7	Wiset Chai Chan	52.14	64.60	74.21	79.06	80.99
8	Ban Mi	52.77	65.12	74.42	79.11	81.96
9	Chai Badan	51.79	64.58	73.53	78.88	81.27
10	Khok Charoen	51.93	64.44	74.08	78.95	81.19
11	Khok Samrong	52.88	65.41	75.17	79.07	81.73
12	Lam Sonthi	51.80	64.22	74.47	78.84	81.01
13	Mueang Lop Buri	53.74	66.12	75.96	79.36	83.30
14	Nong Muang	52.13	64.82	74.29	79.03	81.01
15	Phatthana Nikhom	52.94	65.82	75.13	79.06	82.70
16	Sa Bot	52.24	64.68	74.27	78.94	81.26

Table 7.5 (Continued).

No.	District	October	November	December	January	February
17	Tha Luang	51.86	65.04	73.38	78.88	81.93
18	Tha Wung	52.79	65.48	74.52	79.20	82.39
19	Khlong Luang	51.66	63.86	73.95	78.96	80.32
20	Lam Luk Ka	51.47	64.15	74.24	78.94	80.94
21	Lat Lum Kaeo	50.77	63.48	73.54	78.91	79.07
22	Mueang Pathum Thani	50.53	63.37	73.39	78.95	79.88
23	Nong Suea	52.35	63.96	74.27	79.03	81.08
24	Sam Khok	50.94	63.34	73.52	78.94	79.79
25	Thanyaburi	51.69	63.94	74.14	78.94	80.54
26	Ban Phraek	52.75	65.47	74.72	79.24	83.00
27	Bang Ban	51.87	64.42	74.71	79.12	80.83
28	Bang Pa-In	51.40	64.20	74.46	79.05	80.90
29	Bang Pahan	52.20	64.84	74.83	79.17	81.87
30	Bang Sai	51.40	63.85	74.22	78.96	79.81
31	Bang Sai	51.41	63.91	74.21	78.96	80.28
32	Lat Bua Luang	51.28	63.78	73.92	78.91	79.62
33	Maha Rat	52.58	65.22	74.64	79.15	82.41
34	Nakhon Luang	52.48	65.09	74.84	79.18	82.32
35	Phachi	52.76	65.07	74.86	79.16	82.89
36	Phak Hai	51.81	64.39	74.24	79.05	80.83
37	Phra Nakhon Si Ayutthaya	51.71	64.35	74.84	79.15	80.97
38	Sena	51.48	64.08	74.12	78.94	80.25
39	Tha Ruea	53.22	66.05	75.22	79.32	83.51
40	Uthai	52.20	64.62	74.56	79.10	82.13
41	Wang Noi	52.24	64.36	74.55	79.07	81.48
42	Ban Mo	53.61	66.38	75.67	79.40	84.24
43	Chaloem Phra Kiat	55.03	68.23	80.60	79.52	85.79
44	Don Phut	53.19	65.97	74.97	79.27	83.40
45	Kaeng Khoi	52.99	66.00	76.81	79.30	83.53
46	Muak Lek	52.48	65.49	74.30	78.90	82.60
47	Mueang Saraburi	53.46	65.64	77.48	79.41	83.71
48	Nong Don	53.76	66.13	76.78	79.44	83.79
49	Nong Khae	52.77	65.01	75.02	79.29	83.17
50	Nong Saeng	53.27	65.91	76.70	79.35	83.53
51	Phra Phutthabat	54.64	67.85	79.22	79.45	84.60
52	Sao Hai	53.86	66.99	77.74	79.50	84.13
53	Wang Muang	52.38	65.88	74.65	78.86	82.12
54	Wihan Daeng	53.01	65.02	75.14	79.22	82.77

Table 7.5 (Continued).

No.	District	October	November	December	January	February
55	Bang Rachan	52.31	64.88	74.17	79.08	81.44
56	In Buri	52.29	64.82	74.13	79.09	81.49
57	Khai Bang Rachan	52.32	64.93	74.19	79.08	81.55
58	Mueang Sing Buri	52.37	65.02	74.23	79.06	81.71
59	Phrom Buri	52.62	65.28	74.41	79.15	82.11
60	Tha Chang	52.42	65.08	74.29	79.10	81.81

Table 7.6 The predictive value of monthly PM10 concentration in the summer season at the centroid of each district from the new dataset (October 2020 to February 2021).

No.	District	October	November	December	January	February
1	Chaiyo	42.16	55.78	65.98	78.48	80.07
2	Mueang Ang Thong	42.09	55.79	65.85	78.25	80.06
3	Pa Mok	42.03	55.74	65.80	78.35	80.15
4	Pho Thong	41.94	55.73	65.69	78.16	79.61
5	Samko	41.69	55.74	65.45	78.06	79.29
6	Sawaeng Ha	41.86	55.77	65.47	78.08	79.42
7	Wiset Chai Chan	41.77	55.77	65.72	78.11	79.45
8	Ban Mi	41.90	55.78	65.52	78.45	79.57
9	Chai Badan	41.52	55.78	65.28	78.00	79.09
10	Khok Charoen	41.53	55.75	65.49	77.87	78.78
11	Khok Samrong	42.08	55.80	65.62	78.53	79.51
12	Lam Sonthi	41.61	55.80	65.69	77.87	78.71
13	Mueang Lop Buri	42.59	55.84	65.96	79.01	80.67
14	Nong Muang	41.71	55.78	65.30	78.08	78.58
15	Phatthana Nikhom	42.54	55.83	65.67	78.81	79.89
16	Sa Bot	41.56	55.74	65.34	77.98	78.88
17	Tha Luang	41.87	55.75	65.23	78.17	79.00
18	Tha Wung	42.20	55.84	65.85	78.32	80.09
19	Khlong Luang	41.45	55.71	65.62	77.83	78.79
20	Lam Luk Ka	41.87	55.75	65.51	77.83	79.51
21	Lat Lum Kaeo	40.85	55.72	65.68	76.36	77.68
22	Mueang Pathum Thani	40.51	55.74	65.38	76.75	78.33
23	Nong Suea	41.96	55.72	65.62	77.73	79.92
24	Sam Khok	40.90	55.72	65.75	76.62	78.05
25	Thanyaburi	41.68	55.76	65.33	77.87	79.55
26	Ban Phraek	42.28	55.83	65.87	78.54	80.35
27	Bang Ban	41.92	55.74	65.92	78.07	80.00
28	Bang Pa-In	41.86	55.78	65.85	78.08	79.93

Table 7.6 (Continued).

No.	District	October	November	December	January	February
29	Bang Pahan	41.95	55.79	65.51	78.67	80.32
30	Bang Sai	41.27	55.72	65.48	77.48	78.84
31	Bang Sai	41.40	55.73	65.37	77.46	78.48
32	Lat Bua Luang	41.46	55.75	65.31	77.41	78.34
33	Maha Rat	42.26	55.78	65.59	78.79	80.34
34	Nakhon Luang	42.24	55.81	65.82	78.78	80.55
35	Phachi	42.36	55.82	66.08	79.06	80.63
36	Phak Hai	41.66	55.76	65.50	78.04	79.45
37	Phra Nakhon Si Ayutthaya	41.93	55.74	66.11	78.79	80.02
38	Sena	41.51	55.73	65.64	77.79	79.06
39	Tha Ruea	42.48	55.83	65.77	79.08	81.01
40	Uthai	42.03	55.76	65.89	78.74	80.36
41	Wang Noi	41.74	55.78	65.44	78.25	79.79
42	Ban Mo	42.55	55.87	65.79	79.27	81.03
43	Chaloem Phra Kiat	43.08	55.95	66.70	79.69	82.23
44	Don Phut	42.41	55.81	66.01	78.78	80.80
45	Kaeng Khoi	42.16	55.85	66.27	78.60	80.80
46	Muak Lek	42.04	55.82	65.29	77.95	79.62
47	Mueang Saraburi	42.71	55.80	66.38	79.21	81.15
48	Nong Don	42.53	55.84	66.27	79.29	80.89
49	Nong Khae	42.25	55.82	65.60	78.79	80.40
50	Nong Saeng	42.66	55.82	66.10	79.21	80.92
51	Phra Phutthabat	42.87	55.93	66.49	79.71	81.92
52	Sao Hai	42.94	55.86	66.30	79.35	81.47
53	Wang Muang	42.43	55.81	65.60	78.84	80.15
54	Wihan Daeng	41.92	55.79	65.81	78.73	80.11
55	Bang Rachan	41.92	55.75	65.29	78.14	79.38
56	In Buri	41.97	55.75	65.33	78.07	79.42
57	Khai Bang Rachan	41.94	55.83	65.43	78.31	79.46
58	Mueang Sing Buri	42.06	55.75	65.57	78.33	79.61
59	Phrom Buri	42.18	55.75	65.75	78.57	79.93
60	Tha Chang	42.09	55.82	65.65	78.27	79.72

Table 7.7 The correlation coefficient value for PM10 concentration in the winter season between the existing and new datasets.

Month	Number of samples	Correlation coefficient	Sig.
October	60	0.91**	0.00
November	60	0.89**	0.00
December	60	0.83**	0.00
January	60	0.81**	0.00
February	60	0.91**	0.00
Average		0.87	0.00

**Correlation is significant at the 0.01 level (2-tailed).

According to Table 7.7, the average correlation coefficient value of PM10 concentration in the winter season (October to February) is 0.87. This result indicates that the rural landscape's predictive PM10 concentration in the winter season from two datasets using a suitable model (GWR) provides a very strong positive correlation.

In the meantime, the predictive value of monthly PM10 concentration in the summer season at the centroid of each district from the existing dataset (March 2019 to May 2020) and the new dataset (March 2020 to May 2021) was extracted as a summary in Table 7.8 and Table 7.9. The result of spatial correlation analysis between the predictive value of monthly PM10 concentration in the summer season from the existing dataset and the new dataset is summarized in Table 7.10.

Table 7.8 The predictive value of monthly PM10 concentration in the summer season at the centroid of each district from the existing dataset (March 2019 to May 2020).

No.	District	March	April	May
1	Chaiyo	48.69	44.01	37.17
2	Mueang Ang Thong	48.73	43.89	37.23
3	Pa Mok	48.88	43.96	37.39
4	Pho Thong	48.55	43.84	37.15
5	Samko	48.49	43.74	37.15
6	Sawaeng Ha	48.54	43.78	37.14
7	Wiset Chai Chan	48.61	43.70	37.18
8	Ban Mi	48.33	43.84	37.15
9	Chai Badan	48.46	43.52	37.20
10	Khok Charoen	48.70	43.62	37.14
11	Khok Samrong	48.43	44.01	37.24

Table 7.8 (Continued).

No.	District	March	April	May
12	Lam Sonthi	48.50	43.21	37.12
13	Mueang Lop Buri	49.09	44.55	37.47
14	Nong Muang	48.49	43.64	37.15
15	Phatthana Nikhom	48.74	44.21	37.70
16	Sa Bot	48.43	43.65	37.17
17	Tha Luang	48.47	43.85	37.29
18	Tha Wung	48.57	43.99	37.15
19	Khlong Luang	48.64	43.85	37.20
20	Lam Luk Ka	48.68	44.09	37.25
21	Lat Lum Kaeo	48.56	42.65	36.95
22	Mueang Pathum Thani	48.55	42.99	36.92
23	Nong Suea	48.73	44.29	37.29
24	Sam Khok	48.76	43.20	37.01
25	Thanyaburi	48.59	44.43	37.25
26	Ban Phraek	48.82	44.22	37.24
27	Bang Ban	48.76	44.03	37.55
28	Bang Pa-In	48.75	44.16	37.56
29	Bang Pahan	48.85	44.25	37.54
30	Bang Sai	48.61	43.39	37.45
31	Bang Sai	48.73	43.27	37.26
32	Lat Bua Luang	48.55	43.00	37.15
33	Maha Rat	48.95	44.23	37.31
34	Nakhon Luang	48.85	44.56	37.55
35	Phachi	48.59	44.54	37.48
36	Phak Hai	48.61	43.75	37.29
37	Phra Nakhon Si Ayutthaya	49.35	44.37	37.67
38	Sena	48.63	43.39	37.35
39	Tha Ruea	49.08	44.68	37.57
40	Uthai	48.99	44.43	37.52
41	Wang Noi	49.00	44.30	37.38
42	Ban Mo	49.43	44.79	38.00
43	Chaloem Phra Kiat	51.32	45.73	39.00
44	Don Phut	48.77	44.51	37.38
45	Kaeng Khoi	49.12	44.97	38.48
46	Muak Lek	48.55	44.09	37.63
47	Mueang Saraburi	50.17	44.68	37.54
48	Nong Don	49.07	44.58	37.79

Table 7.8 (Continued).

No.	District	March	April	May
49	Nong Khae	49.25	44.32	37.34
50	Nong Saeng	48.59	44.57	37.51
51	Phra Phutthabat	49.77	45.74	38.44
52	Sao Hai	49.98	44.97	38.18
53	Wang Muang	48.60	44.22	37.78
54	Wihan Daeng	48.48	44.48	37.39
55	Bang Rachan	48.63	43.83	37.14
56	In Buri	48.50	43.83	37.13
57	Khai Bang Rachan	48.59	43.83	37.14
58	Mueang Sing Buri	48.56	43.86	37.14
59	Phrom Buri	48.52	43.94	37.14
60	Tha Chang	48.45	43.89	37.14

Table 7.9 The predictive value of monthly PM10 concentration in the summer season at the centroid of each district from the new dataset (March 2020 to May 2021).

No.	District	March	April	May
1	Chaiyo	57.06	42.93	34.46
2	Mueang Ang Thong	57.08	42.88	34.43
3	Pa Mok	57.10	42.85	34.46
4	Pho Thong	57.02	42.67	34.47
5	Samko	56.92	42.57	34.43
6	Sawaeng Ha	56.99	42.70	34.47
7	Wiset Chai Chan	56.97	42.62	34.42
8	Ban Mi	57.18	42.99	34.42
9	Chai Badan	56.98	42.54	34.44
10	Khok Charoen	57.02	42.62	34.46
11	Khok Samrong	57.14	43.06	34.45
12	Lam Sonthi	56.88	42.43	34.45
13	Mueang Lop Buri	57.27	43.50	34.45
14	Nong Muang	57.04	42.74	34.47
15	Phatthana Nikhom	57.07	43.06	34.46
16	Sa Bot	57.02	42.71	34.44
17	Tha Luang	56.92	42.52	34.44
18	Tha Wung	57.10	43.00	34.46
19	Khlong Luang	56.88	42.94	34.44
20	Lam Luk Ka	56.83	43.39	34.43
21	Lat Lum Kaeo	56.74	41.83	34.41
22	Mueang Pathum Thani	56.77	42.34	34.40

Table 7.9 (Continued).

No.	District	March	April	May
23	Nong Suea	57.05	43.34	34.46
24	Sam Khok	56.93	42.04	34.42
25	Thanyaburi	56.84	43.05	34.44
26	Ban Phraek	57.09	43.09	34.44
27	Bang Ban	56.95	42.49	34.44
28	Bang Pa-In	56.97	42.92	34.45
29	Bang Pahan	57.06	43.13	34.48
30	Bang Sai	56.90	42.22	34.45
31	Bang Sai	56.87	42.17	34.47
32	Lat Bua Luang	56.84	41.90	34.43
33	Maha Rat	57.09	43.08	34.46
34	Nakhon Luang	57.12	43.33	34.46
35	Phachi	57.16	43.46	34.44
36	Phak Hai	56.91	42.47	34.43
37	Phra Nakhon Si Ayutthaya	57.08	43.11	34.45
38	Sena	56.88	42.21	34.44
39	Tha Ruea	57.22	43.49	34.48
40	Uthai	57.07	43.36	34.47
41	Wang Noi	57.06	43.46	34.47
42	Ban Mo	57.23	43.64	34.48
43	Chaloem Phra Kiat	57.71	44.13	34.55
44	Don Phut	57.15	43.28	34.47
45	Kaeng Khoi	57.12	43.74	34.49
46	Muak Lek	56.93	42.88	34.44
47	Mueang Saraburi	57.41	43.78	34.48
48	Nong Don	57.25	43.60	34.47
49	Nong Khae	57.17	43.52	34.43
50	Nong Saeng	57.28	43.60	34.48
51	Phra Phutthabat	57.42	43.96	34.50
52	Sao Hai	57.34	43.93	34.51
53	Wang Muang	56.95	42.95	34.46
54	Wihan Daeng	57.18	43.52	34.43
55	Bang Rachan	57.03	42.70	34.45
56	In Buri	57.13	42.85	34.47
57	Khai Bang Rachan	57.05	42.75	34.45
58	Mueang Sing Buri	57.09	42.83	34.42
59	Phrom Buri	57.07	42.85	34.43
60	Tha Chang	57.06	42.80	34.43

Table 7.10 The correlation coefficient value for PM10 concentration between the existing and new datasets in the summer season.

Month	Number of samples	Correlation coefficient	Sig.
March	60	0.75**	0.00
April	60	0.94**	0.00
May	60	0.76**	0.00
Average		0.82	0.00

**Correlation is significant at the 0.01 level (2-tailed).

According to Table 7.10, the average correlation coefficient value of PM10 concentration in the summer season (March to May) is 0.82. This result indicates that the predictive PM10 concentration in the summer in rural landscapes from two datasets using a suitable model (GWR) provides a very strong positive correlation.

Summary

As a reported result in section 7.2.1, it can be concluded that the predicted PM10 concentration in two seasons in the rural landscape using the GWR model can be accepted in the current study. The correlation coefficient values for PM10 concentration in the winter season between the existing dataset and the new dataset vary from 0.81 to 0.91, with an average value of 0.87. Similarly, the correlation coefficient values between the existing dataset and the new dataset in the summer season vary from 0.75 to 0.94, with an average value of 0.82. These values show a very strong positive relationship, as suggested by Chowdhury, Debsarkar, and Chakrabarty (2015). Additionally, these findings imply that the identified monthly significant factors on PM10 concentration in two seasons from the existing dataset can be managed to mitigate PM10 concentration in rural landscapes. For example, fire radiative power due to burning activity as a significant factor on PM10 concentration in February should be reduced by setting up a schedule for agricultural debris burnt.

7.2.2 Validation of PM2.5 concentration prediction

Like PM10 concentration prediction, the predictive value of monthly PM2.5 concentration in the winter season at the centroid of each district from the existing dataset (October 2019 to February 2020) and the new dataset (October 2020 to February 2021) was extracted using the GWR model, as a summary in Table 7.11 and Table 7.12. The result of spatial correlation analysis between the predictive value of monthly PM2.5 concentration in the winter season from the existing dataset and the new dataset is summarized in Table 7.13.

Table 7.11 The predictive value of monthly PM2.5 concentration in the winter season at the centroid of each district from the existing dataset (October 2019 to February 2020).

No	District	October	November	December	January	February
1	Bang Bon	28.38	35.24	40.00	43.53	44.09
2	Bang Kapi	26.40	33.54	39.53	43.67	44.13
3	Bang Khae	28.04	35.22	40.11	43.57	44.22
4	Bang Khen	27.30	33.77	39.90	43.69	44.29
5	Bang Kho Laem	27.63	34.56	39.87	43.59	44.06
6	Bang Khun Thian	27.81	34.72	39.76	43.36	44.01
7	Bang Na	26.41	33.58	39.31	43.62	43.98
8	Bang Phlat	27.49	34.47	40.17	43.72	44.23
9	Bang Rak	27.77	34.52	39.85	43.71	44.14
10	Bang Sue	27.06	34.55	40.13	43.57	44.22
11	Bangkok Noi	27.92	34.65	40.14	43.74	44.26
12	Bangkok Yai	27.74	34.66	40.09	43.63	44.20
13	Bueng Kum	26.55	33.54	39.59	43.70	44.21
14	Chatuchak	26.81	34.10	40.01	43.69	44.21
15	Chom Thong	27.94	34.85	39.98	43.53	44.08
16	Din Daeng	27.36	33.96	39.81	43.50	44.09
17	Don Mueang	27.19	34.12	40.04	43.81	44.37
18	Dusit	27.75	34.21	40.06	43.58	44.17
19	Huai Khwang	26.82	33.74	39.61	43.52	44.08
20	Khan Na Yao	26.85	33.45	39.51	43.76	44.22
21	Khlong Sam Wa	26.43	33.27	39.32	43.76	44.24
22	Khlong San	27.68	34.57	39.97	43.67	44.12
23	Khlong Toei	26.97	34.08	39.51	43.44	44.00
24	Lak Si	27.09	34.21	40.08	43.82	44.30
25	Lat Krabang	25.60	32.83	39.03	43.77	44.05

Table 7.11 (Continued).

No	District	October	November	December	January	February
26	Lat Phrao	26.88	33.76	39.82	43.53	44.21
27	Min Buri	26.22	32.90	39.21	43.81	44.15
28	Nong Chok	25.97	32.74	38.98	43.82	44.15
29	Nong Khaem	28.09	35.32	40.13	43.53	44.22
30	Pathum Wan	27.72	34.07	39.74	43.62	44.11
31	Phasi Charoen	28.17	34.79	40.11	43.61	44.18
32	Phaya Thai	27.27	34.11	39.94	43.60	44.13
33	Phra Khanong	26.36	33.71	39.34	43.55	44.00
34	Phra Nakhon	27.84	34.41	40.09	43.77	44.20
35	Pom Prap Sattru Phai	27.78	34.17	40.01	43.73	44.19
36	Prawet	26.04	33.15	39.24	43.53	44.03
37	Rat Burana	27.84	34.53	39.83	43.53	44.05
38	Ratchathewi	27.76	33.98	39.81	43.60	44.11
39	Sai Mai	26.69	33.66	39.77	43.73	44.32
40	Samphanthawong	27.87	34.62	39.98	43.67	44.15
41	Saphan Sung	26.01	33.19	39.33	43.66	44.10
42	Sathon	27.49	34.49	39.80	43.66	44.05
43	Suan Luang	26.11	33.60	39.38	43.53	44.05
44	Taling Chan	27.88	34.77	40.13	43.69	44.30
45	Thawi Watthana	27.66	34.99	40.23	43.58	44.31
46	Thon Buri	27.91	34.61	40.01	43.67	44.13
47	Thung Khru	27.42	34.47	39.66	43.51	44.00
48	Vadhana	27.09	33.95	39.46	43.63	44.05
49	Wang Thonglang	26.73	33.63	39.71	43.58	44.12
50	Yan Nawa	27.10	34.32	39.73	43.63	44.01
51	Bang Len	26.73	34.34	40.49	43.65	44.25
52	Don Tum	26.86	34.59	40.51	43.62	44.23
53	Kamphaeng Saen	26.87	34.48	40.52	43.72	44.24
54	Mueang Nakhon Pathom	26.91	35.31	40.52	43.78	44.21
55	Nakhon Chai Si	27.19	35.16	40.42	43.71	44.20
56	Phutthamonthon	27.51	35.17	40.31	43.58	44.23
57	Sam Phran	27.55	35.41	40.28	43.60	44.21
58	Bang Bua Thong	27.48	34.65	40.37	43.83	44.28
59	Bang Kruai	27.51	34.88	40.22	43.68	44.29
60	Bang Yai	27.62	34.93	40.30	43.63	44.24
61	Mueang Nonthaburi	27.22	34.78	40.24	43.69	44.29
62	Pak Kret	27.28	34.61	40.19	43.76	44.28
63	Sai Noi	26.87	34.61	40.45	43.72	44.25
64	Bang Bo	25.33	32.05	38.76	43.63	43.98

Table 7.11 (Continued).

No	District	October	November	December	January	February
65	Bang Phli	26.25	32.84	39.03	43.51	43.99
66	Bang Sao Thong	25.59	32.43	38.88	43.65	44.03
67	Mueang Samut Prakan	26.42	33.25	39.19	43.40	43.97
68	Phra Pradaeng	27.05	34.14	39.52	43.44	43.99
69	Phra Samut Chedi	27.09	34.07	39.46	43.27	43.97
70	Ban Phaeo	27.53	35.77	40.20	43.70	44.10
71	Krathum Baen	27.89	35.45	40.23	43.66	44.12
72	Mueang Samut Sakhon	27.83	35.63	40.02	43.57	44.01

Table 7.12 The predictive value of monthly PM2.5 concentration in the winter season at the centroid of each district from the new dataset (October 2020 to February 2021).

No.	District	October	November	December	January	February
1	Bang Bon	21.93	31.18	38.92	44.85	45.04
2	Bang Kapi	19.80	27.81	34.05	44.65	45.67
3	Bang Khae	21.39	31.17	39.07	44.47	45.54
4	Bang Khen	20.04	27.79	34.16	44.97	45.82
5	Bang Kho Laem	21.13	29.37	36.10	44.50	45.44
6	Bang Khun Thian	20.44	30.17	37.45	44.44	45.30
7	Bang Na	20.43	28.38	34.52	45.00	44.73
8	Bang Phlat	20.53	29.59	36.07	45.28	45.58
9	Bang Rak	21.44	29.26	35.78	44.97	45.41
10	Bang Sue	20.07	28.93	35.13	44.70	45.55
11	Bangkok Noi	20.92	29.73	37.25	44.91	45.60
12	Bangkok Yai	21.06	29.58	37.15	45.08	45.34
13	Bueng Kum	19.42	27.83	34.02	44.70	45.49
14	Chatuchak	19.82	27.98	34.54	45.05	45.41
15	Chom Thong	21.19	30.12	37.60	44.78	45.40
16	Din Daeng	20.33	28.21	34.84	44.54	45.59
17	Don Mueang	19.53	28.07	34.21	45.41	46.55
18	Dusit	20.47	29.38	35.69	44.64	45.91
19	Huai Khwang	20.18	28.27	34.61	44.53	45.15
20	Khan Na Yao	19.32	27.79	33.91	44.87	45.24
21	Khlong Sam Wa	19.36	27.47	33.80	45.17	45.81
22	Khlong San	21.14	29.37	36.35	44.69	45.55
23	Khlong Toei	20.52	28.34	34.98	44.75	45.31
24	Lak Si	19.47	28.08	34.47	45.49	46.08
25	Lat Krabang	19.44	27.14	32.78	44.98	45.28
26	Lat Phrao	19.43	27.83	34.17	44.46	45.76

Table 7.12 (Continued).

No.	District	October	November	December	January	February
27	Min Buri	19.45	27.24	33.40	45.43	45.59
28	Nong Chok	19.73	27.33	33.51	45.51	45.61
29	Nong Khaem	21.33	31.20	39.33	44.44	45.53
30	Pathum Wan	21.17	28.82	35.23	44.99	45.33
31	Phasi Charoen	21.28	30.00	38.10	44.85	45.69
32	Phaya Thai	20.39	28.32	35.11	44.56	45.72
33	Phra Khanong	20.28	28.28	34.54	44.60	45.09
34	Phra Nakhon	20.85	29.45	36.27	44.82	45.54
35	Pom Prap Sattru Phai	21.06	29.35	35.63	45.02	45.42
36	Prawet	19.98	27.72	33.83	44.66	45.36
37	Rat Burana	21.14	29.52	36.50	44.76	45.39
38	Ratchathewi	20.80	28.80	35.41	44.89	45.80
39	Sai Mai	19.26	27.98	34.12	45.17	46.05
40	Samphanthawong	21.13	29.35	36.42	44.92	45.86
41	Saphan Sung	19.49	27.40	33.66	44.80	45.58
42	Sathon	21.28	29.03	35.36	44.75	45.53
43	Suan Luang	20.05	27.93	34.20	44.82	45.32
44	Taling Chan	20.85	30.23	37.80	45.10	46.09
45	Thawi Watthana	20.58	30.62	38.29	44.69	46.37
46	Thon Buri	21.21	29.53	36.85	45.05	45.61
47	Thung Khru	20.73	29.68	36.69	44.83	45.39
48	Vadhana	20.86	28.20	34.71	44.72	45.44
49	Wang Thonglang	19.89	28.16	34.34	44.73	45.67
50	Yan Nawa	21.20	28.75	35.08	44.61	45.34
51	Bang Len	19.35	29.05	35.20	44.87	45.61
52	Don Tum	19.44	29.35	35.41	44.58	45.51
53	Kamphaeng Saen	20.25	29.00	35.08	44.73	45.52
54	Mueang Nakhon Pathom	19.83	30.29	36.73	45.20	45.32
55	Nakhon Chai Si	20.26	30.32	37.55	44.87	45.56
56	Phutthamonthon	20.55	30.41	37.44	44.55	45.63
57	Sam Phran	20.63	31.03	38.44	44.96	45.57
58	Bang Bua Thong	20.32	29.51	36.08	45.57	45.75
59	Bang Kruai	20.15	29.88	37.41	44.73	45.91
60	Bang Yai	19.65	30.05	37.11	44.83	45.60
61	Mueang Nonthaburi	19.70	28.81	35.84	44.90	45.83
62	Pak Kret	19.46	28.32	34.76	45.14	45.59
63	Sai Noi	19.57	29.53	36.01	45.03	45.43
64	Bang Bo	19.18	27.01	32.98	44.91	45.08
65	Bang Phli	20.35	27.69	33.19	44.57	44.93

Table 7.12 (Continued).

No.	District	October	November	December	January	February
66	Bang Sao Thong	19.87	26.90	32.57	44.73	45.48
67	Mueang Samut Prakan	20.06	28.47	34.67	44.59	44.87
68	Phra Pradaeng	20.97	28.78	35.57	44.62	44.88
69	Phra Samut Chedi	20.54	29.28	36.24	44.13	44.61
70	Ban Phaeo	19.80	30.69	37.57	44.80	45.31
71	Krathum Baen	20.82	31.05	38.71	45.12	45.46
72	Mueang Samut Sakhon	20.11	30.81	38.82	44.90	45.36

Table 7.13 The correlation coefficient value for PM2.5 concentration in the winter between the existing and new datasets.

Month	Number of samples	Correlation coefficient	Sig.
October	72	0.71**	0.00
November	72	0.92**	0.00
December	72	0.67**	0.00
January	72	0.78**	0.00
February	72	0.76**	0.00
Average		0.77	0.00

**Correlation is significant at the 0.01 level (2-tailed).

According to Table 7.13, the average correlation coefficient value of PM2.5 concentration in the winter season (October to February) is 0.77. This result indicates that the predictive PM2.5 concentration in the winter season in the urban landscape of the two datasets provides a strong positive correlation.

Meanwhile, the predictive value of monthly PM2.5 concentration in the summer season at the centroid of each district from the existing dataset (March 2019 to May 2020) and the new dataset (March 2020 to May 2021) was extracted as a summary in Table 7.14 and Table 7.15. The result of spatial correlation analysis between the predictive value of monthly PM2.5 concentration in the summer season from the existing dataset and the new dataset is summarized in Table 7.16.

Table 7.14 The predictive value of monthly PM2.5 concentration in the summer season at the centroid of each district from the existing dataset (March 2019 to May 2020).

No.	District	March	April	May
1	Bang Bon	23.31	21.71	16.69
2	Bang Kapi	23.51	22.31	16.77
3	Bang Khae	23.25	21.72	16.73
4	Bang Khen	23.73	22.25	16.83
5	Bang Kho Laem	23.13	21.71	16.69
6	Bang Khun Thian	23.29	21.83	16.71
7	Bang Na	23.20	21.94	16.71
8	Bang Phlat	22.90	21.69	16.77
9	Bang Rak	23.38	21.64	16.75
10	Bang Sue	23.09	21.75	16.78
11	Bangkok Noi	23.09	21.80	16.77
12	Bangkok Yai	23.26	21.73	16.73
13	Bueng Kum	23.57	22.21	16.80
14	Chatuchak	23.26	21.84	16.81
15	Chom Thong	23.08	21.69	16.70
16	Din Daeng	22.86	21.83	16.77
17	Don Mueang	24.04	22.43	16.85
18	Dusit	22.83	21.90	16.78
19	Huai Khwang	23.05	21.82	16.77
20	Khan Na Yao	23.62	22.42	16.80
21	Khlong Sam Wa	23.67	22.46	16.80
22	Khlong San	23.32	21.70	16.71
23	Khlong Toei	23.23	21.62	16.71
24	Lak Si	23.72	22.23	16.83
25	Lat Krabang	23.60	22.17	16.76
26	Lat Phrao	23.48	22.26	16.80
27	Min Buri	23.58	22.37	16.77
28	Nong Chok	23.67	22.17	16.77
29	Nong Khaem	23.33	21.73	16.73
30	Pathum Wan	23.22	21.61	16.77
31	Phasi Charoen	23.17	21.74	16.74
32	Phaya Thai	22.82	21.82	16.78
33	Phra Khanong	23.22	21.96	16.73
34	Phra Nakhon	23.16	21.79	16.78
35	Pom Prap Sattru Phai	23.21	21.72	16.72
36	Prawet	23.35	22.20	16.74
37	Rat Burana	22.95	21.72	16.69

Table 7.14 (Continued).

No.	District	March	April	May
38	Ratchathewi	23.01	21.74	16.76
39	Sai Mai	23.88	22.36	16.84
40	Samphanthawong	23.33	21.71	16.74
41	Saphan Sung	23.51	22.28	16.77
42	Sathon	23.35	21.63	16.71
43	Suan Luang	23.34	22.03	16.74
44	Taling Chan	23.15	21.77	16.78
45	Thawi Watthana	23.22	21.72	16.76
46	Thon Buri	23.22	21.70	16.72
47	Thung Khru	23.05	21.80	16.70
48	Vadhana	23.20	21.74	16.74
49	Wang Thonglang	23.34	22.02	16.79
50	Yan Nawa	23.20	21.68	16.70
51	Bang Len	23.55	21.96	16.77
52	Don Tum	23.56	21.96	16.76
53	Kamphaeng Saen	23.57	22.04	16.77
54	Mueang Nakhon Pathom	23.56	21.93	16.75
55	Nakhon Chai Si	23.52	21.86	16.75
56	Phutthamonthon	23.40	21.80	16.76
57	Sam Phran	23.44	21.81	16.74
58	Bang Bua Thong	23.45	21.88	16.78
59	Bang Kruai	23.14	21.76	16.78
60	Bang Yai	23.31	21.77	16.77
61	Mueang Nonthaburi	23.21	21.87	16.81
62	Pak Kret	23.57	22.01	16.80
63	Sai Noi	23.52	21.85	16.77
64	Bang Bo	23.56	21.98	16.73
65	Bang Phli	23.54	22.25	16.71
66	Bang Sao Thong	23.57	22.30	16.75
67	Mueang Samut Prakan	23.47	22.03	16.70
68	Phra Pradaeng	23.03	21.82	16.70
69	Phra Samut Chedi	23.33	21.94	16.70
70	Ban Phaeo	23.47	21.86	16.74
71	Krathum Baen	23.39	21.78	16.73
72	Mueang Samut Sakhon	23.39	21.86	16.73

Table 7.15 The predictive value of monthly PM2.5 concentration in the summer season at the centroid of each district from the new dataset (March 2020 to May 2021).

No.	District	March	April	May
1	Bang Bon	28.47	22.02	16.11
2	Bang Kapi	28.67	22.27	16.16
3	Bang Khae	28.50	22.00	16.13
4	Bang Khen	28.81	22.17	16.19
5	Bang Kho Laem	28.36	21.93	16.09
6	Bang Khun Thian	28.50	22.13	16.11
7	Bang Na	28.52	22.12	16.12
8	Bang Phlat	28.54	22.02	16.13
9	Bang Rak	28.41	22.05	16.11
10	Bang Sue	28.69	22.09	16.14
11	Bangkok Noi	28.51	22.18	16.13
12	Bangkok Yai	28.47	22.03	16.10
13	Bueng Kum	28.73	22.23	16.17
14	Chatuchak	28.71	22.19	16.16
15	Chom Thong	28.39	22.01	16.10
16	Din Daeng	28.59	22.15	16.13
17	Don Mueang	28.87	22.26	16.20
18	Dusit	28.57	22.13	16.14
19	Huai Khwang	28.60	22.06	16.14
20	Khan Na Yao	28.73	22.29	16.18
21	Khlong Sam Wa	28.81	22.36	16.18
22	Khlong San	28.39	22.02	16.10
23	Khlong Toei	28.48	21.97	16.10
24	Lak Si	28.81	22.13	16.18
25	Lat Krabang	28.67	22.18	16.17
26	Lat Phrao	28.75	22.23	16.17
27	Min Buri	28.75	22.21	16.17
28	Nong Chok	28.80	22.15	16.18
29	Nong Khaem	28.50	22.08	16.13
30	Pathum Wan	28.46	21.90	16.12
31	Phasi Charoen	28.46	21.99	16.12
32	Phaya Thai	28.58	22.10	16.14
33	Phra Khanong	28.53	22.17	16.12
34	Phra Nakhon	28.47	22.07	16.13
35	Pom Prap Sattru Phai	28.47	21.93	16.10
36	Prawet	28.61	22.22	16.15
37	Rat Burana	28.36	21.99	16.09
38	Ratchathewi	28.55	22.06	16.13

Table 7.15 (Continued).

No.	District	March	April	May
39	Sai Mai	28.84	22.23	16.19
40	Samphanthawong	28.43	22.10	16.11
41	Saphan Sung	28.66	22.25	16.17
42	Sathon	28.41	22.01	16.09
43	Suan Luang	28.58	22.11	16.14
44	Taling Chan	28.57	22.10	16.14
45	Thawi Watthana	28.60	22.10	16.14
46	Thon Buri	28.40	22.02	16.10
47	Thung Khru	28.48	22.07	16.11
48	Vadhana	28.54	22.02	16.12
49	Wang Thonglang	28.66	22.22	16.15
50	Yan Nawa	28.39	22.02	16.10
51	Bang Len	28.71	22.09	16.17
52	Don Tum	28.70	22.03	16.16
53	Kamphaeng Saen	28.70	22.20	16.15
54	Mueang Nakhon Pathom	28.66	22.09	16.13
55	Nakhon Chai Si	28.66	21.96	16.13
56	Phutthamonthon	28.65	21.95	16.15
57	Sam Phran	28.59	22.03	16.13
58	Bang Bua Thong	28.72	22.04	16.16
59	Bang Kruai	28.64	22.11	16.15
60	Bang Yai	28.70	22.00	16.15
61	Mueang Nonthaburi	28.70	22.11	16.16
62	Pak Kret	28.81	22.08	16.17
63	Sai Noi	28.72	22.09	16.16
64	Bang Bo	28.64	22.09	16.15
65	Bang Phli	28.62	22.12	16.15
66	Bang Sao Thong	28.64	22.19	16.17
67	Mueang Samut Prakan	28.52	22.04	16.12
68	Phra Pradaeng	28.43	22.05	16.10
69	Phra Samut Chedi	28.49	22.06	16.11
70	Ban Phaeo	28.56	22.00	16.12
71	Krathum Baen	28.54	22.09	16.13
72	Mueang Samut Sakhon	28.54	22.19	16.12

Table 7.16 The correlation coefficient value for PM2.5 concentration between the existing and new datasets in the summer season.

Month	Number of samples	Correlation coefficient	Sig.
March	72	0.67**	0.00
April	72	0.81**	0.00
May	72	0.84**	0.00
Average		0.77	0.00

**Correlation is significant at the 0.01 level (2-tailed).

According to Table 7.16, the average correlation coefficient value of PM2.5 concentration in the summer season (March to May) is 0.77. This result indicates that the predictive PM2.5 concentration in the summer in the urban landscape from the two datasets provides a strong positive correlation.

Summary

As a reported result above in section 7.3.2, it can be concluded that the predicted PM2.5 concentration in two seasons urban landscape using the GWR model can be accepted in the current study as the expected correlation coefficient value should be equal to or more than 0.5. The correlation coefficient values between the existing dataset and the new dataset in the winter season vary from 0.67 to 0.92, with an average value of 0.77. Similarly, the correlation coefficient values between the existing dataset and the new dataset in the summer season vary from 0.67 to 0.84, with an average value of 0.77. These values show a very strong positive relationship, as suggested by Chowdhury, Debsarkar, and Chakrabarty (2015).

Additionally, these findings imply that the identified monthly significant factors on PM2.5 concentration in two seasons from the existing dataset can be managed to mitigate PM2.5 concentration in the urban landscape. For example, brightness temperature, fire radiative power, and fire hotspots as significant factors on PM2.5 concentration in October should be reduced burning activities in the agricultural area, particularly in Nakhon Pathom province.

7.3 Specific characteristics of predictive spatiotemporal PM concentration

Two essential characteristics of predictive spatiotemporal PM concentration by the GWR model, as a suitable model, were summarized in this section. Firstly, the relationship between PM10 and PM2.5 concentration and significant monthly factors was described and discussed based on spatial correlation analysis (pixel by pixel) using the Spatial Modeler module under ERDAS Imagine software. Secondly, the relationship between PM10 and PM2.5 concentration in winter and summer seasons and land use data in 2019 by LDD was described and discussed based on overlay analysis under ESRI ArcMap.

7.3.1 Relationship between monthly PM10 concentration and their factors

7.3.1.1 October 2019 in the winter season

The result of spatial correlation analysis between PM10 concentration in October 2019 and their significant factors: temperature, wind speed, and visibility (see detail in Table 5.30) is reported in Table 7.17.

Table 7.17 Pearson correlation matrix among significant factors and PM10 concentration in October 2019.

Variables	PM10	Temperature	Wind speed	Visibility
PM10	1.00	0.11	0.16	-0.55
Temperature	0.11	1.00	-0.42	-0.06
Wind speed	0.16	-0.42	1.00	0.22
Visibility	-0.55	-0.06	0.22	1.00

From Table 7.17, PM10 concentration in October 2019 shows a higher relationship with visibility than temperature and wind speed, but it depicts a negative direction. As a result, if PM10 concentration increases, visibility tends to decrease due to the effect of PM concentration. This finding shows a consistent linear relationship, as mentioned in Table 3.2.

In contrast, temperature and wind speed positively correlate with PM10 concentration. As a result, if temperature and wind speed, as an influencer on PM concentration, increase, PM10 concentration increases. This finding does not show a consistent linear relationship, as stated in Table 3.2. In fact, if temperature and wind speed increase, PM concentration will decrease. The scatterplot between PM10 concentration and temperature or wind speed is displayed in Figure 7.1. As a result, it indicates that the relationship between PM10 concentration and temperature or wind speed in October 2019 is non-linear form.

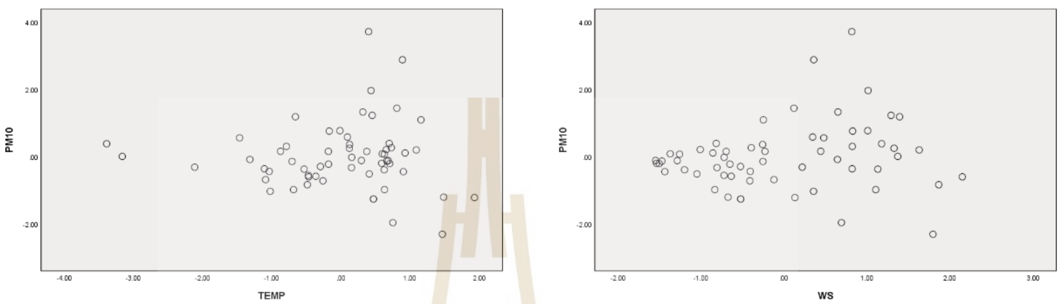

(a) TEMP (b) WS

Figure 7.1 Scatterplot between PM10 concentration in October 2019 and (a) temperature or (b) wind speed.

Moreover, the spatial distribution map of PM10 concentration and significant factors (temperature, wind speed and visibility) is displayed in Figure 7.2. The spatial distribution map of PM10 concentration in October 2019 shows that high PM10 concentration occur in the central part of the study area, particularly in Mueang Lop Buri, Phatthana Nikhom District - Lob Buri province and Chaloem Phra Kiat, Phra Phutthabat District– Saraburi province. At the same time, the low PM10 concentration occurs in the south of the study area, particularly in Mueang Pathum Thani and Lat Lum Kaeo District, Pathum Thani province.

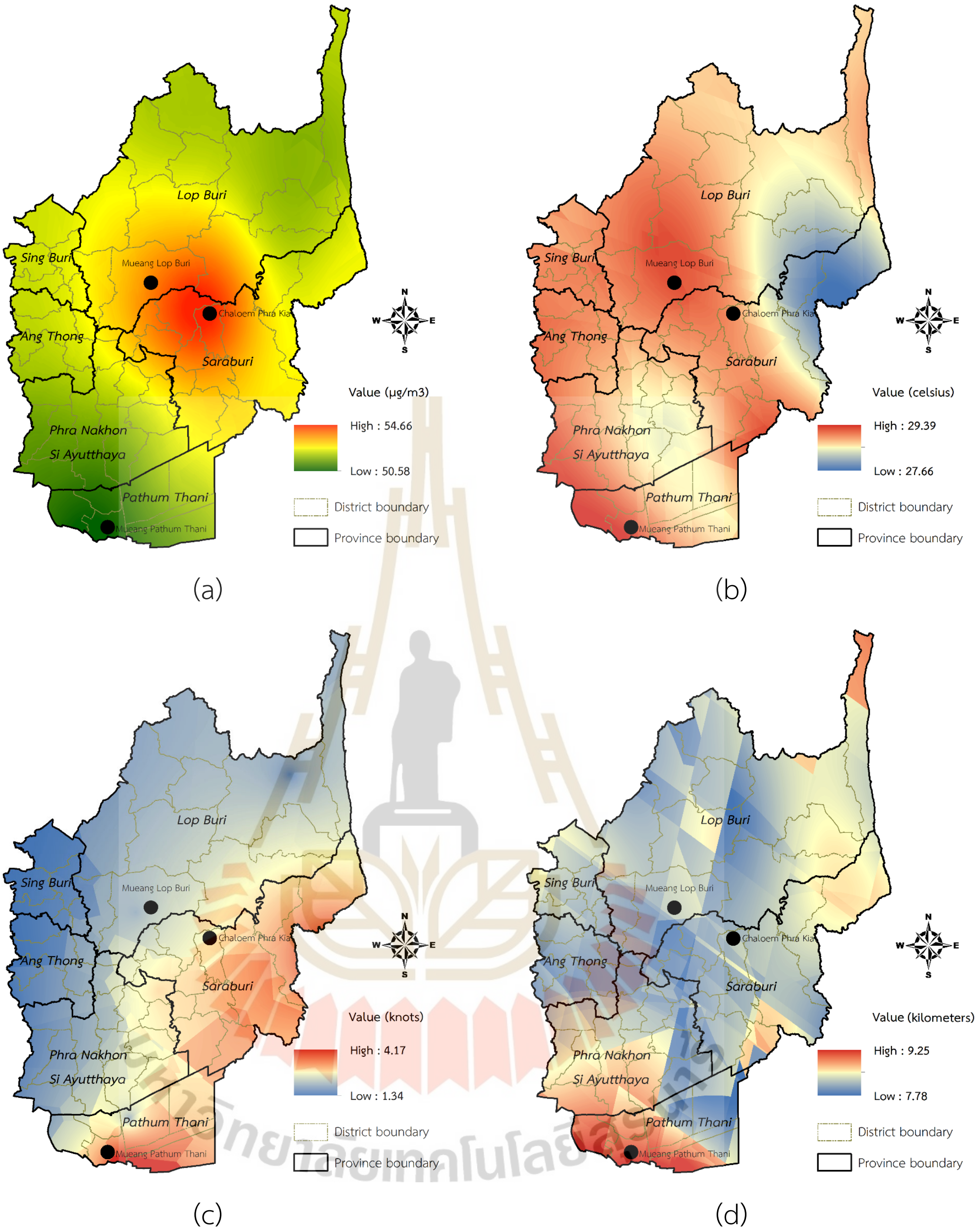

Figure 7.2 Spatial distribution map of (a) PM10 concentration (b) temperature (c) wind speed and (d) visibility.

7.3.1.2 November 2019 in the winter season

The result of spatial correlation analysis between PM10 concentration in November 2019 and their significant factors: wind speed, visibility, and MODIS AOD (see detail in Table 5.31) is reported in Table 7.18.

Table 7.18 Pearson correlation matrix among significant factors and PM10 concentration in November 2019.

Variables	PM10	Wind speed	Visibility	MODIS AOD
PM10	1.00	0.39	-0.31	-0.21
Wind speed	0.39	1.00	0.44	-0.12
Visibility	-0.31	0.44	1.00	0.14
MODIS AOD	-0.21	-0.12	0.14	1.00

From Table 7.18, PM10 concentration in November 2019 shows a positive relationship with wind speed, while it negatively shows a relationship with visibility and MODIS AOD. As a result, if PM10 concentration increases, visibility and MODIS AOD, as the effect of PM10 concentration, tend to decrease. As expected, this finding shows a consistent linear relationship (Table 3.2). In opposite, when wind speed increases, PM10 concentration also increase. This finding does not show a consistent linear relationship as expected in Table 3.2. Basically, wind speed, influencers on PM concentration, increase, and PM10 concentration should decrease. The scatterplot between PM10 concentration and wind speed is displayed in Figure 7.3. As a result, the relationship between PM10 concentration and wind speed in November 2019 shows a non-linear form.

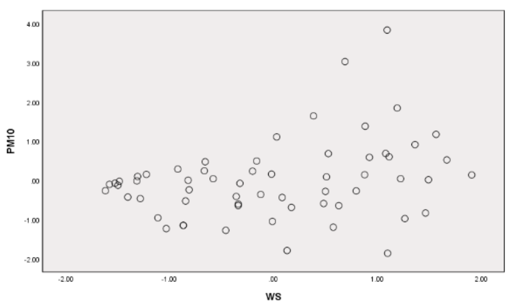

Figure 7.3 Scatterplot between PM10 concentration and wind speed in November 2019.

Moreover, the spatial distribution map of PM10 concentration and significant factors (wind speed, visibility, and MODIS AOD) are displayed in Figure 7.4. The spatial distribution map of PM10 concentration in November 2019 shows the high PM10 concentration occurs in the central part of the study area, particularly Chaloem Phra Kiat, Phra Phutthabat District– Saraburi province. At the same time, the low PM10 concentration occurs in the south of the study area, particularly in Sam Khok District - Pathum Thani province. The trend of the spatial distribution in November 2019 is like October 2019.

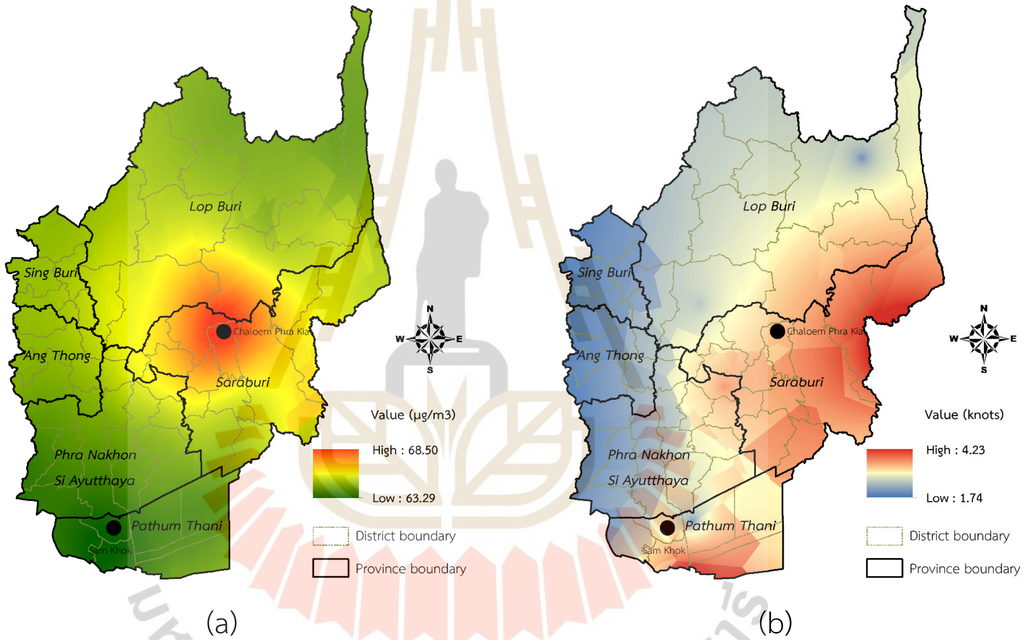

Figure 7.4 Spatial distribution map of (a) PM10 concentration (b) wind speed (c) visibility and (d) MODIS AOD.

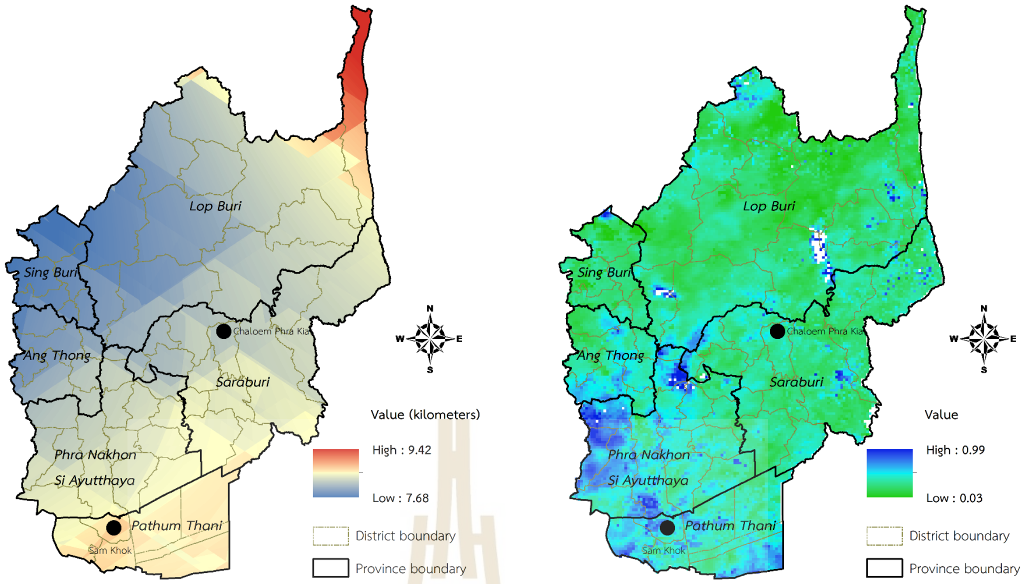

(c) (d)

Figure 7.4 (Continued).

7.3.1.3 December 2019 in the winter season

The result of spatial correlation analysis between PM10 concentration in December 2019 and their significant factors: temperature, wind speed, and visibility (see detail in Table 5.32) is reported in Table7.19.

Table 7.19 Pearson correlation matrix among significant factors and PM10 concentration in December 2019.

Variables	PM10	Temperature	Wind speed	Visibility
PM10	1.00	0.32	0.38	-0.21
Temperature	0.32	1.00	-0.30	-0.47
Wind speed	0.38	-0.30	1.00	0.49
Visibility	-0.21	-0.47	0.49	1.00

As of October 2019, PM10 concentration in December 2019 shows a positive relationship with wind speed and temperature. In contrast, it shows a negative relationship with visibility. As a result, if PM10 concentration increases, visibility, as the effect of PM10 concentration, tends to decrease. This finding shows expected results (Table 3.2). On the contrary, when temperature and wind speed increase, the PM10 concentration also increase. This finding does not show a consistent linear relationship as expected in Table 3.2. Basically, if temperature and wind speed, as influencers on PM concentration, increase, PM10 should decrease. The scatterplots between PM10 concentration and temperature or wind speed are displayed in Figure 7.5. As a result, the relationship between PM10 concentration and temperature or wind speed in December 2019 is non-linear form.

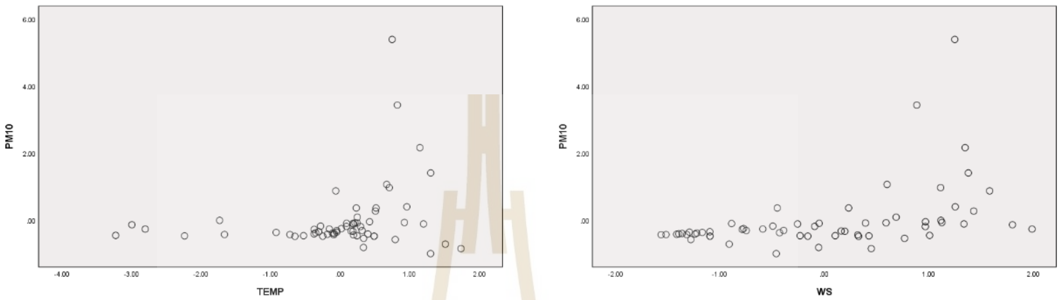

(a) (b)

Figure 7.5 Scatterplot between PM10 concentration and (a) temperature or (b) wind speed.

Moreover, the spatial distribution map of PM10 concentration and significant factors (temperature, wind speed, and visibility) are displayed in Figure 7.6. The spatial distribution map of PM10 concentration in December 2019 shows the high PM10 concentration occurs in the central part of the study area, particularly Chaloem Phra Kiat, Phra Phutthabat District– Saraburi province. At the same time, the low PM10 concentration occurs in the north and south of the study area, particularly in Tha Luang District - Lop Buri province and Mueang Pathum Thani District, Pathum Thani province.

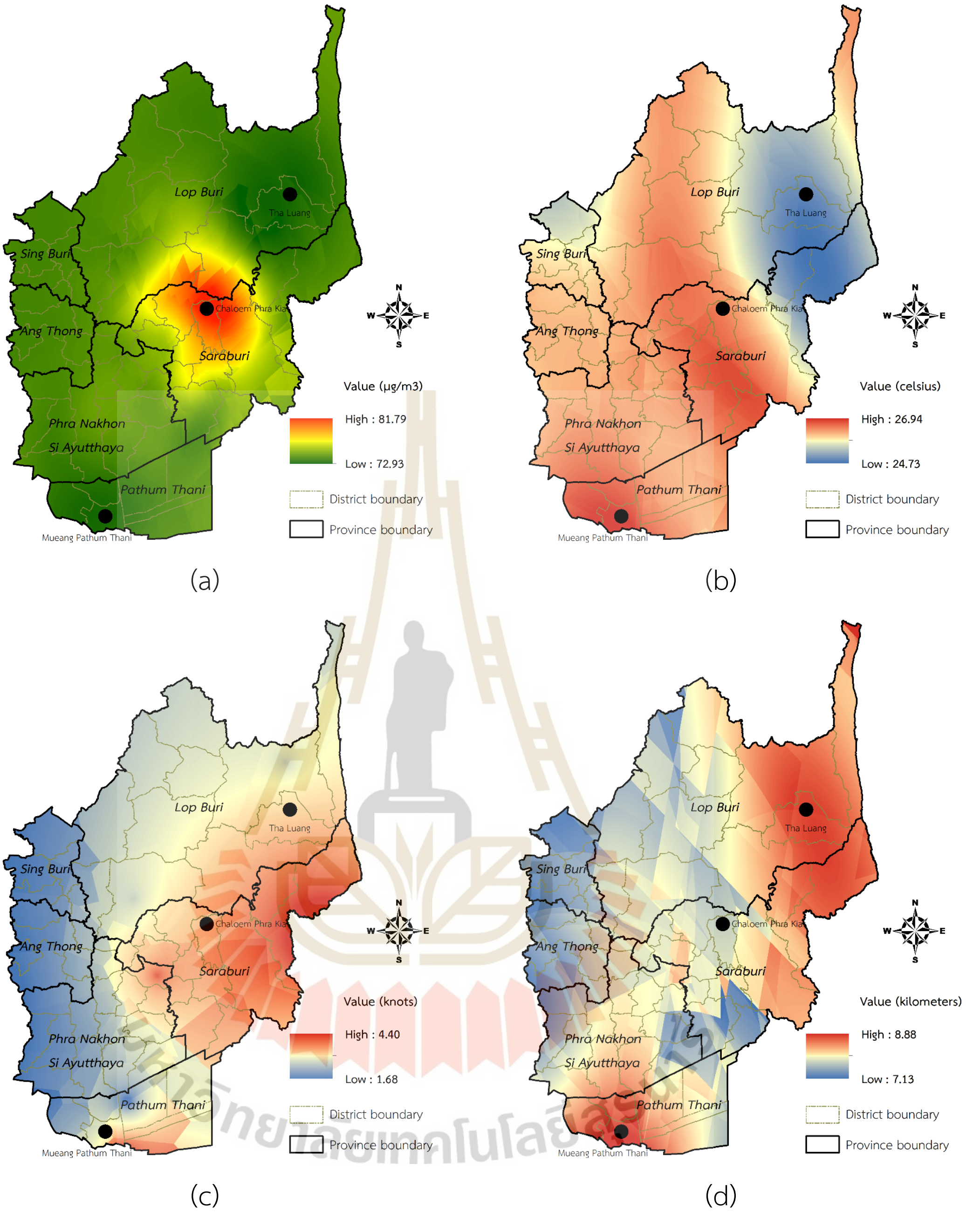

Figure 7.6 Spatial distribution map of (a) PM10 concentration (b) temperature (c) wind speed and (d) visibility.

7.3.1.4 January 2020 in the winter season

The result of spatial correlation analysis between PM10 concentration in January 2020 and their significant factors: temperature and MODIS AOD (see detail in Table 5.33) is reported in Table 7.20.

Table 7.20 Pearson correlation matrix among significant factors and PM10 concentration in January 2020.

Variables	PM10	Temperature	MODIS AOD
PM10	1.00	0.46	-0.12
Temperature	0.46	1.00	0.07
MODIS AOD	-0.12	0.07	1.00

From Table 7.20, PM10 concentration in January 2020 shows a negative relationship with MODIS AOD but a positive relationship with temperature. As a result, if PM10 concentration increase, MODIS AOD, as the effect of PM10 concentration, tends to decrease. This finding shows a consistent linear relationship, as mentioned in Table 3.2. In contrast, when temperature increases, PM10 concentration trends to increase. As expected, this finding does not show a consistent linear relationship (Table 3.2) as the influencer on PM concentration, temperature increases, and PM10 concentration should decrease. The scatterplot between PM10 concentration and temperature is displayed in Figure 7.7. As a result, the relationship between PM10 concentration and temperature is non-linear form.

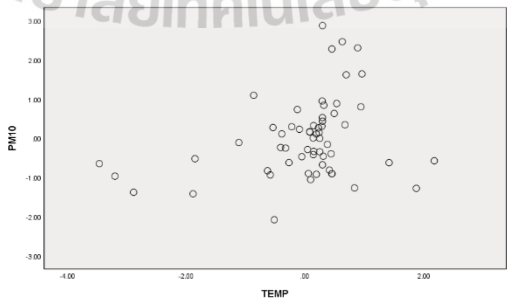

Figure 7.7 Scatterplots between PM10 concentration in January 2020 and temperature.

Moreover, the spatial distribution map of PM10 concentration and significant factors (temperature and MODIS AOD) are displayed in Figure 7.8. The spatial distribution map of PM10 concentration in January 2019 shows the high PM10 concentration in the central part of the study area, particularly Chaloem Phra Kiat, Sao Hai District– Saraburi province. At the same time, the low PM10 concentration occurs in the south of the study area, particularly Lam Sonthi - Lop Buri and Wang Muang District - Saraburi province.

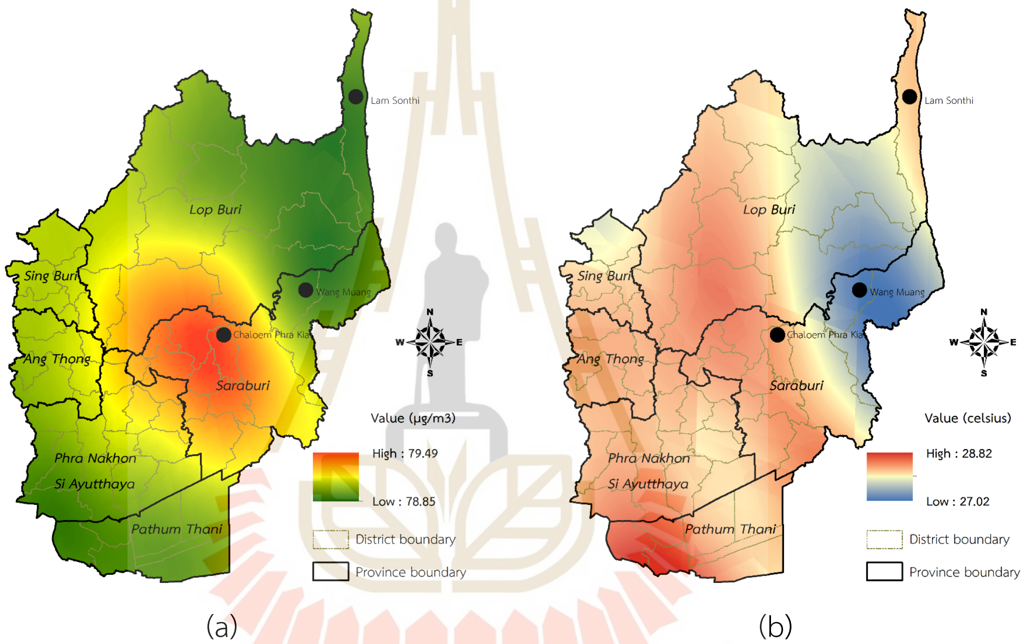

Figure 7.8 Spatial distribution map of (a) PM10 concentration (b) temperature and (c) MODIS AOD.

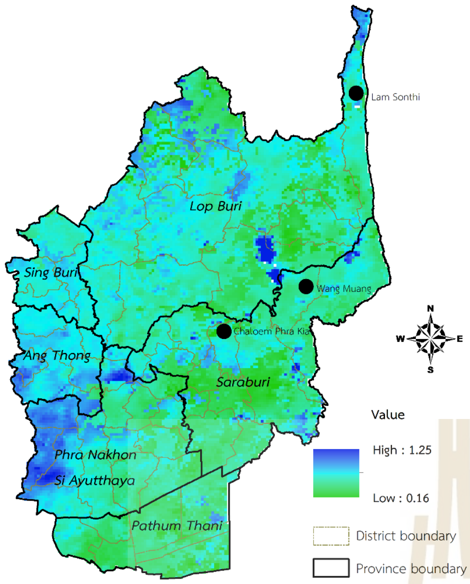

(c)

Figure 7.8 (Continued).

7.3.1.5 February 2020 in the winter season

The result of spatial correlation analysis between PM10 concentration in February 2020 and their significant factors: wind speed and fire radiative power (see detail in Table 5.34) is reported in Table7.21.

Table 7.21 Pearson correlation matrix among significant factors and PM10 concentration in February 2020.

Variables	PM10	Wind speed	Fire radiative power
PM10	1.00	0.39	0.31
Wind speed	0.39	1.00	0.30
Fire radiative power	0.31	0.30	1.00

From Table 7.21, PM10 concentration in February 2020 shows a positive relationship with wind speed and fire radiative power. As a result, if fire radiative power increase, PM10 concentration increase. This finding shows a consistent linear relationship, as mentioned in Table 3.2. However, when wind speed increases, the PM10 concentration also increase. This finding does not show a consistent linear relationship as expected (Table 3.2). Basically, if wind speed, as the influencer on PM concentration, increases, PM10 concentration will decrease. The scatterplot between

PM10 concentration and wind speed is displayed in Figure 7.9. As a result, the relationship between PM10 concentration and wind speed is a non-linear form.

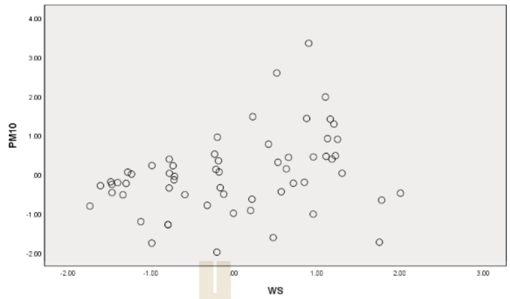

Figure 7.9 Scatterplots between PM10 concentration and wind speed in February 2020.

Moreover, the spatial distribution map of PM10 concentration and significant factors (wind speed and fire radiative power) is displayed in Figure 7.10. The spatial distribution map of PM10 concentration in February 2020 shows the high PM10 concentration occurs in the central part of the study area, particularly Chaloem Phra Kiat, Phra Phutthabat District– Saraburi province. At the same time, the low PM10 concentration occurs in the south of the study area, particularly Lat Lum Kaeo District, Pathum Thani province and Lat Bua Luang - Phra Nakhon Si Ayutthaya province.

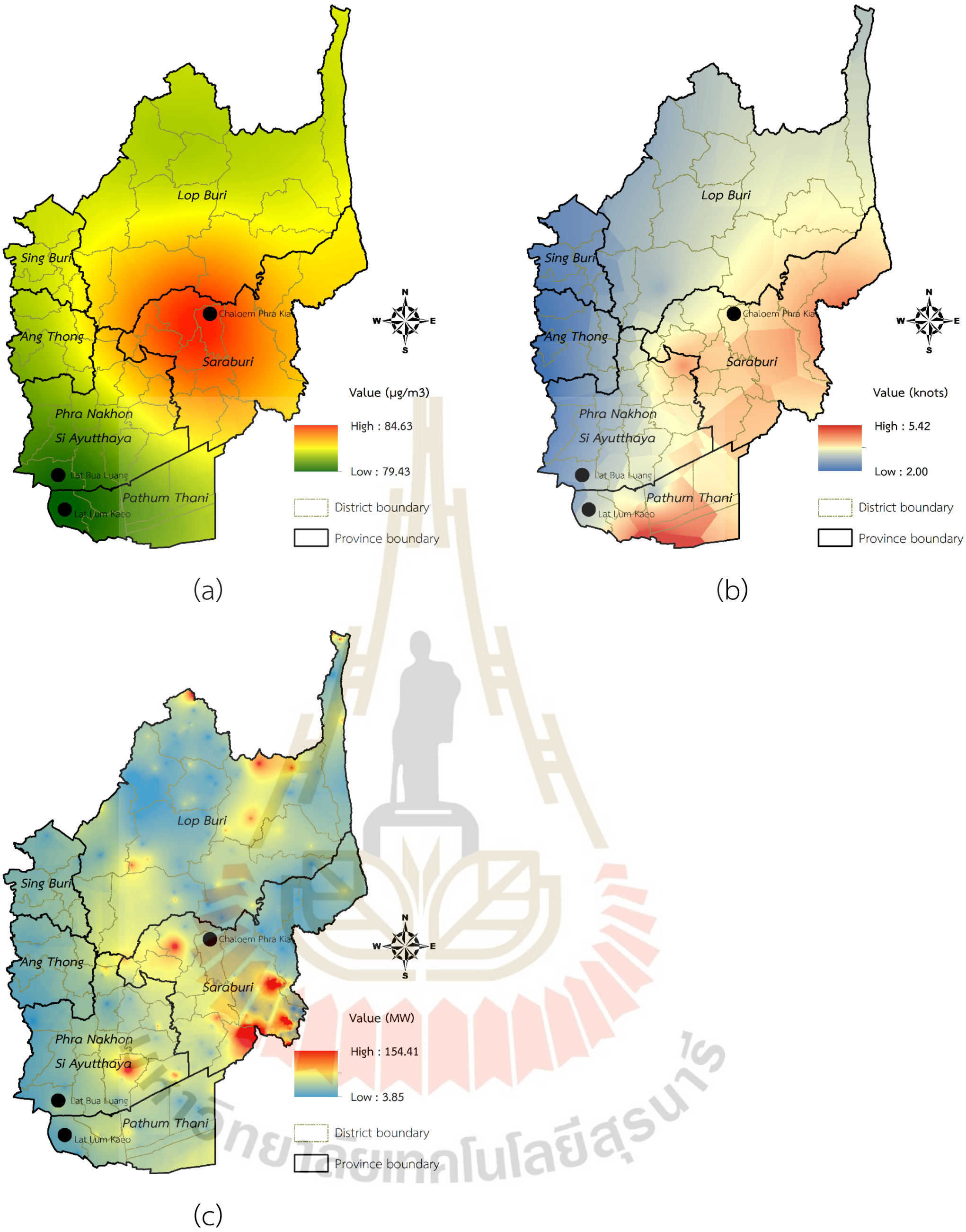

Figure 7.10 Spatial distribution map of (a) PM10 concentration, (b) wind speed and (c) fire radiative power.

7.3.1.6 March 2020 in the summer season

The result of spatial correlation analysis between PM10 concentration in March 2020 and their significant factors: temperature, MODIS AOD, and factory density (see detail in Table 5.35) are reported in Table7.22.

Table 7.22 Pearson correlation matrix among significant factors and PM10 concentration in March 2020.

Variables	PM10	Temperature	MODIS AOD	Factory density
PM10	1.00	-0.47	0.27	0.17
Temperature	-0.47	1.00	-0.10	-0.12
MODIS AOD	0.27	-0.10	1.00	0.03
Factory density	0.17	-0.12	0.03	1.00

From Table 7.22, PM10 concentration in March 2020 shows a negative relationship with temperature but a positive relationship with MODIS AOD and factory density. As a result, if factory density, as a source of PM concentration, increase, PM10 concentration will increase. Likewise, if temperature, as the influencer on PM concentration, increase, PM10 concentration should decrease. These findings show a consistent linear relationship, as mentioned in Table 3.2. On the contrary, PM10 concentration increases, MODIS AOD, as the effect of PM10 concentration, will increase. This phenomenon does not show a consistent linear relationship (Table 3.2). The scatterplot between PM10 concentration and MODIS AOD in March 2020, as shown in Figure 7.11, shows a non-linear form.

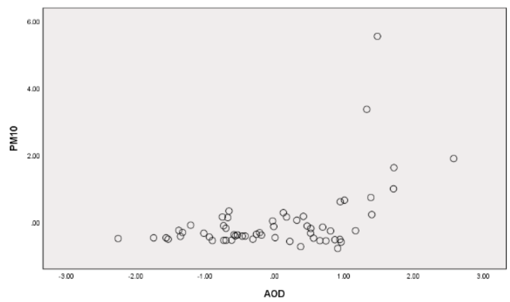

Figure 7.11 Scatterplots between PM10 concentration and MODIS AOD in March 2020.

Moreover, the spatial distribution map of PM10 concentration and significant factors (temperature, MODIS AOD, and factory density) is displayed in Figure 7.12. The spatial distribution map of PM10 concentration in March 2020 shows the high PM10 concentration in the central part of the study area, particularly Chaloem Phra Kiat, Mueang Saraburi District– Saraburi province. At the same time, the low PM10 concentration occurs in the north of the study area, particularly in Ban Mi and Khok Samrong District, Lop Buri province.

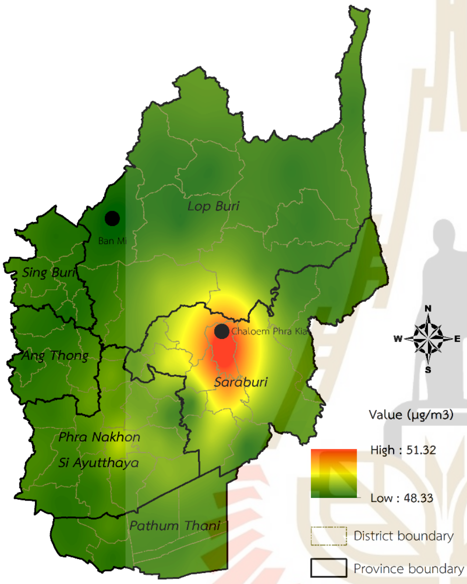

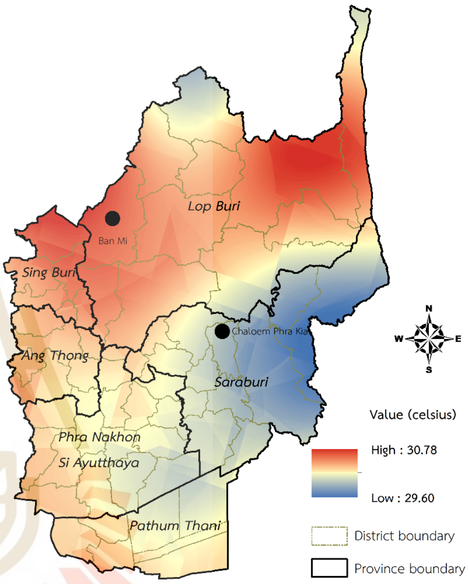

Figure 7.12 Spatial distribution map of (a) PM10 concentration (b) temperature (c) MODIS AOD and (d) factory density.

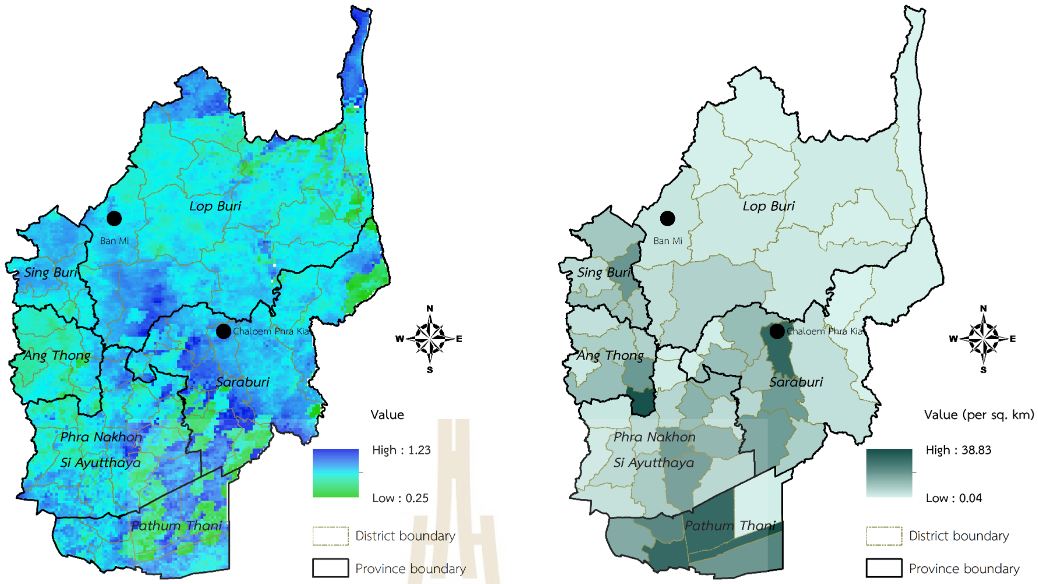

(c) (d)

Figure 7.12 (Continued).

7.3.1.7 April 2020 in the summer season

The result of spatial correlation analysis between PM10 concentration in April 2020 and their significant factors: brightness temperature (see detail in Table 5.36) is reported in Table 7.23.

Table 7.23 Pearson correlation matrix among significant factors and PM10 concentration in April 2020.

Variables	PM10	Brightness temperature
PM10	1.00	0.46
Brightness temperature	0.46	1.00

From Table 7.23, it can be observed that PM10 concentration in April 2020 shows a positive relationship with brightness temperature. This finding shows a consistent linear relationship, as expected. Because if brightness temperature, as the source of PM10 concentration, increases, PM10 concentration should increase.

Moreover, the spatial distribution map of PM10 concentration and significant factors (brightness temperature) is displayed in Figure 7.13. The spatial distribution map of PM10 concentration in April 2020 shows the high PM10 concentration occurs in the central part of the study area, particularly Phra Phutthabat and Chaloem Phra Kiat District– Saraburi province. At the same time, the low PM10 concentration occurs in the south of the study area, particularly Lat Lum Kaeo and Mueang Pathum Thani District - Pathum Thani province.

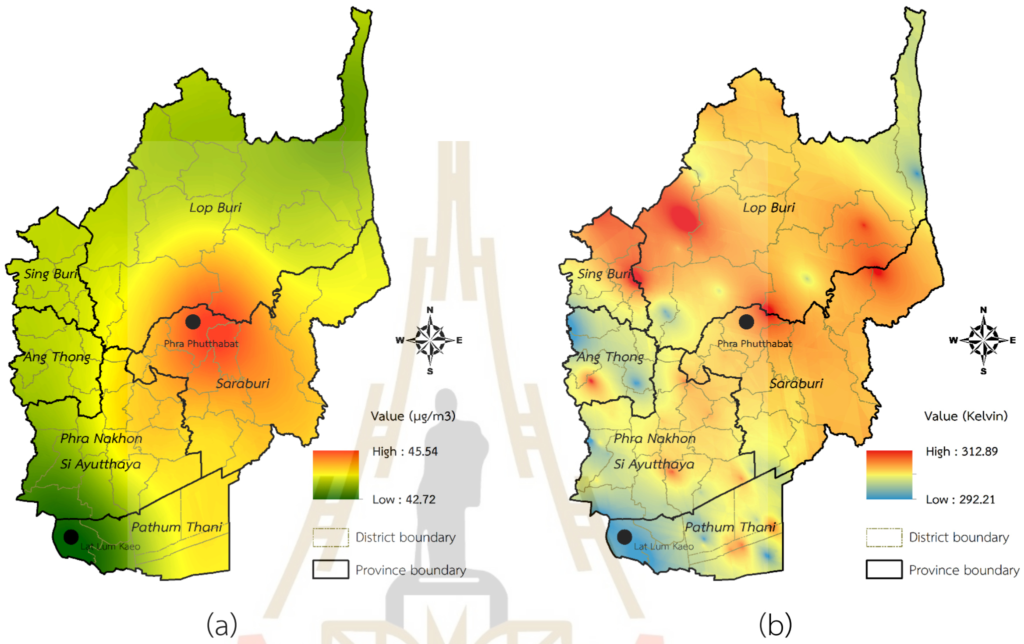

Figure 7.13 Spatial distribution map of (a) PM10 concentration and (b) brightness temperature.

7.3.1.8 May 2020 in the summer season

The result of spatial correlation analysis between PM10 concentration in May 2020 and their significant factors: visibility (see detail in Table 5.37) is reported in Table 7.24.

Table 7.24 Pearson correlation matrix among significant factor and PM10 concentration in May 2020.

Variables	PM10	Visibility
PM10	1.00	-0.22
Visibility	-0.22	1.00

From Table 7.12, it can be observed that PM10 concentration in May 2020 shows a negative relationship with visibility. As a result, if PM10 concentration increases, visibility, as the effect of PM10 concentration, tends to decrease. This finding indicates a consistent linear relationship (Table 3.2).

Moreover, the spatial distribution map of PM10 concentration and significant factor (visibility) is displayed in Figure 7.14. The spatial distribution map of PM10 concentration in May 2020 shows the high PM10 concentration in the central part of the study area, particularly Chaloem Phra Kiat and Kaeng Khoi District– Saraburi province. At the same time, the low PM10 concentration occurs in the south of the study area, particularly in Mueang Pathum Thani and Lat Lum Kaeo District, Pathum Thani province.

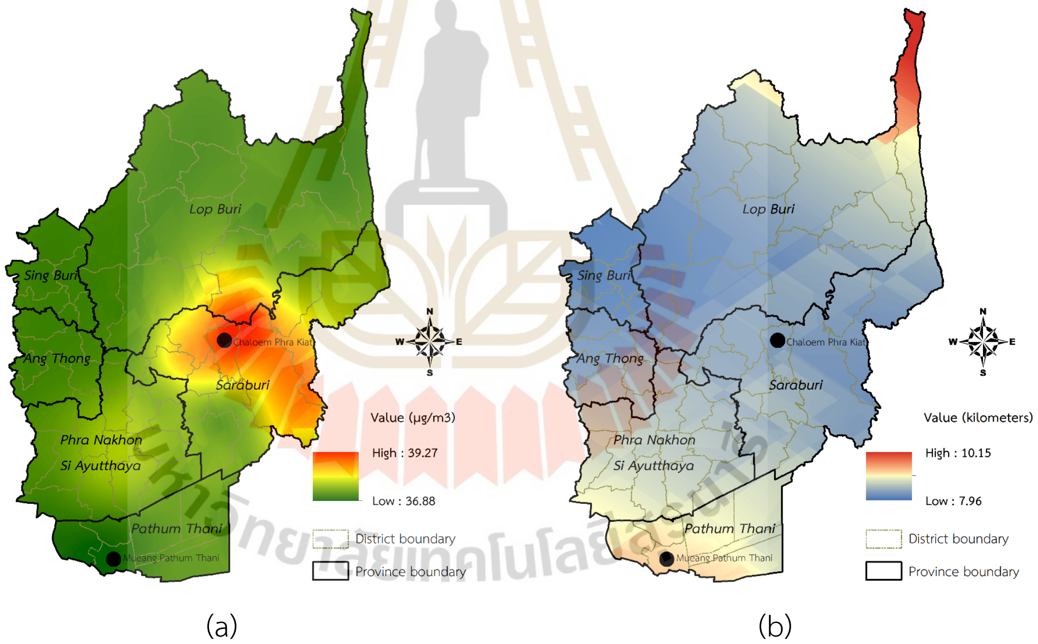

Figure 7.14 Spatial distribution map of (a) PM10 concentration and (b) visibility.

Summary

According to significant factors (Tables 7.17 to 7.24), the relationship between PM10 concentration and significant monthly factors is summarized in Table 7.25 again. As a result, it can be observed that the relationship between temperature and wind speed, as the influencer of PM concentration, is a non-linear form. On the contrary, the relationship between visibility and MOD AOD, as the effect of PM concentration, is linear. Likewise, the relationship between fire radiative power, factory density, and brightness temperature as a source of PM concentration is a linear form.

Table 7.25 Summary of the relationship between PM10 concentration and their significant monthly factors.

Month	TEMP	WS	VIS	AOD	FRP	FD	BT
October	No	No	Yes	N. a.	N. a.	N. a.	N. a.
November	N. a.	No	Yes	Yes	N. a.	N. a.	N. a.
December	No	No	Yes	N. a.	N. a.	N. a.	N. a.
January	No	N. a.	N. a.	Yes	N. a.	N. a.	N. a.
February	N. a.	No	N. a.	N. a.	Yes	N. a.	N. a.
March	Yes	N. a.	N. a.	No	N. a.	Yes	N. a.
April	N. a.	N. a.	N. a.	N. a.	N. a.	N. a.	Yes
May	N. a.	N. a.	Yes	N. a.	N. a.	N. a.	N. a.

Note: 1. Yes represents a linear relationship between PM10 concentration and specific significant factor

2. No represents a non-linear relationship between PM10 concentration and specific significant factor

3. N.a. represents not applied in spatial correlation analysis.

7.3.2 Relationship between monthly PM2.5 concentration and their factors

7.3.2.1 October 2019 in the winter season

The result of spatial correlation analysis between PM2.5 concentration in October 2019 and their significant factors: wind speed, pressure, visibility, MODIS AOD, brightness temperature, fire radiative power, fire hotspot, and elevation (see detail in Table 5.41) is reported in Table 7.26.

Table 7.26 Pearson correlation matrix among significant factors and PM2.5 concentration in October 2019.

Variables	PM2.5	WS	P	VIS	AOD	BT	FRP	FH	ELEV
PM2.5	1.00	-0.30	0.30	0.49	0.63	0.22	-0.18	-0.50	0.20
WS	-0.30	1.00	-0.43	-0.17	0.01	-0.10	0.54	0.02	-0.47
P	0.30	-0.43	1.00	0.04	0.02	-0.10	-0.06	0.16	0.17
VIS	0.49	-0.17	0.04	1.00	0.15	0.35	0.00	-0.53	0.24
AOD	0.63	0.01	0.02	0.15	1.00	-0.07	0.01	-0.27	-0.10
BT	0.22	-0.10	-0.10	0.35	-0.07	1.00	-0.10	-0.28	0.05
FRP	-0.18	0.54	-0.06	0.00	0.01	-0.10	1.00	0.07	-0.38
FH	-0.50	0.02	0.16	-0.53	-0.27	-0.28	0.07	1.00	-0.16
ELEV	0.20	-0.47	0.17	0.24	-0.10	0.05	-0.38	-0.16	1.00

From Table 7.26, PM2.5 concentration in October 2019 shows a negative relationship with wind speed, fire radiative power, and fire hotspot. In contrast, it positively correlates with pressure, visibility, MODIS AOD, brightness temperature, and elevation. As a result, if wind speed, as the influencer of PM2.5 concentration, increase, PM2.5 concentration should decrease. Meanwhile, if pressure, as the influencer of PM2.5 concentration, increase, PM2.5 concentration should increase. In addition, brightness temperature, as a source of PM2.5 concentration increase, will increase PM2.5 concentration. These findings show a consistent linear relationship, as mentioned in Table 3.2.

On the contrary, as mentioned, PM2.5 concentration increases, visibility and MODIS AOD, as the effect of PM concentration, decrease. This finding does not show a consistent linear relationship (Table 3.2). Similarly, this phenomenon occurs with fire radiative power and fire hotspot, as a source of PM concentration, do not show a consistent linear relationship with PM2.5 concentration, as expected. Also, elevation, as the influencer of PM concentration, does not show a consistent linear relationship with PM2.5 concentration, as expected. The scatterplots between PM2.5 concentration and visibility, MODIS AOD, fire radiative power, fire hotspots, and elevation are displayed in Figure 7.15. As a result, the relationships between PM2.5 concentration and visibility, MODIS AOD, fire radiative power, fire hotspots, or elevation are non-linear.

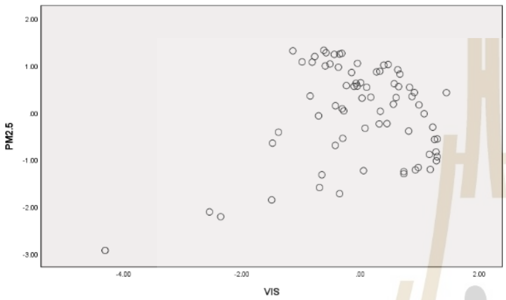

(a

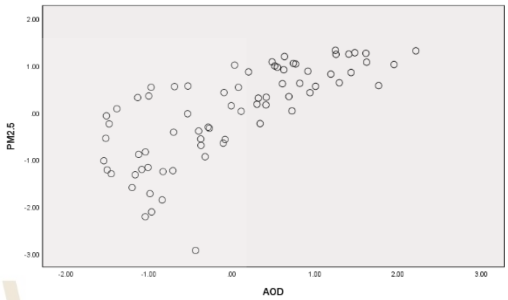

(b)

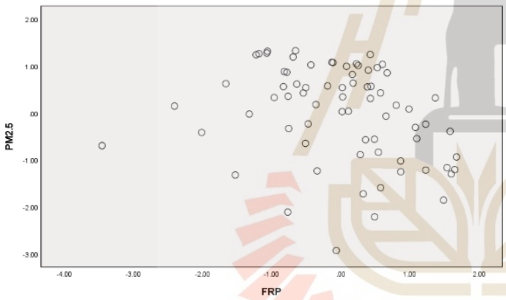

(c)

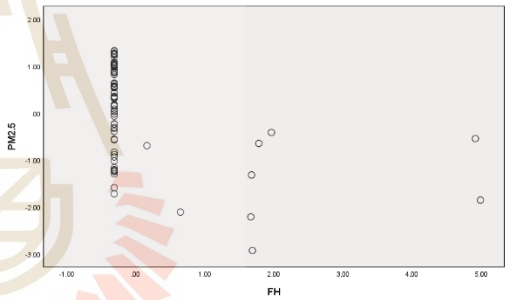

(d)

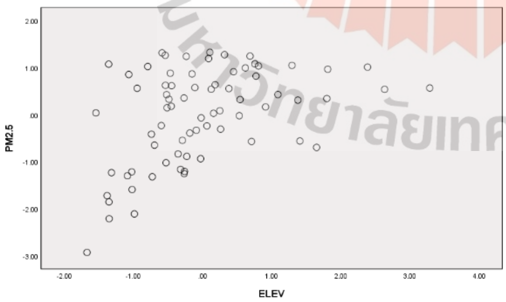

(e)

Figure 7.15 Scatterplots between PM2.5 concentration in October 2019 and (a) visibility, (b) MODIS AOD, (c) fire radiative power, (d) fire hotspots, and (e) elevation.

Moreover, the spatial distribution map of PM2.5 concentration and significant factors (wind speed, pressure, visibility, brightness temperature, fire radiative power, MODIS AOD, fire hotspot, and elevation) is displayed in Figure 7.16. The spatial distribution map of PM2.5 concentration in October 2019 shows the high PM2.5 concentration in the central part of the study area, particularly Bang Bon and Phasi Charoen District – Bangkok province. At the same time, the low PM2.5 concentration occurs in the east of the study area, particularly in Bang Bo and Bang Sao Thong District - Samut Prakan province.

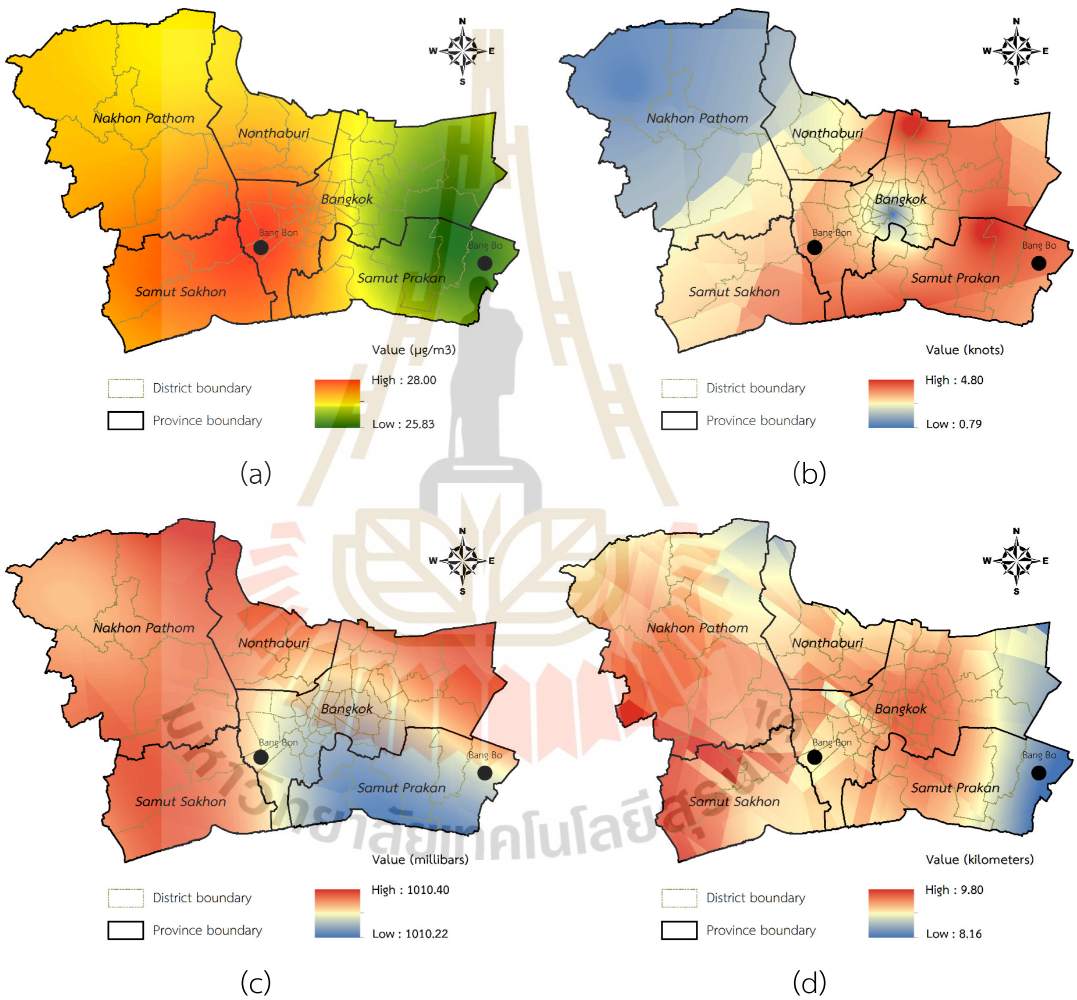

Figure 7.16 Spatial distribution map of (a) PM2.5 concentration (b) wind speed, (c) pressure, (d) visibility, (e) MODIS AOD, (f) brightness temperature, (g) fire radiative power, (h) fire hotspot, and (i) elevation.

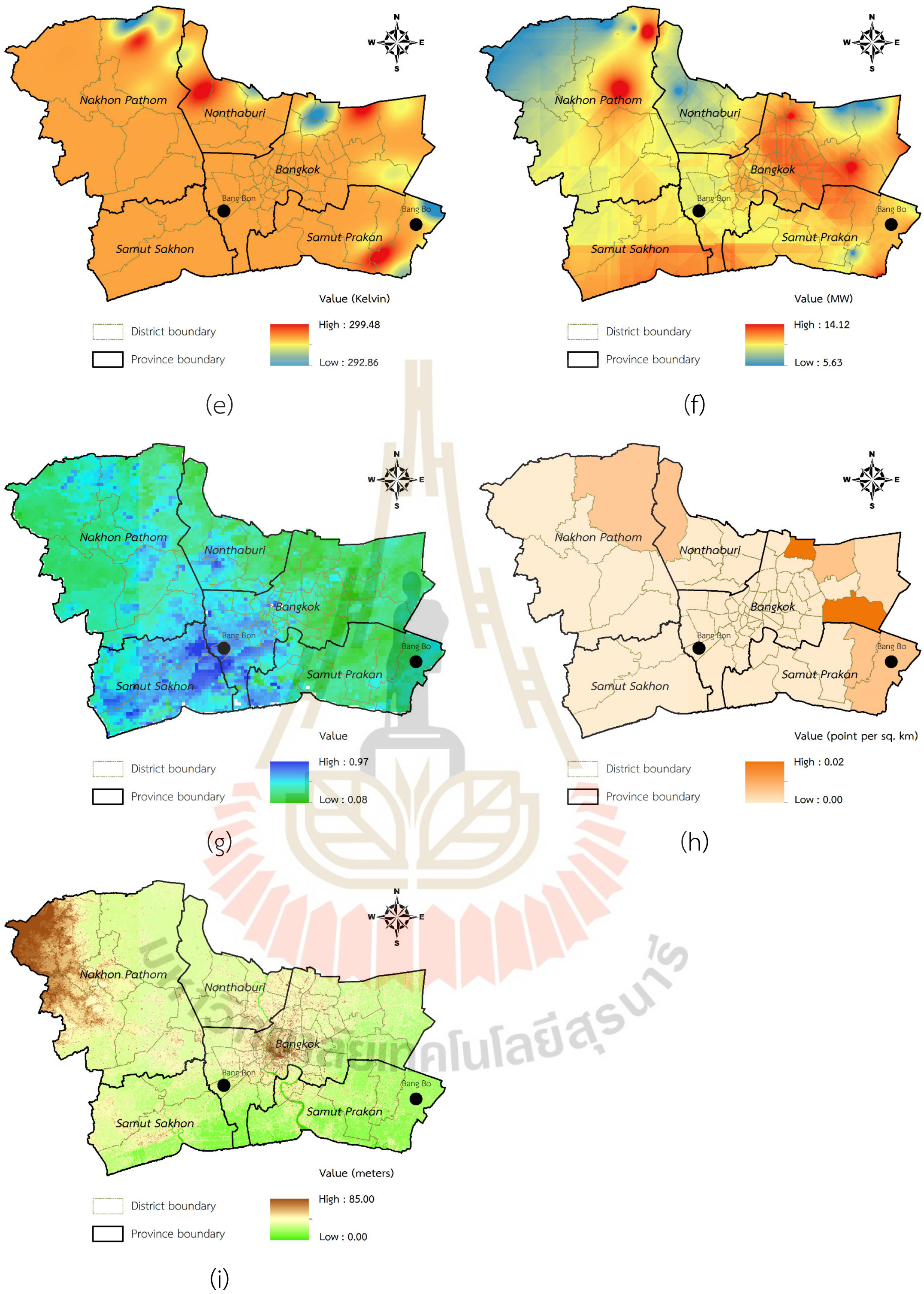

Figure 7.16 (Continued).

7.3.2.2 November 2019 in the winter season

The result of spatial correlation analysis between PM2.5 concentration in November 2019 and their significant factors: visibility and fire radiative power (see detail in Table 5.42) is reported in Table 7.27.

Table 7.27 Pearson correlation matrix among significant factors and PM2.5 concentration in November 2019.

Variables	PM2.5	Visibility	Fire radiative power
PM2.5	1.00	0.40	0.32
Visibility	0.40	1.00	0.27
Fire radiative power	0.32	0.27	1.00

From Table 7.27, PM2.5 concentration in November 2019 shows a positive relationship with visibility and fire radiative power factor. As a result, as a source of PM2.5 concentration, fire radiative power increases, and PM2.5 concentration will increase. This finding shows a consistent linear relationship, as expected.

Conversely, as mentioned above, if PM2.5 concentration increases, visibility, as the effect of PM concentration, increases. This finding does not show a consistent linear relationship as expected (Table 3.2). The scatterplots between PM2.5 concentration and visibility in Figure 7.17 shows a non-linear form.

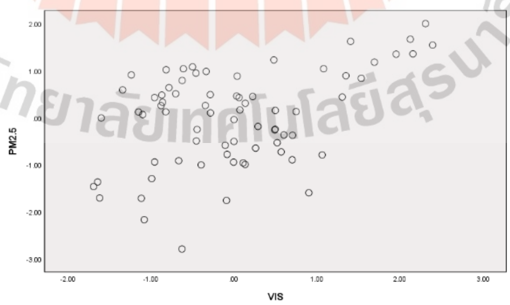

Figure 7.17 Scatterplots between PM2.5 concentration and visibility.

Moreover, the spatial distribution map of PM2.5 concentration and significant factors (visibility and fire radiative power) is displayed in Figure 7.18. The spatial distribution map of PM2.5 concentration in November 2019 shows the high PM2.5 concentration in the west part of the study area, particularly Bang Bon and Phasi

Charoen District – Bangkok province. At the same time, the low PM2.5 concentration occurs in the east of the study area, particularly in Bang Bo and Bang Sao Thong District - Samut Prakan province.

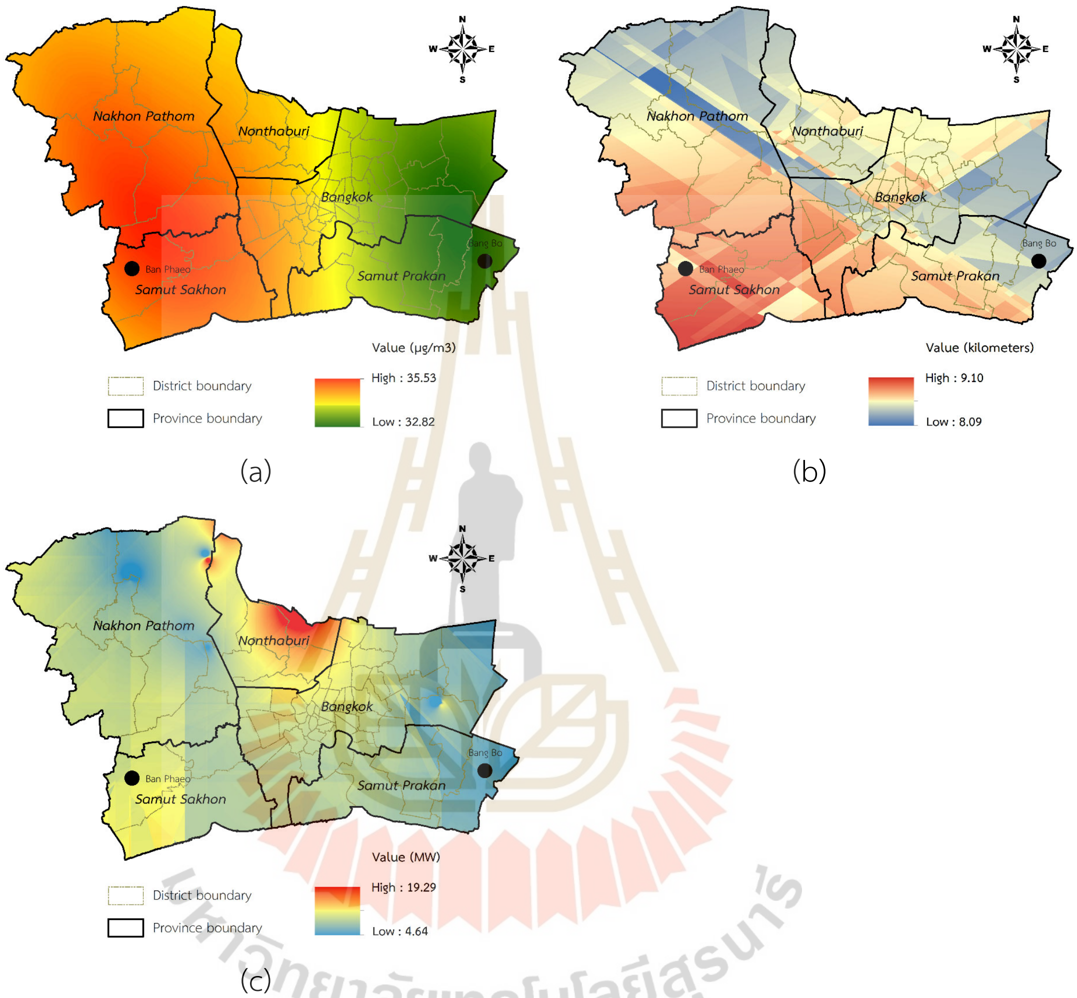

Figure 7.18 Spatial distribution map of (a) PM2.5 concentration (b) visibility and (c) fire radiative power.

7.3.2.3 December 2019 in the winter season

The result of spatial correlation analysis between PM2.5 concentration in December 2019 and their significant factors: wind speed and visibility (see detail in Table 5.43) is reported in Table 7.28.

Table 7.28 Pearson correlation matrix among significant factors and PM2.5 concentration in December 2019.

Variables	PM2.5	Wind speed	Visibility
PM2.5	1.00	-0.69	0.37
Wind speed	-0.69	1.00	-0.05
Visibility	0.37	-0.05	1.00

From Table 7.28, PM2.5 concentration in December 2019 shows a negative relationship with wind speed. As a result, if wind speed, as the influencer of PM concentration, increase, PM2.5 will decrease. This finding does show a consistent linear relationship, as expected.

In contrast, the PM2.5 concentration in December 2019 positively correlates with visibility. As a result, PM2.5 concentration increases, visibility, the effect of PM concentration, will increase. This finding does not show a consistent linear relationship, as expected. The scatterplots between PM2.5 concentration and visibility in Figure 7.19 does not show a linear form.

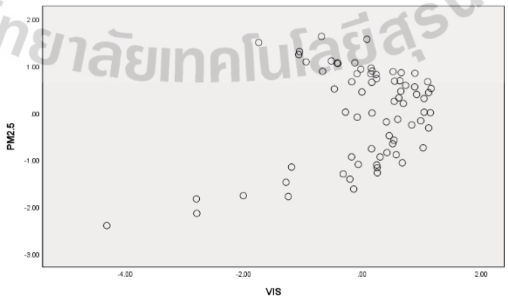

Figure 7.19 Scatterplots between PM2.5 concentration in December 2019 and visibility.

Moreover, the spatial distribution map of PM2.5 concentration and significant factors (wind speed and visibility) is displayed in Figure 7.20. The spatial distribution map of PM2.5 concentration in December 2019 shows the high PM2.5 concentration in the west part of the study area, particularly Kamphaeng Saen and Mueang Nakhon Pathom District – Nakhon Pathom province. At the same time, the low PM2.5 concentration occurs in the east of the study area, particularly in Bang Bo and Bang Sao Thong District - Samut Prakan province.

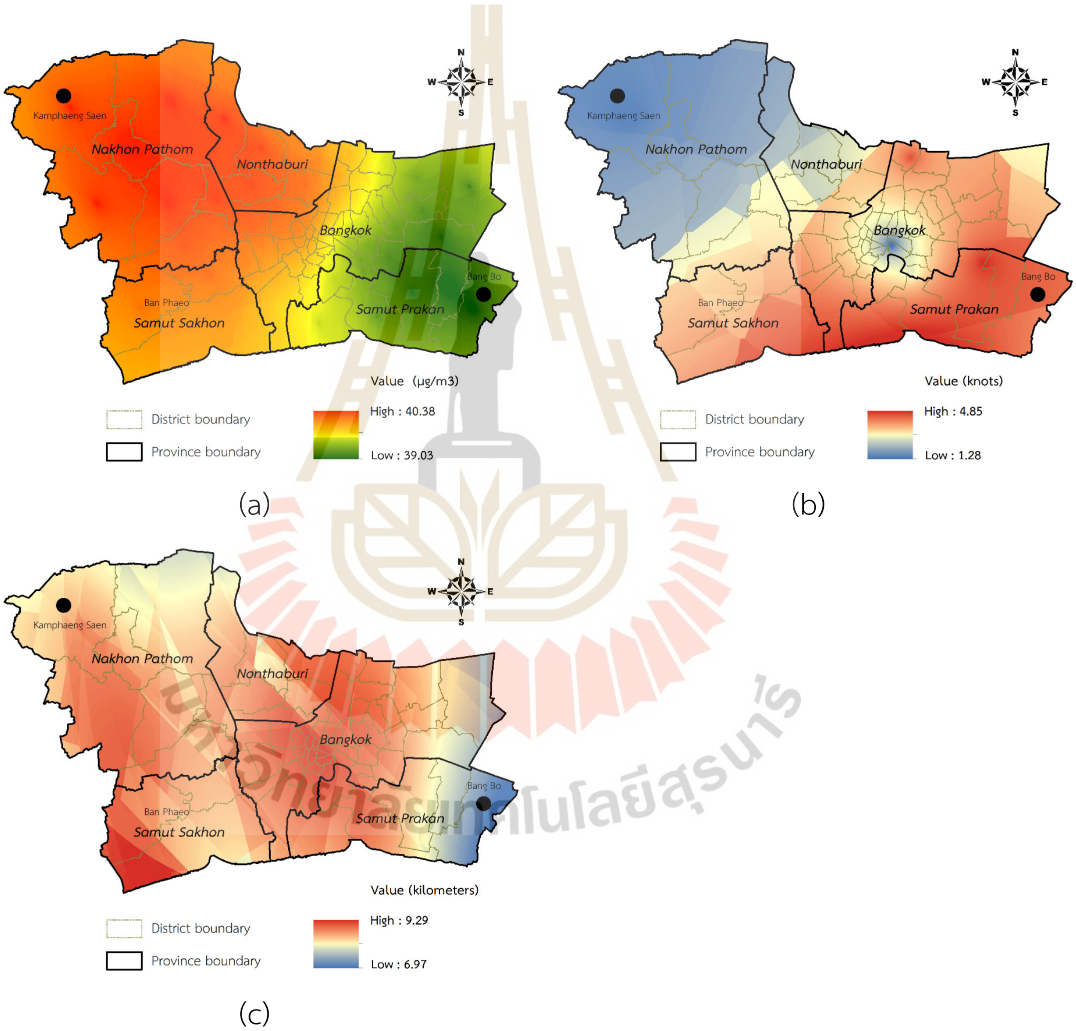

Figure 7.20 Spatial distribution map of (a) PM2.5 concentration, (b) wind speed and (c) visibility.

7.3.2.4 January 2020 in the winter season

The result of spatial correlation analysis between PM2.5 concentration in January 2020 and their significant factors: temperature, visibility, MODIS AOD, fire hotspot, and elevation (see detail in Table 5.44) is reported in Table 7.29.

Table 7.29 Pearson correlation matrix among significant factors and PM2.5 concentration in January 2020.

Variables	PM2.5	TEMP	VIS	AOD	FH	ELEV
PM2.5	1.00	-0.41	-0.17	-0.28	0.16	0.22
TEMP	-0.41	1.00	0.04	-0.37	-0.11	-0.29
VIS	-0.17	0.04	1.00	0.04	-0.53	-0.10
AOD	-0.28	-0.37	0.04	1.00	-0.06	0.10
FH	0.16	-0.11	-0.53	-0.06	1.00	-0.06
ELEV	0.22	-0.29	-0.10	0.10	-0.06	1.00

From Table 7.29, temperature, visibility, MODIS AOD, and fire hotspot show a consistent linear relationship with PM2.5 concentration. In fact, as the influence of PM concentration increases, PM2.5 concentration will decrease. Meanwhile, visibility and MODIS AOD, as the effect of PM concentration, will decrease when PM2.5 increases. Also, fire hotspots, as a source of PM concentration, increase, PM2.5 will increase

On the contrary, elevation positively correlated with PM2.5 in January 2020. These finding does not show a consistent linear relationship as expected. In fact, if elevation, as the influencer of PM2.5 concentration, increase, PM2.5 will decrease. The scatterplot between PM2.5 concentration and elevation is displayed in Figure 7.21. As a result, the relationship between PM10 concentration and the elevation shows a non-linear form.

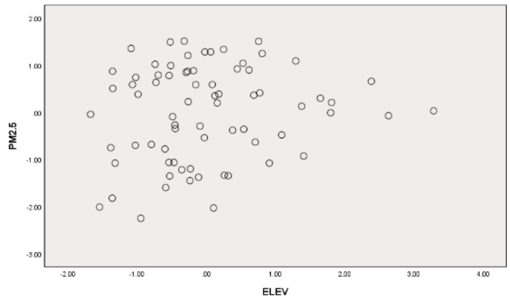

Figure 7.21 Scatterplots between PM2.5 concentration and elevation.

Moreover, the spatial distribution map of PM2.5 concentration and significant factors (wind speed and visibility) is displayed in Figure 7.22. The spatial distribution map of PM2.5 concentration in January 2020 shows the high PM2.5 concentration in the west part of the study area, particularly Bang Bua Thong District – Nonthaburi province and Nong Chok District – Bangkok province. At the same time, the low PM2.5 concentration occurs in the east of the study area, particularly Phra Samut Chedi District - Samut Prakan province and Bang Khun Thian – Bangkok province.

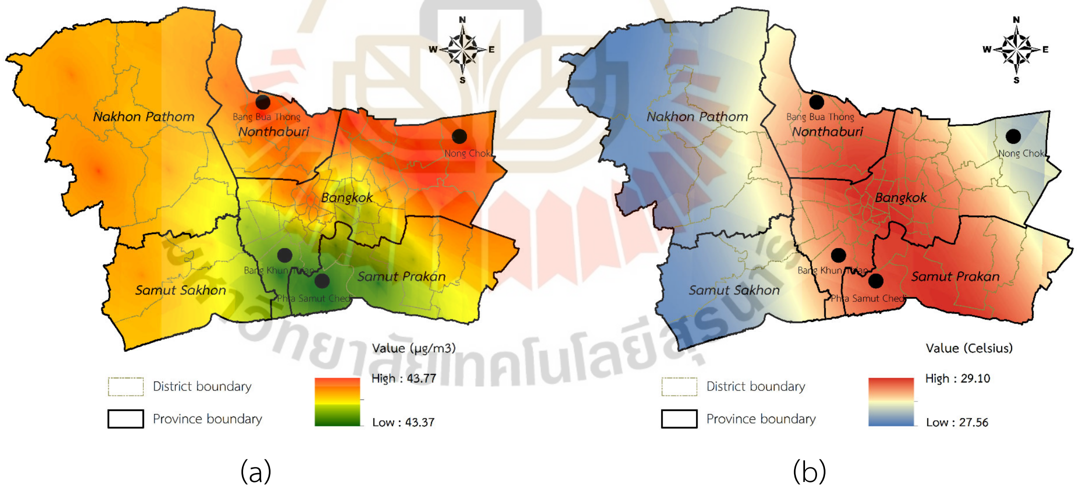

Figure 7.22 Spatial distribution map of (a) PM2.5 concentration (b) temperature, (c) visibility, (d) MODIS AOD, (e) fire hotspot, and (f) elevation.

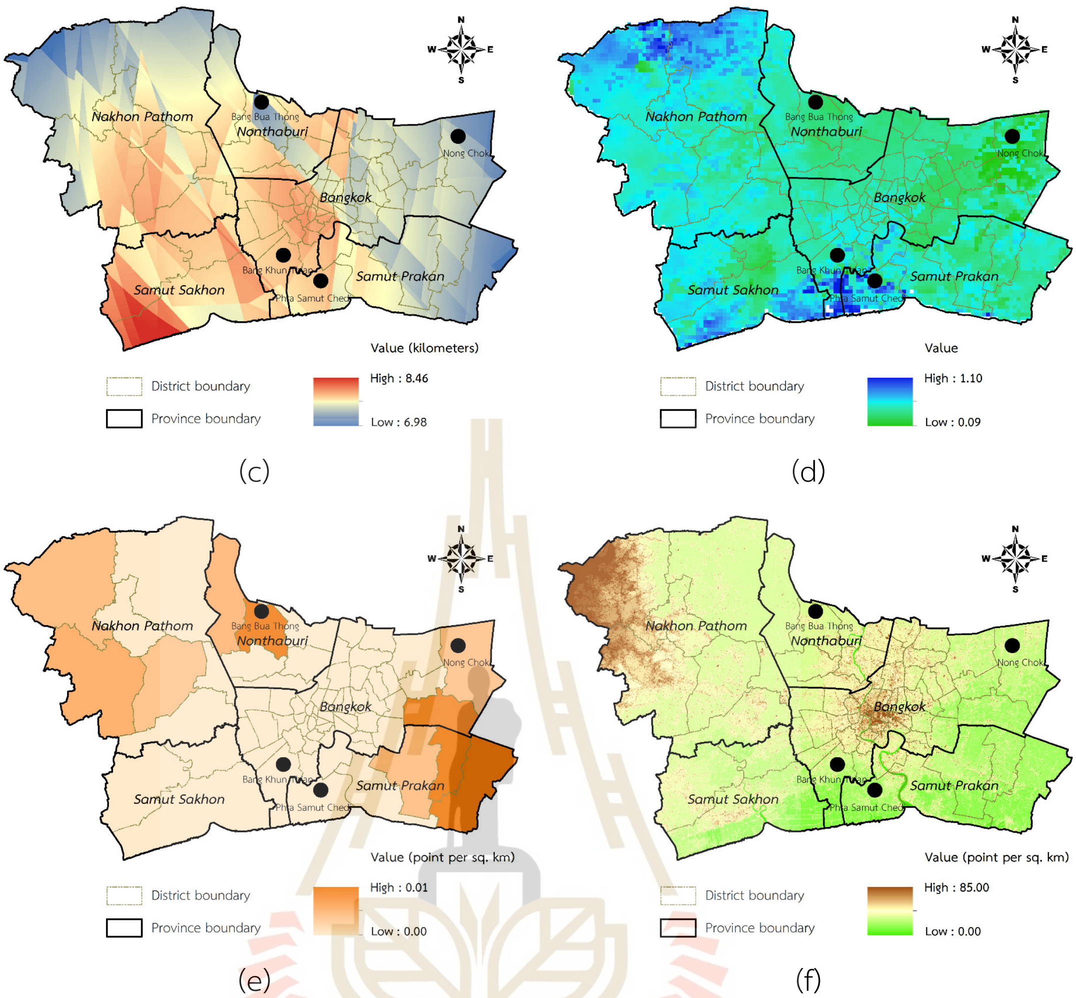

Figure 7.22 (Continued).

7.3.2.5 February 2020 in the winter season

The result of spatial correlation analysis between PM2.5 concentration in February 2020 and their significant factors: relative humidity, wind speed, pressure, fire radiative power, and elevation (see detail in Table 5.45) is reported in Table 7.30.

Table 7.30 Pearson correlation matrix among significant factors and PM2.5 concentration in February 2020.

Variables	PM2.5	RH	WS	P	FRP	ELEV
PM2.5	1.00	-0.48	-0.53	0.30	-0.57	0.30
RH	-0.48	1.00	0.34	0.20	0.00	-0.19
WS	-0.53	0.34	1.00	0.13	0.71	-0.49
P	0.30	0.20	0.13	1.00	-0.13	-1.05
FRP	-0.57	0.00	0.71	-0.13	1.00	-0.35
ELEV	0.30	-0.19	-0.49	-1.05	-0.35	1.00

From Table 7.30, wind speed and pressure showed a consistent linear relationship with PM2.5 concentration in February 2020. In fact, wind speed and pressure, as the influencer of PM concentration, show a negative and positive relationship with PM2.5 concentration, respectively.

On the contrary, as the PM concentration influencer, relative humidity and elevation show a negative and positive relationship with PM2.5 concentration, respectively. These results do not show a consistent linear relationship with PM2.5 concentration in February 2020, as mentioned in Table 3.2. Likewise, fire radiative power negatively affected PM2.5 concentration in February 2020. As a result, it does not show a consistent linear relationship with PM2.5 concentration, as expected. The scatterplots between PM2.5 concentration and relative humidity, fire radiative power, and elevation, as shown in Figure 7.23, shows a non-linear form.

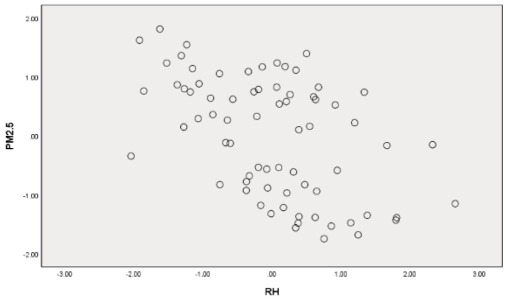

(a)

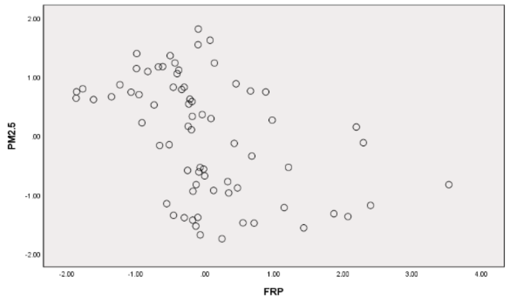

(b)

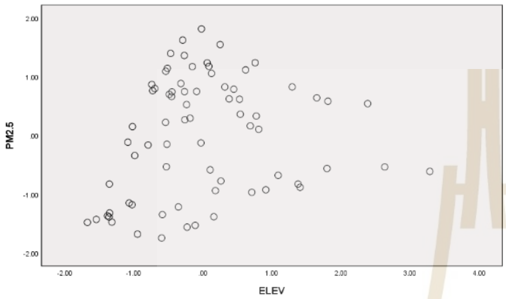

(c)

Figure 7.23 Scatterplots between PM2.5 concentration and (a) relative humidity, (b) fire radiative power, and (c) elevation.

Moreover, the spatial distribution map of PM2.5 concentration and significant factors (wind speed and visibility) is displayed in Figure 7.24. The spatial distribution map of PM2.5 concentration in February 2020 shows the high PM2.5 concentration in the north of the study area, particularly Don Mueang and Sai Mai District – Bangkok province. At the same time, the low PM2.5 concentration occurs in the south of the study area, particularly in Phra Samut Chedi and Mueang Samut Prakan District - Samut Prakan province.

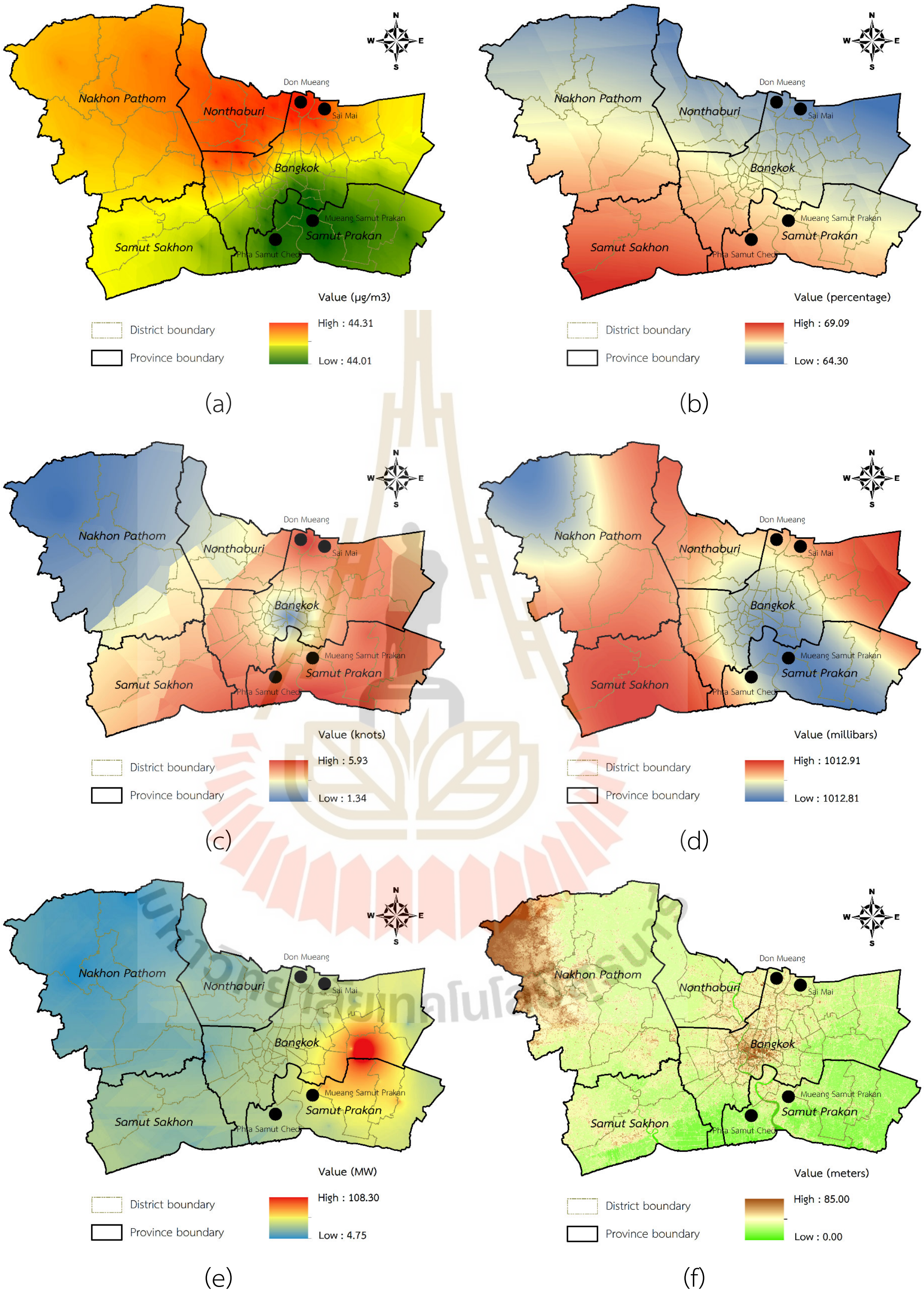

Figure 7.24 Spatial distribution map of (a) PM2.5 concentration (b) relative humidity, (c) wind speed, (d) pressure, (e) fire radiative power, and (f) elevation.

7.3.2.6 March 2020 in the summer season

The result of spatial correlation analysis between PM2.5 concentration in March 2020 and its significant factor: fire radiative power (see detail in Table 5.46) is reported in Table 7.31.

Table 7.31 Pearson correlation matrix among significant factors and PM2.5 concentration in March 2020.

Variables	PM2.5	FRP
PM2.5	1.00	0.40
FRP	0.40	1.00

As a result, in Table 7.31, fire radiative power,.as a source of PM concentration, positively correlates with PM2.5 concentration. This finding indicates a consistent linear relationship, as expected.

Moreover, the spatial distribution map of PM2.5 concentration and significant factor (fire radiative power) is displayed in Figure 7.25. The spatial distribution map of PM2.5 concentration and fire radiative power in March 2020 shows the high value in the same area, particularly Don Mueang and Sai Mai District – Bangkok province. At the same time, the low PM2.5 concentration occurs in the south of the study area, mainly Phaya Thai and Dusit District - Bangkok province.

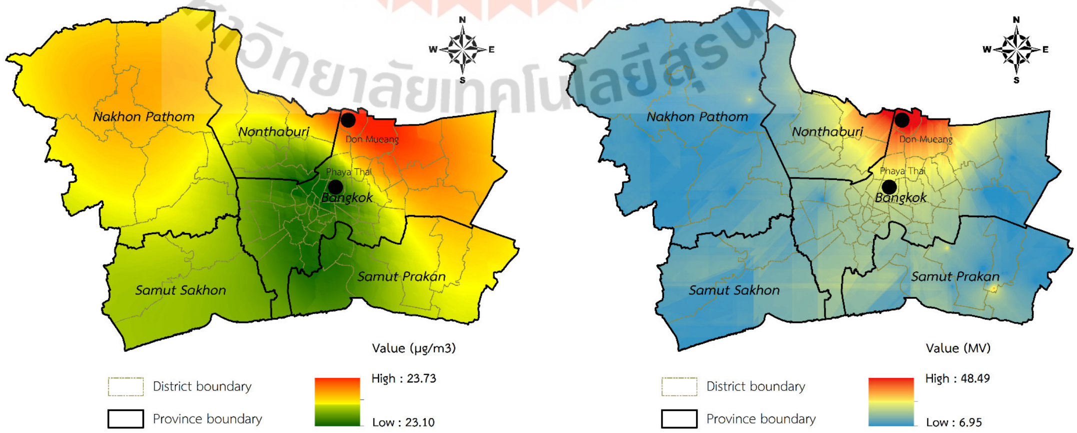

(a) (b)

Figure 7.25 Spatial distribution map of (a) PM2.5 concentration and (b) fire radiative power.

7.3.2.7 April 2020 in the summer season

The result of spatial correlation analysis between PM2.5 concentration in April 2020 and its significant factor: wind speed, visibility, brightness temperature, fire radiative power, MODIS AOD, fire hotspot, and factory density (see detail in Table 5.47) is reported in Table 7.32.

Table 7.32 Pearson correlation matrix among significant factors and PM2.5 concentration in April 2020.

Variables	PM2.5	WS	VIS	BT	FRP	AOD	FH	FD
PM2.5	1.00	0.29	0.10	-0.34	0.20	0.25	0.40	-0.24
WS	0.29	1.00	-0.12	0.30	0.77	0.21	0.13	0.23
VIS	0.10	-0.12	1.00	0.20	0.14	-0.18	-0.28	0.14
BT	-0.34	0.30	0.20	1.00	0.08	-0.01	-0.21	0.19
FRP	0.20	0.77	0.14	0.08	1.00	0.11	0.04	0.31
AOD	0.25	0.21	-0.18	-0.01	0.11	1.00	0.14	-0.10
FH	0.40	0.13	-0.28	-0.21	0.04	0.14	1.00	-0.16
FD	-0.24	0.23	0.14	0.19	0.31	-0.10	-0.16	1.00

From Table 7.32, PM2.5 concentration in April 2020 shows a positive relationship with wind speed, visibility, fire radiative power, MODIS AOD, and fire hotspot. In contrast, it shows a negative effect on brightness temperature and factory density. As a result, if fire radiative power and fire hotspots, as the source of PM2.5 concentration, increase, PM2.5 concentration should decrease. These findings show a consistent linear relationship, as mentioned in Table 3.2.

On the contrary, as mentioned, PM2.5 concentration increases, visibility and MODIS AOD, as the effect of PM concentration, increase. This finding does not show a consistent linear relationship (Table 3.2). Similarly, this phenomenon occurs with brightness temperature and factory density, as a source of PM concentration, show a positive relationship with PM2.5 concentration. Likewise, wind speed, as the influencer of PM concentration, positively correlates with PM2.5 concentration. These do not show a consistent linear relationship with PM2.5 concentration. The scatterplots between PM2.5 concentration and wind speed, visibility, brightness temperature, MODIS AOD, and factory density, as shown in Figure 7.26, show a non-linear form.

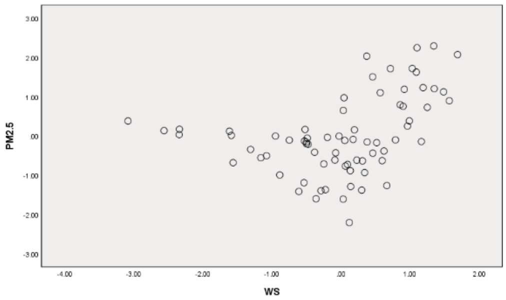

(a)

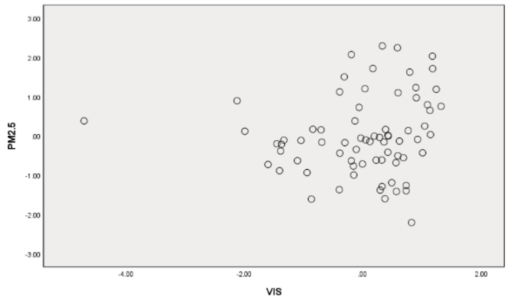

(b)

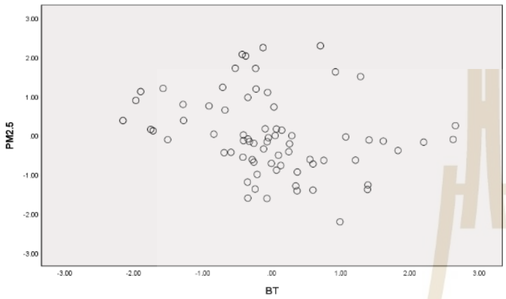

(c)

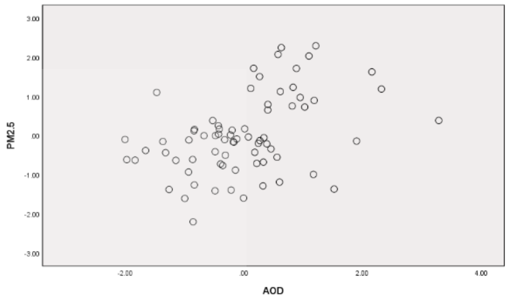

(d)

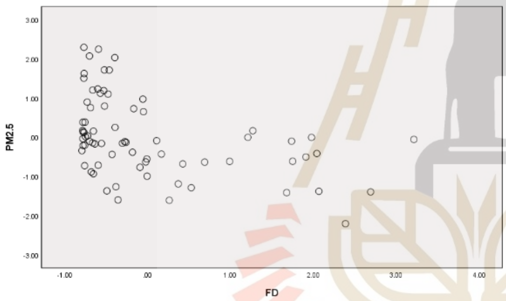

(e)

Figure 7.26 Scatterplots between PM2.5 concentration in April 2020 and (a) wind speed, (b) visibility, (c) brightness temperature, (d) MODIS AOD, and (e) factory density.

Moreover, the spatial distribution map of PM2.5 concentration and significant factors (wind speed, visibility, brightness temperature, fire radiative power, MODIS AOD, fire hotspot, factory density) are displayed in Figure 7.27. The spatial distribution map of PM2.5 concentration and fire radiative power in April 2020 shows the high value in the same area, particularly Khlong Sam Wa and Don Mueang District – Bangkok province. At the same time, the low PM2.5 concentration occurs in the south of the study area, mainly Pathum Wan and Khlong Toei District - Bangkok province.

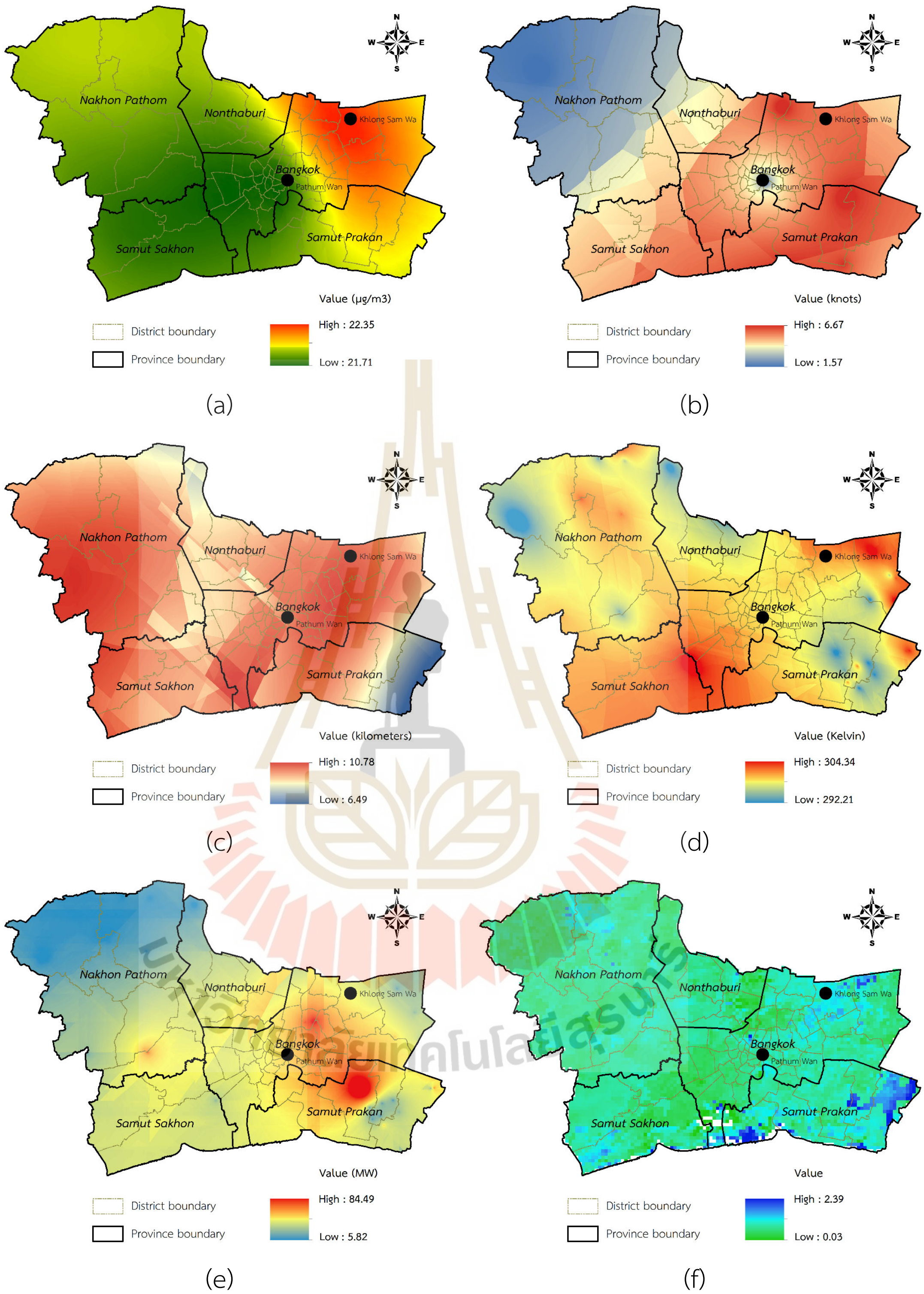

Figure 7.27 Spatial distribution map of (a) PM2.5 concentration and (b) wind speed, (c) visibility, (d) brightness temperature, (e) fire radiative power, (f) MODIS AOD, (g) fire hotspot, (h) factory density.

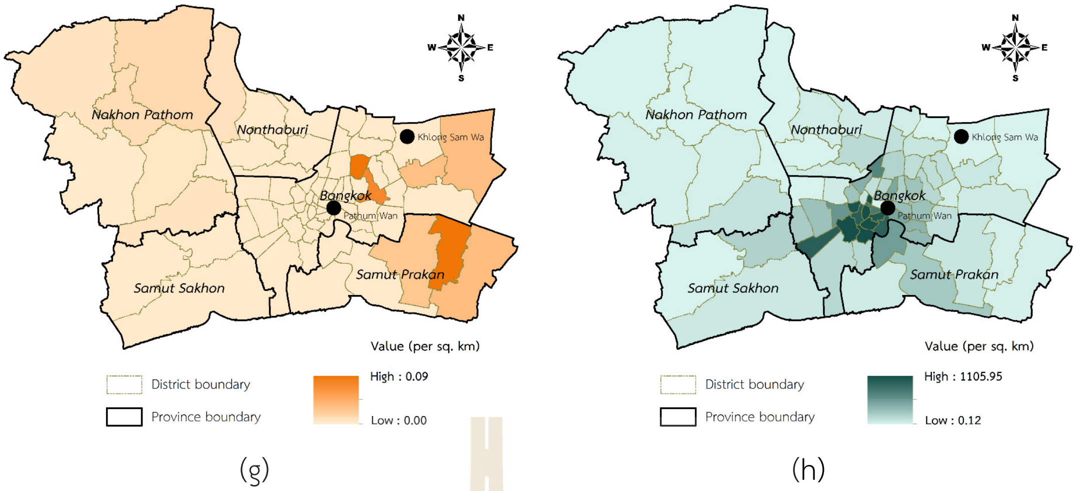

Figure 7.27 (Continued).

7.3.2.8 May 2020 in the summer season

The significant factors for PM2.5 concentration in May 2020 are wind speed, visibility, brightness temperature, factory density, and elevation (see detail in Table 5.48). At the same time, the correlation coefficient values between these variables and PM2.5 concentration are reported in Table 7.33.

Table 7.33 Pearson correlation matrix among significant factors and PM2.5 concentration in May 2020.

Variables	PM2.5	WS	VIS	BT	FD	ELEV
PM2.5	1.00	-0.37	-0.59	0.18	-0.32	0.23
WS	-0.37	1.00	-0.10	-0.24	0.23	-0.49
VIS	-0.59	-0.10	1.00	0.05	0.05	0.08
BT	0.18	-0.24	0.05	1.00	-0.07	0.08
FD	-0.32	0.23	0.05	-0.07	1.00	0.04
ELEV	0.23	-0.49	0.08	0.08	0.04	1.00

From Table 7.33, PM2.5 concentration in May 2020 shows a negative relationship with wind speed, visibility, and factory density. However, at the same time, it shows a positive relationship between brightness temperature and elevation. As a result, if PM2.5 concentration increases, wind speed and visibility, as the influence and the effect of PM2.5 concentration, respectively, tend to decrease. Likewise, when brightness temperature, as a source of PM2.5 concentration, increases, PM2.5 concentration increases. This finding shows a consistent linear relationship, as expected.

On the contrary, when factory density increase, PM10 concentration decrease. As elevation increases, PM10 concentration increases. These findings do not show a consistent linear relationship as expected. In fact, if factory density, as a source factor on PM2.5 concentration, increase, PM2.5 will increase. Likewise, if elevation, as the influencer of PM2.5 concentration, increases, PM2.5 concentration will decrease. The scatterplots between PM2.5 concentration and factory density and elevation are displayed in Figure 7.28. As a result, the relationship between PM10 concentration and factory density and elevation is a non-linear form.

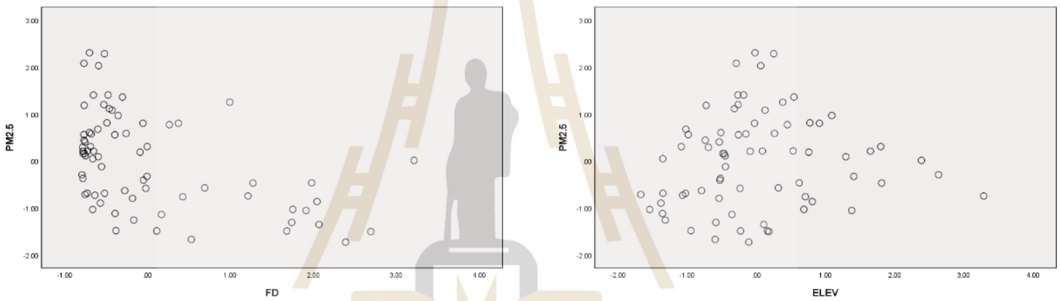

(a) (b)

Figure 7.28 Scatterplots between PM2.5 concentration in May 2020 and (a) factory density and (b) elevation.

Moreover, the spatial distribution map of PM2.5 concentration and significant factors (wind speed, visibility, brightness temperature, factory density, and elevation) is displayed in Figure 7.29. The spatial distribution map of PM2.5 concentration in May 2020 shows the high PM2.5 concentration in the central part of the study area, particularly Don Mueang and Sai Mai District – Bangkok province. At the same time, the low PM10 concentration occurs in the east of the study area, particularly Bang Bon and Bang Kho Laem District - Bangkok province.

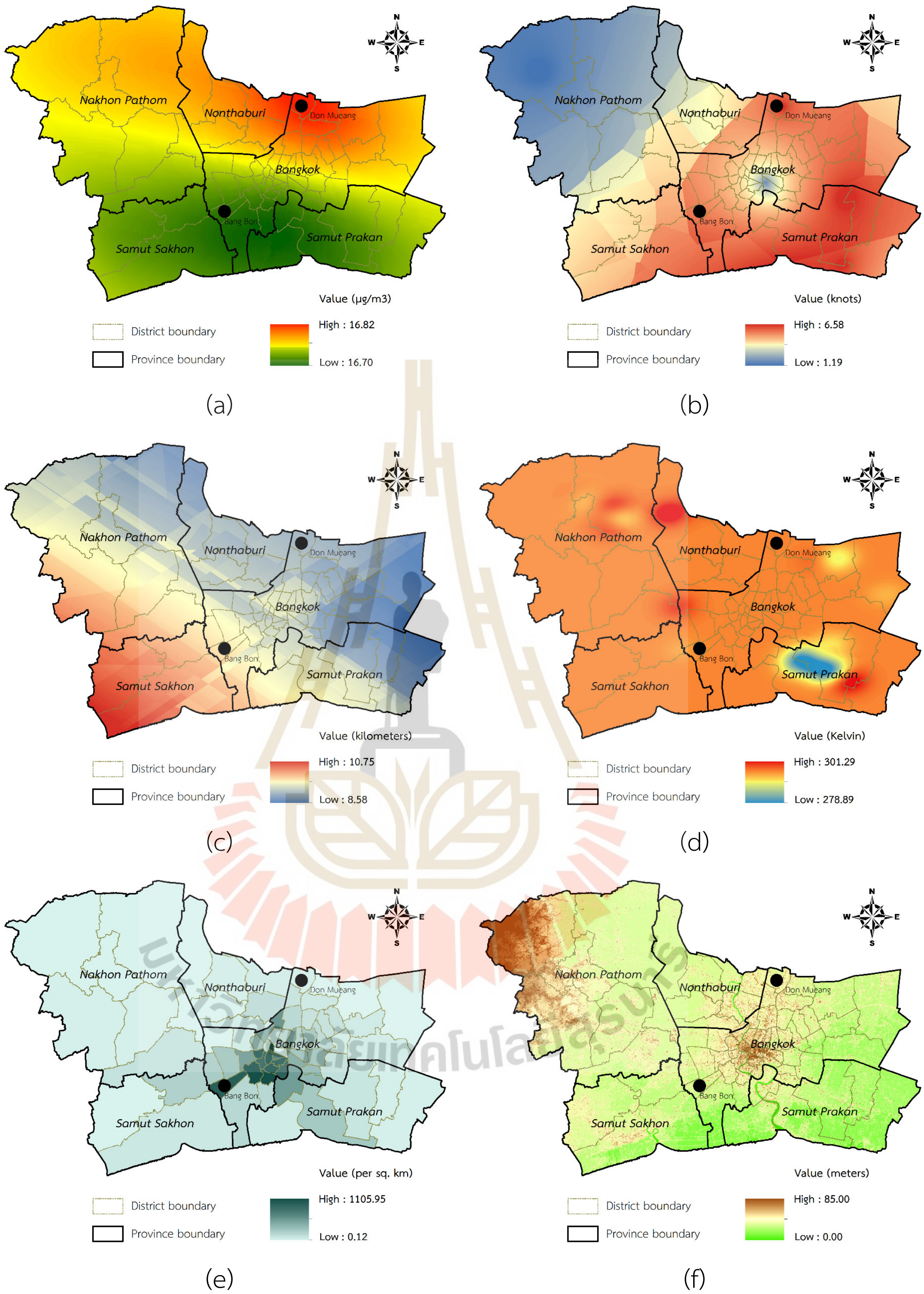

Figure 7.29 Spatial distribution map of (a) PM2.5 concentration (b) wind speed, (c) visibility, (d) brightness temperature, (e) factory density and (f) elevation.

Summary

According to significant factors (Tables 7.26 to 7.33), the relationship between PM2.5 concentration and significant monthly factors is summarized in Table 7.34 again. As a result, it can be observed that the relationship between temperature, wind speed, relative humidity and pressure, as the influencer of PM concentration, is primarily linear. On the contrary, the relationship between visibility and MOD AOD, as the effect of PM concentration, is non-linear. Likewise, the relationship between fire radiative power, brightness temperature, fire hot spot, factory density, and elevation as a source of PM concentration is non-linear. The relationship between elevation and PM2.5 concentration in all identified months shows a non-linear form since elevation variations as static data in the urban landscape are small.

Table 7.34 Summary of the relationship between PM2.5 concentration and their significant monthly factors.

Month	Influencer of PM concentration				Effect of PM concentration		Source of PM concentration				
	TEMP	WS	RH	P	VIS	AOD	FRP	BT	FH	FD	ELEV
October	N. a	Yes	N. a	Yes	No	No	No	Yes	No	N. a	No
November	N. a	N. a	N. a	N. a	No	N. a	Yes	N. a	N. a	N. a	N. a
December	N. a	Yes	N. a	N. a	No	N. a	N. a	N. a	N. a	N. a	N. a
January	Yes	N. a	N. a	N. a	Yes	Yes	N. a	N. a	Yes	N. a	No
February	N. a	Yes	No	Yes	N. a	N. a	No	N. a	N. a	N. a	No
March	N. a	N. a	N. a	N. a	N. a	N. a	Yes	N. a	N. a	N. a	N. a
April	N. a	No	N. a	N. a	No	No	Yes	No	Yes	No	N. a
May	N. a	Yes	N. a	N. a	Yes	N. a	N. a	Yes	N. a	No	No

Note: 1. Yes represents a linear relationship between PM2,5 concentration and specific significant factor

2. No represents a non-linear relationship between PM2,5 concentration and specific significant factor

3. N.a. represents not applied in spatial correlation analysis.

7.3.3 Relationship between seasonal PM concentration and land use data

The relationship between seasonal PM 10 and PM2.5 concentration in winter and summer and land use data in 2019 of LDD were described and discussed in the following sections.

7.3.3.1 PM 10 concentration classification and land use data

PM10 concentration classification in winter and summer seasons using the standard deviation method with one standard deviation interval size for identifying the relationship with land use types in 2019 is displayed in Figure 7.30.

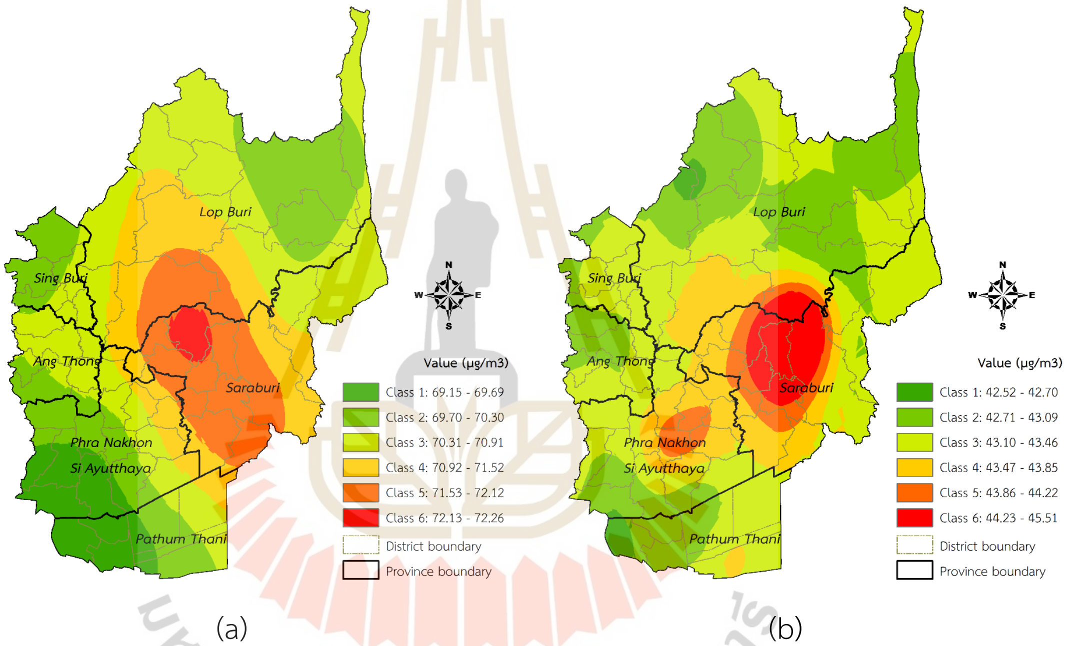

Figure 7.30 Spatial distribution of PM10 concentration classification in (a) winter and (b) summer.

The result of overlay analysis between PM10 classification in winter and summer and land use in 2019 was reported in Tables 7.35 and 7.36, respectively.

Table 7.35 Area of PM10 concentration classification in winter in each land use type.

PM10 classification in winter	Area of land use type in sq. km					
	Urban	Agriculture	Forest	Waterbody	Miscellaneous	Total
Class 1: 69.15-69.69 μg/m^3	366.59	895.68	0.07	64.42	76.47	1,403.22
Class 2: 69.70-70.30 μg/m^3	490.29	2,567.34	200.16	145.74	144.72	3,548.25
Class 3: 70.31-70.91 μg/m^3	516.41	3,632.65	831.53	308.26	139.96	5,428.81
Class 4: 70.92-71.52 μg/m^3	289.86	1,921.11	557.67	60.53	84.80	2,913.98
Class 5: 71.53-72.12 μg/m^3	347.15	1,405.40	365.28	53.41	130.11	2,301.35
Class 6: 72.13-72.26 μg/m^3	35.20	155.08	20.34	2.67	18.10	231.39
Total	2,045.49	10,577.26	1,975.05	635.04	594.16	15,827.00

From Table 7.35, the most dominant PM10 concentration in winter is Class 3, with a value between 70.31 and 70.91 μg/m^3. The least dominant class is Class 6, with a PM10 concentration between 72.13 and 72.26 μg/m^3.

At the same time, the major land use type, agriculture, which covers an area of about 66.83% of the total land, is located in Class 2 (69.70-70.30 μg/m^3) and Class 3 (70.31-70.91 μg/m^3) and cover area about 5,560 sq. km or about 53% of total agriculture area. On the contrary, minor land use type, miscellaneous land, which covers an area of about 3.75% of the total land, is located in Class 2 (69.70-70.30 μg/m^3) and Class 3 (70.31-70.91 μg/m^3) and cover area about 225 sq. km or about 38% of total miscellaneous land.

Table 7.36 Area of PM10 concentration classification in summer in each land use type.

PM10 classification in summer	Area of land use type in sq. km					
	Urban	Agriculture	Forest	Waterbody	Miscellaneous	Total
Class 1: 42.52-42.70 μg/m^3	31.69	193.46	9.26	7.19	7.05	248.65
Class 2: 42.71-43.09 μg/m^3	566.41	3,528.33	416.45	277.14	137.62	4,925.95
Class 3: 43.10-43.46 μg/m^3	736.48	4,285.34	1,080.38	234.93	224.66	6,561.79
Class 4: 43.47-43.85 μg/m^3	399.27	1,598.90	203.88	71.35	103.37	2,376.78
Class 5: 43.86-44.22 μg/m^3	181.56	495.48	104.98	29.08	43.17	854.28
Class 6: 44.23-45.51 μg/m^3	130.07	475.74	160.10	15.34	78.29	859.54
Total	2,045.49	10,577.26	1,975.05	635.04	594.17	15,827.00

On the contrary, the most dominant PM10 concentration in summer is Class 3, with a value between 43.10 and 43.46 μg/m^3. The least dominant class is Class 1, with a PM10 concentration between 42.52 and 42.70 μg/m^3. See detail in Table 7.36.

At the same time, the major land use type, agriculture, which covers an area of about 66.83% of the total land, is located in Class 2 (42.71-43.09 μg/m^3) and Class 3 (43.10-43.46 μg/m^3) and cover area about 7,814 sq. km or about 74% of total agriculture area. On the contrary, minor land use type, miscellaneous land, which covers an area of about 3.75% of the total land, is located in Class 2 (42.71-43.09 μg/m^3) and Class 3 (43.10-43.46 μg/m^3) and cover area about 362.28 sq. km or about 38% of total miscellaneous land.

The percentage of each LULC type in each PM10 concentration class in winter and summer are reported in Figures 7.31 and 7.32, respectively.

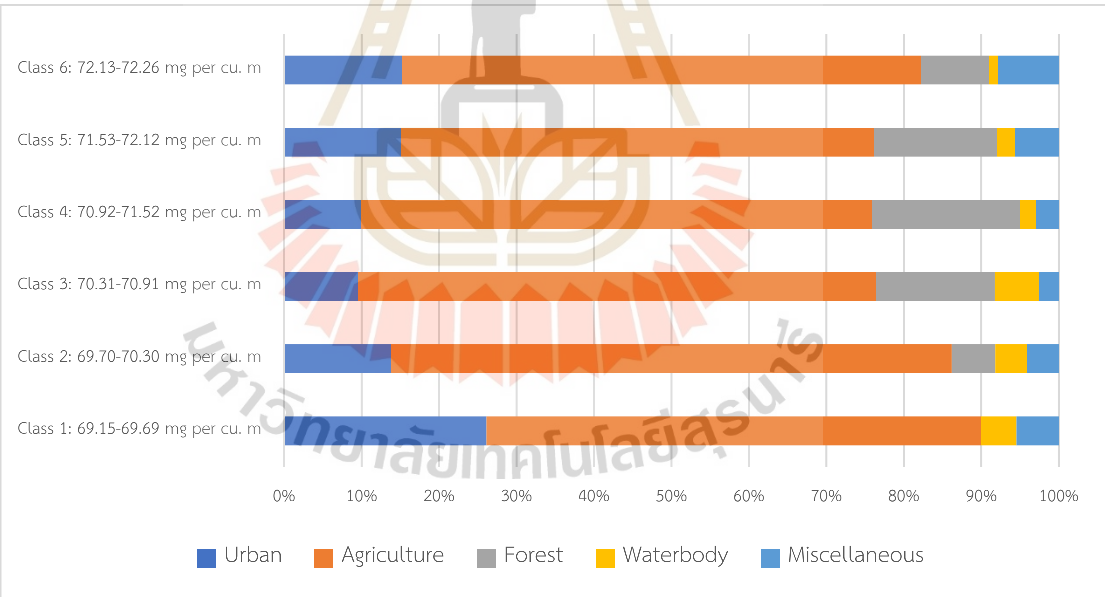

Figure 7.31 Percentage of each LULC type in each PM10 concentration class in the winter season.

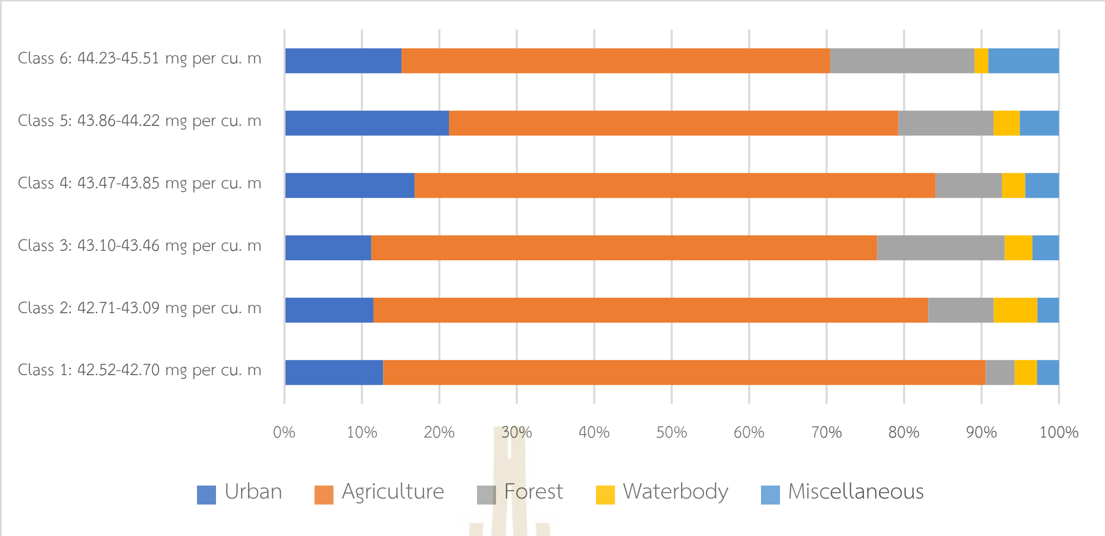

Figure 7.32 percentage of each LULC type in each PM10 concentration class in the summer season.

These findings indicate the significance of agriculture on PM10 concentration in the winter and summer seasons.

7.3.3.2 PM2.5 concentration classification and land use data

PM2.5 concentration classification in winter and summer seasons using the standard deviation method with one standard deviation interval size for identifying the relationship with land use types in 2019 is displayed in Figure 7.33.

The result of overlay analysis between PM2.5 classification in winter and summer and land use in 2019 was reported in Tables 7.37 and 7.38, respectively.

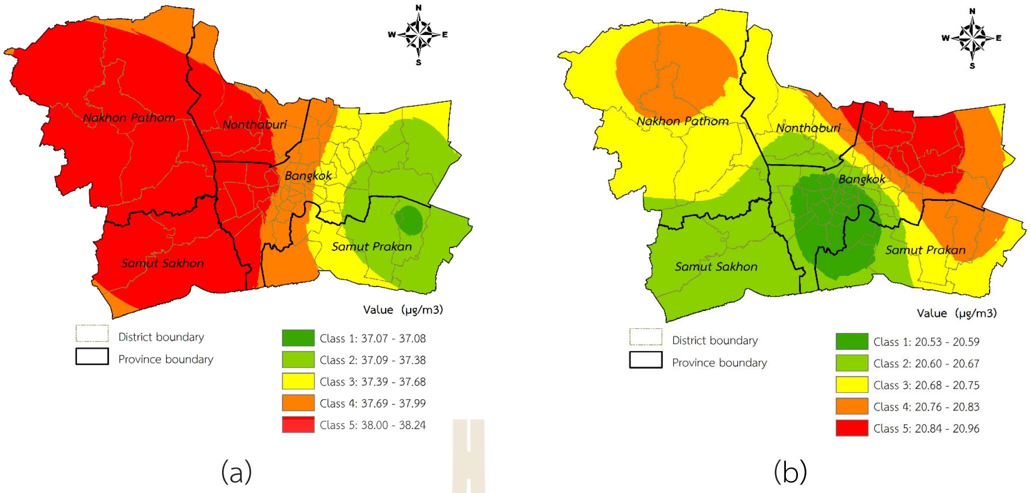

Figure 7.33 Spatial distribution of PM2.5 concentration classification in (a) winter and (b) summer.

Table 7.37 Area of PM2.5 concentration classification in winter in each land use type.

PM2.5 classification in winter	Area of land use type in sq. km					
	Urban	Agriculture	Forest	Waterbody	Miscellaneous	Total
Class 1: 37.07-37.08 µg/m^3	6.89	34.76	0.00	1.39	1.28	44.33
Class 2: 37.09-37.38 µg/m^3	461.35	419.62	4.75	33.07	73.34	992.13
Class 3: 37.39-37.68 µg/m^3	404.93	132.35	8.16	29.29	30.19	604.92
Class 4: 37.69-37.99 µg/m^3	493.71	370.21	10.33	60.58	43.15	977.98
Class 5: 38.00-38.24 µg/m^3	1,065.17	2,059.76	33.88	128.99	272.84	3,560.63
Total	2,432.06	3,016.70	57.12	253.32	420.80	6,180.00

As a result, the most dominant PM2.5 concentration in winter is Class 5, with a value between 37.69 and 37.99 µg/m^3. The least dominant class is Class 1, with a PM2.5 concentration between 37.07 and 37.08 µg/m^3. See detail in Table 7.37.

At the same time, the major land use type, agriculture, which covers an area of about 48.80 % of the total land, is located in Class 5 (38.00-38.24 µg/m^3) and Class 2 (37.09-37.38 µg/m^3) and cover area about 2,479.38 sq. km or about 82.20% of total agriculture area. On the contrary, minor land use type, forest land, which covers an area of about 0.92% of the total land, is located in Class 5 (38.00-38.24 µg/m^3) and Class 2 (37.09-37.38 µg/m^3) and cover area about 38.63 sq. km or about 67.63% of total forest land.

Table 7.38 Area of PM2.5 concentration classification in summer in each land use type.

PM2.5 classification in summer	Area of land use type in sq. km					
	Urban	Agriculture	Forest	Waterbody	Miscellaneous	Total
Class 1: 20.53-20.59 μg/m^3	344.90	99.63	10.93	28.31	29.47	513.23
Class 2: 20.60-20.67 μg/m^3	666.08	801.18	40.01	82.37	133.29	1,722.93
Class 3: 20.68-20.75 μg/m^3	637.89	1,276.03	6.18	81.36	146.16	2,147.61
Class 4: 20.76-20.83 μg/m^3	445.26	746.66	0.00	48.06	80.21	1,320.19
Class 5: 20.84-20.96 μg/m^3	337.93	93.21	0.00	13.22	31.67	476.03
Total	2,432.06	3,016.70	57.12	253.32	420.80	6,180.00

On the contrary, the most dominant PM2.5 concentration in summer is Class 3, with a value between 20.68 and 20.75 μg/m^3. The least dominant class is Class 5, with a PM2.5 concentration between 20.84 and 20.96 μg/m^3. See detail in Table 7.38.

At the same time, the major land use type, agriculture, which covers an area of about 48.80 % of the total land, is located in Class 3 (20.68-20.75 μg/m^3) and Class 2 (20.60-20.67 μg/m^3) and cover area about 2,077 sq. km or about 68.86% of total agriculture area. On the contrary, minor land use type, forest land, which covers an area of about 0.92% of the total land, is located in Class 2 (20.60-20.67 μg/m^3) and Class 1 (20.53-20.59 μg/m^3) and cover area about 51 sq. km or about 89.19% of total forest land.

Meanwhile, the percentage of each LULC type in each PM2.5 concentration class in winter and summer are reported in Figures 7.34 to 7.35, respectively.

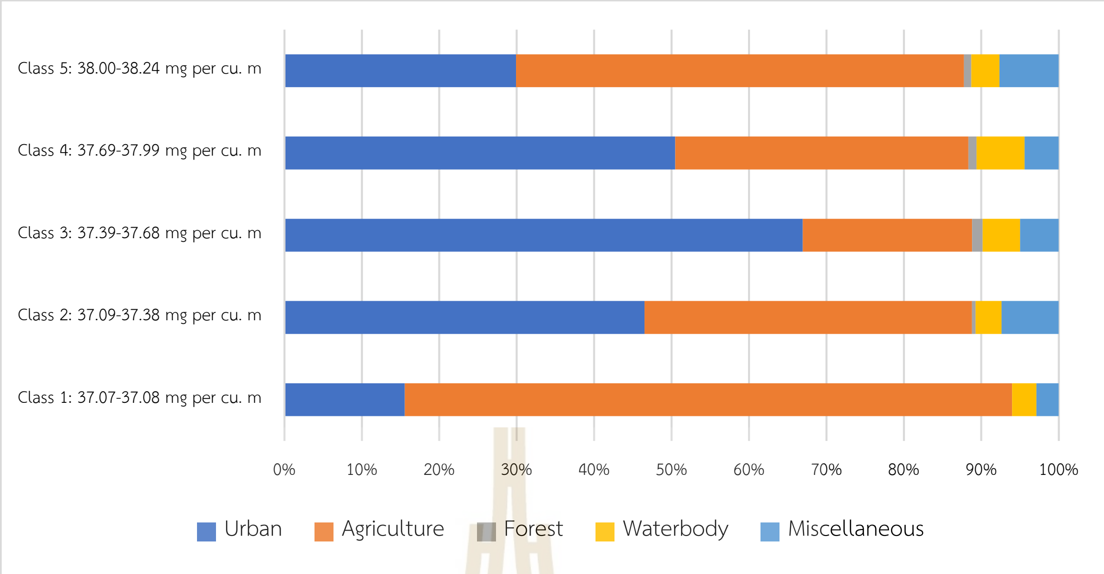

Figure 7.34 Percentage of each LULC type in each PM2.5 concentration class in the winter season.

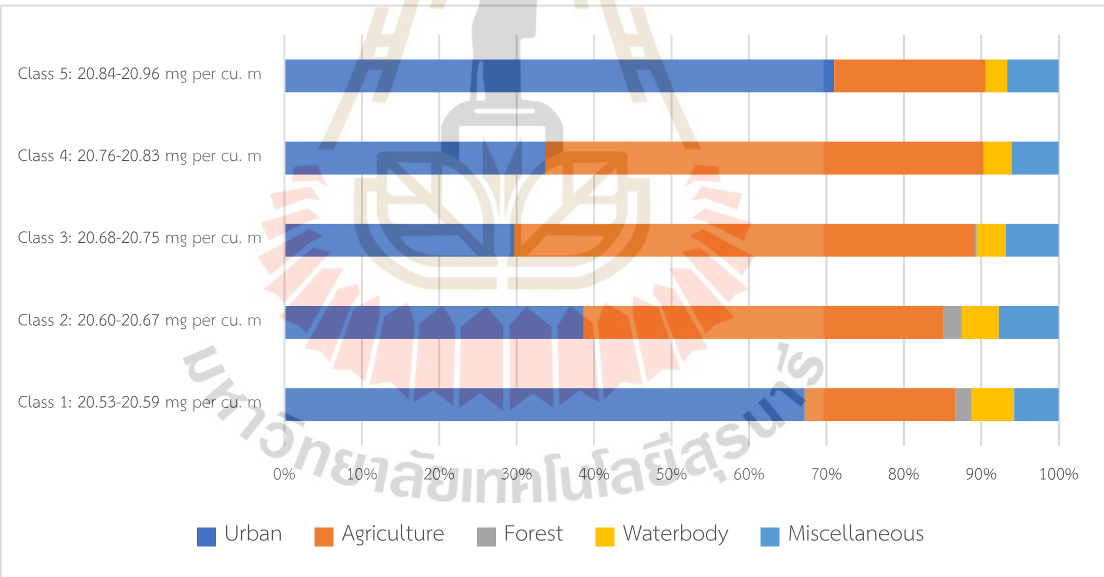

Figure 7.35 Percentage of each LULC type in each PM2.5 concentration class in the summer season.

These findings indicate the significance of urban and agriculture on PM2.5 concentration in the winter and summer seasons.

CHAPTER VIII

CONCLUSION AND RECOMMENDATIONS

This chapter first presents the conclusion of four main results, which were reported in detail according to the research objectives in four chapters, including (1) data collection and preparation, (2) significant spatiotemporal factors on PM concentration, (3) prediction of spatiotemporal particulate matter concentration, and (4) suitable spatiotemporal model for pm concentration prediction and validation. Then, some recommendations are suggested for future research and development.

8.1 Conclusion

8.1.1 Data collection and preparation

Standard interpolation methods were selected to identify an optimum method for the selected dependent and independent variables between October 2019 and May 2020. As a result, the SCK with the J-Bessel function was optimum for ground-level PM concentration. The SCK with J-Bessel function was optimum for relative humidity. The SCK with the Hole Effect function was optimum for temperature. The RBF with Spline with Tension and One Sector was optimum for wind speed. The SCK with Stable function was optimum for pressure. The OCK with the Hole Effect function was optimum for visibility. The SCK with Stable function and RBF with Spline with Tension and Eight Sector function was optimum for brightness temperature and fire radiative power

Meanwhile, the remaining independent variables, including MODIS AOD, NDVI, BUI, road density, factory density, elevation fire hotspot, population density, and GPP, were prepared by spatial analysts.

After that, mean and standard deviation values at the district level of all dependent and independent variables were extracted using the zonal statistics analysis. Then, all prepared variables were normalized using the Z-score method for significant spatiotemporal factors on PM concentration.

8.1.2 Significant spatiotemporal factors on PM concentration

The dependent and independent variables on PM10 concentration in the rural landscape and PM2.5 concentration in the urban landscape in the winter season (October 2019 to February 2020) and summer season (March 2020 to May 2020) were applied to identify significant spatiotemporal factors using multicollinearity test and the ordinary least squares (OLS) regression.

As a result, the OLS regression equations on PM10 concentration in each month in the winter showed the AICc from 140.10 to 178.47, with an average of 159.13, while the adjusted R-squared varied from 0.13 to 0.59, with an average of 0.39. On the contrary, the OLS regression equations on PM10 concentration in each month in the summer showed the AICc from 157.49 to 187.73, with an average of 168.61, while the adjusted R-squared varied from 0.20 to 0.43, with an average of 0.27. The significant factors on PM10 concentration in winter and summer were five and five. Additionally, three common factors on PM10 concentration, namely temperature, visibility, and MODIS AOD, were identified in both seasons. Two significant factors on PM10 concentration were only found in the winter season, including wind speed and fire radiative power. On the contrary, two significant factors on PM10 concentration, factory density and brightness temperature, were only found in the summer season.

Meanwhile, the OLS regression equations on PM2.5 concentration in each month in the winter showed the AICc from 114.36 to 194.85, with an average of 154.33, while the adjusted R-squared varied from 0.27 to 0.77, with an average of 0.55. On the contrary, the OLS regression equations on PM2.5 concentration in each month in the summer showed the AICc from 168.59 to 192.42, with an average of 178.67, while the adjusted R-squared varied from 0.32 to 0.50, with an average of 0.42. There were seven common factors on PM2.5 concentration in both seasons: wind speed, visibility, brightness temperature, fire radiative power, MODIS AOD, fire hotspot, and elevation. Furthermore, it was found that three significant factors on PM2.5 concentration were only found in the winter season, including relative humidity, temperature, and pressure. In contrast, one significant factor in PM2.5 concentration, factory density, was only found in the summer season.

8.1.3 Prediction of spatiotemporal PM concentration

The significant factors on PM10 and PM2.5 concentration were separately applied to predict monthly concentration using the GWR and MEM models.

As a result, the PM10 concentration predictions using the GWR model in the winter showed a value from 50.53 to 85.79 mg/m^3, with an average of 70.64 mg/m^3. The maximum value was in February. Monthly Thailand AQI classifications were satisfactory to moderate, while US EPA AQI classifications were good to moderate. In contrast, the PM10 concentration predictions using the GWR model in the summer showed a value from 36.92 to 51.32 mg/m^3, with an average of 43.43 mg/m^3. The maximum value was in March. According to Thailand and US EPA standards, monthly AQI classifications were excellent and good, respectively.

Meanwhile, the PM10 concentration predictions using the MEM model in the winter showed a value from 50.68 to 84.59 mg/m^3, with an average of 70.63 mg/m^3. The maximum value was in February. Monthly Thailand AQI classifications were satisfactory to moderate, while US EPA AQI classifications were good to moderate. In contrast, the PM10 concentration predictions using the MEM model in the summer showed a value between 37.08 to 50.81 mg/m^3, with an average of 43.40 mg/m^3. The maximum value was in March. According to Thailand and US EPA standards, monthly AQI classifications were excellent and good, respectively.

In the meantime, PM2.5 concentration predictions using the GWR model in the winter showed a value from 25.33 to 44.37 mg/m^3, with an average of 37.80 mg/m^3. The maximum value was in February. Monthly Thailand AQI classifications were satisfactory to moderate, while the US EPA AQI classifications were moderate to unhealthy for the sensitive group. In contrast, PM2.5 concentration prediction using the GWR model in the summer showed a value from 16.69 to 24.04 mg/m^3, with an average of 20.67 mg/m^3. The maximum value was in March. According to Thailand and US EPA standards, monthly AQI classifications were excellent and moderate, respectively.

Meanwhile, PM2.5 concentration prediction using the MEM model in the winter showed a value from 25.45 to 44.36 mg/m^3, with an average of 37.80 mg/m^3. The maximum value was in February. Monthly Thailand AQI classifications were satisfactory to moderate, while US EPA AQI classifications were moderate to unhealthy for the sensitive group. In contrast, PM2.5 concentration prediction using the MEM model in the summer showed a value from 16.68 to 23.75 mg/m^3, with an average of 20.67 mg/m^3. The maximum value was in March. According to Thailand and US EPA standards, monthly AQI classifications were excellent and moderate, respectively.

8.1.4 Suitable spatiotemporal model for PM concentration prediction and validation

The reported AICc values from spatiotemporal PM10 and PM2.5 concentration prediction between GWR and MEM models were used to determine a suitable model for PM concentration prediction. The average AICc values of PM10 concentration prediction in rural landscapes using the GWR model in the winter and summer seasons were 97.92 and 113.03, respectively. On the contrary, average AICc values of PM10 concentration prediction in rural landscapes using the MEM model were 155.49 and 164.77. The result showed that the average AICc value of the GWR model was lower than the MEM. Thus, the GWR model was suitable for spatiotemporal PM10 concentration prediction in both seasons. In the meantime, the average AICc values of PM2.5 concentration prediction in urban landscapes using the GWR model in the winter and summer seasons were 73.86 and 122.55, respectively. At the same time, the average AICc values of PM2.5 concentration prediction in urban landscapes using the MEM model were 168.61 and 186.67. Therefore, the GWR model was also suitable for spatiotemporal PM2.5 concentration prediction in both seasons.

The spatial distribution map of PM10 concentration showed the high frequency of the high PM10 concentration that occurred in the central part of the rural landscape, particularly northern parts of Saraburi and the south of Lop Buri province. At the same time, the low PM10 concentration occurred in the south of the study area, mainly in Pathum Thani province and the south of Phra Nakhon Si Ayutthaya province. It can be observed that the most dominant factors on PM10 concentration based on spatial correlation analysis were consistent with the derived result using OLS regression analysis.

The spatial distribution map of PM2.5 concentration showed the high frequency of the high PM2.5 concentration occurring in the western part of the urban landscape, particularly Nakhon Pathom, Samut Sakhon, Nonthaburi, and the west side of Bangkok. At the same time, the low PM2.5 concentration occurred in the east part of the study area, particularly Samut Prakan and the east side of Bangkok. It can be observed that the most dominant factors on PM2.5 concentration based on spatial correlation analysis were consistent with the derived result using OLS regression analysis.

Moreover, the GWR model as a suitable model was reapplied to a newly collected and prepared dataset in the winter and summer seasons (between October 2020 and May 2021) to validate the prediction of spatiotemporal PM10 and PM2.5 concentration using Pearson correlation analysis. As a result, the correlation coefficient values for PM10 concentration in the winter season between the existing dataset and the new dataset varied from 0.81 to 0.91, with an average value of 0.87. Similarly, the correlation coefficient values for PM10 concentration in the summer season between the existing dataset and the new dataset varied from 0.75 to 0.94, with an average value of 0.82. So, the predicted PM10 concentration with the same significant monthly factors in two seasons in the rural landscape using the GWR model could be accepted in the current study. Likewise, the correlation coefficient values for PM2.5 concentration in the winter season between the existing dataset and the new dataset varied from 0.67 to 0.92, with an average value of 0.77.

Similarly, the correlation coefficient values for PM2.5 concentration in the summer season between the existing dataset and the new dataset varied from 0.67 to 0.84, with an average value of 0.77. Thus, the predicted PM2.5 concentration with the same significant monthly factors in two seasons in the rural landscape using the GWR model can be accepted in the current study. The predicted PM2.5 concentration with the same significant monthly factors in two seasons in the urban landscape using the GWR model could be accepted in this study.

8.2 Recommendations

Many objectives were explored in this study, including significant spatiotemporal factors for identifying spatiotemporal PM concentration predictions and predicting suitable spatiotemporal models for PM concentration in the winter and summer seasons that are separate in rural and urban landscapes. Therefore, the possible expected recommendations and implications could be made for further studies as the following.

(1) The predicted PM concentration using the GWR model in this study is the critical data source for the effect of PM on human health. So, PM exposure to human health regarding diseases such as tuberculosis, allergy, diabetes, and respiratory disease should be investigated based on the predicted PM data and the existing database of the Department of Disease Control, Ministry of Public Health. For example, Xing, Xu, Shi, and Lian (2016) reported smog levels have increased throughout China, resulting in the deterioration of air quality, raising worldwide concerns. PM2.5 can deeply penetrate into the lung, irritate and corrode the alveolar wall, and consequently impair lung function. Especially the elderly and those with pre-existing cardiopulmonary problems should be more cautious of PM2.5 pollution and minimize outdoor PM2.5 exposure. Polichetti, Cocco, Spinali, Trimarco, and Nunziat (2009) reported health effects to depend not only on the level of PM concentration in the air but also on its particular internal composition. The effect of PM produced by tobacco smoke can give rise to cardiovascular injury.

(2) This study predicted the PM concentration using the GWR and MEM models with a linear regression algorithm. However, all significant factors do not correlate perfectly with PM concentration (Filonchyk, Yan, and Li, 2018; Mahmoud, 2012). Thus, non-linear regression algorithms that include exponential, logarithmic, logistic, machine learning, land use regression (LUR) models, etc., should be examined to predict PM concentration. For example, Zaman, Kanniah, Kaskaoutis, and Latif (2021) applied machine learning models (random forest and support vector regression) to predict PM2.5 concentration nationally in Malaysia by combining satellite aerosol retrievals with ground-based pollutants and meteorological factors. The model provided a satisfactory prediction of PM2.5 concentration across Malaysia and allowed continuous monitoring of the pollution levels in remote areas without measurement networks. Moreover, Yang, Chen, and Liang (2017) used the LUR model to explore the effect of land use on PM2.5 in urban areas. The model indicates the dominant factor was the traffic conditions, and land use can significantly affect the PM2.5 levels.

(3) Data from light scattering or beta ray instruments should be considered for data verification. The previous study by Panta, Wimonthanasit, Chaithanu, Sampattagul, and Yawootti (2018) studied suitable devices for measuring airborne PM; the result

showed a high correlation between the light scattering device and the Beta Ray device as certified by the Pollution Control Department.

(4) This study used MODIS (Moderate Resolution Imaging Spectroradiometer from Terra and Aqua MAIAC AOD data product at 1 km spatial resolution. However, many satellite sensors have been used to measure AOD. They calibrated and validated, such as VIIRS (Visible Infrared Imaging Radiometer) from Suomi-NPP and AHI (Advanced Himawari Imager) from Himawari-8. Besides, Aerosol Robotic Network (AERONET) established by NASA and PHOTONS can provide an accurate ground measurement of AOD (Wang et al., 2020). In addition, AERONET and MODIS AOD are very similar and can be used instead in the case of missing data (Nisantzi et al., 2012; Segura, Estellés, Utrillas, and Martínez-Lozano, 2017).

REFERENCES

REFERENCES

Antonis S. Manolis, and Theodora A. Manolis. (2013). Air Pollution in the Metropolis: A Lurking Health Trap. *Hospital Chronicles*. *8*(3), 103-111.

Apte, J. S., Brauer, M., Cohen, A. J., Ezzati, M., and Pope, C. A. (2018). Ambient PM2.5 Reduces Global and Regional Life Expectancy. *Environmental Science & Technology Letters*. *5*(9), 546-551.

Arslan, S., and Aybek, A. (2012). *Particulate Matter Exposure in Agriculture*. Air Pollution. A Comprehensive Perspective. London: IntechOpen.

Bardossy, A. (2002). *Introduction to Geostatistics*. Germany: Institute of Hydraulic Engineering University of Stuttgart.

Berrick, S. (2020). *MCD14DL*. [On-line]. Available: https://earthdata.nasa.gov/earth-observation-data/near-real-time/firms/c6-mcd14dl#ed-firms-attributes

Bevans, R. (2021). *An introduction to the Akaike information criterion.* [On-line]. Available: https://www.scribbr.com/statistics/akaike-information-criterion/

Cao, W., Hu, J., and Yu, X. (2009, 12-14 Aug. 2009). *A Study on Temperature Interpolation Methods Based on GIS.* Paper presented at the 17th International Conference on Geoinformatics, Fairfax, VA, USA.

Chen, Z., Cai, J., Gao, B., Xu, B., Dai, S., He, B., and Xie, X. (2017). Detecting the causality influence of individual meteorological factors on local PM2.5 concentration in the Jing-Jin-Ji region. *Scientific Reports*. *7*, 1-11.

Chowdhury, A. K., Debsarkar, A., and Chakrabarty, S. (2015). Novel Methods for Assessing Urban Air Quality: Combined Air and Noise Pollution Approach. *Journal of Atmospheric Pollution*. *3*(1), 1-8.

Chu, Y., Liu, Y., Li, X., Liu, Z., Lu, H., Lu, Y., Mao, Z., Chen, X., Li, N., Ren, M., Liu, F., Tian, L., Zhu, Z., and Xiang, H. (2016). A Review on Predicting Ground PM2.5 Concentration Using Satellite Aerosol Optical Depth. *Atmosphere*. *7*(10), 129.

Chudnovsky, A. A., Koutrakis, P., Kloog, I., Melly, S., Nordio, F., Lyapustin, A., Wang, Y., and Schwartz, J. (2014). Fine particulate matter predictions using high resolution Aerosol Optical Depth (AOD) retrievals. *Atmospheric Environment*. *89*, 189-198.

Cohen, J. (1988). *Statistical Power Analysis for the Behavioral Sciences*. (2nd ed). New York: Lawrence Erlbaum Associates.

Czernecki, B., Półrolniczak, M., Kolendowicz, L., Marosz, M., Kendzierski, S., and Pilguj, N. (2017). Influence of the atmospheric conditions on PM10 concentrations in Poznan, Poland. *Journal of Atmospheric Chemistry*. *74*(1), 115-139.

Deligiorgi, D., and Philippopoulos, K. (2011). Spatial Interpolation Methodologies in Urban Air Pollution Modeling: Application for the Greater Area of Metropolitan Athens, Greece. *Advanced Air Pollution*. 341-362.

Devkota, J. U. (2021). Statistical analysis of active fire remote sensing data: examples from South Asia. *Environmental Monitoring and Assessment*. *193*, 608.

ESRI. (2015a). *ArcGIS 10.3.1 Help*. Interpolation. Redlands, California: Environmental Systems Research Insitute, Inc.

ESRI. (2015b). *ArcGIS 10.3.1 Help*. Regression analysis basics. Redlands, California: Environmental Systems Research Insitute, Inc.

European Environment Agency. (2016). *Air quality standards under the Air Quality Directive, and WHO air quality guidelines.* [On-line]. Available: https://www.eea.europa.eu/data-and-maps/figures/air-quality-standards-under-the

Ferrero, L., Riccio, A., Ferrini, B. S., D'Angelo, L., Rovelli, G., Casati, M., Angelini, F., Barnaba, F., Gobbi, G. P., Cataldi, M., and Bolzacchini, E. (2019). Satellite AOD conversion into ground PM10, PM2.5 and PM1 over the Povalley (Milan, Italy) exploiting information on aerosol vertical profiles, chemistry, hygroscopicity and meteorology. *Atmospheric Pollution Research*. *10*, 1895-1912.

Filonchyk, M., Yan, H., and Li, X. (2018). Temporal and spatial variation of particulate matter and its correlation with other criteria of air pollutants in Lanzhou, China, in spring-summer periods. *Atmospheric Pollution Research*. *9*, 1100-1110.

Fotheringham, A. S., Brunsdon, C., and Charlton, M. (2002). *Geographically Weighted Regression: the analysis of spatially varying relationships*. Chichester: John Wiley & Sons Ltd.

Galindo, N., Varea, M., Gil-Moltó, J., Yubero, E., and Nicolás, J. (2011). The Influence of Meteorology on Particulate Matter Concentrations at an Urban Mediterranean Location. *Water, Air, & Soil Pollution*. *215*, 365-372.

Ghorani, A. A., Riahi, Z. B., and Balali, M. M. (2016). Effects of air pollution on human health and practical measures for prevention in Iran. *Journal of research in medical sciences*. *21*, 65.

Giles, H. R. (2015). *Meteorological Measurements and Instrumentation*. (1 ed). Advancing Weather and Climate Science Series. West Sussex: John Wiley & Sons, Ltd.

Giraldo, R., Herrera, L., and Leiva, V. (2020). Cokriging Prediction Using as Secondary Variable a Functional Random Field with Application in Environmental Pollution. *mathematics*. *8*, 1305.

Gradka, R., and Kwinta, A. (2018). A Short Review Of Interpolation Methods Used For Terrain Modeling. *Geomatics, Land management and Landscape*. *4*, 29-47.

Grgurić, S., Križan, J., Gašparac, G., Antonić, O., Špirić, Z., Mamouri, R. E., Christodoulou, A., Nisantzi, A., Agapiou, A., Themistocleous, K., Fedra, K., Panayiotou, C., and Hadjimitsis, D. (2014). Relationship between MODIS based Aerosol Optical Depth and PM10 over Croatia. *Central European Journal of Geosciences*. *6*, 2-16.

Gu, Y. (2019). *Estimating PM2.5 Concentrations Using 3 km MODIS AOD Products: A Case Study in British Columbia, Canada*. Master of Science, University of Waterloo.

Guo, Y., Tang, Q., Gong, D. Y., and Zhang, Z. (2017). Estimating ground-level PM2.5 concentrations in Beijing using a satellite-based geographically and temporally weighted regression model. *Remote Sensing of Environment*. *198*, 140-149.

Guo, Y., and Zhang, X. (2014). Analysis of the Pollution Characteristics and Influence Factors of PM2.5 in Chinese main capital city. *Advanced Materials Research*. *1023*, 247-251.

Hamer, M. S., Franklin, M., Chau, K., Garay, M., and Kalashnikova, O. (2020). Spatiotemporal Characteristics of the Association between AOD and PM over the California Central Valley. *Remote Sensing*. *12*, 685.

Harnkijroong, T., and Panich, N. (2013, 6-7 December). *Influence Of Meteorological Factors On PM10 at Roadside Of Bangkok*. Paper presented at the 10th National Kasetsart University Kamphaeng Saen conference, Nakhon Pathom.

He, Q., Gu, Y., and Zhang, M. (2020). Spatiotemporal trends of PM2.5 concentrations in central China from 2003 to 2018 based on MAIAC-derived high-resolution data. *Environment International*. *137*, 105536.

He, Q., and Huang, B. (2018). Satellite-based mapping of daily high-resolution ground PM2.5 in China via space-time regression modeling. *Remote Sensing of Environment*. *206*, 72-83.

Health Effects Institute. (2020). *Health impact.* [On-line]. Available: https://www.stateofglobalair.org/

Jantakat, Y., and Ongsomwang, S. (2011). Assessing The Effect Of Incorporating Topographical Data With Geostatistical Interpolation For Monthly Rainfall And Temperature In Ping Basin, Thailand. *Suranaree Journal of Science and Technology*. *18*(2), 123-139.

Jensen, J. R. (2015). *Introductory digital image processing: a remote sensing perspective*. (4th ed). Pearson Series in Geographic Information Science. Glenview: Pearson Education, Inc.

Jiang, M., Sun, W., Yang, G., and Zhang, D. (2017). Modelling Seasonal GWR of Daily PM2.5 with Proper Auxiliary Variables for the Yangtze River Delta. *Remote Sensing*. *9*, 346.

Kanabkaew, T. (2013). Prediction of Hourly Particulate Matter Concentrations in Chiangmai, Thailand Using MODIS Aerosol Optical Depth and Ground-Based Meteorological Data. *EnvironmentAsia*. *6*(2), 65-70.

Keskin, M., and Özdoğu, K. (2011). *Comparison Of Interpolation Methods For Meteorological Data* Geomatics Engineering, Istanbul Technical University.

Kim, K. H., Kabir, E., and Kabir, S. (2015). A review on the human health impact of airborne particulate matter. *Environment International*. *74*, 136-143.

Kliengchuay, W., Meeyai, A. C., Worakhunpiset, S., and Tantrakarnapa, K. (2018). Relationships between Meteorological Parameters and Particulate Matter in Mae Hong Son Province, Thailand. *International Journal of Environmental Research and Public Health*. *15*, 2801.

Kloog, I., Koutrakis, P., Coull, B. A., Lee, H. J., and Schwartz, J. (2011). Assessing temporally and spatially resolved PM2.5 exposures for epidemiological studies using satellite aerosol optical depth measurements. *Atmospheric Environment*. *45*, 6267-6275.

Kong, L., Xin, J., Zhang, W., and Wang, Y. (2016). The empirical correlations between PM2.5, PM10 and AOD in the Beijing metropolitan region and the PM2.5, PM10 distributions retrieved by MODIS. *Environmental Pollution*. *216*, 350-360.

Kulshreshtha, P. (2019). *Effects of Air Pollution on Human Health***.** Air Pollution: Sources, Impacts and Controls. Oxfordshire: CAB International.

Kumar, A., Gupta, I., Brandt, J., Kumar, R., Dikshit, A. K., and Patil, R. S. (2016). Air quality mapping using GIS and economic evaluation of health impact for Mumbai City, India. *Journal of the Air & Waste Management Association*. *66*(5), 470-481.

Kuo, P.-F., Huang, T.-E., and Putra, I. G. B. (2021). Comparing Kriging Estimators Using Weather Station Data and Local Greenhouse Sensors. *Sensors*. *21*(5), 1853.

Land Development Department. (2019). *Provincial land use in Thailand.* [On-line]. Available: https://www.ldd.go.th/www/lek_web/web.jsp?id=18662

Lee, H. J., Coull, B. A., Bell, M. L., and Koutrakis, P. (2012). Use of satellite-based aerosol optical depth and spatial clustering to predict ambient PM2.5 concentrations. *Environmental Research*. *118*, 8-15.

Lee, H. J., Liu, Y., Coull, B. A., Schwartz, J., and Koutrakis, P. (2011). A novel calibration approach of MODIS AOD data to predict PM2.5 concentrations. *Atmospheric Chemistry and Physics*. *11*, 7991-8002.

Levy, R., and Hsu, C. (2015). *Collection-6 Terra Product Descriptions: MOD04_L2.* [On-line]. Available: https://modaps.modaps.eosdis.nasa.gov/services/about/products/c6/MOD04_L2.html

Levy, R., and Hsu, C. (2019). *MODIS Aerosol Product.* [On-line]. Available: https://modis.gsfc.nasa.gov/data/dataprod/mod04.php

Levy, R. C. (2009). *The dark-land MODIS collection 5 aerosol retrieval: algorithm development and product evaluation***.** Satellite aerosol remote sensing over land. New York: In association with Praxis Publishing.

Li, X., Chen, X., Yuan, X., Zeng, G., León, T., Liang, J., Chen, G., and Yuan, X. (2017). Characteristics of Particulate Pollution (PM2.5 and PM10) and Their Spacescale-Dependent Relationships with Meteorological Elements in China. *Sustainability*. *9*, 2330.

Lin, G., Fu, J., Jiang, D., Hu, W., Dong, D., Huang, Y., and Zhao, M. (2014). Spatio-Temporal Variation of PM2.5 Concentrations and Their Relationship with Geographic and Socioeconomic Factors in China. *International Journal of Environmental Research and Public Health*. *11*, 173-186.

Loboda, T. V., Hall, J. V., and Baer, A. (2017). *ABoVE: Wildfire Date of Burning within Fire Scars across Alaska and Canada, 2001-2019*. Tennessee, USA: ORNL Distributed Active Archive Center.

Luo, J., Du, P., Samat, A., Xia, J., Che, M., and Xue, Z. (2017). Spatiotemporal Pattern of PM2.5 Concentrations in Mainland China and Analysis of Its Influencing Factors using Geographically Weighted Regression. *Scientific Reports*. *7*, 40607.

Lyapustin, A., and Wang, Y. (2018). *MODIS Multi-Angle Implementation of Atmospheric Correction (MAIAC) Data User's Guide*.

Ma, Z., Liu, Y., Zhao, Q., Liu, M., Zhou, Y., and Bi, J. (2016). Satellite-derived high resolution PM2.5 concentrations in Yangtze River Delta Region of China using improved linear mixed effects model. *Atmospheric Environment*. *133*, 156-164.

Mahmoud, R. M. M. (2012). *Study of the suspended particulate matter concentrations in the atmosphere of Qena, Upper Egypt*. M. Sc. in Atmospheric Physics, South Valley University.

Mehrotra, S., Bardhan, R., and Ramamritham, K. (2016, 15-17 June). *Built form determinants of urban land surface temperature: A case of Mumbai.* Paper presented at the Sustainable Built Environment (SBE) Regional Conference Zurich 2016, Zurich.

Meng, X., Fu, Q., Ma, Z., Chen, L., Zou, B., Zhang, Y., Xue, W., Wang, J., Wang, D., Kan, H., and Liu, Y. (2016). Estimating ground-level PM10 in a Chinese city by combining satellite data, meteorological information and a land use regression model. *Environmental Pollution*. *208*, 177-184.

Ni, X., Cao, C., Zhou, Y., Cui, X., and Singh, R. P. (2018). Spatio-Temporal Pattern Estimation of PM2.5 in Beijing-Tianjin-Hebei Region Based on MODIS AOD and Meteorological Data Using the Back Propagation Neural Network. *Atmosphere*. *9*, 105.

Ozturk, D., and Kilic, F. (2016). Geostatistical Approach for Spatial Interpolation of Meteorological Data. *Annals of the Brazilian Academy of Sciences*. *88*(4), 2121-2136.

Panta, S., Wimonthanasit, P., Chaithanu, K., Sampattagul, S., and Yawootti, A. (2018, 06/14). *A Comparison of Beta Ray and Light Scattering Technique for PM2.5 and PM10 in Chiangmai.* Paper presented at the 14th Conference on Energy Network of Thailand, Rayong.

Polichetti, G., Cocco, S., Spinali, A., Trimarco, V., and Nunziat, A. (2009). Effects of particulate matter (PM10, PM2.5 and PM1) on the cardiovascular system. *Toxicology*. *261*, 1-8.

Pollution Control Department. (2018). *Thailand's air quality information.* [On-line]. Available: http://air4thai.pcd.go.th/webV2/

Ponomarev, E. I., Shvetsov, E. G., and Usataya, Y. O. (2018). Determination of the Energy Properties of Wildfires in Siberia by Remote Sensing. *Atmospheric and Oceanic Physics*. *54*(9), 979-985.

Prasomsup, W. (2017). *Spatial Evaluation And Prediction Of Urban Heat Island Phenomena In Bangkok And Its Vicinity*. Doctor of Philosophy in Geoinformatics, Suranaree University of Technology.

Prasomsup, W., Piyatadsananon, P., Aunphoklang, W., and Boonrang, A. (2020). Extraction Technic for Built-up Area Classification in Landsat 8 Imagery. *International Journal of Environmental Science and Development*. *11*(1), 15-20.

Remer, L. A., Brogniez, C., Cairns, B., Hsu, N. C., Kahn, R., Stammes, P., Tanré, D., and Torres, O. (2013). *MODIS/AQUA/TERRA*. Aerosol Remote Sensing. Heidelberg: Springer.

Remer, L. A., Kaufman, Y. J., Tanre, D., Mattoo, S., Chu, D. A., Martins, J. V., Li, R. R., Ichoku, C., Levy, R. C., Kleidman, R. G., Eck, T. F., Vermote, E., and Holben, B. N. (2005). The MODIS Aerosol Algorithm, Products, and Validation. *The Journal of the Atmospheric Sciences*. *62*(4), 947-973.

Remer, L. A., Mattoo, S., Levy, R. C., Heidinger, A., Pierce, R. B., and Chin, M. (2012). Retrieving aerosol in a cloudy environment: aerosol product availability as a function of spatial resolution. *Atmospheric Measurement Techniques*. *5*, 1823-1840.

Sajjadi, S. A., Zolfaghari, G., Adab, H., Allahabadi, A., and Delsouz, M. (2017). Measurement and modeling of particulate matter concentrations: Applying spatial analysis and regression techniques to assess air quality. *MethodsX*. *4*, 372-390.

Segura, S., Estellés, V., Utrillas, M. P., and Martínez-Lozano, J. A. (2017). Long term analysis of the columnar and surface aerosol relationship at an urban European coastal site. *Atmospheric Environment*. *167*, 309-322.

Shonk, J. (2013). *Introducing Meteorology: A Guide to Weather*. Edinburgh Dunedin Academic Press Ltd.

Sonwani, S., and Maurya, V. (2019). *Impact of Air Pollution on the Environment and Economy*. Air Pollution: Sources, Impacts and Controls. Oxfordshire: CAB International.

Syafrijon, Marzuki, Emriadi, and Pratama, R. (2018). Relationship Between MODIS-based Aerosol Optical Depth and PM10 over Sumatra to Overcome the Limitations of Air Quality Monitoring Data Availability. *Oriental Journal Of Chemistry*. *34*(4), 2163-2169.

Thai PBS WORLD. (2019). *Prolonged air pollution can cause economic loss up to 6 billion baht.* [On-line]. Available: https://www.thaipbsworld.com/prolonged-air-pollution-can-cause-economic-loss-up-to-6-billion-baht/

The Thaiger & The Nation. (2019). *Bangkok smog to hit Thailand in the tourism pocket.* [On-line]. Available: https://thethaiger.com/news/bangkok/bangkok-smog-to-hit-thailand-in-the-tourism-pocket

U.S. Environmental Protection Agency. (2018). *Technical Assistance Document for the Reporting of Daily Air Quality – the Air Quality Index (AQI)***.** NC: Research Triangle Park.

Unal, Y. S., Toros, H., Deniz, A., and Incecik, S. (2011). Influence of meteorological factors and emission sources on spatial and temporal variations of PM10 concentrations in Istanbul metropolitan area. *Atmospheric Environment*. *45*, 5504-5513.

Veraverbeke, S., Sedano, F., Hook, S. J., Randerson, J. T., Jin, Y., and Rogers, B. M. (2014). Mapping the daily progression of large wildland fires using MODIS active fire data. *International Journal of Wildland Fire*. *23*, 655-667.

Vorapracha, P., Phonprasert, P., Khanaruksombat, S., and Pijarn, N. (2015). A Comparison of Spatial Interpolation Methods for predicting concentrations of Particle Pollution (PM10). *International Journal of Chemical, Environmental & Biological Sciences*. *3*(4), 302-306.

Wang, Q., Li, S., Zeng, Q., Sun, L., Yang, J., and Lin, H. (2020). Retrieval and Validation of AOD from Himawari-8 Data over Bohai Rim Region, China. *Remote Sensing*. *12*(20).

Wang, S., Huang, G. H., Lin, Q. G., Li, Z., Zhang, H., and Fan, Y. R. (2014). Comparison of interpolation methods for estimating spatial distribution of precipitation in Ontario, Canada. *International journal of climatology*. *34*, 3745-3751.

Wei, Q., Zhang, L., Duan, W., and Zhen, Z. (2019). Global and Geographically and Temporally Weighted Regression Models for Modeling PM2.5 in Heilongjiang, China from 2015 to 2018. *Environmental Research and Public Health*. *16*, 5107.

Wiseman, C. L. S., and Zereini, F. (2010). *Airborne Particulate Matter: Sources, Composition and Concentration***.** Urban Airborne Particulate Matter: Origin, Chemistry, Fate and Health Impacts. Berlin: Springer.

Wong, D. W., Yuan, L., and Perlin, S. A. (2004). Comparison of spatial interpolation methods for the estimation of air quality data. *Journal of Exposure Analysis and Environmental Epidemiology*. *14*, 404-415.

World Health Organization. (2013). *Health effects of particulate matter: Policy implications for countries in eastern Europe, Caucasus and central Asia***.** Copenhagen: WHO Regional Office for Europe.

World Health Organization. (2020). *Gross Domestic Product (GDP), per capita, international $ (PPP-adjusted).* [On-line]. Available: https://www.who.int/data/gho/indicator-metadata-registry/imr-details/1145

World Health Organization. (2021). *Ambient (outdoor) air pollution.* [On-line]. Available: https://www.who.int/news-room/fact-sheets/detail/ambient-(outdoor)-air-quality–and-health

Wu, L. (2010). *Mixed effects models for complex data*. (1st ed). Boca Raton: Chapman & Hall/CRC.

Xing, Y.-F., Xu, Y.-H., Shi, M.-H., and Lian, Y.-X. (2016). The impact of PM2.5 on the human respiratory system. *Journal of Thoracic Disease*. *8*(1), E69-E74.

Xue, T., Zheng, Y., Tong, D., Zheng, B., Li, X., Zhu, T., and Zhang, Q. (2019). Spatiotemporal continuous estimates of PM2.5 concentrations in China, 2000–2016: A machine learning method with inputs from satellites, chemical transport model, and ground observations. *Environment International*. *123*, 345-357.

Yalçin, E. (2005). Cokriging and its effect on the estimation precision. *The Journal of The South African Institute of Mining and Metallurgy*. *105*, 223-228.

Yang, H., Chen, W., and Liang, Z. (2017). Impact of Land Use on PM2.5 Pollution in a Representative City of Middle China. *International Journal of Environmental Research and Public Health*. *14*, 462.

You, W., Zang, Z., Pan, X., Zhang, L., and Chen, D. (2015). Estimating PM2.5 in Xi'an, China using aerosol optical depth: A comparison between the MODIS and MISR retrieval models. *Science of The Total Environment*. *505*, 1156-1165.

You, W., Zang, Z., Zhang, L., Li, Y., Pan, X., and Wang, W. (2016). National-Scale Estimates of Ground-Level PM2.5 Concentration in China Using Geographically Weighted Regression Based on 3 km Resolution MODIS AOD. *Remote Sensing*. *8*, 184.

Zaman, N. A. F. K., Kanniah, K. D., Kaskaoutis, D. G., and Latif, M. T. (2021). Evaluation of Machine Learning Models for Estimating PM2.5 Concentrations across Malaysia. *Applied Sciences*. *11*(7326).

Zhang, G., Rui, X., and Fan, Y. (2018). Critical Review of Methods to Estimate PM2.5 Concentrations within Specified Research Region. *International Journal of Geo-Information*. *7*, 368.

Zhang, K., Leeuw, G. d., Yang, Z., Chen, X., Su, X., and Jiao, J. (2019). Estimating Spatio-Temporal Variations of PM2.5 Concentrations Using VIIRS-Derived AOD in the Guanzhong Basin, China. *Remote Sensing*. *11*(22), 2679.

Zhang, P., and Shen, T. (2015). Comparison of different spatial interpolation methods for atmospheric pollutant PM2.5 by using GIS and Spearman correlation. *Journal of Chemical and Pharmaceutical Research*. *7*(12), 452-469.

Zhang, T., Zeng, C., Gong, W., Wang, L., Sun, K., Shen, H., Zhu, Z., and Zhu, Z. (2017). Improving Spatial Coverage for Aqua MODIS AOD Using NDVI-Based Multi-Temporal Regression Analysis. *Remote Sensing*. *9*, 340.

Zheng, Y., Zhang, Q., Liu, Y., Geng, G., and He, K. (2016). Estimating ground-level PM2.5 concentrations over three megalopolises in China using satellite-derived aerosol optical depth measurements. *Atmospheric Environment*. *124*, 232-242.

APPENDIX

APPENDIX

THE GEOGRAPHICAL COORDINATES OF MONITORING STATIONS

Table 1 The PM concentration monitoring stations.

No.	Station_ID	Station_Name	Latitude	Longitude	PM10	PM2.5
1	02t	Bansomdejchaopraya Rajabhat University	13.7330	100.4882	●	●
2	03t	Highway NO.3902 km.13 +600	13.6365	100.4143	●	●
3	05t	Thai Meteorological Department	13.6661	100.6057	●	●
4	08t	Prabadang Rehabiltation Center	13.664	100.5434	●	●
5	10t	National Housing Authority Klongchan	13.7795	100.6457	●	●
6	11t	National Housing Huaykwang	13.7755	100.5692	●	●
7	12t	Nonsi Witthaya School	13.7080	100.5473	●	●
8	13t	EGAT	13.8072	100.5063	●	●
9	14t	Highway District	13.7055	100.3157	●	●
10	16t	South Bangkok Power Plant	13.618	100.5562	●	●
11	17t	Residence for Dept. of Mineral Resources	13.6522	100.5318	●	●
12	18t	City Hall, Samut Prakan	13.5992	100.5973	●	●
13	19t	National Housing Authority Bangplee	13.5703	100.7859	●	●
14	20t	Bangkok University Rangsit Campus	14.0375	100.6051	●	●
15	21t	Ayutthaya Witthayalai School	14.3522	100.5654	●	●
16	22t	Sukhothai Thammathirat Open University	13.9079	100.5356	●	●
17	24t	Na Phralan Police Station	14.6858	100.8720	●	●
18	25t	Khao Noi Fire Station	14.5263	100.9261	●	●
19	26t	Environmental Office 8 Ratchaburi	13.5326	99.8149	●	●
20	27t	Samut Sakhon Wittayalai School	13.5505	100.2643	●	●
21	28t	Pluakdaeng District Health Office	12.9738	101.2128	●	●
22	29t	Health Promotion Hospital Maptaput	12.7086	101.1661	●	●
23	30t	Agricultural Office	12.6715	101.2759	●	●
24	31t	Field Crop Research Center, Rayong	12.7351	101.1356	●	●
25	32t	Laem Chabang Municipal Stadium	13.1192	100.9186	●	●
26	33t	Health Promotion Hospital Bankhaohin	13.0546	101.0981	●	●

Table 1 (Continued).

No.	Station_ID	Station_Name	Latitude	Longitude	PM10	PM2.5
27	34t	Environment Agency Section 13, Chonburi	13.3551	100.9778	●	●
28	41t	Nakhon Sawan Irrigation Project	15.6863	100.1105	●	●
29	46t	Hydrogeological Group Water Resources Regional Office4 khon kaen	16.4453	102.8353	●	●
30	50t	Chulalongkorn Hospital	13.7300	100.5364	●	●
31	52t	Thonburi Power Sub-Station	13.7276	100.4866	●	●
32	53t	Chokchai Police Station	13.7954	100.5929	●	●
33	54t	National Housing Authority Dindaeng	13.7626	100.5504	●	●
34	59t	The Government Public Relations Department	13.7831	100.5405	●	●
35	60t	Municipality Office Tungsadao	13.5886	101.2864	●	●
36	61t	Bodindecha Sing Singhaseni School	13.7696	100.6146	●	●
37	71t	Sriaranyothai Kindergarten	13.6921	102.5021	●	●
38	74t	Government Complex, Rayong	12.7063	101.181	●	●
39	77t	Bu Yai Bai Hall Station	13.9342	101.587	●	●
40	79t	Kanchanaburi Meteorological Station	14.0224	99.5361	●	●
41	81t	Water reservoir	13.8321	100.0580	●	●
42	bkp56t	Din Dang, Bangkok	13.7619	100.5586	●	●
43	bkp57t	Phra Kanong District Office	13.6915	100.6146	●	●
44	bkp58t	Rat Burana District Office	13.6821	100.5061	●	●
45	bkp59t	Ratchathewi District Office	13.7591	100.5346	●	●
46	bkp60t	Dusit District Office	13.7767	100.5210	●	●
47	bkp61t	National Economic and Social Development Council Office	13.7563	100.5143	●	●
48	bkp62t	Odeon Circus	13.7371	100.5127		●
49	bkp63t	Army Apartment Sam Sen	13.7836	100.5345		●
50	bkp64t	Wang Thonglang District Office	13.7790	100.6223		●
51	bkp65t	Samyan Mitrtown	13.7331	100.5283		●
52	bkp66t	Bangrak Lovely Plaza	13.7261	100.5281		●
53	bkp67t	Sathon District Office	13.7078	100.5268		●
54	bkp68t	Thanon Tok Intersection	13.6973	100.4972		●
55	bkp69t	Bank of Ayuthaya Head Office Yan Nawa	13.6792	100.5469		●
56	bkp70t	Soi Sukhumwit 63 Roadside Wattana	13.7221	100.5846	●	●
57	bkp71t	Suan Luang District Office	13.7311	100.6517	●	●
58	bkp72t	Big C Supercenter Bang Na	13.6680	100.6353	●	●
59	bkp73t	Kasertsart University	13.8399	100.5756		●
60	bkp74t	Don Mueng District Office	13.9110	100.5949	●	●

Table 1 (Continued).

No.	Station_ID	Station_Name	Latitude	Longitude	PM10	PM2.5
61	bkp75kp	Sai Mai District Office	13.8960	100.6606	●	●
62	bkp76t	Bang Kapi District Office	13.7665	100.6478		●
63	bkp77t	Suan Sayam-Ram Intra Intersection	13.7994	100.6825	●	●
64	bkp78t	Lat Krabang Hospital	13.7221	100.7841		●
65	bkp79t	Chaloem Phrakiat Rama 9 Park Min Buri	13.8136	100.7321	●	●
66	bkp80t	Nong Chok District Office	13.8554	100.8627	●	●
67	bkp81t	Seacon Square	13.6956	100.6476	●	●
68	bkp82t	Mahaisawan Intersection	13.7052	100.4847		●
69	bkp83t	Library under King Taksin Bridge	13.7197	100.5088		●
70	bkp84t	Tha phra Intersection	13.7294	100.4744	●	●
71	bkp85t	Bangkok Noi Train Police Station	13.7596	100.4811		●
72	bkp86t	Phutthamonthon 1 - Borommaratchachonnani Intersection	13.7808	100.4267	●	●
73	bkp87t	Thon Buri Market Sanam Luang 2	13.7463	100.3551	●	●
74	bkp88t	Siam University	13.7187	100.4539		●
75	bkp89t	Ma Charean Roadside, Petcha Kasem 8	13.7056	100.3432	●	●
76	bkp90t	Bang Bon 5 Market	13.6392	100.3730	●	●
77	bkp91t	King Mongkut's University of Technology Thonburi	13.6510	100.4967	●	●
78	bkp92t	Phra Nakhon District Office	13.7642	100.4991		●
79	bkp93t	Huai Khwang District Office	13.7768	100.5795	●	●
80	bkp94t	Khlong Toei District Office	13.7085	100.5837		●
81	bkp95t	Bang Sue District Office	13.8096	100.5379		●
82	bkp96t	Ladphrao District Office	13.8036	100.6075	●	●
83	bkp97t	Lak Si District Office	13.8874	100.5792		●
84	bkp98t	Bang Khen District Office	13.8736	100.5958		●
85	bkp99t	Saphan Sung District Office	13.7689	100.6857	●	●
86	bkp100t	Bueng Kum District Office	13.7852	100.6692		●
87	bkp101t	Khlong Sam Wa District Office	13.8599	100.7040	●	●
88	bkp102t	Chomthong District Office	13.6778	100.4839	●	●
89	bkp103t	Bang Phlat District Office	13.7940	100.5050		●
90	bkp104t	Bang Khae District Office	13.6963	100.4090	●	●
91	bkp105t	Bang Khun Thian District Office	13.6599	100.4359	●	●
Sum of stations for PM concentrations interpolation method					68	91

Table 2 The meteorological stations.

No.	Station_ID	Station_Name	Latitude	Longitude	RH	TEMP	WS	P	VIS
1	400201	Station Nakhon Sawan	15.6718	100.1324	●	●	●	●	●
2	400301	Takfa Agromet	15.3494	100.5303	●	●	●	●	●
3	402301	Chainat Agromet	15.1500	100.1833	●	●	●	●	●
4	415301	Ayutthaya Agromet	14.5347	100.7250	●		●	●	●
5	417201	Nakorn Nayok	14.36222	101.39278			●	●	●
6	419301	Pathum Thani Agromet	14.1000	100.6167	●		●	●	●
7	423301	Chachoengsao Agromet	13.5156	101.4583	●	●	●	●	●
8	424301	Station Ratchaburi	13.4893	99.7924	●	●	●	●	●
9	425201	Station Suphan Buri	14.4744	100.1389	●	●	●	●	●
10	425301	U Thong Agromet	14.3036	99.8647	●	●	●	●	●
11	426201	Station Lop Buri	14.7997	100.6450	●	●	●	●	●
12	426401	Station Bua Chum	15.2667	101.1874	●	●	●	●	●
13	429201	Station Pilot Station, Samut Prakan	13.3939	100.5994	●	●	●	●	●
14	429301	Samutprakan Agromet	13.5167	100.7617	●	●	●	●	●
15	429601	Station Suvarnabhumi Airport	13.6864	100.7675	●	●	●	●	●
16	430201	Station Prachin Buri	14.0584	101.3693	●	●	●	●	●
17	430401	Station Kabin Buri	13.9833	101.7072	●	●	●	●	●
18	431201	Station Nakhon Ratchasima	14.9683	102.0860	●	●	●	●	●
19	431301	Pakchong Agromet	14.6439	101.3319	●	●	●	●	●
20	431401	Station Chok Chai	14.7189	102.1686	●	●	●	●	●
21	438201	Samut Songkram	13.40778	100.03222					●
22	440201	Station Aranya Prathet	13.7000	102.5833	●	●	●	●	●
23	440401	Station Sa Kaew	13.7889	102.0347	●	●	●	●	●
24	450201	Station Kanchanaburi	14.0225	99.5358	●	●	●	●	●
25	450401	Station Thong Phaphum	14.7422	98.6364	●	●	●	●	●
26	451301	Nakornpathom Agromet	14.0117	99.9700	●	●	●	●	●
27	455201	Station Bangkok Metropolis	13.7264	100.5600	●	●	●	●	●
28	455203	Station Bangkok Port Khlong Toei	13.7069	100.5681	●	●	●	●	●
29	455301	Bangna Agromet	13.6664	100.6061	●	●	●	●	●
30	455601	Station Don Muang Airport	13.9192	100.6050	●	●	●	●	●
31	459201	Station Chon Buri	13.3667	100.9833	●	●	●	●	●
32	459202	Station Ko Sichang	13.1617	100.8019	●	●	●	●	●

Table 2 (Continued).

No.	Station_ID	Station_Name	Latitude	Longitude	RH	TEMP	WS	P	VIS
33	459203	Station Phatthaya	12.9200	100.8694	●	●	●	●	●
34	459204	Station Sattahip	12.6833	100.9833	●	●	●	●	●
35	459205	Station Laem Chabang	13.0769	100.8758	●	●	●	●	●
36	465201	Station Phetchaburi	12.9994	100.0606	●	●	●	●	●
37	478201	Station Rayong	12.6322	101.3436	●	●	●	●	●
38	478301	Huai Pong Agromet	12.7333	101.1333	●	●	●	●	●
39	480201	Station Chanthaburi	12.6167	102.1133	●	●	●	●	●
40	480301	Phliu Agromet	12.5086	102.1731	●	●	●	●	●
41	501201	Station Khlong Yai	11.7667	102.8833	●	●	●	●	●
Sum of stations for Meteorological data interpolation method					39	37	40	40	41

CURRICULUM VITAE

Name Miss. Pirada Tongprasert

Date of Birth June 19, 1985

Place of Birth Nan

Education Background

2007: Bachelor of Science in Geography,
Faculty of Social Sciences, Kasetsart University,
Thailand.

2014: Master of Science in Geoinformatics,
Faculty of Social Sciences, Chiang Mai University,
Thailand.

Position and Place of work

2015-Present: Lecturer,
Faculty of Humanities and Social Sciences,
Kamphaeng Phet Rajabhat University, Thailand.